Coordination and Reactivity of Ligands with Unconventional 'Donors'

Chenxi Ma

A thesis submitted for the degree of Doctor of Philosophy

of

The Australian National University

November 2018

Declaration

This thesis is an account of the research undertaken between February 2015 and November 2018 at the Research School of Chemistry, The Australian National University. Except where due reference has been made, the work contained in this thesis is my own.

Chenxi Ma

November 2018

Acknowledgements

The past few years have been a wonderful yet challenging time. It would not have been the same without the support from friends, colleagues and family.

Thank you, Tony, for your unwavering support throughout my candidature. Your enthusiasm for chemistry and breadth of knowledge is inspirational, and I have learnt so much under your guidance. It was exciting heading to work knowing there will be a new idea (or project!) from you waiting around the corner. Thank you for believing in me and encouraging me to achieve more than I ever could have imagined. Thank you, Mark S, for your kindness and generosity, especially for making sure I had lunch to eat and spoiling me with delicious food!

It has been a privilege to work with the members of the Hill group, past and present: Stephen, Manab, Caitlin, Annie, Jas, Yong-Shen, Richie, Kass, Natalie, Jane, Richard, Kedar, Takao, Tim, Anders, Ben, Harrison, Chee Sheng, Liam, Ryan and Steve. Thank you all for the friendship, the company in the lab and office, and many memorable moments during our conference adventures.

Thank you to Professor Kempe for giving me the opportunity to carry out four months of research in Bayreuth, Germany, which was a priceless and unforgettable experience. Thank you to my friends and colleagues for warmly welcoming me into the group and Germany, giving me a sense of belonging from the moment I arrived. Thank you Fabian, Freddie, Melanie, Meli, Nick, Robin, Mara, Andy, Heidi and Martin.

Thank you, Mark E and Geoff, for the advice and guidance from my undergraduate to postgraduate years, and for offering me opportunities to teach on numerous occasions. Each opportunity has been an incredible learning experience.

Thank you, Jas, for teaching me crystallography (on both crystals and Olex!) and Tony Willis for the advice on the challenging structures. Thank you, Anitha, for patiently running mass spectrometric analysis on my air sensitive compounds. Thank you, Chris Blake, for the guidance during the variable temperature experiments.

Thank you, Ben, Yong-Shen, Fabian, Craig and Jas for taking the time out of your busy schedule to read my thesis and provide feedback. Thank you, Craig for solving all my Word formatting woes.

Thank you An, Celeste, Craig, Fabian and Michael, for understanding when I go MIA during busy periods of my candidature and for being a pillar of support in your own unique ways.

Thank you to my family for the unwavering unconditional love and support, for raising me to be who I am today and for all the delicious food.

Abstract

This thesis describes investigations into tridentate *facial* or *meridional* ligand frameworks that feature unconventional 'donors' including boron, aluminium and silicon and their coordination chemistry with transition metals. Inclusion of electropositive elements within the ligand framework are of interest as they impart unique properties to their corresponding complexes and contrasts that of conventional donors such as phosphorus, nitrogen and sulfur.

Chapter one provides an introduction that includes a survey of relevant literature of pincer and scorpionate chemistry.

In Chapter two, the series of complexes [Ru(X)(CO)(PPh_3){κ^3-*H,S,S'*-$H_2B(mt)_2$}] (X = H, Cl, SePh, BCat, $SiCl_3$, $SiMe_3$) was synthesised for spectroscopic and structural comparisons to gain insight into perturbations on the B–H–Ru interaction affected by the *trans* X ligand. The *trans* influence of the X ligand on the δ_H chemical shift of the borohydride B–*H*–Ru group was assessed. Ligands of strong *trans* influence resulted in a B–H···Ru interaction consisting of more borohydride character while those of weaker *trans* influence resulted in a B···H–Ru interaction with metallohydridic character. The osmium complex [OsH(CO)(PPh_3){κ^3-*H,S,S'*-$H_2B(mt)_2$}] served as a further (5d transition metal) point of comparison. When the *trans* ligand was a σ-organyl (X = Ph, CH=CHPh), the complexes [Ru(X)(CO)(PPh_3){κ^3-*H,S,S'*-$H_2B(mt)_2$}] were observed as transient species *en route* to the ruthenaboratrane [Ru{κ^3-*B,S,S'*-$BH(mt)_2$}(CO)(PPh_3)$_2$].

In Chapter three, a convenient one-pot synthesis from [RuHCl(CO)(PPh_3)$_3$] was developed for the first doubly-bridged ruthenaboratrane [Ru{κ^3-*B,S,S'*-$BH(mt)_2$}(CO)(PPh_3)$_2$] (Ru→B), which can alternatively be obtained using [Ru(Ph)Cl(CO)(PPh_3)$_2$]. Trace amounts of [Ru(C≡CPh)(CO)(PPh_3){κ^3-*H,S,S'*-$BH(mt)_2$}] and [Ru(κ^2-*N,S*-mt)(Ph)(CO)(PPh_3)$_2$] were crystallographically identified during the syntheses. The reactivity of the Ru→B bond was explored for oxidative conversion to the κ^3-*H,S,S* mode of coordination. The reactions revealed either a plethora of products indicative of ligand degradation or no reaction, which suggests a robust M→B interaction. The complex [Ru{κ^3-*B,S,S'*-$BH(mt)_2$}(CO)(PPh_3)$_2$] was shown to serve as a

useful precursor to access further examples of doubly-bridged ruthenaboratrane complexes. Phosphine substitution reactions of [Ru{κ^3-*B,S,S'*-BH(mt)$_2$}(CO)(PPh$_3$)$_2$] afforded the monosubstituted products [Ru{κ^3-*B,S,S'*-BH(mt)$_2$}(CO)(PPh$_3$)(L)] (L = CO, PMe$_2$Ph) and the disubstituted products [Ru{κ^3-*B,S,S'*-BH(mt)$_2$}(CO)(L)$_2$] (L = PMe$_2$Ph, P(OMe$_3$)) and [Ru{κ^3-*B,S,S'*-BH(mt)$_2$}(CO)(Z-Ph$_2$PCH=CHPPh$_2$)]. These complexes consistently feature an elongated ruthenium phosphorus bond *trans* to boron compared to that *trans* to sulfur, confirming a pronounced *trans* influence exerted by the Ru→B bond. Comparisons were made to sulfur-based metallaboratranes, including the triply-bridged series [Ru{κ^4-*B,S,S',S''*-B(mt)$_3$}(CO)(PR$_3$)] (PR$_3$ = PMe$_2$Ph, PCy$_3$, P(OMe)$_3$), which were synthesised and characterised. No general trends concerning the M→B interaction were identified from the complexes assessed, reflecting the constraints of chelation in different ligand frameworks and metals.

In Chapter four, the synthesis of aluminium based ligands was explored and yielded the novel aluminium pro-ligand, Li[H$_2$Al(mt)$_2$].THF. Coordination of the [H$_2$Al(mt)$_2$]$^-$ ligand to transition metal precursors allowed spectroscopic observation of the desired products on ruthenium, osmium and rhenium, but ligand degradation precluded isolation of complexes with an intact [H$_2$Al(mt)$_2$]$^-$ unit. The greater reactivity and metal-mediated lability of Li[H$_2$Al(mt)$_2$].THF compared to the Na[H$_2$B(mt)$_2$] ligand was a recurrent feature.

In Chapter five, coordination of the *o*-phenylenediamine-based silane HPhSi(NCH$_2$PPh$_2$)$_2$C$_6$H$_4$-1,2 to metal precursors afforded rhodium(III), rhodium(I), iridium and osmium complexes. A third preparatory method toward the reported complex [RhHCl{SiPh(NCH$_2$PPh$_2$)$_2$C$_6$H$_4$-1,2}(PPh$_3$)] was discovered with use of [RhCl(CO)(PPh$_3$)$_2$]. The iridium analogue [IrHCl{SiPh(NCH$_2$PPh$_2$)$_2$C$_6$H$_4$-1,2}(PPh$_3$)] and [RhHCl{SiCl(NCH$_2$PPh$_2$)$_2$C$_6$H$_4$-1,2}(PPh$_3$)] were similarly synthesised. Preparative routes to rhodium(I) square planar complex [Rh{SiPh(NCH$_2$PPh$_2$)$_2$C$_6$H$_4$-1,2}(PPh$_3$)] were explored and include dehydrohalogenation of octahedral rhodium(III) complexes and a direct synthesis pathway from [RhH(PPh$_3$)$_4$]. The strong σ-donating properties of the silyl unit was evident by elongation of the bond *trans* to silicon in crystallography studies. Complex [Rh{SiPh(NCH$_2$PPh$_2$)$_2$C$_6$H$_4$-1,2}(PPh$_3$)] displayed facile ligand addition and substitution with dihydrogen, carbon monoxide and norbornadiene to give [RhH$_2$\{SiPh(NCH$_2$PPh$_2$)$_2$C$_6$H$_4$-1,2}(PPh$_3$)], [Rh{SiPh(NCH$_2$PPh$_2$)$_2$C$_6$H$_4$-1,2}(CO)(PPh$_3$)],

[Rh{SiPh(NCH_2PPh_2)$_2C_6H_4$-1,2}$(CO)_2$] and [Rh{SiPh(NCH_2PPh_2)$_2C_6H_4$-1,2}(C_7H_8)]. Direct synthesis resulted in the first benzosiladiazole based osmium complex [OsCl{SiPh(NCH_2PPh_2)$_2C_6H_4$-1,2}(PPh_3)] from [$OsCl_2(PPh_3)_3$] and HPhSi(NCH_2PPh_2)$_2C_6H_4$.

The Appendix Chapter details the reaction of pro-ligands $H_2C(NCH_2PR_2)_2C_{10}H_6$-1,8 (R = Cy, Ph) with iridium precursors. Pro-ligand $H_2C(NCH_2PCy_2)_2C_{10}H_6$-1,8 was found to readily react with iridium(I) chloro-bridged dimers through double C–H activation to afford iridium(III) NHC complex *trans*-[IrH_2Cl{$C(NCH_2PCy_2)_2C_{10}H_6$}]. The *trans* hydrides in [IrH_2Cl{$C(NCH_2PCy_2)_2C_{10}H_6$}] hindered reductive elimination of dihydrogen. However, the complex underwent spontaneous hydride substitution upon solvation in chloroform, which afforded *cis*-[$IrHCl_2${$C(NCH_2PCy_2)_2C_{10}H_6$}]. Hydride replacement reactions were similarly observed for the diphenylphosphine supported trihydride complex, [IrH_3{$C(NCH_2PPh_2)_2C_{10}H_6$}].

Contents

Abbreviations

General

3c2e, 2c2e	3-centre 2-electron, 2-centre 2-electron
Ac	acetyl
Ar	aryl
^{n}Bu, ^{t}Bu	butyl, *tert*-butyl
Bz	benzoyl
cat.	catalyst
Cy	cyclohexyl
DFT	density functional theory
e.s.d.	estimated standard deviation
Et	ethyl
fac	facial
h	hour(s)
Me	methyl
mer	meridional
min	minute(s)
ML_n	generalised metal fragment (M) with n ligands (L)
NHC	N-heterocyclic carbene
^{i}Pr	*iso*-propyl
Ph	phenyl
r.t.	room temperature
VE	valence electron(s)

Spectroscopy/Spectrometry

δ_{nuclei}	chemical shift, expressed in ppm
$^{n}J_{AB}$	n-bond coupling between nuclei A and B, expressed in Hz
$\{^{1}H\}$	Proton decoupled NMR experiment
cm^{-1}	wavenumber(s)
h.h.w.	half height width
HMBC	heteronuclear multiple-bond correlation

HSQC	heteronuclear single quantum coherence
HR-ESI MS	high resolution electrospray ionisation mass spectrometry
LR-ESI MS	high resolution electrospray ionisation mass spectrometry
IR	infrared
m/z	mass-to-charge ratio
NMR	nuclear magnetic resonance
pm	picometer
ppm	parts per million
s, d, t, t^v, br	singlet, doublet, triplet, virtual triplet, broad

Solvents, Reagents and Ligands

$[BAr^F{}_4]^-$	tetrakis(3,5-bis(trifluoromethyl)phenyl)borate
Bpin	pinacolato boron
COD	1,5-cyclooctadiene
COE	cyclooctene
Cp	η^5-cyclopentadienyl
Cp*	η^5-pentamethylcyclopentadienyl
DCM	dichloromethane
dba	dibenzylideneacetone
depe	1,2-bis(diethylphosphino)ethane
DMSO	dimethyl sulfoxide
dppe	1,2-bis(diphenylphosphino)ethane
dppen	1,2-bis(diphenylphosphino)ethylene
Et_2O	diethyl ether
HBCat	catecholborane
Hmt	methimazole
mt	methimazolyl
LDA	lithium diisopropylamide
Mes	mesityl (2,4,6-trimethylphenyl)
NBD	norbornadiene
NCMe or MeCN	acetonitrile
OTf	trifluoromethansulfonate

pip	piperidine
py	pyridine
pz	pyrazolyl
TEEDA	*N,N,N',N'*-tetramethylethylenediamine
THF	tetrahydrofuran

Complexes

The complexes in this thesis are numbered according to the following:

L Chapter.number refers to literature compounds. A number followed by a letter of the alphabet (a–w) refers to isomers or derivatives in complexes of similarity (e.g. variation at the metal, substituents, anion or cation).

Chapter.number refers to compounds prepared in this work. A number followed by x or y refers to by-products or decomposition products. A number followed by a letter of the alphabet (a–w) refers to isomers.

Chapter 1

Overview of Pincer and Poly(azolyl)borate Chemistry

1.1 General Introduction

The research in this thesis describes ligand design and complex synthesis in the broad fields of pincer and soft scorpionate organometallic chemistry. Both pincer and scorpionate complexes typically consist of terdentate ligands, with a plethora of examples of each available in literature. The key distinguishing feature is that pincer complexes usually feature *meridional* coordination whereas scorpionate systems are predominantly *facial* coordinating (Figure 1.1). Where these coordinative definitions of the two fields were once viewed as distinct, advancements in both have revealed exceptions that illustrate the delicate (circumstantial) balance between *meridional* and *facial* coordination (i.e. either conformation is possible depending on the environment around the metal centre).

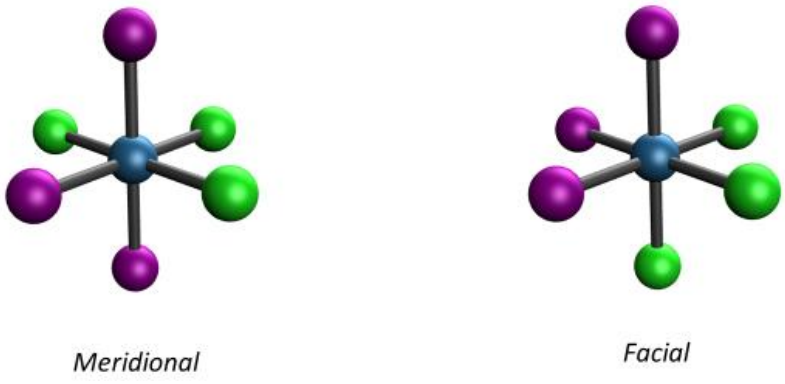

Figure 1.1: General representation of *meridional* pincer and *facial* scorpionate coordination.

Systems offering geometric flexibility prove beneficial in catalysis in directing the site of reactivity. The occupation of three adjacent coordination sites in a *fac*-bound ligand directs reactivity to the other face of the complex. In comparison, a *mer*-bound ligand provides access to unsaturated square planar complexes, which are renowned in their role in catalysis (e.g., group 10 metal complexes in cross coupling reactions).[1] Furthermore, an attractive feature of pincer and scorpionate terdentate ligands is the potential for hemilability,[2] which for these ligands involves dissociation of one group from the metal while the other two remain firmly held by chelation. The benefits are two-fold and include generation of a vacant coordination site through hemilability and re-coordination of the ligand donor group conferring a more long-lived system. Therefore, understanding the factors that dictate geometric coordination preference could aid in sophisticated targeted ligand design.

The enormous field of pincer complexes and their applications has been collated into books,[3,4] and reviews with particular emphasis on catalysis.[5-17] As there is an impressive body of literature available on pincer complexes, this chapter only briefly summarises the progress in this field with selected highlights on the applications of the complexes. A similarly substantial amount of research has been carried out on the scorpionate class of ligands, with summaries available for complexes of tris(azolyl)borates.[18-20] However, the chemistry of $Bm^{R'}$ has yet to be reviewed and thus a review is provided in Section 1.3.

Aspects of the following introductory chapter have contributed to a comprehensive review that is to be submitted for publication. As such, the chapter contains material that is beyond the specific scope of the research to be discussed in the subsequent chapters and instead provides a broader context.

1.2 Pincers

1.2.1 Classical Pincers and General Advancements

In 1976, Moulton and Shaw reported complexes featuring the *meridionally* coordinated PCP tridentate ligand (Figure 1.2).[21] This was shortly followed by reports from van Koten on the NCN framework.[22] The installation of the ligands in Figure 1.2 was achieved by activation of the C–H bond in pro-ligand $(P^tBu_2CH_2)_2C_6H_4$-2,6, forming ligand $(P^tBu_2CH_2)_2C_6H_3$-2,6 on the corresponding metal centre. The area remained generally underexplored until the 1990s where pincer complexes of second and third row late transition metals were shown to be effective in the fields of catalysis, molecular recognition and supramolecular chemistry.[5,23,24]

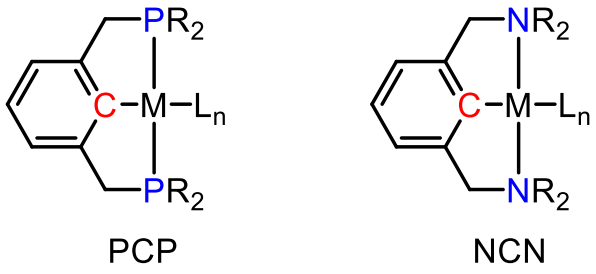

Figure 1.2: Early examples of organometallic pincer complexes.

Coined in 1989 by van Koten, the term 'pincer' was initially used to describe terdentate ligands with a central anionic carbon and two flanking units that coordinate to the metal centre in a rigid *meridional* geometry. The field has since shown tremendous growth, owing to the impressive modularity of the ligand and the high thermal stability of the tridentate coordination mode. The definition of pincers has broadened to describe any *mer*-bound tridentate ligand. The general formula denoted by [ML_n(EYE)] in Figure 1.3 refers to a pincer ligand (EYE) coordinated to a metal (M) with co-ligands (L_n).

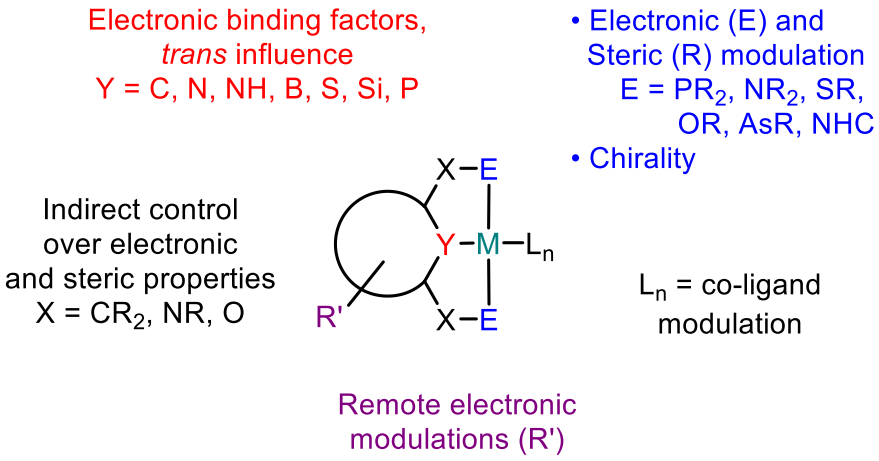

Figure 1.3: General structure of a pincer complex and areas of modulation. NHC = N-Heterocyclic Carbene.

Modulations include the nature of the equatorial (Y) and flanking (E) donors, which are neutral or ionic and feature many of the p-block elements. The two E donor groups are not necessarily identical, and the ligand can be classified based on symmetry.[12] Palindromic (EYE) ligands dominate the majority of the field and non-palindromic (e.g. NNP, NCP) present an avenue of further variation. The spacer (X) controls the size of the ring formed by the pincer ligand, which are commonly five or six membered rings, but more recently has provided a focus for non-innocent behaviour. The backbone can be aliphatic or aromatic with substituents (R'). These modulations combined have a direct influence on the steric (including chirality) and electronic properties, allowing access to many complexes through fine-tuning of the ligand.

Meridional coordination is particularly prevalent for classical pincer systems featuring sp^2 hybridised C and N central donors, which impose planarity on the ligand. However, examples of *fac* coordination are known. Roddick and co-workers showed the reaction of *mer*-[IrHCl(PCP)(C_2H_4)] **L1.1** (Scheme 1.1) with bidentate ligands results in folding of the pincer scaffold affording *fac*-[Ir(PCP)(LL)] (LL = norbornadiene, 1,5-cyclooctadiene,

$P(C_2F_5)_2CH_2CH_2P(C_2F_5)_2$).[25] The non-*meridional* coordination of the PCP ligand in **L1.2** was attributed to the strongly π-accepting $P(CF_3)_2$ groups preferring to be *cis* disposed to avoid competition for dπ-back-bonding that would arise from a mutually *trans* coordination.

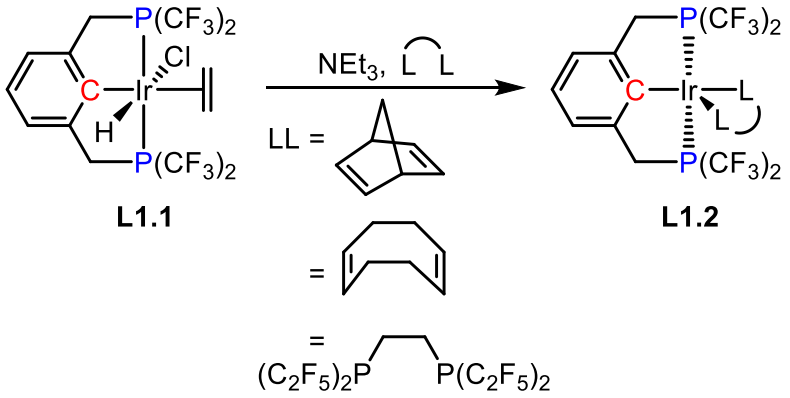

Scheme 1.1: Dehydrohalogenation of *mer*-[IrHCl(PCP)(C_2H_4)] **L1.1** to *fac*-[Ir(PCP)(LL)] **L1.2**.

Since the introduction of archetypical carbon-based pincer scaffolds, other backbones featuring heteronuclear functionality have been developed. These include amido, silyl, phosphido and boryl moieties as the central donor. The incorporation of reactive groups such as N-heterocyclic carbenes (NHC), boryl and silyl donors within the tridentate system confers stabilisation of these units *via* chelation. Due to the abundance of pincers in the literature and extensive reviews, it is impossible to provide complete coverage of all areas here. Therefore, the subsequent sections aim to provide a brief introduction to pincers featuring NHCs, and recent advances in the field of boryl and silyl pincer complexes, relevant to the work to follow.

1.2.2 Non-conventional Pincers

1.2.2.1 N-Heterocyclic Carbene Pincers

The inclusion of NHC units within pincer ligands has introduced great structural diversity with NHCs being incorporated at any position in the EYE pincer framework. Common patterns include NHCs at the two E positions (CYC) or less commonly as the central Y donor of the pincer system. The variety of pincer ligands containing NHC units and their corresponding complexes across the periodic table has been thoroughly reviewed, with discussions mainly focused on CYC based complexes.[17,26-29]

The first examples of NHC-based pincers of the CYC framework (lutidine based **[L1.3]**$^+$ and **[L1.4]**$^+$) were introduced in 2001 (Figure 1.4). Numerous derivatives, including those of (meta)-xylyl with carbon as the equatorial donor have since been reported.[30,31]

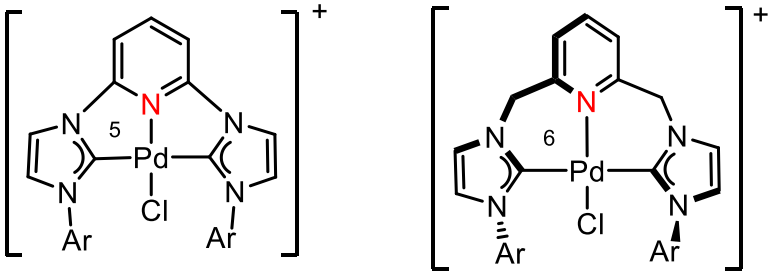

[L1.3]$^+$ **[L1.4]**$^+$

Figure 1.4: First examples of NHC-based pincer ligands.

The ligand backbone of **[L1.3]**$^+$ and **[L1.4]**$^+$ differ at the spacer (X), by an additional methylene group in **[L1.4]**$^+$, which increases the size of each ring of the chelate from five to six. Consequently, complexes of similar framework to **[L1.4]**$^+$ may adopt characteristic C_2 conformation, as shown in atropisomers **L1.5a** and **L1.5b** (Figure 1.5). Dynamic interconversion occurs between the atropisomers in solution, demonstrating conformational fluxionality despite the rigidity of the pincer ligand.[32-35] Experimental and computational studies of palladium(II) CNC complexes suggest that the fluxionality proceeds through C_s symmetric intermediates with partial or complete dissociation of the lutidine donor.[34] A recent report by Chaplin on the rhodium(I) CNC complex **[L1.6]**BAr^F_4 (BAr^F_4 = tetrakis(3,5-bis(trifluoromethyl)phenyl)borate) showed that atropisomerisation was enhanced by reversible coordination of CO.[32]

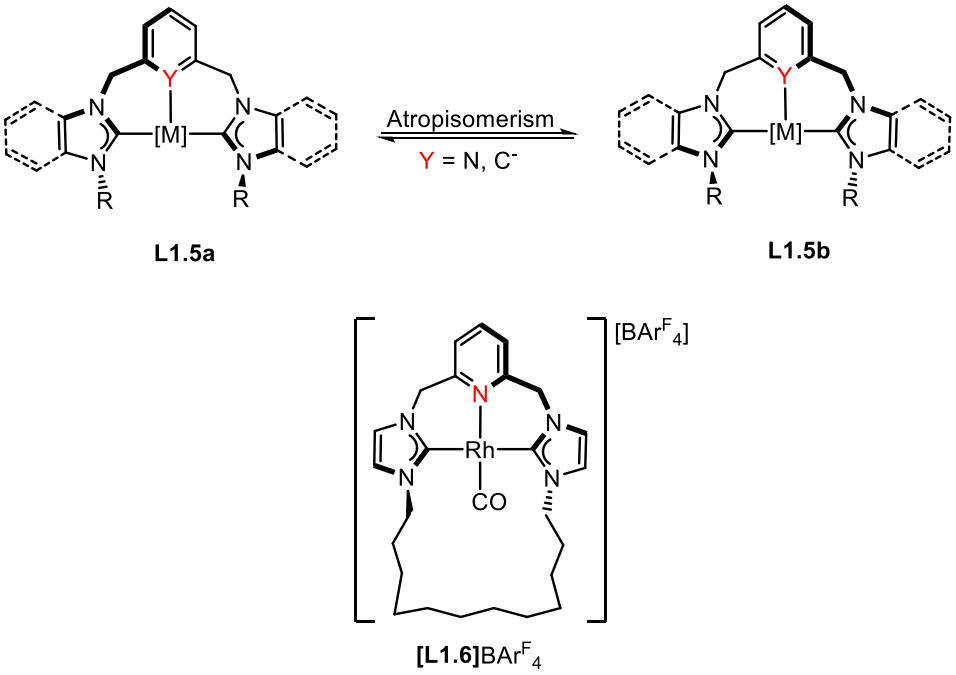

Figure 1.5: Fluxional equilibrium between **L1.5a** and **L1.5b**, and example complex **[L1.6]**BAr$^F_4$.

Compared to the CYC complexes, the complexes featuring an E(NHC)E system with a NHC core have received less attention and will be of focus here as they are most relevant to the work in this thesis (See Appendix chapter). In particular, metal complexes featuring the P(NHC)P [6,6]-(benz)imidazolium (**L1.7**–**[L1.9]**$^+$)[36-43] and [5,5]-(benz)imidazolium (**L1.10**–**[L1.12]**$^+$)[44-47] scaffolds are summarised in Figure 1.6.

Nearly all the complexes in Figure 1.6 display *mer* coordination of the pincer ligand, except for the flexible alkyl variants of **L1.7**[37] and **[L1.9]**$^+$.[43] The phosphaferrocenyl-substituted NHC ligand in **[L1.9]**$^+$ was crystallographically shown by Ganter and co-workers to be *fac*-binding (P–Ru–P 105.03(14)°).[43] This might be attributed to the pentamethylcyclopentadienyl ligand (Cp*) in **[L1.9]**$^+$ that occupies one face of the metal, thus enforcing *fac* coordination of the P(NHC)P system. However, the phosphaferrocenyl-substituted NHC ligand is similarly *fac*-bound in the Mo(CO)$_3$ derivative where no geometric constraints are imposed by the carbonyl ligands.[43] As such, the *fac* geometry may not simply be a consequence of the accommodation of another *fac* co-ligand.

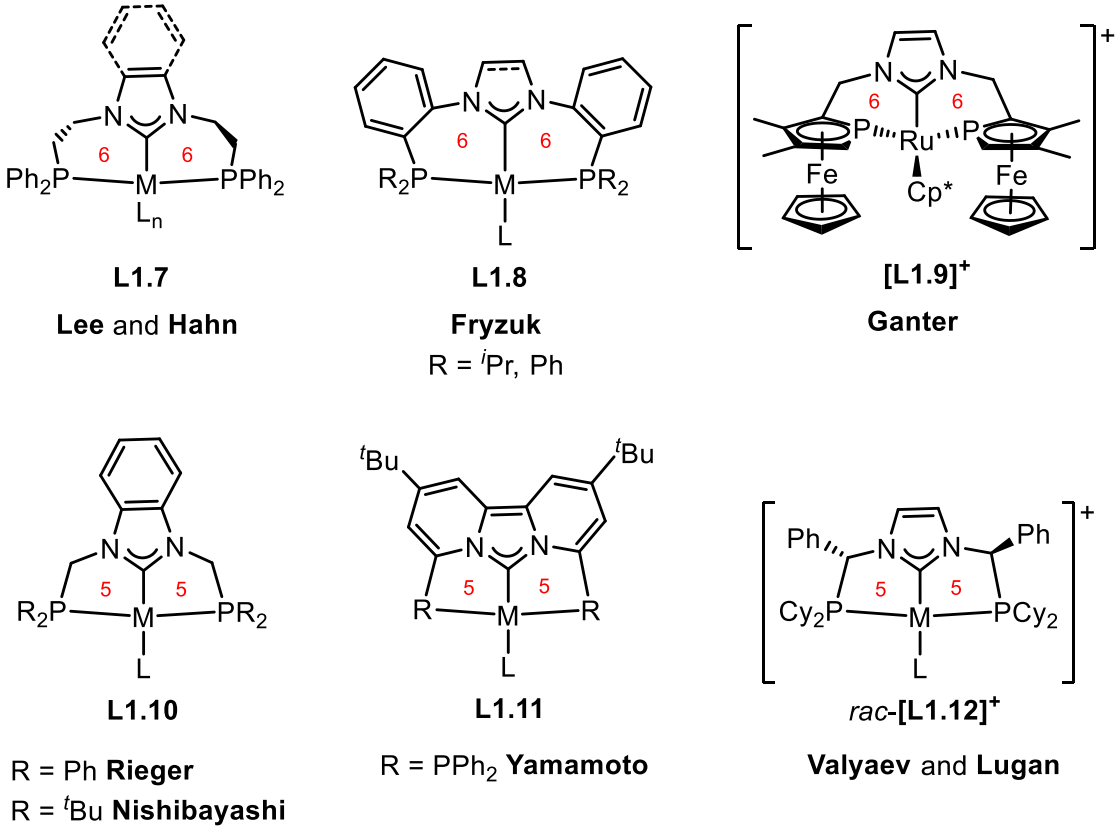

Figure 1.6: Examples of [6,6]- and [5,5]-membered P(NHC)P metal complexes.

The P(NHC)P ligands are commonly obtained as imidazolium salts, as the precursor to carbene ligands. Similar strategies are used in the activation of these salts, as known for non-chelate azolium precursors. One common method to install P(NHC)P systems onto metals involved using silver as a carbene transfer agent. Complexes of the form **L1.7**[36-39] are prepared analogous to the steps illustrated in Scheme 1.2 with the benzimidazolium system.[39] Deprotonation of the imidazolium salt **[L1.13]**Cl by Ag_2O generates the corresponding silver complex **L1.14**. Subsequent carbene transfer from silver to metal reagents such as $[PtCl_2(PhCN)_2]$ and $[PdCl_2(COD)]$ affords complexes **[L1.15a]**Cl and **[L1.15b]**Cl, respectively.[39] This process is driven by cleavage of the weak NHC–Ag bond and precipitation of the silver halide side product.

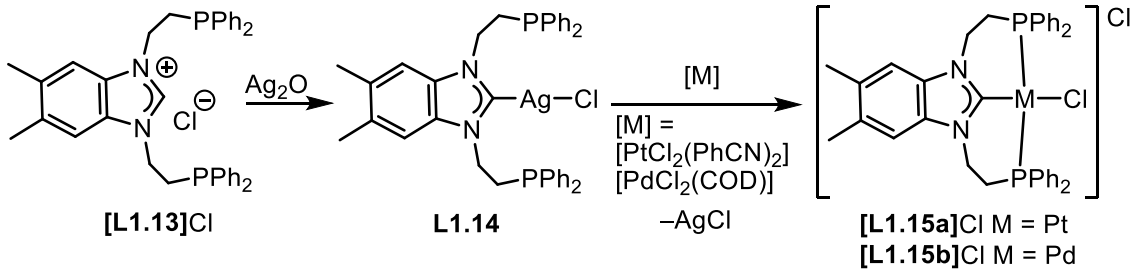

Scheme 1.2: Activation of imidazolium salts with silver and subsequent carbene transfer reactions.

Transmetallation from early to late transition metals has also been used as a synthetic strategy to install carbene pincers onto late transition metals. Recently, Bourissou and co-workers demonstrated the preparation of the SCS palladium complex **[L1.19]**$^-$ (Scheme 1.3) from transmetallation with zirconium precursors generated from the reaction of 1,3-bis(thiophosphinoyle)indene pro-ligand **L1.16** and $[Zr(NMe_2)_4]$.[48] The more stable zirconium precursor **L1.17** was isolated and converted to **L1.18** through thermolysis prior to use. Transmetallation onto platinum was similarly efficient.[48]

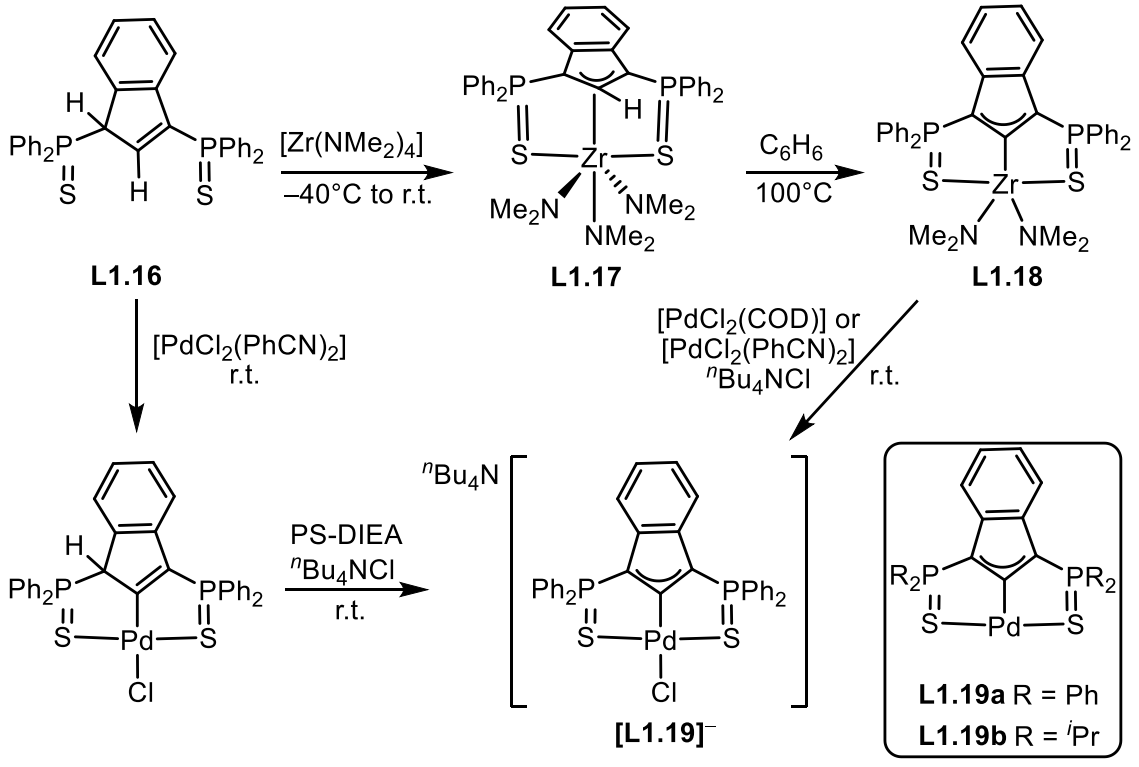

Scheme 1.3: Preparation of **[L1.19]**$^-$ from transmetallation pathway or C–H activation/deprotonation pathway (PS-DIEA = polystyrene-supported diisopropylethylamine).

An alternative route to **[L1.19]**$^-$ was employed in 2011 which involved C–H activation of **L1.16** to $[PdCl_2(PhCN)_2]$, followed by deprotonation of the resulting palladium complex by polystyrene-supported diisopropylethylamine (PS-DIEA) (Scheme 1.3).[49,50] Complex **[L1.19]**$^-$ and the non-halogenated derivatives **L1.19a** and **L1.19b** have been demonstrated as effective catalysts in a range of transformations. These include imine allylation,[51] cycloisomerisation of *N*-tosyl alkynylamides to form five to seven membered ring alkylidene lactams,[52] cycloisomerisation of functionalised and internal alkynoic acids,[53] and carboxylative cyclisation of propargylamines.[54] Greater catalytic activity of the SCS based palladium complexes (**L1.19**) was favoured for an electron rich indenediide framework[51] and attributed to the cooperation between the metal centre and the indenediide backbone. The non-innocence of the indenediide ligand was confirmed through experimental, computational and kinetic studies[52-56] and are rare examples of cooperative catalysis with palladium.

The activation of imidazolium pincer precursors to their corresponding carbene functionality has been widely demonstrated through deprotonation by an external base or a basic co-ligand. Deprotonation of **[L1.20a]**PF_6 by $KN(SiMe_3)_2$ affords the isolable carbene **L1.21** (Scheme 1.4).[57] However, due to the sensitivity of free carbenes, the preferred method involves the generation of the carbene *in situ* and subsequent reaction with metal precursors. This was applied by the groups of Rieger and Nishibayashi in the synthesis of complexes **[L1.22a]**PF_6, **L1.22b** and **L1.23**.[47]

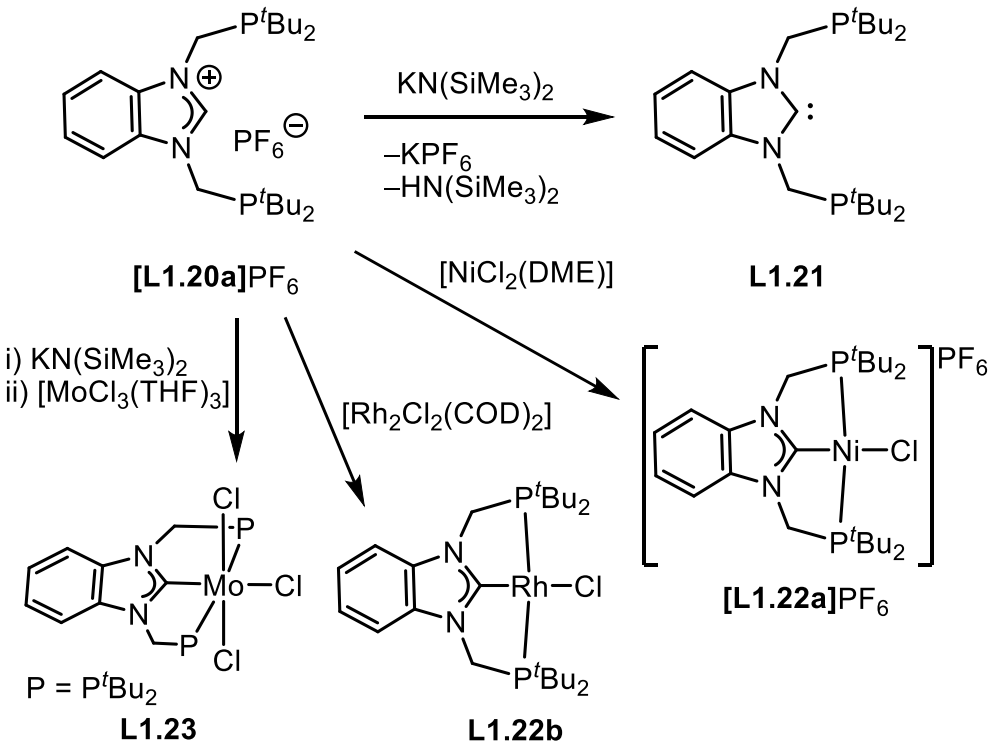

Scheme 1.4: Generation of free carbene **L1.21** from **L1.20a** and synthesis of P(NHC)P complexes **[L1.22a]**PF_6, **L1.22b** and **L1.23**.

Nishibayashi reported the dimerization of complex **L1.23** to **L1.24** (Scheme 1.5) upon treatment with sodium-mercury amalgam under a nitrogen atmosphere.[57] The dinitrogen-bridged complex **L1.24** was found to be an efficient catalyst in the fixation of nitrogen, liberating 100 equivalents of ammonia per molybdenum centre.[57] The catalytic activity of **L1.24** is greater than dinitrogen-bridged PNP pincer complexes (e.g. $[\{Mo(N_2)_2(P^tBu_2CH_2)_2C_5H_3N)\}_2(\mu\text{-}N_2)]$, which achieved 13 equivalents of ammonia per molybdenum centre)[58] and are comparable to scorpionate systems based on the tris(*o*-diisopropylphosphinophenyl)borane ligand (e.g. $[Fe\{\kappa^4\text{-}B,P,P',P''\text{-}B(C_6H_4P^iPr_2\text{-}2)_2\}][BAr^F{}_4]$, which yields 84 equivalents of ammonia per iron)[59].

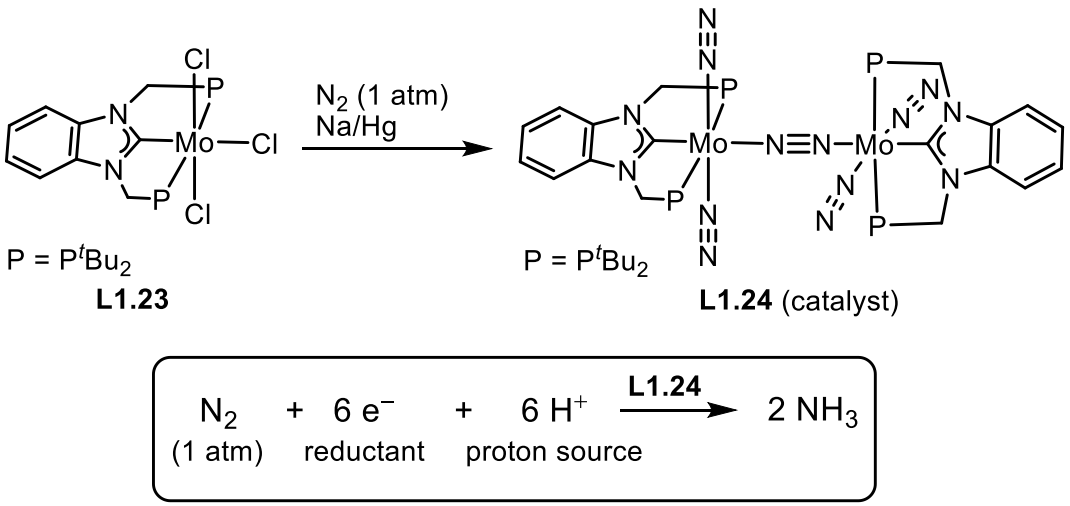

Scheme 1.5: Synthesis of nitrogen fixation catalyst **L1.24** and ammonia formation under ambient conditions.

Deprotonation of the imidazolium C–H can also be achieved by use of a basic co-ligand, such as the methoxide ligand in precursor $[Rh_2(OCH_3)_2(COD)_2]$. As exemplified in Scheme 1.6, the complexation of **[L1.20b]**PF_6 to $[Rh_2(OCH_3)_2(COD)_2]$ proceeds through benzimidazolium deprotonation and subsequent hydrogenation to produce **[L1.25a]**PF_6 or **[L1.25b]**PF_6.[46]

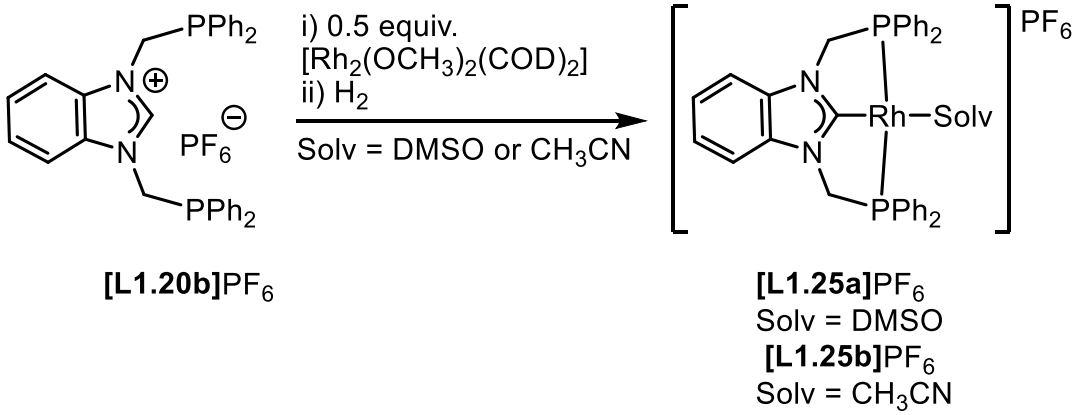

Scheme 1.6: Deprotonation of **[L1.20b]**PF_6 by basic co-ligand in the preparation of **[L1.25a]**PF_6 and **[L1.25b]**PF_6.

In some cases, oxidative addition of the imidazolium C–H bond upon coordination to a metal precursor has provided access to NHC pincer complexes.[40,42,47] Thomas and co-workers showed that direct C–H activation of imidazolium salt **[L1.26]**PF_6 afforded NHC pincer complexes **[L1.29]**PF_6 and **[L1.30]**PF_6 (Scheme 1.7).[42] The analogous reaction with the imidazolium chloride salt **[L1.26]**Cl led to complexes devoid of C–H activation (**L1.27** and **L1.28**), and are implicated as intermediates of arrested C–H activation.

Activation of the C–H bond in **L1.27** and **L1.28** was promoted *via* halide abstraction with $TlPF_6$, generating complexes **[L1.29]**PF_6 and **[L1.30]**PF_6, respectively.[42]

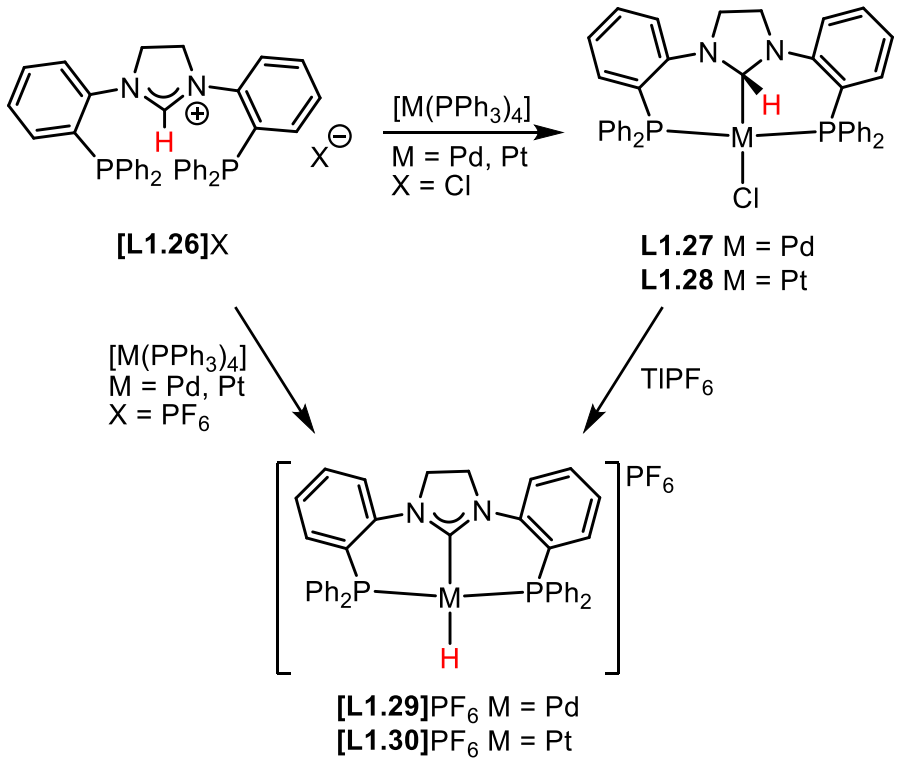

Scheme 1.7: Preparation of NHC pincer complexes **[L1.29]**PF_6 and **[L1.30]**PF_6 through direct C–H oxidative addition of **[L1.26]**X and *via* the intermediate complexes **L1.27** and **L1.28**.

In a recent publication, Nishibayashi and co-workers prepared complexes **[L1.31]**PF_6 and **[L1.32]**PF_6 through oxidative addition of **[L1.20a]**PF_6 to rhodium(I) and iridium(I) precursors (Scheme 1.8).[47] However, in this case no intermediates of arrested C–H activation was isolated. Thus, the reactivity patterns of the C–H activation pathway remain to be better understood, and as such, the complexation of pincer ligands through C–H activation processes is further addressed in the Appendix chapter.

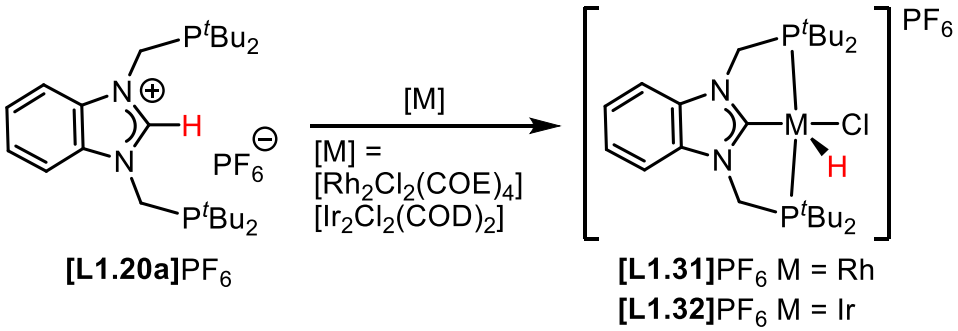

Scheme 1.8: Formation of **[L1.31]**PF_6 and **[L1.32]**PF_6 from oxidative addition of imidazolium salt **[L1.20a]**PF_6.

1.2.2.2 Boron-based pincers

Tridentate scaffolds with boron as a ligating element have gained increasing popularity in the last decade. Early examples shown in Figure 1.7 include metallaboratranes on iridium (**L1.33a**, **L1.33b**)[60] and rhodium (**L1.34**)[61] that feature a central M(donor)→B(acceptor) bond. In 2009, Mirkin and co-workers introduced examples of carborane-based pincer complexes incorporating SBS **L1.35** and SeBSe **L1.36** donor sets.[62] Around the same time, Yamashita and Nozaki developed the benzoboradiazole $HB(NCH_2P^tBu_2)_2C_6H_4$-1,2 (PBP) pincer pro-ligand (abbreviated as ^{Ph}PNNP(BH)),[63] which has since led to the synthesis of boryl pincer complexes on iridium,[64,65] rhodium,[66,67] ruthenium,[68-72] osmium,[70,72] platinum,[73] nickel[74-77] and cobalt[75,78] (generalised as **L1.37**); and investigations into their catalytic applications.

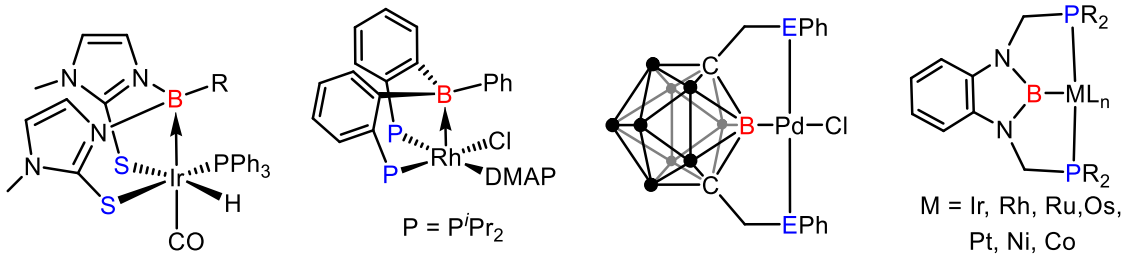

L1.33a R = H
L1.33b R = mt

L1.34

L1.35 E = S
L1.36 E = Se

L1.37

Figure 1.7: Tridentate boron-based complexes (mt = methimazolyl, DMAP = 4-dimethylaminopyridine).

In contrast to the polar covalent M(donor)→B(acceptor) bonding in complexes **L1.33a**, **L1.33b** and **L1.34**, complexes **L1.35**–**L1.37** contain a strong σ-donating boryl unit with an empty p-orbital that might be stabilised by competing π-bonding from the metal or π-donor substituents on boron (Figure 1.8). The π-donation from the metal to the boryl unit is generally accepted as rather weak and becomes weaker when the boron is surrounded by π-donor substituents.[79]

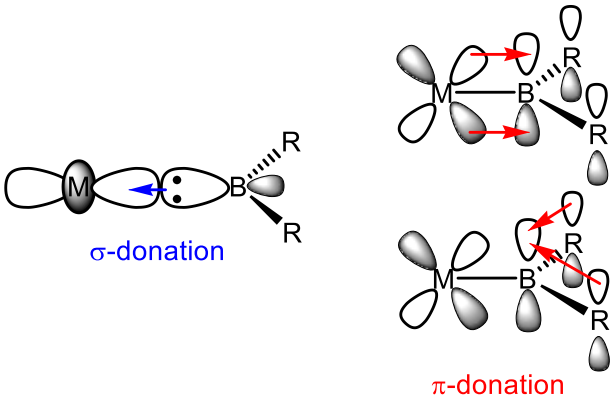

Figure 1.8: Bonding modes between metal (M) and boron (B) with substituents (R).

The polarisation of the B–H bond is inverse of the C–H bond (i.e. $B^{\delta+}$–$H^{\delta-}$ and $C^{\delta-}$–$H^{\delta+}$), which renders the hydrogen on boron hydridic. The synthesis of complexes of the form **L1.37** typically occurs through oxidative addition of the B–H bond in ^{Ph}PNNP(BH), which is exemplified by the examples in Scheme 1.9. Activation of the B–H bond upon coordination to an Ir(I) precursor provided the first boryl pincer complex **L1.38**,[63] and the rhodium analogue **L1.39** was similarly prepared.[66]

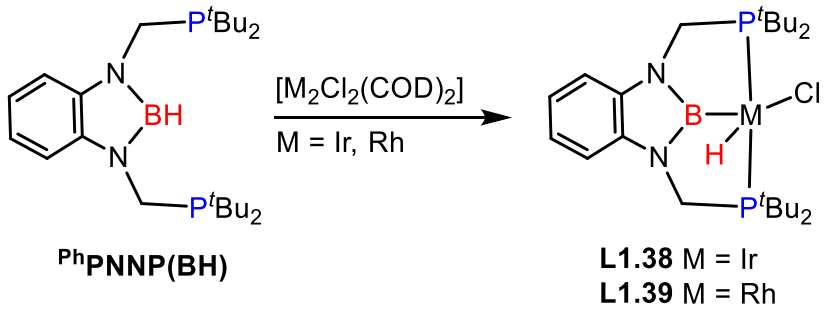

^{Ph}PNNP(BH)

L1.38 M = Ir
L1.39 M = Rh

Scheme 1.9: Coordination of the ^{Ph}PNNP(BH) ligand to form iridium (**L1.38**) and rhodium (**L1.39**) complexes.

The structures of complexes **L1.38** and **L1.39** were both established by crystallographic studies as distorted trigonal bipyramidal geometry. No interaction between the boron atom and hydride was inferred in **L1.38**, whereas a weak B···H interaction was present in the rhodium analogue **L1.39**, which was inferred from spectral and crystallographic data, and supported by DFT calculations.[66] Anion exchange could be effected on **L1.39** (*via* reaction with AgOTf) to displace the chloride by triflate to form complex **L1.40** (Scheme 1.10).[66] Subsequent treatment of **L1.40** with $LiCH_2SiMe_3$ afforded a low-coordinate T-shaped rhodium polymer **L1.41**, which was stabilised by C–H σ-interactions and the strong *trans* influence of the boryl ligand. The strong *trans* influence of boryls

has been previously proven by structural parameters and computationally interrogated.[63,72,80] The combination of low coordinative saturation at rhodium in complex **L1.41** and a σ-donating boryl unit creates a more electron rich metal centre, resulting in the high reactivity of the complex towards oxidative cleavage of polar O–H and non-polar σ-C–C bonds.[66,67]

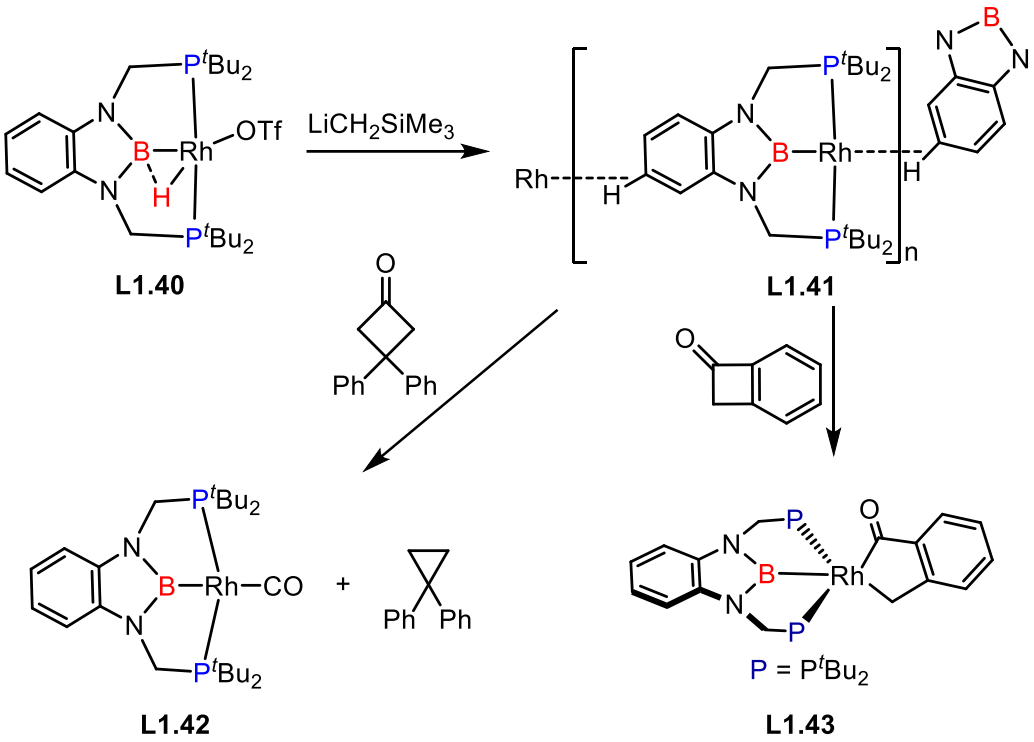

Scheme 1.10: Preparation of **L1.41** and subsequent selective C–C bond activation reactions.

The cleavage of C–C bonds in cyclobutenones by oxidative addition to **L1.41** proceeds readily at ambient temperature (Scheme 1.10).[67] The reaction of **L1.41** with 3,3-diphenylcyclobutan-1-one affords the product of decarbonylation, 1,1-diphenylcyclopropane, and carbonyl complex **L1.42**. However, when the benzocyclobutenone was used, selective C–C cleavage at the sp^3 α-carbon led to **L1.43** as the product of oxidative addition.

In many cases, the boryl group serves as an innocent spectator group within the pincer framework. However, a recent number of examples have suggested the participation of the boryl unit in hydrogenolysis. An attractive feature of reversible hydrogen shuttling mediated by boryl pincer complexes is the potential for these complexes to aid in hydrogen storage. In 2013, Peters reported the reversible reaction of **L1.44** (Scheme 1.11) with dihydrogen to form **L1.45**, demonstrating the conversion between

boryl and dihydroborate conformation.[78] In contrast, Yamashita and co-workers showed retention of the Ru(H_2)–B interaction in the synthesis of **L1.46** and **L1.47** (Scheme 1.11).[71] Computational studies (DFT and AIM analysis) on the bonding in **L1.46** and **L1.47** suggests a 2-centre 2-electron (2c2e) Ru^{IV}–B bond that is bridged by hydrides, whereas the coordination of tetraborate BH_4^- in **L1.47** is predominately ionic. These complexes have been used in hydrogenation catalysis including olefin hydrogenation (**L1.44**)[78] and aldehyde hydrogenation (**L.47**).[71]

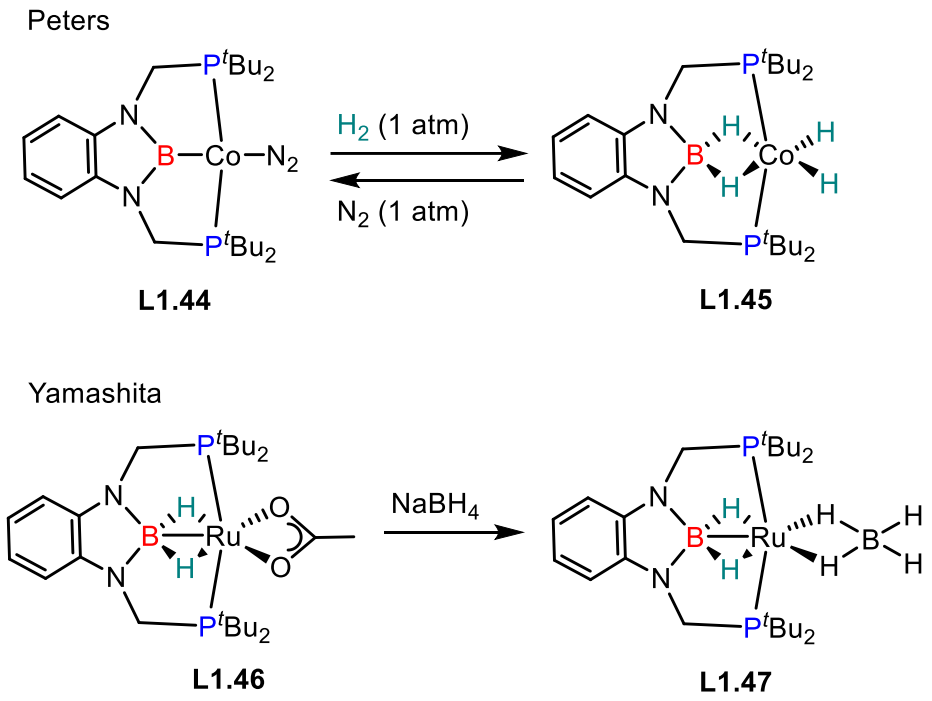

Scheme 1.11: Dihydridoborate pincer complexes.

In other cases a dihydridoborate complex is not isolated, such as in the reaction of nickel complex **L1.48** with dihydrogen that instead resulted in nickel hydride complex **L1.49** (Scheme 1.12).[74] Computational experiments by Rodríguez and López-Serrano suggested the formation of **L1.49** proceeded with cooperation of the Ni–B bond, involving a σ-B–H nickel intermediate structure and elimination of methane.[74] Complex **L1.49** can be obtained through an alternative route from [(PBP)Ni(OTf)] and Mg^{i}Pr$_2$.[75] The groups of Peters and Rodríguez and López-Serrano further exploited **L1.49** in olefin hydrogenation and activation of CO_2.[75-77] Specifically, Rodríguez and López-Serrano recently reported on **L1.49** as an effective catalyst, for the hydrosilation of carbon dioxide to bis(silyl)acetal derivatives in the presence of $B(C_6F_5)_3$. The reaction readily proceeds with insertion of CO_2 into the Ni–H bond to form the formate complex **L1.50**.[76,77]

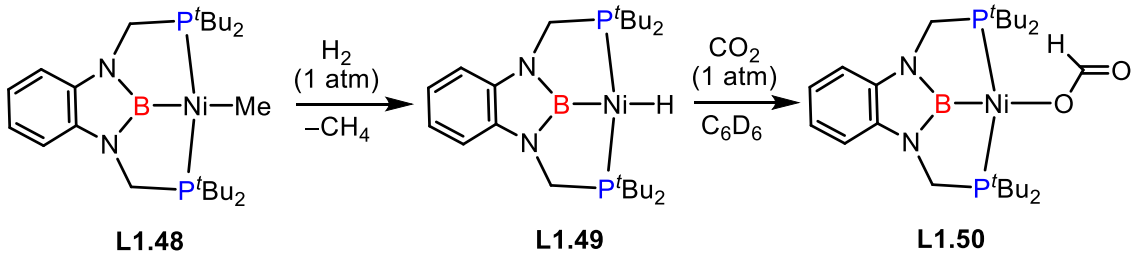

L1.48 **L1.49** **L1.50**

Scheme 1.12: Reactivity of boryl pincer nickel complexes.

From the literature discussed thus far, boron-based pincer complexes have demonstrated potential in catalysis, with the ligand behaving circumstantially as an ancillary or spectator. Whilst boron-based ligands and their derived complexes are well established, those of aluminium are relatively underexplored. Therefore, investigations into aluminium ligand design and corresponding complexes are detailed in Chapter 4.

1.2.2.3 Silicon-based pincers

Both boron and silicon lie along the metal-nonmetal divide and are expected to have similar properties (diagonal relationship). These include strong σ-donor properties that create an electron rich metal centre that predisposes the complex towards reactivity and activation of small molecules. The rapid development of pincer and scorpionate type silicon-based ligands and corresponding complexes has recently been summarised.[81]

Out of all the subgroups within the field of pincers, complexes featuring silicon derived tridentate ligands exhibit a tendency for flexible coordination in the *mer* or *fac* mode. This is a corollary of the sp^3-hybridised silicon that favours a tetrahedral geometry, which is more comfortably accommodated by *fac* coordination than in the planar orientation defined by *mer* coordination.

Complexes ligated by a PSiP scaffold shown as the general representation **L1.54** (Figure 1.9) make up a large portion of tridentate Si-based complexes in the literature, which appear to prefer *mer* coordination but have been known to circumstantially adopt *fac* coordination. Complexes of the PSiP framework will be revisited and investigated in Chapter 5. A general overview of silicon-based tridentate ligands is covered here.

Tridentate ligands featuring Si as the central donor shown in Figure 1.9 include **L1.51** and **L1.52** with SSiS ligand sets that have been known to adopt *fac* coordination.[82,83] Conversely, the NSiN ligand in complex **L1.53** predominately exhibits *fac*-binding[84-86] but has been noted in *mer* coordination to satisfy the electronic requirements at the metal centre (e.g., square planar Pt(II)).[87]

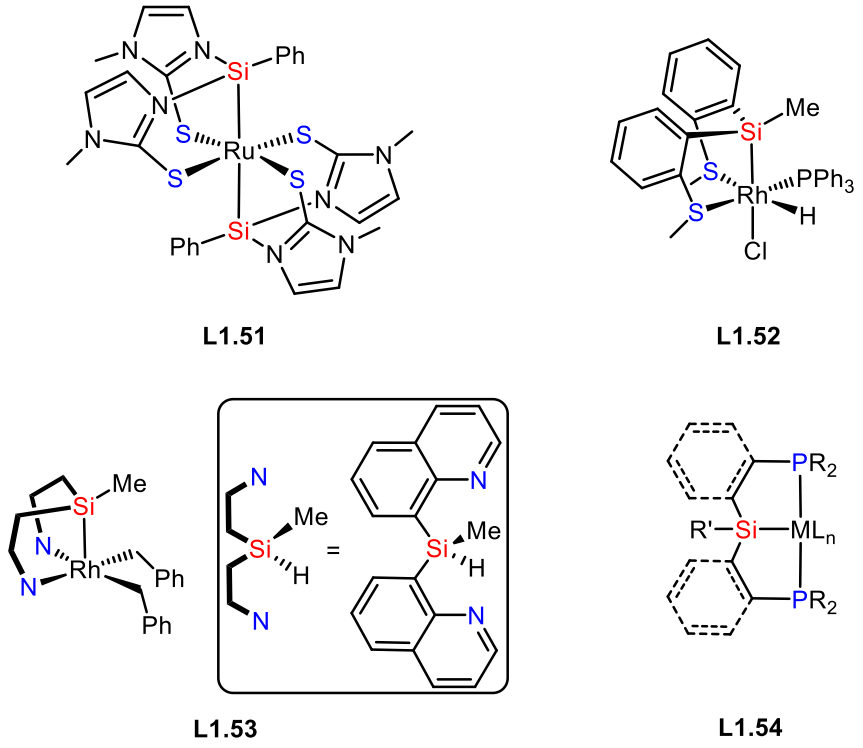

Figure 1.9: Selected examples of DSiD (D = S, N, P) complexes.

Alternative architectures include silicon-based groups at the pincer arms, incorporating one to three groups, with two groups most commonly encountered in literature. The selected examples of SiDSi ligands in Figure 1.10 feature heteroatoms (Si, P, O, N) as central donors (D).

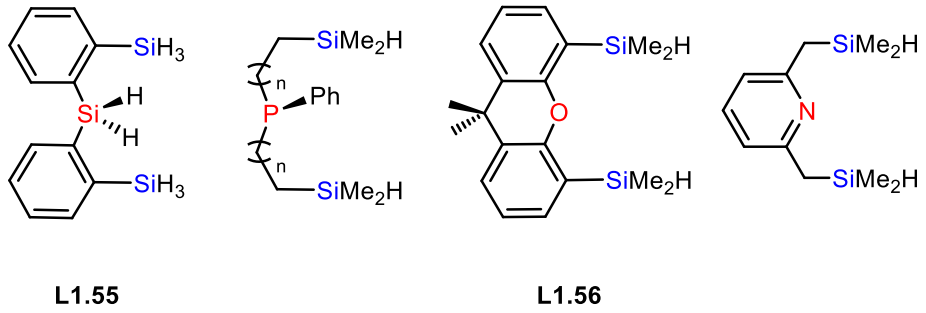

Figure 1.10: Selected examples of SiDSi (D = Si, P, O, N) ligands and complexes.

The coordination of silanes typically proceeds through Si–H activation, resulting in either full oxidative addition of the Si–H bond onto the metal or occasionally partial interactions between the silicon, hydride and metal (η^2-Si–H). Both modes of bonding were noted in Shimada and Tanaka's report on the coordination of SiSiSi pro-ligand **L1.55** to [Ni(depe)(PEt_3)$_2$] (Scheme 1.13).[88] The resulting complex **L1.57** had a η^2-Si–H interaction, indicative of arrested Si–H activation, that was confirmed through crystallographic studies. Additionally, the complex showed hydride fluxionality on the NMR time scale at 20°C, however stabilised at low temperatures (–80°C) to the nickel(IV) complex **L1.57a** that contains a formal Ni–H instead of η^2-Si–H bonding. The absence of an η^2-Si–H interaction was further supported by spectroscopic data and DFT calculations.

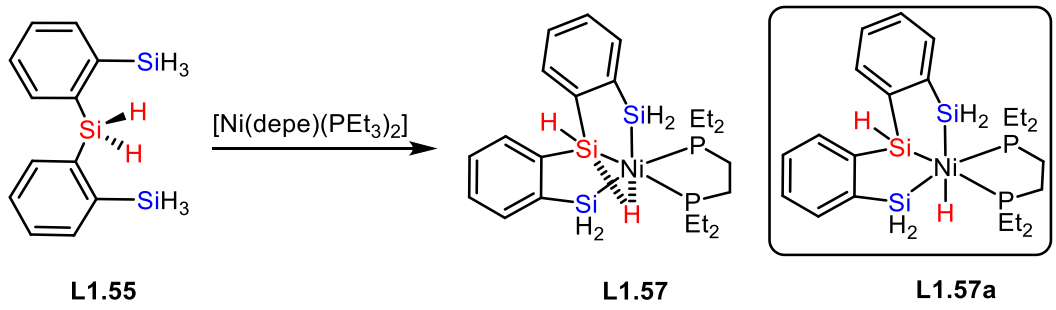

L1.55 **L1.57** **L1.57a**

Scheme 1.13: Synthesis of nickel complexes **L1.57** and **L1.57a** featuring different extents of Si–H activation; depe = 1,2-bis(diethylphosphino)ethane.

The delicate balance between η^2-Si–H agostic coordination and complete Si–H activation (in forming a terminal hydride complex) is further exemplified in complex **L1.58**, which is stabilised by two η^2-Si–H interactions from the arms of the SiPSi pincer (Scheme 1.14).[89] Despite the solution stability of **L1.58**, subjecting the sample to vacuum results in complex **L1.59** as the product of dehydrogenation and concomitant Si–H activation. The small energy barrier for dehydrogenation ($\Delta_r G_{298}$ = +16.9 kJ mol^{-1}) renders possible conversion between **L1.58** and **L1.59**, and hence the Si–H activation, reversible. Thus, the unsaturated 16 VE complex **L1.59** is unmasked *via* dehydrogenation of **L1.58**.

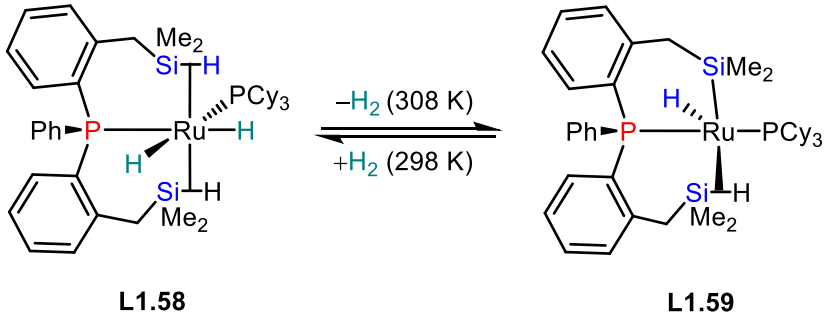

L1.58 **L1.59**

Scheme 1.14: Stabilisation of complexes **L1.58** and **L1.59** by η^2-Si–H interactions.

Reactive complexes can also be unmasked through hemilability of ligands such as SiOSi **L1.56** (xantsil, Figure 1.10). Developed and investigated by Tobita and co-workers, the ether oxygen of **L1.56** is typically labile, generating unsaturated complexes that are susceptible to further reactivity.[90-94] As demonstrated in Scheme 1.15, the oxygen in κ^3-*Si,O,Si* **L1.60a** is labile and affords the coordinatively unsaturated κ^2-*Si,Si* **L1.60b**, which is inferred from the subsequent reaction with nitriles to yield complexes **L1.61a** and **L1.61b**.[90,93] The hemilability of xansil complexes is an attractive feature in catalysis, finding application in alkene hydrogenation[94,95], *o*-C–H silylation/hydrogenation[96] and *o*-C–H silylation/hydrosilation[97].

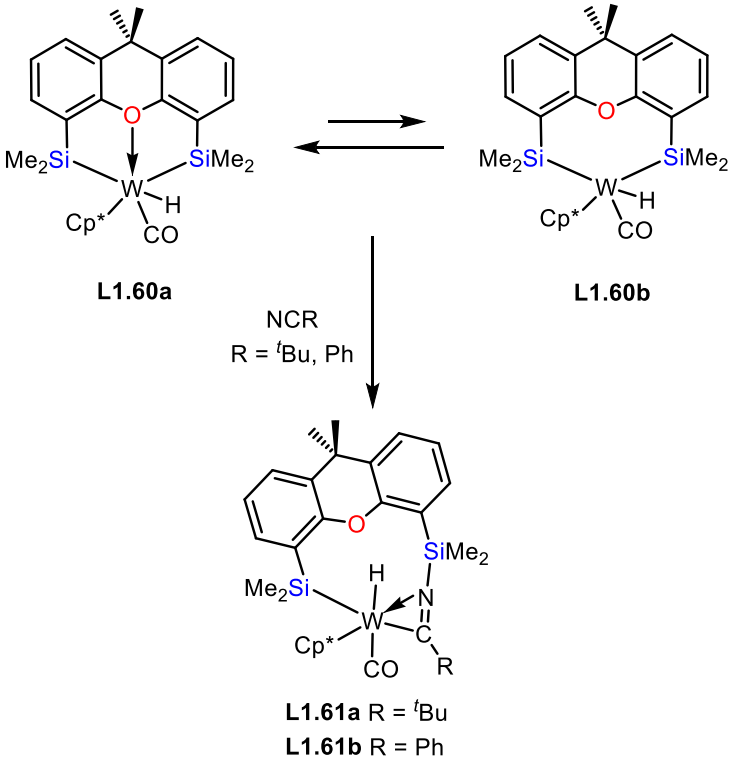

Scheme 1.15: Hemilability of the SiOSi (**L1.56**) ligand between complexes **L1.60a** and **L1.60b** (Cp* = pentamethylcyclopentadiene).

1.3 Poly(azolyl)borates

1.3.1 Introduction and Applications

Independently developed by Reglinski and Parkin, the $Bm^{R'}$ and $Tm^{R'*}$ ligand families are considered soft congeners (S donors) of Trofimenko's ubiquitous poly(pyrazolyl)borates (N donors) (Bp/Bp* and Tp/Tp*, Figure 1.11). Guided by the perceived analogy and promising reactivity of Trofimenko's poly(pyrazolyl)borates,[98-100] the coordination chemistry of $Tm^{R'}$ and $Bm^{R'}$ has grown apace over the last two decades. During this time the synthesis of complexes featuring the $Tm^{R'}$ ligand has been a key focus of research. However, the in some ways more intriguing $Bm^{R'}$ analogue has nevertheless enjoyed extensive study and coordination to many elements within the periodic table. Advances in the chemistry of $Tm^{R'}$ have been reviewed previously,[101-103] and the field continues to flourish with some 45 publications released since then (2009). Herein, research involving the $Bm^{R'}$ ligand up to January 2018 are discussed and comparisons to the tris analogue ($Tm^{R'}$) and other scorpionate systems are made where appropriate.

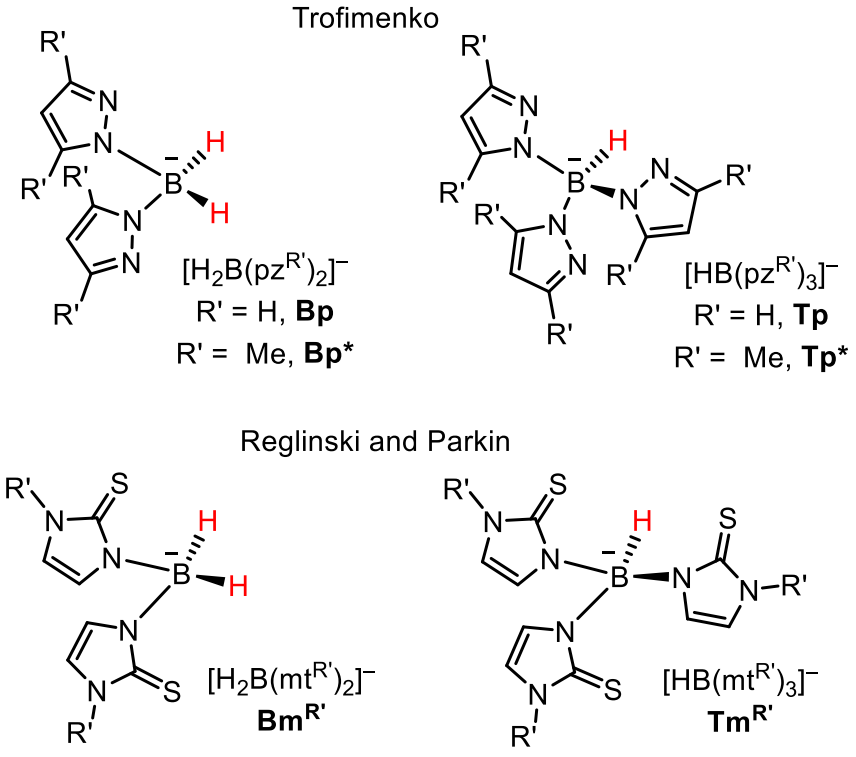

Figure 1.11: Bis- and tris(azolyl)borates of pyrazolyl and methimazolyl.

*R' refers to the N-substituent. Since most of the examples are derived from N-methyl-2-mercaptoimidazole (Hmt, methimazole), the absence of an R' superscript implies R' = Me.

1.3.1.1 Applications

The $Tm^{R'}$ and $Bm^{R'}$ ligands have been extensively studied in bioinorganic (biomimetic) applications to model the sulfur groups within metalloenzymes. They are considered 'tame thiolates'[104] with somewhat reduced tendency for oligomerization *via* μ-S bridges. Early applications included modelling for the active site of Liver Alcohol Dehydrogenase (LADH) of sulfur-rich composition that consists of one histidine and two cysteine residues, which are involved in the coordination to zinc.[105] Similarly, the NiFe-hydrogenase from *Desulfovibrio gigas* possesses a sulfur-rich active site that was modelled with the $Tm^{R'}$ and $Bm^{R'}$ ligand systems.

Furthermore, these ligands are widely exploited in the design of radiopharmaceuticals. Developed by Santos and co-workers, an extensive range of $[HRB(mt^{R'})_2]^-$ (R = H, Me, Ph; R' = Me, ^{t}Bu, *p*-Tol, Bz) and related derivatives, including modification of olefinic substituents, have been coordinated to *fac*-$[M(CO)_3]^+$ (M = Re, ^{99}Tc, ^{99m}Tc). The versatility in ligand modification, provides easy access to complexes comprised of a range of different physical-chemical properties. The aerobic and hydrolytic stability of the corresponding complexes (generally robust BH–M interaction) make them particularly suitable for radiopharmaceutical application.[106-108]

1.3.2 Ligand Synthesis

The $Tm^{R'}$ and $Bm^{R'}$ ligands were pursued as the soft congeners of the well-studied poly(pyrazolyl)borates founded by Trofimenko in 1966.[18,98,109] The synthesis of poly(pyrazolyl)borates is achieved through melting the alkali borohydride and a suitable equivalent of pyrazole. The extent of substitution on the boron was controlled by the temperature of the melt (bis 110°C, tris 180°C, tetra >210°C), and was monitored by volumetric hydrogen evolution.

Utilising a similar synthetic strategy with sodium borohydride and methimazole, Reglinski obtained the $Tm^{R'}$ salt,[110,111] while Parkin concurrently developed the $Bm^{R'}$ variant in toluene at 50°C.[105,112] These ligands are henceforth referred to as $[HB(mt^{R'})_3]^-$ and $[H_2B(mt^{R'})_2]^-$. Subsequent reports on the synthesis of these ligands involve reactions in solvent under reflux or heating at suitably elevated temperatures. The sodium derivatives $Na[H_2B(mt^{R'})_2]$ (R' = Me, Bz, ^{t}Bu, *p*-Tol) were developed by the groups of

Rabinovich and Hill, from the reaction of $NaBH_4$ with the appropriate methimazole in a THF reflux.[113,114] The solvent facilitated reactions proceeded more selectively and with higher isolated yields (70–95%) than reactions performed neat.

Functionalisation of the methimazolyl backbone has been reported by Santos and co-workers.[115] These include the symmetric $Na[H_2B(mt^{Me}_{R''})_2]$ (where the $mt^{Me}_{R''}$ group is **1**, **2** or **3**; Table 1.1), which were prepared by the reaction of $NaBH_4$ with the functionalised methimazole in THF under reflux. The asymmetric analogues $Li[HPhB(mt^{Me})(mt^{Me}_{R''})]$ can also be prepared from subsequent reaction of $Li(PhBH_3)$ with methimazole to generate $Li[H_2PhB(mt^{Me})]$ followed by reflux in THF with the functionalised methimazole.[115] The range of ligands and areas of modification discussed above are summarised in Table 1.1.

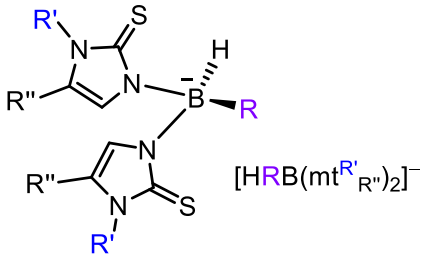

M^+	R	R'	R''	Ref.
Li	H	Me or Mes	H	105
	Me, Ph	Me	H	107
	Ph	Me	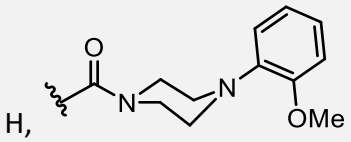	115
	Ph	Me	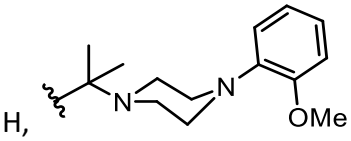	115
Na	H	Me, Bz, ^{t}Bu, *p*-Tol, C_6H_4Cl-4, C_6H_4Me-4 or $C_6H_4NO_2$-4	H	113, 114, 166
	H	Me	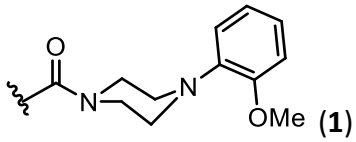 (**1**)	115
	H	Me	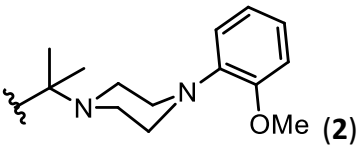 (**2**)	115
	H	Me	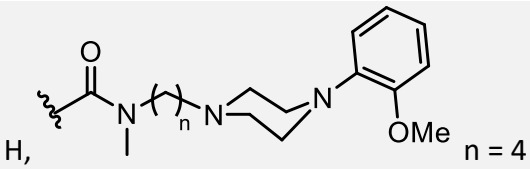 n = 4	162
	H	Me	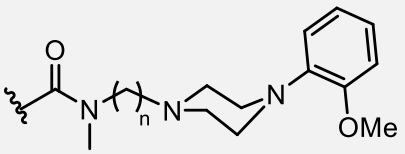 n = 4 (**3**)	162

Table 1.1: Substituted [HRB(mt$^{R'}_{R''}$)$_2$] or Bm$^{R'}$. NB: In most cases R'' = H and thus the formula is shown as [HRB(mt$^{R'}$)$_2$] or abbreviated as Bm$^{R'}$ for simplicity.

The substituents on boron can also be varied to assess the impact on the coordination chemistry of the ligands (Table 1.1). Santos and co-workers reported the reaction of $Li(RBH_3)$ with the appropriate equivalent of methimazole at room temperature (Me) or reflux (Ph) to form $Li[H(R)B(mt^{Me})_2]$ (where R = Me or Ph).[107] As the focus of this introduction is on bis-substituted borate ligands and their reactivity, modifications on boron are only considered for non-coordinating units (e.g. alkyl, aryl, halide). However, it is noteworthy that the field has grown to encompass hybrid scorpionates involving mixed heterocyclic systems on the boron.[116]

Other extensions to the field of bis-substituted sulfur based scorpionates include the heterocycles **4**–**10** in Figure 1.12.[117-123]

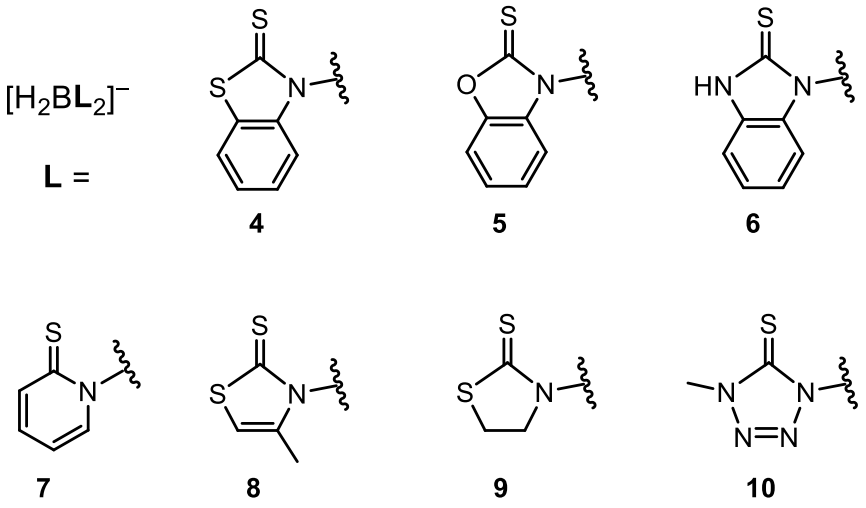

Figure 1.12: Heterocycle derivatives of the $[H_2BL_2]^-$ ligand.

1.3.3 Coordination Modes

The $Bm^{R'}$ ligand displays versatile coordination in mononuclear complexes. The variety of coordination modes adopted by $Bm^{R'}$ are summarised in Figure 1.13. Four coordination outcomes have been documented; i. simple monodentate coordination (**A**) ii. bidentate chelation (**B**), iii. tridentate coordination where a B–H group engages in 3-center-2-electron (3c2e) bonding with the metal (**C**), and iv. metallaboratrane formation *via* B–H activation (**D**).

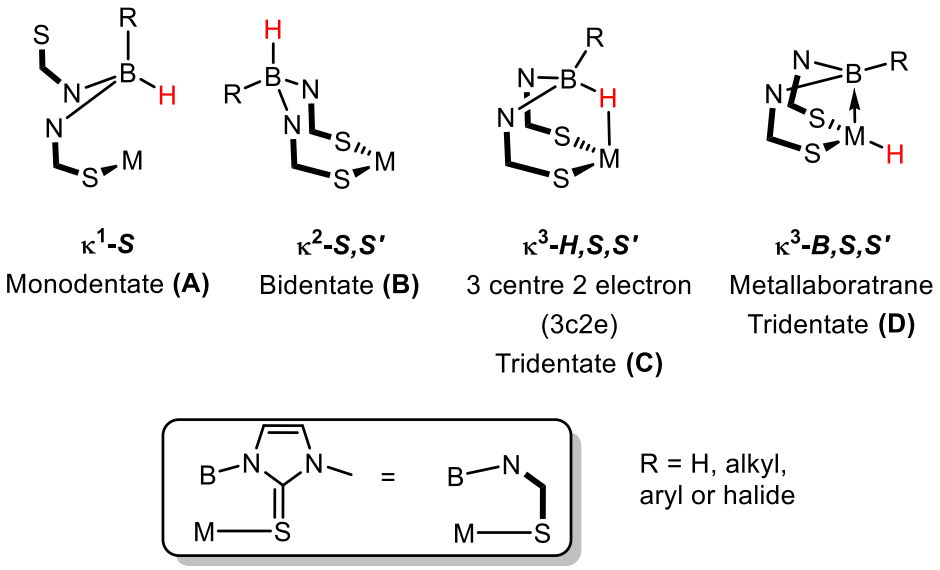

Figure 1.13: Coordination modes of the $Bm^{R'}$ ligand.

Perusal of the Cambridge Crystallography Data Centre (CCDC) reveals **B** and **C** as the most common coordination modes with 49 and 48 structural reports, respectively. The κ^2-*S,S′* mode is encountered most often with rhenium and κ^3-*H,S,S′* with ruthenium. Monodentate κ^1-*S* coordination of $Bm^{R'}$ is rare and typically occurs with metals that favour linear coordination, e.g. Au(I) or when a more suitable (stronger) donor or chelate is present. Examples are limited to the complexes $Na[\kappa^1\text{-}H_2B(mt^{Me})_2].3H_2O$, $[Re(CO)_3(H_2NCH_2CH_2NH_2)\{\kappa^1\text{-}H_2B(mt^{Me})_2\}]$, $[Au(PEt_3)\{\kappa^1\text{-}H_2B(mt^{Me})_2\}]$, $[TlMe_2\{\kappa^1\text{-}H_2B(mt^{Me})_2\}]_n$.[124-127] While the metallaboratrane mode of coordination is prevalent for $Tm^{R'}$, the bonding motif is rare for $Bm^{R'}$ with $[IrH\{\kappa^3\text{-}B,S,S'\text{-}BH(mt^{Me})_2\}(CO)(PPh_3)]$ being the only example. The study of metallaboratrane complexes is detailed in Chapter 3 of this thesis.

There has been an appreciable amount of work in $Bm^{R'}$ chemistry with most examples involving d-block elements. As inferred from the structures within the CCDC, the scope of $Bm^{R'}$ chemistry is summarised in Figure 1.14.

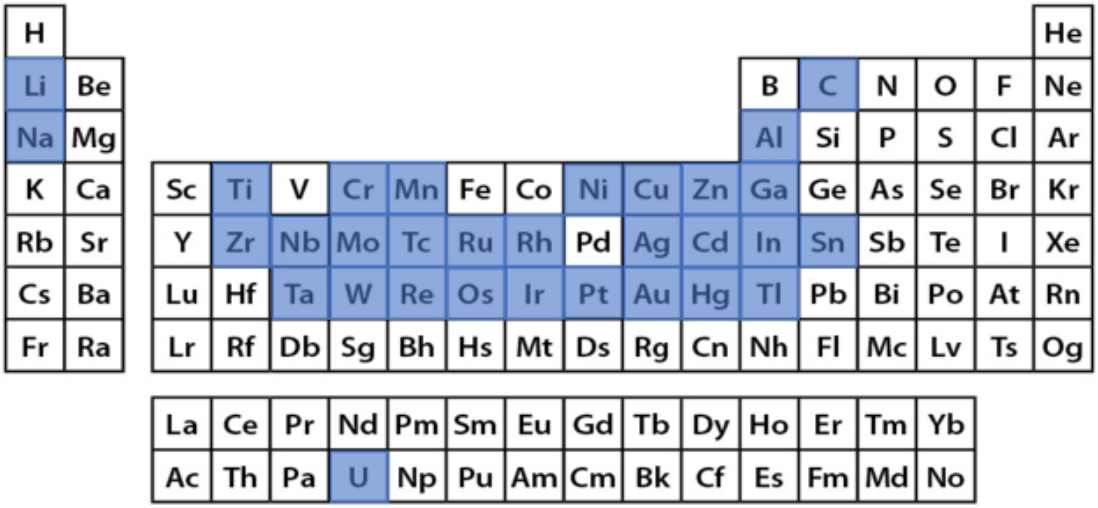

Figure 1.14: Elements (in blue) for which structurally authenticated $Bm^{R'}$ complexes are known.

1.3.3.1 The M–H–B Interaction

The structural data in the Cambridge Crystallographic Database illustrates that the κ^3-*H,S,S'* coordination mode is particularly prevalent within $Bm^{R'}$ chemistry. Indeed, this is even encountered in some $Tm^{R'}$ complexes in preference to the more anticipated κ^3-*S,S',S''* mode. This recurrent feature between the metal, hydrogen and boron is best represented as a 3-centre 2-election (3c2e) interaction. Such interactions have been observed in early classical scorpionate chemistry, with the first examples dating back to the early 1970's for dihydrobis(dimethylpyrazolyl)borates (Bp*) complexes.[128,129]

However, accumulation of evidence over the last two decades since the discovery of $Tm^{R'}$ and $Bm^{R'}$ shows that B–H–M interactions are particularly favourable for these ligands. This is presumed to be a consequence of the flexibility of the increased chelate size relative to the pyrazolyl congeners (BNNM *cf.* BNCSM cages respectively, Figure 1.15), and in the case of $Tm^{R'}$ ligands, the geometric constraints associated with the bicyclo-[3.3.3] $B(NCS)_3M$ connectivity that requires twisting of the cage from local C_{3v} to (chiral) C_3 geometry.

Figure 1.15: Geometric implications from B–H–M Ring Size.

The nature of the B–H–M interaction was the subject of considerable debate and is often described as 'agostic' in literature. The term 'agostic' was first coined by Green and Brookhart to define the interaction between C–H and transition metals.[130,131] A study of the isoelectronic complexes [Rh(COD){κ^3-*H,S,S'*-$H_2B(mt^{Me})_2$}] and [Rh(COD){κ^3-*H,S,S'*-$H_2C(mt^{Me})_2$}]BF_4 showed respective B–H···Rh and C–H···Rh interactions in the crystal structure of each complex.[132] This suggests the use of 'agostic' may be appropriate to describe both C–H···M and B–H···M interactions, notwithstanding the disparate bond polarities involved ($C–H^{\delta+}$ *cf.* $B–H^{\delta-}$).

The interaction between the B–H group and the metal can be visualised as the two extreme forms in Scheme 1.16. Representation a) depicts the electron pair in a B–H σ-bond donating to a vacant orbital on the metal, whereas the alternative b) envisages a borane acting as a Lewis acid to a metal hydride.[133] The latter would appear to be more relevant for early transition metals where the hydride exhibits more hydridic than protic character. The bonding in complexes is expected to lie somewhere between the two extremes.

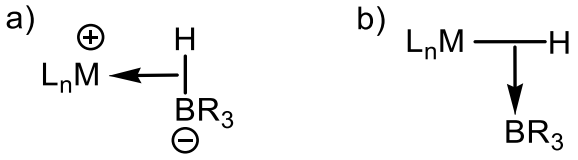

Scheme 1.16: Representations of B–H–M interactions.

The B–H–M interaction is generally persistent and apparent in the proton NMR spectra, revealing a useful diagnostic handle for determining the presence of such associations. Whilst the terminal B–H of $H_nB(mt)_{4-n}$ ligands are characteristically observed as broad resonances in the positive region of the ^1H NMR spectrum, the B–H–M hydrogen resonance with greater hydridic character is commonly located at lower frequency ($\delta_H < 0$). In addition to ^1H NMR data, the occurrence of a B–H–M interaction is present in infrared spectra around 2000–2200 cm^{-1}, whereas the terminal B–H band is distinct, falling within the region 2300–2500 cm^{-1}.

Given the variety of coordination modes adopted by $Bm^{R'}$ ligands, the question of potential *hemilability* of the B–H–M interaction (i.e. an equilibrium between the κ^3-*H,S,S'* and κ^2-*S,S'* coordination modes) arose. Complex **L1.62** (Scheme 1.17) is reported by Santos and co-workers to be stable towards aerobic oxidation, hydrolysis

and coordinating solvents such as alcohols, dimethyl sulfoxide, tetrahydrofuran or acetonitrile. However, the B–H–Re interaction is susceptible to cleavage by neutral (σ + π) ligands such as imidazole, *tert*-butylisonitrile, triphenylphosphine and 4-(dimethylamino)pyridine, to allow mono-addition at the metal centre (κ^2-*S,S'*). A large excess (5 equivalents) of the extraneous ligand is required to coerce complete addition and in all cases, except *tert*-butylisonitrile (**L1.63b**), the κ^3-*H,S,S'* coordination appears to be favoured and is reformed on standing of solutions of **L1.63a,c-f**.[106,125]

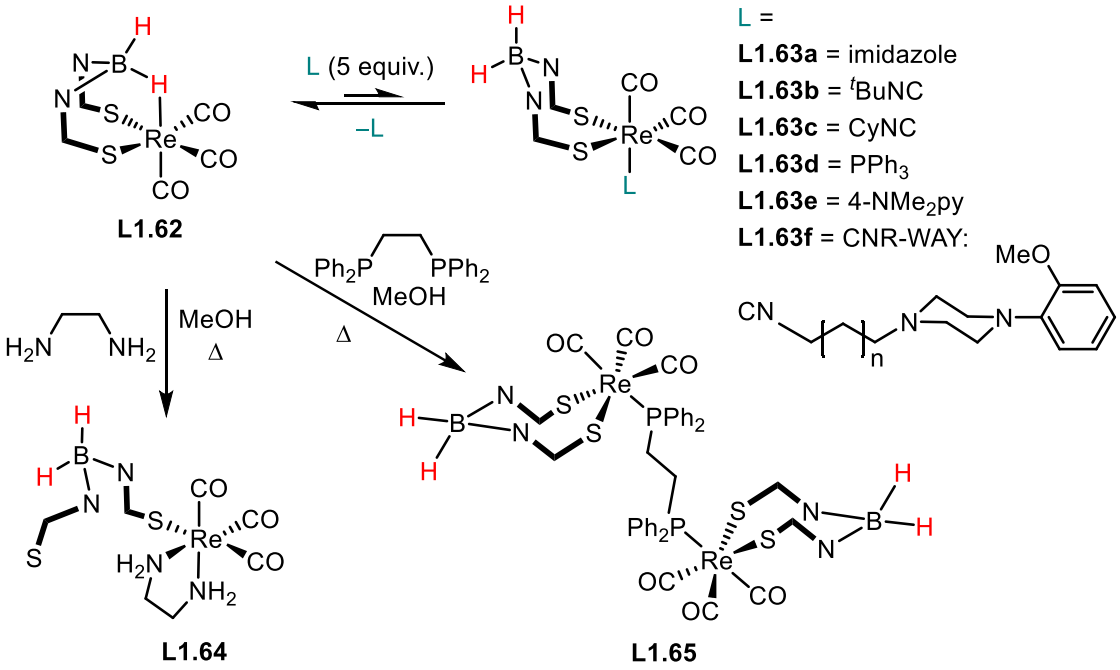

Scheme 1.17: Hemilability of BH–Re in complex **L1.62**, where n = 2, 3, 4.

The more sterically demanding cyclohexylisonitrile and bioactive functionalised piperazinyl isonitriles (CNR-WAY) were also suitable monodentate co-ligands to cleave the B–H–Re bond under a methanol reflux.[134] The intense ν_{CO} bands of these complexes are visualised in the IR spectra between 1870–2040 cm^{-1}, distinct from those of the isonitriles that are found near ν_{CN} 2200 cm^{-1}. The affinity of the piperazinyl isonitriles (CNR-WAY) complexes **L1.63f** toward 5-HT_{1A} receptors in rat brain homogenates were tested and showed that the longest linker length (n = 3) had the greatest affinity and selectivity.

When **L1.62** was treated with neutral bidentate ligands, the hard N-donors of ethylenediamine cleaved the B-H–Re interaction with replacement of a thione donor to accommodate *cis* bidentate coordination, thereby creating a pendent κ^1-*S* borate unit in **L1.64**. In contrast, the softer 1,2-bis(diphenylphosphino)ethane (dppe) ligand yields the dimetallic product **L1.65** upon cleavage of just the B–H–Re interaction.

In contrast to the reported lability of the B–H–Re association in complex **L1.62**, the isoelectronic complex **L1.66** (Scheme 1.18) was found to be inert to substitution by triphenylphosphine under ambient conditions.[135] The expected complex **L1.67** was alternatively accessed through reaction of $[W(NO)(CO)_2(PPh_3)_2]PF_6$ and $Na[H_2B(mt^{Me})_2]$. Given the robust B–H–Re interaction in **L1.66**, it was anticipated that PPh_3 would be labile in **L1.67** to allow reformation of the B–H–Re bond, however, this was not observed spectroscopically.

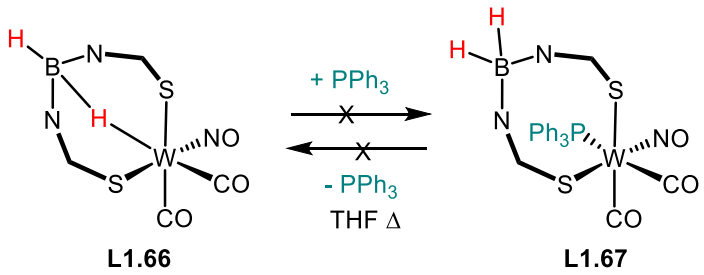

L1.66 **L1.67**

Scheme 1.18: Robust B–H–W interaction towards PPh_3 substitution.

Further rare cases of *hemilability* exist despite the plethora of examples in the literature that support the robust nature of the B–H–M interaction. Kuwata and Ikariya found reversible coordination of carbon monoxide between the complexes **L1.68**[136] and **L1.69**[137] (Scheme 1.19) that proceeds through facile cleavage and reformation of the BH–Ru linkage. Conversely, the liberation of CO from **L1.69** was only achieved *via* a toluene reflux.

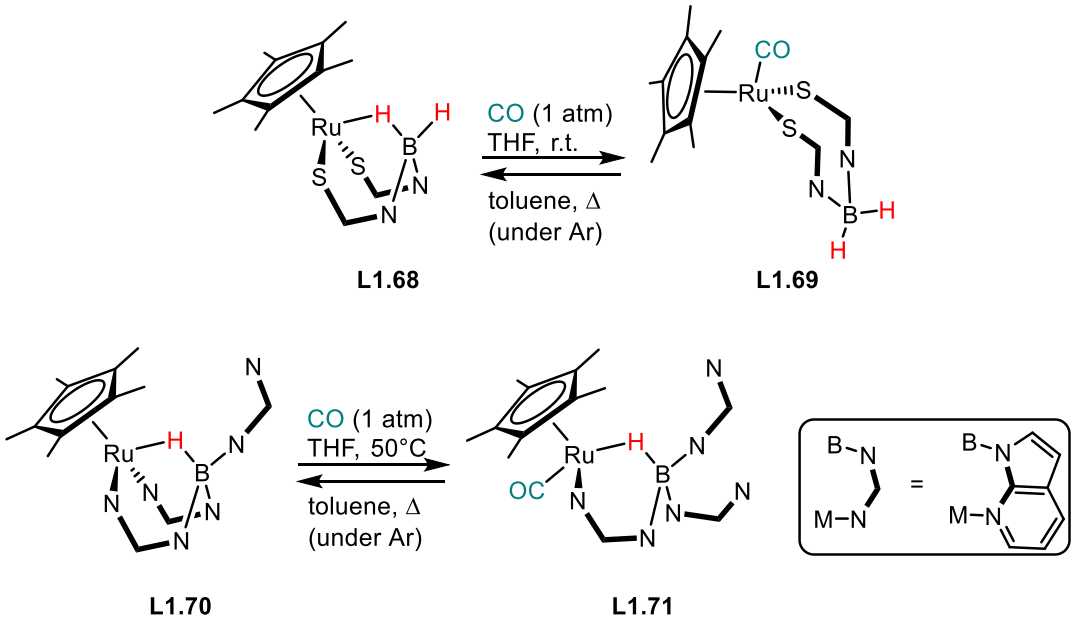

Scheme 1.19: Reversible CO coordination through exchange of binding modes: κ^3-*H,S,S'* **L1.68** and κ^2-*S,S'* **L1.69**; κ^3-*H,N,N'* **L1.70** and κ^2-*H,N* **L1.71**.

In the analogous complex featuring tris(azaindolyl)borate **L1.70** (Scheme 1.19), 3c2e B–H–Ru coordination (κ^3-*H,N,N'*) is preferred over κ^3-*N,N',N''*. In contrast to the facile displacement of BH–Ru in **L1.68**, this B–H–Ru linkage remains intact in the presence of CO, which instead substitutes an azaindolyl unit forming κ^2-*H,N* bound **L1.71**.[137]

Coordination exchange is more commonly observed for $Bm^{R'}$ complexes than the $Tm^{R'}$ derivatives, suggesting greater coordinative flexibility of the former. Nevertheless, facile κ^3-*S,S',S''* and κ^3-*H,S,S'* coordination exchange was reported by Goh and co-workers for the complexes $[Ru^{III}\{HB(mt^{Me})_3\}(Cp^*)]^+$ and $[Ru^{II}\{HB(mt^{Me})_3\}(Cp^*)]$.[138] In the solid state the complexes adopt κ^3-*S,S',S''*coordination and readily exchange to κ^3-*H,S,S'* binding in solution.

The pronounced tendency towards B–H–M bonding is further exemplified in the selective formation of $[Mn(CO)_3\{\kappa^3\text{-}H,S,S'\text{-}H_2B(mt^{Me})_2\}]$ despite the presence of additional coordinating ligands (triphenylphosphine, pyridine, 2,6-dimethylphenylisocyanide) in five-fold excess in the reaction of $[MnBr(CO)_5]$ with $Na[H_2B(mt^{Me})_2]$.[139]

1.3.4 Reactivity

1.3.4.1 Main Group

The coordination chemistry of $Bm^{R'}$ with the main group elements is mainly limited to those in group 13 and of carbon and tin from group 14. A recent comprehensive review by Reglinski and Spicer detailed the advances of anionic scorpionate ligands within the p-block, showing the breadth of the field of anionic scorpionates.[140] The key developments relating to $Bm^{R'}$ complexes are highlighted in this section.

Group 13

The first $Bm^{R'}$ complex of indium, $[InBr_2\{H_2B(mt^{Me})_2\}]$, was synthesised in 2006 by Rabinovich from the reaction of $InBr_3$ with $Na[H_2B(mt^{Me})_2]$. The molecular structure was established *via* a crystallographic study and revealed a distorted tetrahedral environment at indium with a $[InS_2Br_2]$ core.[141] Subsequent research by Parkin and co-workers extended examples within group 13 to aluminium, gallium, indium and thallium. Their findings summarised in Scheme 1.20 include the general reaction $M'X_3$ (M' = Al, Ga, In, Tl) with $M[H_2B(mt^{R'})]$ (M = Li, Na, Tl; R' = Me, ^{t}Bu) to afford complexes of the form $[H_2Bm^{R'}]M'X_2$ **L1.72–L1.76a-c** and $[H_2Bm^{R'}]_2M'X$ **L1.77a-c**.[127] The molecular structures of complexes $[H_2Bm^{R'}]M'X_2$ **L1.72–L1.76a-c** determined by X-ray crystallography show a chair-like configuration for the $[H_2Bm^{R'}]M'$ moiety.

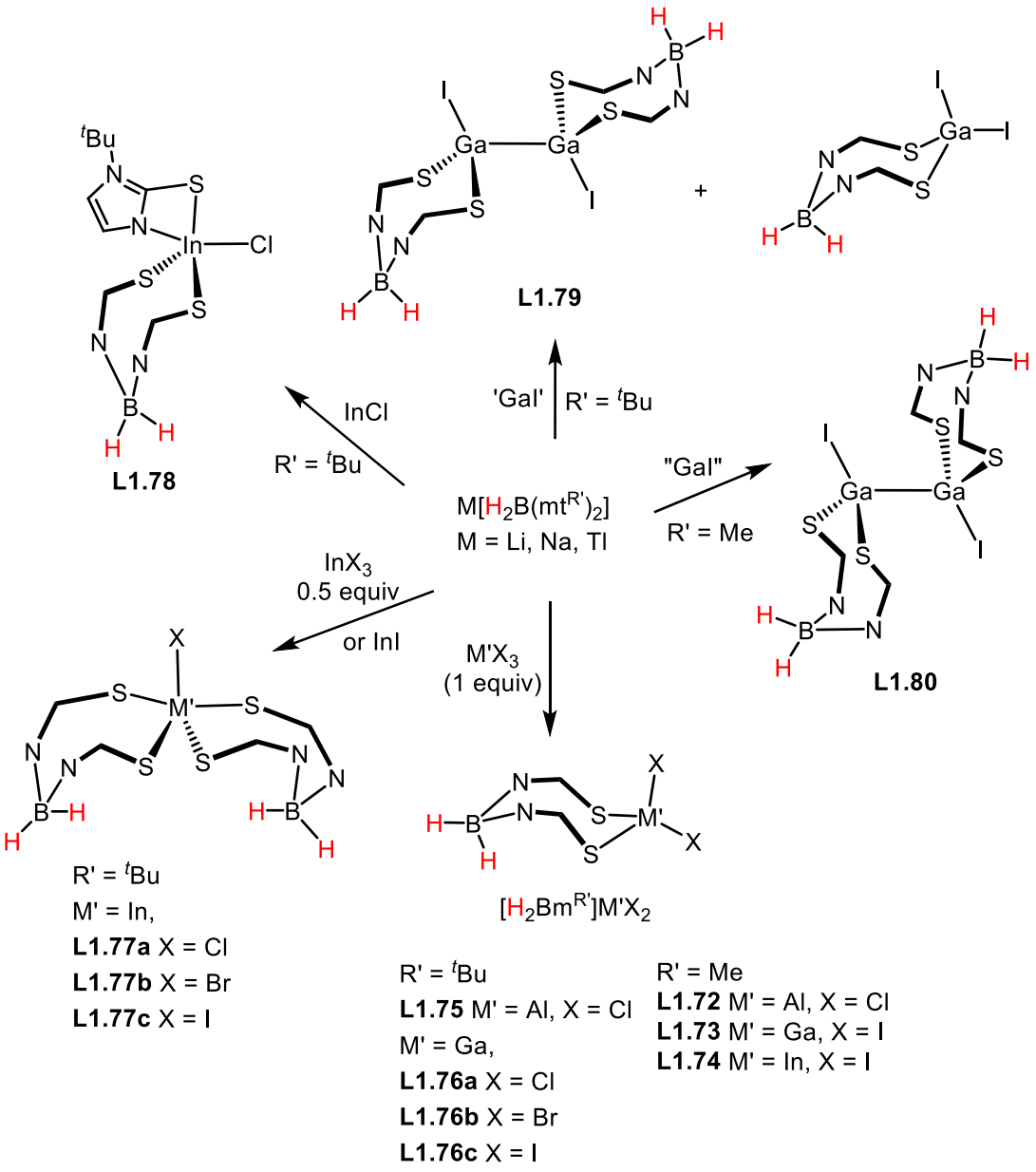

Scheme 1.20: $[H_2B(mt^{R'})_2]^-$ complexes of aluminium, gallium and indium.

The indium complexes **L1.77a-c** and **L1.78** were crystallographically determined to feature a trigonal bipyramidal geometry at indium, whilst mononuclear and dinuclear gallium(II) complexes were accessible from 'GaI'. The reactive 'GaI' species was generated *via* Green's method involving the ultrasonic irradiation of gallium metal, I_2 and alkyl iodides.[142] For the sterically demanding $[H_2B(mt^{tBu})_2]^-$ in **L1.79**, the ligands are directed away from the Ga–Ga bond while the analogous complex **L1.80** consists of less sterically repulsive $[H_2B(mt^{Me})_2]^-$ ligands that rest over the Ga–Ga bond.

Early examples of $Bm^{R'}$ thallium complexes were reported by Parkin and co-workers, and include the polymeric $[Tl\{\kappa^3\text{-}H,S,S'\text{-}B(mt^{Me})_2\}]_x$ synthesised from metathesis of $[Li\{\kappa^3\text{-}H,S,S'\text{-}B(mt^{Me})_2\}]_2$ with $Tl(O_2CMe)$.[112] Through a similar procedure, Rabinovich and

co-workers prepared N-derivatised complexes Tl[κ^3-*H,S,S'*-$H_2B(mt^{R'})_2$] (R' = Me, Bz, ^{t}Bu, *p*-Tol) **L1.81a-d** from reaction of Na[$H_2B(mt^{R'})_2$] and Tl(O_2CMe) (Scheme 1.21).[143] In contrast to the polymeric [Tl{κ^3-*H,S,S'*-$B(mt^{Me})_2$}]$_x$ complex, the ^{t}Bu analogue exists as two crystallographically independent molecules with weak B–H···Tl interactions (**L1.81c**, Scheme 1.21). The aforementioned thallium(I) complexes are commonly utilised as transfer agents of $Bm^{R'}$ ligands, typically resulting in a cleaner transfer than the corresponding sodium derivatives.[112,144] One example is use of Tl[$H_2B(mt^{R'})$] (R' = Bz, *p*-Tol) in the synthesis of [Mn(CO)$_3${κ^3-*H,S,S'*-$H_2B(mt^{R'})_2$}].[139]

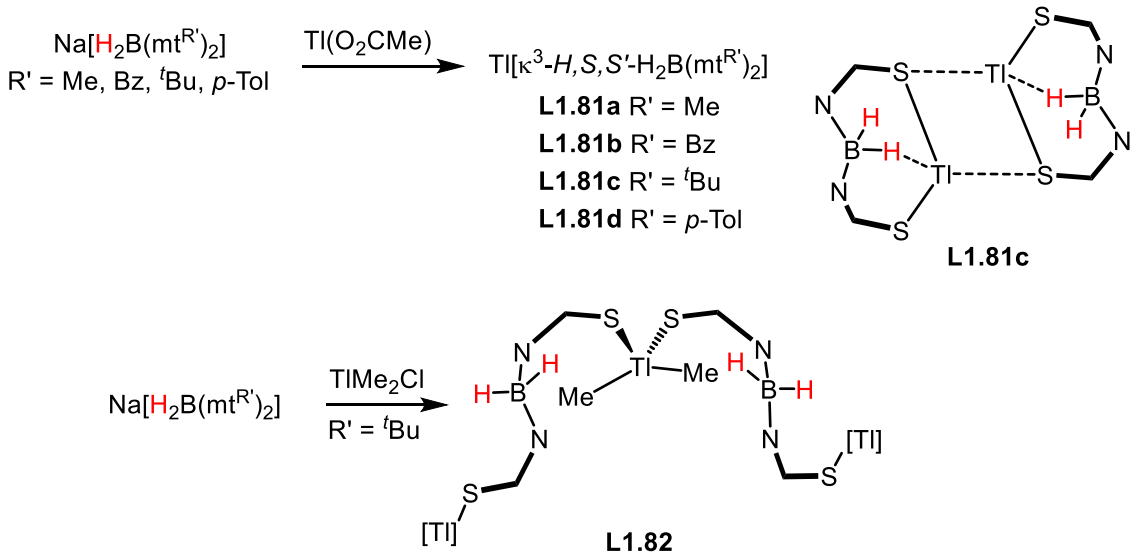

Scheme 1.21: $Bm^{R'}$ complexes of thallium.

Complex **L1.82** (Scheme 1.21) is likewise polymeric but features an uncommon four-coordinate trivalent thallium, which is unusual due to the inert pair effect dictating the preference for thallium to exist in the +1 state as monovalent compound.[127] While the other [$H_2Bm^{R'}$]M'X_2 complexes adopt a tetrahedral coordination environment, the environment around thallium in **L1.82** resembles a see-saw geometry.

<u>Group 14</u>

In 2004, Hill and co-workers noted dichloromethane acting as an non-innocent solvent, reacting with $Bm^{R'}$ and $Tm^{R'}$ under long reaction times to form poorly soluble dithioacetal salts [{κ^2-$H_{4-n}B(mt^{Me})_n$}CH_2]Cl.H_2O (n = 2, 3).[145] These reactions took place both in the presence and absence of a metal reagent. The molecular structure of [{κ^2-$H_2B(mt^{Me})_2$}CH_2]Cl.H_2O **[L1.83]**Cl (Figure 1.16) is comprised of an eight membered

ring in a chair conformation, thereby preventing potential interaction of B–H and the CH_2 groups.

Analogous to the formation of the heterocyclic salt **[L1.83]**Cl from dichloromethane, direct reaction of Me_2SnCl_2 with $Na[H_2B(mt^{Me})_2]$ results in $[Me_2Sn\{\kappa^2\text{-}S,S'\text{-}H_2B(mt^{Me})_2\}]Cl$ **[L1.84]**Cl.[146] Both **[L1.83]**$^+$ and **[L1.84]**$^+$ are structurally similar (as shown in Figure 1.16), with the notable difference of a subtended C1–Sn1–C2 angle (159.8°) deviating from ideal tetrahedral geometry at tin.

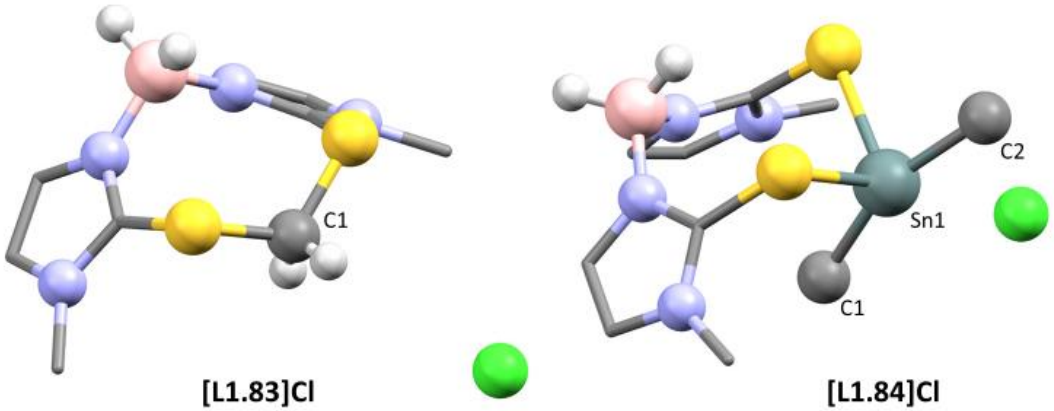

Figure 1.16: Molecular structures of **[L1.83]**Cl and **[L1.84]**Cl.

Stannyl reagents have been utilised as transfer agents of $[H_2B(mt)_2]^-$ or $[HB(mt)_3]^-$ ligands. For example, $Ph_3Sn[HB(mt^{Me})_3]$ has been reacted with Group 5 and 6 precursors, whereas reaction of Me_2SnCl_2 or $[Me_2Sn(mt^{Me})_2BH_2]Cl$ with appropriate molybdenum precursors afforded the bimetallic complex $[Mo(SnClMe_2)(CO)_3\{\mu\text{-}S\text{:}\kappa^3\text{-}H,S,S'\text{-}H_2B(mt^{Me})_2\}]$ **L1.97**.[146,147] Further discussion can be found under Group 5 and 6 (Section 1.3.4.2).

1.3.4.2 Transition Metal Chemistry

Group 3

No complexes of $[H_2B(mt^{R'})_2]^-$ with Group 3 metals (Sr and Y) have been reported.

Group 4

Studies prior to 2005 have predominantly focussed on coordination of $Bm^{R'}$ ligands to mid to late transition metals (Group 6 onwards). From a hard and soft acid and base (HSAB) perspective, the combination of soft sulfur donors with hard Lewis acidic metal centres might be discouraged. On the contrary, chelation and the π-basicity of the ligand might be expected to offset the HSAB incompatibility. Direct reaction of $[H_2B(mt^{R'})_2]^-$ sources with group 4 and 5 metal halides were complicated by redox and/or ligand hydrolysis (degradation), resulting in intractable mixtures, which was attributed to the highly electrophilic nature of the metal centre. Similar complications have been reported for the installation of poly(pyrazolyl)borate and $Tm^{R'}$ ligands into early transition metal complexes.[147-150] Therefore, alternative synthetic strategies were employed and are discussed for Groups 4 and 5.[133,147,148,151]

Direct reaction of $Na[H_2B(mt^{Me})_2]$ with $TiCl_4$ or $[TiCl_4(THF)_2]$ led to intractable mixtures, which may be due to the high Lewis acidity of the titanium(IV) reagents. The first $Bm^{R'}$ complex of group 4, $[Ti(=NCMe_3)\{H_2B(mt^{Me})_2\}_2]$ **L1.85**, was reported in 2006 by Hill and synthesised from two equivalents of $Na[H_2B(mt)_2]$ with Mountford's imido complex, $[Ti(=NCMe_3)Cl_2(py)_3]$.[148] There was no observation of the intermediate containing only one $[H_2B(mt)_2]^-$ unit, $[Ti(=NCMe_3)Cl(py)\{H_2B(mt^{Me})_2\}]$, even if limiting amounts of $Na[H_2B(mt)_2]$ were used. The molecular structure of **L1.85** reveals an interesting bonding situation where the two $[H_2B(mt)_2]^-$ ligands exhibit different coordination modes within the same molecule; the κ^2-*S,S'* bound ligand provides a cleft for the κ^3-*H,S,S'* coordinated ligand to fit into (Figure 1.17). The binuclear complex $[Ti_2(\mu\text{-}NCMe_3)_2(\mu\text{-}mt)_2(\kappa^2\text{-}mt)Cl]$ **L1.86** was obtained as a trace product and serves as an example of ligand degradation (Figure 1.17).

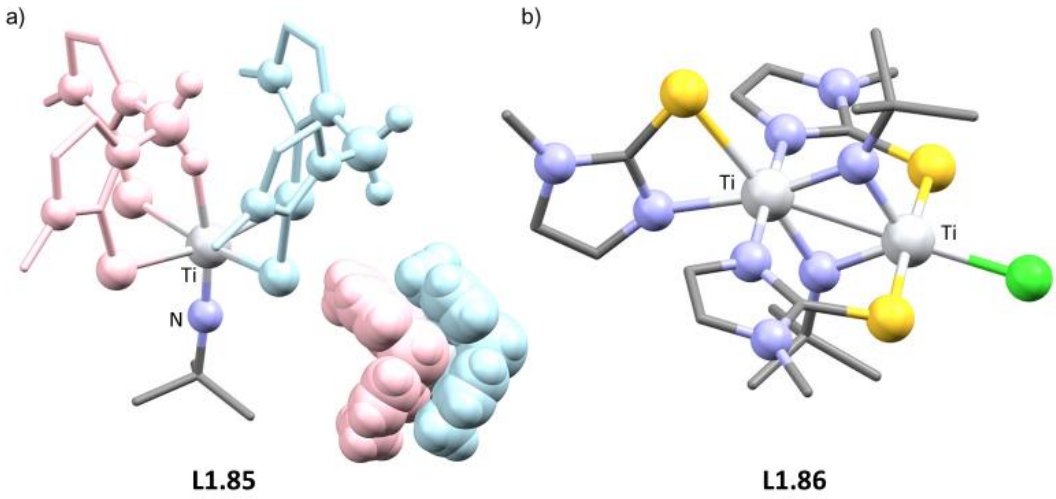

Figure 1.17: Molecular structures of a) Bm titanium complex **L1.85** and b) titanium methimazole based degradation product **L1.86**.

The series of zirconium complexes [ZrCl(η-C_8H_8)(κ^2-L)] (L = $H_2B(pz)_2$ **L1.87**, $HB(pzMe_2)_3$ **L1.88**, $H_2B(mt^{Me})_2$ **L1.89**) were synthesised from the precursor [$ZrCl_2$(η-C_8H_8)(THF)] and the appropriate borate salt.[151,152] Complex **L1.89** is the first example of the $Bm^{R'}$ ligand on zirconium. All complexes showed electronic unsaturation (16 VE) despite the capability of the ligands to contribute to coordination saturation by forming a further bond to the metal (either *via* B–H–Zr bonding or, in the case of $HB(pzMe_2)_3$, tridentate κ^3-*N,N',N''* coordination). Consequently, this would increase the metal coordination number to adopt a four-coordinate piano stool geometry. A comparison of the molecular structures is summarised in Figure 1.18, which confirms the absence of κ^3-*H,S,S'* coordination, instead showing the preferential binding of η-C_8H_8 over further chelation of the borate ligands. For comparison, the absence of η-C_8H_8 in Parkin's [$ZrCl_2$(η-C_5H_5){κ^3-*S,S',S''*-$HB(mt^{Me})_3$}] does allow tridentate coordination to establish electronic saturation at zirconium.[153] In contrast to $H_2B(pz)_2$ (**L1.87**) and $HB(pzMe_2)_3$ (**L1.88**) which adopt boat geometries upon chelation, the Bm^{Me} in **L1.89** shows the BH_2 group twisted away from the zirconium centre.

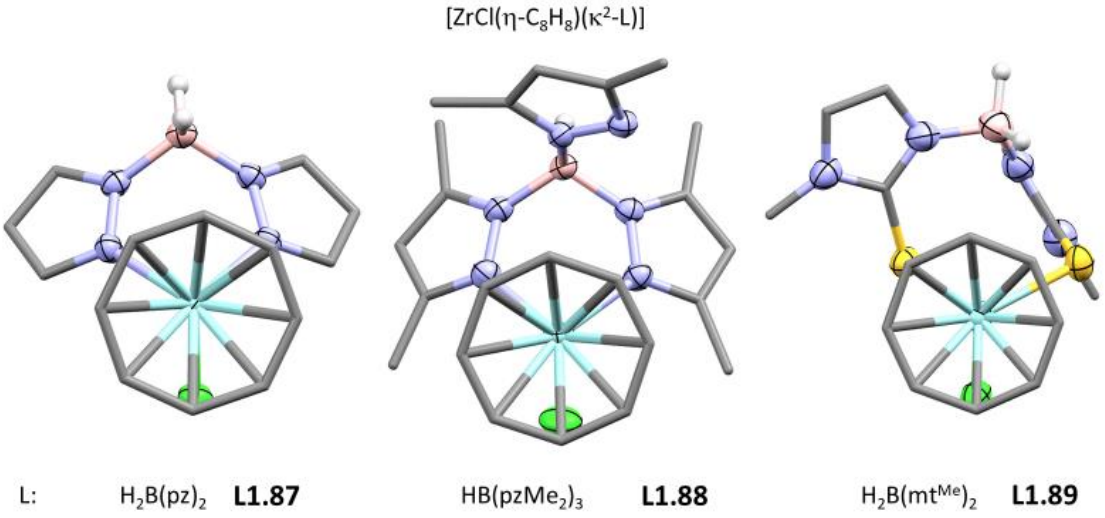

Figure 1.18: Molecular structure comparison of zirconium complexes **L1.87**–**L1.89** $[ZrCl(\eta\text{-}C_8H_8)(\kappa^2\text{-}L)]$ (L = $H_2B(pz)_2$, $HB(pzMe_2)_3$, $H_2B(mt^{Me})_2$).

No hafnium complexes of $[H_2B(mt^{R'})_2]^-$ have been reported.

Group 5

No vanadium complexes with $[H_2B(mt^{R'})_2]^-$ ligand(s) have been reported.

Given the complications in the direct reaction of $Bm^{R'}$ salts with group 5 halides (M_2Cl_{10}), organotin derivatives were utilised as transfer agents. When $Ph_3Sn[HB(mt^{Me})_3]$ was treated with $[MCl_4(\eta\text{-}C_5H_5)]$ (M = Nb, Ta), the anticipated products $[MCl_3(\eta\text{-}C_5H_5)\{\kappa\text{-}HB(mt^{Me})_3\}]$ eluded isolation and instead crystallographic studies revealed chloro(methimazolyl)borato complexes $[MCl_3(\eta\text{-}C_5H_5)\{HClB(mt^{Me})_2\}]$ (M = Nb, Ta **L1.90** Figure 1.19) were instead formed.[147] In each case, the $[HClB(mt^{Me})_2]^-$ ligand coordinates in a κ^2-*S,S'* mode where B–H···M or B–Cl···M bonding is precluded by the sterically encumbered metal centre.

The formation of the $[HClB(mt^{Me})_2]^-$ unit ultimately involves the transfer of a chloro group from the metal to boron and cleavage of mt. Two mechanistic possibilities were considered. Since the chloro group is located *exo* to the metal, one pathway is envisaged as the separation of $Ph_3Sn[HB(mt^{Me})_3]$ into $Ph_3Sn(mt^{Me})$ and $HB(mt^{Me})_2$, followed by abstraction of a chloride from the metal by $HB(mt^{Me})_2$. An alternative route considers the abstraction of an mt group from $[MCl_3(\eta\text{-}C_5H_5)\{\kappa\text{-}HB(mt^{Me})_3\}]$ by $ClSnPh_3$.

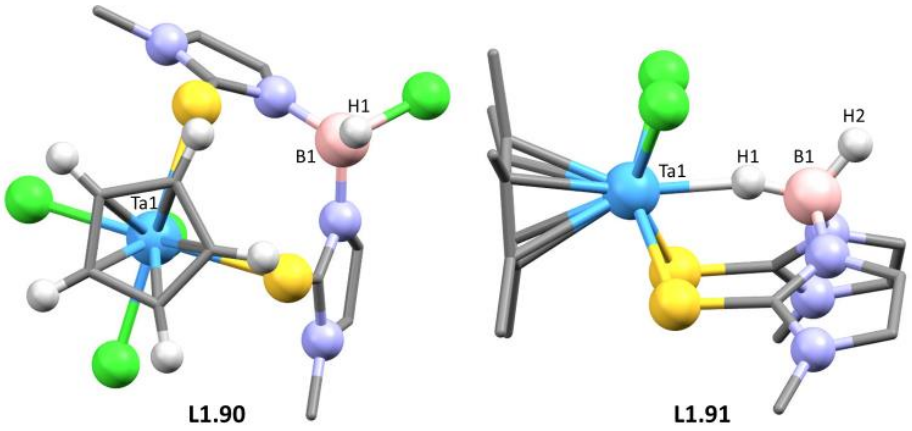

Figure 1.19: Molecular structures of **L1.90** and **L1.91**.

When the bulkier metal precursor [$TaCl_4(\eta\text{-}C_5Me_5)$] was reacted with less sterically demanding $Na[H_2B(mt^{Me})_2]$, the complex $[TaCl_2(\eta\text{-}C_5Me_5)\{\kappa^3\text{-}H,S,S'\text{-}H_2B(mt^{Me})_2\}]$ **L1.91** was formed and is the first example of a group 5 $Bm^{R'}$ complex.[133] The Ta–H–B geometry is nearly linear (163(6)°), distinct from the usual geometric range of 85.40–131.98° of related complexes in the CCDC.

Group 6

The half sandwich chromium(III) complexes, **L1.92**–**L1.94**, reported in the joint work by Leong and Goh are the only reported $Bm^{R'}$ complexes of chromium (Scheme 1.22).[154] The formation of **L1.92** follows from treatment of $Na[H_2B(mt^{Me})_2]$ with $[Cr_2Br_4(Cp^*)_2]$, and subsequent bromide abstraction by $AgPF_6$ in acetonitrile and toluene to provide the respective products, **[L1.94]**PF_6 and **[L1.93]**PF_6. The weak B–H–Cr interaction in **[L1.93]**PF_6 is instantly cleaved upon dissolution in acetonitrile to form **[L1.94]**PF_6.

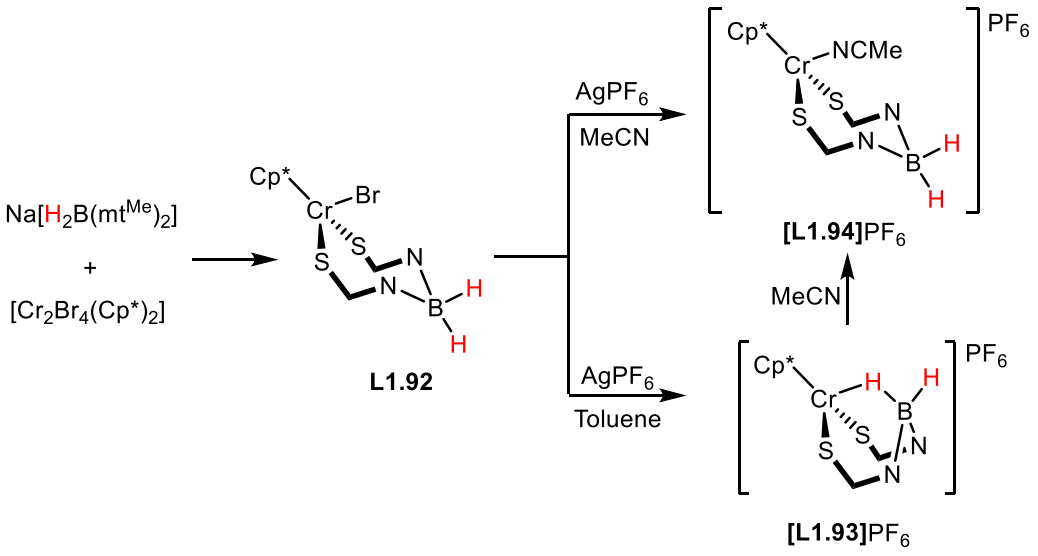

Scheme 1.22: $Bm^{R'}$ complexes of chromium.

Studies into the synthesis of molybdenum $Bm^{R'}$ complexes have been carried out by Hill and co-workers (Scheme 1.23) and readily provides access to thiocarbamoyl, stannyl, nitrosyl derivatives and a diheterotrimetallic complex.[114,135,146,155] The thiocarbamoyl complex **L1.95** could be prepared *via* two routes: i) the sequential reaction of $[Mo(pip)_2(CO)_4]$ (pip = piperidine) with $Na[H_2B(mt^{Me})_2]$ followed by Me_2NCSCl; or ii) treatment of complex **L1.96** with $Na[H_2B(mt^{Me})_2]$. High yields (80–82%) were obtained from both preparative routes.[114] Notable features include the higher symmetry observed in the ^1H and $^{13}C\{^1H\}$ NMR of **L1.95**, despite the static crystal structure containing no evidence of symmetry, which suggests that there is fluxionality in solution. The large discrepancy in the Mo–S bond lengths of the two thione donors, 2.5859(9) and 2.4864(10) Å, was attributed to the disparate *trans* influences of the carbonyl and thiocarbamoyl ligands.

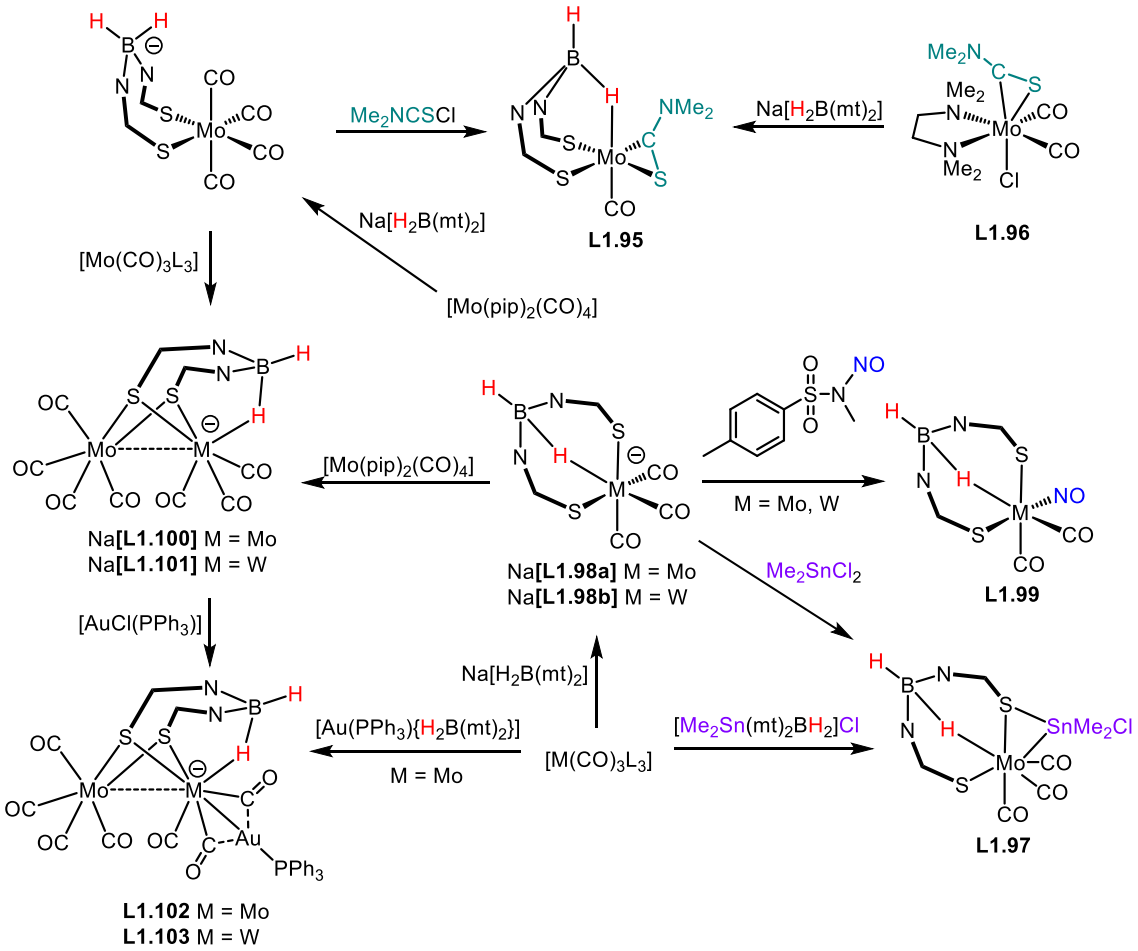

Scheme 1.23: $Bm^{R'}$ molybdenum complexes (pip = piperidine, L = NCMe, $L_3 = \eta^6$-C_7H_8).

The molybdenum stannyl complex **L1.97** is accessible through two preparative pathways (Scheme 1.23).[146] One strategy features consecutive reaction of $[Mo(CO)_3(NCMe)_3]$ with $Na[H_2B(mt^{Me})_2]$ to form intermediate Na**[L1.98a]** that is subsequently treated with Me_2SnCl_2. Alternatively the $[Me_2Sn(mt^{Me})_2BH_2]Cl$ group remains intact when engaging with $[Mo(CO)_3(\eta^6\text{-}C_7H_8)]$ and the resulting complex **L1.97** can be considered as interrupted oxidative addition of the S–Sn bond. In contrast, the analogous reaction with $Ph_3Sn[HB(mt^{Me})_3]$ affords C_3-symmetric $[Mo(SnPh_3)(CO)_3\{\kappa^3\text{-}S,S',S''\text{-}HB(mt^{Me})_3\}]$ where complete Sn–S rupture occurs.

$Bm^{R'}$ Nitrosyl complexes (**L1.99**) are obtained from the treatment of Na**[L1.98a]** (generated *in situ* from $[Mo(CO)_6]$ and $Na[H_2B(mt^{Me})_2]$) with *N*-methyl-*N*-nitroso-*p*-toluenesulfonamide (Diazald®) as a mild source of NO^+ (Scheme 1.23). The tungsten analogue was similarly synthesised, although it can also be obtained through the alternative pathway commencing from pre-isolated $[W(CO)_3(NCMe)_3]$.[135,156]

Bimetallic coordination of $Bm^{R'}$ *via* sulfur bridges was demonstrated in the synthesis of complexes Na**[L1.100]**–Na**[L1.103]**. Complex Na**[L1.100]** was accessible through two synthetic pathways (Scheme 1.23): sequential reaction of $[Mo(pip)_2(CO)_4]$, $Na[H_2B(mt^{Me})_2]$ and $[Mo(CO)_3L_3]$ or through initial treatment of $[Mo(CO)_3L_3]$ with $Na[H_2B(mt^{Me})_2]$ followed by $[Mo(pip)_2(CO)_4]$ (L = NCMe, $L_3 = \eta^6\text{-}C_7H_8$). The resulting anionic complex **[L1.100]**$^-$ can be generated *in situ* as Na**[L1.100]** or isolated as the bis(triphenylphosphine)iminium (PPN) salt by metathesis with [PPN]Cl.[155] The connectivity of the **[L1.100]**$^-$ unit was confirmed through X-ray crystallography as the anion in the bimetallic salt $[Au_2\{\mu^2\text{-}H_2B(mt^{Me})_2\}(PEt_3)_2][Mo_2\{\mu^2\text{-}H_2B(mt^{Me})_2\}(CO)_7]$ **L1.147**, which is discussed under Group 11 (Figure 1.22).

Subsequent treatment of **[L1.100]**$^-$ with $[AuCl(PPh_3)]$ affords the diheterotrimetallic complex **L1.102**. Crystallographic studies confirmed the connectivity in **L1.102** and showed that only modest structural rearrangement was required to accommodate the $Au(PPh_3)$ fragment (Figure 1.20). The retention of the B–H–Mo interaction depicted in the molecular structure was further supported by the IR and ^{1}H NMR data.

The long Mo–Mo separation of 3.879 Å is beyond covalent bonding distance, as anticipated for d^6–d^6 centres. An alternate construction of the Mo_2Au core begins with the insertion of $[Mo(CO)_3(\eta^6\text{-}C_7H_8)]$ into the Au–S bond of $[Au(PPh_3)\{\kappa^2\text{-}S,S'\text{-}$

$H_2B(mt^{Me})_2$}]. Following the first pathway, the sequential reaction of Na**[L1.98b]**, [Mo(pip)$_2$(CO)$_4$], and [AuCl(PPh$_3$)] yields the triheterometallic complex **L1.103** with comparable similarities to the diheterotrimetallic analogue.

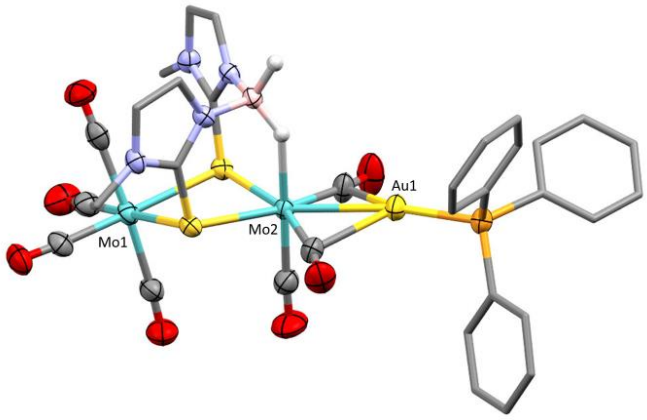

Figure 1.20: Molecular structure of diheterotrimetallic complex **L1.102**.

The Bm$^{R'}$ unit can be incorporated into an alkylidyne complex, such as **L1.104** generated from [Mo(≡CC$_6$H$_2$Me$_3$-2,4,6)X(CO)$_2$(py)$_2$] (X = Cl, Br) and Na[H$_2$B(mt^{Me})$_2$] (Scheme 1.24).[157] Synthesis of the tungsten analogue was unsuccessful, however the complex [W(≡CC$_6$H$_2$Me$_3$-2,4,6)(CO)$_2${H$_2$B(mt^{Me})$_2$}] was proposed to be an intermediate, with the final product being identified as **L1.105**. Complex **L1.105** featured (at that time) unprecedented ligation of [H$_2$B(mt^{Me})$_2$]$^-$ in two different coordination modes, κ^3-*H,S,S'* and κ^2-*S,S'*, within the same complex.

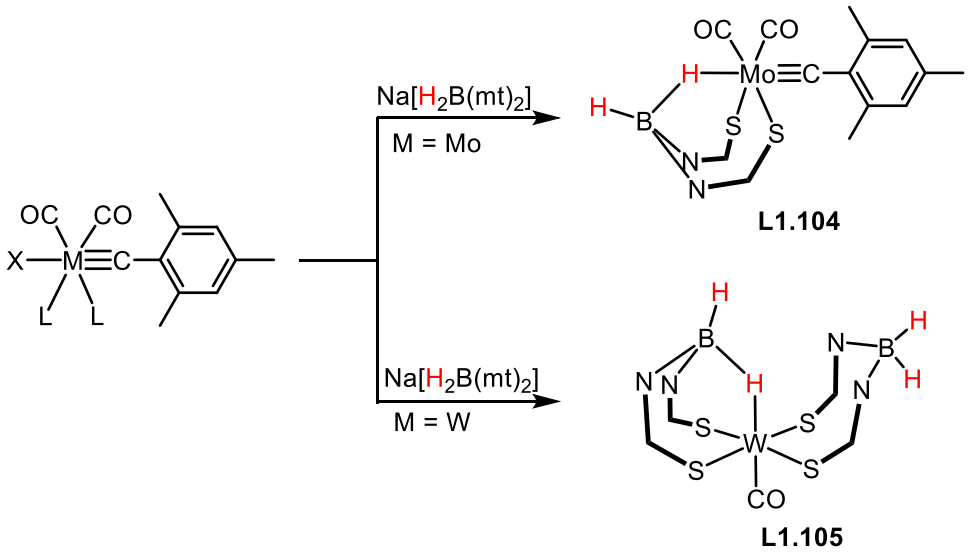

Scheme 1.24: Bm$^{R'}$ alkylidyne complexes **L1.104** and **L1.105.** L = pyridine (py), 3,5-dimethylpyrazole (Hpz*); X = Cl, Br.

Given the coexistent coordination of the two $[H_2B(mt^{Me})_2]^-$ units in **L1.105**, the coordinative unsaturation (16 VE) of the complex is particularly remarkable given that coordinative saturation (18 VE) could be easily attained by tridentate coordination of both $[H_2B(mt^{Me})_2]^-$ ligands. The presence of only one B–H–W interaction appears to be dictated by electronic factors and the d^4 tungsten(II) centre is further stabilised by π-basic thione donors. The coordinative unsaturation of **L1.105** raises the possibility of coordination mode interconversion between the two borate ligands, which were invariant on the ^{1}H NMR timescale over the temperature range of 20–70°C, followed by decomposition into methimazole at higher temperatures.[157]

Other examples of $Bm^{R'}$ tungsten complexes include the monoalkyne complexes **L1.106** and **L1.107**, which can be accessed *via* reaction of $Na[H_2B(mt^{Me})_2]$ with the alkyne precursors $[WI_2(HC{\equiv}CSiMe_3)_2(CO)_2]$ or $[WI_2(MeC{\equiv}CMe)_2(CO)(NCMe)]$ (Scheme 1.25).[158]

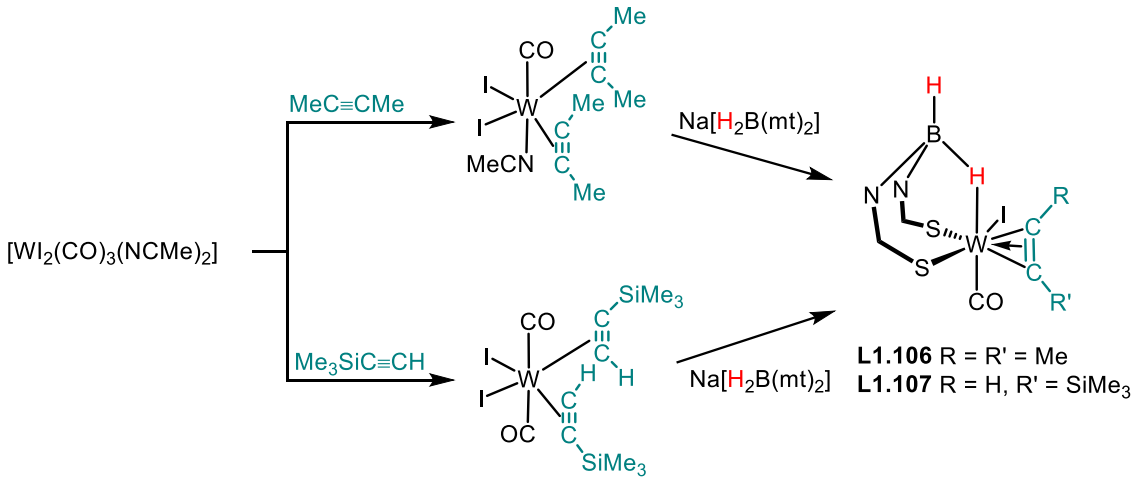

Scheme 1.25: $Bm^{R'}$ monoalkyne complexes of tungsten.

Group 7

The coordination chemistry of $Tm^{R'}$ and $Bm^{R'}$ of group 7 was primarily directed toward the preparation of radiopharmaceuticals with ^{99m}Tc and $^{186/188}$Re isotopes. The lightest member of the triad wasn't explored until 2005, when Rabinovich and co-workers reported manganese(I) tricarbonyl complexes **L1.108** (R' = Me, R = H, Ph; and R' = Bz, ^{t}Bu, *p*-Tol, R = H).[139] As depicted in Scheme 1.26, the complexes were obtained by reaction of $[MnBr(CO)_5]$ with the salts $Na[H_2B(mt^{R'})]$ (R' = Me, ^{t}Bu), $Li[HPhB(mt^{Me})]$ or $Tl[H_2B(mt^{R'})]$ (R' = Bz, *p*-Tol). Cleaner reactions were obtained with the (albeit toxic) thallium reagents.

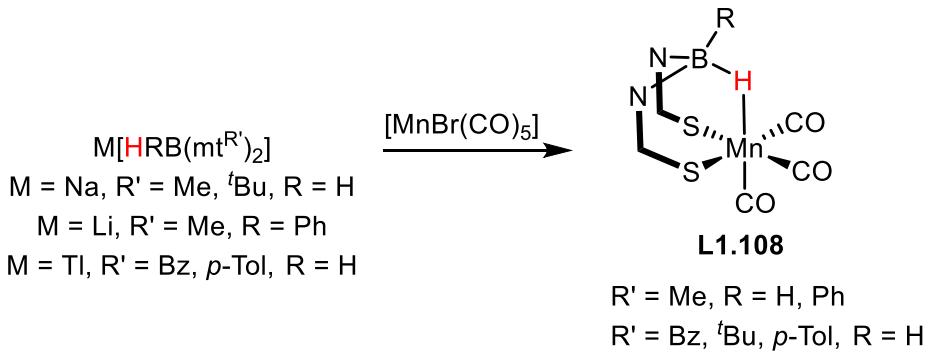

Scheme 1.26: Synthesis of $Bm^{R'}$ manganese complexes with varying N-substituent (R') and B-substituent (R).

The R' substituent affects the solubility of the complex in decreasing order Me ~ *p*-Tol > ^{t}Bu > Bz and exerts a small change to the electron density at the metal centre, observed by the somewhat lower ν_{CO} stretching frequencies of the more basic alkyl-substituted ligands (R = Me, Bz, ^{t}Bu) relative to the *p*-Tol analogue.

The group of Santos has extensively studied $Bm^{R'}$ and $Tm^{R'}$ complexes of rhenium and technetium. As reviews on this area by Santos and Rabinovich are available,[101,159,160] the work described herein will focus on the main advancements in $Bm^{R'}$ chemistry. Complexes of the form $[M(CO)_3\{\kappa^3\text{-}H,S,S'\text{-}H_2B(mt^{R'})_2\}]$ (M = Re **L1.62**, ^{99}Tc **L1.109**) are obtained from the reaction of *fac*-$[M(CO)_3]^+$ precursors with a suitable $Bm^{R'}$ ligand (Scheme 1.27).[106] Complex $[Re(CO)_3\{\kappa^3\text{-}H,S,S'\text{-}H_2B(mt^{Me})_2\}]$ **L1.62** has been previously discussed in Section 1.3.3.1 (Scheme 1.17) with respect to B–H–M *hemilability*. Another route to **L1.62** includes the reaction of complex **L1.110** (Scheme 1.27) featuring less substituted borate $[H_3B(mt^{Me})]^-$ and one equivalent of methimazole, demonstrating that the addition of an mt^- unit to $[H_3B(mt^{Me})]^-$ occurs within the rhenium coordination sphere. Analogous reactivity of complex **L1.110** with other heterocycles allows access to heteroscorpionates, such as those of benzo(methimazolyl) **L1.111** and pyrazolyl **L1.112** (Scheme 1.27).[161]

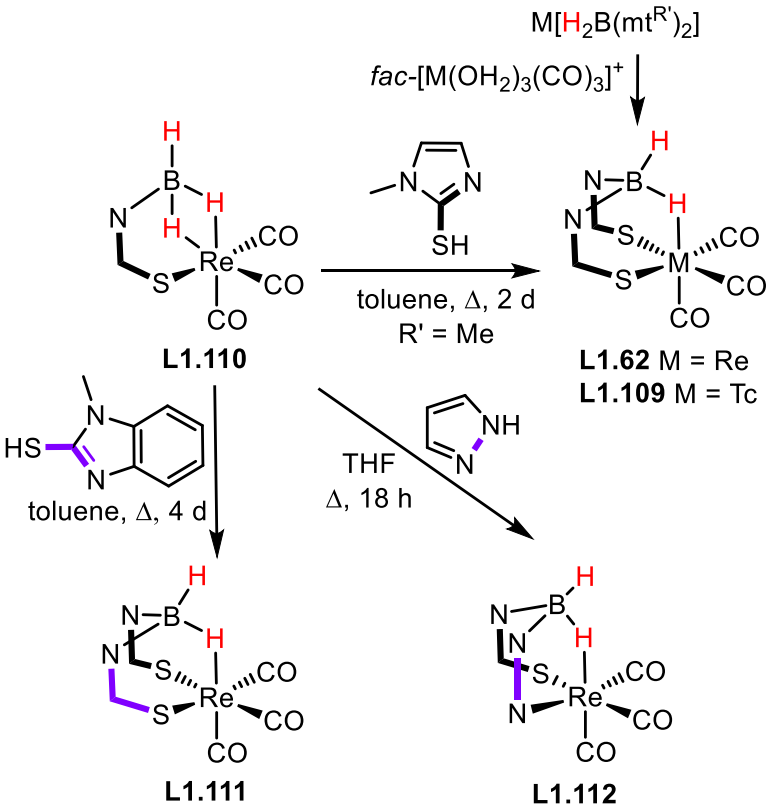

Scheme 1.27: Synthetic pathways to rhenium **L1.62** and technetium **L1.109** complexes, and heteroscorpionates **L1.111** and **L1.112**.

Other early examples include introduction of a substituent (R) on boron to give [Re(CO)$_3${κ^3-*H,S,S'*-HRB(mt^{Me})$_2$}] (R = Me, Ph), which showed C_s symmetry in the solid state as confirmed *via* crystallographic studies.[107] In each case a robust BH–Re interaction persisted even in coordinating solvents. In contrast, the related Tm$^{R'}$ complex [Re(CO)$_3${κ^3-*S,S',S''*-HB(mt^{Me})$_3$}] is of C_3 symmetry with the rhenium and borohydride group lying on the crystallographic *3* axis.[107] The B···Re distance of [Re(CO)$_3${κ^3-*H,S,S'*-RHB(mt^{Me})$_2$}] (R = Me, Ph) complexes was slightly greater than the unsubstituted [H$_2$B(mt^{Me})$_2$]$^-$ analogues (2.91(1) and 2.92(2) Å *cf*. 2.832(12) Å) on rhenium indicating that the substituent on the boron has no substantial effect on coordination behaviour.[107]

Borate ligands functionalised at the olefinic backbone also coordinate to the rhenium precursor [NEt$_4$]$_2$[ReBr$_3$(CO)$_3$] in a κ^3-*H,S,S'* fashion, yielding symmetric [Re(CO)$_3${κ^3-*H,S,S'*-H$_2$B(mt$^{Me}_{R''}$)$_2$}] and asymmetric [Re(CO)$_3${κ^3-*H,S,S'*-PhHB(mt$^{Me}_{R''}$)(mt^{Me})}] complexes (R'' = **1**, **2** Table 1.1).[115] Longer linkers were utilised in the synthesis of [M(CO)$_3${κ^3-*H,S,S'*-H$_2$B(mt$^{Me}_{R''}$)$_2$}] and [Re(CO)$_3${κ^3-*H,S,S'*-H$_2$B(mt$^{Me}_{R''}$)(mt^{Me})}] (M = Re,

^{99m}Tc, R'' = **3** Table 1.1).[162] The latter rhenium complexes were shown to exhibit excellent affinity as radioactive probes for 5-HT_{1A} serotonergic receptors.

Group 8

No iron complexes of $[H_2B(mt^{R'})_2]^-$ have been reported, while coordination of $Bm^{R'}$ to ruthenium has enjoyed extensive study and includes homoleptic examples in addition to a range of ruthenium precursors with differing co-ligands. The homoleptic complex **L1.113** (Scheme 1.28) has been independently reported by Zhang, and by Reglinski and Spicer.[163,164] Both preparatory routes involve the reaction of $[RuCl_2(DMSO)_4]$ with two equivalents of $M[H_2B(mt^{Me})_2]$ (M = K, Zhang; Na, Reglinski and Spicer), albeit under different temperature and solvents (THF, r.t and acetonitrile reflux, respectively). The two hydrides from the κ^3-*H,S,S'* coordinated ligands are consistently *cis* disposed in the octahedral complex.

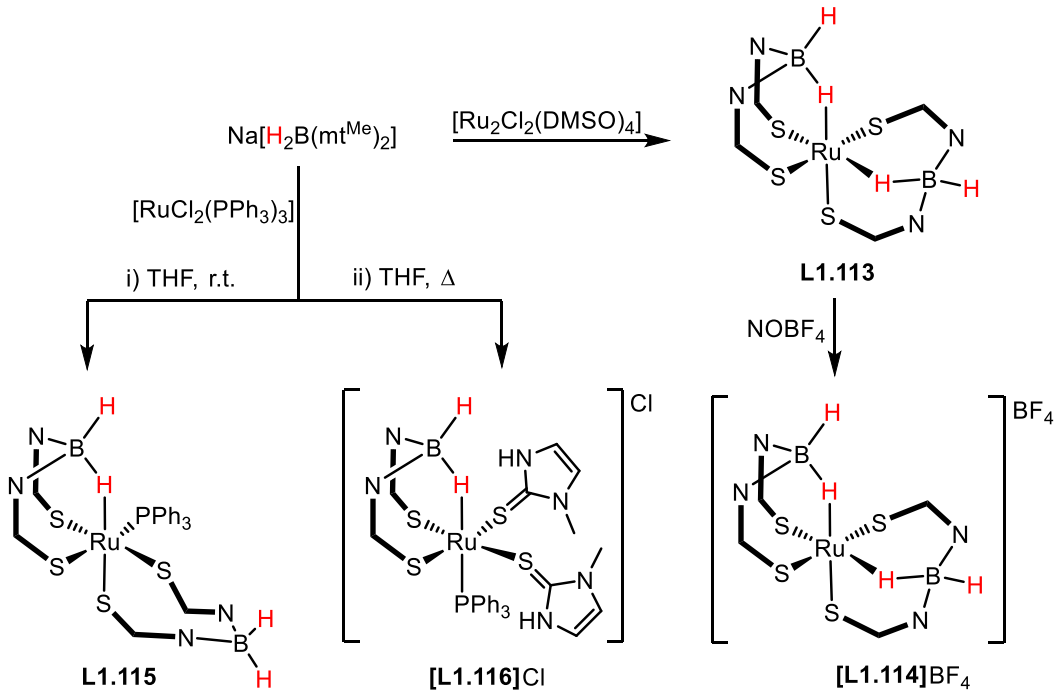

Scheme 1.28: Reaction of $Na[H_2B(mt^{Me})_2]$ with ruthenium precursors $[RuCl_2(L)_n]$ (L = PPh_3, n = 3; L = DMSO, n = 4).

Reglinski and Spicer demonstrated the oxidation of **L1.113** by $NOBF_4$ to give [**L1.114**]BF_4 (Scheme 1.28). Whilst the octahedral molecular structure was maintained on oxidation from Ru(II) to Ru(III), the IR band of the terminal B–H moiety shifts to higher wavenumbers (2377 *cf.* 2438 cm^{-1}). Attempts to install nitrosyl into the coordination

sphere of ruthenium *via* direct reaction ($NOBF_4$, NO, NOBr) or by introduction of the ligand onto a ruthenium nitrosyl chloride adduct '$Ru(NO)Cl_3$' were unsuccessful.[164]

When $[RuCl_2(PPh_3)_3]$ and two equivalents of $K[H_2B(mt^{Me})_2]$ were reacted in THF at two different temperatures (Scheme 1.28), Zhang and co-workers obtained complexes **L1.115** (from room temperature) and **[L1.116]**Cl (from reflux).[163] The coordination of free methimazole in **[L1.116]**Cl is presumably due to $Bm^{R'}$ degradation during the synthesis.

The co-existence of $Bm^{R'}$ and $Tm^{R'}$ ligands with ruthenium arene and Cp* moieties has been investigated by the collaborative work of Leong and Goh. The combination of $Na[H_2B(mt^{Me})_2]$ with ruthenium dimers $[Ru_2Cl_4(C_6Me_6)_2]$ or $[Ru_2(OMe)_2(Cp^*)_2]$ at a 2:1 ratio led to the respective complexes **[L1.117]**Cl and **L1.68**, featuring tridentate κ^3-*H,S,S'* coordination (Scheme 1.29).[136] Kuwata and Ikariya and co-workers showed **L1.68** was reactive towards CO in forming **L1.69** through *hemilability* of the BH–M association.[137]

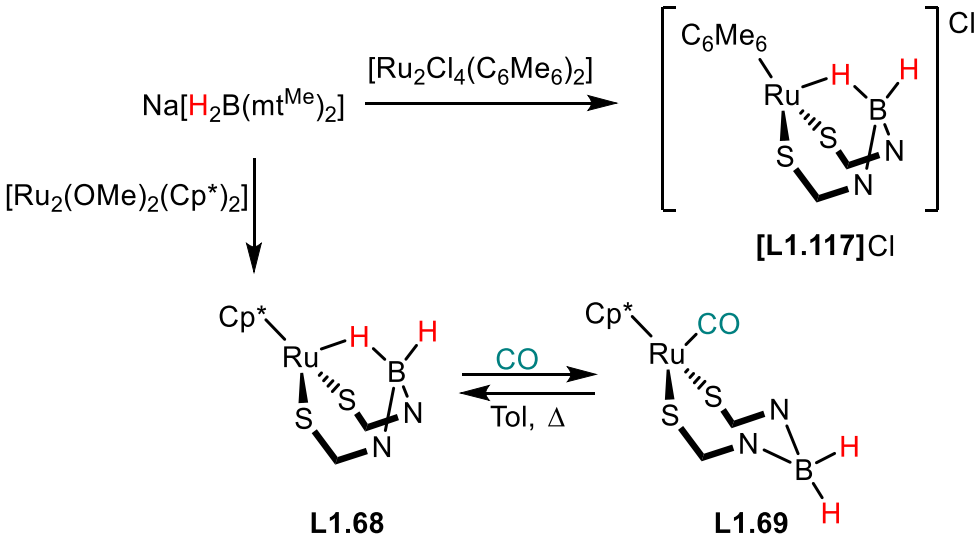

Scheme 1.29: Reaction of $Na[H_2B(mt^{Me})_2]$ with ruthenium dimers.

The $Tm^{R'}$ analogues were concurrently reported, albeit with κ^3-*S,S',S''* coordination.[136,138] Complexes $[Ru\{HB(mt^{Me})_3\}(Cp^*)]Cl$ and $[Ru\{HB(mt^{Me})_3\}(Cp^*)]$ exhibited solution isomerisation involving fluxionality between κ^3-*H,S,S'* and κ^3-*S,S',S''* coordination modes. In contrast, no fluxional equilibrium was evident (in variable temperature NMR studies and cyclic voltammetry) for **[L1.117]**Cl and **L1.68**. In particular, complex **[L1.117]**Cl was significantly harder to oxidise than its neutral Cp* derivative **L1.68**.

Further examples of $Bm^{R'}$ ruthenium complexes include **L1.118**[165] and the series **L1.119a-c**[166] (R' = C_6H_4Cl-4, C_6H_4Me-4, $C_6H_4NO_2$-4) synthesised from reaction of $Na[H_2B(mt^{Me})_2]$ and the respective precursors $[RuHCl(PPh_3)_3]C_6H_5Me$ and $[RuHCl(CO)(PPh_3)_3]$ (Scheme 1.30). When complexes **L1.119a-c** were heated under reflux in chloroform or treated with Br_2 or I_2, the hydride was replaced with the respective halide to give complexes **L1.120a-c** (X = Cl, Br, I).[166,167]

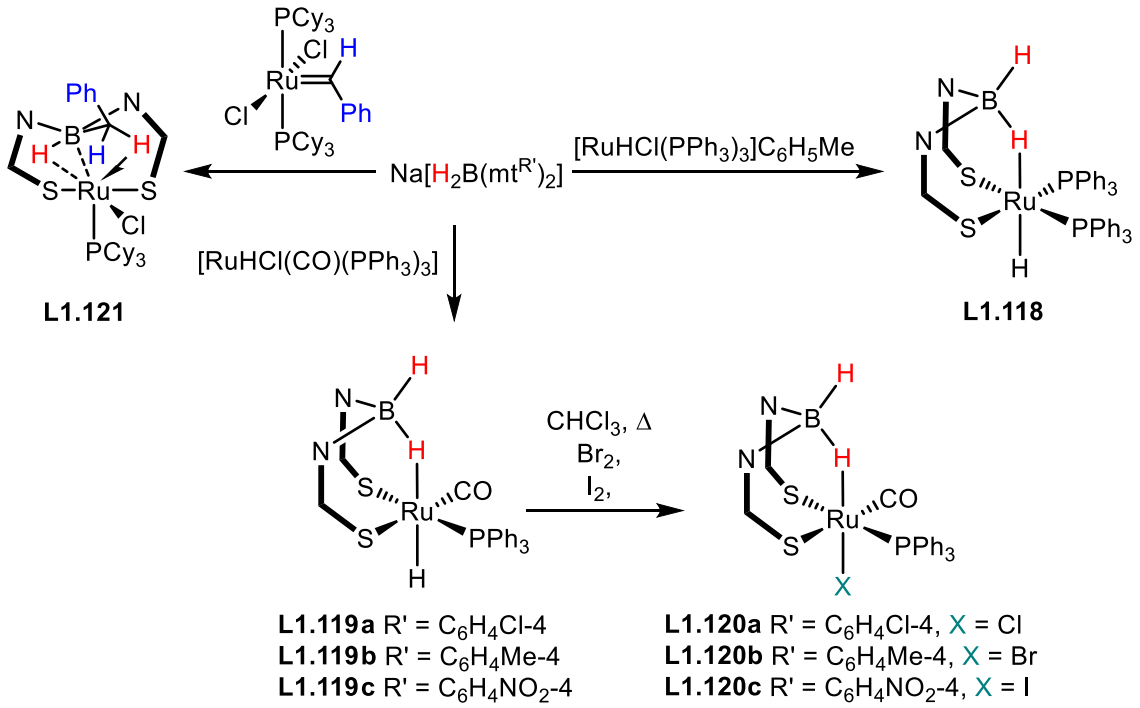

Scheme 1.30: Further examples of $Bm^{R'}$ ruthenium complexes.

Owen reported the unusual reactivity of $Na[H_2B(mt^{Me})_2]$ with Grubbs' catalyst in the formation of complex $[RuCl(PCy_3)\{\kappa^4\text{-}HB(CH_2Ph)(mt^{Me})_2\}]$ **L1.121** (Scheme 1.30), which is suggested to represent the novel interception of an intermediate in hydride transfer between boron and ruthenium.[168]

Osmium $Bm^{R'}$ complexes are comparably rare and the synthesis of the only example to date, $[OsH(CO)(PPh_3)\{\kappa^3\text{-}H,S,S'\text{-}H_2B(mt^{R'})_2\}]$, has been prepared in this work (Chapter 2).

Group 9

Whilst no cobalt complexes of $[H_2B(mt^{R'})_2]^-$ have been reported, the heavier group 9 elements have been explored extensively, with the first report featuring iridium in complexes **L1.122** and **L1.123** (Scheme 1.31). Prepared from treatment of Vaska's complex *trans*-$[IrCl(CO)(PPh_3)_2]$ with $Na[HB(mt^{Me})_3]$ and $Na[H_2B(mt^{Me})_2]$ (Scheme 1.31),

L1.122 and **L1.123** were additionally recognised as the first iridaboratrane complexes, with a characteristic Ir→B dative bond in κ^3-*B,S,S'* coordination of the $RB(mt)_2$ (R = H, mt) moiety.[60,169]

Notably, these complexes were the first examples of metallaboratranes with a M→B interaction supported by only two methimazolyl buttresses. Despite the greater flexibility of the dibuttressed cage compared to the κ^4-*B,S,S',S''* tricyclo-[3.3.3.0] motif of $Tm^{R'}$ based metallaboratranes, no relaxation to the electronically favoured square planar analogue was observed, highlighting the structural rigidity of the Ir→B linkage. The carbon sulfide analogues **L1.124** and **L1.125** were similarly prepared (Scheme 1.31), however these were comparably less stable in solution than their carbon monoxide counterparts.[169]

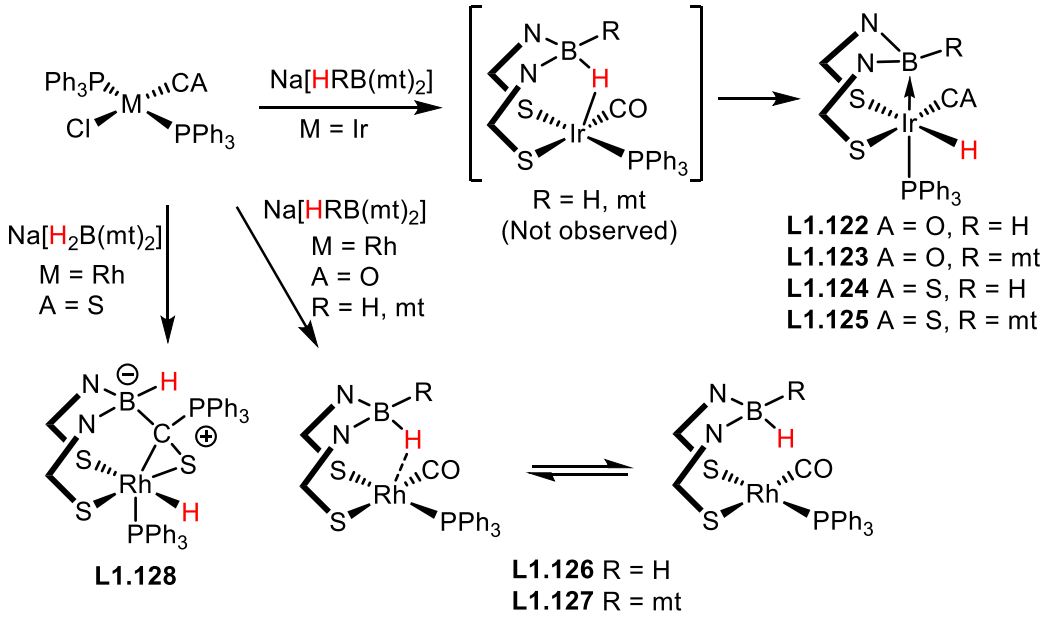

Scheme 1.31: Schematic summary of $[MCl(CA)(PPh_3)_2]$ (M = Rh, Ir; A = O, S) reactivity with $Na[HRB(mt^{Me})_2]$ (R = H, mt).

In contrast, reduced propensity for oxidative addition upon going from 5d (Ir) to 4d (Rh), resulted in a lack of B–H activation, and instead led to formation of the borates **L1.126** and **L1.127** (Scheme 1.31). In the solid state both complexes display B–H–Rh bonding (κ^3-*H,S,S'*), which is lost in solution owing to the suspected prominence of the square planar geometry (κ^2-*S,S'*). Unexpectedly, the reaction with $[RhCl(CS)(PPh_3)_2]$ resulted in novel phosphaboration of the thiocarbonyl ligand to provide complex **L1.128**.[170] As the migration of PPh_3 to CS is unprecedented, the proposed mechanistic conjecture

accounting for the formation of **L1.128** was proposed to be CS insertion into the M→B bond.

The reactivity of $Na[H_2B(mt^{R'})_2]$ towards rhodium chloro-bridged dimers is summarised in Scheme 1.32, involving simple metathesis and are further illustrations of B–H–Rh interactions.[132,171] Reaction with $[Rh_2Cl_2(COD)_2]$ provided the mononuclear complex **L1.129** where the COD ligand could be readily replaced by CO and CNXyl ligands to give the respective complexes, **L1.130** and **L1.131**.[132] Similar to **L1.126** and **L1.127**, the presence of B–H–Rh bonds in complex **L1.129** differed in the solution and solid state. The 3c2e interaction was absent in solution IR, concomitant with the presence of two terminal B–H vibrations (2344, 2303 cm^{-1}); but weakly determined in the molecular structure and solid-state IR spectrum (2192 cm^{-1}).

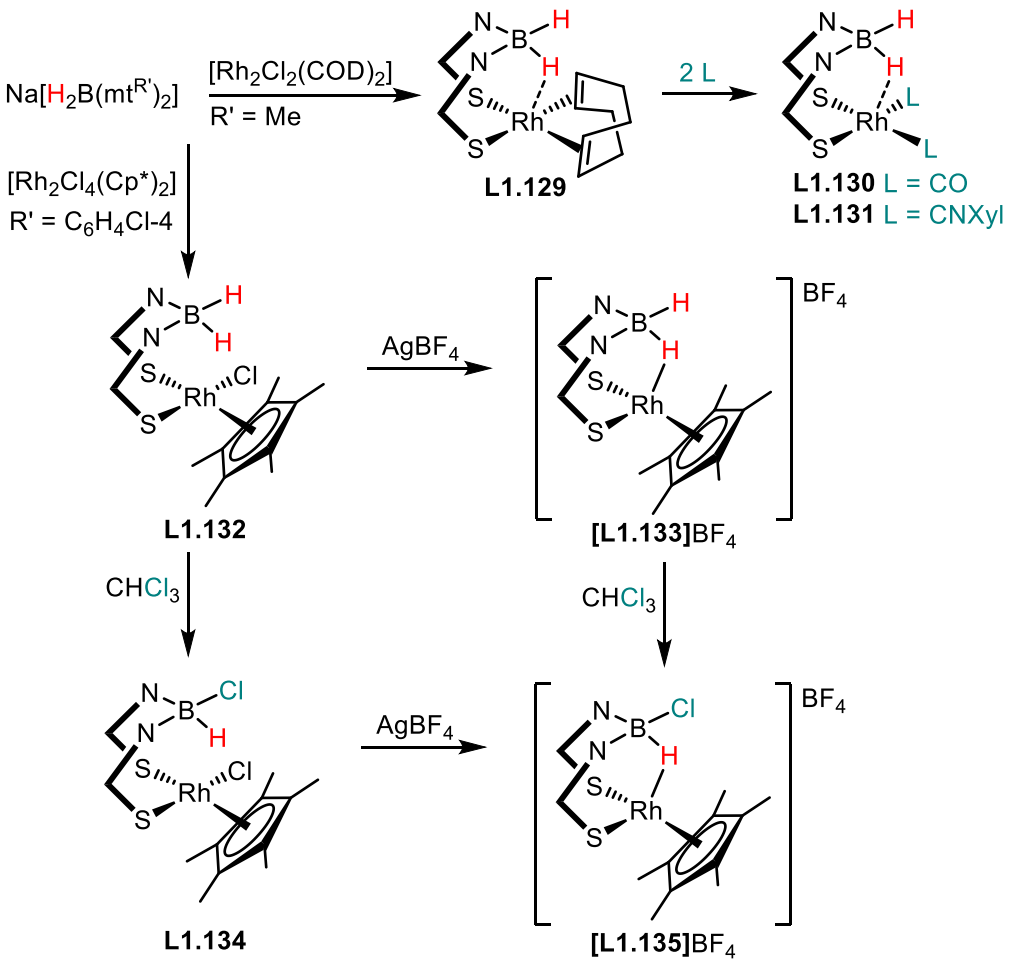

Scheme 1.32: Schematic summary of $Na[H_2B(mt^{R'})_2]$ reactivity with rhodium precursors and subsequent reactions (Xyl = $C_6H_3Me_2$-2,6).

When the precursor $[Rh_2Cl_4(Cp^*)_2]$ with the non-labile Cp* ligand was used, complex **L1.132** was formed, revealing only κ^2-*S,S'* coordination (Scheme 1.32). The complex was subsequently subjected to chloride abstraction by $AgBF_4$ to yield **[L1.133]**BF_4 featuring an established B–H–Rh bond.[171] Both complexes are prone to boron chlorination in chloroform to generate **L1.134** and **[L1.135]**BF_4 respectively.

Group 10

To model the sulfur rich NiFe hydrogenase active site, Rabinovich prepared the homoleptic **L1.136** (Scheme 1.33) from aqueous/methanolic solutions of $NiCl_2.6H_2O$ and $Na[H_2B(mt^{Me})_2]$ (1:2 ratio).[172] The NiS_4H_2 core features κ^3-*S,S',H* coordination of each ligand in a distorted octahedral geometry. The susceptibility of complex **L1.136** to irreversible electrochemical reduction and oxidation was established through cyclic voltammetry.

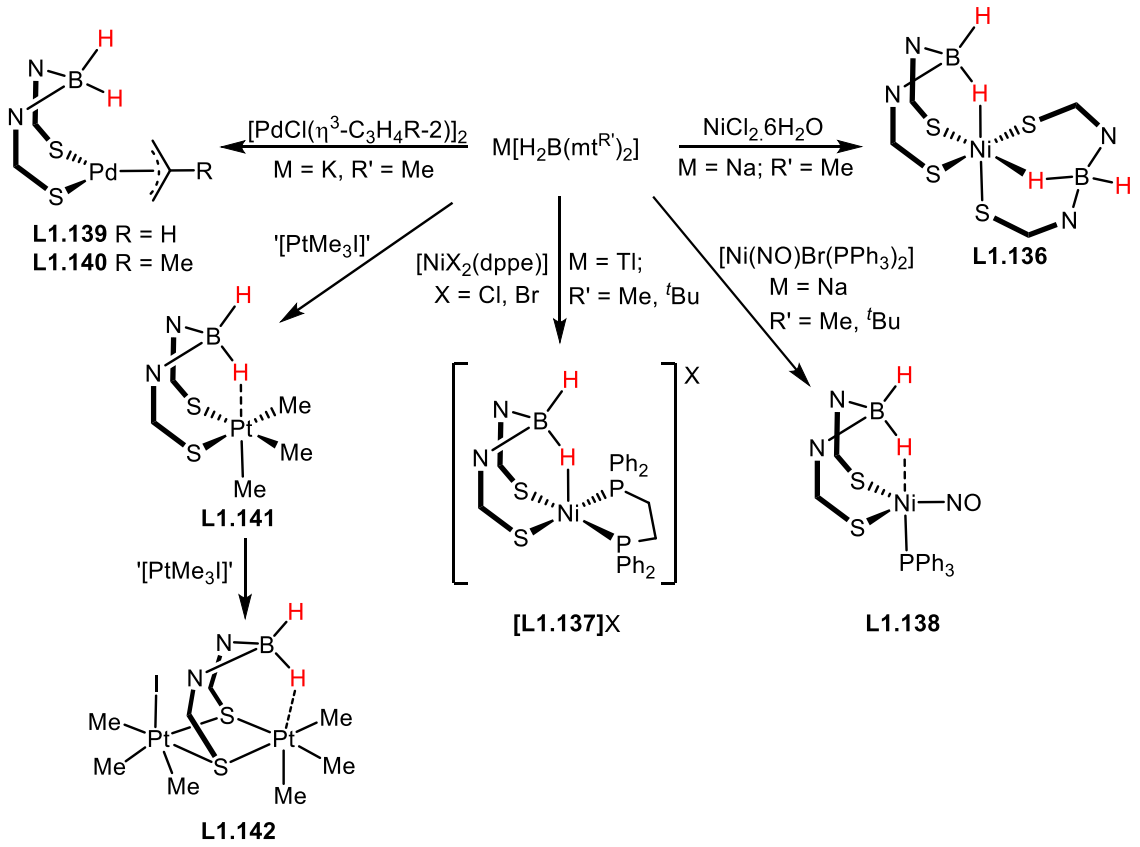

Scheme 1.33: Summary of $Na[H_2B(mt^{R'})_2]$ reactivity with Group 10 precursors.

Heteroleptic Ni(II) complexes such as **[L1.137]**X can be synthesised from $[NiX_2(dppe)]$ (X = Cl, Br) with the appropriate thallium salt $Tl[H_2B(mt^{R'})_2]$ (R' = Me, ^{t}Bu), affording the first structurally characterised complexes to possess a $[NiP_2S_2H]$ core (Scheme 1.33).[144]

The complexes are distorted square pyramidal featuring B–H–Ni bonding with a Ni···H distance of 1.99(4) Å. The $Tm^{R'}$ derivative [Ni(dppe){$HB(mt^{p\text{-tol}})_3$}]Cl similarly exhibits preferential κ^3-*S,S',H* coordination over κ^3-*S,S',S''* and has a comparable Ni···H distance of 2.15(4) Å, given the lack of precision in metal-hydride bond lengths.[144]

Furthermore, Rabinovich developed the first few examples of $Bm^{R'}$ and $Tm^{R'}$ nickel nitrosyl complexes, **L1.138** and [Ni(NO){$HB(mt^{R'})_3$}] (R' = *p*-Tol, ^{t}Bu), from [Ni(NO)Br$(PPh_3)_2$] and the suitable borate salt.[173] Whilst both featured tripodal binding, the latter supported tridentate κ^3-*S,S',S''* chelation of the ligand to the nickel centre, whereas **L1.138** coordinated *via* the κ^3-*H,S,S'* mode with a weak intramolecular Ni–H–B interaction, which completes the trigonal bipyramidal geometry adopted by the complex.

Compared to nickel, $Bm^{R'}$ chemistry of palladium and platinum have been less studied. Whilst palladium and platinum chemistry of $Tm^{R'}$ is dominated by metallaboratrane motifs, parallel chemistry with the $Bm^{R'}$ analogue have proven to be elusive. However, the reaction of [PdCl(η^3-C_3H_4R-2)]$_2$ (R = H, Me) with K[$H_2B(mt^{Me})_2$] does yield complexes **L1.139** and **L1.140** (Scheme 1.33), for which NMR spectroscopy indicates the absence of agostic B–H–Pd interactions even at low temperatures (–70°C).[174]

Since the discovery of the di- and zero valent platinaboratranes of $Tm^{R'}$ complexes [PtH{κ^4-*B,S,S',S''*-$B(mt^{Me})_3$}(PPh_3)]Cl and [Pt{κ^4-*B,S,S',S''*-$B(mt^{Me})_3$}(PPh_3)] (Pt→B) in 2004, the preparation of similar structures supported by two methimazolyl bridges was pursued.[175] Pope's complex $[PtMe_3I]_4$ was used as the platinum precursor in these investigations. However, the stable κ^3-*H,S,S'* complex **L1.141** was obtained, or when the reaction was halted prematurely, crystals of dinuclear complex **L1.142** were isolated (Scheme 1.33).[176] Both complexes displayed remarkable thermal stability and resisted reductive elimination of CH_4 or C_2H_6 that might result in boratrane formation. An intact B–H bond was observed even for the tris analogue [$PtMe_3${κ^3-*S,S',S''*-$HB(mt^{Me})_3$}], which remained consistently robust at comparatively high temperatures.

Using the precursor [$PtCl_2(PPh_3)_2$] that first led to platinaboratrane formation with the $HB(mt^{Me})_3$ system, a similar methodology was investigated with $[H_2B(mt^{Me})_2]^-$.[174] However, the only product that was isolated in appreciable quantities was the previously reported platinaboratrane complex, [PtH{κ^4-*B,S,S',S''*-$B(mt^{Me})_3$}(PPh_3)]Cl.[174,175]

Given the well documented B–N cleavage of poly(azolyl)borate ligands and facile nucleophilic substitution of moieties on the boron (particularly in mixed scorpionate ligand synthesis), the transfer of a methimazolyl unit from one boron to another was presumed for the formation of [PtH{κ^4-*B,S,S',S''*-B(mt^{Me})$_3$}(PPh_3)]Cl. Other platinum precursors attempted with K[$H_2B(mt^{Me})_2$] include [PtCl(η^3-C_3H_4R-2)]$_n$ (R = H, n = 4; R = Me, n = 2), [$PtCl_2(PEt_3)_2$] and [$PtCl_2(NCR')_2$] (R' = Me, Ph). A mixture resulted in all cases and evaded purification, despite spectroscopic evidence for metallaboratrane formation.

Group 11

The coordination chemistry of $Bm^{R'}$ with coinage metals has predominately concerned copper and silver, with few examples involving gold.

During investigations into the coordination of Li[$HB(mt^{Me})_3$] to coinage metals by Reglinski and Parkin, the copper and silver bis-variants [M(PPh_3){$HPhB(mt^{Me})_2$}] were identified through crystallography as side products produced from trace amounts of [$HPhB(mt^{Me})_2$].[177] These complexes featured trigonal planar geometry about the metal and κ^3-*H,S,S'* bonding of the ligand.

The attempted synthesis of [$Bu_4N]_2[WS_4Cu_4\{H_2B(mt^{Me})_2Cl_2\}$] from sequential reaction of CuCl, [$Bu_4N]_2[WS_4]$ and Na[$H_2B(mt^{Me})_2$] unexpectedly afforded trinuclear **L1.143** (Figure 1.21), which was the first Bm^{Me} complex with a nuclearity greater than two. A rational synthesis of this complex has yet to emerge since direct combination of CuCl and Na[$H_2B(mt^{Me})_2$] was reported to provide polymeric material. The molecular structure of this trinuclear cluster reveals a highly unsymmetrical complex. The Cu_3 triangle features a direct Cu–Cu bond, and two longer interactions between the copper centres (2.8641(11) for Cu–Cu *cf.* 3.1498(11) and 3.5388(15) Å). With the omission of direct Cu···Cu bonds, the geometry around each Cu is distorted trigonal planar secured by Cu···H interaction from a nearby BH_2 moiety.

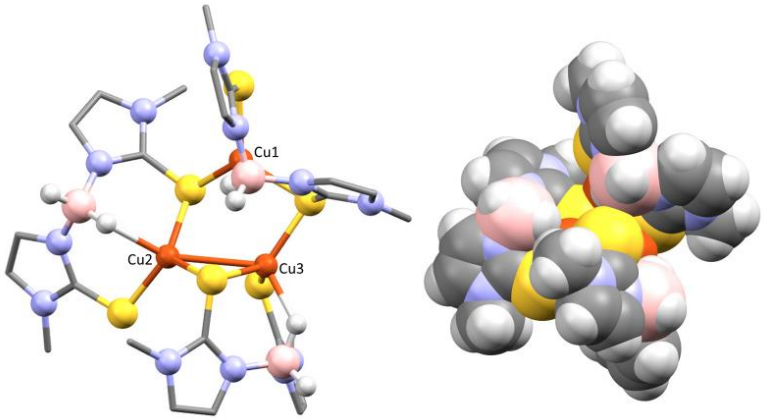

Figure 1.21: Molecular structure of trinuclear **L1.143** complex.

The crystallographic study of the three coordinate gold complex **L1.145** (Scheme 1.34) was initially reported by Fackler and co-workers (synthesised from $[Au(NO_3)(PPh_3)]$) and complete characterisation later obtained by Hill by reaction of $Na[H_2B(mt^{Me})_2]$ with $[AuCl(PPh_3)]$.[155,178] The crystal study revealed a distorted trigonal environment about the gold, consistent with the geometry of the silver analogue **L1.144** reported by Beheshti and Clegg. Both complexes are trigonal planar geometry with markedly different M–S distances between the two S donors in each complex (Ag: 2.4779(13) *cf.* 2.5398(12) Å; Au: 2.3511(8) *cf.* 2.8155(12) Å).[179]

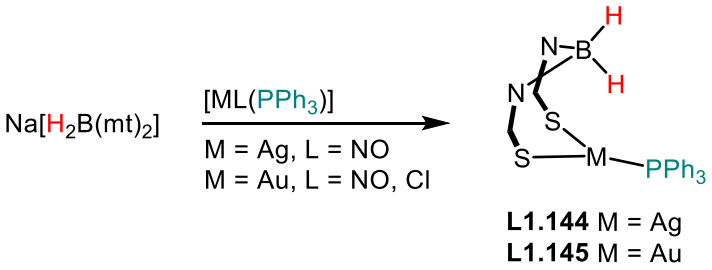

Scheme 1.34: Examples of silver and gold $Bm^{R'}$ complexes.

The reactivity of complex **L1.145** with molybdenum and tungsten precursors was discussed under Group 6, specifically, in the formation of diheterotrimetallic $[Mo_2Au\{\mu\text{-}H_2B(mt^{Me})_2\}(CO)_7(PPh_3)]$ **L1.102** and triheterometallic $[MoWAu\{\mu\text{-}H_2B(mt^{Me})_2\}(CO)_7(PPh_3)]$ **L1.103** complexes.[155] In contrast to complex **L1.145** of κ^2-*S,S'* coordination, the triethylphosphine analogue **L1.146** synthesised from $[AuBr(PEt_3)]$ and $Na[H_2B(mt^{Me})_2]$ has the ligand adopting monodentate coordination through sulfur (κ^1-*S*), a potential reflection of the greater electron donating properties of PEt_3 compared to PPh_3.[126] Monodentate coordination is generally rare for the strongly

chelating $[H_2B(mt^{Me})_2]^-$ and $[HB(mt^{Me})_3]^-$ ligands. Notwithstanding the expected preference for chelation, the related $Tm^{R'}$ species $[Au(PEt_3)\{PhB(mt^{Me})_3\}]$ likewise coordinates through a single sulfur donor.[177] This reflects the preference of gold(I) complexes to adopt a linear geometry at gold in the presence of other donors in multidentate ligands that are available for coordination.

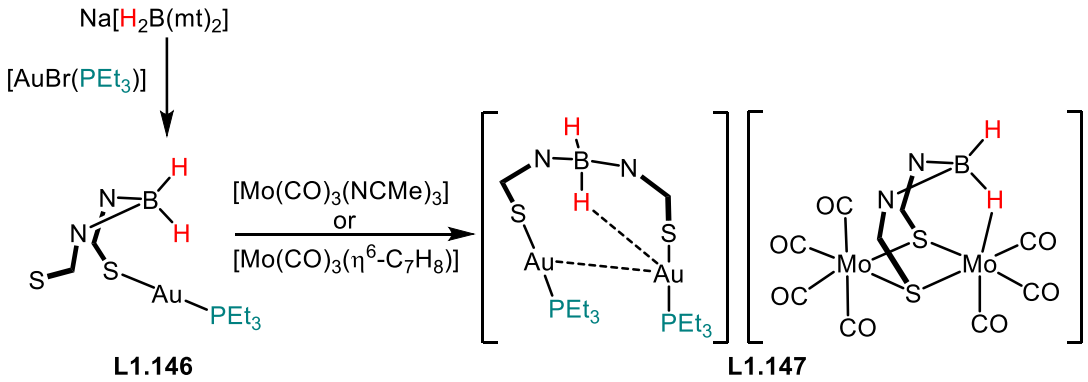

Scheme 1.35: Synthesis of bimetallic salt **L1.147**.

Whilst the complexes $[MoMAu\{\mu\text{-}H_2B(mt^{Me})_2\}(CO)_7(PPh_3)]$ (M = Mo **L1.102**, W **L1.103**) were generated from coordination of **L1.145** (Group 6, Scheme 1.23), reaction of triethylphosphine analogue **L1.146** with $[Mo(CO)_3(NCMe)_3]$ or $[Mo(CO)_3(\eta^6\text{-}C_7H_8)]$ produced the bimetallic salt **L1.147** (Scheme 1.35). A notable feature in the molecular structure of **L1.147** is the two distinct coordination modes for the $[H_2B(mt^{Me})_2]^-$ ligands, which bridge the two gold centres in the cation and between two molybdenum centres in the anion (Figure 1.22).

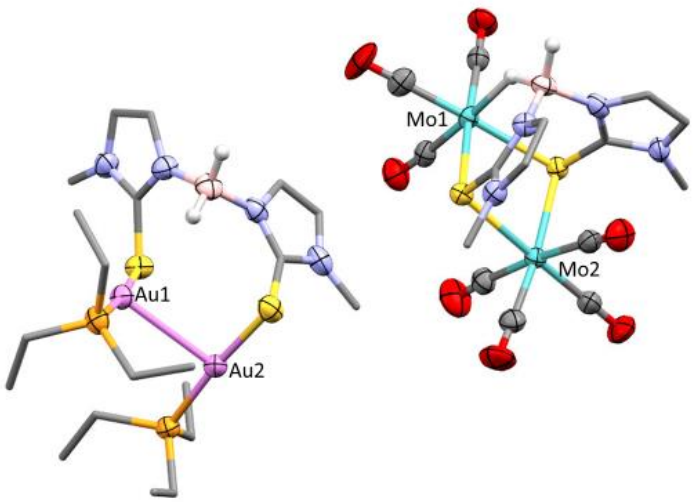

Figure 1.22: Crystal structure of $[Au_2\{\mu^2\text{-}H_2B(mt^{Me})_2\}(PEt_3)_2][Mo_2\{\mu^2\text{-}H_2B(mt^{Me})_2\}(CO)_7]$ **L1.147**.

Group 12

Coordination to zinc has been extensively studied, driven by the potential application to enzyme modelling. Formation of zinc complexes include reaction of $Li[H_2B(mt)_2]_2$ with $Tl(O_2CMe)$ and subsequent metathesis with ZnI_2 or $ZnMe_2$, to yield **L1.148** and **L1.149** respectively (Scheme 1.36).[112] Direct reaction of $Li[H_2B(mt^{Mes})_2]_2$ with $Zn(NO_3)_2$ affords nitrate stabilised complex **L1.150**. The molecular structures of monomeric complexes **L1.148**–**L1.150** show coordination by two sulfur donors to the zinc centre, which is further supported by a B–H–Zn interaction (κ^3-*H,S,S'* coordination).[105,112]

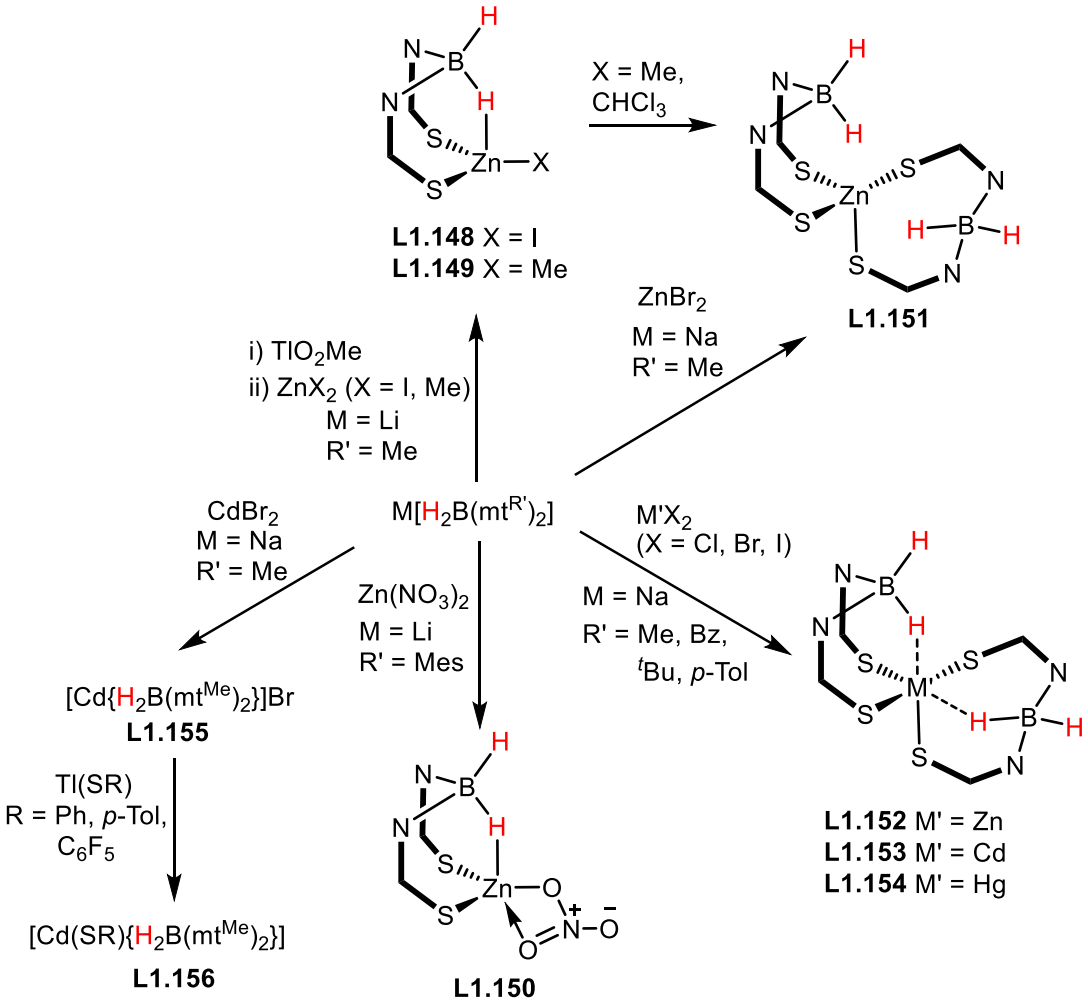

Scheme 1.36: Schematic summary of $Na[H_2B(mt^{R'})_2]$ reactivity with Group 12 precursors.

Parkin and co-workers reported the formation of homoleptic **L1.151** from the redistribution of **L1.149** in $CHCl_3$. In contrast to the heteroleptic $[Zn(X)\{\kappa^3\text{-}H,S,S'\text{-}H_2B(mt^{Mes})_2\}]$ complexes **L1.148**–**L1.150**, the homoleptic complex **L1.151** features a tetrahedral $[ZnS_4]$ core where B–H···Zn interactions are not present.[112]

An alternative route to **L1.151** was reported in 2003 by Rabinovich and co-workers that involves the direct reaction of $ZnBr_2$ with $Na[H_2B(mt^{Me})_2]$ (1:2 ratio).[113] This general method was applied to all members of the triad (zinc, cadmium and mercury). A combination of $M'X_2$ with the appropriate $Na[H_2B(mt^{R'})_2]$ ligand gives complexes of the form $[M'\{\kappa^3\text{-}H,S,S'\text{-}B(mt^{R'})_2\}_2]$ (where M' = Zn **L1.152**, Cd **L1.153**, Hg **L1.154**; R' = Me, Bz, ^{t}Bu, *p*-Tol).[113] These were the first examples of homoleptic $Bm^{R'}$ cadmium and mercury complexes. Crystallographic studies of $[Cd\{\kappa^3\text{-}H,S,S'\text{-}H_2B(mt^{Me})_2\}_2]$ and $[M'\{\kappa^3\text{-}H,S,S'\text{-}H_2B(mt^{tBu})_2\}_2]$ (M' = Zn, Cd, Hg) reveal a distorted tetrahedral $[M'S_4]$ core with weak B–H···M' interactions.

In the work of Rabinovich and co-workers, a series of cadmium(II) thiolate complexes $[Cd(SR)\{H_2B(mt^{Me})_2\}]$ (R = Ph, *p*-Tol, C_6F_5) **L1.156** was readily prepared from metathesis of $[CdBr\{H_2B(mt^{Me})_2\}]$ with Tl(SR) (Scheme 1.36).[180] The cadmium precursor complex **L1.155** was obtained in almost quantitative yield (95%), whereas attempts to isolate the chlorido or iodo variants resulted in homoleptic **L1.153**. The molecular structure of $[Cd(\mu\text{-}S\text{-}p\text{-}C_6H_4Me)\{H_2B(mt^{Me})_2\}]_2$ shows dimeric thiolato-bridged cadmium centres, $\kappa^3\text{-}H,S,S'$ coordinated borate units, and provides the first example of a five coordinate $[CdS_4H]$ complex.[180] Unlike the more sterically demanding mononuclear $Tm^{R'}$ complexes, $[Cd(SPh)\{HB(mt^{p\text{-}Tol})_3\}]$ and $[Cd(SC_6F_5)\{HB(mt^{tBu})_3\}]$, the $Bm^{R'}$ analogues are more prone to dinucleation.[181]

1.3.4.3 F-Block Chemistry

There are no examples of $Tm^{R'}$ and $Bm^{R'}$ lanthanide complexes to date. In the actinide series, examples are limited to uranium. The reaction of $[UI_3(THF)_4]$ with $M[HRB(mt^{Me})_2]$ (M = Na, R = H; M = Li, R = Ph) yielded uranium(III) complexes $[U(THF)_3\{\kappa^3\text{-}H,S,S'\text{-}H(R)B(mt^{Me})_2\}_2][BPh_4]$.[182] These complexes are formally nine-coordinate and adopt a distorted trigonal prismatic geometry, as established by crystallographic studies (Figure 1.23). The THF ligands are labile and readily displaced by other coordinating solvents such as acetonitrile and pyridine. Similar to homoleptic complexes of first row transition metal complexes, each $[HRB(mt^{Me})_2]^-$ moiety coordinates through the two thione donors and a B–H···U interaction resulting in two six membered rings and one eight membered ring of 'boatlike' configuration. Coordination of $Tm^{R'}$ and $Bm^{R'}$ ligands to other elements within the f-block presents as a potential future avenue.

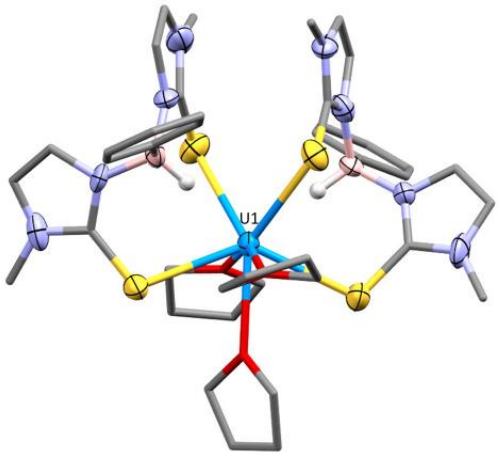

Figure 1.23: Crystal structure of $[U(THF)_3\{\kappa^3\text{-}H,S,S'\text{-}HPhB(mt^{Me})_2\}_2]^+$.

1.3.5 Conclusion

The last two decades has seen rapid advances in the field of $Tm^{R'}$ and $Bm^{R'}$ coordination chemistry since the introduction of the ligands by Reglinski and Parkin. Of the total 506 entries in the CCDC of $Tm^{R'}$ and $Bm^{R'}$ complexes combined, 102 entries (20%) were of the latter. The scope of the $Bm^{R'}$ field, although much less explored than that of $Tm^{R'}$, encompasses complexes primarily from the d-block and further examples with the remaining blocks of the periodic table. Coordination chemistry to ruthenium has been most studied in the d-block, Group 13 elements in the p-block, and there are limited examples in the s and f-blocks; with the latter restricted to only uranium.

Through the work of Santos, the $Tm^{R'}$ and $Bm^{R'}$ ligands are illustrated as fundamental building blocks of Re and Tc complexes for use in radiopharmacology. Structures of the first-row (bio-available) transition metals were investigated as models for the metallic core within metalloenzymes. The impressive coverage of the periodic table for $Bm^{R'}$ complexes could be in part, attributed to the flexibility of the ligand in accessing a variety of coordination modes. Less sterically encumbered than their $Tm^{R'}$ counterparts and lacking the possibility of κ^3-*S,S',S''* coordination, the $Bm^{R'}$ complexes are predisposed toward stabilisation by κ^3-*H,S,S'* bonding, although many structures involve κ^2-*S,S'* coordination. Coordination modes κ^1-*S* and κ^3-*B,S,S'* (M→B) are comparatively rarer.

Although there remain gaps to fill in the basic coordination chemistry of $Tm^{R'}$ and $Bm^{R'}$ systems, it is envisaged that the research will take two directions depending on whether the B–H group remains non-reactive or participates in subsequent chemistry. The most apparent non-innocence of the B–H group is the hemilability of the B–H–M interactions. Although such an interaction is widely encountered, the factors that dictate hemilability are by no means apparent at this stage.

A second point of reactivity, only rarely encountered so far, includes the direct participation of the B–H bond in reactions, e.g., Owen's alkylidene hydroboration and Hill's thiocarbonyl phosphaboration. The proximity of a pendant borohydride group to a substrate bound to a Lewis acidic metal may provide an ideal stage for substrate modification.

Furthermore, the relationship between M{κ^3-*H,S,S'*-$H_2B(mt)_2$} and the metallaboratrane tautomer H–M{κ^3-*B,S,S'*-$HB(mt)_2$} raises the possibility of hydrogen shuttling between boron (whereupon it is hydridic) and a transition metal (characteristically protic), in a hydrogen umpolung. These and no doubt many other directions yet to emerge suggest that the $Bm^{R'}$ class will for some time remain intriguing ligands for further study.

1.4 Summary

The comprehensive discussion presented in this Chapter serves to emphasise the reactivity of complexes with multidentate ligands featuring electropositive (B, Al, Si) donors, which are underexplored compared to those of more electronegative elements. Significant differences are expected for electropositive elements due to the (reverse) polarisation of the $E^{\delta+}$–$H^{\delta-}$ bond.

Extensive reactivity is exhibited by the $Bm^{R'}$ ligand, coordinating to elements across the periodic table from main group, late transition metals, actinide and even to early transition metals. Rapid advancement of the field is owing to the versatility of the $Bm^{R'}$ ligand in adopting various coordination modes (κ^1-*S*, κ^2-*S,S'*, κ^3-*H,S,S'*, κ^3-*B,S,S'*) in both mononuclear and cluster complexes. Although the κ^3-*H,S,S'* mode is commonly observed, making up 48% of structurally reported $Bm^{R'}$ complexes, little is known about the nature of the B–H–M interaction. Thus, the work in Chapter 2 investigates the effect of *trans* ligand variation on the B–H–M interaction. The metallaboratrane mode of

coordination κ^3-*B,S,S'* (M→B) is rare for $Bm^{R'}$, with only one example in literature prior to the work in this thesis. Further examples of metallaboratrane complexes buttressed by two methimazolyl units are introduced in Chapter 3, followed by studies of their reactivity.

A recurring theme of the boron pincer and scorpionate systems is hydrogen shuttling between the boron and metal. The electronics at boron also flexibly adopt σ-donating (boryl) or σ-accepting (borane) character depending on the ligand scaffold. As the heavier analogue of boron, aluminium-based ligands and complexes are relatively less studied. The highly electropositive nature of aluminium compared to boron engenders the possibility of new or enhanced reactivity as well as expected parallels to boron chemistry. The synthesis of aluminium-based ligands and subsequent coordination studies are explored in Chapter 4.

Inclusion of silicon within a multidentate ligand scaffold offers properties such as flexible coordination (*mer*/*fac*) and strong *trans* influence. The formation of Si–H···M type interactions are frequently encountered, which can mask potential reactivity. Flexible PSiP scaffolds have been well studied while those of N-heterocyclic silanes have received little attention. The stabilisation of electropositive silicon by π-donating nitrogens might impart different reactivity than the PSiP scaffolds. Coordination and reactivity studies of N-heterocyclic silanes are detailed in Chapter 5.

As the lighter analogue of silicon, carbenes are recognised for their strong electron donating properties as support ligands in catalytic systems. Numerous preparative routes to N-heterocyclic carbenes have been reported and include transfer from silver agents, transmetallation, deprotonation by external or internal base and oxidative addition. N-heterocyclic carbene formation *via* C–H activation is beneficial as it avoids the handling of reactive free carbene species. However, there are relatively few examples with a dihydroperimidine based framework and the mechanism behind C–H activation is not well understood. These areas will be addressed in the Appendix Chapter.

1.5 References

(1) Roy, D.; Uozumi, Y. *Adv. Synth. Catal.* **2018**, *360*, 602.
(2) Jeffrey, J. C.; Rauchfuss, T. B. *Inorg. Chem.* **1979**, *18*, 2658.
(3) *The Chemistry of Pincer Compounds*; Morales-Morales, D.; Jensen, C. G. M., Eds.; Elsevier Science, 2011.
(4) *Pincer Compounds Chemistry and Applications*; Morales-Morales, D., Ed.; Elsevier Science, 2018.
(5) Valdés, H.; Garcia-Eleno, M. A.; Canseco-Gonzalez, D.; Morales-Morales, D. *ChemCatChem* **2018**, *10*, 3136.
(6) Choi, J.; MacArthur, A. H. R.; Brookhart, M.; Goldman, A. S. *Chem. Rev.* **2011**, *111*, 1761.
(7) Kumar, A.; Bhatti, T. M.; Goldman, A. S. *Chem. Rev.* **2017**, *117*, 12357.
(8) Gunanathan, C.; Milstein, D. *Chem. Rev.* **2014**, *114*, 12024.
(9) Selander, N.; Szabo, K. J. *Chem. Rev.* **2011**, *111*, 2048.
(10) Benito-Garagorri, D.; Kirchner, K. *Acc. Chem. Res.* **2008**, *41*, 201.
(11) Valdés, H.; Gonzalez-Sebastian, L.; Morales-Morales, D. *J. Organomet. Chem.* **2017**, *845*, 229.
(12) Peris, E.; Crabtree, R. H. *Chem. Soc. Rev.* **2018**, *47*, 1959.
(13) Lawrence, M. A. W.; Green, K.-A.; Nelson, P. N.; Lorraine, S. C. *Polyhedron* **2018**, *143*, 11.
(14) Balakrishna, M. S. *Polyhedron* **2018**, *143*, 2.
(15) Albrecht, M.; van Koten, G. *Angew. Chem. Int. Ed.* **2001**, *40*, 3750.
(16) van der Boom, M. E.; Milstein, D. *Chem. Rev.* **2003**, *103*, 1759.
(17) Pugh, D.; Danopoulos, A. A. *Coord. Chem. Rev.* **2007**, *251*, 610.
(18) Trofimenko, S. *Chem. Rev.* **1993**, *93*, 943.
(19) Spicer, M. D.; Reglinski, J. *Eur. J. Inorg. Chem.* **2009**, 1553.
(20) Owen, G. R. *Chem. Soc. Rev.* **2012**, *41*, 3535.
(21) Moulton, C. J.; Shaw, B. L. *J. Chem. Soc., Dalton Trans.* **1976**, 1020.
(22) van Koten, G.; Timmer, K.; Noltes, J. G.; Spek, A. L. *J. Chem. Soc., Chem. Commun.* **1978**, 250.
(23) Elacqua, E.; Lye, D. S.; Weck, M. *Acc. Chem. Res.* **2014**, *47*, 2405.
(24) Serrano-Becerra, J. M.; Morales-Morales, D. *Curr. Org. Synth.* **2009**, *6*, 169.
(25) Adams, J. J.; Arulsamy, N.; Roddick, D. M. *Organometallics* **2011**, *30*, 697.
(26) Andrew, R. E.; González-Sebastián, L.; Chaplin, A. B. *Dalton Trans.* **2016**, *45*, 1299.
(27) Storey, C. M.; Cook, H. P.; Chaplin, A. B. In *Pincer Compounds*; Morales-Morales, D., Ed.; Elsevier: 2018, p 173.
(28) Asay, M. In *Pincer Compounds*; Morales-Morales, D., Ed.; Elsevier: 2018, p 431.
(29) Denny, J. A.; Lang, G. M.; Hollis, T. K. In *Pincer Compounds*; Morales-Morales, D., Ed.; Elsevier: 2018, p 251.
(30) Tulloch, A. A. D.; Danopoulos, A. A.; Tizzard, G. J.; Coles, S. J.; Hursthouse, M. B.; Hay-Motherwell, R. S.; Motherwell, W. B. *Chem. Commun.* **2001**, 1270.
(31) Peris, E.; Loch, J. A.; Mata, J.; Crabtree, R. H. *Chem. Commun.* **2001**, 201.
(32) Andrew, R. E.; Ferdani, D. W.; Ohlin, C. A.; Chaplin, A. B. *Organometallics* **2015**, *34*, 913.
(33) Watarai, N.; Kawasaki, H.; Azumaya, I.; Yamasaki, R.; Saito, S. *Heterocycles* **2009**, *79*, 531.
(34) Miecznikowski, J. R.; Gründemann, S.; Albrecht, M.; Mégret, C.; Clot, E.; Faller, J. W.; Eisenstein, O.; Crabtree, R. H. *Dalton Trans.* **2003**, 831.
(35) Schultz, K. M.; Goldberg, K. I.; Gusev, D. G.; Heinekey, D. M. *Organometallics* **2011**, *30*, 1429.
(36) Lee, H. M.; Zeng, J. Y.; Hu, C.-H.; Lee, M.-T. *Inorg. Chem.* **2004**, *43*, 6822.
(37) Chiu, P. L.; Lee, H. M. *Organometallics* **2005**, *24*, 1692.
(38) Zeng, J. Y.; Hsieh, M.-H.; Lee, H. M. *J. Organomet. Chem.* **2005**, *690*, 5662.
(39) Hahn, F. E.; Jahnke, M. C.; Pape, T. *Organometallics* **2006**, *25*, 5927.
(40) Steinke, T.; Shaw, B. K.; Jong, H.; Patrick, B. O.; Fryzuk, M. D. *Organometallics* **2009**, *28*, 2830.
(41) Shaw, B. K.; Patrick, B. O.; Fryzuk, M. D. *Organometallics* **2012**, *31*, 783.

(42) Pan, B.; Pierre, S.; Bezpalko, M. W.; Napoline, J. W.; Foxman, B. M.; Thomas, C. M. *Organometallics* **2013**, *32*, 704.
(43) Willms, H.; Frank, W.; Ganter, C. *Chem. Eur. J.* **2008**, *14*, 2719.
(44) Fuku-en, S.-i.; Yamamoto, J.; Kojima, S.; Yamamoto, Y. *Chem. Lett.* **2014**, *43*, 468.
(45) Valyaev, D. A.; Filippov, O. A.; Lugan, N.; Lavigne, G.; Ustynyuk, N. A. *Angew. Chem. Int. Ed.* **2015**, *54*, 6315.
(46) Plikhta, A.; Poethig, A.; Herdtweck, E.; Rieger, B. *Inorg. Chem.* **2015**, *54*, 9517.
(47) Matoba, K.; Eizawa, A.; Nishimura, S.; Arashiba, K.; Nakajima, K.; Nishibayashi, Y. *Synthesis* **2018**, *50*, 1015.
(48) Monot, J.; Merceron-Saffon, N.; Martin-Vaca, B.; Bourissou, D. *J. Organomet. Chem.* **2017**, *829*, 37.
(49) Oulie, P.; Nebra, N.; Ladeira, S.; Martin-Vaca, B.; Bourissou, D. *Organometallics* **2011**, *30*, 6416.
(50) Nebra, N.; Lisena, J.; Saffon, N.; Maron, L.; Martin-Vaca, B.; Bourissou, D. *Dalton Trans.* **2011**, *40*, 8912.
(51) Lisena, J.; Monot, J.; Mallet-Ladeira, S.; Martin-Vaca, B.; Bourissou, D. *Organometallics* **2013**, *32*, 4301.
(52) Espinosa-Jalapa, N. A.; Ke, D.; Nebra, N.; Le Goanvic, L.; Mallet-Ladeira, S.; Monot, J.; Martin-Vaca, B.; Bourissou, D. *ACS Catal.* **2014**, *4*, 3605.
(53) Nebra, N.; Monot, J.; Shaw, R.; Martin-Vaca, B.; Bourissou, D. *ACS Catal.* **2013**, *3*, 2930.
(54) Brunel, P.; Monot, J.; Kefalidis, C. E.; Maron, L.; Martin-Vaca, B.; Bourissou, D. *ACS Catal.* **2017**, *7*, 2652.
(55) Monot, J.; Brunel, P.; Kefalidis, C. E.; Espinosa-Jalapa, N. A.; Maron, L.; Martin-Vaca, B.; Bourissou, D. *Chem. Sci.* **2016**, *7*, 2179.
(56) Nicolas, E.; Martin-Vaca, B.; Mezailles, N.; Bourissou, D.; Maron, L. *Eur. J. Inorg. Chem.* **2013**, *2013*, 4068.
(57) Eizawa, A.; Arashiba, K.; Tanaka, H.; Kuriyama, S.; Matsuo, Y.; Nakajima, K.; Yoshizawa, K.; Nishibayashi, Y. *Nat. Commun.* **2017**, *8*, 14874.
(58) Arashiba, K.; Miyake, Y.; Nishibayashi, Y. *Nat. Chem.* **2010**, *3*, 120.
(59) Chalkley, M. J.; Del Castillo, T. J.; Matson, B. D.; Roddy, J. P.; Peters, J. C. *ACS Cent. Sci.* **2017**, *3*, 217.
(60) Crossley, I. R.; Hill, A. F.; Willis, A. C. *Organometallics* **2005**, *24*, 1062.
(61) Bontemps, S.; Gornitzka, H.; Bouhadir, G.; Miqueu, K.; Bourissou, D. *Angew. Chem. Int. Ed.* **2006**, *45*, 1611.
(62) Spokoyny, A. M.; Reuter, M. G.; Stern, C. L.; Ratner, M. A.; Seideman, T.; Mirkin, C. A. *J. Am. Chem. Soc.* **2009**, *131*, 9482.
(63) Segawa, Y.; Yamashita, M.; Nozaki, K. *J. Am. Chem. Soc.* **2009**, *131*, 9201.
(64) Segawa, Y.; Yamashita, M.; Nozaki, K. *Organometallics* **2009**, *28*, 6234.
(65) Tanoue, K.; Yamashita, M. *Organometallics* **2015**, *34*, 4011.
(66) Hasegawa, M.; Segawa, Y.; Yamashita, M.; Nozaki, K. *Angew. Chem. Int. Ed.* **2012**, *51*, 6956.
(67) Masuda, Y.; Hasegawa, M.; Yamashita, M.; Nozaki, K.; Ishida, N.; Murakami, M. *J. Am. Chem. Soc.* **2013**, *135*, 7142.
(68) Hill, A. F.; Lee, S. B.; Park, J.; Shang, R.; Willis, A. C. *Organometallics* **2010**, *29*, 5661.
(69) Miyada, T.; Yamashita, M. *Organometallics* **2013**, *32*, 5281.
(70) Hill, A. F.; McQueen, C. M. A. *Organometallics* **2014**, *33*, 1977.
(71) Miyada, T.; Kwan, E. H.; Yamashita, M. *Organometallics* **2014**, *33*, 6760.
(72) McQueen, C. M. A.; Hill, A. F.; Sharma, M.; Singh, S. K.; Ward, J. S.; Willis, A. C.; Young, R. D. *Polyhedron* **2016**, *120*, 185.
(73) Ogawa, H.; Yamashita, M. *Dalton Trans.* **2013**, *42*, 625.
(74) Curado, N.; Maya, C.; Lopez-Serrano, J.; Rodriguez, A. *Chem. Commun.* **2014**, *50*, 15718.
(75) Lin, T.-P.; Peters, J. C. *J. Am. Chem. Soc.* **2014**, *136*, 13672.
(76) Rios, P.; Rodriguez, A.; Lopez-Serrano, J. *ACS Catal.* **2016**, *6*, 5715.
(77) Rios, P.; Curado, N.; Lopez-Serrano, J.; Rodriguez, A. *Chem. Commun.* **2016**, *52*, 2114.

(78) Lin, T.-P.; Peters, J. C. *J. Am. Chem. Soc.* **2013**, *135*, 15310.
(79) Dang, L.; Lin, Z.; Marder, T. B. *Chem. Commun.* **2009**, 3987.
(80) Zhu, J.; Lin, Z.; Marder, T. B. *Inorg. Chem.* **2005**, *44*, 9384.
(81) Simon, M.; Breher, F. *Dalton Trans.* **2017**, *46*, 7976.
(82) Hill, A. F.; Neumann, H.; Wagler, J. *Organometallics* **2010**, *29*, 1026.
(83) Azpeitia, S.; Fernandez, B.; Garralda, M. A.; Huertos, M. A. *Eur. J. Inorg. Chem.* **2016**, *2016*, 2891.
(84) Stradiotto, M.; Fujdala, K. L.; Tilley, T. D. *Chem. Commun.* **2001**, 1200.
(85) Sangtrirutnugul, P.; Stradiotto, M.; Tilley, T. D. *Organometallics* **2006**, *25*, 1607.
(86) Sangtrirutnugul, P.; Tilley, T. D. *Organometallics* **2007**, *26*, 5557.
(87) Sangtrirutnugul, P.; Tilley, T. D. *Organometallics* **2008**, *27*, 2223.
(88) Chen, W.; Shimada, S.; Tanaka, M.; Kobayashi, Y.; Saigo, K. *J. Am. Chem. Soc.* **2004**, *126*, 8072.
(89) Montiel-Palma, V.; Muñoz-Hernández, M. A.; Cuevas-Chávez, C. A.; Vendier, L.; Grellier, M.; Sabo-Etienne, S. *Inorg. Chem.* **2013**, *52*, 9798.
(90) Begum, R.; Komuro, T.; Tobita, H. *Chem. Commun.* **2006**, 432.
(91) Begum, R.; Komuro, T.; Tobita, H. *Chem. Lett.* **2007**, *36*, 650.
(92) Okazaki, M.; Yamahira, N.; Gabrillo Minglana, J. J.; Komuro, T.; Ogino, H.; Tobita, H. *Organometallics* **2008**, *27*, 918.
(93) Komuro, T.; Begum, R.; Ono, R.; Tobita, H. *Dalton Trans.* **2011**, *40*, 2348.
(94) Komuro, T.; Furuyama, K.; Kitano, T.; Tobita, H. *J. Organomet. Chem.* **2014**, *751*, 686.
(95) Komuro, T.; Arai, T.; Kikuchi, K.; Tobita, H. *Organometallics* **2015**, *34*, 1211.
(96) Komuro, T.; Kitano, T.; Yamahira, N.; Ohta, K.; Okawara, S.; Mager, N.; Okazaki, M.; Tobita, H. *Organometallics* **2016**, *35*, 1209.
(97) Kitano, T.; Komuro, T.; Ono, R.; Tobita, H. *Organometallics* **2017**, *36*, 2710.
(98) Trofimenko, S. *J. Am. Chem. Soc.* **1966**, *88*, 1842.
(99) Trofimenko, S. *The Coordination Chemistry of Polypyrazolylborate Ligands*; Imperial College Press: London, 1999.
(100) Pettinari, C. *Scorpionates II: Chelating Borate Ligands*; Imperial College Press: London, 2008.
(101) Reglinski, J.; Spicer, M. D. *Curr. Bioact. Compd.* **2009**, *5*, 264.
(102) Smith, J. M. *Comments Inorg. Chem.* **2008**, *29*, 189.
(103) Rabinovich, D. *Struct. Bonding* **2006**, *120*, 143.
(104) Seebacher, J.; Shu, M.; Vahrenkamp, H. *Chem. Commun.* **2001**, 1026.
(105) Kimblin, C.; Hascall, T.; Parkin, G. *Inorg. Chem.* **1997**, *36*, 5680.
(106) Garcia, R.; Paulo, A.; Domingos, A.; Santos, I.; Ortner, K.; Alberto, R. *J. Am. Chem. Soc.* **2000**, *122*, 11240.
(107) Garcia, R.; Paulo, A.; Domingos, A.; Santos, I. *J. Organomet. Chem.* **2001**, *632*, 41.
(108) Silva, F.; Fernandes, C.; Campello, M. P. C.; Paulo, A. *Polyhedron* **2017**, *125*, 186.
(109) Trofimenko, S. *Polyhedron* **2004**, *23*, 197.
(110) Garner, M.; Reglinski, J.; Cassidy, I.; Spicer, M. D.; Kennedy, A. R. *Chem. Commun.* **1996**, 1975.
(111) Reglinski, J.; Garner, M.; Cassidy, I. D.; Slavin, P. A.; Spicer, M. D.; Armstrong, D. R. *J. Chem. Soc., Dalton Trans.* **1999**, 2119.
(112) Kimblin, C.; Bridgewater, B. M.; Hascall, T.; Parkin, G. *Dalton* **2000**, 891.
(113) Alvarez, H. M.; Tran, T. B.; Richter, M. A.; Alyounes, D. M.; Rabinovich, D.; Tanski, J. M.; Krawiec, M. *Inorg. Chem.* **2003**, *42*, 2149.
(114) Foreman, M. R. S. J.; Hill, A. F.; Tshabang, N.; White, A. J. P.; Williams, D. J. *Organometallics* **2003**, *22*, 5593.
(115) Garcia, R.; Xing, Y.-H.; Paulo, A.; Domingos, A.; Santos, I. *J. Chem. Soc., Dalton Trans.* **2002**, 4236.
(116) Pellei, M.; Lobbia, G. G.; Papini, G.; Santini, C. *Mini-Rev. Org. Chem.* **2010**, *7*, 173.
(117) Ahmad, N.; Alam, M.; Kumar, P.; Hashmi, A. A.; Wahab, R. *Asian J. Chem.* **2013**, *25*, 10386.

(118) Imran, M.; Neumann, B.; Stammler, H.-G.; Monkowius, U.; Ertl, M.; Mitzel, N. W. *Dalton Trans.* **2014**, *43*, 1267.
(119) Maria, L.; Moura, C.; Paulo, A.; Santos, I. C.; Santos, I. *J. Organomet. Chem.* **2006**, *691*, 4773.
(120) Joshi, R.; Ahmad, N.; Ahmad Khan, S.; Adil Hashmi, A. *J. Coord. Chem.* **2010**, *63*, 906.
(121) Imran, M.; Mix, A.; Neumann, B.; Stammler, H.-G.; Monkowius, U.; Bleckenwegner, P.; Mitzel, N. W. *Dalton Trans.* **2014**, *43*, 14737.
(122) Wang, Y.-L.; Cao, R.; Bi, W.-H. *Polyhedron* **2005**, *24*, 585.
(123) Dyson, G.; Hamilton, A.; Mitchell, B.; Owen, G. R. *Dalton Trans.* **2009**, 6120.
(124) Rajasekharan-Nair, R.; Moore, D.; Chalmers, K.; Wallace, D.; Diamond, L. M.; Darby, L.; Armstrong, D. R.; Reglinski, J.; Spicer, M. D. *Chem. Eur. J.* **2013**, *19*, 2487.
(125) Garcia, R.; Domingos, A.; Paulo, A.; Santos, I.; Alberto, R. *Inorg. Chem.* **2002**, *41*, 2422.
(126) Hill, A. F.; Smith, M. K.; Tshabang, N.; Willis, A. C. *Organometallics* **2010**, *29*, 473.
(127) Yurkerwich, K.; Coleman, F.; Parkin, G. *Dalton Trans.* **2010**, *39*, 6939.
(128) Kosky, C. A.; Ganis, P.; Avitabile, G. *Acta Crystallogr., Sect. B* **1971**, *27*, 1859.
(129) Cotton, F. A.; Jeremic, M.; Shaver, A. *Inorg. Chim. Acta* **1972**, *6*, 543.
(130) Brookhart, M.; Green, M. L. H. *J. Organomet. Chem.* **1983**, *250*, 395.
(131) Brookhart, M.; Green, M. L. H.; Wong, L. L. *Prog. Inorg. Chem.* **1988**, *36*, 1.
(132) Crossley, I. R.; Hill, A. F.; Humphrey, E. R.; Smith, M. K. *Organometallics* **2006**, *25*, 2242.
(133) Hill, A. F.; Smith, M. K.; Wagler, J. *Organometallics* **2008**, *27*, 2137.
(134) Garcia, R.; Paulo, A.; Domingos, A.; Santos, I.; Pietzsch, H. J. *Synth. React. Inorg., Met.-Org., Nano-Met. Chem.* **2005**, *35*, 35.
(135) Abernethy, R. J.; Foreman, M. R. S. J.; Hill, A. F.; Tshabang, N.; Willis, A. C.; Young, R. D. *Organometallics* **2008**, *27*, 4455.
(136) Kuan, S. L.; Leong, W. K.; Goh, L. Y.; Webster, R. D. *J. Organomet. Chem.* **2006**, *691*, 907.
(137) Saito, T.; Kuwata, S.; Ikariya, T. *Chem. Lett.* **2006**, *35*, 1224.
(138) Kuan, S. L.; Leong, W. K.; Goh, L. Y.; Webster, R. D. *Organometallics* **2005**, *24*, 4639.
(139) Graham, L. A.; Fout, A. R.; Kuehne, K. R.; White, J. L.; Mookherji, B.; Marks, F. M.; Yap, G. P. A.; Zakharov, L. N.; Rheingold, A. L.; Rabinovich, D. *Dalton Trans.* **2005**, 171.
(140) Reglinski, J.; Spicer, M. D. *Coord. Chem. Rev.* **2015**, *297-298*, 181.
(141) Hill, S. C.; Jones, D. S.; Rabinovich, D. *Acta Crystallogr., Sect. E: Struct. Rep. Online* **2006**, *62*, m702.
(142) Green, M. L. H.; Mountford, P.; Smout, G. J.; Speel, S. R. *Polyhedron* **1990**, *9*, 2763.
(143) Alvarez, H. M.; Gillespie, P. A.; Gause, C. D.; Rheingold, A. L.; Golen, J. A.; Rabinovich, D. *Polyhedron* **2004**, *23*, 617.
(144) Alvarez, H. M.; Tanski, J. M.; Rabinovich, D. *Polyhedron* **2004**, *23*, 395.
(145) Crossley, I. R.; Hill, A. F.; Humphrey, E. R.; Smith, M. K.; Tshabang, N.; Willis, A. C. *Chem. Commun.* **2004**, 1878.
(146) Foreman, M. R. S. J.; Hill, A. F.; Smith, M. K.; Tshabang, N. *Organometallics* **2005**, *24*, 5224.
(147) Hill, A. F.; Smith, M. K. *Chem. Commun.* **2005**, 1920.
(148) Hill, A. F.; Smith, M. K. *Dalton Trans.* **2005**, 28.
(149) Hubert-Pfalzgraf, L. G.; Riess, J. G. *Inorg. Chim. Acta* **1981**, *47*, 7.
(150) Hubert-Pfalzgraf, L. G.; Tsunoda, M. *Polyhedron* **1983**, *2*, 203.
(151) Hill, A. F.; Smith, M. K. *Organometallics* **2007**, *26*, 3900.
(152) Kablitz, H.-J.; Wilke, G. *J. Organomet. Chem.* **1973**, *51*, 241.
(153) Buccella, D.; Shultz, A.; Melnick, J. G.; Konopka, F.; Parkin, G. *Organometallics* **2006**, *25*, 5496.
(154) Kuan, S. L.; Leong, W. K.; Webster, R. D.; Goh, L. Y. *Organometallics* **2012**, *31*, 273.
(155) Cade, I. A.; Hill, A. F.; Tshabang, N.; Smith, M. K. *Organometallics* **2009**, *28*, 1143.
(156) Tate, D. P.; Knipple, W. R.; Augl, J. M. *Inorg. Chem.* **1962**, *1*, 433.
(157) Abernethy, R. J.; Hill, A. F.; Neumann, H.; Willis, A. C. *Inorg. Chim. Acta* **2005**, *358*, 1605.
(158) Hill, A. F.; Tshabang, N.; Willis, A. C. *Eur. J. Inorg. Chem.* **2007**, 3781.
(159) Santos, I.; Paulo, A.; Correia, J. D. G. *Top. Curr. Chem.* **2005**, *252*, 45.

(160) Garcia, R.; Paulo, A.; Santos, I. *Inorg. Chim. Acta* **2009**, *362*, 4315.
(161) Videira, M.; Moura, C.; Datta, A.; Paulo, A.; Santos, I. C.; Santos, I. *Inorg. Chem.* **2009**, *48*, 4251.
(162) Garcia, R.; Gano, L.; Maria, L.; Paulo, A.; Santos, I.; Spies, H. *JBIC, J. Biol. Inorg. Chem.* **2006**, *11*, 769.
(163) Wang, X.-Y.; Ma, Q.; Duan, T.; Chen, Q.; Zhang, Q.-F. *Inorg. Chim. Acta* **2012**, *384*, 281.
(164) Rajasekharan-Nair, R.; Darby, L.; Reglinski, J.; Spicer, M. D.; Kennedy, A. R. *Inorg. Chem. Commun.* **2014**, *41*, 11.
(165) Abernethy, R. J.; Hill, A. F.; Tshabang, N.; Willis, A. C.; Young, R. D. *Organometallics* **2009**, *28*, 488.
(166) Ma, Q.; Jia, A.-Q.; Chen, Q.; Shi, H.-T.; Leung, W.-H.; Zhang, Q.-F. *J. Organomet. Chem.* **2012**, *716*, 182.
(167) Foreman, M. R. S. J.; Ma, C.; Hill, A. F.; Otten, N. E.; Sharma, M.; Tshabang, N.; Ward, J. S. *Dalton Trans.* **2017**, *46*, 14957.
(168) Rudolf, G. C.; Hamilton, A.; Orpen, A. G.; Owen, G. R. *Chem. Commun.* **2009**, 553.
(169) Crossley, I. R.; Hill, A. F.; Willis, A. C. *Organometallics* **2010**, *29*, 326.
(170) Crossley, I. R.; Hill, A. F.; Willis, A. C. *Organometallics* **2007**, *26*, 3891.
(171) Fan, F.-F.; Ma, Q.; Jia, A.-Q.; Huang, X.-H.; Zhang, Q.-F. *J. Coord. Chem.* **2014**, *67*, 1309.
(172) Alvarez, H. M.; Krawiec, M.; Donovan-Merkert, B. T.; Fouzi, M.; Rabinovich, D. *Inorg. Chem.* **2001**, *40*, 5736.
(173) Maffett, L. S.; Gunter, K. L.; Kreisel, K. A.; Yap, G. P. A.; Rabinovich, D. *Polyhedron* **2007**, *26*, 4758.
(174) Crossley, I. R.; Hayes, J. *J. Organomet. Chem.* **2012**, *716*, 285.
(175) Crossley, I. R.; Hill, A. F. *Organometallics* **2004**, *23*, 5656.
(176) Crossley, I. R.; Hill, A. F.; Willis, A. C. *Organometallics* **2005**, *24*, 4889.
(177) Dodds, C. A.; Garner, M.; Reglinski, J.; Spicer, M. D. *Inorg. Chem.* **2006**, *45*, 2733.
(178) Mohamed, A. A.; Rabinovich, D.; Fackler, J. P. *Acta Crystallogr., Sect. E: Struct. Rep. Online* **2002**, *58*, m726.
(179) Beheshti, A.; Clegg, W.; Nobakht, V.; Mehr, M. P.; Russo, L. *Dalton Trans.* **2008**, 6641.
(180) Philson, L. A.; Alyounes, D. M.; Zakharov, L. N.; Rheingold, A. L.; Rabinovich, D. *Polyhedron* **2003**, *22*, 3461.
(181) Bakbak, S.; Incarvito, C. D.; Rheingold, A. L.; Rabinovich, D. *Inorg. Chem.* **2002**, *41*, 998.
(182) Maria, L.; Domingos, A.; Santos, I. *Inorg. Chem.* **2001**, *40*, 6863.

Chapter 2

Bis(methimazolyl)borate Complexes of Ruthenium

2.1 Introduction

The flexibility of the $Bm^{R'}$ and $Tm^{R'}$ ligand systems enables access to a range of coordination modes. As noted in Chapter 1, numerous structures of $HRB(mt)_2$ (R = alkyl, aryl, halide) based complexes feature κ^3-*H,S,S'* coordination. Extending the search, the κ^3-*H,S,S'* coordination mode has also been reported for frameworks with a third coordinating group present, such as in Tm and hybrid scorpionate systems, where there is competing potential for κ^3-*S,S',S''* or κ^3-*N,S,S'* coordination. Combined, this makes 72 structures (13%, of 560 total hits in the CCDC) that display κ^3-*H,S,S'* coordination. The most examples were observed with ruthenium.

The prevalence of this coordination mode may suggest thermal stability and mechanistically, potential metallaboratrane (M→B) formation in the event that the B–H–M 3c2e interaction progresses towards BH activation. These complexes are summarised in Table 2.1 with selected crystallographic and spectroscopic properties. The large variation of the complexes in Table 2.1 (i.e. different ligand sets and overall complex charge) makes meaningful comparisons of the B–H–Ru interaction difficult, compounded by imprecise crystallographic location of hydrogen atom positions.

Complex	Ru–H–B [°]	Ru···B [Å]	δ_{BHRu} [ppm]	δ_{B} [ppm]	ν_{CO} (cm^{-1})
$[Ru(Bm)_2]$ *,[1]	136	2.672	n.g	n.g	n/a
$[Ru(Bm)_2]$ [2]	151	2.660	−14.7	n.g	n/a
$[Ru(PPh_3)(Bm)_2]$ [2]	151	2.677	−14.3	n.g	n/a
$[RuH(PPh_3)_2(Bm)]$ *,[3]	137	2.778	−5.70	n.g	n/a
$[Ru(C_5Me_5)(Bm)]$ [4]	140	2.815	−7.83	n.g	n/a
$[Ru(PPh_3)(Hmt)_2(Bm)]$ +,[2]	148	2.774	−14.7	n.g	n/a
$[Ru(Bm)_2]^+$ *,[1]	144	2.757	n.g	n.g	n/a
$[Ru(C_6Me_6)(Bm)]^+$ [4]	151	2.799	−10.9	n.g	n/a
$[Ru(mt^{Ar})(PPh_3)\{HB(mt^{Ar})_3\}]$ [5]	145	2.634	−3.46	n.g	n/a
$[RuH(CO)(PPh_3)(Tm)]$ [6]	136	2.834	−3.87	−2.13	1941
$[RuI(CO)(PPh_3)\{H_2B(mt^{Ar})_2\}]$ [7]	131	2.672	n.g	−6.08	1968
$[RuBr(CO)(PPh_3)\{H_2B(mt^{Ar})_2\}]$ [7]	127	2.682	n.g	−6.51	1960
$[RuH(CO)(PPh_3)\{H_2B(mt^{ptol})_2\}]$ [7]	134	2.763	−5.37	−6.60	1934
$[RuH(CO)(PPh_3)\{H_2B(mt^{Ar})_2\}]$ [7]	132	2.759	−5.34	−6.66	1945
$[RuH(PPh_3)_2(Tm)]$ [8]	142	2.931	−3.89	1.60	n/a
$[RuH(CO)(PPh_3)(Tm)]$ *,[9]	139	2.858	−3.72	n.g	1944
$[Ru(mt)(PPh_3)(Tm)]$ [9]	126	2.637	−3.53	n.g	n/a
$[RuCl(dmso)_2(Tm)]$ [3]	141	2.817	−9.02	0.99	n/a
$[RuH(SiEt_3)(CO)(PPh_3)(Tm)]$ [10]	138	2.925	n.g	n.g	n.g
$[Ru(C_6Me_6)\{HB(mt)_2(pz)\}]^+$ [11]	128	2.834	−10.6	n.g	n/a
$[Ru(C_5Me_5)\{HB(mt)_2(pz)\}]$ [11]	141	2.910	−7.20	n.g	n/a

Table 2.1: Structural data for $Ru\{\kappa^3\text{-}H,S,S'\text{-}H_nB(mt)_{4-n}\}$ complexes. Bm = $\kappa^3\text{-}H,S,S'\text{-}H_2B(mt)_2$, Tm = $\kappa^3\text{-}H,S,S'\text{-}HB(mt)_3$, pz = pyrazolyl, Ar = N-(4-chlorophenyl)-2-mercaptoimidazolyl. *Mean value for multiple crystallographically independent metrics in the molecule(s).

Accordingly, in this chapter the synthesis of a series of complexes of the form [Ru(X)(CO)(PPh_3){κ^3-*H,S,S'*-$H_2B(mt)_2$}] (X = H, Cl, SePh, BCat, $SiCl_3$, $SiMe_3$) is described, where all considerations were kept constant with the exception of the *trans* X ligand. Aspects of this work have formed the basis of a recent publication.[10] Some of the complexes have, where indicated, been observed previously in the Hill group with however, only partial characterisation. Therefore, revised synthetic protocols were implemented to achieve complete characterisation and the collation of the series [Ru(X)(CO)(PPh_3){κ^3-*H,S,S'*-$H_2B(mt)_2$}] (X = H, Cl, SePh, BCat, $SiCl_3$, $SiMe_3$) for which perturbations on the B–H–Ru interaction by the *trans* X group could be investigated.

2.2 Bis(methimazolyl)borate Complexes of Ruthenium

2.2.1 Synthesis of [RuH(CO)(PPh_3){κ^3-*H,S,S'*-$H_2B(mt)_2$}]

Complex [RuH(CO)(PPh_3){κ^3-*H,S,S'*-$H_2B(mt)_2$}] **2.1** was synthesised from [RuHCl(CO)(PPh_3)$_3$] and Na[$H_2B(mt)_2$] *via* modification of the procedure reported by Tshabang,[12] incorporating longer reaction times and a shorter work-up (Scheme 2.1).

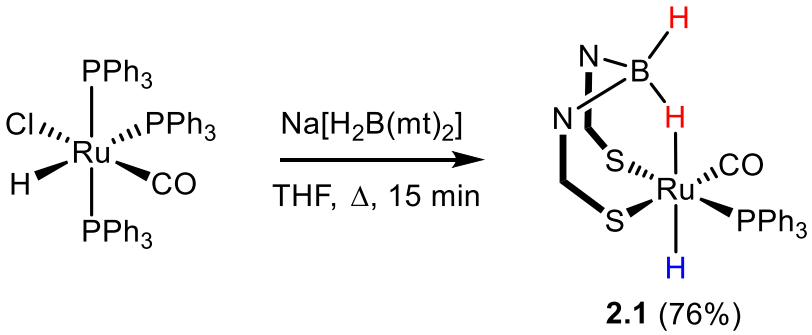

2.1 (76%)

Scheme 2.1: Synthesis of complex **2.1**.

The dichloromethane solution IR spectrum reveals stretching bands for all three hydridic environments at 2110 ν_{RuH}, 2201 ν_{BHRu}, 2399 ν_{BH} cm^{-1}, as well as a strong CO stretch at 1936 cm^{-1}.

The ^{1}H NMR spectrum exhibits two resonances in the hydride region characteristic of a formally metal bound hydride as a sharp doublet coupling to the neighbouring *cis*-phosphine (δ_H = –12.22, $^{2}J_{HP}$ = 23.1 Hz) and the B–H–Ru hydride (δ_H = –5.42), which is broadened by the quadrupolar boron nuclei (^{10}B and ^{11}B)*. The asymmetry (C_1) of the complex was represented by distinct methyl resonances at δ_H = 3.10 and 3.57, and a separate environment for each of the four olefinic protons. Owing to the quadrupolar ^{10}B and ^{11}B nuclei, a broadened signal $\delta_B \approx$ –5.52 resulted in both ^{11}B (h.h.w. = 276 Hz) and ^{11}B{^{1}H} NMR (h.h.w. = 142 Hz) spectra such that for **2.1** and many of those to follow, $^{1}J_{BH}$ was not generally resolved.

The phosphine resonance observed at δ_P = 56.7 in the ^{31}P{^{1}H} NMR spectrum was consistent with the single phosphine environment present in the molecular structure of **2.1** (Figure 2.1). The κ^3-*H,S,S'* coordinated $H_2B(mt)_2$ unit illustrated in Figure 2.1 was consistent with the spectroscopically inferred B–H–Ru interaction. Crystallographically determined hydrogen atom locations are low in precision and accuracy, particularly of those near heavy atoms. Notwithstanding this caveat, the ruthenium hydrides in **2.1** were located and refined isotropically, revealing a longer Ru1–H1 bond from the 3c2e interaction (Ru1–H1 1.86(2) Å) than the terminal ruthenium hydride (Ru1–H11 1.58(3) Å). This was attributed to the strong *trans* influence of the terminal hydride and the geometric impacts of chelation.

*Boron has two NMR active isotopes ^{10}B (I = 3) and ^{11}B (I = $^{3}/_{2}$) that are naturally abundant at 19.6% and 80.4% respectively. The resonance for coupled nuclei is expected to appear as a non-binomial, i.e., 1:1:1:1 quartet overlayed with a smaller septet. Due to the short relaxation time of both quadrupolar ^{10}B and ^{11}B nuclei, a broadened signal results where the multiplets are poorly resolved unless the boron experiences a highly symmetric electric field, e.g., $[BH_4]^-$ or are thermally decoupled. A rare counter example is provided by $[RuCl(DMSO)_2\{\kappa^3$-*H,S,S'*-$HB(mt)_3\}]^3$ where both ^{11}B and ^{10}B associated multiplets are sharp and well-resolved for the B–**H**–Ru resonance in the ^{1}H NMR spectrum.

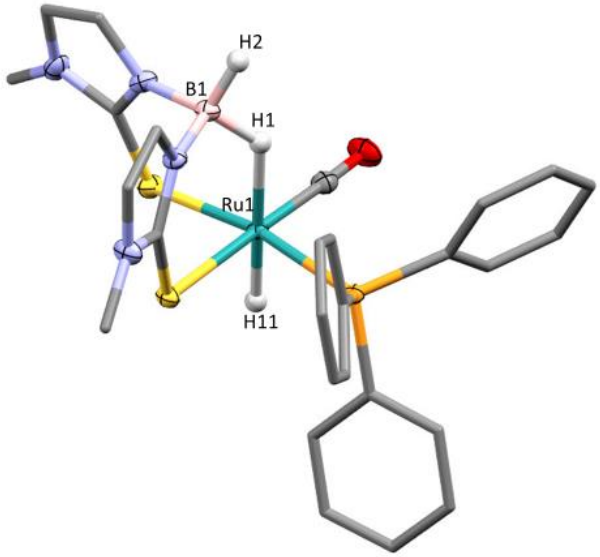

Figure 2.1: Molecular structure of [RuH(CO)(PPh_3){κ^3-*H,S,S'*-$H_2B(mt)_2$}] **2.1** (organic hydrogen atoms omitted, phenyl groups simplified, displacement ellipsoids shown at 50% probability). Selected bond lengths (Å) and angles (°): B1···Ru1 2.796(2), B1–H1 1.22(2), B1–H2 1.12(3), Ru1–H1 1.86(2), Ru1–H11 1.58(3), B1–H1–Ru1 128.6(17), H1–Ru1–H11 177.0(12).

Former members of the Hill group have briefly investigated the lack of reactivity of [RuH(CO)(PPh_3){κ^3-*H,S,S'*-$H_2B(mt)_2$}] towards bases and the *hemilability* of the B–H–Ru interaction toward neutral ligands.[12,13] Late transition metal hydrides may possess protic character, with Brønsted acidities dependent on the metal and its corresponding surrounding environment (ligand set, oxidation state and charge).[14] Treatment of complex **2.1** with $KN(SiMe_3)_2$, LiN^iPr_2 and ^{n}BuLi (in order of increasing basicity) resulted in no observed reactivity in all cases.[13] Similarly, attempts to displace the B–H–Ru interaction by exposure to an excess of PPh_3 (the synthesis of **2.1** involved liberation of PPh_3), CO (1 atm), or HC≡CR (R = H, Ph, ^{t}Bu) were unsuccessful, from which the inertness of the B–H–Ru 3c2e bond may be inferred (Scheme 2.2).[12] The apparently robust B–H–Ru interaction stands in contrast to the facile reversible cleavage of the B–H–Re interaction within Santos' [$Re(CO)_3${κ^3-*H,S,S'*-$H_2B(mt)_2$}] system, which was achieved by a five-fold excess of PPh_3 and other neutral ligands.[15] Additionally, complex [Ru{κ^3-*H,S,S'*-$H_2B(mt)_2$}(Cp*)] undergoes reversible coordination of CO to [Ru(CO){κ^2-*S,S'*-$H_2B(mt)_2$}(Cp*)] *via* opening of the B–H–Ru interaction.[16]

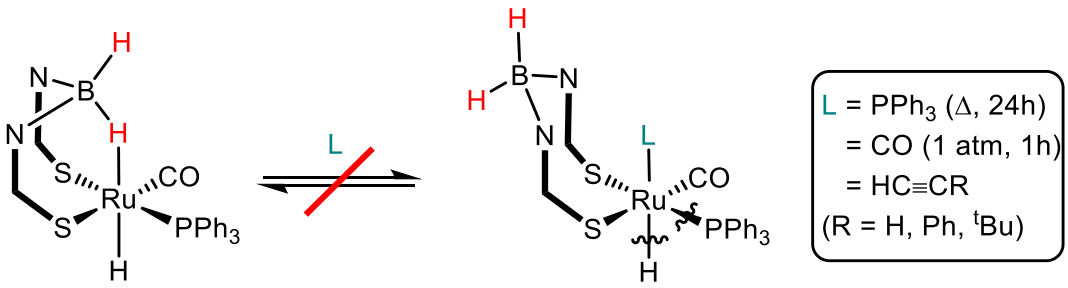

Scheme 2.2: Reactivity of **2.1** towards potential ligands.[12]

Despite evidence of the robust B–H–Ru interaction and a lack of Brønsted acidity for the metal hydride, the acquisition of the $^{13}C\{^{1}H\}$ NMR spectrum of **2.1** in $CDCl_3$ was accompanied by slow conversion to $[RuCl(CO)(PPh_3)\{H_2B(mt)_2\}]$. This is consistent with the report by Zhang, where the ruthenium hydride in the related analogue $[RuH(CO)(PPh_3)\{H_2B(mt^{R'})_2\}]$ (R' = C_6H_4Cl-4) was replaced by a chloride to afford $[RuCl(CO)(PPh_3)\{H_2B(mt^{R'})_2\}]$.[7] This itself seems counterintuitive in that the hydride is considered to be a ligand that usually exerts a strong *trans* influence and *trans* effect.

2.2.2 Synthesis of $[RuCl(CO)(PPh_3)\{\kappa^3\text{-}H,S,S'\text{-}H_2B(mt)_2\}]$

The intentional synthesis of $[RuCl(CO)(PPh_3)\{\kappa^3\text{-}H,S,S'\text{-}H_2B(mt)_2\}]$ **2.2** (Scheme 2.3) on a preparative scale was achieved in chloroform slowly at room temperature or more quickly in chloroform under reflux.

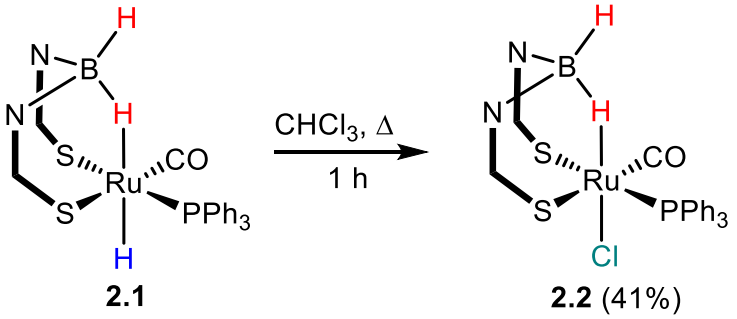

2.1 **2.2** (41%)

Scheme 2.3: Synthesis of complex **2.2**.

The distinct ruthenium hydride resonance of **2.1** disappears over the course of the reaction while the B–H–Ru resonance shifts dramatically upfield to δ_H = –18.11. Of the three 'hydridic' hydrogens B–H, B–H–Ru and Ru–H, the terminal ruthenium hydride was selectively substituted by chloride. The formulation of **2.2** is supported by spectroscopy, mass spectrometry and a crystallographic study. A shift to higher frequency for the ν_{BH} (2431 cm^{-1}) and ν_{CO} (1973 cm^{-1}) absorptions was observed in the dichloromethane solution IR spectrum of **2.2**, suggesting a comparatively less electron rich metal centre

than **2.1**. Drawing similarities to **2.1**, the C_1-symmetric system of **2.2** is similarly represented by distinct methyl and olefin environments, manifested in the ^{1}H and $^{13}C\{^{1}H\}$ NMR spectra. The carbonyl carbon was observed as a doublet at δ_C = 198.2 and showed coupling to phosphorus ($^{2}J_{CP}$ = 11.6 Hz). The phosphorus and boron nuclei gave rise to resonances at the respective chemical shifts, δ_P = 36.3 and δ_B = –7.36. The sodium adduct of **2.2** was detected in the HR-ESI+ mass spectrum and the formulation was further confirmed through X-ray analysis of crystals grown from chloroform (Figure 2.2a). Spectroscopic features are similar in the various derivatives of **2.1** to be described such that only the interesting unique features will be discussed. Generic features will subsequently be discussed collectively (*vide infra*). Spectroscopic and crystallographic comparisons of the complexes within the series [Ru(X)(CO)(PPh_3){κ^3-*H,S,S'*-$H_2B(mt)_2$}] (X = H, Cl, SePh, BCat, $SiCl_3$, $SiMe_3$) **2.1**–**2.6** will also be discussed collectively in Section 2.2.6.

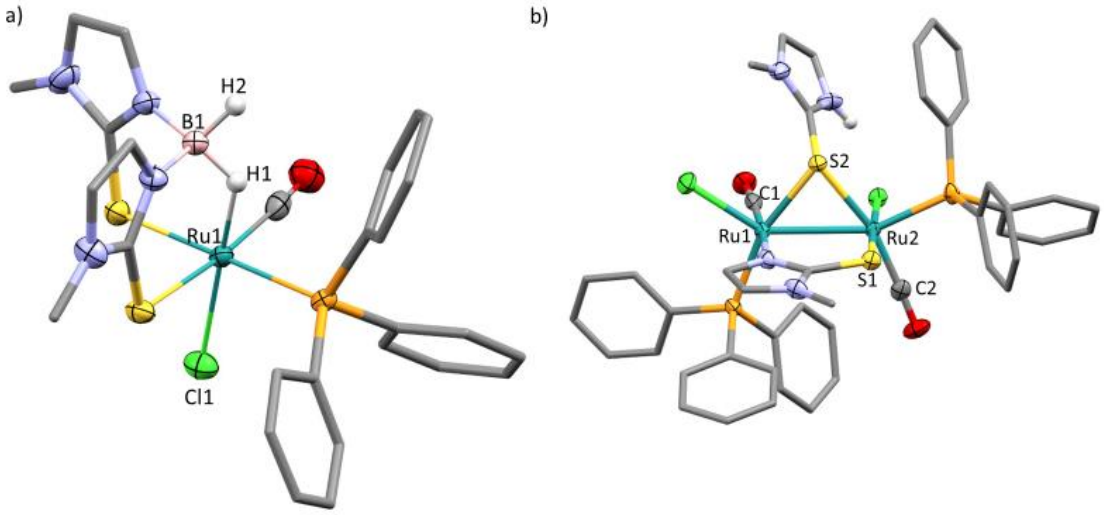

Figure 2.2: a) Molecular structure of [RuCl(CO)(PPh_3){κ^3-*H,S,S'*-$H_2B(mt)_2$}] **2.2**.$CHCl_3$ (solvent omitted, CH hydrogen atoms omitted, phenyl groups simplified, displacement ellipsoids shown at 50% probability). Selected bond lengths (Å) and angles (°): B1···Ru1 2.651(3), B1–H1 1.18(3), B1–H2 1.14(3), Ru1–H1 1.74(3), Ru1–Cl1 2.4186(6), B1–H1–Ru1 130(2), H1–Ru1–Cl1 175.5(11). b) [Ru_2(μ-S-mtH)(μ-mt)$Cl_2(CO)_2(PPh_3)_2$] **2.2x** (aryl hydrogen atoms omitted, phenyl groups simplified, displacement ellipsoids shown at 50% probability). Selected bond lengths (Å) and angles (°): Ru1–Ru2 2.9195(3), Ru1–S2 2.4567(7), Ru2–S1 2.3777(7), Ru1–C1 1.845(4), Ru2–C2 1.842(3), Ru2–S2–Ru1 73.130(19), S2–Ru2–Ru1 53.637(17), S2–Ru1–Ru2 53.232(16).

Prolonged exposure of **2.2** to chloroform results in the formation of insoluble red crystals that were identified as $[Ru_2(\mu\text{-S-mtH})(\mu\text{-mt})Cl_2(CO)_2(PPh_3)_2]$ **2.2x** through an X-ray diffraction study (Figure 2.2b). The molecular structure of **2.2x** depicts coordination of two distinct methimazolyl units obtained from $[H_2B(mt)_2]^-$ ligand degradation, bridged between the two ruthenium centres in μ-S and μ-S,N modes respectively. The formally non-bonded Ru1–Ru2 distance is comparable to the average range for the 5380 entries in the CCDC (2.9195(3) *cf.* 2.575–3.136 Å). The methimazole bridged through the thione donor forms a scalene triangle with the ruthenium centres. It is perhaps noteworthy that whilst two methimazolyl groups are widely encountered as pairwise bridging ligands, examples where one coordinates through both nitrogen and sulfur while the second bridges solely through sulfur are scarce. The complex **2.2x** and rhodium dimer $[Rh_2(\mu\text{-S-mtH})(\mu\text{-mt})(COD)_2]$ (mtH = 1-methyl-4-tert-butylimidazole-2-thiolate) appear to be the only crystallographically established examples.[17]

2.2.3 Synthesis of $[Ru(SePh)(CO)(PPh_3)\{\kappa^3\text{-}H,S,S'\text{-}H_2B(mt)_2\}]$

Complex $[Ru(SeH)(CO)(PPh_3)\{\kappa^3\text{-}H,S,S'\text{-}H_2B(mt)_2\}]$ was only detected in trace amounts through an X-ray crystallography study in the reaction of **2.1** with PhSeSePh (0.5 equivalent) performed by Otten,[13] and represents only the second structural report of a ruthenium hydroselenide complex, following that of Mizobe and Hidai for the binuclear complex $[Ru_2(\mu\text{-SeH})_2Cl_2(MeC_6H_4{}^i\text{Pr-}4)_2]$.[18]

Driven by the rarity of ruthenium hydroselenide complexes, the preparation of $[Ru(SeH)(CO)(PPh_3)\{\kappa^3\text{-}H,S,S'\text{-}H_2B(mt)_2\}]$ was investigated by treatment of **2.1** with elemental (grey) selenium (Scheme 2.4). There was, however, no spectroscopic evidence of Se insertion into the Ru–H bond over 21 hours at room temperature, and the only observed reaction was slow conversion of **2.1** to **2.2** owing to the $CDCl_3$ solvent.

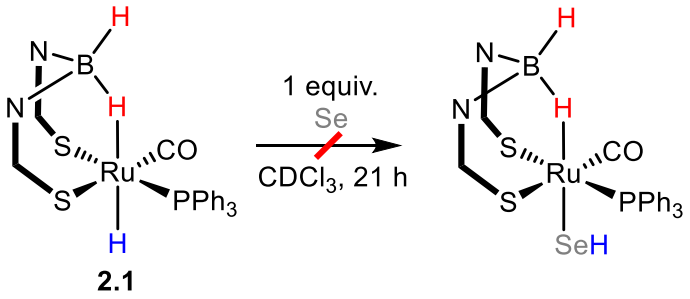

Scheme 2.4: Attempted synthesis of $[Ru(SeH)(CO)(PPh_3)\{\kappa^3\text{-}H,S,S'\text{-}H_2B(mt)_2\}]$.

Given that some metal hydrides react with diarylsulfides to yield arylthiolato complexes, an analogy was drawn for diselenides.[19] Accordingly, reaction of **2.1** with one equivalent of PhSeSePh was found to provide [Ru(SePh)(CO)(PPh_3){κ^3-*H,S,S'*-$H_2B(mt)_2$}] **2.3** in a modest 66% yield (Scheme 2.5). Complex **2.3** is spectroscopically similar to **2.1** with the noteworthy loss of the ruthenium hydride doublet resonance in the ^1H NMR spectrum and shift of the B–H–Ru resonance to δ_H = –12.00. The $^{31}P\{^1H\}$ and $^{11}B\{^1H\}$ NMR spectra revealed single phosphorus and boron environments at the respective shifts of δ_P = 39.70 and δ_B = –5.50.

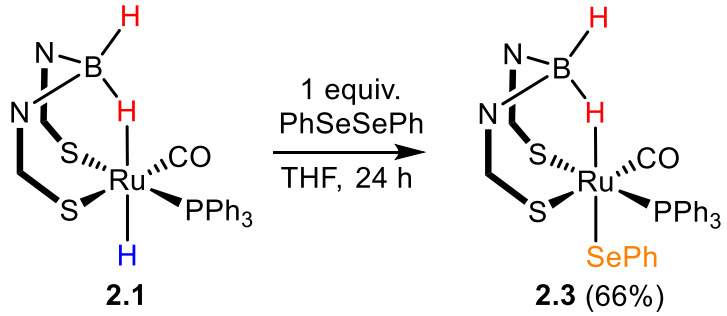

Scheme 2.5: Synthesis of complex **2.3**.

The formulation of **2.3** was further confirmed by mass spectrometry and an X-ray diffraction study (Figure 2.3). In contrast to the rare reports of hydroselenide complexes, ruthenium arylselenato complexes are more common and particularly prevalent within bridging and chelating frameworks. The coordinatively unsaturated [Ru($SeC_6HMe_4)_4$(NCMe)] adopts a trigonal bipyramidal geometry and consists of a longer axial Ru–Se bond length than the three equatorial bond lengths (2.496 *cf.* 2.316–2.330 Å, respectively).[20] Examples of simple non-chelated ruthenium selenolates that comply with the 18 electron rule include [Ru(SeC≡CR)($PPh_3)_2$(η-C_5H_5)] (R = Ph, $SiMe_3$, C≡W$(CO)_2$Tp*) and [Ru{$SeCOC_6H_3(NO_2)_2$-3,5}$(CO)_2$(η-$C_5H_4{}^t$Bu)].[21-23] The Ru–Se bond length within these structures span a range of 2.500–2.547 Å and the Ru–Se bond length of 2.5254(6) Å in **2.3** lies within this range, whilst the Ru1–Se1–C2 angle of 113.19(16)° is unremarkable.

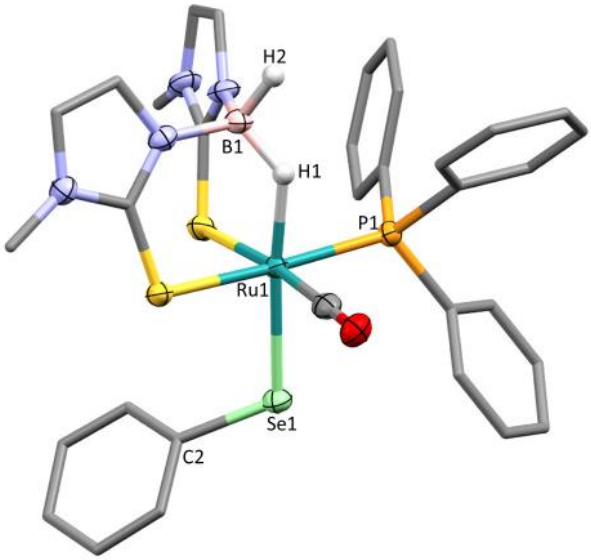

Figure 2.3: Molecular structure of [Ru(SePh)(CO)(PPh_3){κ^3-*H,S,S'*-$H_2B(mt)_2$}] **2.3** (organic hydrogen atoms omitted, phenyl groups simplified, displacement ellipsoids shown at 50% probability). Selected bond lengths (Å) and angles (°): B1···Ru1 2.723(5), B1–H1 1.23(6), B1–H2 1.17(6), Ru1–H1 1.79(6), Ru1–Se1 2.5254(6), Se1–C2 1.927(5), B1–H1–Ru1 128(4), H1–Ru1–Se1 175(2), Ru1–Se1–C2 113.19(16).

2.2.4 Synthesis of [Ru(X)(CO)(PPh_3){κ^3-*H,S,S'*-$H_2B(mt)_2$}] (X = BCat, $SiCl_3$, $SiMe_3$)

The persistence of the robust B–H–Ru interaction in the presence of the strongly *trans* influential hydride ligand prompted the exploration of other ligands renowned for their strong *trans* influences. Of superlative *trans* influential strength are σ-boryls and σ-silyls, and these empirical observations are supported by the computational studies of Lin and Marder.[24] The synthetic approach to these complexes begun with introduction of the *trans* ligand of interest to the ruthenium through reaction of [RuHCl(CO)(PPh_3)$_3$] with HBCat, $HSiCl_3$ or H_2C=CH$SiMe_3$. Thus, complexes [Ru(BCat)Cl(CO)(PPh_3)$_2$][25] and [Ru($SiMe_3$)Cl(CO)(PPh_3)$_2$][26] were obtained from literature procedures while [Ru($SiCl_3$)Cl(CO)(PPh_3)$_2$] **2.5a** was prepared based on the synthetic approach reported by Roper for the corresponding osmium analogue (Scheme 2.6).[27]

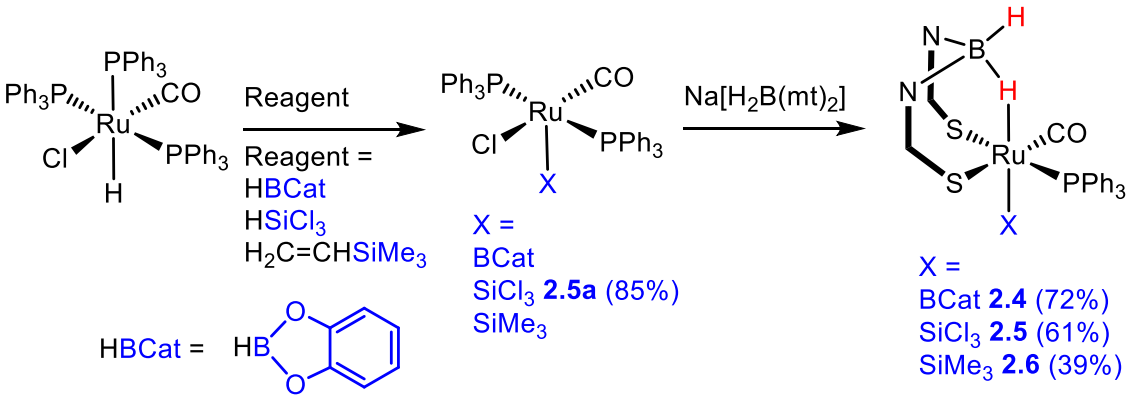

Scheme 2.6: Synthetic approaches to complexes **2.4**–**2.6** through coordinatively unsaturated precursors [Ru(X)Cl(CO)(PPh_3)$_2$].

The formation of the new intermediate **2.5a** was supported by spectroscopic data that show only aromatic resonances in the ^{1}H NMR spectrum (δ_H = 7.01–7.86) and a single environment in the ^{31}P{^{1}H} NMR spectra (δ_P = 34.8) consistent with the *trans* PPh_3 ligands. The presence of two PPh_3 was substantiated by the triplet coupling of the CO carbon in the ^{13}C{^{1}H} NMR spectrum (δ_C = 198.7, $^2J_{CP}$ = 12.5 Hz). Whilst the molecular ion was not observed by mass spectrometry, the acetonitrile adducts of both chloride isotopologues were detected.

The synthesis of [Ru(X)(CO)(PPh_3){κ^3-*H,S,S'*-$H_2B(mt)_2$}] (X = BCat **2.4**, $SiCl_3$ **2.5**, $SiMe_3$ **2.6**) was achieved through a general procedure that involved reaction of [Ru(X)Cl(CO)(PPh_3)$_2$] with Na[$H_2B(mt)_2$] in THF at room temperature for 2–25 hours. Spectroscopic and mass spectrometric data of **2.4**–**2.6** are similar and are therefore discussed collectively with highlights of the key distinguishing features. All complexes were detected in HR-ESI+ MS as the sodium and/or acetonitrile adducts. The B–H–Ru interaction was observed as broad resonances upfield of TMS in the ^{1}H NMR spectra (δ_H = –3.09 **2.4**, –5.74 **2.5**, –3.50 **2.6**). The ^{31}P{^{1}H} resonances span a range of δ_P = 40.7–48.7, while the ^{11}B{^{1}H} resonances of the BH_2 unit fall within the narrow range of δ_B = –4.7 to –5.4. For complex **2.4**, ^{11}B resonances corresponding to the BH_2 and BCat moieties appeared in distinct regions of the spectrum (Figure 2.4), consistent with pre-established chemical shift ranges for ruthenium σ-boryls (δ_{BCat} = 52.3) and borates (δ_{BH2} = –5.4).[28]

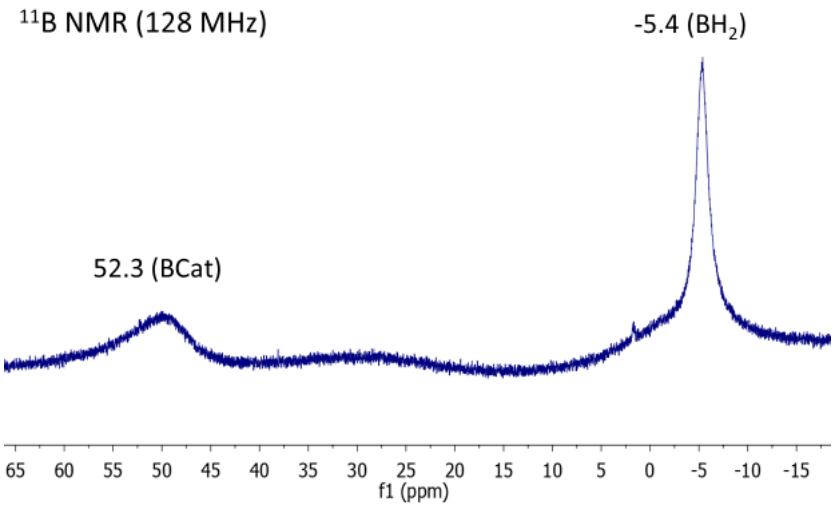

Figure 2.4: The ^{11}B NMR spectrum (128 MHz, $CDCl_3$) of complex **2.4**.

The molecular structures of **2.4** and **2.5** were determined previously within the group. In the present work numerous attempts to acquire crystallographic quality crystals of **2.6** resulted in the precipitation of amorphous powders. During an attempt to recrystallise **2.5** in dichloromethane/ethanol, the ruthenium dimer $[Ru_2(\mu\text{-}Hmt)_2Cl_4(CO)_2(PPh_3)_2]$ **2.5x** was obtained as a decomposition product (Figure 2.5) and illustrates the propensity for the $[H_2B(mt)_2]^-$ ligand to degrade into its constituent methimazoles, although the fate of the extruded boron is unknown.

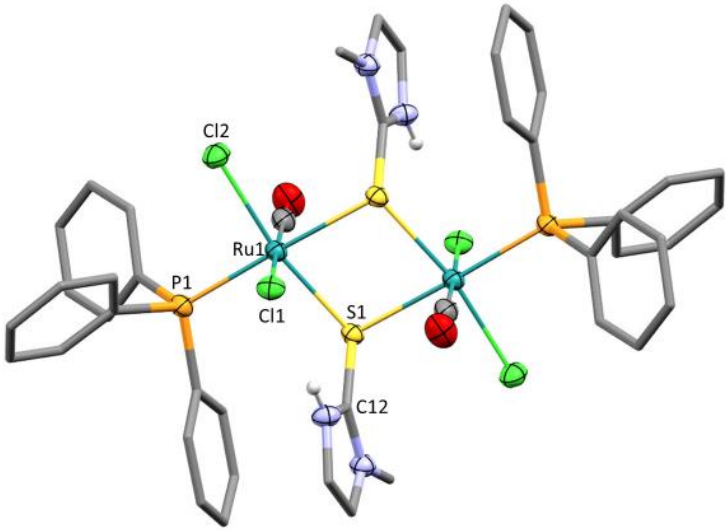

Figure 2.5: Molecular structure of $[Ru_2(\mu\text{-}Hmt)_2Cl_4(CO)_2(PPh_3)_2]$ **2.5x** (CH hydrogen atoms omitted, phenyl groups simplified, displacement ellipsoids shown at 50% probability). Selected bond lengths (Å) and angles (°): Ru1–Cl1 2.4678(6), Ru1–Cl2 2.4139(6), Ru1–S1 2.4139(6), Ru1–P1 2.3269(6), S1–Ru1–P1 97.68(2), S1–Ru1–Cl2 169.85(2), S1–Ru1–Cl1 93.51(2). The molecule lies on a crystallographic inversion centre such that only half the molecule is unique.

2.2.5 Attempted Synthesis of [Ru(X)(CO)(PPh$_3$){κ^3-*H,S,S'*-H$_2$B(mt)$_2$}] (X = Ph, CH=CHPh)

The complexes discussed thus far have involved X ligands that are unlikely to serve as a hydrogen acceptor. When the X group is a σ-organyl such as Ph or CH=CHPh, the possibility of hydrogen elimination (as benzene or styrene) arises. This was demonstrated in the synthesis of the first ruthenaboratrane [Ru{κ^4-*B,S,S',S''*-B(mt)$_3$}(CO)(PPh$_3$)][29,30] (Scheme 2.7) from the reaction of [Ru(X)Cl(CO)(PPh$_3$)$_2$] (X = Ph, CH=CHPh, CH=CHCPh$_2$OH, CH=CH(C$_6$H$_4$Me-4)) and Na[HB(mt)$_3$], with extrusion of X–H.

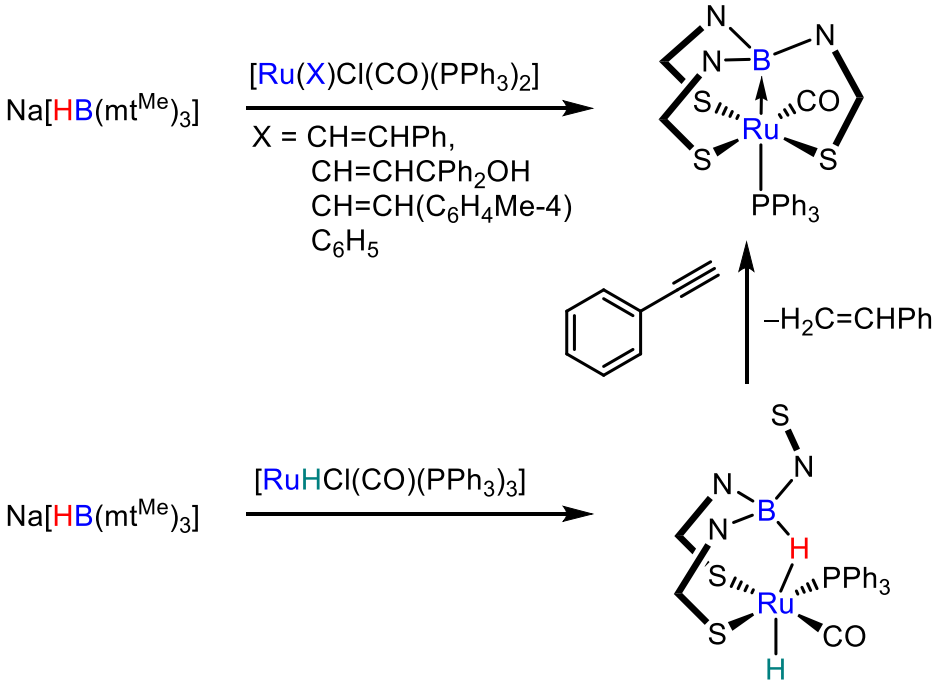

Scheme 2.7: Synthetic pathways to ruthenaboratrane [Ru{κ^4-*B,S,S',S''*-B(mt)$_3$}(CO)(PPh$_3$)].

Upon replacing the hydrogen accepting σ-organyl (X) with a hydride ligand, ruthenaboratrane formation was impeded and allowed isolation of the thermally stable hydrido intermediate [RuH(CO)(PPh$_3$){κ^3-*H,S,S'*-HB(mt)$_3$}] (Scheme 2.7).[6] Formation of the ruthenaboratrane could then be induced by addition of ethynylbenzene to afford subsequent elimination of styrene. The main implications include the inferred BH–Ru *hemilability* to allow initial coordination/hydroruthenation of ethynylbenzene and the participation of a hydrogen acceptor co-ligand in the elimination process (of X–H).

Notwithstanding the hydrogen accepting potential of σ-organyls, the synthesis of $[Ru(X)(CO)(PPh_3)\{\kappa^3\text{-}H,S,S'\text{-}H_2B(mt)_2\}]$ (X = Ph, CH=CHPh) was pursued through an analogous synthetic pathway to complexes **2.4**–**2.6** (i.e., through the unsaturated precursor $[Ru(X)Cl(CO)(PPh_3)_2]$, X = Ph,[31] CH=CHPh[32,33]). The NMR scale reactions of $[Ru(X)Cl(CO)(PPh_3)_2]$ (X = Ph, CH=CHPh) with $Na[H_2B(mt)_2]$ in $CDCl_3$ were monitored by ^1H and $^{31}P\{^1H\}$ NMR spectroscopy and revealed the transient formation of non-isolable species formulated as $[Ru(X)(CO)(PPh_3)\{\kappa^3\text{-}H,S,S'\text{-}H_2B(mt)_2\}]$ (X = Ph **2.7**, CH=CHPh **2.8**) followed by subsequent conversion to a complex postulated to be the doubly-bridged ruthenaboratrane $[Ru\{\kappa^3\text{-}B,S,S'\text{-}BH(mt)_2\}(CO)(PPh_3)_2]$ **3.1**. The spectra for the progress of both reactions are similar, with the Ph variant in Figure 2.6 proceeding with fewer side products.

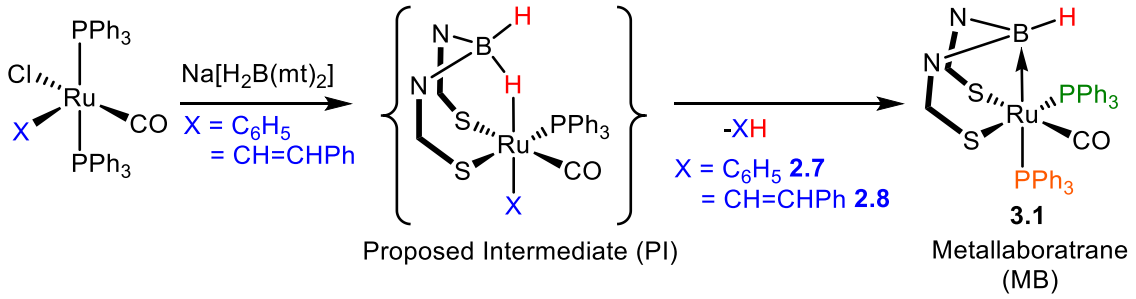

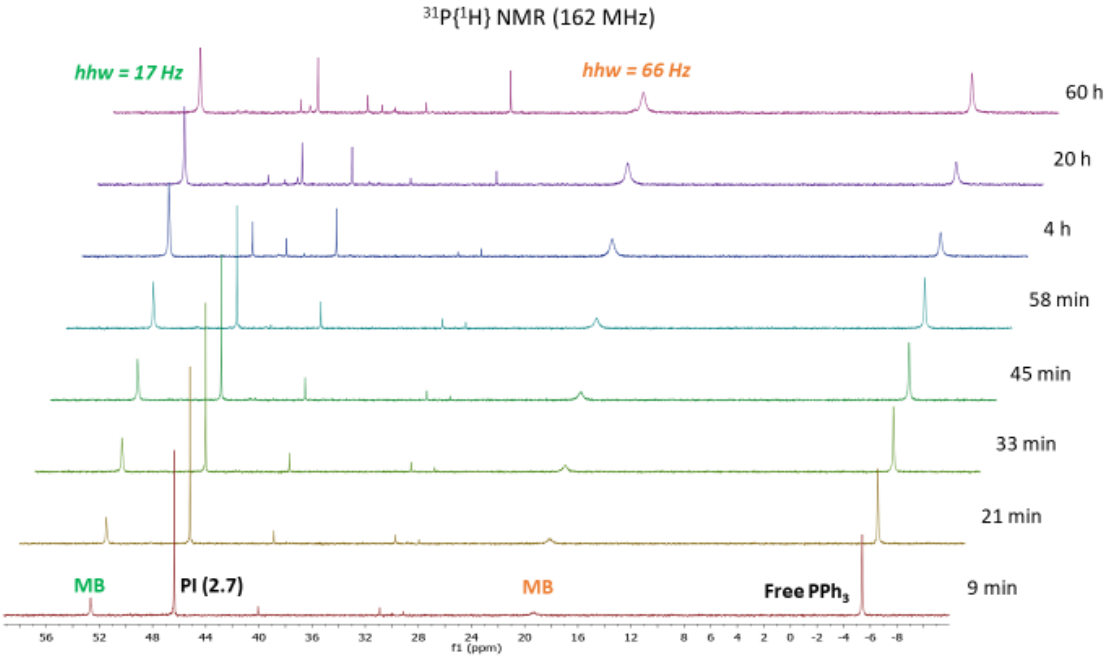

Figure 2.6: Attempted synthesis of $[Ru(Ph)(CO)(PPh_3)\{\kappa^3\text{-}H,S,S'\text{-}H_2B(mt)_2\}]$ monitored by $^{31}P\{^1H\}$ NMR spectroscopy (162 MHz, $CDCl_3$, 25°C).

As shown in Figure 2.6, facile formation of **2.7** (δ_P = 46.4) resulted within 9 minutes upon dissolution of [Ru(Ph)Cl(CO)(PPh_3)$_2$] and Na[$H_2B(mt)_2$] in $CDCl_3$. Minor broad resonances at δ_P = 52.7 and 19.3 were also present. The κ^3-*H,S,S'* 3c2e coordination in **2.7** is unstable ($t_{½}$ = 33 min), as observed by the disappearance of the singlet at δ_P = 46.4 and an increase in those of the minor product. The resonances δ_P = 52.7 and 19.3 were assigned as the ruthenaboratrane **3.1**, where the half height width value of each resonance provides an indication of the phosphine environment. The phosphine located *trans* to the Ru→B bond (δ_P = 19.3, h.h.w. = 66 Hz) would be expected to exhibit significant broadening through coupling with the quadrupolar boron (^{11}B, ^{10}B) nuclei, compared to that positioned *trans* to a thione donor (δ_P = 52.7, h.h.w. = 17 Hz). The ^{1}H NMR data for the reaction depicted in Figure 2.6 is consistent with the initial formation of **2.7,** notably by a broad singlet at δ_H = –7.13 suggestive of a 3c2e B–H–Ru interaction, which slowly diminishes to afford a spectrum devoid of hydride resonances.

The reaction of [Ru(CH=CHPh)Cl(CO)(PPh_3)$_2$] and Na[$H_2B(mt)_2$] proceeded similarly with numerous resonances (>8) observed in the ^{31}P{^{1}H} NMR spectrum within 5 minutes, with the major product (δ_P = 44.9) and corresponding hydride resonance (δ_H = –6.64) assigned as **2.8**. Spectroscopic (NMR, IR) and spectrometric (MS) data were acquired from the *in situ* (t ≈ 0) generation of complexes **2.7** and **2.8**. The sodium adducts of **2.7** and **2.8** were detected in the HR-ESI+ mass spectrum, along with the [M+H]$^+$ peak of complex **3.1**. IR bands associated with the B–H–Ru interaction in **2.7** and **2.8** were observed at 2092 and 2089 cm^{-1}, respectively. The stretching frequencies of the CO ligand are higher in **2.7** (1934 cm^{-1}) and **2.8** (1943 cm^{-1}) than for **3.1** (1900 cm^{-1}). A higher CO stretching frequency is associated with a Ru(II) centre compared to a lower value for Ru(0), as exemplified in Roper's respective Ru(II) and Ru(0) complexes, [Ru(O_2)(CO)$_2$(PPh_3)$_3$] (1945 cm^{-1}) and [Ru(CO)$_2$(PPh_3)$_3$] (1905 cm^{-1}).[34] Therefore, the nature of the ruthenium centre was inferred as Ru(II) in **2.7** and **2.8** and Ru(0) in **3.1**. The preparative scale synthesis and reactivity of **3.1** are explored in Chapter 3.

2.2.6 Analysis and Comparison of Complexes

The synthesis and characterisation of the complexes [Ru(X)(CO)(PPh_3){κ^3-*H,S,S'*-$H_2B(mt)_2$}] (X = H, Cl, SePh, BCat, $SiCl_3$, $SiMe_3$) **2.1**–**2.6** provides a series that, in keeping all ligands equal, allows focus on the influence of the *trans* X ligand on the 3c2e B–H–Ru interaction.

Trans influence has been a long-accepted concept in transition metal chemistry, as a thermodynamic (ground state) component of the *trans* effect[†] and describes the influence that ligands can exert to weaken the bond to which they are *trans* coordinated.[35] Observable changes include M–X bond distance, ν_{MX} vibrational frequency or force constant, and NMR coupling constants (e.g., $^1J_{MX}$). Mechanistic considerations are described by the kinetic *trans* effect, and together with the *trans* influence, make up the *trans* effect defined by Basolo and Pearson as *"the labilization of ligands trans to certain other ligands"*.[36] A variety of techniques have been utilised to quantify the effects of *trans* influence including crystallographic data and computational studies, which are summarised in reviews on octahedral and square planar geometries.[37-41] A generally accepted method of rationalising *trans* influence is the polarisation model first proposed by Grinberg and Nekrasov.[37] Their model details the competition between *trans* disposed ligands for bonding to the metal centre, which may occur through electrostatic charge, σ-covalency or both.

Initial analysis of the current work explored the combined structural data of the series collated in Table 2.2 (below) and that of the literature in Table 2.1 (Section 2.1). Notably, due to the lack of precision in the location of the hydrogen positions near heavy metals, X-ray diffraction is not the technique of choice for the study of hydrogens atoms. Thus, the direct Ru–H bond in the B–H–Ru interaction was not considered sufficiently precise and indirect parameters such as the RuHB angle and Ru···B distance were analysed instead. The RuHB angle and Ru···B distance should be more accurately measured than the Ru–H bond and represent, to some extent, the nature of the B–H–Ru interaction. The B–H–Ru angle spans 126–151° and with typically an e.s.d. of 2°, the 25° variation barely falls within the limits of significance, given the accepted value for statistical significance is 6 x e.s.d = 24°. The deviation of the Ru···B distance (2.634–2.931 Å, e.s.d. 0.002 Å) is statistically significant (12 e.s.d.). Statistical significance aside, a recurrent general trend is that the B–H involved in the 3c2e bonding is longer than of the terminal B–H bond. Furthermore, a plot of δ_B against the Ru···B distance shows no dominant correlation.

[†] The kinetic trans effect may also arise from transition state stabilisation, e.g., with π-donor ligands capable of moderating the decrease in electron density at the metal as ligands depart. As a feature of a transition state, this may not normally be readily measured.

Despite the lack of substantial variation in the complexes in Table 2.1 and Table 2.2, the data are nevertheless informative as the following was noted: i) N-substituent variation (e.g. Me to larger groups C_6H_4Cl-4 or *p*-tol) has little chemical impact, consistent with their remote location.[42] ii) The presence of a third coordinating unit on the boron (mt, pz) does not influence the Ru–H–B and Ru···B distances. iii) Oxidation of the metal centre results in longer Ru···B distances (e.g., $[Ru(Bm)_2]^{n+}$, n = 0, 1) due to the BH_2 group moving away from the ruthenium. Although an increase in the Lewis acidity of the ruthenium upon oxidation is expected to pull the BH_2 group closer, the concurrent effect of π-donation from the thione donors into the previously filled t_2g set (Ru^{II} t_2g^6 *cf.* Ru^{III} t_2g^5) presumably dominates. The contraction of the thione donors towards the ruthenium(III) centre (3 pm) occludes access of the σ-donating B–H unit.

Complex	**Ru–H–B [°]**	**Ru···B [Å]**	**δ_{BHRu} [ppm]**	**δ_B [ppm]**	**ν_{CO} (cm^{-1})**	**δ_P [ppm]**	***r*RuCl^a [Å]**
[Ru(X)(CO)(PPh_3)(Bm)] = Ru–X							*trans*-[Ru(X)Cl(PMe_3)$_4$]
Ru-H **2.1**	129	2.796	–5.42	–5.52	1926	56.7	2.640
Ru-Cl **2.2**	130	2.651	–18.11	–7.36	1963	36.3	2.542
Ru-BCat **2.4**	138	2.897	–3.09	–4.98	1939	47.2	2.693
Ru-$SiCl_3$ **2.5**	137	2.830	–5.74	–4.70	1970	40.7	2.594
Ru-SePh **2.3**	128	2.724	–12.00	–5.50	1945	39.7	2.588
Ru-SeH	131	2.663	-	-	-		-
Ru-$SiMe_3$ **2.6**	-	-	–3.50	–4.81	1906	48.7	2.678
Ru-Ph **2.7**	-	-	–7.13	–6.59	1934	46.4	2.695
Ru-CH=CHPh **2.8**	-	-	–6.64	–5.82	1943	44.8	2.681 ^{b}

Table 2.2: Data for the series: [Ru(X)(CO)(PPh_3){κ^3-*H,S,S'*-$H_2B(mt)_2$}] (X = H, Cl, SePh, BCat, $SiCl_3$, $SiMe_3$) **2.1**–**2.6**, and transient complexes [Ru(X)(CO)(PPh_3){κ^3-*H,S,S'*-$H_2B(mt)_2$}] (X = Ph, CH=CHPh). ^{a}Ru–Cl bond length calculations for *trans*-[Ru(X)Cl(PMe_3)$_4$] performed on DFT: B3LYP-LanL2DZ level of theory by Professor Anthony Hill. ^{b}Calculations for $CH{=}CH_2$.

In the absence of any significant correlation of the combined data in Tables 2.1 and 2.2, attention was directed towards the data in Table 2.2 in more detail. Attempts to probe the effect of the varied *trans* ligands *via* the *cis* CO ligand showed no correlation between the CO stretching frequency and the parameters in Table 2.2. However, the

plot of the hydride shift δ_{BHRu} against the B···Ru distance in Figure 2.7 showed reasonable correlation (R^2 = 0.93), which suggested that the closer the BH group approaches the metal, the greater the metal hydride character, where the hydride resonance moves to lower frequency due to shielding by the metal (Figure 2.7, bottom right). Conversely, the top representation in Figure 2.7 depicts the weak donation of the B–H electron pair to the metal centre. This implies that the farther the B···Ru distance the more BH character the B–H···M interaction possesses. This was favoured for ligands (X) of strong *trans* influence (σ-donating H, $SiCl_3$, BCat). The complexes discussed fall within the spectrum outlined by the two bonding extremes in Figure 2.7, which resemble those observed for Si–H adducts of transition metals.[43]

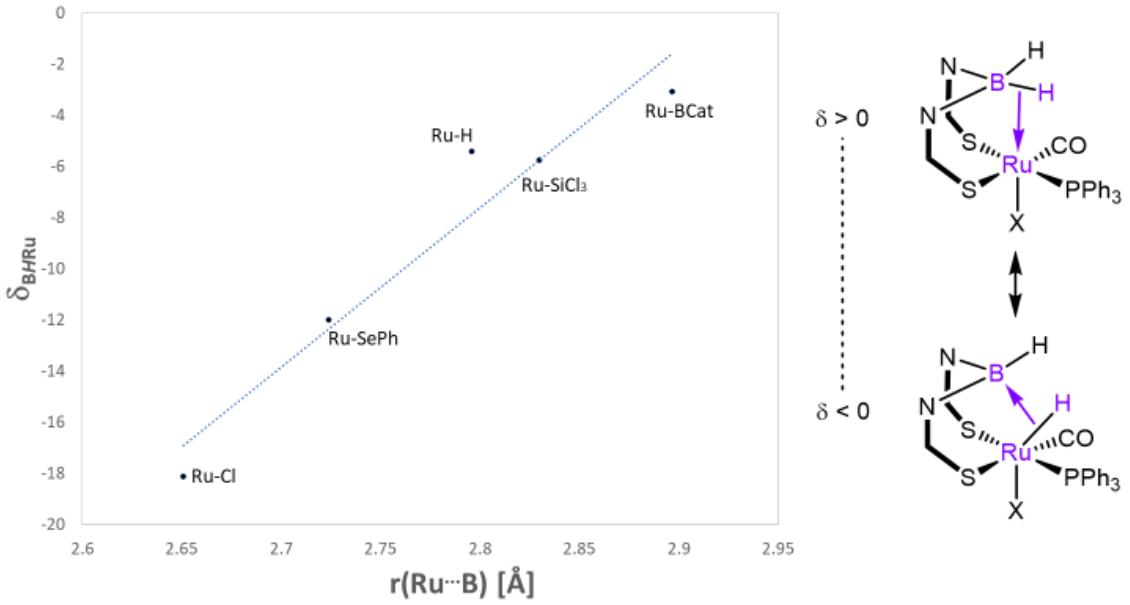

Figure 2.7: Relationship between hydrogen chemical shift in B***H***Ru and Ru···B distance for the complexes [Ru(X)(CO)(PPh_3){κ³-*H,S,S'*-$H_2B(mt)_2$}].

The issue of utilising an appropriate methodology arises when examining *trans* influence. To the author's knowledge, there is no one systematic method to quantify the wide range of ligands that could be used. Based on the computational studies performed by Lin and Marder on complexes *trans*-[Pt(X)(Cl)(PMe_3)$_2$] with *trans* ligand X (of various monovalent ligands),[24] the X ligands considered in this chapter fall into the *trans* influence order of:

$$SiMe_3 > BCat > HC{=}CH_2 > H > C_6H_5 > SiCl_3 > Cl > SePh$$

Analogous to their approach, calculations (DFT: B3LYP-LanL2DZ) were performed on the octahedral series *trans*-[Ru(X)Cl(PMe_3)$_4$] to determine the Ru–Cl bond length (Table 2.2) and assess the *trans* potency of the X ligands investigated in this chapter. A plot of the hydride shift δ_{BHRu} against the Ru–Cl distance in Figure 2.8 shows reasonably good correlation (R^2 = 0.83) with X = $SiCl_3$ as the only outlier. The presence of electronegative halides on silyl ligands has been associated with π-accepting properties.[44] The plot is consistent with the conclusions drawn from the analysis of structures within the CCDC, which were carried out by See and Kozina. They suggested that *trans* influence is greatest with strong σ-donating ligands, whereas a lesser effect is observed for chloride ligands.[37] This is represented by the longer Ru–Cl bond length in [Ru(X)Cl(PMe_3)$_4$] for Ru–X (where X = BCat, Ph, $CH{=}CH_2$, $SiMe_3$, H) compared to the chloride complex [$RuCl_2$(PMe_3)$_4$] (average 2.677 *cf.* 2.542 Å).

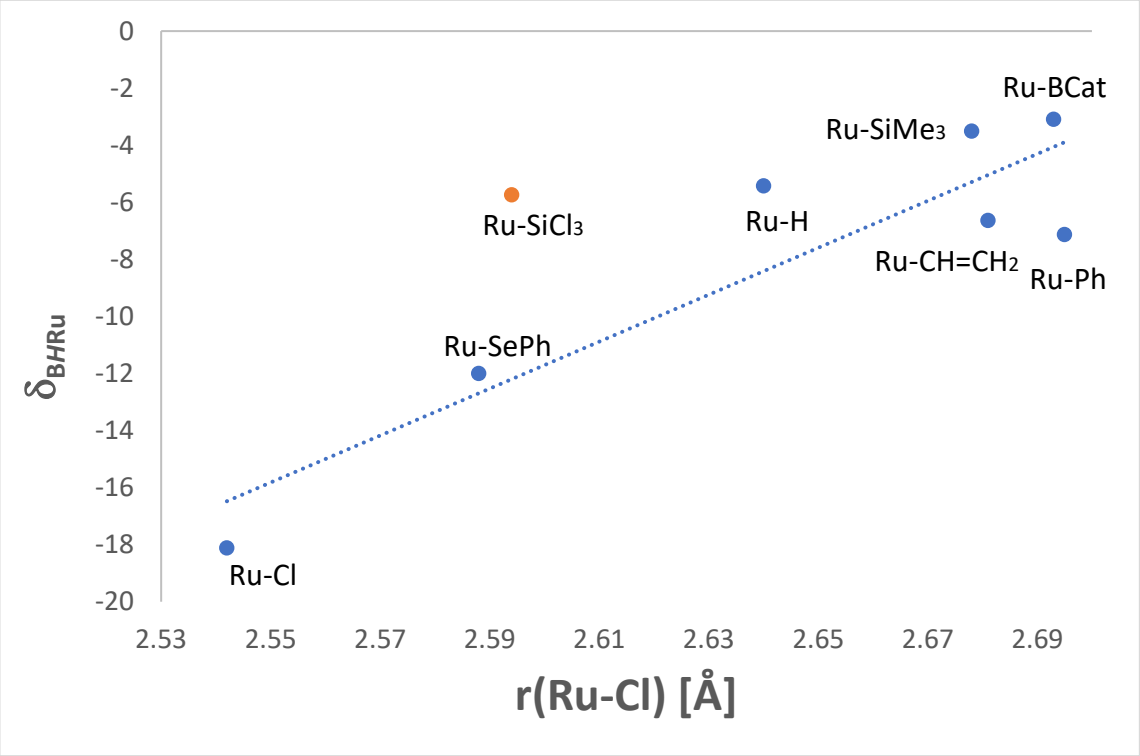

Figure 2.8: Relationship between the hydrogen chemical shift of B***H***Ru in complexes [Ru(X)(CO)(PPh_3)(κ^3-*H,S,S'*-$H_2B(mt)_2$}] and the calculated Ru–Cl distance in the complexes *trans*-[Ru(X)Cl(PMe_3)$_4$]. Ru–$SiCl_3$ not included in the trendline.

2.2.7 Synthesis of [OsH(CO)(PPh$_3$){κ^3-*H,S,S'*-H$_2$B(mt)$_2$}]

As apparent in this chapter, there is a comparatively large number of poly(azolyl)borate ruthenium complexes that feature B–H–Ru 3c2e interactions. In contrast, those of osmium complexes are underexplored. Reports of mononuclear B–H–Os 3c2e interactions are primarily concerned with κ^2-*H,H* tetrahydroborate derivatives[45,46] and metallapolyborane[47-53] clusters. The limited number of examples of simple R$_2$B–H–Os interactions are summarised in Figure 2.9.

Marder and Baker's [OsH(PMe$_3$)$_3${κ^2-*H,P*-HB(CH$_2$PMe$_2$)C$_8$H$_{14}$}] complex being the first simple example, was prepared from the insertion of 9-BBN into cyclometallated [OsH(CH$_2$PMe$_2$)(PMe$_3$)$_3$].[54] Further examples emerged two decades later in Hill's [OsCl$_2${κ^3-*H,P,P'*-HB(NCH$_2$PPh$_2$)$_2$C$_6$H$_4$}(PPh$_3$)][55] illustrating arrested B–H activation, and reports from Esteruelas of simple 3c4e interactions in [OsH$_2$Cl{κ^2-*B,H*-HBCH$_2$Ph}(P^{i}Pr$_3$)(IDipp)] (IDipp = bis(diisopropylphenyl)imidazolylidene),[56] [OsH{κ^2-*H,S*-HSBNR$_2$}(CO)(P^{i}Pr$_3$)$_2$] (R = H, Me; R$_2$ = H^{t}Bu),[57] [OsH$_2${κ^2-*H,H*-H$_2$BCH$_2$Ph}(P^{i}Pr$_3$)(IDipp)],[58] [OsH$_2$Cl{κ^2-*B,H*-HBR}(P^{i}Pr$_3$)$_2$] (R = NMe$_2$, O(CMe$_2$)$_2$OBPin, H^{t}Bu)[59] and [OsHX(η^2-H-BR){κ^3-*P,O,P*-xant(P^{i}Pr$_2$)$_2$}] (X = H, R = Bpin, BCat; X = Cl, R = BCat).[60]

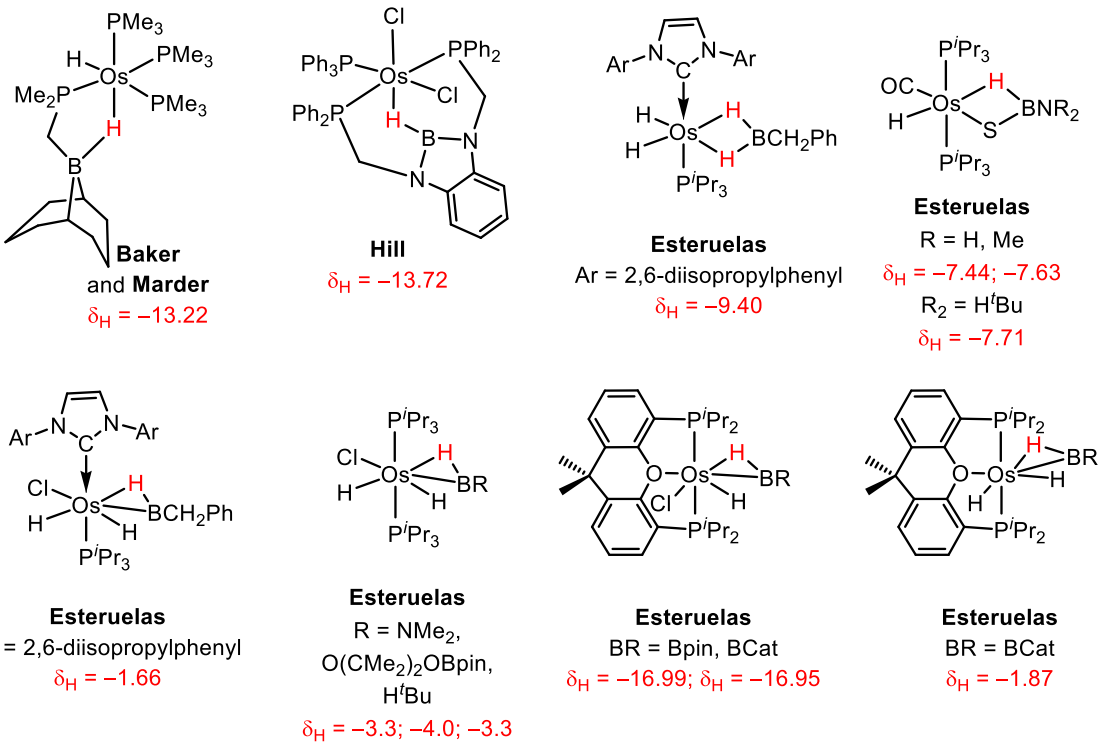

Figure 2.9: Mononuclear B–H–Os interactions and their corresponding ^{1}H NMR hydride shift.

Complex [OsH(CO)(PPh_3){κ^3-*H,S,S'*-$H_2B(mt)_2$}] **2.9** was initially observed by Otten in this group and structurally determined with geometric similarities to the ruthenium analogue **2.1**. The crystals of the two complexes are isostructural and consist of the same ligand set that coordinate around the metal centre to form an octahedral complex. The bond lengths between the metal and the ligands are almost identical (e.g. Os–P 2.325(1) and Os–C 1.824(5) Å *cf.* Ru–P 2.3028(4) and Ru–C 1.840(2) Å). The geometric similarities between **2.1** and **2.9** are expected given the similar covalent radii of ruthenium and osmium (r_{cov}(Ru) = 1.46 *cf.* r_{cov}(Os) = 1.44). Complex **2.9** was prepared herein (Scheme 2.8) with modifications to the initial procedure, utilising a simple dichloromethane/ethanol work-up to afford white crystalline solids of **2.9** in improved yields (73%).

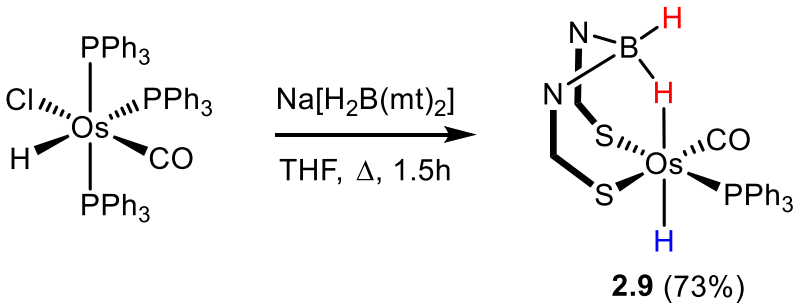

2.9 (73%)

Scheme 2.8: Synthesis of complex **2.9**.

Both the solid state and solution (CH_2Cl_2) IR spectra showed osmium hydride (ν_{OsH} = 1952 cm^{-1} [ATR]; 1955 cm^{-1} [solution]) and terminal BH (ν_{BH} = 2399; 2408 cm^{-1}) bands. The B–H–Os was observed as a broad resonance in the ^{1}H NMR spectrum at δ_H = –6.82, consistent with the wide range of chemical shifts noted for the complexes in Figure 2.9. The terminal osmium hydride resonated as a sharp well-resolved doublet at δ_H = –13.23 with coupling to the *cis*-PPh_3 ($^2J_{HP}$ = 18.2 Hz). Other spectroscopic features within the ^{1}H and ^{13}C{^{1}H} NMR spectra bear resemblance to the ruthenium derivative **2.1**. The ^{31}P nucleus appeared at δ_P = 19.7 in the ^{31}P{^{1}H} NMR spectrum and the ^{11}B resonance was broadened at δ_B = –6.47. The formulation of **2.9** was further supported by mass spectrometry.

The isolation of **2.9** contributes a κ^3-*H,S,S'* bonding model from which analogies may be drawn to further understand the intermediate structures in the mechanism of the formation of osmaboratrane [Os{κ^4-*B,S,S',S''*-$B(mt)_3$}(CO)(PPh_3)].[61] The osmaboratrane ultimately forms from the reaction of [Os(Ph)Cl(CO)(PPh_3)$_2$] and Na[$HB(mt)_3$].

The intermediate isolated from an ether suspension was postulated to be [Os(Ph)(CO)(PPh_3)$_2${κ^2-*S,S'*-HB(mt)$_3$}], *albeit* not conclusively confirmed due to facile conversion to the osmaboratrane [Os{κ^4-*B,S,S',S''*-B(mt)$_3$}(CO)(PPh_3)] upon solvation. As observed for transient species **2.7** (Figure 2.6), the hydrogen accepting properties of the phenyl moiety leads to ruthenaboratrane formation, whereas the B–H activation/reductive elimination process is impeded for **2.1** and similarly for **2.9**. Therefore, with inference from the series of **2.1**–**2.9**, the likely formulation of the intermediate is most likely [Os(Ph)(CO)(PPh_3){κ^3-*H,S,S'*-HB(mt)$_3$}].

2.3 Conclusion

A series of complexes of the form [Ru(X)(CO)(PPh_3){κ^3-*H,S,S'*-H_2B(mt)$_2$}] (X = H, Cl, SePh, BCat, $SiCl_3$, $SiMe_3$) **2.1**–**2.6** was synthesised for spectroscopic and structural comparisons to gain insight into perturbations on the B–H–Ru interaction affected by the *trans* X ligand. A loose correlation between the *trans* influence of the X ligand and the chemical shift (δ_H) of the borohydride group (B*H*Ru) was inferred. For ligands (X) of strong *trans* influence (σ-donating H, $SiCl_3$, BCat) the B–H–Ru interaction possessed more borohydride character (B–H···Ru), whereas those of weaker *trans* influence showed stronger B–H–Ru interactions that comprised more of metallohydridic character (B···H–Ru).

The osmium complex [OsH(CO)(PPh_3){κ^3-*H,S,S'*-H_2B(mt)$_2$}] **2.9** served as a comparison between 4d and 5d transition metals and provided insight into the coordination modes of intermediates in the formation of osmaboratrane [Os{κ^4-*B,S,S',S''*-B(mt)$_3$}(CO)(PPh_3)]. The complexes [Ru(X)(CO)(PPh_3){κ^3-*H,S,S'*-H_2B(mt)$_2$}] (X = Ph **2.7**, CH=CHPh **2.8**) were transient species *en route* to [Ru{κ^3-*B,S,S'*-BH(mt)$_2$}(CO)(PPh_3)$_2$] **3.1**, the synthesis and reactivity of which will be explored in Chapter 3.

2.4 References

(1) Rajasekharan-Nair, R.; Darby, L.; Reglinski, J.; Spicer, M. D.; Kennedy, A. R. *Inorg. Chem. Commun.* **2014**, *41*, 11.
(2) Wang, X.-Y.; Ma, Q.; Duan, T.; Chen, Q.; Zhang, Q.-F. *Inorg. Chim. Acta* **2012**, *384*, 281.
(3) Abernethy, R. J.; Hill, A. F.; Tshabang, N.; Willis, A. C.; Young, R. D. *Organometallics* **2009**, *28*, 488.
(4) Kuan, S. L.; Leong, W. K.; Goh, L. Y.; Webster, R. D. *J. Organomet. Chem.* **2006**, *691*, 907.
(5) Zhu, H.; Ma, Q.; Jia, A.-Q.; Chen, Q.; Leung, W.-H.; Zhang, Q.-F. *Inorg. Chim. Acta* **2013**, *405*, 427.
(6) Foreman, M. R. S. J.; Hill, A. F.; Owen, G. R.; White, A. J. P.; Williams, D. J. *Organometallics* **2003**, *22*, 4446.
(7) Ma, Q.; Jia, A.-Q.; Chen, Q.; Shi, H.-T.; Leung, W.-H.; Zhang, Q.-F. *J. Organomet. Chem.* **2012**, *716*, 182.
(8) Jimenez-Tenorio, M.; Puerta, M. C.; Valerga, P. *Organometallics* **2009**, *28*, 2787.
(9) Wang, X.-Y.; Shi, H.-T.; Wu, F.-H.; Zhang, Q.-F. *J. Mol. Struct.* **2010**, *982*, 66.
(10) Foreman, M. R. S. J.; Ma, C.; Hill, A. F.; Otten, N. E.; Sharma, M.; Tshabang, N.; Ward, J. S. *Dalton Trans.* **2017**, *46*, 14957.
(11) Kuan, S. L.; Leong, W. K.; Webster, R. D.; Goh, L. Y. *Organometallics* **2012**, *31*, 5159.
(12) Tshabang, N. PhD Thesis, The Australian National University, 2005.
(13) Otten, N. E. Honours Thesis, The Australian National University, 2015.
(14) Moore, E. J.; Sullivan, J. M.; Norton, J. R. *J. Am. Chem. Soc.* **1986**, *108*, 2257.
(15) Garcia, R.; Paulo, A.; Domingos, A.; Santos, I.; Ortner, K.; Alberto, R. *J. Am. Chem. Soc.* **2000**, *122*, 11240.
(16) Saito, T.; Kuwata, S.; Ikariya, T. *Chem. Lett.* **2006**, *35*, 1224.
(17) Miranda-Soto, V.; Perez-Torrente, J. J.; Oro, L. A.; Lahoz, F. J.; Martin, M. L.; Parra-Hake, M.; Grotjahn, D. B. *Organometallics* **2006**, *25*, 4374.
(18) Seino, H.; Mizobe, Y.; Hidai, M. *New J. Chem.* **2000**, *24*, 907.
(19) Lee, C.-L.; Chisholm, J.; James, B. R.; Nelson, D. A.; Lilga, M. A. *Inorg. Chim. Acta* **1986**, *121*, L7.
(20) Millar, M.; O'Sullivan, T.; De Vries, N.; Koch, S. A. *J. Am. Chem. Soc.* **1985**, *107*, 3714.
(21) Sunada, Y.; Hayashi, Y.; Kawaguchi, H.; Tatsumi, K. *Inorg. Chem.* **2001**, *40*, 7072.
(22) Hill, A. F.; Manzano, R. A.; Sharma, M.; Ward, J. S. *Organometallics* **2015**, *34*, 361.
(23) Jibril, I.; Esmadi, F. T.; Al-Masri, H.; Zsolnai, L.; Huttner, G. *J. Organomet. Chem.* **1996**, *510*, 109.
(24) Zhu, J.; Lin, Z.; Marder, T. B. *Inorg. Chem.* **2005**, *44*, 9384.
(25) Irvine, G. J.; Roper, W. R.; Wright, L. J. *Organometallics* **1997**, *16*, 2291.
(26) Marciniec, B.; Pietraszuk, C. *Organometallics* **1997**, *16*, 4320.
(27) Clark, G. R.; Rickard, C. E. F.; Roper, W. R.; Salter, D. M.; Wright, L. J. *Pure Appl. Chem.* **1990**, *62*, 1039.
(28) Hermanek, S. *Chem. Rev.* **1992**, *92*, 325.
(29) Hill, A. F.; Owen, G. R.; White, A. J. P.; Williams, D. J. *Angew. Chem. Int. Ed.* **1999**, *38*, 2759.
(30) Crossley, I. R.; Foreman, M. R. S. J.; Hill, A. F.; Owen, G. R.; White, A. J. P.; Williams, D. J.; Willis, A. C. *Organometallics* **2008**, *27*, 381.
(31) Bohle, D. S.; Clark, G. R.; Rickard, C. E. F.; Roper, W. R.; Wright, L. J. *J. Organomet. Chem.* **1988**, *358*, 411.
(32) Torres, M. R.; Vegas, A.; Santos, A.; Ros, J. *J. Organomet. Chem.* **1986**, *309*, 169.
(33) Werner, H.; Meyer, U.; Peters, K.; Von Schnering, H. G. *Chem. Ber.* **1989**, *122*, 2097.
(34) Cavit, B. E.; Grundy, K. R.; Roper, W. R. *J. Chem. Soc., Chem. Commun.* **1972**, 60.
(35) Pidcock, A.; Richards, R. E.; Venanzi, L. M. *J. Chem. Soc. A* **1966**, 1707.
(36) Basolo, F. *Prog. Inorg. Chem.* **1962**, *4*, 381.
(37) See, R. F.; Kozina, D. *J. Coord. Chem.* **2013**, *66*, 490.
(38) Appleton, T. G.; Clark, H. C.; Manzer, L. E. *Coord. Chem. Rev.* **1973**, *10*, 335.

(39) Kukushkin, Y. N. *Usp. Khim.* **1974**, *43*, 1689.
(40) Hartley, F. R. *Chem. Soc. Rev.* **1973**, *2*, 163.
(41) Coe, B. J.; Glenwright, S. J. *Coord. Chem. Rev.* **2000**, *203*, 5.
(42) Foreman, M. R. S. J.; Hill, A. F.; White, A. J. P.; Williams, D. J. *Organometallics* **2003**, *22*, 3831.
(43) Corey, J. Y. *Chem. Rev.* **2016**, *116*, 11291.
(44) Manojlovic-Muir, L.; Muir, K. W.; Ibers, J. A. *Inorg. Chem.* **1970**, *9*, 447.
(45) Frost, P. W.; Howard, J. A. K.; Spencer, J. L. *J. Chem. Soc., Chem. Commun.* **1984**, 1362.
(46) Esteruelas, M. A.; Lopez, A. M.; Mora, M.; Onate, E. *Organometallics* **2015**, *34*, 941.
(47) Beckett, M. A.; Greenwood, N. N.; Kennedy, J. D.; Thornton-Pett, M. *J. Chem. Soc., Dalton Trans.* **1986**, 795.
(48) Alcock, N. W.; Jasztal, M. J.; Wallbridge, M. G. H. *J. Chem. Soc., Dalton Trans.* **1987**, 2793.
(49) Bould, J.; Rath, N. P.; Barton, L. *Acta Crystallogr., Sect. C: Cryst. Struct. Commun.* **1996**, *C52*, 1388.
(50) Bould, J.; Crook, J. E.; Greenwood, N. N.; Kennedy, J. D. *J. Chem. Soc., Dalton Trans.* **1991**, 185.
(51) Balagurova, E. V.; Cheredilin, D. N.; Kolomnikova, G. D.; Tok, O. L.; Dolgushin, F. M.; Yanovsky, A. I.; Chizhevsky, I. T. *J. Am. Chem. Soc.* **2007**, *129*, 3745.
(52) Bould, J.; Kennedy, J. D.; Thomas, R. L.; Rath, N. P.; Barton, L. *Acta Crystallogr., Sect. C: Cryst. Struct. Commun.* **2001**, *C57*, 1245.
(53) McQuade, P.; Hupp, K.; Bould, J.; Fang, H.; Rath, N. P.; Thomas, R. L.; Barton, L. *Inorg. Chem.* **1999**, *38*, 5415.
(54) Baker, R. T.; Calabrese, J. C.; Westcott, S. A.; Marder, T. B. *J. Am. Chem. Soc.* **1995**, *117*, 8777.
(55) Hill, A. F.; McQueen, C. M. A. *Organometallics* **2014**, *33*, 1977.
(56) Buil, M. L.; Cardo, J. J. F.; Esteruelas, M. A.; Fernandez, I.; Onate, E. *Organometallics* **2014**, *33*, 2689.
(57) Esteruelas, M. A.; Fernandez, I.; Lopez, A. M.; Mora, M.; Onate, E. *Organometallics* **2014**, *33*, 1104.
(58) Buil, M. L.; Cardo, J. J. F.; Esteruelas, M. A.; Fernandez, I.; Onate, E. *Organometallics* **2015**, *34*, 547.
(59) Esteruelas, M. A.; Fernandez-Alvarez, F. J.; Lopez, A. M.; Mora, M.; Onate, E. *J. Am. Chem. Soc.* **2010**, *132*, 5600.
(60) Esteruelas, M. A.; Fernandez, I.; Garcia-Yebra, C.; Martin, J.; Onate, E. *Organometallics* **2017**, *36*, 2298.
(61) Foreman, M. R. S. J.; Hill, A. F.; White, A. J. P.; Williams, D. J. *Organometallics* **2004**, *23*, 913.

Chapter 3

Poly(methimazolyl)borane Complexes of Ruthenium

3.1 Introduction

3.1.1 Metallaboratranes

The long-postulated dative (polar covalent) M→B bond was first authenticated in 1999 with the isolation and structural characterisation of the complexes [M{κ^4-*B,S,S',S''*-B(mt^{Me})$_3$}(CO)(PPh$_3$)] (M = Ru, Os). These were described as metallaboratranes, consisting of tricyclo-[3.3.3.0] cage structures featuring a transannular dative metal-boron bond.[1]

Since their discovery, metallaboratrane complexes of Tm$^{R'}$ with Group 8 to 10 metals have been reported by Hill (Os,[2] Ru,[1,3] Rh,[4-6] Ir,[7] Pt[8-10]), Parkin (Fe,[11] Pd,[12] Rh and Ir,[13] Ni[14]), Rabinovich (Co[15]), Tatsumi (Ni[16]), Connelly (Rh[17]) and Zhang (Ru[18]). Initial examples of metallaboratrane complexes included metal centres of low formal oxidation state (Ru^0, Os^0)[1,2,19],* whereas it was later shown that metal-boron dative bonding was also viable for metals in positive oxidation states (Rh^I, Ir^I, Pt^{II})[4,10,20]. The structurally characterised complexes are displayed in Figure 3.1. The various geometries adopted by these complexes has been a topic for discussion.[21]

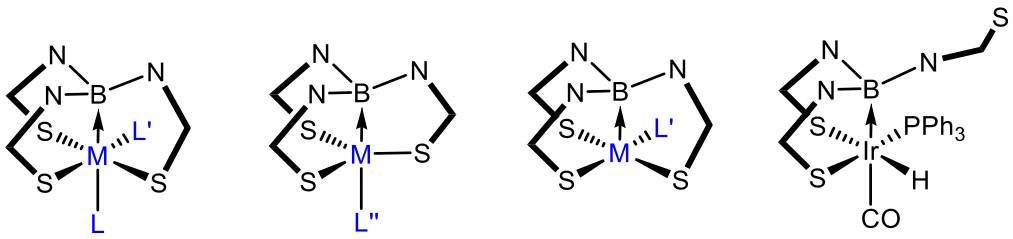

MLL' Ru(CO)(PPh$_3$), Ru(CO)(CNC$_6$H$_2$Me$_3$), Ru(CO)(CNCMe$_3$), Ru(CS)(PPh$_3$)
Os(CO)(PPh$_3$), Fe(CO)$_2$
RhCl(PPh$_3$), Rh(PMe)$_2^+$, Rh(PPh$_3$)(CNC$_6$H$_2$Me$_3$), Rh(PPh$_3$)(CNC$_6$H$_3$Me$_2$)
IrCl(PPh$_3$), PtI$_2$, PtH(PPh$_3$)$^+$

ML'' Co(PPh$_3$)$^+$, NiCl, Ni(NCS), Ni(N$_3$), Ni(OCOMe), Pd(PMe$_3$)

ML' Rh(PPh$_3$)$^+$

Figure 3.1: Crystallographically authenticated metallaboratrane complexes.

There has been considerable debate on the nature of the bonding. In particular, the allocation of the valence electrons within metallaboratrane systems to either the metal or boron has been contentious.[13,21-24] Most complexes reported to date favour a M→B

* Formal oxidation state assignment allocates the bonding pair of electrons to the more electronegative element (Pauling electronegativities: B = 2.04; Ru, Os = 2.20).

bonding representation that suggests the partial donation of two electrons from the metal-based orbital to the Lewis acidic B centre, i.e., a polar-covalent or dative bond.[†] As a corollary of this bonding, metallaboratrane complexes are particularly prevalent for electron-rich metals with high d-occupancies (d^n $n \geq 8$, Group 8 onwards). In contrast, the earlier metals (Groups 3-7) in commonly encountered oxidation states lack the appropriate number of electrons to satisfy the bonding requirement for a σ-basic metal centre.

As numerous metallaboratrane complexes are derived from B–H activation of Tm^R ligands, this led to speculation about the contribution of the chelated tricyclo-[3.3.3.0] cage to the stability of the complex. Initial arguments suggest that metallaboratrane dative bonding was a consequence of the geometric proximity of the metal and boron, which was constrained by the tricyclo-[3.3.3.0] cage. In 2005, the less geometrically constrained iridaboratranes [IrH{κ^3-*B,S,S'*-B(mt^{Me})$_3$}(CO)(PPh_3)] **L3.1** and [IrH{κ^3-*B,S,S'*-HB(mt^{Me})$_2$}(CO)(PPh_3)] **L3.2** were reported (Scheme 3.1).[20] The M→B interaction is favoured in **L3.1** despite the potential for the Tm ligand to coordinate in the κ^3-*S,S',S''* mode. This showed that the predilection for M→B dative bonding was not simply a response to fortuitous geometric juxtaposition of boron and iridium. Metallaboratrane complexes supported by two buttresses are rare, and iridaboratrane **L3.2** is thus far the only reported isolated example derived from $Bm^{R'}$.

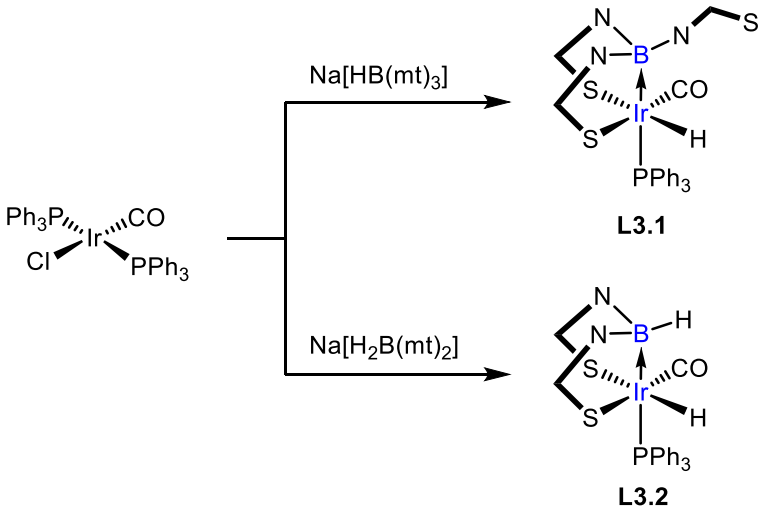

Scheme 3.1: Synthesis of iridaboratranes **L3.1** and **L3.2**.

[†] The M→B notation is used from here onwards to emphasise the polar-covalent (dative) nature of metal-boron bonding in metallaboratranes, as suggested in the literature.[22] It is appreciated that conventional ligands also exhibit (reverse) dative bonding, e.g. Ph_3P→M, which are implicit by line drawings.

3.1.2 Mechanistic Discussion

The driving force behind metallaboratrane formation is attributable to a confluence of appropriate d-orbital occupancy, geometric factors and metal σ basicity. Their formation can be facilitated by the presence of a σ-organyl co-ligand as a hydrogen acceptor through irreversible elimination of RH (where the H is from the borate ligand). This is the case in the reaction of $[M(R)Cl(L)(PPh_3)_2]$ (ML = RuCO, OsCO, Ru(CS), RhCl; R = aryl, vinyl) with $Na[HB(mt^{Me})_3]$. However, the presence of a hydrogen acceptor is not crucial to metallaboratrane formation, as is exemplified by the synthesis of $[PtH\{\kappa^4\text{-}B,S,S',S''\text{-}B(mt^{Me})_3\}(PPh_3)]Cl$ from $[PtCl_2(PPh_3)_2]$.[25] In other cases, the $[HB(mt)_3]^-$ ligand coordinates in a tridentate κ^3-*S,S',S''* mode where the B–H moiety remains intact. For $[PtMe_3\{\kappa^3\text{-}S,S',S''\text{-}HB(mt^{Me})_3\}]$, no isomerisation to the κ^3-*S,S',H* mode occurs even under prolonged forcing conditions (24 hour toluene reflux), although the corresponding κ^3-*H,S,S'*-Bm^{Me} complex $[PtMe_3\{\kappa^3\text{-}H,S,S'\text{-}H_2B(mt^{Me})_2\}]$ is known. The conditions that lead to metallaboratrane formation are thus intriguing and vary considerably.

One postulated mechanism involves the initial formation of an elusive intermediate with B–H–M connectivity. The B–H bond is subsequently cleaved by electron donation from the appropriately π-basic metal to the B–H σ* orbital, ultimately resulting in the formation of a metallaboratrane (Scheme 3.2a). Evidence for this mechanistic pathway was obtained from isolation of the intermediate complex bicyclo-[3.3.0] iridaboratrane **L3.1**.[20]

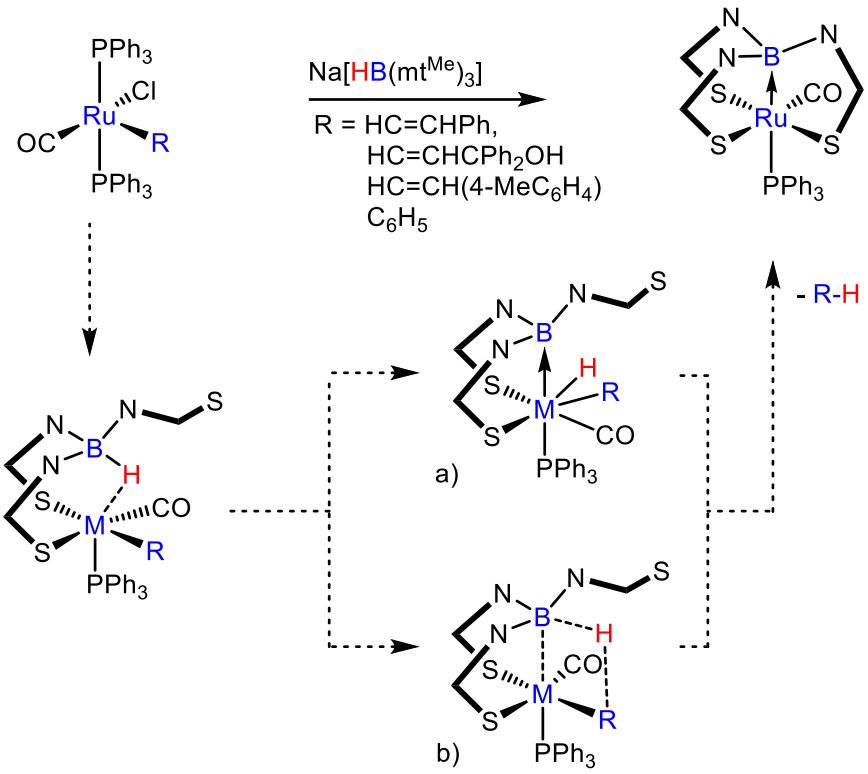

Scheme 3.2: Mechanistic conjecture regarding metallaboratrane formation through a) sequential insertion and reductive elimination and b) concerted σ-metathesis.

Another potential mechanistic pathway to metallaboratranes involves concerted σ-metathesis between the B–H and Ru–H bonds (Scheme 3.2b). Owen suggested that the complex [RuCl(PCy$_3$){κ^4-HB(CH$_2$Ph)(mt^{Me})$_2$}] **L3.3** (Scheme 3.3), obtained from Grubbs' catalyst and Na[H$_2$B(Mt^{Me})$_2$], represented a midway point of hydride migration between the metal and boron.[26] Established through an X-ray diffraction study, the structure revealed *trans*-coordinated sulfur donors of the Bm-derived ligand and interaction between the ruthenium with the B–H and benzyl methylene unit. The location of the metal associated hydrogens was further supported by DFT calculations. Deuterium labelling studies with Na[D$_2$B(mt^{Me})$_2$] showed that formation of the benzyl group was irreversible, consistent with the observed migration of one hydrogen/deuterium from the borate moiety. Ultimately, migration of the benzyl fragment and rearrangement to a wider S–Ru–S angle affords complex **L3.3**. The *trans*-disposition of the usually facially coordinating Bm$^{R'}$ ligand remains uncommon.

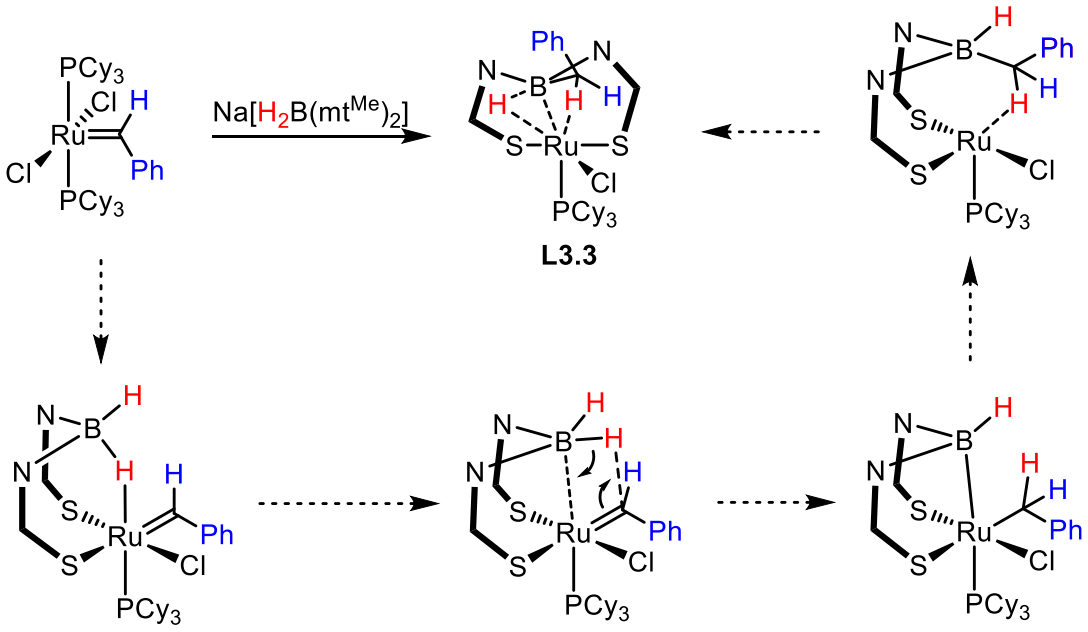

Scheme 3.3: Proposed mechanism of hydride migration in the formation of **L3.3**.

Of intrigue is the rate of the final step in metallaboratrane formation for $Tm^{R'}$ tricyclo-[3.3.3.0] systems, specifically, the chelation of the third methimazolyl donor. A solution of complex [Rh(CO)(PPh_3){κ^3-*H,S,S'*-HB(mt^{Me})$_3$}] **L3.4** partially converts into rhodaboratrane [Rh{κ^4-*B,S,S',S''*-B(mt^{Me})$_3$}(CO)(PPh_3)]Cl **[L3.6]$^+$** with no observation of the B–H activated intermediate, [RhH{κ^3-*B,S,S'*-B(mt^{Me})$_3$}(CO)(PPh_3)] **L3.5** (Scheme 3.4). The analogous reaction between Vaska's complex [IrCl(CO)(PPh_3)$_2$] and $NaTm^{Me}$ afforded exclusively the B–H activated product [IrH{κ^3-*B,S,S'*-B(mt^{Me})$_3$}(CO)(PPh_3)] **L3.8**, rapidly bypassing the inferred B–H–Ir 3c2e coordinated complex [Ir(CO)(PPh_3){κ^3-*H,S,S'*-HB(mt^{Me})$_3$}] **L3.7**. Relative to the rhodium derivative, the conversion to the iridaboratrane [Ir{κ^4-*B,S,S',S''*-B(mt^{Me})$_3$}(CO)(PPh_3)]Cl **[L3.9]$^+$** was much slower. Greater conversion could be effected by addition of HCl to iridaboratrane **L3.8**, or treatment of rhodaboratrane **L3.4** with [Fe(η-C_5H_5)$_2$]PF_6/NH^iPr_2.[7,17] Together these observations suggested that B–H activation is less favourable and hydride replacement is more facile at rhodium than iridium.

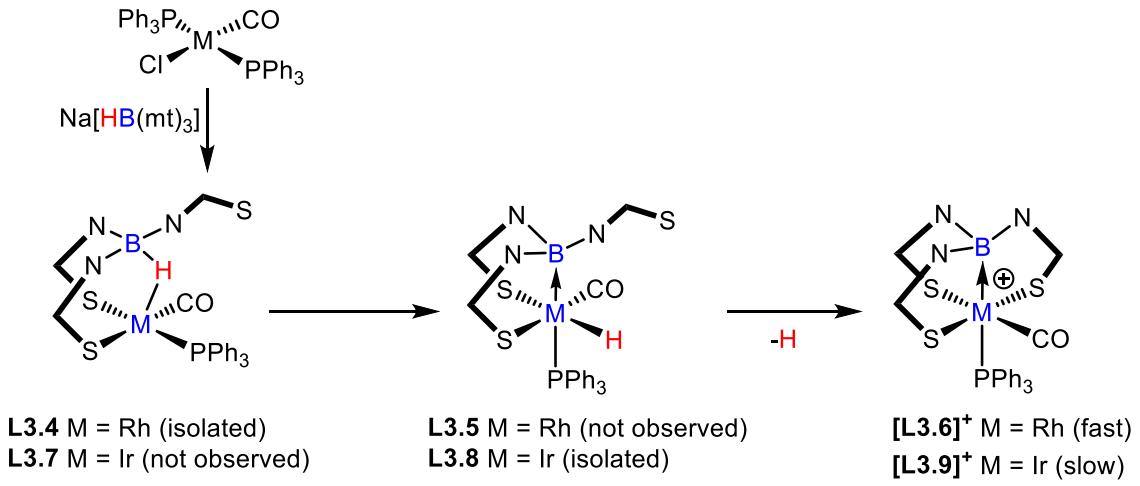

L3.4 M = Rh (isolated)
L3.7 M = Ir (not observed)

L3.5 M = Rh (not observed)
L3.8 M = Ir (isolated)

[L3.6]$^{+}$ M = Rh (fast)
[L3.9]$^{+}$ M = Ir (slow)

Scheme 3.4: Comparison of final coordination step in metallaboratrane formation for rhodium and iridium systems.

Given that activation of a bridging B–H–M moiety is the key feature in the formation of metallaboratranes, the resulting M→B bond housed within the tricyclo-[3.3.3.0] framework is suspected of having non-reactive innocent behaviour. Whilst this holds true for the bulk of $Tm^{R'}$ complexes in the literature, reversible M→B bond formation was observed during ligand substitution studies of [PtH{κ^4-*B,S,S',S''*-B(mt^{Me})$_3$}(PTol$_3$)]Cl **[L3.10]**Cl (Tol = C_6H_4Me-4) with the phosphines PR_3 (R = Me, Et) (Scheme 3.5).[9] The resulting complexes were formulated as [Pt(PR$_3$)$_2${κ^2-*S,S'*-HB(mt^{Me})$_3$}]Cl (R = Me **[L3.11a]**Cl, Et **[L3.11b]**Cl) in which the migration of the platinum hydride to boron reconstitutes a B–H bond. This likely proceeds through unobserved intermediates (or transition states) with B–H–M 3c2e interactions [Pt(PTol$_3$){κ^3-*H,S,S'*-HB(mt^{Me})$_3$}]Cl **[L3.10a]**Cl and subsequent PR_3 coordination to generate [Pt(PR$_3$)(PTol$_3$){κ^{2-}*S,S'*-HB(mt^{Me})$_3$}]Cl **[L3.10b]**Cl.

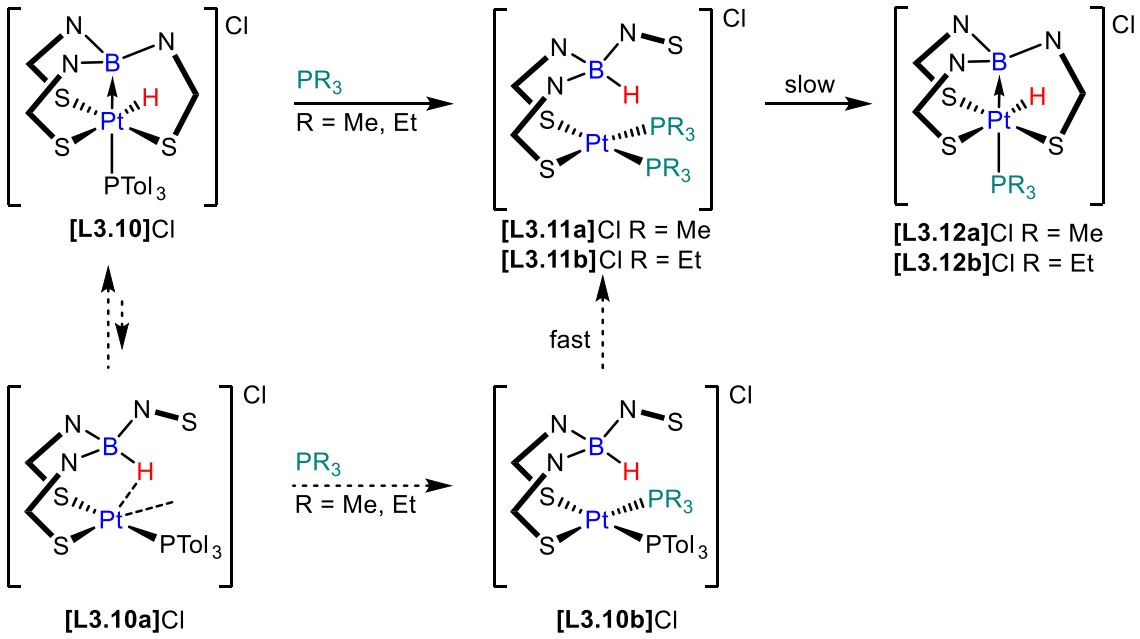

Scheme 3.5: Reversible M→B bond formation with mechanistic conjecture. Tol = C_6H_4Me-4.

In solution, complexes **[L3.11a]**Cl and **[L3.11b]**Cl show reformation of the M→B bond, albeit slowly and in low conversion (30-50%), to yield the metallaboratrane complexes [PtH{κ^4-*B,S,S′,S″*-B(mt^{Me})$_3$}(PR$_3$)]Cl (**[L3.12a]**Cl and **[L3.12b]**Cl); thereby confirming that B–H bond formation preceded phosphine substitution. The greater Tolman cone angle of PEt$_3$ (132°) relative to PMe$_3$ (118°) was suggested to encourage faster conversion to [PtH{κ^4-*B,S,S′,S″*-B(mt^{Me})$_3$}(PR$_3$)]Cl (50% conversion with PEt$_3$ *cf.* 30% for PMe$_3$).

Cleavage of the M→B bond has been further demonstrated by Parkin in 1,2-addition reactions across the M→B bond for iron and nickel metallaboratranes, [Fe{κ^4-*B,S,S′,S″*-B(mt^{tBu})$_3$}(CO)$_2$] **L3.13** and [NiY{κ^4-*B,S,S′,S″*-B(mt^{tBu})$_3$}] (Y = Cl, NCS, N$_3$) **L3.15** (Scheme 3.6).[11,14] Reaction of **L3.13** with CHX$_3$ (X = Cl, Br), I$_2$ in CHCl$_3$ or (PhCO$_2$)$_2$ affords the respective products [FeX′{κ^3-*S,S′,S″*-XB(mt^{tBu})$_3$}]$^+$ (X = X′: Cl **[L3.14a]$^+$**, Br **[L3.14b]$^+$**), [FeI{κ^3-*S,S′,S″*-ClB(mt^{tBu})$_3$}]$^+$ **[L3.14d]$^+$**, and [Fe(O$_2$CPh){κ^3-*S,S′,S″*-(O$_2$CPh)B(mt^{tBu})$_3$}]$^+$ **[L3.14c]$^+$**. For complex **L3.15**, reaction with I$_2$ yields [NiI{κ^3-*S,S′,S″*-XB(mt^{tBu})$_3$}] (X = Cl, NCS, N$_3$) **L3.16d**, while the reaction of [NiCl{κ^4-*B,S,S′,S″*-B(mt^{tBu})$_3$}] with CHCl$_3$, CHBr$_3$ or XeF$_2$ generates [NiX′{κ^3-*S,S′,S″*-ClB(mt^{tBu})$_3$}] (X′ = Cl **L3.16a**, Br **L3.16b**, and [NiCl{κ^3-*S,S′,S″*-FB(mt^{tBu})$_3$}] **L3.16c** respectively. Similar M→B bond cleavage reactions have been reported by Peters for ferraboratranes buttressed by a triphosphinoborane scaffold.[27,28]

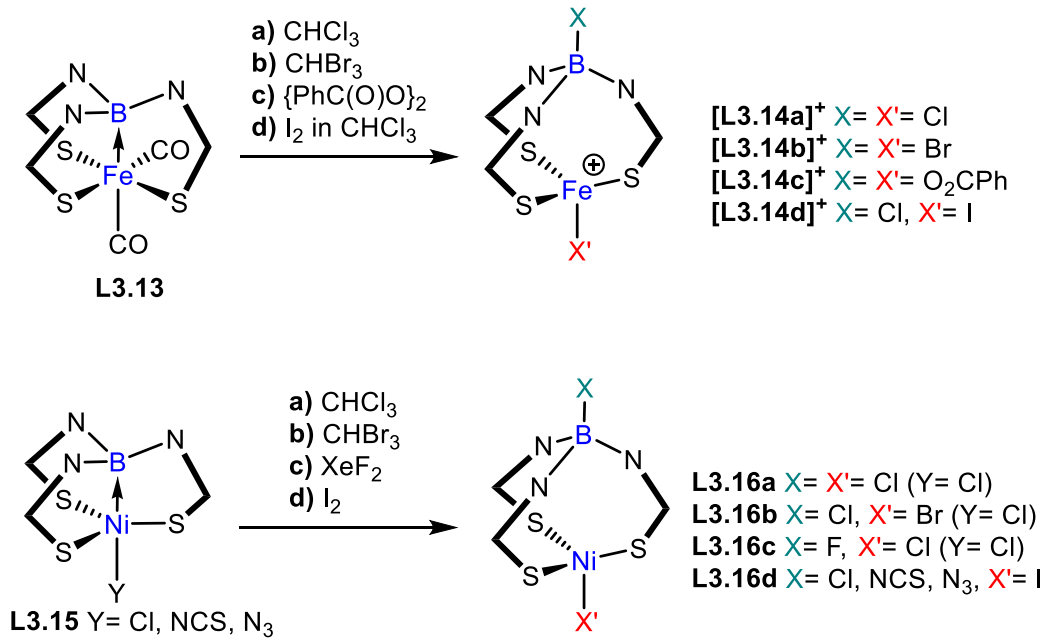

Scheme 3.6: Addition across the M→B bond in metallaboratranes of iron and nickel.

In contrast to Parkin's report, reaction of platinaboratrane [Pt{κ⁴-*B,S,S',S''*-B(mt^{Me})$_3$}(PPh$_3$)] **L3.17** with Cl_2, Br_2, I_2 or MeI (Scheme 3.7) resulted in retention of the Pt→B interaction. Instead, oxidative halogenation occurred on the platinum centre to yield the octahedral platinaboratranes [Pt{κ⁴-*B,S,S',S''*-B(mt^{Me})$_3$}XX'] **L3.18** (X = X' = Cl, Br; X = Me, X' = I).[8] The Pt→B interaction also remains intact in the reverse process, e.g., dehydrochlorination of platinum(II) **L3.18**.[10] The lack of reactivity of the Pt→B bond in **L3.17** compared to the readily cleaved Ni→B bond in **L3.15** is consistent with Bourissou's experimental and theoretical calculations on ambiphilic triphosphinoborane systems that show a stronger Pt→B interaction than Ni→B.[29]

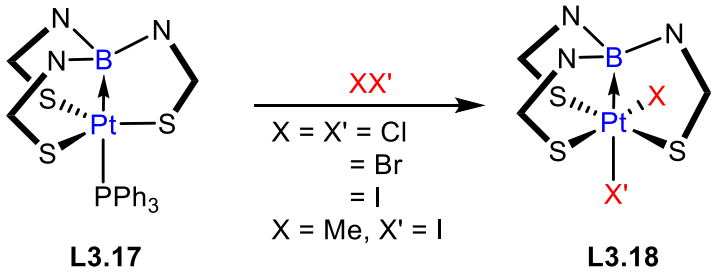

Scheme 3.7: Oxidative addition reactions of platinum(0) complex **L3.17**.

3.2 Synthesis of [Ru{κ³-*B,S,S'*-BH(mt)₂}(CO)(PPh₃)₂]

The attempted synthesis of [Ru(X)(CO)(PPh₃){κ³-*H,S,S'*-H₂B(mt)₂}] (X = Ph **2.7**, CH=CHPh **2.8**) described in Chapter 2 revealed an unstable B–H–Ru interaction where subsequent elimination of XH yields [Ru{κ³-*B,S,S'*-BH(mt)₂}(CO)(PPh₃)₂] **3.1** as the first doubly-bridged ruthenaboratrane. The observation of **2.7** and **2.8** *en route* to **3.1** provides further support for the mechanism of metallaboratrane formation, which proceeds through a κ³-*H,S,S'* coordinated intermediate (Scheme 3.2) as proposed for the Tm analogue [Ru{κ⁴-*B,S,S',S''*-B(mt)₃}(CO)(PPh₃)].[19] In the previous chapter, ^{1}H and ^{31}P{^{1}H} NMR spectral data and HR-ESI+ MS measurements collected from NMR scale reactions support the formation of complex **3.1**. Given the rarity of doubly-bridged metallaboratrane complexes, a preparative scale synthesis of **3.1** was explored.

The seminal report detailing the formation of the metallaboratrane [Ru{κ⁴-*B,S,S',S''*-B(mt)₃}(CO)(PPh₃)] was performed in dichloromethane. When the reaction was carried out in diethyl ether, non B–H activated intermediates of the form [Ru(R)(CO)(PPh₃){κ³-*S,S',S''*-HB(mt)₃}] (R = CH=CHPh₂OH, CH=CH₂, CH=CH(4-MeC₆H₄), C₆H₅) precipitated from solution.[1,19] Characterisational data were, however, rather limited and equivocal due to rapid evolution of these intermediates to the metallaboratrane upon dissolution in solvents suitable for spectroscopic studies. The NMR scale experiment in $CDCl_3$ leading to **3.1** *via* complex **2.7** provided approximately 8 products (Chapter 2). Therefore, by analogy to the tri-buttressed metallaboratrane, it was envisaged that a more controlled reaction may ensue from the reaction of [Ru(Ph)Cl(CO)(PPh₃)₂] with Na[H₂B(mt)₂] as a diethyl ether suspension (Scheme 3.8).

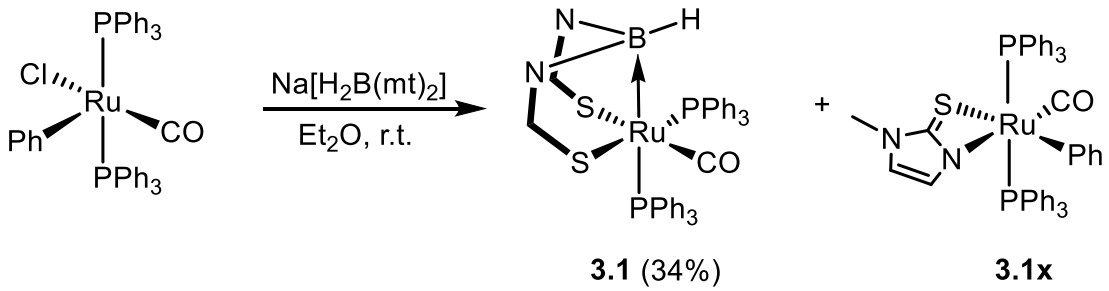

3.1 (34%) **3.1x**

Scheme 3.8: Preparative scale synthesis of **3.1** from [Ru(Ph)Cl(CO)(PPh₃)₂].

The initially orange suspension lightened in colour over 15 hours to yield a beige solid. The IR (ATR) spectrum of the solid revealed two CO bands at 1893 and 1910 cm^{-1}, where the low stretching frequency of the former was consistent with the electron-rich

formally Ru(0) centre of **3.1**. A band was also noted at 2316 cm^{-1} and is characteristic of a terminal borohydride. In the ^{1}H and $^{31}P\{^{1}H\}$ NMR spectra of the solid, two products were identified as **3.1** and the previously reported complex [Ru(Ph)(κ^2-*N,S*-mt)(CO)(PPh_3)$_2$] **3.1x** (in a respective 4:1 ratio).[30] The NMR and IR data of **3.1x** were consistent with the reported values (δ_P = 40.0, IR = ν_{CO} 1908 cm^{-1}). The impurity **3.1x** was removed by washing with diethyl ether, albeit compromising the isolated yield (34%) of **3.1**. Crystals of **3.1** and **3.1x** suitable for X-ray diffraction were obtained from slow evaporation of a diethyl ether solution of the crude sample (Figure 3.2). The molecular structure of **3.1x** was first reported by Wilton-Ely as a dichloromethane solvate. The non-solvated structure in Figure 3.2b shows structural similarities to Wilton-Ely's report and calls for little comment.

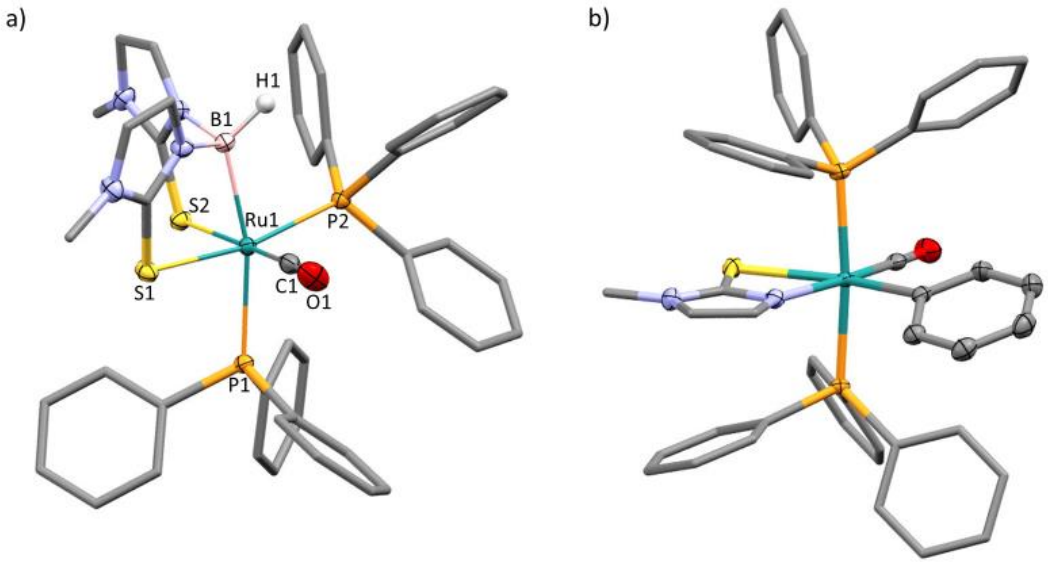

Figure 3.2: a) Molecular structure of [Ru{κ^3-*B,S,S'*-BH(mt)$_2$}(CO)(PPh_3)$_2$] **3.1**.$C_4H_{10}O$ (solvent omitted, organic hydrogen atoms omitted, phenyl groups simplified, displacement ellipsoids shown at 50% probability). Selected bond lengths (Å) and angles (°) of **3.1**: B1–Ru1 2.2463(16), B1–H1 1.17(2),[‡] Ru1–P1 2.4766(4), Ru1–P2 2.3045(4), Ru1–C1 1.8336(16), H1–B1–Ru1 123.3(13), N2–B1–H1 104.7(12), N3–B1–H1 106.1(12), B1–Ru1–P1 166.36(4), B1–Ru1–P2 84.13(4), P1–Ru1–P2 108.061(13). b) Non-solvated [Ru(Ph)(κ^2-*N,S*-mt)(CO)(PPh_3)$_2$] **3.1x**.

The formulation of **3.1** was confirmed by an X-ray crystallography study and spectroscopic, mass spectrometry and analytical data. The molecular structure of **3.1**

[‡] Where applicable, the hydrogen on boron (B1–H1) in the molecular structures reported in this chapter, was located on a Fourier Difference map and refined isotropically.

(Figure 3.2a) reveals a distorted octahedral geometry at ruthenium and a distorted tetrahedral geometry about boron with angles in the range of 104.7(12)–123.2(13)°. The Ru1–B1 bond length of 2.2463(16) Å in **3.1** is comparatively longer than found in the corresponding Tm analogue (2.161(5) Å; 17 e.s.d.) but, as expected, shorter than the Ru···B distance in the κ^3-*H,S,S'* complexes **2.1**–**2.5** which span the range 2.651–2.897 Å. Considering the comparable covalent radii of ruthenium and iridium (r_{cov}(Ru) = 1.46, r_{cov}(Ir) = 1.41),[§] the Ru1–B1 bond distance of 2.2463(16) Å in **3.1** is similar to the Ir→B bond in [IrH{κ^3-*B,S,S'*-BH(mt)$_2$}(CO)(PPh$_3$)], which has a bond distance of 2.210(5) Å.

Notably, the two Ru–P bonds shown in Figure 3.2a are significantly different in length (Ru1–P1 2.4766(4) *cf.* Ru1–P2 2.3045(4) Å, 430 e.s.d.), where the phosphine *trans* to boron exhibits a far longer bond than that *trans* to sulfur. The disparity of the Ru–P bond lengths in **3.1** and derivatives are discussed in Section 3.6. In contrast to the analogous Tm complex, [Ru{κ^4-*B,S,S',S''*-B(mt)$_3$}(CO)(PPh$_3$)], with only one triphenylphosphine for investigations into substitution reactivity, the two triphenylphosphines within complex **3.1** are available as potential sites for substitution.

The low symmetry of complex **3.1** (C_1) was reflected in the two distinct methyl resonances in the ^{1}H NMR spectrum at δ_H = 3.07 and 3.33, as well as four signals at δ_H = 6.04, 6.15, 6.50 and 6.58 (d, $^3J_{HH}$ ≈ 1.8 Hz) associated with each separate ^{1}H environment in the olefinic backbone. Consistent with the ^{1}H NMR spectrum, ^{13}C{^{1}H} NMR spectroscopy allowed the two methyl and four olefinic resonances of the methimazolyl group to be identified.

Despite the broadening of the borohydride resonance by the quadrupolar boron nuclei (^{10}B and ^{11}B), the BH resonance was located at δ_H = 4.07. A single boron environment was detected at δ_B = 4.12 in the ^{11}B{^{1}H} NMR spectrum, which is downfield of the boron signal in complexes **2.1**–**2.5**, consistent with a borane unit compared to the borate moiety of the latter. The resonance in the ^{11}B NMR spectrum was similarly broad (h.h.w. = 455 Hz), and thus precluded the resolution of B–H coupling constants in the ^{1}H-coupled spectrum.

[§] The second and third row transition metals are known to have similar covalent radii, owing to the lanthanide contraction.

As observed in the NMR scale experiments detailed in Chapter 2, the two phosphine environments were located at δ_P = 19.3 and 52.7 (C_6D_6), where the broadness of the latter resonance suggested coordination *trans* to the boron. To assess whether the two phosphines in **3.1** exchange on the NMR timescale, variable temperature NMR experiments were performed. The two phosphine environments remain stationary at δ_P = 21.1 and 52.8 throughout the temperature range 25–75°C (in d_8-toluene), suggesting no exchange was occurring between the two phosphines. However, progressive broadening of the resonance of the PPh_3 *trans* to boron (δ_P = 21.1) was observed in the ^{31}P NMR spectra with increasing temperature, merging into the baseline at 66°C, whereas the resonance of PPh_3 *trans* to sulfur (δ_P = 52.8) remained consistently sharp. The absence of free PPh_3 (δ_P = –5.3) allowed ligand association and dissociation processes to be excluded. As the broadening is markedly greater for the PPh_3 bound *trans* to boron than that *trans* to sulfur, this might reflect the effect of the temperature dependent nuclear quadrupole spin-lattice relaxation time of the boron nucleus[31] (thermal decoupling)[32,33] on the phosphorus nuclei. Although sharpening of the boron resonance is expected at higher temperatures, it is currently unclear how this effect translates into nuclei that are coordinated *trans* and share the same metal orbital.

The formation of metallaboratrane **3.1** occurs with the extrusion of arene or alkene, from ruthenium precursors [Ru(Ph)Cl(CO)(PPh_3)$_2$] or [Ru(CH=CHPh)Cl(CO)(PPh_3)$_2$] respectively. These reagents can be obtained from treatment of [RuHCl(CO)(PPh_3)$_3$] with mercuric reagents (HgR_2; R = Ph, CH=CHPh).[34,35] An alternate and less toxic route to complex [Ru(CH=CHPh)Cl(CO)(PPh_3)$_2$] is *via* hydroruthenation of phenylacetylene.[36,37] Generation of [Ru(CH=CHPh)Cl(CO)(PPh_3)$_2$] and subsequent use *in situ* was explored in a one-pot methodology for the synthesis of **3.1**. The one-pot synthesis includes reaction of [RuHCl(CO)(PPh_3)$_3$] with phenylacetylene to form [Ru(CH=CHPh)Cl(CO)(PPh_3)$_2$] *in situ*, which is subsequently treated with Na[H_2B(mt)$_2$] for 18 hours to afford complex **3.1** in a 61% yield (Scheme 3.9). The synthesis has been successfully scaled up to 2-3 grams with similar yields (43–58%).

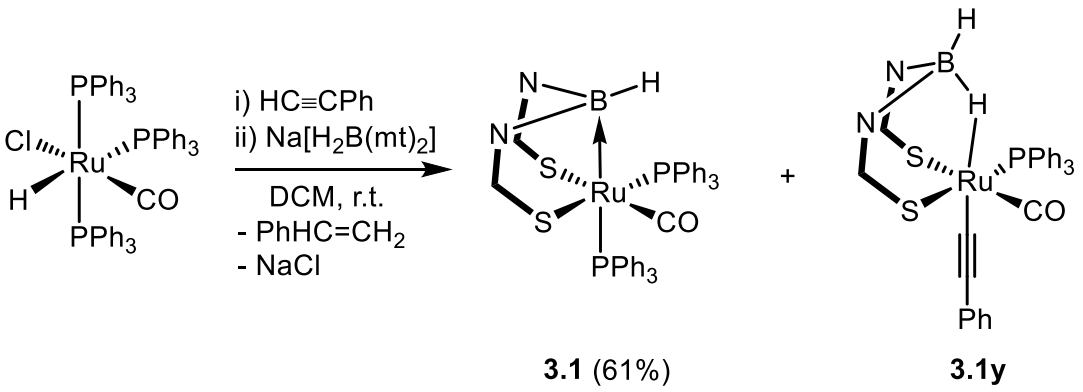

Scheme 3.9: One-pot synthesis of **3.1** and identification of **3.1y** by-product.

This preparatory route generates *ca* 3% of by-products that resonate at δ_P = 38.0, 41.7 and 50.2 in the $^{31}P\{^1H\}$ NMR spectrum. Through an X-ray crystallography study, one by-product was identified as [Ru(C≡CPh)(CO)(PPh_3){κ^3-*H,S,S'*-$H_2B(mt)_2$}] **3.1y** (Figure 3.3). Complex **3.1y** was only obtained in quantities sufficient for X-ray crystallography experiments. The molecular structure of **3.1y** consists of the same ligand set, '[Ru(CO)(PPh_3){$H_2B(mt)_2$}]', as the complexes **2.1**–**2.5**, with the borate ligand similarly facially capping the ruthenium centre in a κ^3-*H,S,S'* coordination mode. The structural features of complex **3.1y** fall within the range established by the series **2.1**–**2.5** in Chapter 2. Key features of **3.1y** include the Ru···B distance of 2.740 Å (*cf.* 2.651–2.897 Å) and B–H–Ru angle of 134(3)° (*cf.* 128–138°).

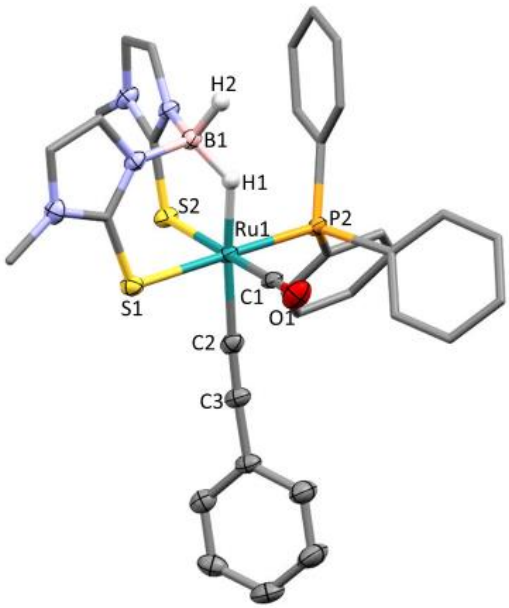

Figure 3.3: Molecular structure of [Ru(C≡CPh)(CO)(PPh_3){κ^3-*H,S,S'*-$H_2B(mt)_2$}] **3.1y**.$CHCl_3$ (solvent omitted, organic hydrogen atoms omitted, phenyl groups simplified, displacement ellipsoids shown at 50% probability). Selected bond lengths (Å) and angles (°): B1···Ru1 2.740, B1–H1 1.24(4), B1–H2 1.19(4), Ru1–H1 1.74(4), Ru1–P1 2.3228(6), Ru1–C1 1.864(2), Ru1–C2 2.028(3), C2–C3 1.200(4), C3–C4 1.448(3), B1– H1–Ru1 134(3), H1–Ru1–C2 173.3(14), S2–Ru1–P1 176.25(2), S1–Ru1–P1 87.20(2), S1–Ru1–S2 89.82(2).

The mechanistic pathways in the formation of **3.1y** are shown in Scheme 3.10, which is adapted from a report by Echavarren and co-workers on the mechanistic elucidation of phenylacetylene oligomerisation and polymerisation processes facilitated by ruthenium(II) complexes.[38] The relationship between the ruthenium hydride [RuHCl(CO)(PPh_3)$_3$] and styryl [Ru(CH=CHPh)Cl(CO)(PPh_3)$_2$] complexes is shown in Scheme 3.10. Conversion of [Ru]–H to [Ru]–CH=CHPh occurs readily with an excess of phenylacetylene, whereas the reverse reaction involving β-hydride elimination of the styryl group to reform phenylacetylene and [Ru]–H requires heating (≈80°C). The proposed mechanism for **3.1y** involves further reactivity of [Ru]–CH=CHPh with phenylacetylene, involving coordination and migratory insertion processes to form (i). This is followed by oxidative addition of another phenylacetylene molecule and reductive elimination of the diene in (ii) to give [Ru]–C≡CPh. Reaction of this coordinatively unsaturated/labile [Ru]–C≡CPh complex with Na[$H_2B(mt)_2$] subsequently gives **3.1y**.

As the one-pot synthesis of **3.1** was performed at room temperature, the [Ru]–CH=CHPh complex generated *in situ* was envisaged to immediately react with $Na[H_2B(mt)_2]$ resulting in the desired product **3.1**. Therefore, the derivative pathway towards **3.1y** was perceived as a minor side reaction.

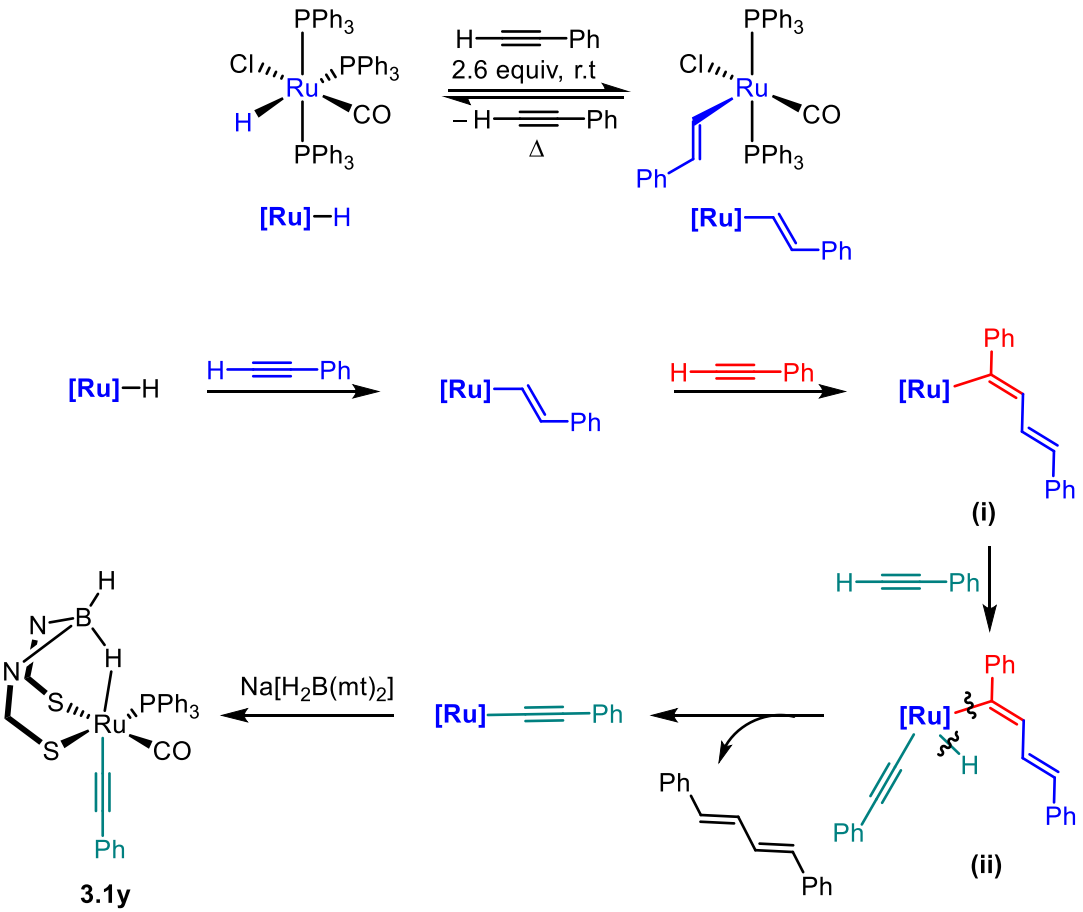

Scheme 3.10: Proposed mechanism for the formation of **3.1y**.

Another mechanistic consideration is the potential for the transient $[Ru(CH{=}CHPh)(CO)(PPh_3)\{\kappa^3\text{-}H,S,S'\text{-}H_2B(mt)_2\}]$ **2.8** complex to engage in further reaction with phenylacetylene to form the acetylide unit in **3.1y**. This would require creation of a vacant coordination site on the coordinatively saturated **2.8**, presumably from *hemilabile* dissociation of the BH–Ru bond of the κ^3-*H,S,S'* bound borate ligand. Whilst conversion to **3.1** precludes isolation of **2.8** (Chapter 2), the series of analogous complexes $[Ru(X)(CO)(PPh_3)\{\kappa^3\text{-}H,S,S'\text{-}H_2B(mt)_2\}]$ **2.1**–**2.5** would suggest a fairly robust κ^3-*H,S,S'* coordination. This was explored by treatment of **2.1** with phenylacetylene in $CDCl_3$ at room temperature where insertion into a ruthenium-hydride bond might be expected, thereby affording **3.1y** (Scheme 3.11). Instead, no reaction between the two reagents was detected.

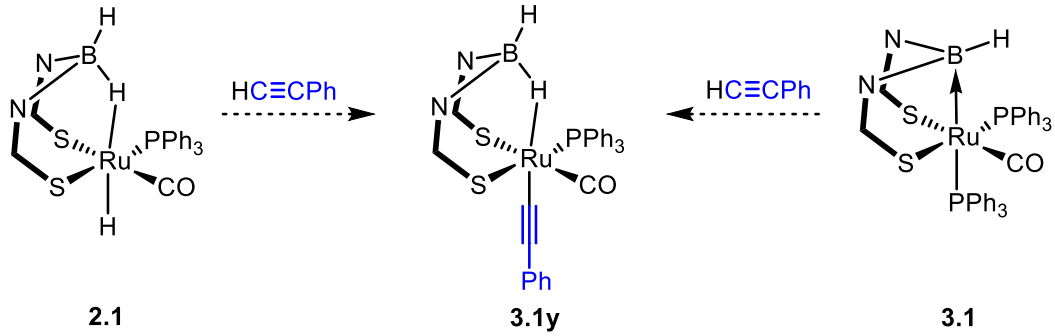

Scheme 3.11: Attempted synthesis of **3.1y** from complexes **2.1** and **3.1**.

An alternate synthesis of the complex through treatment of **3.1** with phenylacetylene was also explored (Scheme 3.11) where the M→B interaction might conceivably rupture upon oxidation (alkynyl C–H activation) at the metal centre. However, no reaction ensued, which is unsurprising given previous (albeit limited) reports on the comparatively inert M→B interaction in metallaboratranes.[39]

3.2.1 Chapter Aims

Given the rarity of metallaboratranes with two methimazolyl buttresses (two examples) and the greater potential for reactivity offered by a more flexible and less sterically encumbered system, the research detailed in this chapter describes investigations into the reactivity of complex **3.1**. As depicted in Figure 3.4, complex **3.1** offers the opportunity to explore reactivity of the metallaboratrane bond and substitution studies at the two phosphines.

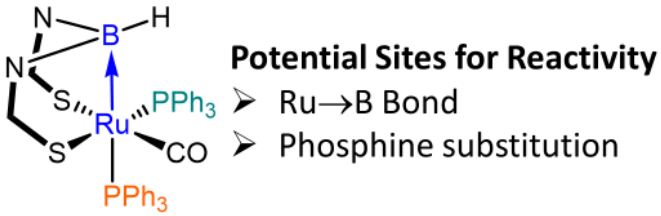

Figure 3.4: Areas of investigation in complex **3.1**.

Potential reagents suitable for substitution of the triphenylphosphine ligands include olefins, isonitriles and other phosphines. The use of phosphines of varying steric and electronic properties was expected to provide insight into the reactivity of **3.1** and influence the ligands that comprise the ruthenium coordination sphere. In 1970, Tolman introduced ligand cone angle (θ_T) as a quantitative measure of steric effects and compared the carbonyl stretching frequency in $[Ni(CO)_3L]$ (L = triply connected

phosphorus ligands) to determine the net electron donor-acceptor properties of L. Selected values are shown in Table 3.1.[40,41] To gain an understanding of the substitution process in **3.1**, phosphines of a range of electronic (σ-basic/π-acidic) and steric properties were chosen and shown in purple in Table 3.1.

Phosphine (L)	ν (cm^{-1})	θ_T (°)	Phosphine (L)	ν (cm^{-1})	θ_T (°)
$P(^tBu)_3$	2056	182	$P(OMe)Ph_2$	2072	132
PCy_3	**2056**	**170**	$PHPh_2$	2073	128
$P(^iPr)_3$	2059	160	$P(O^iPr)_3$	2076	130
PBu_3	2060	132	$P(OEt)_3$	2076	109
PEt_3	2062	132	PH_2Ph	2077	101
$P(NMe_2)_3$	2062	157	**$P(OMe)_3$**	**2080**	**107**
PMe_3	**2064**	**118**	PH_3	2083	87
PMe_2Ph	**2065**	**122**	$P(OPh)_3$	2085	128
$P(CH_2Ph)_3$	2066	165	$P(C_6F_5)_3$	2090	184
PPh_3	**2069**	**145**	PCl_3	2097	125

Table 3.1: The electronic ν_{CO} (cm^{-1}) and steric θ_T (°) properties for the phosphorus ligands in $[Ni(CO)_3L]$. Phosphine ligands used in this project are labelled in purple.

3.3 Reactivity of the Ru→B Bond in $[Ru\{\kappa^3\text{-}B,S,S'\text{-}BH(mt)_2\}(CO)(PPh_3)_2]$

The potential of the M→B interaction to engage in reactions has long been of interest, with contrasting differences between the reactivity of the complexes (Scheme 3.6 and Scheme 3.7). In particular, interconversion between coordination modes κ^3-*B,S,S'* and κ^3-*H,S,S'* *via* hydride migration from the metal centre (as discussed above for $[PtH\{\kappa^4\text{-}B,S,S',S''\text{-}B(mt^{Me})_3\}(PTol_3)]Cl$ **[L3.10]**Cl) has yet to be observed for the Bm system. Whilst some reactions can be inferred to proceed through a κ^3-*H,S,S'* bound species (as for **[L3.10]**Cl), coordination mode interchange is generally not observed, but of potential interest as a means of reversing the polarity (umpolung) of the hydrogen atom ($M–H^{\delta+}$ *cf.* $B–H^{\delta-}$).

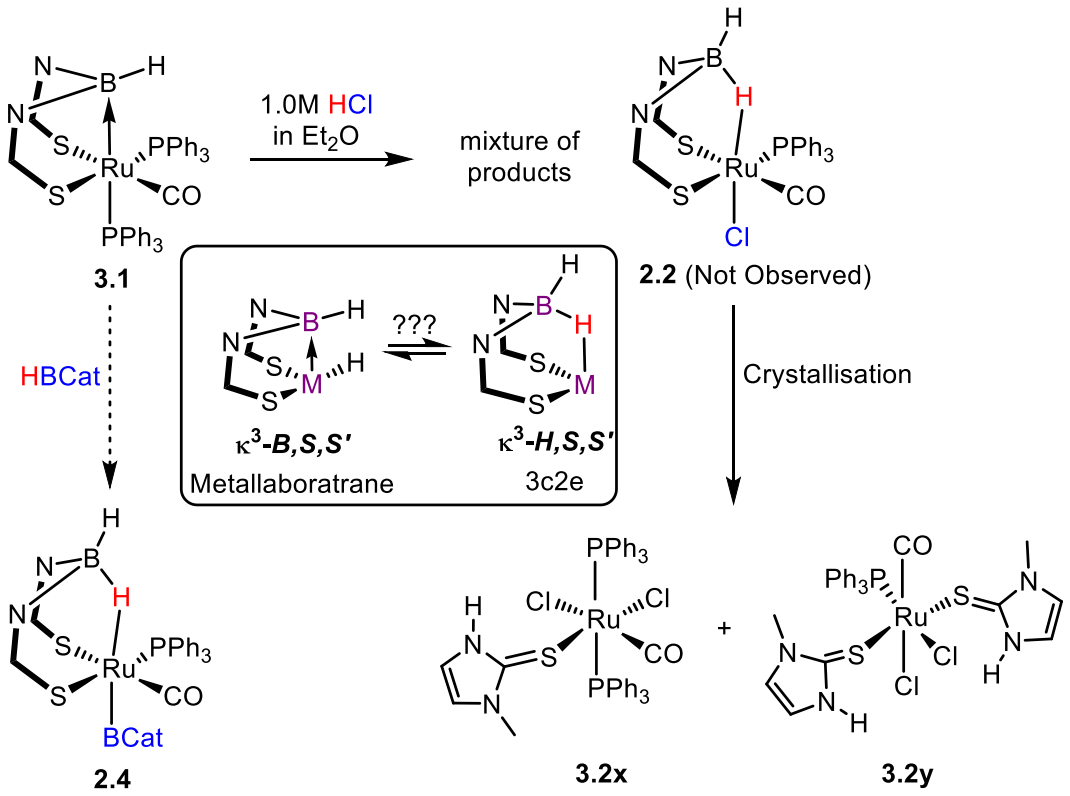

Scheme 3.12: Reactions investigating the reversibility of the κ^3-*B,S,S'* and κ^3-*H,S,S'* coordination modes.

Treatment of **3.1** with HBCat or HCl might be anticipated to lead to the known products **2.4** and **2.2**, respectively (Scheme 3.12). However, the Ru→B interaction remained intact in the presence of HBCat and no reaction resulted. In the reaction of **3.1** with one equivalent of 1.0M HCl, a mixture of products was obtained within one hour. Numerous resonances were observed in the $^{31}P\{^{1}H\}$ NMR spectrum at δ_P = 19.1, 28.1, 35.7, 45.2, 50.0 and 55.2, with no evidence for the expected product **2.2**. The ^{1}H NMR was also absent of the expected resonances associated with **2.2**. Increasing the reaction time to 24 hours did not alter the ratio of these products. Attempts to identify the products formed through crystallisation from chloroform/*n*-pentane afforded a mixture of complexes $[RuCl_2(CO)(PPh_3)_2(Hmt)]$ **3.2x** and $[RuCl_2(CO)(PPh_3)(Hmt)_2]$ **3.2y**, from which purified **3.2y** was isolated. The formulation of complexes **3.2x** and **3.2y** was confirmed by X-ray diffraction (Figure 3.5).

The bond lengths and angles of **3.2x** and **3.2y** are consistent with other reported structures of thione-bound mercaptoimidazole ligands on Ru(II) centres.[18,42-44] For example, the Ru–S bond lengths of 2.3845(6) Å (**3.2x**) and 2.4128(12), 2.4240(11) Å (**3.2y**) show little deviation from the range established by the literature complexes

(2.391–2.553 Å).[18,42-44] Similarly, the Ru1–S1–C2 angle of 115.59(9)° (**3.2x**) and 112.20(16), 112.46(14)° (**3.2y**) lie within the range 106.96–119.16°.

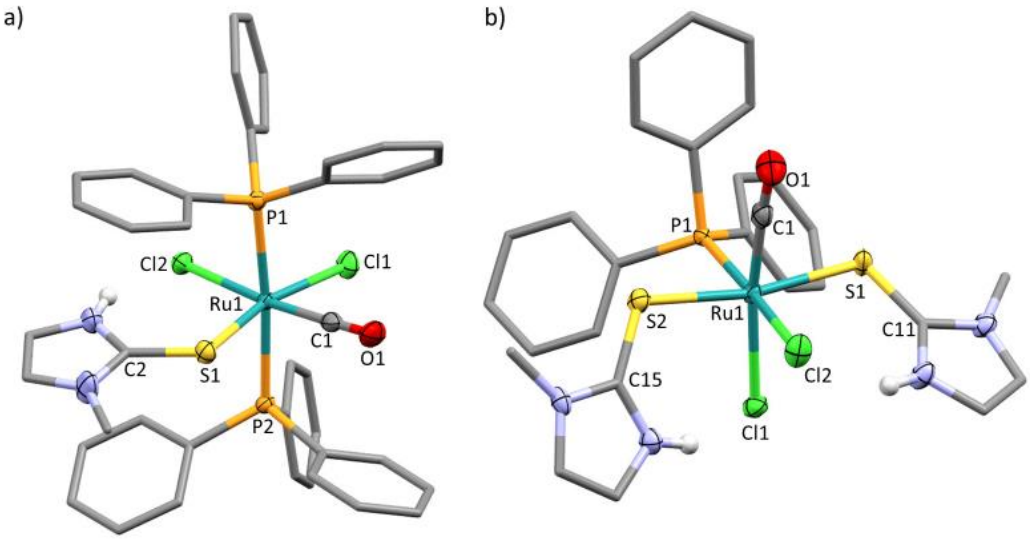

Figure 3.5: a) Molecular structure of $[RuCl_2(CO)(PPh_3)_2(Hmt)]$ **3.2x**.$CHCl_3$ (solvent omitted, CH hydrogen atoms omitted, phenyl groups simplified, displacement ellipsoids shown at 50% probability). Selected bond lengths (Å) and angles (°) of **3.2x**: Ru1–Cl1 2.4351(6), Ru1–Cl2 2.4841(6), Ru1–S1 2.3845(6), Ru1–P1 2.3982(6), Ru1–P2 2.4239(6), Ru1–C1 1.833(3), Ru1–S1–C2 115.59(9), S1–Ru1–Cl1 165.87(2), P1–Ru1–P2 175.03(2), C1–Ru1–Cl2 174.40(8). b) $[RuCl_2(CO)(PPh_3)(Hmt)_2]$ **3.2y** (CH hydrogen atoms omitted, phenyl groups simplified, displacement ellipsoids shown at 50% probability). Selected bond lengths (Å) and angles (°) of **3.2y**: Ru1–Cl1 2.4804(11), Ru1–Cl2 2.4763(11), Ru1–S1 2.4128(12), Ru1–S2 2.4240(11), Ru1–P1 2.3110(11), Ru1–C1 1.827(5), Ru1–S1–C11 112.20(16), Ru1–S2–C15 112.46(14), S1–Ru1–S2 169.21(4), P1–Ru1–Cl2 175.58(4), C1–Ru1–Cl1 170.99(14).

The molecular structure of **3.2y** is consistent with spectroscopic data. The IR spectrum shows one CO band (1961 cm^{-1}) while the coordination of two methimazole groups was inferred through ^1H NMR integration of methimazole environments relative to the triphenylphosphine co-ligand. The triphenylphosphine co-ligands in the purified sample of **3.2y** gives rise to a resonance at δ_P = 45.1 in the $^{31}P\{^1H\}$ NMR spectrum and **3.2x** was identified at δ_P = 19.1. Additionally, both complexes were observed by HR-ESI+ mass spectrometry.

The platinaboratrane $[Pt\{\kappa^4\text{-}B,S,S',S''\text{-}B(mt^{Me})_3\}(PPh_3)]$ **L3.17** reacted with Br_2, I_2 and MeI at the Pt(0) centre to generate Pt(II) complexes in preference to reaction at the Pt→B bond. In contrast, the coordinative saturation at the Ru(0) centre within **3.1** may deter

reactivity at the metal centre, such that reactivity of the Ru→B might instead be anticipated. Treatment of **3.1** with Br_2 or I_2 resulted in instant darkening of the reaction mixture from yellow to brown (Br_2) or red (I_2). A plethora of products was detected by $^{31}P\{^1H\}$ NMR spectroscopy in both reactions (Br_2: ≈20 resonances, I_2: ≈10 resonances). The absence of B*H*Ru hydride resonances in the ^1H NMR spectra of these reactions excluded the possibility of complexes with κ^3-*H,S,S'* coordinated $BHX(mt)_2$ (X = Br, I) units. In the Br_2 reaction, the broadness of the dominant resonance at δ_P = 48.2 was inferred as the retention of the Ru→B bond in a new complex. The mass spectrum of the I_2 reaction mixture contained peaks at *m/z* = 1145.6 in the LR-ESI(+) mass spectrum that was attributed to $[Ru(CO)(PPh_3)_2\{\kappa^2$-*S,S'*-$I_2B(mt)_2\}]$, whereas the product of oxidative addition at ruthenium $[RuI_2\{\kappa^2$-*S,S'*-$BH(mt)_2\}(CO)(PPh_3)]$ (expected around *m/z* = 883) was not observed. On the contrary, the band at 1966 cm^{-1} in the IR spectrum of the reaction mixture of higher frequency than **3.1** (1893 cm^{-1}) was inferred as a product of oxidative addition with a somewhat electron rich (π-basic) Ru(II) centre. Attempts to crystallographically identify the complexes formed in each reaction were unsuccessful as only amorphous powder was obtained.

The greater reactivity of **3.1** in these reactions compared to the oxidative halogenation of platinaboratrane **L3.17** (Scheme 3.7) may be due to the presence of the reductive B–H group as well as the more flexible di-buttressed system. The relatively exposed boron centre of **3.1** (Figure 3.6a) compared to the Tm analogue (Figure 3.6b) may predispose **3.1** towards more reactive pathways. Although not observed here, the two triphenylphosphines in **3.1** could present as potential sites for dissociation and reactivity, further confounding the distribution of products obtained (X_2PPh_3: δ_P = 49.2 X = Br,[45] 44.8 X = I [46]).

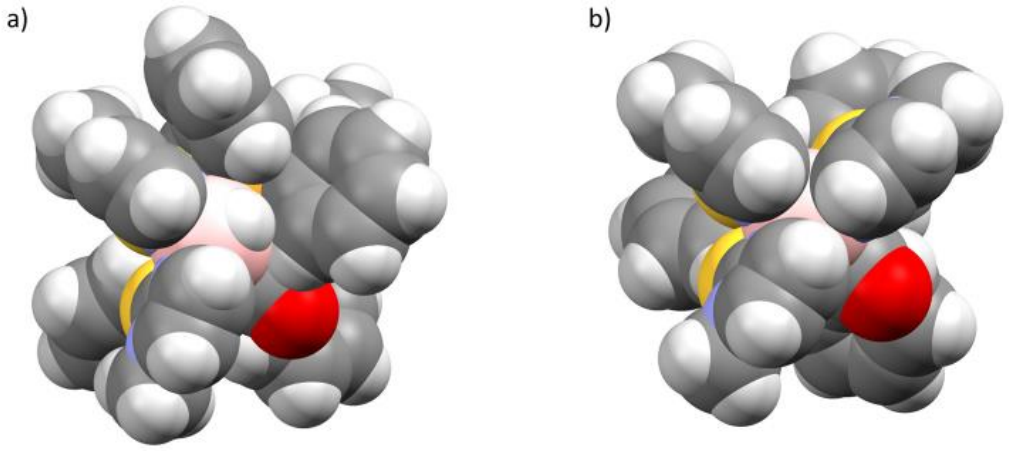

Figure 3.6: Space-filling diagrams of a) **3.1** and b) [Ru{κ^4-*B,S,S',S''*-B(mt^{Me})$_3$}(CO)(PPh$_3$)] that illustrate the exposure at boron. Elements: B (pink), H (white), C (grey), O (red), S (yellow), N (blue).

Whilst the investigations into the reactivity of the Ru→B interaction reported here are only preliminary and far from exhaustive, the lack of clean reactivity at the dative bond is already an emerging feature. The bond is unreactive towards C–H (Scheme 3.11) or B–H (Scheme 3.12) oxidative addition and the presence of acid ultimately encourages decomposition of **3.1** through protonation of the methimazolyl moiety.

Given the challenges faced thus far in encouraging a clean and directed reaction at the Ru→B interaction, it was envisaged that modification of the co-ligands (PPh$_3$) may present an alternative approach to gain insight into the nature of the dative bond.

3.4 Substitution Reactions of [Ru{κ^3-*B,S,S'*-BH(mt)$_2$}(CO)(PPh$_3$)$_2$]

3.4.1 Synthesis of [Ru{κ^3-*B,S,S'*-BH(mt)$_2$}(CO)$_2$(PPh$_3$)]

Previous research in the Hill group has briefly explored the lability of the phosphine ligand in Tm complex [Ru{κ^4-*B,S,S',S''*-B(mt^{Me})$_3$}(CO)(PPh$_3$)] as a way to access new ruthenaboratrane complexes. The displacement of PPh$_3$ (Scheme 3.13) was found to occur reversibly with carbon monoxide and irreversibly with isonitriles (CNR; R = ^{t}Bu, C$_6$H$_3$Me$_2$-2,6, C$_6$H$_2$Me$_3$-2,4,6).[3] The coordination sphere of this complex is not especially cluttered, suggesting an electronic rather than steric origin for this phosphine lability that calls for further scrutiny.

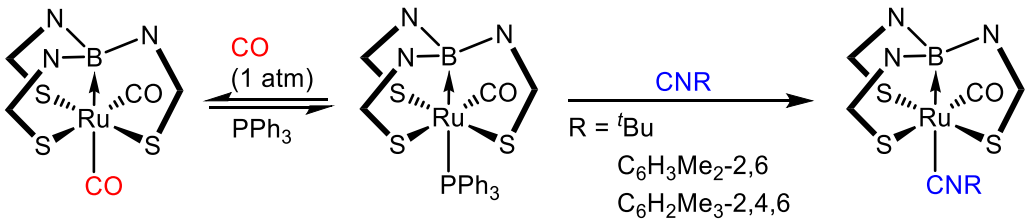

Scheme 3.13: Phosphine substitution of ruthenaboratrane [Ru{κ⁴-*B,S,S',S''*-B(mt^{Me})$_3$}(CO)(PPh$_3$)].

By analogy, complex **3.1** presents as a viable precursor to further examples of rare doubly-bridged ruthenaboratrane complexes. While the Tm complex has only one site of reactivity for phosphine substitution, the presence of two chemically distinct phosphine ligands in **3.1** may offer an opportunity to further explore the *trans* effect of a M→B association upon substitution selectivity. Particularly, insight could be gained into the comparable influence of the Ru→B and Ru–S units, *trans* to which the phosphines are located.

Facile and clean substitution of triphenylphosphine was achieved by passing CO through a solution of **3.1** in THF for 15 minutes to selectively yield [Ru{κ^3-*B,S,S'*-BH(mt)$_2$}(CO)$_2$(PPh$_3$)] **3.3** (CO *trans* to S), with no evidence for isomer **3.3a** where CO is *trans* to boron (Figure 3.7). The conversion of **3.1** to symmetric **3.3** proceeded with increased symmetry (C_1 to C_s) as inferred from the ^{1}H NMR spectrum (Figure 3.7). This was manifest by the replacement of the two distinct methyl resonances in **3.1** by one resonance in **3.3** (δ_H = 3.43). The four independent olefinic proton resonances similarly simplified to two environments at δ_H = 6.62 and 6.69 [ABCD to (AB)$_2$].

The ^{13}C{^{1}H} NMR spectrum contained fewer resonances, as expected for C_s **3.3** compared to C_1 **3.1**. Notably, only one phosphine environment was present in the ^{31}P{^{1}H} NMR spectrum of **3.3** at δ_P = 20.1, the broadness of which implies coordination *trans* to the boron. The spectrum measured *in situ* included a resonance due to liberated PPh$_3$, which was sharp, confirming that exchange with the coordinated PPh$_3$ did not occur on the ^{31}P{^{1}H} NMR timescale. Furthermore, an absence of the resonance at δ_P = 52.7 corresponding to the equatorial phosphine of **3.1** suggested replacement at this position by the CO ligand. Replacement of one phosphine by CO was further confirmed by IR spectroscopy, which showed two ν_{CO} associated bands (CH_2Cl_2: 1913, 1984 cm^{-1}).

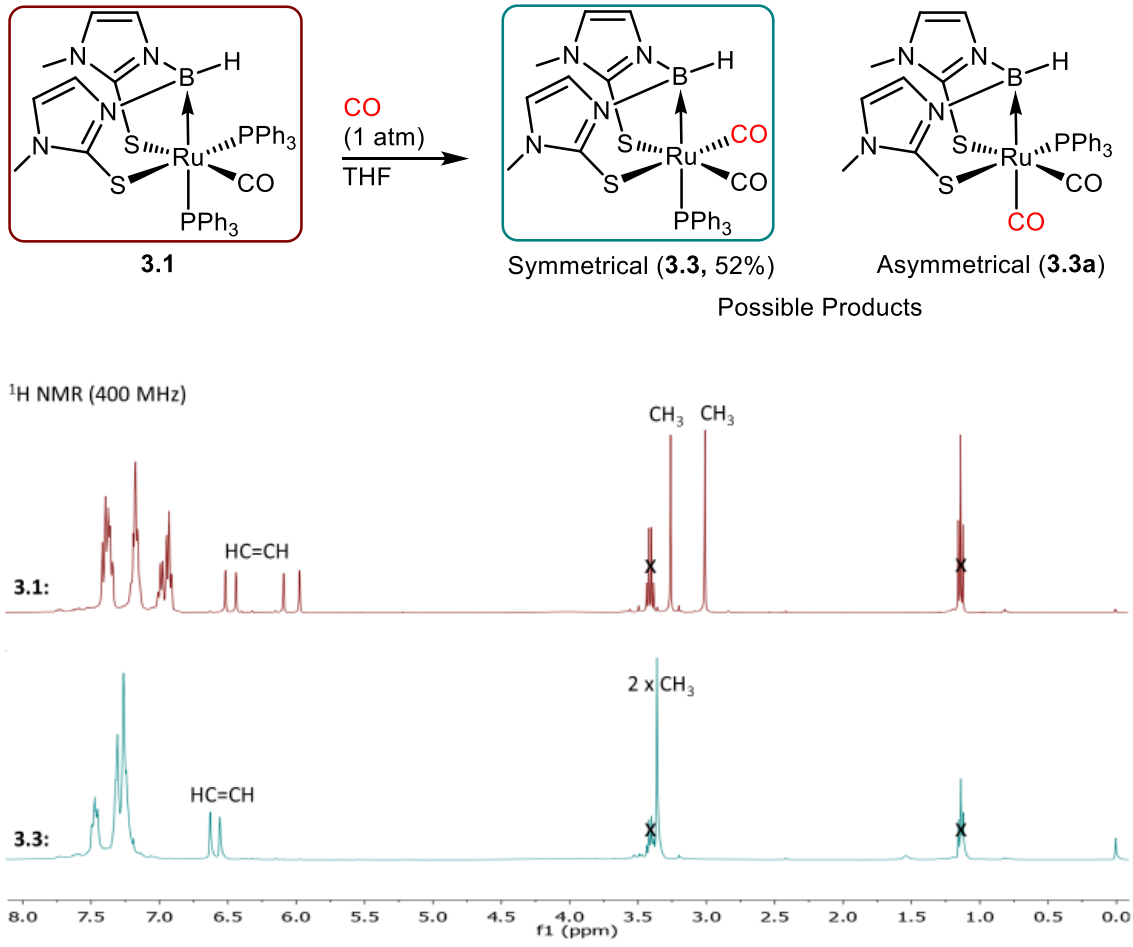

Figure 3.7: Synthesis of **3.3** supported by increased symmetry observed in the ^{1}H NMR spectrum in $CDCl_3$ (X = Et_2O).

The X-ray diffraction analysis of single crystals of **3.3** (Figure 3.8) was consistent with the symmetrical product formulation inferred from spectroscopic data. In contrast to **3.1**, the space-filling diagram of **3.3** revealed less steric encumbrance on the plane occupied by the two CO ligands. The mitigation of steric congestion associated with replacement of the phosphine *trans* to sulfur by CO is expected to be greater than at the position *trans* to BRu, which may provide a rationale for the observed selectivity. In addition, the introduction of π-acidic CO is electronically favourable in relieving the electron density of the rich Ru(0) metal centre, favouring substitution. It should be noted that a dissociative pathway would involve a five-coordinate intermediate, the lifetime of which could be sufficient to allow *pseudo*-rotation, i.e., the ultimate stereochemistry adopted need not necessarily reflect the site of initial dissociation. Detailed discussion of the molecular structure of complex **3.3** will be addressed collectively with further examples in Section 3.6.

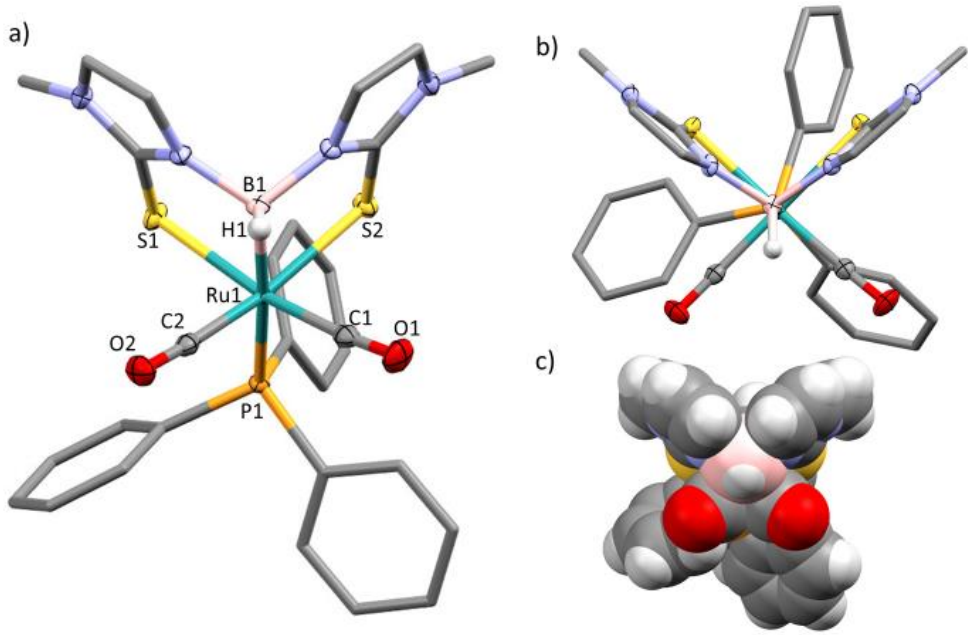

Figure 3.8: a), b) Molecular structure of [Ru{κ^3-*B,S,S'*-BH(mt)$_2$}(CO)$_2$(PPh$_3$)] **3.3**.CHCl$_3$ (solvent omitted, organic hydrogen atoms omitted, phenyl groups simplified, displacement ellipsoids shown at 50% probability). Selected bond lengths (Å) and angles (°): B1–Ru1 2.237(2), B1–H1 1.03(4), Ru1–P1 2.4740(5), Ru1–C1 1.861(2), Ru1–C2 1.855(2), H1–B1–Ru1 117(2), B1–Ru1–P1 173.72(6), B1–Ru1–C1 82.18(9), B1–Ru1–C2 81.16(9), C1–Ru1–C2 91.77(10). c) Space-filling diagram of **3.3**.

In contrast to the reversible CO coordination in [Ru{κ^4-*B,S,S',S''*-B(mt^{Me})$_3$}(CO)(PPh$_3$)], subjecting a crude sample of **3.3** to vacuum did not result in reformation of **3.1**. The persistence of complex **3.3** was instead noted by ^{1}H and ^{31}P{^{1}H} NMR spectroscopy, which suggested irreversible coordination of the CO ligand. Together these observations indicate that coordination of CO *trans* to the Ru→B linkage is less favourable than coordination *trans* to the π-basic thione donors.

3.4.2 Synthesis of Complexes [Ru{κ^3-*B,S,S'*-BH(mt)$_2$}(CO)(PMe$_2$Ph)(PPh$_3$)] and [Ru{κ^3-*B,S,S'*-BH(mt)$_2$}(CO)(PMe$_2$Ph)$_2$]

Ligand exchange investigations were continued with the range of electronically and sterically variant phosphines highlighted (purple) in Table 3.1. The reaction with an excess of PMe$_3$ proceeded cleanly within one hour to give the mono-substitution product [Ru{κ^3-*B,S,S'*-BH(mt)$_2$}(CO)(PMe$_3$)(PPh$_3$)], the nature of which was inferred from NMR spectroscopic data. The ^{31}P{^{1}H} NMR spectrum revealed the downfield shift of resonances for both phosphine environments relative to **3.1**, where the broad peak at δ_P = –29.6 suggests the triphenylphosphine ligand was located *trans* to the boron, with the doublet at δ_P = 58.7 ($^1J_{PC}$ = 11.3 Hz) corresponding to coordinated PMe$_3$.

Integration of the $^{31}P\{^{1}H\}$ NMR resonances was indicative of the liberation of one equivalent of triphenylphosphine. Despite the clean reaction observed by NMR spectroscopy, the inferred product [Ru{κ^3-*B,S,S'*-BH(mt)$_2$}(CO)(PMe$_3$)(PPh$_3$)] eluded isolation, which could be owing to the lability and/or volatility of PMe$_3$. Therefore, investigations were continued with the less volatile PMe$_2$Ph, which has electronic and steric similarities to PMe$_3$.

Similar to the reactivity observed with PMe$_3$, complex **3.1** was treated with an excess of PMe$_2$Ph at room temperature to afford the mono-substituted product, [Ru{κ^3-*B,S,S'*-BH(mt)$_2$}(CO)(PMe$_2$Ph)(PPh$_3$)] **3.4** (Scheme 3.14). Interestingly, substitution of the second phosphine was not observed spectroscopically under these reaction conditions, despite the presence of excess PMe$_2$Ph. The spectral data resemble those of [Ru{κ^3-*B,S,S'*-BH(mt)$_2$}(CO)(PMe$_3$)(PPh$_3$)]. The broad resonance at δ_P = –17.2 was attributed to the *trans* (RuB) PPh$_3$ ligand, while the relatively sharp doublet at δ_P = 56.9 ($^1J_{PC}$ = 11.3 Hz) was assigned as the smaller PMe$_2$Ph ligand occupying the position *trans* to sulfur. The use of PMe$_2$Ph over the more symmetrical PMe$_3$ is advantageous in that the two methyl groups may provide an indication of the local symmetry of the complex. The asymmetric nature of **3.4** was noted by ^{1}H NMR spectroscopy with the diastereotopic methyl groups from PMe$_2$Ph resonating as chemically inequivalent doublets at δ_H = 1.28 ($^2J_{HP}$ = 5.5 Hz) and 1.43 ($^2J_{HP}$ = 5.3); whilst the remaining ^{1}H signals are similar to that of **3.1**. Although crystals of **3.4** suitable for X-ray diffraction studies were not obtained, the formulation of **3.4** was further supported by mass spectrometry and elemental analysis.

Following the overnight acquisition of a pure sample of **3.4**, the $^{13}C\{^{1}H\}$ NMR spectrum revealed several (≈6) resonances in the methyl region where the methimazolyl unit is typically located (δ_C = 33.5–34.2). The corresponding resonances in the ^{1}H NMR spectrum were distinct and the three products **3.4**, isomer **3.4a** and the product of double substitution [Ru{κ^3-*B,S,S'*-BH(mt)$_2$}(CO)(PMe$_2$Ph)$_2$] **3.5** were formulated (Scheme 3.14). The decomposition of **3.4** occurred within 10 minutes of solvation in CDCl$_3$ and stabilised to a relative ratio of 2:3:5 for **3.4**, **3.5**, **3.4a** at room temperature. The formation of these products was initially suspected to be due to the residual acidity of CDCl$_3$. However, a similar ratio of products formed when the less acidic CD$_2$Cl$_2$ was used as the characterisation solvent.

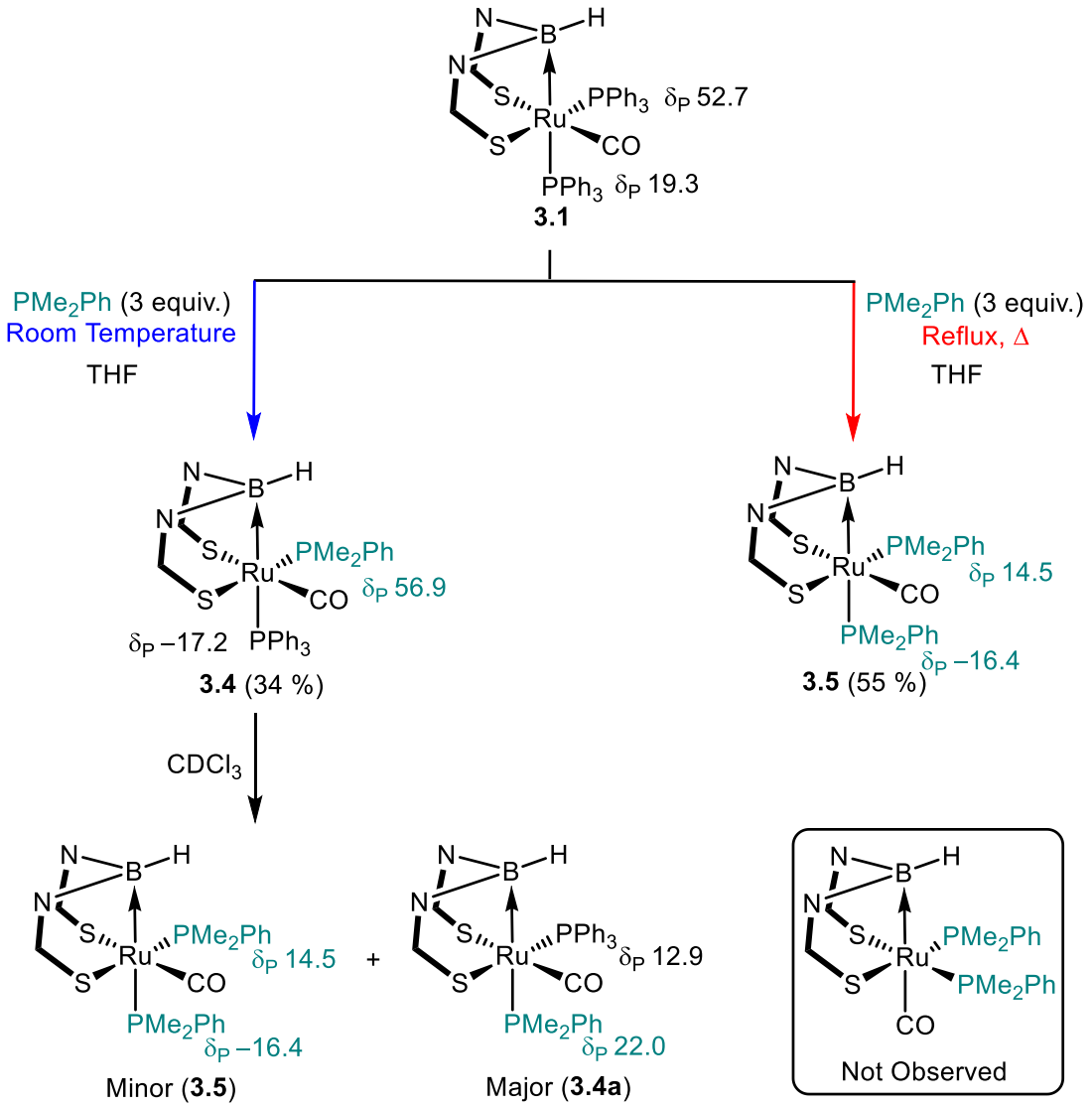

Scheme 3.14: Temperature dependent substitution of triphenylphosphine in **3.1**.

To encourage conversion of **3.4** to complexes **3.5** and **3.4a** that were previously observed in $CDCl_3$, an aliquot of the crude reaction mixture of **3.4** in THF was briefly heated to reflux. The NMR spectra showed the clean partial conversion of **3.4** to complex **3.5**, with no evidence for the other product (**3.4a**) or the C_s-symmetric isomer of **3.5**. Full conversion of **3.4** to **3.5** could be achieved by performing the same reaction under THF reflux for 18 hours (Scheme 3.14). The formation of **3.5** over this time period was accompanied by an increased complexity of the methyl region in the ^{1}H NMR spectrum (δ_H = 1.27–1.48). This is due to the four chemically inequivalent methyl environments of the two PMe_2Ph ligands, which resonate as doublets within this region, whereas two doublets would be expected for C_s-**3.5**. Four distinct methyl resonances from PMe_2Ph were also present in the $^{13}C\{^1H\}$ NMR spectrum. Two of the PMe_2Ph methyl groups couple to the chemically inequivalent phosphines in a doublet of doublet multiplicity at

δ_C = 15.6 ($^1J_{CP}$ = 31.2, $^3J_{CP}$ = 3.3 Hz) and 18.6 ($^1J_{CP}$ = 32.3, $^3J_{CP}$ = 4.2 Hz), while the other two environments appear only as doublets at δ_C = 16.3 ($^1J_{CP}$ = 13.6 Hz) and 19.4 ($^1J_{CP}$ = 16.2 Hz). This effect may be attributed to the relative angle of the methyl carbon to the other phosphine atom (Karplus-type relationship, Figure 3.9b). Although rotation about the Ru–P bond in solution is expected, the steric properties of the phenyl moiety could dictate conformational preferences (Figure 3.9c). Coordination of two PMe_2Ph ligands was further ascertained by the respective sharp doublet and broad singlet phosphine environments at δ_P = 14.5 ($^2J_{PC}$ = 12.3 Hz) and –16.4 in the $^{31}P\{^1H\}$ NMR spectrum.

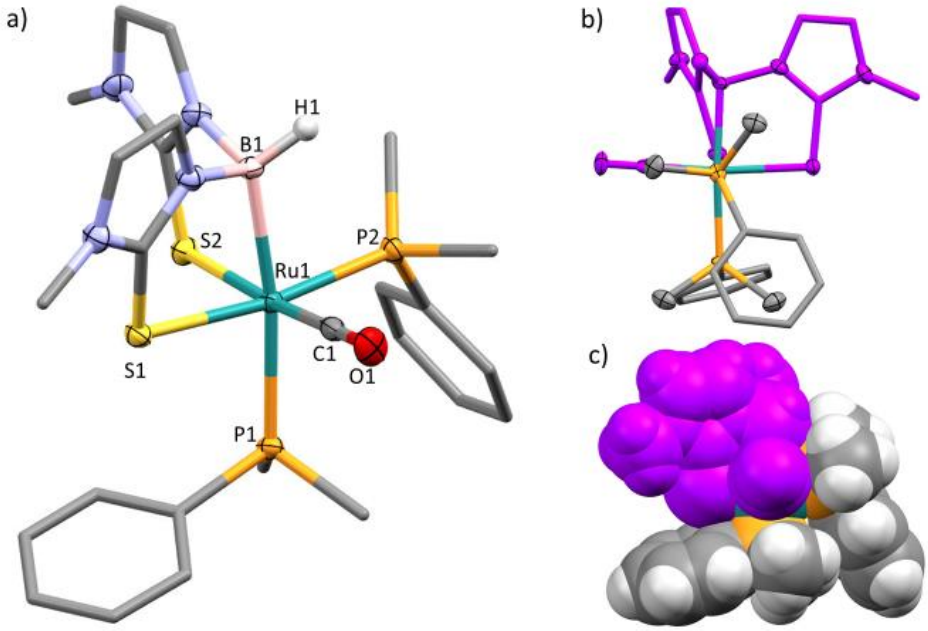

Figure 3.9: a) Molecular structure of [Ru{κ^3-*B,S,S'*-BH(mt)$_2$}(CO)(PMe_2Ph)$_2$] **3.5** (organic hydrogen atoms omitted, phenyl groups simplified, displacement ellipsoids shown at 50% probability). Selected bond lengths (Å) and angles (°): B1–Ru1 2.253(4), B1–H1 1.09(6), Ru1–P1 2.4095(9), Ru1–P2 2.2876(9), Ru1–C1 1.821(4), H1–B1–Ru1 120(3), B1–Ru1–P1 171.51(11), B1–Ru1–P2 88.00(11), B1–Ru1–C1 88.78(16), P1–Ru1–P2 99.57(3). b) PMe_2Ph groups emphasised and c) space-filling diagram.

The formulation of the isomerised complex **3.4a** was further confirmed through a process of elimination in the ^1H and $^{31}P\{^1H\}$ NMR spectra of resonances corresponding to **3.4** and **3.5** (Figure 3.10)**.** The methyl environments of **3.4a** in Figure 3.10 consist of two distinct doublets for the PMe_2Ph ligand (δ_H = 1.23, 1.45, $^2J_{HP}$ = 8.5 Hz), whereas the downfield resonances (δ_H = 3.19, 3.24) correspond to the chemically inequivalent *N*-methyl groups of the methimazolyl backbone. The olefinic signals of all three products reside in a similar chemical shift range of 6.40–6.58 ppm, which occluded the unambiguous assignment of the resonances that result from **3.4a**. The two dominant

resonances in the $^{31}P\{^{1}H\}$ NMR spectrum further support the assignment of **3.4a**. Consistent with the ruthenaboratrane complexes discussed thus far in this chapter, the two phosphine environments resolved as a broadened signal at δ_P = 22.0 and a sharp doublet at δ_P = 12.9 ($^{2}J_{PP}$ = 11.4 Hz), which were postulated as PMe_2Ph and PPh_3 respectively.

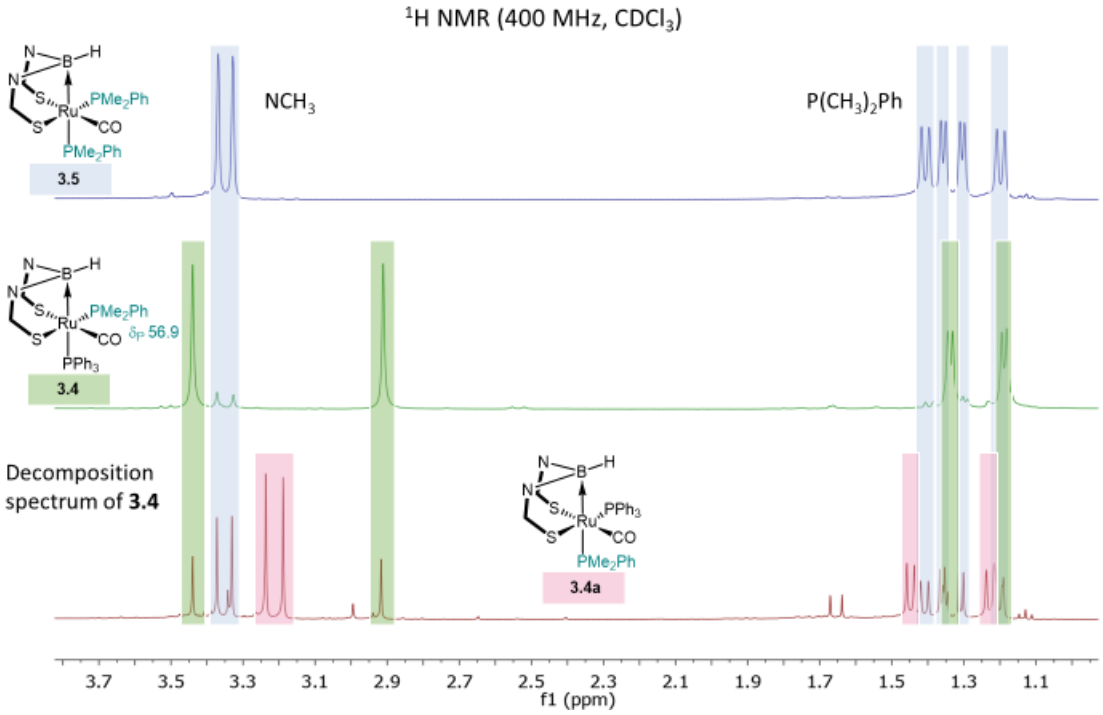

Figure 3.10: Comparison of the methyl regions in the ^{1}H NMR spectra of **3.5**, **3.4** and the decomposition spectrum of **3.4** in $CDCl_3$ to identify isomer **3.4a**.

3.4.3 Synthesis of [Ru{κ^3-*B,S,S'*-BH(mt)$_2$}(CO){P(OMe)$_3$}$_2$]

Compared to PMe_3 and PMe_2Ph, trimethylphosphite has a smaller steric profile and greater π-acidity. Treatment of **3.1** with three equivalents of $P(OMe)_3$ for 18 hours at room temperature yielded the product of double substitution, the complex [Ru{κ^3-*B,S,S'*-BH(mt)$_2$}(CO){P(OMe)$_3$}$_2$] **3.6**. Whilst the crude $^{31}P\{^{1}H\}$ NMR spectrum revealed several (≈10) resonances, **3.6** was evident as the major species and could be purified through recrystallisation from diethylether and *n*-pentane. The formulation of **3.6** was established by NMR spectroscopy, IR, mass spectrometry, elemental analysis and single crystal X-ray diffraction study (Figure 3.11).

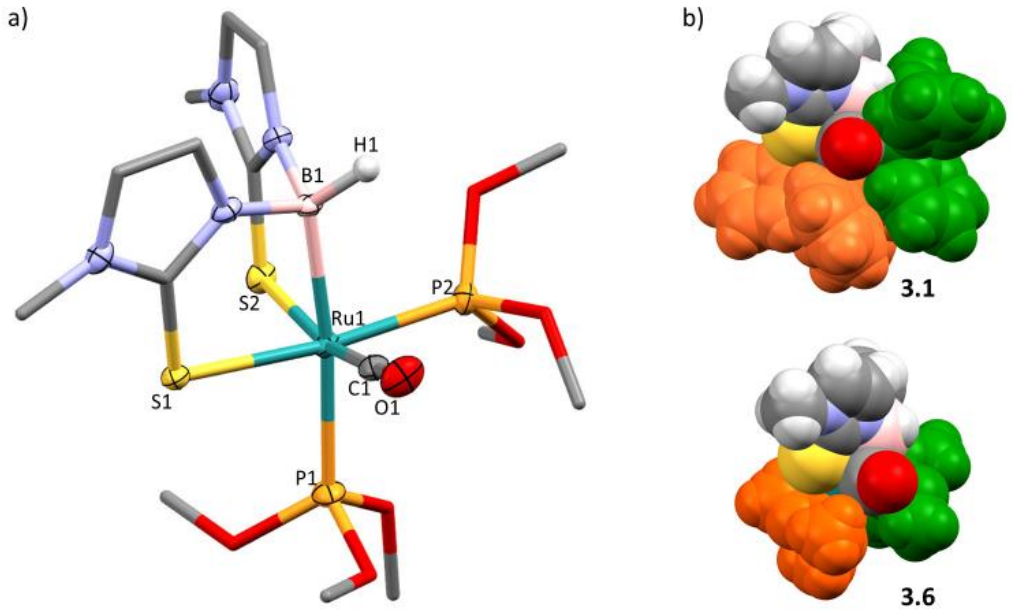

Figure 3.11: a) Molecular structure of [Ru{κ^3-*B,S,S'*-BH(mt)$_2$}(CO){P(OMe)$_3$}$_2$] **3.6** (organic hydrogen atoms omitted, phenyl groups simplified, displacement ellipsoids shown at 50% probability). Selected bond lengths (Å) and angles (°) for **3.6**: B1–Ru1 2.252(3), B1–H1 1.17(5), Ru1–P1 2.3604(8), Ru1–P2 2.2341(8), Ru1–C1 1.835(3), H1–B1–Ru1 122(3), B1–Ru1–P1 173.33(9), B1–Ru1–P2 86.67(9), B1–Ru1–C1 81.66(13), P1–Ru1–P2 99.56(3). b) Space-filling comparison between complexes **3.1** and **3.6**.

In addition to the characteristic resonances resulting from the BH(mt)$_2$ moiety in the ^{1}H NMR spectrum, doublets at δ_H = 3.56 ($^3J_{HP}$ = 10.8 Hz) and 3.67 ($^3J_{HP}$ = 11.1 Hz), are consistent with the coordination of two P(OMe)$_3$ ligands. Given the electronegative inductive effects of the methoxy substituents, the two P(OMe)$_3$ resonances were observed as a doublet at δ_P = 151.1 ($^2J_{PC}$ = 19.4 Hz) and a broad singlet at δ_P = 153.7; downfield compared to complexes **3.1** and **3.3**–**3.5**, as expected.

The replacement of both triphenylphosphine ligands in **3.1** by P(OMe)$_3$ was further supported by an absence of signals in the aromatic region in the ^{1}H and ^{13}C{^{1}H} NMR spectra, and the emergence of shifts in the methoxy region. The effect of the quadrupolar boron nuclei appears to extend to the methyl carbon of the P(OMe)$_3$ ligand coordinated *trans*, which results in broadening of the resonance (δ_C = 50.8). The resonance of the equatorial phosphite ligand remains unaffected, appearing as a sharp doublet (δ_C = 52.0, $^2J_{CP}$ = 5.9 Hz).

One notable difference in the reactivity of **3.1** with PMe$_2$Ph or PMe$_3$ compared to P(OMe)$_3$ is the ease of PPh$_3$ substitution. Single substitution predominately occurs with the electron rich alkyl phosphines at room temperature, and the introduction of a

second equivalent can be achieved only at elevated temperatures. In contrast, substitution with $P(OMe)_3$ occurs readily at room temperature with replacement of both triphenylphosphines. This may be due to the greater potential of π-acidic $P(OMe)_3$ to stabilise the electron rich Ru(0) centre than PPh_3 and is reflected by the IR shift to higher frequency from 1893 cm^{-1} (**3.1**) to 1921 cm^{-1} (**3.6**). Furthermore, the replacement of bulky PPh_3 ligands with $P(OMe)_3$ may be sterically favourable as evident from the space-filling diagrams in Figure 3.11b (θ_T° = 145 and 107° respectively).

3.4.4 Attempted Synthesis of [Ru{κ³-*B,S,S'*-BH(mt)₂}(CO)(PCy₃)(PPh₃)]

The synthesis of the PCy_3 variant of **5.1** was pursued through two synthetic strategies, which were based on the methodology used for the formation of the analogous Tm complex [Ru{κ⁴-*B,S,S',S''*-B(mt)₃}(CO)(PCy₃)]. Preliminary work by Tshabang showed complex [Ru{κ⁴-*B,S,S',S''*-B(mt)₃}(CO)(PCy₃)] could be formed *via* two synthetic pathways (Scheme 3.15).[47] The first route involved substitution of the PPh_3 ligand in [Ru{κ⁴-*B,S,S',S''*-B(mt)₃}(CO)(PPh₃)] (the Tm analogue of **3.1**) for PCy_3. The second pathway involved the reaction of precursor [Ru(Ph)Cl(CO)(PCy₃)₂] and Na[HB(mt)₃]. Direct substitution afforded a mixture at equilibrium that could not be converted to a single product, whilst the complex [Ru{κ⁴-*B,S,S',S''*-B(mt)₃}(CO)(PCy₃)] was isolated *via* the second synthetic pathway, which obviates the presence of competitive PPh_3.

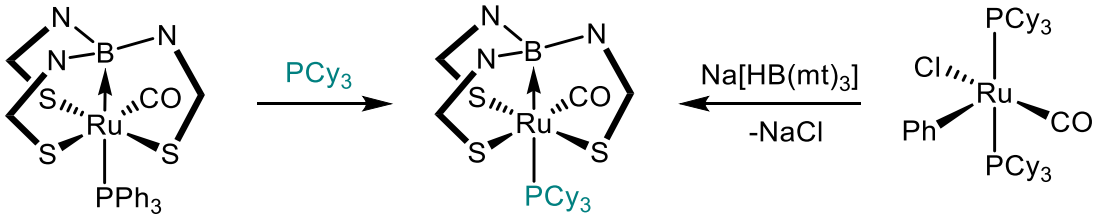

Scheme 3.15: Synthetic pathways to [Ru{κ⁴-*B,S,S',S''*-B(mt)₃}(CO)(PCy₃)] by Tshabang.

Similar synthetic strategies were employed in the synthesis of complexes [Ru{κ³-*B,S,S'*-BH(mt)₂}(CO)(PCy₃)(PPh₃)] **3.7** and [Ru{κ³-*B,S,S'*-BH(mt)₂}(CO)(PCy₃)₂] **3.7a** (Scheme 3.16). It should be noted that whilst the sterically congested *cis*-Ru(PCy₃)₂ fragment is understandably rare, it is not unknown.[48-53]

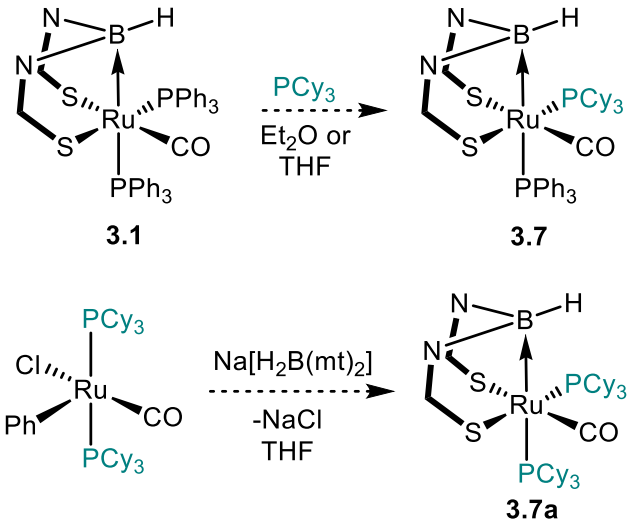

Scheme 3.16: Synthetic pathways toward complexes [Ru{κ^3-*B,S,S'*-BH(mt)$_2$}(CO)(PCy$_3$)(PPh$_3$)] **3.7** or [Ru{κ^3-*B,S,S'*-BH(mt)$_2$}(CO)(PCy$_3$)$_2$] **3.7a**.

The room temperature reaction of **3.1** with two equivalents of PCy$_3$ in THF for 20 hours yielded starting material, PCy$_3$, free PPh$_3$ and numerous minor products (≈10 resonances in the ^{31}P{^{1}H} NMR spectrum comprising *ca* 28% of the total phosphorus present). The broad resonance of free PPh$_3$ (h.h.w. = 52 Hz) indicated the occurrence of dynamic phosphine exchange processes. Heating at reflux for four hours facilitated further development of the resonances associated with the minor products and concurrent disappearance of the starting material (**3.1**). In contrast to the unheated reaction mixture, the sharp resonance of the free PPh$_3$ led to the inference that no dynamic phosphine exchange was occurring. The anticipated complex [Ru{κ^3-*B,S,S'*-BH(mt)$_2$}(CO)(PCy$_3$)(PPh$_3$)] **3.7** could not be conclusively identified. Further attempts with one equivalent of PCy$_3$ at room temperature and at reflux, in Et$_2$O and THF, showed either no reaction or produced ^{1}H and ^{31}P{^{1}H} NMR spectra that were similarly abundant in unidentifiable resonances.

To eliminate the possible complication of mixed PPh$_3$/PCy$_3$ coordination, the synthesis of the PCy$_3$ analogue of **3.1** was pursued through the reaction of Na[H$_2$B(mt)$_2$] with [Ru(Ph)Cl(CO)(PCy$_3$)$_2$] in THF. The solution IR spectrum of the crude reaction in THF displays a CO band of low stretching frequency 1898 cm^{-1}, amongst others (ν_{CO} = 1918, 1988 cm^{-1}). This is indicative of ruthenium in the zero-oxidation state and falls within the range 1877–1921 cm^{-1} established by the ruthenaboratrane complexes synthesised thus far in this chapter. The presence of free benzene (δ_H = 7.36) in the ^{1}H NMR spectrum was consistent with expected extrusion of HPh during ruthenaboratrane formation.

Whilst the IR spectrum showed promise, the four sharp resonances of equal intensity in the $^{31}P\{^{1}H\}$ NMR spectrum suggested the absence of coordination *trans* to the boron. However, the sharpness of the product resonances would imply an absence of fluxional Berry-*pseudo* rotation processes typical by five-coordinate complexes. Despite numerous crystallisation experiments, only amorphous powder unsuitable for X-ray diffraction studies was obtained.

The complications associated with the introduction of PCy_3 may be both steric and electronic in nature. The steric bulk of the PCy_3 ligand is considerably greater than that of PPh_3 (θ_T° = 170, PCy_3 *cf.* 145, PPh_3), and therefore it may be sterically unfavourable to accommodate two adjacent around the ruthenium centre. From the substitution reactions investigated thus far, the substitution process appears to be most facile and favoured for π-acidic ligands, whereas the σ-basicity of the PCy_3 ligand may disfavour its coordination to the electron rich Ru(0) centre.

3.4.5 Synthesis of [Ru{κ^3-*B,S,S'*-BH(mt)$_2$}(CO)(Z-Ph$_2$PCH=CHPPh$_2$)]

The replacement of both PPh_3 ligands in **3.1** in the synthesis of complexes **3.5** and **3.6** naturally led to extension of the chemistry to bidentate ligands. Given the *cis* arrangement of the PPh_3 ligands in **3.1**, *Z*-1,2-bis(diphenylphosphino)ethylene (dppen), was envisaged as a suitable bidentate ligand to ensure chelation.

The conversion of **3.1** to [Ru{κ^3-*B,S,S'*-BH(mt)$_2$}(CO)(Z-Ph$_2$PCH=CHPPh$_2$)] **3.8** took place in THF under reflux for 43 hours, where phosphine substitution was evident by the development of two downfield resonances at δ_P = 70.6 (d, $^2J_{PC}$ = 8.1) and 50.8 (broad). The vinylic hydrogen resonances were embedded within the aromatic region and located from $^1H^{13}C$ HSQC experiments as multiplets at δ_H = 7.91 and 7.97. The corresponding $^{13}C\{^1H\}$ NMR signals appear as two doublet of doublets at δ_C = 148.1 ($^1J_{CP}$ = 26.6, $^2J_{CP}$ = 26.6) and 149.0 ($^1J_{CP}$ = 35.8, $^2J_{CP}$ = 45.5). The C_1 symmetry of **3.8** and the rigidity of the ethylene backbone renders each phenyl group on dppen inequivalent. The molecular structure of **3.8** was confirmed by an X-ray diffraction study (Figure 3.12).

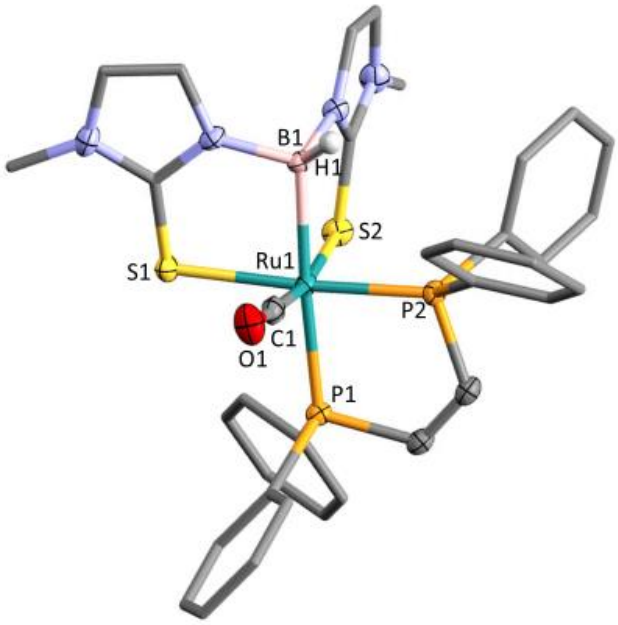

Figure 3.12: Molecular structure of [Ru{κ^3-*B,S,S'*-BH(mt)$_2$}(CO)(Z-Ph$_2$PCH=CHPPh$_2$)] **3.8** (organic hydrogen atoms omitted, phenyl groups simplified, displacement ellipsoids shown at 50% probability). Selected bond lengths (Å) and angles (°): B1–Ru1 2.231(2), B1–H1 1.09(4), Ru1–P1 2.3636(5), Ru1–P2 2.2719(5), Ru1–C1 1.848(2), H1–B1–Ru1 121(2), B1–Ru1–P1 175.39(6), B1–Ru1–P2 91.81(6), B1–Ru1–C1 86.26(9), P1–Ru1–P2 85.293(19).

3.4.6 Other Attempted Substitution Reactions

Despite the promising phosphine substitution reactions discussed thus far, complex **3.1** appeared reluctant to undergo clean reactions with other ligands. Several reactions were investigated, and their outcomes of generally non-isolable products or complex mixtures are depicted in Scheme 3.17.

Inspired by the irreversible coordination of isonitriles in the analogous complex [Ru{κ^4-*B,S,S',S''*-B(mt)$_3$}(CO)(PPh$_3$)] (Scheme 3.13, Section 3.4.1),[3] reactions with ^{t}BuNC and the less nucleophilic MesNC were explored. Whilst **3.1** reacts readily with ^{t}BuNC and MesNC at room temperature, liberating free PPh$_3$, difficulties in purification precluded the isolation of the desired products, [Ru{κ^3-*B,S,S'*-BH(mt)$_2$}(CNR)(CO)(PPh$_3$)] (R = ^{t}Bu, Mes).

The infrared spectrum measured at two hours of the reaction between **3.1** and ^{t}BuNC in THF contained numerous overlapping peaks at 2109–2200 cm^{-1}, as well as free ^{t}BuNC (2070 cm^{-1}). The dominant bands at ν_{CN} = 2134 and ν_{CO} = 1924 cm^{-1} may be evidence of the product of mono-substitution, [Ru{κ^3-*B,S,S'*-BH(mt)$_2$}(CN^{t}Bu)(CO)(PPh$_3$)].

Although a stoichiometric amount of MesNC was used in the reaction with **3.1**, incomplete reactivity was inferred by the presence of free MesNC (ν_{CN} = 2112 cm^{-1}) in the IR spectrum after an extended period (43 hours). A plethora of resonances was present in the $^{31}P\{^{1}H\}$ NMR spectrum (≈11) and persisted following recrystallisation from THF/*n*-pentane. The IR spectrum similarly showed a mixture of products, including the postulated product [Ru{κ^3-*B,S,S'*-BH(mt)$_2$}(CNMes)(CO)(PPh$_3$)] (ν_{BH} = 2360, ν_{CN} = 2088, and ν_{CO} = 1919 cm^{-1}) and an unidentified carbonyl containing complex at ν_{CO} = 1954 cm^{-1}. Neither further attempts of fractional crystallisation nor column chromatography resulted in the isolation of pure material.

Treatment of **3.1** with HC_5Me_5 (HCp*) was envisaged as a potential alternate route to Kuwata and Ikariya's complex, [Ru(CO){κ^2-*S,S'*-H_2B(mt)$_2$}(Cp*)],[54] and concomitantly probes phosphine substitution and Ru→B reactivity. No reaction occurred at room temperature and raising the temperature to 80°C resulted in a mixture of products. These results unsurprisingly parallel findings in Section 3.3 on the reactivity of the Ru→B bond.

Intriguing activity has been observed in the synthesis of thiocarbonyl metallaboratranes. The synthesis of the rhodaboratrane [RhH(CS)(PPh$_3$){BH(mt)$_2$}] was confounded by the formation of the unexpected CS insertion product [RhH(PPh$_3$){η^2-(C,S),κ^2-*S',S''*-SC(PPh$_3$)BH(mt)$_2$}] (Chapter 1, Scheme 1.31).[7] In contrast, the preparation of ruthenium CS complex [Ru{κ^4-*B,S,S',S''*-B(mt)$_3$}(CS)(PPh$_3$)] from [Ru(CH=CH$_2$)Cl(CS)(PPh$_3$)$_2$] was relatively straightforward.[3] Addition of CS_2 to **3.1** resulted in no reaction at room temperature, while elevated temperatures led to the decomposition of the borane ligand into methimazole.

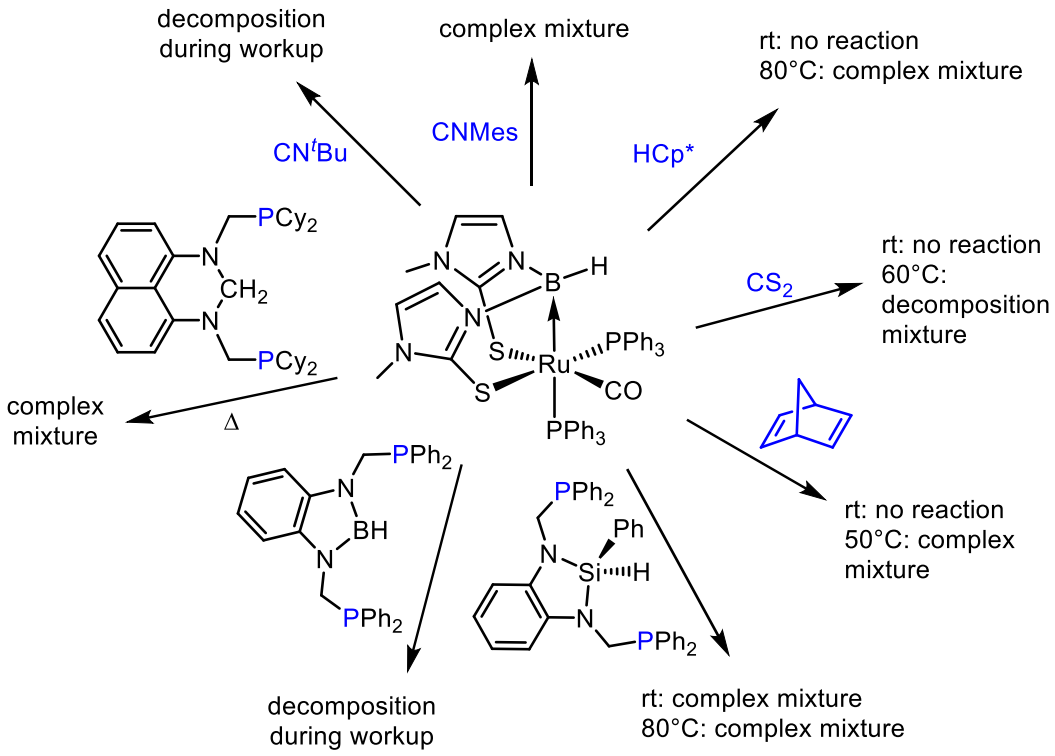

Scheme 3.17: Results of attempted phosphine substitution reactions of **3.1**.

Given the successful synthesis and isolation of **3.8**, other multidentate ligands such as norbornadiene and pincer pro-ligands were considered. Whilst many pincer complexes in the literature feature ligands of tridentate coordination (Chapter 1), some pro-ligands have been reported to behave as simple bidentate phosphine ligands or bridging ligands without direct involvement of the central donor atom.[55-59] Furthermore, arrested B–H or Si–H activation has been reported for borane and silane based frameworks.[57,60-62] Selected examples are illustrated in Figure 3.13.

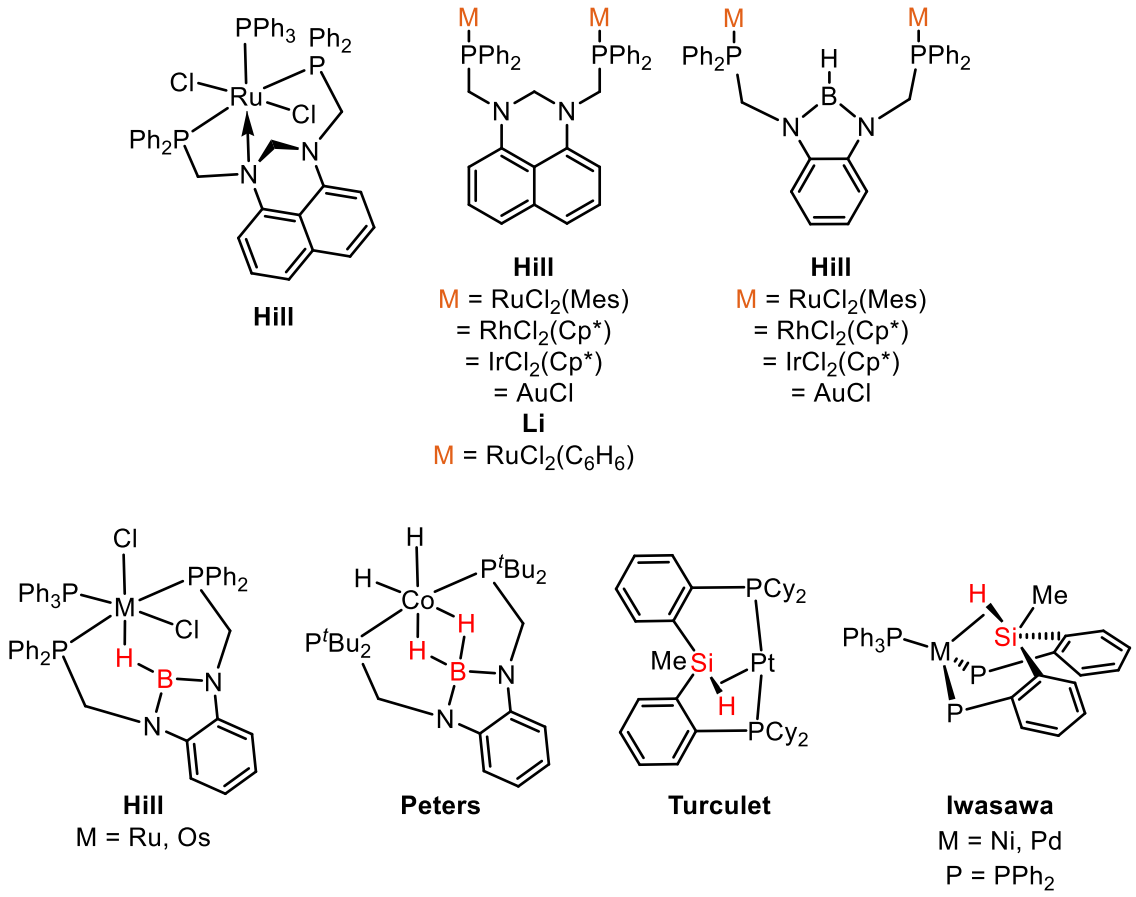

Figure 3.13: Selected examples of innocent behaviour of pincer ligands in coordination chemistry.

The reaction of **3.1** with norbornadiene or the pincer pro-ligands illustrated in Figure 3.13 ultimately resulted in a complex mixture of products that were difficult to separate. The most promising reaction was with the borane pro-ligand ^{Ph}PNNP(BH) with new resonances observed at δ_P = 53.7 and 17.2 in the $^{31}P\{^1H\}$ NMR spectrum of the reaction mixture. However, upon recrystallisation only an inseparable mixture of three products was obtained. The absence of hydride resonances in the ^1H NMR spectra for the borane and silane ligands argues against the presence of B–H and Si–H *agostic* complexes.

Owen's report on the metal-borane pincer complexes [M{κ^3-*B,S,S'*-BH(mp)$_2$}(PPh$_3$)] (M→B; M = Pt **L3.19**, Pd **L3.20**, mp = 2-mercaptopyridinyl) illustrated the coordinative flexibility of the 'BH(mp)' group.[63] The 'BH(mp)' unit typically coordinates facially, but in **L3.19** and **L3.20** the nearly *trans*-disposed sulfurs exhibit more meridional-like coordination similar to that of pincer scaffolds (S–M–S angle: **L3.19** 161.14(3), **L3.20** 158.88(2)°). Inspired by this result, **3.1** was treated with the hydride abstractor

$[CPh_3][PF_6]$ to assess the potential of **3.1** to relax to meridional coordination upon BH hydride abstraction (Scheme 3.18).

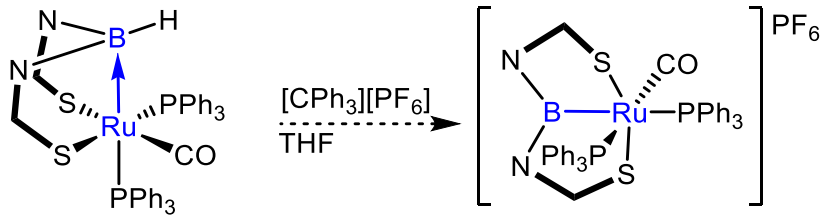

3.1 **3.9**

Scheme 3.18: Attempted hydride abstraction reaction of **3.1** with $[CPh_3][PF_6]$.

Within two hours, the solution IR(THF) showed significant shift of the ν_{CO} band from 1899 cm^{-1} in **3.1** to 1931 and 1972 cm^{-1}. This suggests a change in electronic nature of the ruthenium centre as expected from the progression of a neutral to cationic complex. The absence of a BH stretching band was also noted in the IR spectrum. Both the ^{1}H and $^{31}P\{^{1}H\}$ NMR spectra revealed broad resonances. In the crude $^{31}P\{^{1}H\}$ spectrum, the major product was identified at δ_P = 39.6 accompanied by distinct resonances corresponding to PF_6 (δ_P = –142.9) and free PPh_3. The broadness of the latter may imply the occurrence of rapid exchange processes. Attempts to identify the product through X-ray diffraction analysis of crystals obtained from slow evaporation of a benzene/*n*-pentane solution of **3.9** afforded the complex $[RuF(CO)(PPh_3)_2(Hmt)_2]PF_6$ **3.9x** (Figure 3.14). The cation of **3.9x** features a terminal fluoride, the coordination of which is stabilised by bifurcated hydrogen bonding to two N–H groups from Hmt co-ligands.

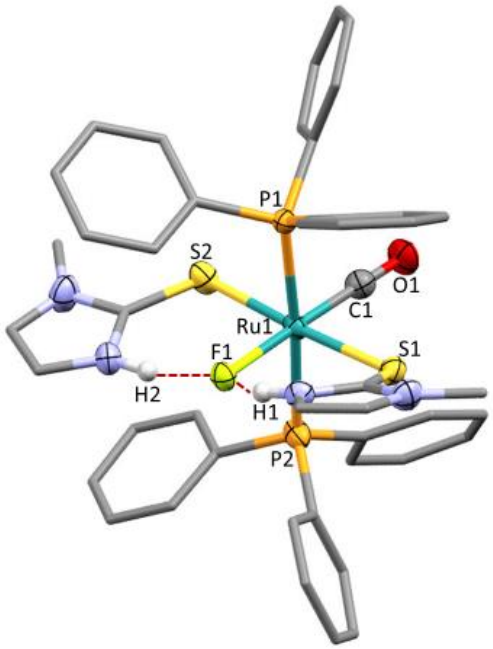

Figure 3.14: Molecular structure of decomposition product $[RuF(CO)(PPh_3)_2(Hmt)_2]^+$ **3.9x**.C_6H_6 (solvent and PF_6^- anion omitted, CH hydrogen atoms omitted, phenyl groups simplified, displacement ellipsoids shown at 50% probability). Selected bond lengths (Å) and angles (°): Ru1–F1 2.098(2), Ru1–S1 2.4338(10), Ru1–S2 2.4238(11), Ru1–P1 2.3970(9), Ru1–P2 2.4277(10), Ru1–C1 1.818(4), F1–Ru1–C1 177.70(15), S1–Ru1–F1 91.60(7), S2–Ru1–F1 92.30(7). HF bonding represented as red dotted lines.

The molecular structure depicted in Figure 3.14 is unlikely to be the complex inferred from the NMR data, as the ^{1}H NMR spectrum was devoid of N–H resonances associated with the methimazole ligands and a sharp singlet would be expected from the *trans*-disposed PPh_3 ligands in the $^{31}P\{^1H\}$ NMR spectrum.

The orientation of the methimazole groups may be influenced by subtle $H^{\delta+}$ and $F^{\delta-}$ attractive forces with approximate distances of 1.627 (H2–F1) and 1.764 Å (H1–F1). The Ru–F distance of 2.098(2) Å in **3.9x** lies within the range established by simple ruthenium fluoride complexes such as $[RuF_2(CO)(PPh_3)_2]$[64] and $[RuHF(CO)(PPh_3)_3]$,[65] and NHC derivatives reported by Pregosin and Whittlesey[65] (2.011–2.099 Å).

3.5 Synthesis of $[Ru\{\kappa^4\text{-}B,S,S',S''\text{-}B(mt)_3\}(CO)(PR_3)]$ ($R = PMe_2Ph$, $P(OMe)_3$, PCy_3)

As there are limited examples of dibuttressed ruthenaboratrane complexes, the Tm derivatives act as the closest point of comparison. Preliminary results were obtained by Tshabang on the Tm series $[Ru\{\kappa^4\text{-}B,S,S',S''\text{-}B(mt)_3\}(CO)(PR_3)]$ ($R = PMe_2Ph$, $P(OMe)_3$,

PCy_3), however, with only partial characterisation.[47] The syntheses of these complexes was revisited for comparative purposes and complete characterisation was obtained.[**]

As shown in Scheme 3.19, the complexes [Ru{κ^4-*B,S,S',S''*-B(mt)$_3$}(CO)(PMe_2Ph)] **3.10** and [Ru{κ^4-*B,S,S',S''*-B(mt)$_3$}(CO){$P(OMe)_3$}] **3.11** were prepared by the substitution of PPh_3 from the parent ruthenaboratrane [Ru{κ^4-*B,S,S',S''*-B(mt)$_3$}(CO)(PPh_3)]. The complex [Ru{κ^4-*B,S,S',S''*-B(mt)$_3$}(CO)(PCy_3)] **3.12** was produced from reaction of Na[HB(mt)$_3$] and [Ru(Ph)Cl(CO)(PCy_3)]. Improvements to Tshabang's procedures in the preparation of **3.10** and **3.11**, including performing the reactions in THF followed by diethylether workup are detailed in the experimental (Chapter 7).

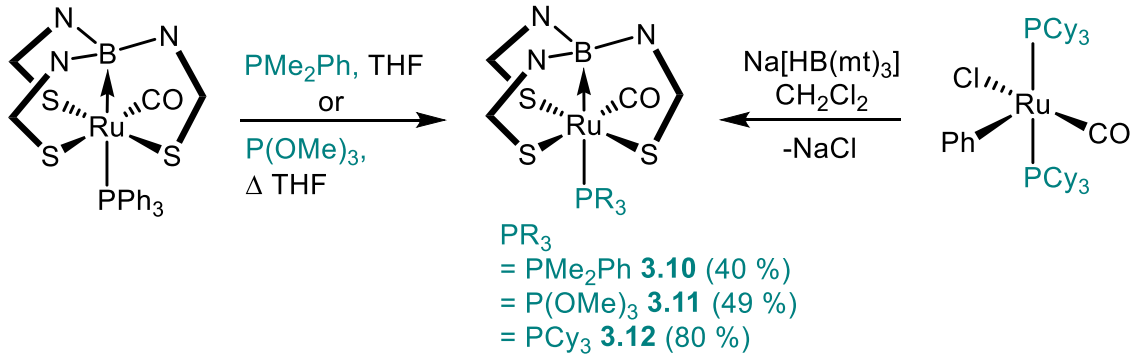

Scheme 3.19: Synthesis of [Ru{κ^4-*B,S,S',S''*-B(mt)$_3$}(CO)(PR_3)] (R = PMe_2Ph, $P(OMe)_3$, PCy_3), through improvements to Tshabang's procedures.

The ^1H, $^{13}C\{^1H\}$ and $^{31}P\{^1H\}$ spectroscopic data of **3.10** were consistent with previously reported.[47] In addition to these data, the bridgehead boron was located in the ^{11}B NMR spectrum as a singlet resonance at δ_B = 15.4 and the sodium adduct of **3.10** was observed in the HR-ESI+ mass spectrum at *m/z* = 641.0121 $[M + Na]^+$. Crystals suitable for X-ray diffraction studies were obtained from slow evaporation of a dichloromethane/*n*-pentane solution of **3.10** (Figure 3.15). Crystallographic details are discussed collectively with **3.1** and derivatives in the next section.

[**] The work in Section 3.5 has formed the basis for the recent publication:
Foreman, M. R. St.-J.; Hill, A. F.; Ma, C.; Tshabang, N.; White, A. J. P., *Dalton Trans.* **2019**, *48*, 209.

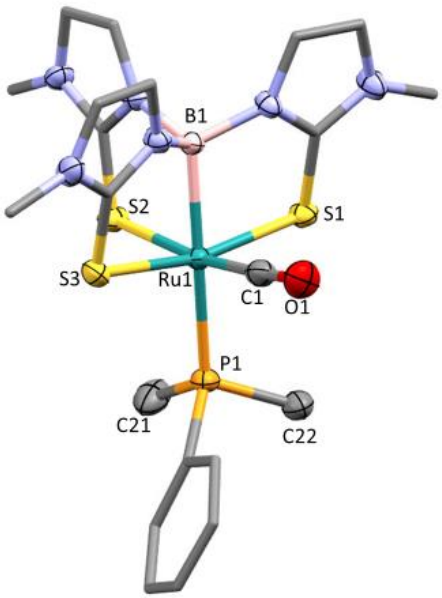

Figure 3.15: Molecular structure of [Ru{κ^4-*B,S,S′,S″*-B(mt)$_3$}(CO)(PMe$_2$Ph)] **3.10** (hydrogen atoms omitted, phenyl groups simplified, displacement ellipsoids shown at 50% probability). Selected bond lengths (Å) and angles (°): B1–Ru1 2.174(3), Ru1–P1 2.4170(7), Ru1–S1 2.3881(7), Ru1–S2 2.4938(7), Ru1–S3 2.4071(8), Ru1–C1 1.813(3), B1–Ru1–P1 173.56(8), S1–Ru1–P1 92.97(2), S2–Ru1–P1 89.52(2), S3–Ru1–P1 100.99(3).

The methodology formerly used to synthesise **3.11** involved heating the reaction under reflux in *n*-hexane followed by recrystallisation. An alternate procedure developed in the current work features heating ruthenaboratrane [Ru{κ^4-*B,S,S′,S″*-B(mt)$_3$}(CO)(PPh$_3$)] and six equivalents of P(OMe)$_3$ at reflux in THF for 16 hours. The precipitation of **3.11** from THF allowed the convenient isolation of the yellow product through filtration in 49% yield, without need for further purification.

The resonance of the P(OMe)$_3$ group in **3.11** was observed at δ_P = 159.1 as a broad singlet far downfield in the $^{31}P\{^1H\}$ NMR spectrum than the formerly reported value of –87.4 ppm. Given that both P(OMe)$_3$ ligands in the analogous complex **3.6** resonate at δ_P = 151.1 and 153.7, the similarly downfield resonance at δ_P = 159.1 was deemed plausible for **3.11**. Despite numerous crystallisation attempts, the crystals obtained were too small for X-ray diffraction analysis. However, further data were obtained to support the formulation of **3.11**, which included $^{13}C\{^1H\}$, ^{11}B NMR and mass spectrometry data. Successful substitution of the PPh$_3$ ligand for P(OMe)$_3$ was evident by the absence of signals in the aromatic region and the presence of the methoxy carbon resonance at δ_C = 50.8.

As complex **3.12** cannot be obtained cleanly through substitution of PPh_3 in [Ru{κ^4-*B,S,S',S''*-B(mt)$_3$}(CO)(PPh_3)] by PCy_3 (Scheme 3.15, Section 3.4.4), it was prepared through the direct reaction pathway following Tshabang's procedure. The IR, ^{1}H and ^{31}P{^{1}H} NMR spectroscopy agreed with previous values obtained by Tshabang. The formulation of **3.12** was supported by further characterisation obtained in the form of ^{13}C{^{1}H}, ^{11}B NMR and mass spectrometry. Coordination of the PCy_3 group was ascertained by the four carbon environments observed at δ_C = 26.9–35.3, with ^{13}C-^{31}P coupling constants in the range of 2.2–9.4 Hz.

The broad bridgehead boron resonance for complexes **3.10**, **3.11** and **3.12** was located at the same shift of δ_B = 15.4, which may suggest that the boron environment is rather insensitive to the steric and electronic variation of the *trans* phosphine. For structural comparison purposes, the molecular structure of **3.12** was obtained from slow evaporation of a dichloromethane and *n*-pentane solution and solved in a triclinic P–1 crystal system.[47] The structural features are discussed in the sections to follow.

3.6 Analysis and Comparison of Data

The series of complexes of the form [Ru{κ^3-*B,S,S'*-BH(mt)$_2$}(CO)(L$_1$)(L$_2$)] synthesised from phosphine substitution reactions of **3.1** allow assessment of the effect of various ligands on the Ru→B bond, with comparison to the Tm derivatives, [Ru{κ^4-*B,S,S',S''*-B(mt)$_3$}(CO)L]. The key structural features of complexes [Ru{κ^3-*B,S,S'*-BH(mt)$_2$}(CO)(L$_1$)(L$_2$)] (**3.1**, **3.3**–**3.6**, **3.8**) and [Ru{κ^4-*B,S,S',S''*-B(mt)$_3$}(CO)L] (PPh_3,[1] **3.10**–**3.12**) are summarised in Table 3.2.

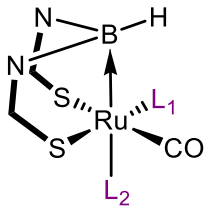

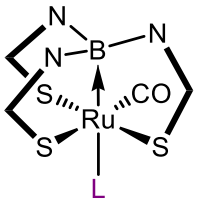

Complex [Ru{BH(mt)$_2$}CO(L$_1$)(L$_2$)] Ru – L	**Ru→B [Å]**	**δ_B (ppm)**	**ν_{CO} cm^{-1}**	**Ru – P (L$_1$) [Å]**	**Ru – P (L$_2$) [Å]**	**d(L$_2$)/ d(L$_1$)**
L$_1$, L$_2$ = PMe$_2$Ph **3.5**	2.253(4)	5.00	1877	2.288(1)	2.4094(8)	1.053
L$_1$ = PMe$_2$Ph, L$_2$ = PPh$_3$ **3.4**	-	5.13	1890	-	-	-
L$_1$ and L$_2$ = PPh$_2$C$_2$H$_2$PPh$_2$ **3.8**	2.231(2)	5.05	1905	2.2720(5)	2.3637(6)	1.040
L$_1$, L$_2$ = PPh$_3$ **3.1**	2.246(2)	4.12	1893	2.3044(4)	2.4766(4)	1.075
L$_1$, L$_2$ = P(OMe)$_3$ **3.6**	2.252(3)	3.80	1921	2.2340(9)	2.3604(9)	1.057
L$_1$ = CO, L$_2$ = PPh$_3$ **3.3**	2.237(2)	2.97	1913, 1984	n/a	2.4741(5)	n/a
[Ru{B(mt)$_3$}CO(L)]						
L = PCy$_3$ **3.12**	2.168(3)	15.4	1871	n/a	2.4894(7)	n/a
L = PMe$_2$Ph **3.10**	2.174(3)	15.4	1882	n/a	2.4170(7)	n/a
L = PPh$_3$ [1]	2.161(7)	17.1	1888	n/a	2.435(1)	n/a
L = P(OMe)$_3$ **3.11**	-	15.4	1894	n/a	-	n/a

Table 3.2: Structural data for complexes of the series [Ru{κ^3-*B,S,S'*-BH(mt)$_2$}(CO)(L$_1$)(L$_2$)] and [Ru{κ^4-*B,S,S',S''*-B(mt)$_3$}(CO)(L)].

The [Ru{κ^3-*B,S,S'*-BH(mt)$_2$}CO(L$_1$)(L$_2$)] series is ordered by increasing CO stretching frequency. This trend represents the relative decrease of electron density at the ruthenium and parallels the progressive change of electronic properties of the phosphine ligands from σ-basic to π-acidic. At the two extremes, greater electron density at the metal is expected for complex **3.5** with PMe$_2$Ph (σ-basic phosphine) compared to **3.6**, bearing π-acidic P(OMe)$_3$. Consistent with this observation, the ν_{CO} stretching frequency of **3.5** is some 44 cm^{-1} lower than **3.6**, signifying that greater back bonding occurs in the Ru–CO interaction of the former than the latter. A similar trend is noted for the [Ru{κ^4-*B,S,S',S''*-B(mt)$_3$}CO(L)] series, but the electronic variation at the metal is less pronounced than the [Ru{κ^3-*B,S,S'*-BH(mt)$_2$}CO(L$_1$)(L$_2$)] series with ν_{CO} values ranging from 1871–1894 cm^{-1}.

The Ru–L_2 bond distance (*trans* to B) in [Ru{κ^3-*B,S,S'*-$BH(mt)_2$}$CO(L_1)(L_2)$] is consistently longer than that of Ru–L_1 (*trans* to S) independent of the coordinated phosphine. This disparity in bond lengths is likely a reflection of the *trans* directing potential between the π-donating thione donor and that of the Ru$\rightarrow$B interaction, with substantial *trans* influence observed for the latter.[5] Elongation of the ligand *trans* to B (M–L) has been previously noted for metallaboratranes of different metals: $[PtI_2\{\kappa^4\text{-}B,S,S',S''\text{-}B(mt^{tBu})_3\}]$[8] ($\pi$-donor I), $[Rh\{\kappa^4\text{-}B,S,S',S''\text{-}B(mt^{Me})_3\}(PMe_3)_2]^+$ [5] (σ-donor PMe_3) and $[Fe\{\kappa^4\text{-}B,S,S',S''\text{-}B(mt^{tBu})_3\}(CO)_2]$[11] ($\pi$-acidic CO).[8] In each case the M–L bond *trans* to B was longer than that *trans* to S, despite the electronic differences of the monodentate ligands. The effect was most pronounced for the platinum complex, followed by rhodium and iron. However, the presence of different metals may compromise the generality of the trend, whereas the series [Ru{κ^3-*B,S,S'*-$BH(mt)_2$}$CO(L_1)(L_2)$] may provide a more reliable comparison given that the moiety 'Ru{$BH(mt)_2$}CO' was kept constant.

To assess the extent of the disparity between the bond lengths of Ru–L_2 and Ru–L_1, the ratio $d(L_2)/d(L_1)$ was used as a comparative measure. A larger value of $d(L_2)/d(L_1)$ reflects greater deviation between the Ru–L_2 and Ru–L_1 bond distances. Of the comparable complexes in the [Ru{κ^3-*B,S,S'*-$BH(mt)_2$}$CO(L_1)(L_2)$] series, the *trans* influence was greatest for mild σ-donor/π-acceptor PPh_3 **3.1**, followed by π-acceptor $P(OMe)_3$ **3.6** and σ-donor PMe_2Ph **3.5** ($d(L_2)/d(L_1)$ ratio in Table 3.2). This trend is inconsistent to that above, which had the opposite order for the σ-donor and π-acceptor. However, the differences between the L_2/L_1 ratios of PMe_2Ph and $P(OMe)_3$ were minimal (1.053 *cf.* 1.057) despite their contrasting electronic properties. This may favour a steric argument as PMe_2Ph and $P(OMe)_3$ both have smaller cone angles (θ_T° = 122 and 107 respectively) than that of PPh_3 (θ_T° = 145). Interestingly, the disparity in bond length was found to be the least pronounced in complex **3.8** with the bidentate dppen ligand ($d(L_2)/d(L_1)$ ratio = 1.040), which may reflect the constraints of chelation over electronic considerations. However, no viable correlation could be inferred between the elongated Ru–L_2 bond and the Ru$\rightarrow$B bond distance.

The array of values for the Ru→B bond distance in Table 3.2 show no consistent trend, suggesting that the Ru→B interaction is insensitive to the electronic and steric properties of the phosphines. The Ru→B bonds within both the [Ru{κ^3-*B,S,S'*-BH(mt)$_2$}CO(L$_1$)(L$_2$)] and [Ru{κ^4-*B,S,S',S''*-B(mt)$_3$}CO(L)] series span the remarkably small range of 2.231(2)–2.253(4) Å and 2.161(7)–2.174(7) Å, respectively. Within each series, the variation is not significant (5 e.s.d.s). The shorter Ru→B distance in the [Ru{κ^4-*B,S,S',S''*-B(mt)$_3$}CO(L)] series is likely a geometric consequence enforced by the tricyclo-[3.3.3.0] cage that draws the metal-boron closer than the bicyclo-[3.3.0] supported cage.

Tricoordinate boranes are typically planar ($\Sigma°BX_3 \approx 360°$), with pyramidalisation of the boron attending interaction with a metal (M→BX$_3$; ideal tetrahedron $\Sigma°BX_3 \approx 328°$). Thus, the degree of pyramidalisation at the boron environment was used to estimate the strength of the Ru→B bond.[29,66] Notwithstanding the usual caveats associated with the precision of hydrogen atom positions in X-ray analysis, the angle sum $\Sigma°BX_3$ of angles a + b + c (Figure 3.16) of the complexes in the [Ru{κ^3-*B,S,S'*-BH(mt)$_2$}CO(L$_1$)(L$_2$)] series span a comparatively narrow range of 317.5–326.1°, flanked by **3.1** and **3.3**. A narrower range of 324.9–325.9° was established by the [Ru{κ^4-*B,S,S',S''*-B(mt)$_3$}CO(L)] series. The geometry around boron deviates far from planarity in both series. This suggests a stronger M→B interaction than Bourissou's Group 9, 10 and 11 metallaboratranes which feature an ambiphilic di- or tri- phosphinoborane ligand adopting larger (more trigonal) $\Sigma°BX_3$ values (e.g. Group 10, M→B: 341.8–336.7°, for ligands see Scheme 4.6, Chapter 4).[29,66] The variation of pyramidalisation is most remarkable between **3.1** and **3.3** where the smaller $\Sigma°BX_3$ value (greater pyramidalisation) of **3.1** may result from the greater steric imposition of PPh$_3$ on the boron environment than CO. A steric effect may be inferred from the increase in $\Sigma°BX_3$ from PPh$_3$ to CO (Figure 3.16), with no significant deviation in the Ru→B length within the series [Ru{κ^3-*B,S,S'*-BH(mt)$_2$}CO(L$_1$)(L$_2$)].

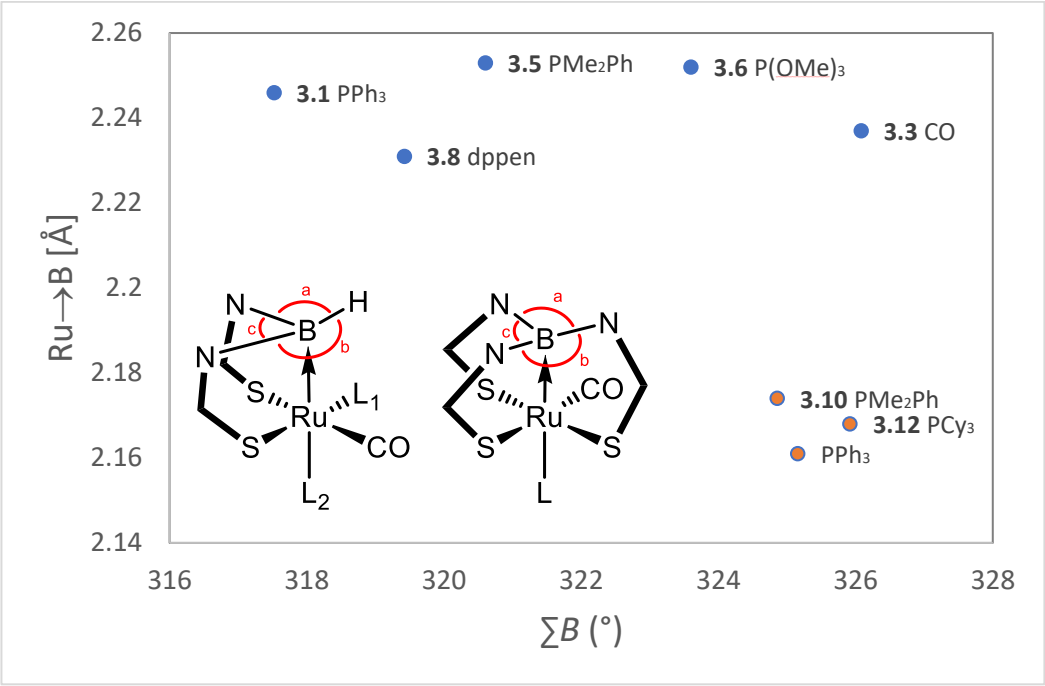

Figure 3.16: Lack of relationship between the Ru→B distance and the pyramidalization sum around the boron ($\Sigma°BX_3$) for complexes [Ru{κ^3-*B,S,S'*-BH(mt)$_2$}CO(L$_1$)(L$_2$)] (blue, **3.1**, **3.3**, **3.5**, **3.6**, **3.8**) and [Ru{κ^4-*B,S,S',S''*-B(mt)$_3$}CO(L)] (orange, **3.10**, **3.12**, PPh$_3$[1]).

With limited examples of doubly bridged ruthenaboratranes, comparisons were extended to crystallographically established sulfur-based metallaboratranes of other metal centres and tricyclo-[3.3.3.0] ruthenaboratranes (Table 3.3).

Complex (κ^4-*B,S,S',S''*)	Ru→B [Å]	δ_B (ppm)	Complex (κ^3-*B,S,S'*)	M→B [Å]	δ_B (ppm)
[Ru{B(mt)$_2$(mp)}(CO)(PPh$_3$)][67]	2.146(7)	n.g	**L3.2** [20]	2.210(5)	n.g
[Ru{B(mp)$_3$}(CO)(PPh$_3$)][67]	2.093(5)	32.5	**L3.19** [63] *	2.101(4)	15.2
[Ru{B(mt)$_3$}(CNMes)(CO)][3]	2.147(4)	n.g	**L3.20** [63] *	2.093(3)	12.5
[Ru{B(mt)$_3$}(CN^{t}Bu)(CO)][3]	2.175(7)	14.6	**L3.21** [68]	2.053(3)	8.0
[Ru{B(mt)$_3$}(CS)(PPh$_3$)][3]	2.153(7)	n.g	**L3.22** [69]	2.14(1)	10.2
[Ru{B(mt^{Ar})$_3$}(CO)(PPh$_3$)][18]	2.17(2)	n.g	**L3.23** [70]	2.142(8)	10.4
			L3.24 [71]	2.13(2)	–13.6

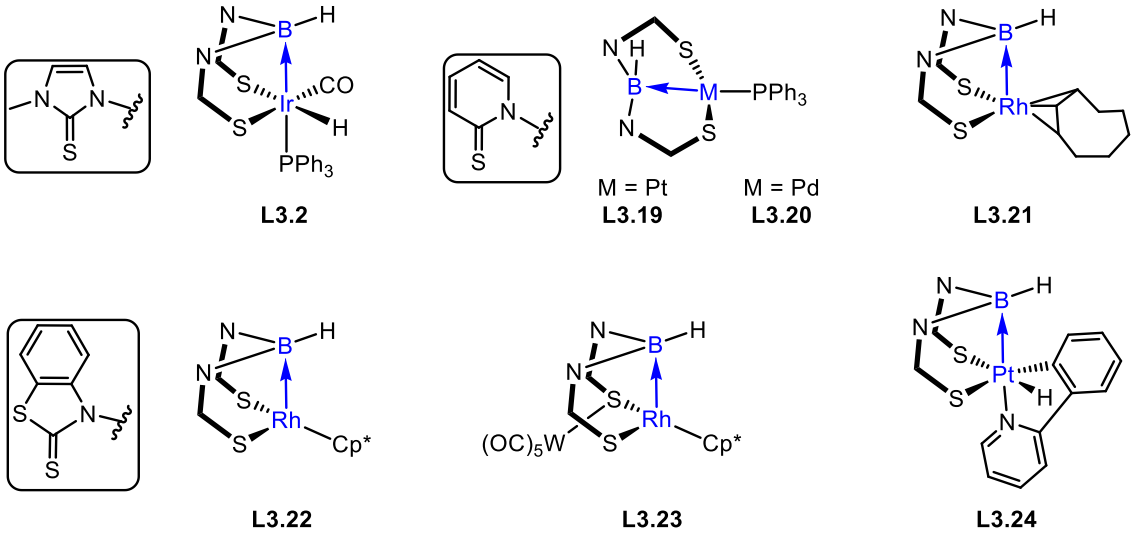

Table 3.3: Structural data for tricyclo-[3.3.3.0] ruthenaboratranes and assorted di-buttressed metallaboratranes **L3.2**, **L3.19**–**L3.24**. Ar = N-(4-chlorophenyl)-2-mercaptoimidazolyl and mp = 2-mercaptopyridinyl. *Mean value for multiple crystallographically independent metrics in the molecule(s). n.g. = not given.

The combined data from Table 3.2 and Table 3.3 are represented in Figure 3.17 as a plot of the ^{11}B NMR chemical shift against the M→B distance. Unfortunately, not all δ_B chemical shifts were reported for the complexes in Table 3.3. The Bm and Tris series independently occupy narrow ranges. The one outlier in the Tris series is the complex [Ru{κ^4-*B,S,S',S''*-B(mp)$_3$}(CO)(PPh$_3$)], which is supported by the 2-mercaptopyridinyl framework, instead of the 2-mercaptoimidazolyl system as for the other complexes within the series. Thus, variation in chemical shift may be expected from the different ligand framework. The di-buttressed complexes in Table 3.3 span a more scattered range, which can be attributed to the greater variation in both ligand and metal centre. The donating ability of the transition metal to boron varies in a triad and between groups

as determined for triphosphinoborane metallaboratrane complexes. Stronger M→B interactions were computationally and experimentally evaluated for the heavier analogues of group 9, 10 and 11.[29,72] It is unsurprising that no trends were collectively inferred from the scattered data points in Figure 3.17 given the variation of metals and constraints of chelation imposed by the di- or tri-buttressed ligand frameworks in the complexes assessed.

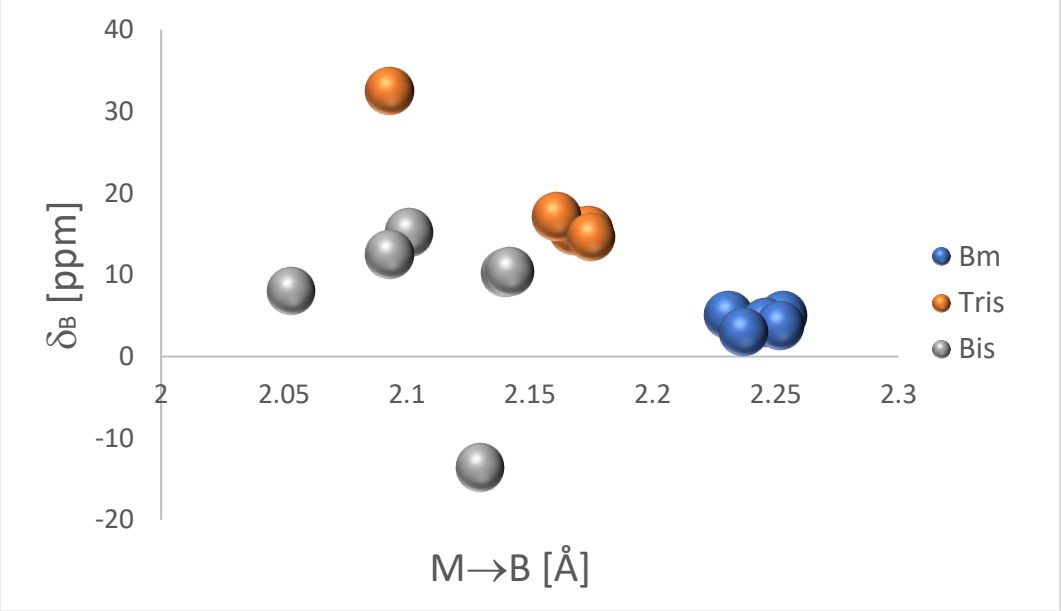

Figure 3.17: Relationship between the ^{11}B NMR chemical shift and the M→B distance for complexes in Table 3.2 and Table 3.3. Bm = [Ru{κ^3-*B,S,S'*-BH(mt)$_2$}CO(L$_1$)(L$_2$)] (**3.1**, **3.3**, **3.5**, **3.6**, **3.8**). Tris = [Ru{κ^4-*B,S,S',S''*-B(mt)$_3$}CO(L)] (**3.10**, **3.12**, PPh$_3$[1]) and derivatives in Table 3.3. Bis = complexes **L3.2**, **L3.19**–**L3.24** in Table 3.3.

3.6.1 Reactivity and Mechanism

The boron centre of Bm complexes **3.1**, **3.3**, **3.5**, **3.6** and **3.8** is comparatively more exposed than that in the Tm complexes **3.10** and **3.12**. Consequently, the boron of the Bm complexes may be predisposed towards further reactivity, which may be due to the presence of the B–H unit. Thus, accounting for the tendency of these complexes to evolve to several decomposition and by-products during the investigations in this chapter. In contrast, the bridgehead boron in the series in **3.10** and **3.12** is housed within three methimazolyl supports in a more rigidly braced tricyclo-[3.0.0.0] framework. Consistent with the expected enhanced stability, the complexes [Ru{κ^4-*B,S,S',S''*-B(mt)$_3$}CO(L)] (L = PMe$_2$Ph, P(OMe)$_3$, PCy$_3$) exhibited greater solution stability than [Ru{κ^3-*B,S,S'*-BH(mt)$_2$}CO(L$_1$)(L$_2$)].

In mechanistic considerations, the remarkable *trans* influence exerted by the Ru→B linkage would, in theory, be expected to predispose the elongated *trans* ligand (L_2) toward displacement over L_1 in the phosphine substitution reactions of **3.1**. Yet the contrary result was observed in the formation of **3.3** and **3.4**, where the CO and PMe_2Ph ligands *ultimately* occupied the equatorial position. Two potential mechanistic pathways are postulated; simple displacement (of L_1) at the equatorial position or alternatively, the initial dissociation of L_2 (PPh_3) followed by low energy rearrangement in the ensuing five-coordinate complex (*cf.* Berry *pseudo*-rotation), which then proceeds to react with the incoming ligand. No evidence of an intermediate species was observed in the reaction NMR at t ≈ 0 upon combination of **3.1** and PMe_2Ph. Although, this does not distinguish between facile phosphine substitution or rapid rearrangement, and the mechanism remains to be confirmed. Rearrangement after coordination seems unlikely for the *pseudo*-octahedral complexes, given that there was no evidence for site exchange from ^{31}P NMR measurements.

Previous qualitative discussion on the nature of the ligand *trans* to the Ru→B linkage suggests a slight preference for the stronger σ-donor ligands to occupy this position.[5] Whilst this may hold true for dicarbonyl complex **3.3**, the *trans* position in **3.4** is taken by the less σ-basic PPh_3 rather than PMe_2Ph. Electronic considerations aside, the greater steric bulk of PPh_3 over PMe_2Ph may dictate its preference for coordination *trans* to the boron (θ_T° = 145, PPh_3 *cf.* 122, PMe_2Ph).

3.7 Conclusion

A convenient one-pot synthesis for the first doubly-bridged ruthenaboratrane [Ru{κ^3-*B,S,S'*-BH(mt)$_2$}(CO)(PPh_3)$_2$] **3.1** has been developed, with the crystallographic identification of by-products [Ru(Ph)(κ^2-*N,S*-mt)(CO)(PPh_3)$_2$] **3.1x** and [Ru(C≡CPh)(CO)(PPh_3){κ^3-*H,S,S'*-H_2B(mt)$_2$}] **3.1y**.

The Ru→B linkage in **3.1** was resistant to cleavage to assume a κ^2-*S,S'* coordination mode from κ^3-*B,S,S'*. The robust nature of the linkage was evident from the lack of reactivity with HBCat or HC≡CPh; whereas degradation of **3.1** to a mixture of products occurred in the reactions with HCl, Br_2 and I_2. Decomposition upon oxidative

halogenation to $(t_{2g})^6$-Ru(II) most likely reflects the lack of occupied metal orbitals of σ-symmetry to sustain Ru→B bonding.

Complex **3.1** was shown to be a useful precursor to further ruthenaboratranes. The triphenylphosphine ligands in **3.1** were readily displaced to afford products of single or double substitution. The degree of substitution was found to be dependent on temperature and the electronic properties of the phosphine. Facile single substitution was demonstrated at room temperature to produce the complexes [Ru{κ^3-*B,S,S'*-BH(mt)$_2$}(CO)$_2$(PPh$_3$)] **3.3** and [Ru{κ^3-*B,S,S'*-BH(mt)$_2$}(CO)(PMe$_2$Ph)(PPh$_3$)] **3.4**. Double substitution was thermally promoted to produce [Ru{κ^3-*B,S,S'*-BH(mt)$_2$}(CO)(PMe$_2$Ph)$_2$] **3.5** and [Ru{κ^3-*B,S,S'*-BH(mt)$_2$}(CO)(Z-Ph$_2$PCH=CHPPh$_2$)] **3.8**. In contrast, [Ru{κ^3-*B,S,S'*-BH(mt)$_2$}(CO){P(OMe)$_3$}$_2$] **3.6** was generated at room temperature reflecting the retro-donating capacity of the π-acidic P(OMe)$_3$ to stabilise the low-valent metal centre. Crystallographic analysis revealed a consistent trend where the Ru–P bond *trans* to boron is elongated relative to that *trans* to sulfur, confirming a pronounced *trans* influence by the Ru→B bond. No general trends were inferred from the collective comparison of di- and tri-buttressed sulfur-based metallaboratrane systems.

3.8 Future Work

Within this chapter six examples of previously unknown doubly-bridged ruthenaboratrane complexes were introduced to the field of metallaboratranes, with discussion around the reactivity of the Ru→B linkage. There remains considerable potential for further investigations into the reactivity at the boron and metal.

Functionalisation of the BH moiety may provide access to heteroscorpionate systems to allow the examination of the conversion from the doubly-bridged system to the tris-system. Another potential avenue for exploration is borylene [:BR] chemistry, which has attracted increasing popularity recently with a steady library of transition metal stabilised (terminal) borylenes reported by the Braunschweig group.[73-75] Reduction at the boron of **3.1** (or an appropriate BX (X = Cl, Br, I) derivative) could lead to a redistribution of electronics such that a Ru=B interaction may ensue (i.e. σ-acceptor → σ-donor umpolung of the boron). Alternatively, hydride abstraction may in principle result in conversion to σ-boryls (i.e. σ -donor, σ-acceptor boron).

3.9 References

(1) Hill, A. F.; Owen, G. R.; White, A. J. P.; Williams, D. J. *Angew. Chem. Int. Ed.* **1999**, *38*, 2759.

(2) Foreman, M. R. S. J.; Hill, A. F.; White, A. J. P.; Williams, D. J. *Organometallics* **2004**, *23*, 913.

(3) Crossley, I. R.; Foreman, M. R. S. J.; Hill, A. F.; Owen, G. R.; White, A. J. P.; Williams, D. J.; Willis, A. C. *Organometallics* **2008**, *27*, 381.

(4) Crossley, I. R.; Foreman, M. R. S. J.; Hill, A. F.; White, A. J. P.; Williams, D. J. *Chem. Commun.* **2005**, 221.

(5) Crossley, I. R.; Hill, A. F.; Willis, A. C. *Organometallics* **2006**, *25*, 289.

(6) Crossley, I. R.; Hill, A. F.; Humphrey, E. R.; Willis, A. C. *Organometallics* **2005**, *24*, 4083.

(7) Crossley, I. R.; Hill, A. F.; Willis, A. C. *Organometallics* **2010**, *29*, 326.

(8) Crossley, I. R.; Hill, A. F.; Willis, A. C. *Organometallics* **2008**, *27*, 312.

(9) Crossley, I. R.; Hill, A. F. *Dalton Trans.* **2008**, 201.

(10) Crossley, I. R.; Hill, A. F. *Organometallics* **2004**, *23*, 5656.

(11) Figueroa, J. S.; Melnick, J. G.; Parkin, G. *Inorg. Chem.* **2006**, *45*, 7056.

(12) Pang, K.; Quan, S. M.; Parkin, G. *Chem. Commun.* **2006**, 5015.

(13) Landry, V. K.; Melnick, J. G.; Buccella, D.; Pang, K.; Ulichny, J. C.; Parkin, G. *Inorg. Chem.* **2006**, *45*, 2588.

(14) Pang, K.; Tanski, J. M.; Parkin, G. *Chem. Commun.* **2008**, 1008.

(15) Mihalcik, D. J.; White, J. L.; Tanski, J. M.; Zakharov, L. N.; Yap, G. P. A.; Incarvito, C. D.; Rheingold, A. L.; Rabinovich, D. *Dalton Trans.* **2004**, 1626.

(16) Senda, S.; Ohki, Y.; Hirayama, T.; Toda, D.; Chen, J.-L.; Matsumoto, T.; Kawaguchi, H.; Tatsumi, K. *Inorg. Chem.* **2006**, *45*, 9914.

(17) Lopez-Gomez, M. J.; Connelly, N. G.; Haddow, M. F.; Hamilton, A.; Orpen, A. G. *Dalton Trans.* **2010**, *39*, 5221.

(18) Qin, Y.; Ma, Q.; Jia, A.-Q.; Chen, Q.; Zhang, Q.-F. *J. Coord. Chem.* **2013**, *66*, 1405.

(19) Foreman, M. R. S. J.; Hill, A. F.; Owen, G. R.; White, A. J. P.; Williams, D. J. *Organometallics* **2003**, *22*, 4446.

(20) Crossley, I. R.; Hill, A. F.; Willis, A. C. *Organometallics* **2005**, *24*, 1062.

(21) Owen, G. R. *Transition Met. Chem.* **2010**, *35*, 221.

(22) Hill, A. F. *Organometallics* **2006**, *25*, 4741.

(23) Parkin, G. *Organometallics* **2006**, *25*, 4744.

(24) Sircoglou, M.; Bontemps, S.; Mercy, M.; Saffon, N.; Takahashi, M.; Bouhadir, G.; Maron, L.; Bourissou, D. *Angew. Chem. Int. Ed.* **2007**, *46*, 8583.

(25) Crossley, I. R.; Hill, A. F.; Willis, A. C. *Organometallics* **2005**, *24*, 4889.

(26) Rudolf, G. C.; Hamilton, A.; Orpen, A. G.; Owen, G. R. *Chem. Commun.* **2009**, 553.

(27) Moret, M.-E.; Peters, J. C. *J. Am. Chem. Soc.* **2011**, *133*, 18118.

(28) Suess, D. L. M.; Peters, J. C. *J. Am. Chem. Soc.* **2013**, *135*, 4938.

(29) Sircoglou, M.; Bontemps, S.; Bouhadir, G.; Saffon, N.; Miqueu, K.; Gu, W.; Mercy, M.; Chen, C.-H.; Foxman, B. M.; Maron, L.; Ozerov, O. V.; Bourissou, D. *J. Am. Chem. Soc.* **2008**, *130*, 16729.

(30) Wilton-Ely, J. D. E. T.; Honarkhah, S. J.; Wang, M.; Tocher, D. A.; Slawin, A. M. Z. *Dalton Trans.* **2005**, 1930.

(31) Lowman, D. W.; Ellis, P. D.; Odom, J. D. *J. Magn. Resonance* **1972**, *8*, 289.

(32) Beall, H.; Bushweller, C. H.; Dewkett, W. J.; Grace, M. *J. Amer. Chem. Soc.* **1970**, *92*, 3484.

(33) Bushweller, C. H.; Beall, H.; Grace, M.; Dewkett, W. J.; Bilofsky, H. S. *J. Amer. Chem. Soc.* **1971**, *93*, 2145.

(34) Rickard, C. E. F.; Roper, W. R.; Taylor, G. E.; Waters, J. M.; Wright, L. J. *J. Organomet. Chem.* **1990**, *389*, 375.

(35) Bohle, D. S.; Clark, G. R.; Rickard, C. E. F.; Roper, W. R.; Wright, L. J. *J. Organomet. Chem.* **1988**, *358*, 411.

(36) Torres, M. R.; Vegas, A.; Santos, A.; Ros, J. *J. Organomet. Chem.* **1986**, *309*, 169.

(37) Werner, H.; Meyer, U.; Peters, K.; Von Schnering, H. G. *Chem. Ber.* **1989**, *122*, 2097.
(38) Echavarren, A. M.; López, J.; Santos, A.; Montoya, J. *J. Organomet. Chem.* **1991**, *414*, 393.
(39) Braunschweig, H.; Dewhurst, R. D. *Dalton Trans.* **2011**, *40*, 549.
(40) Tolman, C. A. *J. Am. Chem. Soc.* **1970**, *92*, 2953.
(41) Tolman, C. A. *J. Am. Chem. Soc.* **1970**, *92*, 2956.
(42) Taher, D.; Al-Noaimi, M.; Mohammad, S.; Corrigan, J. F.; MacDonald, D. G.; El-khateeb, M. *Inorg. Chim. Acta* **2010**, *363*, 4134.
(43) Parsons, S.; Mclachlan, F.; Bailey, P.; Davidson, J.; Johnstone, R. *CSD Communication* **2006**.
(44) Landgrafe, C.; Sheldrick, W. S. *J. Chem. Soc., Dalton Trans.* **1996**, 989.
(45) Bricklebank, N.; Godfrey, S. M.; Mackie, A. G.; McAuliffe, C. A.; Pritchard, R. G.; Kobryn, P. J. *J. Chem. Soc., Dalton Trans.* **1993**, 101.
(46) M. Godfrey, S.; A. McAuliffe, C.; Mushtaq, I.; G. Pritchard, R.; M. Sheffield, J. *J. Chem. Soc., Dalton Trans.* **1998**, 3815.
(47) Tshabang, N. PhD Thesis, The Australian National University, 2005.
(48) Borowski, A. F.; Sabo-Etienne, S.; Donnadieu, B.; Chaudret, B. *Organometallics* **2003**, *22*, 4803.
(49) Gloaguen, Y.; Alcaraz, G.; Pecharman, A.-F.; Clot, E.; Vendier, L.; Sabo-Etienne, S. *Angew. Chem. Int. Ed.* **2009**, *48*, 2964.
(50) Ayed, T.; Barthelat, J.-C.; Tangour, B.; Pradere, C.; Donnadieu, B.; Grellier, M.; Sabo-Etienne, S. *Organometallics* **2005**, *24*, 3824.
(51) Delpech, F.; Sabo-Etienne, S.; Chaudret, B.; Daran, J.-C. *J. Am. Chem. Soc.* **1997**, *119*, 3167.
(52) Delpech, F.; Sabo-Etienne, S.; Daran, J.-C.; Chaudret, B.; Hussein, K.; Marsden, C. J.; Barthelat, J.-C. *J. Am. Chem. Soc.* **1999**, *121*, 6668.
(53) Hussein, K.; Marsden, C. J.; Barthelat, J.-C.; Rodriguez, V.; Conejero, S.; Sabo-Etienne, S.; Donnadieu, B.; Chaudret, B. *Chem. Commun.* **1999**, 1315.
(54) Saito, T.; Kuwata, S.; Ikariya, T. *Chem. Lett.* **2006**, *35*, 1224.
(55) Hill, A. F.; McQueen, C. M. A. *Organometallics* **2014**, *33*, 1909.
(56) Fu, Q.; Zhang, L.; Yi, T.; Zou, M.; Wang, X.; Fu, H.; Li, R.; Chen, H. *Inorg. Chem. Commun.* **2013**, *38*, 28.
(57) McQueen, C. M. A.; Hill, A. F.; Ma, C.; Ward, J. S. *Dalton Trans.* **2015**, *44*, 20376.
(58) Hill, A. F.; Ma, C.; McQueen, C. M. A.; Ward, J. S. *Dalton Trans.* **2016**, *Submitted*.
(59) Sung, S.; Ang, A.; Hill, A. F.; Ma, C.; Kong, R. Y.; Ward, J. S.; Young, R. D. *Eur. J. Inorg. Chem.* **2018**, *2018*, 2855.
(60) Lin, T.-P.; Peters, J. C. *J. Am. Chem. Soc.* **2013**, *135*, 15310.
(61) Mitton, S. J.; McDonald, R.; Turculet, L. *Angew. Chem. Int. Ed.* **2009**, *48*, 8568.
(62) Takaya, J.; Iwasawa, N. *Dalton Trans.* **2011**, *40*, 8814.
(63) Zech, A.; Haddow, M. F.; Othman, H.; Owen, G. R. *Organometallics* **2012**, *31*, 6753.
(64) Brewer, S. A.; Coleman, K. S.; Fawcett, J.; Holloway, J. H.; Hope, E. G.; Russell, D. R.; Watson, P. G. *J. Chem. Soc., Dalton Trans.* **1995**, 1073.
(65) Reade, S. P.; Nama, D.; Mahon, M. F.; Pregosin, P. S.; Whittlesey, M. K. *Organometallics* **2007**, *26*, 3484.
(66) Bontemps, S.; Sircoglou, M.; Bouhadir, G.; Puschmann, H.; Howard, J. A. K.; Dyer, P. W.; Miqueu, K.; Bourissou, D. *Chem. Eur. J.* **2008**, *14*, 731.
(67) Owen, G. R.; Hugh Gould, P.; Charmant, J. P. H.; Hamilton, A.; Saithong, S. *Dalton Trans.* **2010**, *39*, 392.
(68) Dyson, G.; Zech, A.; Rawe, B. W.; Haddow, M. F.; Hamilton, A.; Owen, G. R. *Organometallics* **2011**, *30*, 5844.
(69) Anju, R. S.; Roy, D. K.; Mondal, B.; Yuvaraj, K.; Arivazhagan, C.; Saha, K.; Varghese, B.; Ghosh, S. *Angew. Chem. Int. Ed.* **2014**, *53*, 2873.
(70) Roy, D. K.; De, A.; Panda, S.; Varghese, B.; Ghosh, S. *Chem. Eur. J.* **2015**, *21*, 13732.

(71) Neshat, A.; Shahsavari, H. R.; Mastrorilli, P.; Todisco, S.; Haghighi, M. G.; Notash, B. *Inorg. Chem.* **2018**, *57*, 1398.
(72) Kameo, H.; Hashimoto, Y.; Nakazawa, H. *Organometallics* **2012**, *31*, 4251.
(73) Bauer, J.; Braunschweig, H.; Damme, A.; Carlos, J. O.; Kramer, J.-H. T.; Radacki, K.; Shang, R.; Siedler, E.; Ye, Q. *J. Am. Chem. Soc.* **2013**, *135*, 8726.
(74) Braunschweig, H.; Kramer, T.; Radacki, K.; Shang, R.; Siedler, E.; Werner, C. *Chem. Sci.* **2014**, *5*, 2271.
(75) Braunschweig, H.; Shang, R. *Inorg. Chem.* **2015**, *54*, 3099.

Chapter 4

Investigation of Aluminium-based Pro-ligands and Complexes

4.1 Introduction

The field of scorpionate chemistry is rich with boron-based ligand frameworks, whereas the heavier analogue aluminium has received limited attention. Similarly, boryl-based pincer systems have been investigated since their introduction by Yamashita and Nozaki in 2009,[1] with research directed to aluminium only recently emerging. As the third most abundant metal in the earth's crust, aluminium exists in minerals as aluminium oxides and hydroxides. It also plays a dominant role in numerous industrial applications, best known for Lewis acid catalysis, and in an organometallic context as co-catalyst methylaluminoxane (MAO, $[Al(CH_3)_xO_y]_n$) in Ziegler-Natta olefin polymerisation for the production of unbranched alkanes.[2] In contrast to boron, directly bonded transition metal-aluminium organometallic complexes are rare, particularly those of 3-coordinate aluminyls, i.e. involving 2c2e sp^2 M–AlR_2 species, although tetrahydroaluminate complexes involving 3c2e AlHM bonding are well represented. This no doubt reflects the greater reactivity of aluminium compared to boron, a consequence of the more highly electropositive (ionic) nature of aluminium (Pauling electronegativity 1.61 [Al] *cf.* 2.04 [B]). Group 13 elements are typically found in the M(III) oxidation state whereas the lower M(I) state occurs for all except boron.[3] It is noteworthy that boron has non-metal properties while aluminium is considered a metal despite some chemical similarities to boron.

4.1.1 Aluminium-based Coordination Chemistry

Early examples of transition metal aluminium complexes date back to 1965 with Brunner's reported synthesis of the 1:1 $Cp_2WH_2.AlMe_3$ adduct **L4.1a**, where the 'Cp_2WH_2' unit was believed to act as a Lewis base to the Lewis acid $AlMe_3$ moiety.[4] This formulation was based on IR and low temperature NMR spectroscopic data that eliminated the possibility of bridged species **L4.1b**, but was later disproved in 1984 by Caulton. Through crystallographic means the structure was instead revealed as the hydride bridged species **L4.1c** featuring five coordinate aluminium (Scheme 4.1).[5] This provides an alternative structural representation for the subsequent compounds **L4.2–L4.4** prepared by Storr and Thomas, although yet to be confirmed through single crystal analysis.[6] Another example of a terminal aluminium hydride bridged species established by crystallographic studies is $[ReH_4(\eta^2\text{-}H_2AlMe_2)(PPh_2Me)_2]$, where the $[H_2AlMe_2]^-$ unit is η^2 bound to rhenium through two hydrides.[7]

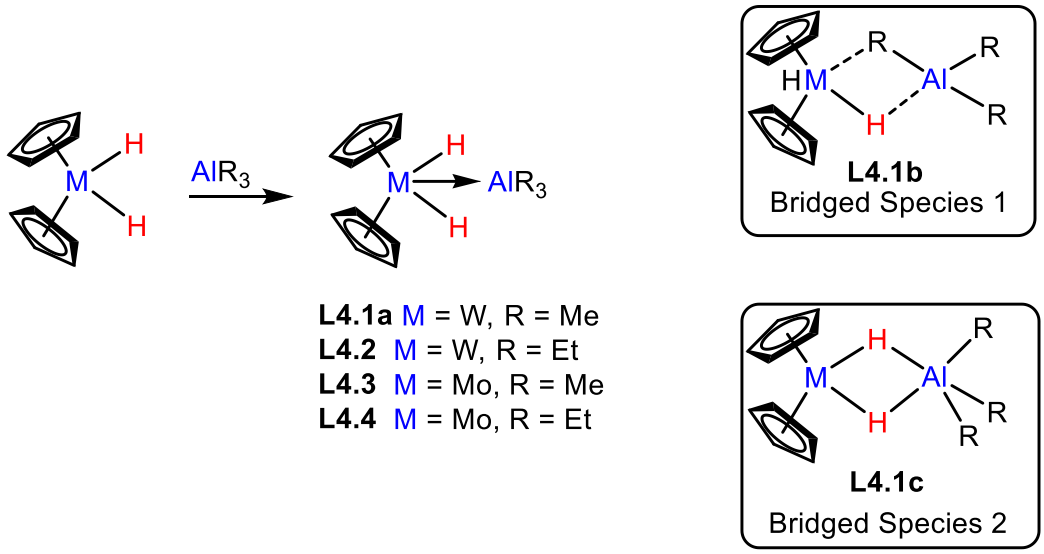

Scheme 4.1: Lewis Acid – Base adducts and bridged species of the form $[MH_2(Cp)_2].AlR_3$ (M = Mo, W; R = Me, Et) **L4.1a–L4.4**.

Following Brunner's report, the alkane elimination potential of related molybdenum and tungsten adducts with organo-aluminium derivatives AlR_3 (R = Me, Et, Ph) and $AlMe_2H$ was investigated by Storr and Thomas.[6] Solutions of **L4.2–L4.4** in benzene underwent slow decomposition at room temperature accompanied by the evolution of alkane. No alkane elimination was observed for **L4.1a** over prolonged periods at room temperature, as might be expected due to the increased basicity of the metal down a group (Mo to W) within the d-block. Replacing alkyl substituents on aluminium with hydrogen results in reduced σ-stabilisation of aluminium and thus the preparation of stable $[MH_2(Cp)_2].AlH_3$ 'adducts' was unsuccessful. The $AlMe_2H$ based analogues demonstrate preferential elimination of dihydrogen over alkane, perhaps an indication of the greater reactivity of the aluminium hydrogen bond compared to the aluminium carbon bond.

Three decades later, two different covalent Ir–Al interactions were established in complexes **L4.5** and **L4.6** (Scheme 4.2), depending on the choice of the alkyl aluminium reagent used.[8] A Lewis acid-Lewis base adduct **L4.5** was formed with $AlPh_3$ where the dative Ir–Al interaction is supported by two hydrogens. In contrast, double deprotonation of $[IrH_2(PMe_3)(Cp^*)]$ by $AlEt_3$ resulted in direct Ir–Al covalent bonds in dimer **L4.6**.

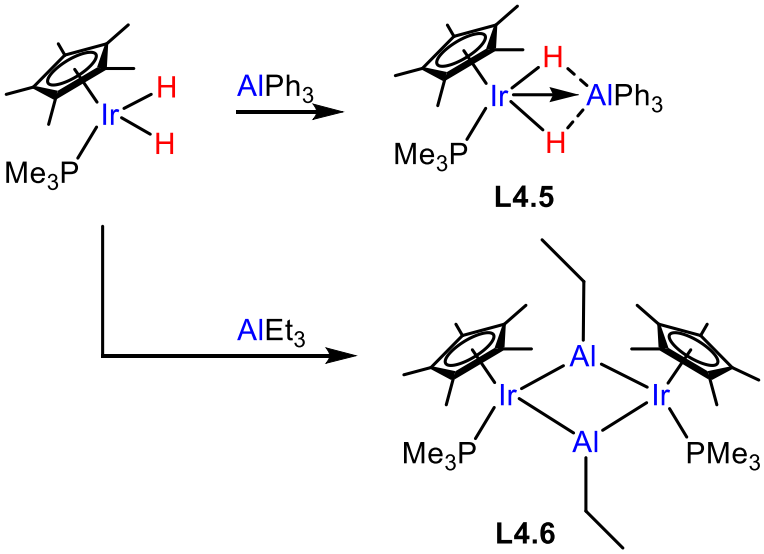

Scheme 4.2: Iridium-aluminium heterobimetallics showing dative Ir→Al interaction **L4.5** and Ir–Al covalent bond **L4.6**.

Prior to this discovery, the first example of an unbridged transition metal-aluminium complex containing a direct iron-aluminium bond was discovered by Burlitch and Hughes (Scheme 4.3).[9] A crystallographic study of $[Et_4N][Fe(AlPh_3)(CO)_2(Cp)]$ $[Et_4N]$**[L4.7]**$^-$ showed that the anionic complex is composed of a direct Fe–Al bond (2.510(2) Å) and was the first example of an organometallic compound featuring an Fe–Al bond. Another illustration of an unbridged transition metal-aluminium interaction is provided by $[Rh(AlMe_2Cl)_2(PMe_3)_2(Cp)]$ **L4.8** with a rhodium-aluminium bond length of 2.458(1) Å.[10]

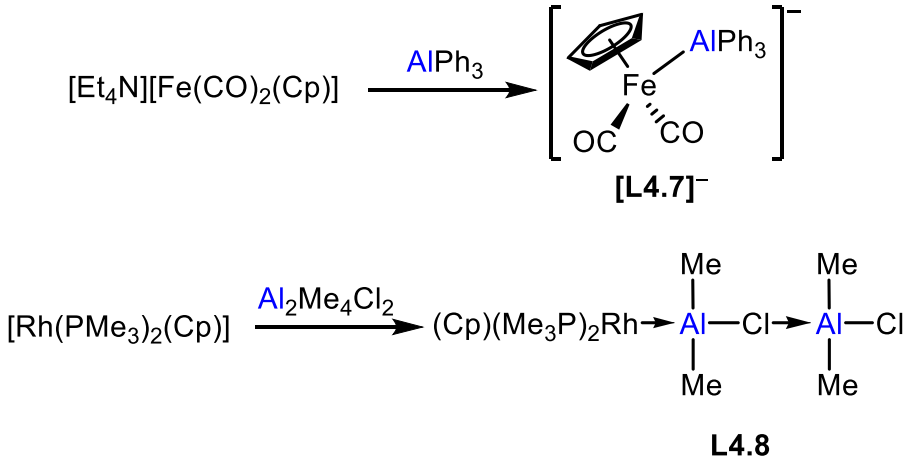

Scheme 4.3: Examples of unbridged transition metal-aluminium complexes by Burlitch and Hughes (**[L4.7]**$^-$) and Mayer and Calabrese (**L4.8**).

Braunschweig and co-workers developed the first examples of heteroleptic NHC-phosphane-platinum(0) (**L4.10**, **L4.11** and **L4.13**), homoleptic NHC-platinum(0) (**L4.12**) and homoleptic phosphane-platinum(0) complexes (Scheme 4.4),[11-13] where the strong σ-donation of the NHC leads to enhanced Lewis basicity of the complex.[13,14] The NHC-platinum-phosphane complexes **L4.10–L4.13** were generated *via* ligand displacement of precursor [$Pt(PR_3)_2$] (R = Cy, ^{i}Pr). The corresponding Lewis base/acid platinum(0)-aluminium halide adducts were also synthesised (**L4.9a**–**L4.9e**, **L4.13a** and **L4.13b**) and provide further illustration of unsupported metal only Lewis pairs (MOLPs).

Spectroscopic assessment of the complexes provided preliminary evidence of the increased density around platinum, owing to the strong σ-donating properties of the NHC ligand. Through computational studies it was found that the electronic effect of $P^{i}Pr_3$ was similar to that of the NHC ligands, IMes and SIMes.[13] Structural analysis of the platinum(0)-aluminium halide complexes (**L4.9a-b**, **L4.9d-e**, **L4.13a**, **L4.11**) ascertained the connectivity between aluminium and platinum, and showed little deviation in the Al–Pt bond length (2.368(2)–2.386(1) Å). Additionally, the ^{27}Al nucleus was located around δ_{Al} = 41.3–68.9 with the one bond ^{27}Al-^{195}Pt coupling constants determined in the magnitude range of 1933–2200 Hz. The current library of unsupported metal-only dative bonded complexes encompasses s-, p- and d-block Lewis acids that participate in the formation of MOLPs of the form [$(Cy_3P)_2Pt\rightarrow ECl_n$] (E = Be, Al, Ga, Zr, n = 2, 3, 4).[11,12,15,16] The molecular structures of these complexes consistently feature an unusual T-shaped geometry about the platinum. This geometry is similarly present in complexes of the geminal PAl ligand [$Mes_2PC(=CHPh)Al^{t}Bu_2$], which comprises of a strained four-membered cyclic (M→AlCP) structure that has found application in the fixation and activation of small molecules.[17,18]

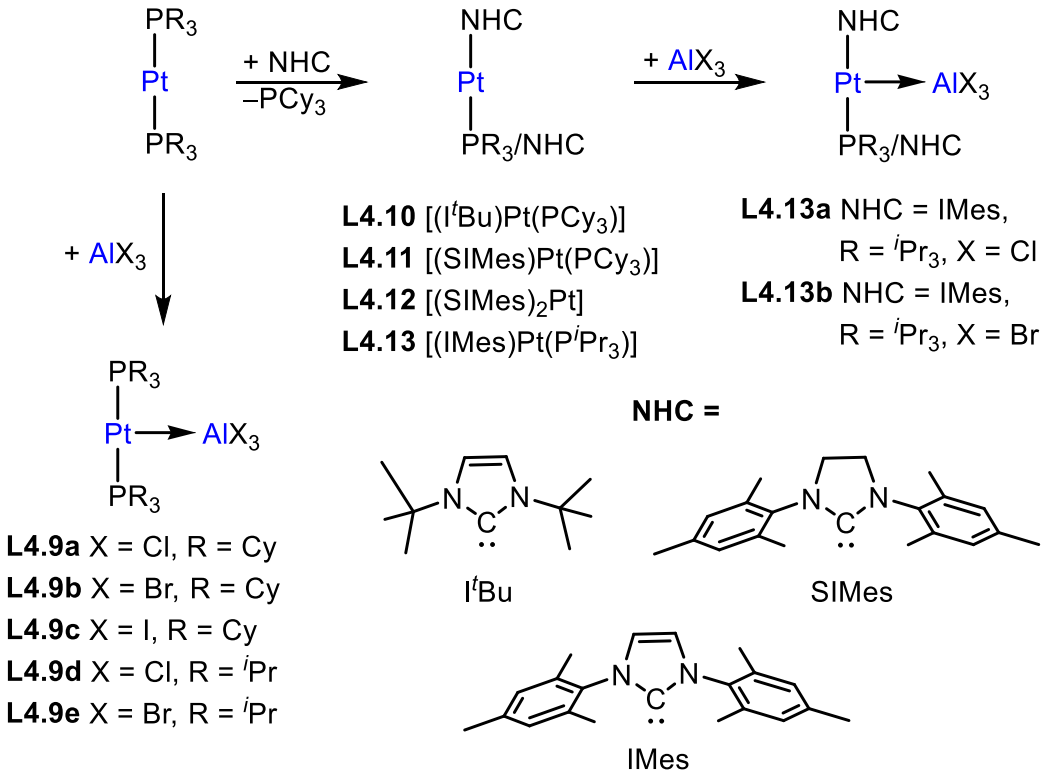

Scheme 4.4: Platinum(0)-aluminium halide complexes prepared by Braunschweig and co-workers.

Aluminium based pro-ligands of the form $[AlR_xH_y]^n$ (n = 3-x-y) are rarely isolated independently and are instead more commonly stabilised by ether solvated lithium ion(s). Stalke isolated the reactive intermediates **L4.14** (mono-substituted) and **L4.15** (di-substituted) *en route* to the formation of $Al[N(Me_3Si)_2]_3$, illustrated from crystallographic data reproduced in Figure 4.1.[19]

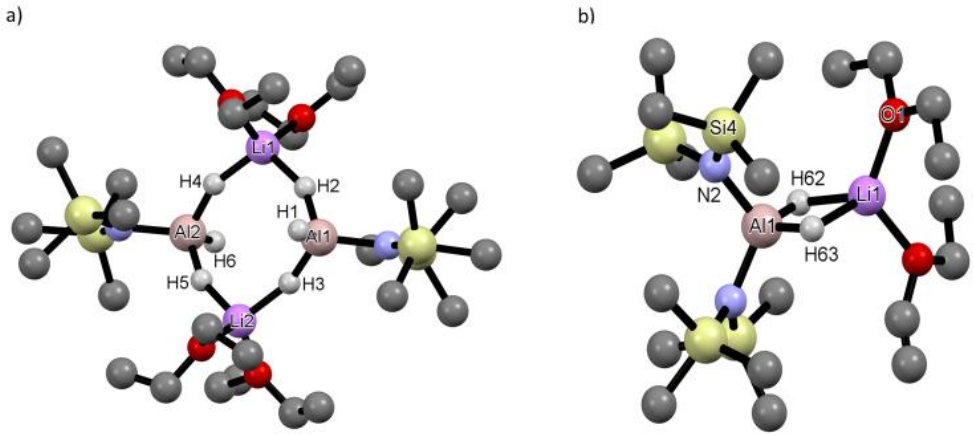

Figure 4.1: Crystal structure of a) $[H_3AlN(Me_3Si)_2Li.2Et_2O]_2$ **L4.14** and b) $H_2Al[N(Me_3Si)_2]_2Li.2Et_2O$ **L4.15** by Stalke (alkyl hydrogen atoms omitted).

In the solid-state compound **L4.14** exists as a dimer with two $[H_3AlN(Me_3Si)_2]^-$ units bridged by $[Li(OEt_2)_2]^+$ with Li–H contacts, where the average contact distance is 1.777 and 1.610 Å for Al–H. Similarly, in the monomeric structure of di-substituted compound **L4.15** the aluminium hydrides are bridged by lithium concomitantly coordinated to two ether molecules. Effervescence of the crystals was observed at temperatures higher than –30°C for **L4.14** and +5°C for **L4.15**. The decomposition occurs presumably with the loss of dihydrogen and provides an indication to the (in)stability of these complexes.

Four coordinate aluminium compounds of greater stability typically feature an organoaluminium 'AlR_2' unit enclosed within the walls of sterically encumbered scaffolds. Mason utilised the dipyrromethene (deprotonated form: *N,N*) backbone with an appropriate organoaluminium source to produce the monomeric compounds (*N,N*)AlR_2 (R = Me, ^{t}Bu, Ph, H, **L4.16a–d**) in Scheme 4.5.[20]

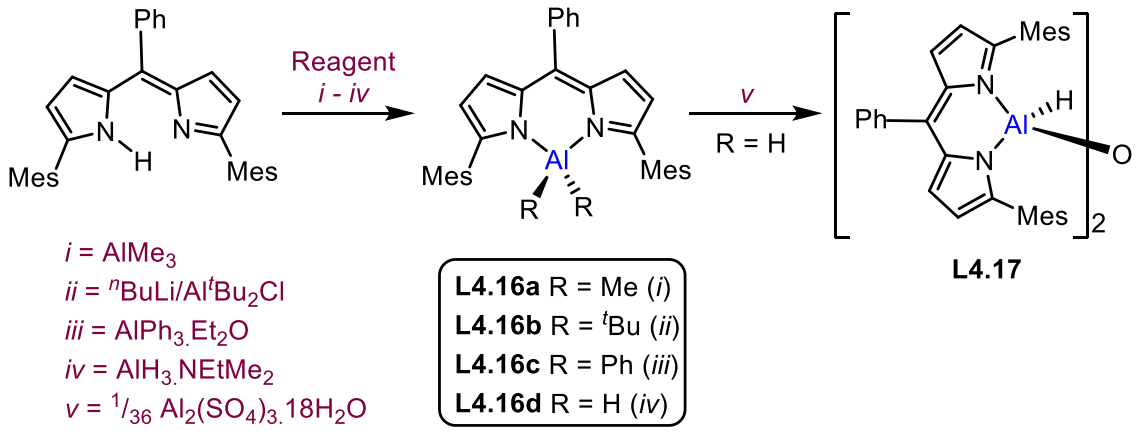

Scheme 4.5: Monomeric dipyrromethene complexes **L4.16a–d** and bimetallic oxo-bridged dimer **L4.17**.

The alkyl and aryl analogues are surprisingly tolerant and stable in air and moisture (for a short period of time) and can be purified *via* column chromatography. Alkyl aluminium complexes of the bulky β-diketiminate backbone prepared by Smith are similarly stable.[21] Dihydride **L4.16d** has greater reactivity than **L4.16a–c** and forms dimer **L4.17** upon exposure to moisture. Compound **L4.17** can be independently synthesised *via* controlled hydrolysis with aluminium sulfate hydrate. The preference of aluminium to adopt higher coordination numbers than boron was evident by the straightforward synthesis and isolation of **L4.17**. The analogous boron derivative has evaded isolation, instead existing as the three-coordinate borenium cation $[(N,N)BH]^+$.[22]

In the last decade the 'Frustrated Lewis Pairs' (FLPs) concept has attracted growing interest owing to the catalytic applications of compounds featuring both Lewis acid and Lewis base components within the same molecular framework. First reported by Stephan and Erker,[23] main group FLPs typically consist of a Lewis basic phosphine and a Lewis acidic borane separated through steric 'frustration', which prevents quenching of both components. FLPs have been shown to participate in metal-free dihydrogen activation as surveyed in a recent review.[24] The extension to involve transition metals as the Lewis acid (early TM) or Lewis base (middle/late TM) component is a developing avenue, though much previously reported chemistry may be reinterpreted within this conceptual framework.[25] In addition, ambiphilic ligands containing Lewis acid and Lewis base functionalities have been developed and those of group 13 elements are shown in Scheme 4.6.[26-32] Of particular interest are the di-substituted (**L4.19**) and tri-substituted (**L4.18**) phosphinoaluminium ligands.

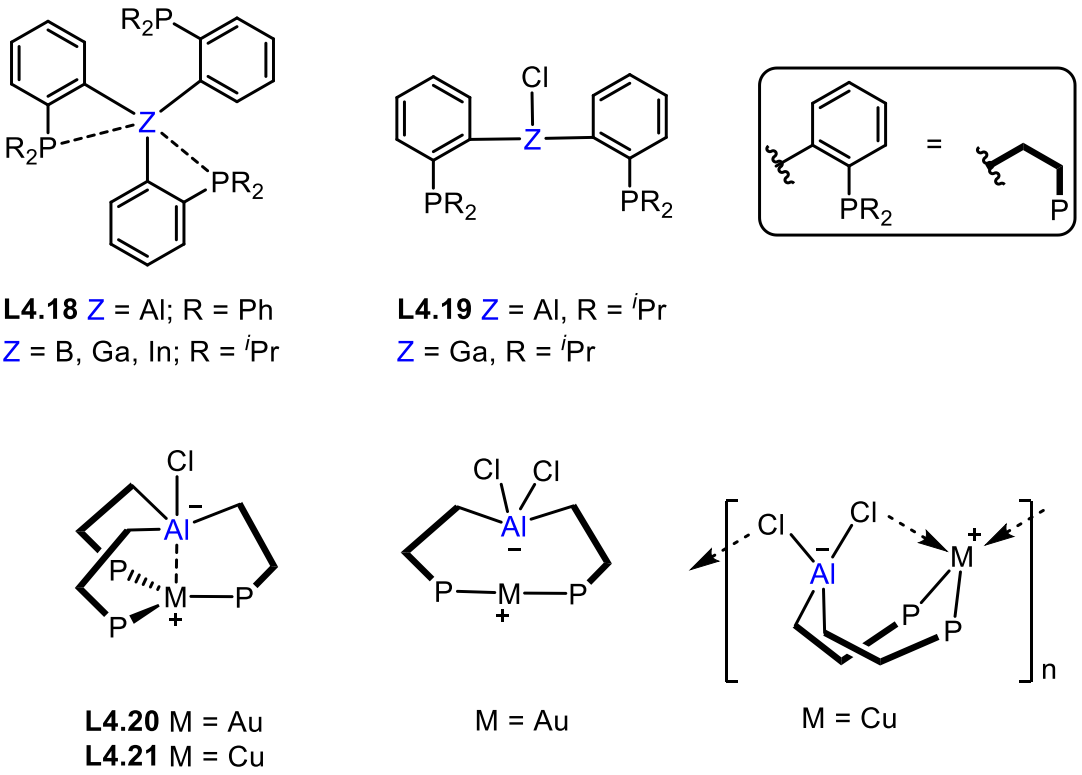

L4.18 Z = Al; R = Ph
Z = B, Ga, In; R = ^{i}Pr

L4.19 Z = Al, R = ^{i}Pr
Z = Ga, R = ^{i}Pr

L4.20 M = Au
L4.21 M = Cu

M = Au

M = Cu

Scheme 4.6: Aryl bridged ambiphilic ligands of Group 13 elements.
Complexes of trisubstituted and disubstituted ambiphilic aluminium ligands (P = P^{i}Pr$_2$).

While the triphosphinoborane ligand can form metallaboratranes with group 9–11 metals, the aluminium tri- and di-substituted derivatives prefer to exist as zwitterionic complexes of gold and copper through M–X activation (Scheme 4.6).[27,30,31,33]

Based on crystallographic and computational analysis the M–Al interaction in **L4.20** and **L4.21** was considered weak relative to the boron based variant, and is thus more appropriately described as zwitterionic.

As an extension to the well-studied poly(pyrazolyl)borate chemistry, poly(pyrazolyl)aluminate ligands are prepared *via* treatment of a solution of $LiAlH_4$ in diethyl ether with 2, 3 or 4 equivalents of 3,5-disubstituted pyrazoles, Ph_2pzH, $^{i}Pr_2pzH$ or Me^{t}BupzH (Scheme 4.7).[34,35]

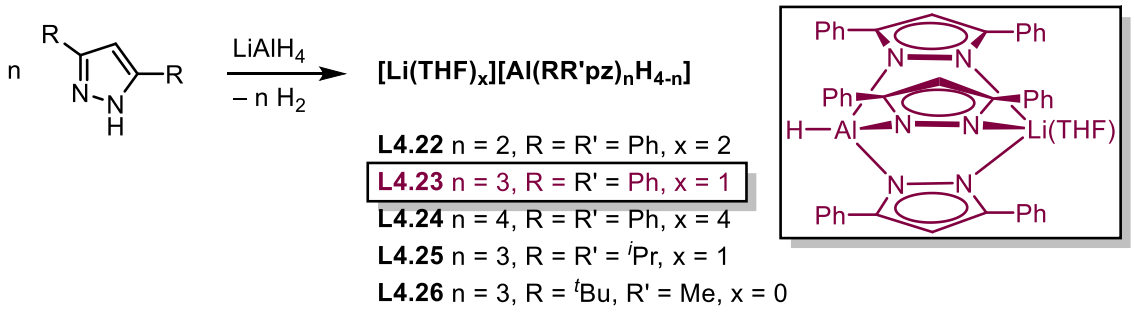

Scheme 4.7: Synthesis of poly(pyrazolyl)aluminate ligands **L4.22**–**L4.26**, with the structure of **L4.23** is shown as an illustration of the analogy to hydrotris(pyrazolyl)borate (Tp).

The reactivity of ligand **L4.23** was investigated through reaction with a range of metal halides MCl_2 (M = Zn, Mg, Co, Mn, Fe, Ni, Cu) at ambient temperature. Coordination of **L4.23** to zinc was achieved through successful displacement of the lithium(THF) unit by zinc, ascertained *via* spectroscopic and crystallographic analysis. In contrast, reaction with the other metal halides (Mg, Co) resulted in cleavage of the Al–N bond and pyrazolate transfer; consistent with the absence of Al–H IR absorptions and confirmed in X-ray diffraction studies. Furthermore, reduction of the metal was common for MCl_2 (where M = Mn, Fe, Ni, Cu) and occurs through hydride transfer from aluminium to the metal followed by subsequent reductive elimination. This accounts for the observed formation of insoluble black precipitates, presumed to be the metal. These degradation pathways are similar to that observed of the Tm and Bm chemistry. Cleavage of Ga–N bonds during attempted installation of pyrazolyl and methimazolyl gallate ligands was also a recurrent observation in the early and eventually abandoned chemistry of these ligands.[36,37]

The most recent advancements in the field include the synthesis and coordination of **L4.27** and **L4.29** to late transition metals (Scheme 4.8).[38-40] The selected examples in Scheme 4.8 demonstrate the successful isolation of an aluminium ligand supported by a PNNNP framework with stabilisation of the transition metal centre by the phosphine arms. Takaya and Iwasawa's **L4.28** displayed high catalytic activity for the hydrosilation of CO_2 and Sakaki and Nakao's **L4.30** contained an aluminyl ligand of sufficient Lewis acidity to coordinate pyridine.

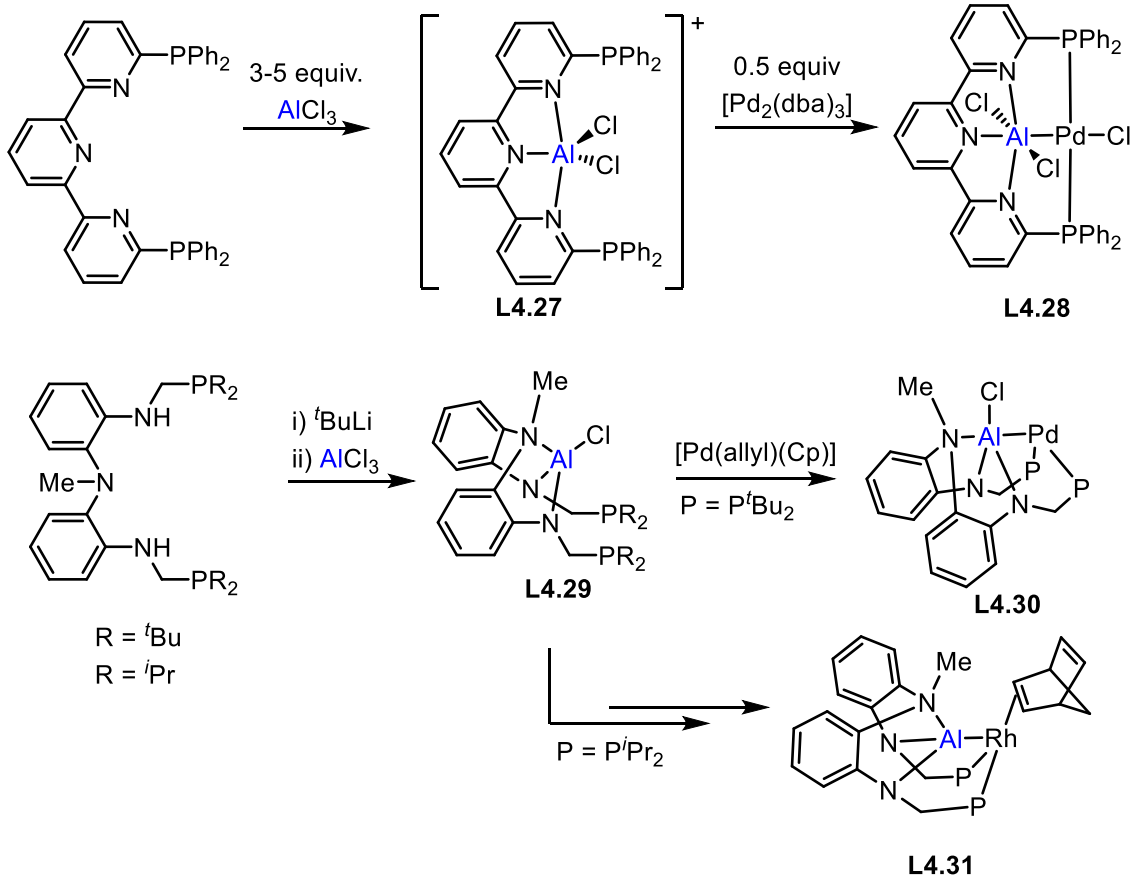

Scheme 4.8: Synthesis of aluminium ligands supported by PNNNP framework **L4.27** and **L4.29**, and coordination to late transition metals (**L4.28**, **L4.30** and **L4.31**).

With established protocols in bis(methimazolyl)borate chemistry and given the limited examples of aluminium bearing tridentate ligands present in the literature, this chapter details the design of coordination pro-ligands that feature a reactive aluminium centre (of the form $R_2AlH_2^-$ and R_3AlH^-) for subsequent coordination to receptive metal substrates.

4.2 Synthesis of Aluminium-based Pro-ligands

The successful development of pincer pro-ligands of non-conventional donors (B, Si) and the fertile field of poly(methimazolyl)borate coordination chemistry (Chapter 1) begs exploration into incorporation of aluminium units within the pincer and scorpionate scaffolds.

Attempts to prepare the benzoaluminadiazole pincer pro-ligand (**4.1a** or **4.1b**, Scheme 4.9) *via* treatment of $(HNCH_2PPh_2)_2C_6H_4$-1,2 (^{Ph}PNNP) with $LiAlH_4$ appeared promising as deduced from NMR spectroscopy. The ^{Ph}PNNP starting material (δ_P = –18.4) was consumed within two hours of the reaction and a new resonance emerged in the $^{31}P\{^1H\}$ NMR spectrum at δ_P = –19.7. Removal of the solvent produced a gummy oily residue that did not yield crystals suitable for an X-ray diffraction study despite numerous attempts.

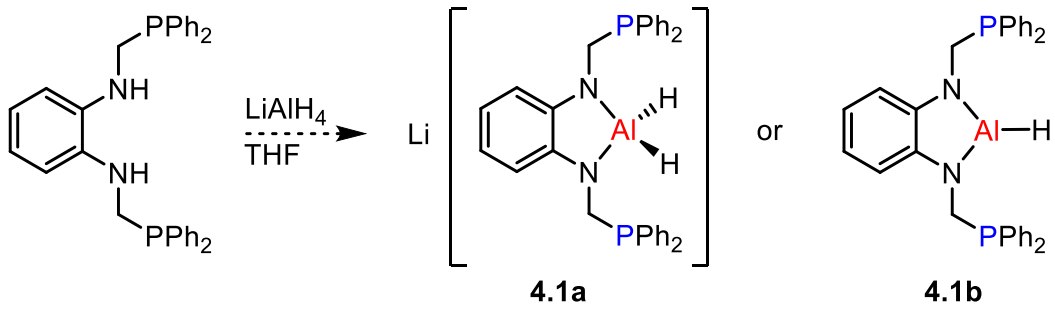

4.1a **4.1b**

Scheme 4.9: Attempted synthesis of aluminium-based ^{Ph}PNNP pincer ligand.

Depending on the substitution pattern at the aluminium centre, two possible products were postulated, anionic R_2AlH_2 **4.1a** or neutral R_2AlH **4.1b**. To identify the product formed, an ^{27}Al NMR experiment was performed. Due to the quadrupolar nature of the ^{27}Al nucleus, the $^1J_{AlH}$ coupling constant could not be discerned from the apparent broad singlet (δ_{Al} = 103.7).* Furthermore, both ESI(+) and ESI(-) mass spectra returned unidentifiable peaks, although either form of the pro-ligand would have been expected to be hydrolytically sensitive, with little likelihood of enduring ESI conditions (acetonitrile or methanol matrices).

* The NMR active aluminium isotope ^{27}Al nuclei is 100% abundant with spin $I=5/2$. The coupled nuclei are expected to appear as a doublet (when coupled to one ^{1}H). However, the short relaxation time of quadrupolar ^{27}Al nuclei results in a broadened signal where the multiplets are poorly resolved except in the case of a highly symmetric electric field, e.g., $[AlH_4]^-$; the ^{27}Al resonance for $LiAlH_4$ was observed at δ_{Al} = 100.3 as a quintet $^1J_{AlH}$ = 175.5 Hz.

It was envisaged the nature of the ligand might be clarified from coordination to a metal substrate. The ruthenium precursor $[Ru(Ph)Cl(CO)(PPh_3)_2]$ is commonly used in reactions with boron-based tridentate ligands, such as in the synthesis of boryl pincer complex $[Ru\{B(NCH_2PPh_2)_2C_6H_4\text{-}1,2\}Cl(CO)(PPh_3)]$[41] and ruthenaboratrane $[Ru\{\kappa^4\text{-}B,S,S',S''\text{-}B(mt)_3\}(CO)(PPh_3)_2]$.[42] The addition of $[Ru(Ph)Cl(CO)(PPh_3)_2]$ to a solution of the ligand that was generated *in situ* resulted in instantaneous formation of black insoluble residue and a yellow supernatant. The ^1H and ^{31}P NMR spectra of the supernatant contained a mixture of resonances (≈10), with the known dihydride complex $[RuH_2(CO)(PPh_3)_3]$[43] and triphenylphosphine as the major components of the mixture.

The rigidity of the ^{Ph}PNNP system may impose geometric restrictions, particularly for anionic **4.1a** where a tetrahedral Al centre may be expected. The ease of handling and accurate weighing for subsequent metal coordination reactions was also complicated by the oily nature of the isolated ligand. Therefore, it was envisaged that a methimazole based scorpionate system, where the ligands are typically obtained as solid salts, might be an attractive alternative. Treatment of methimazole (Hmt) in THF with $LiAlH_4$ led to the formation of $Li[H_2Al(mt)_2]$ **4.2** (Scheme 4.10), the lithium-aluminium analogue of the well-studied $Na[H_2B(mt)_2]$.

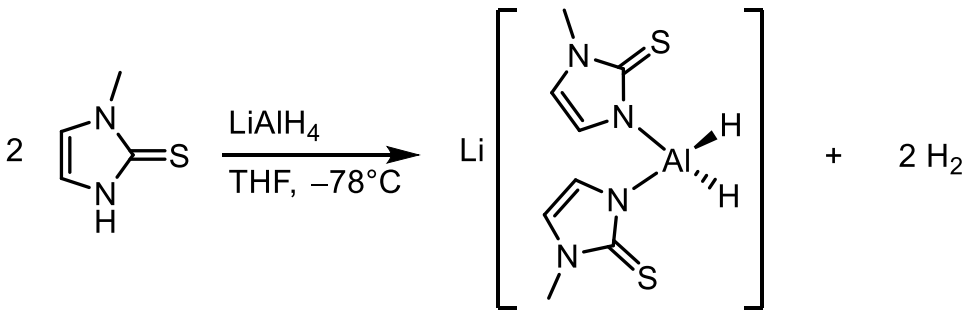

4.2

Scheme 4.10: Synthesis of $Li[H_2Al(mt)_2]$ ligand.

The formulation of **4.2** follows from spectroscopic data and was confirmed by a single crystal X-ray diffraction study (Figure 4.2). The ^1H NMR spectrum of **4.2** showed a downfield shift of all resonances relative to the starting material. The chemically inequivalent olefinic resonances were resolved as a doublet ($^3J_{HH}$ = 2.0 Hz) and a broad singlet at the respective shifts at δ_H = 5.91 and 6.71. The broad singlet is presumably a manifestation of the quadrupolar effects of the aluminium nuclei on the olefinic proton four bonds away. An extremely broadened singlet at δ_H = 4.72 (h.h.w. = 326 Hz) was

inferred to be due to Al–H. Additionally, the ν_{AlH} absorption was found in both the solid -state and tetrahydrofuran solution IR spectra at 1815 cm^{-1} and 1800 cm^{-1} (broad) respectively. A broad resonance was observed at δ_{Al} = 126.9 in the ^{27}Al NMR spectrum, indicative of the unsymmetrical environment around aluminium.

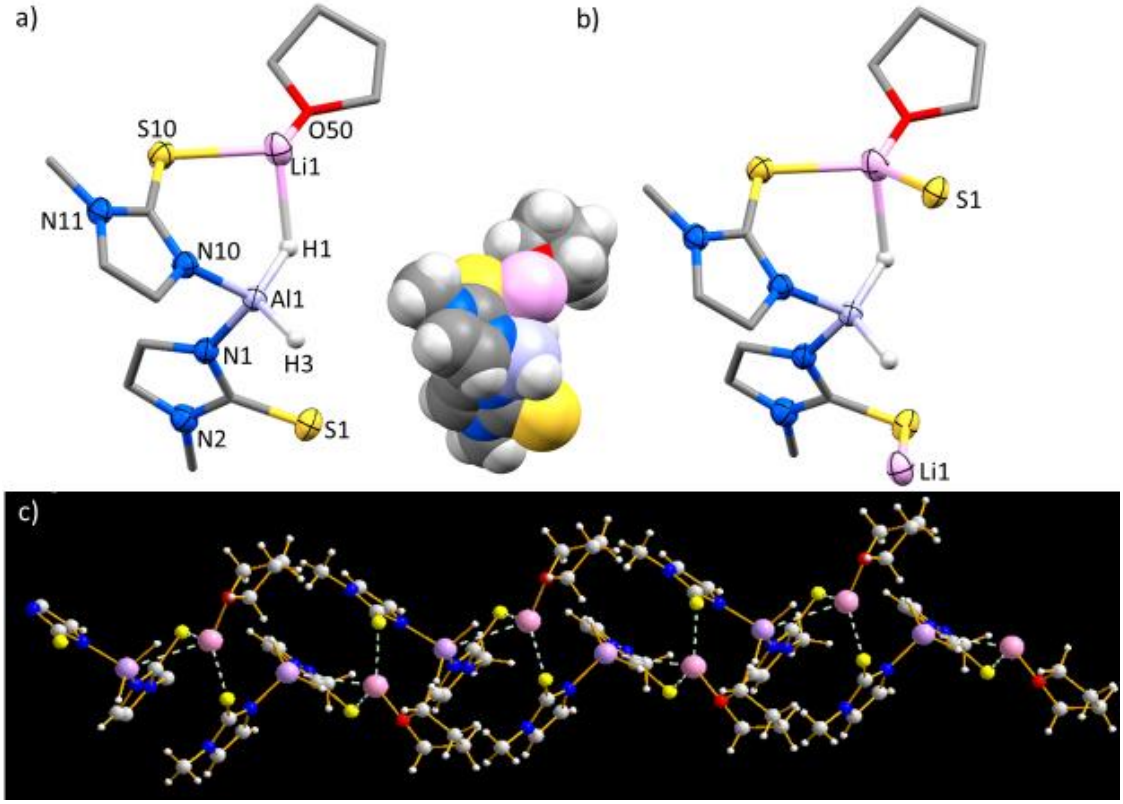

Figure 4.2: a) Molecular structure of $Li[H_2Al(mt)_2].THF$ **4.2** in a crystal as the asymmetric unit b) polymer contact point through Li1–S1 and c) polymeric representation (CH hydrogens omitted, displacement ellipsoids shown at 50% probability). Selected bond lengths (Å) and angles (°): Al1–H1 1.53(2), Al1–H3 1.54(2), Al1–N1 1.908(1), Al1–N10 1.914(1), S1–C1 1.711(2), S10–C10 1.707(2), N1–Al1–N10 98.89(6), N1–Al1–H1 107.1(8), N10–Al1–H1 113.3(8), N1–Al1–H3 111.7(8), N10–Al1–H3 106.3(8), H1–Al1–H3 118.0(11). Aluminium-bound hydrogen atomic coordinates were located from a Fourier Difference map and refined isotropically.

Analysis of the crystal structure revealed the solid state structure of $Li[H_2Al(mt)_2].THF$ is polymeric and comprises of a $[Li(THF)]^+$ unit bound to both an aluminium hydride (H1) and a sulfur atom (S10) (Figure 4.2c). The measured distance of Li1–H1 (2.12 Å) is greater than that of bridging lithium hydrogen interactions in the solid state structure of $LiAlH_4$ (1.88–2.00 Å).[34] In comparison, the asymmetric unit cell of the sodium borate analogue, $Na[\kappa^1\text{-}H_2B(mt^{Me})_2].3H_2O$, contains a '$Na(OH_2)_2$' unit bound to the sulfur atom of $[H_2B(mt^{Me})_2]^-$.[44] There are no appreciable interactions between the sodium and the

nearest boron hydride, although the approximate Na–H distance of 2.584 Å falls within the range 2.03(1)–2.7(2) Å established by complexes in the CCDC that have a Na–HBH unit. The molecular structures of both the borate and aluminate salts feature a distorted tetrahedral geometry at the respective boron and aluminium centres. However, the distortion is more pronounced for **4.2** with a N1–Al–N10 angle of 98.89(6)° (*cf.* N–B–N angle of 107.6(1)°), which might be influenced by the aluminium existing as a part of a 6-membered chelate ring compared to the non-chelated boron centre.

Compound **4.2** is air and moisture sensitive, decomposing in air to methimazole within 30 minutes in the solid state. This is in direct contrast to the $Na[H_2B(mt)_2]$ salt, which can be isolated and stored under air. The sodium-aluminium derivative $Na[H_2Al(mt)_2]$ was expected to have lesser Lewis acidity than lithium salt **4.2**. However, attempts to prepare $Na[H_2Al(mt)_2]$ from $NaAlH_4$ and methimazole returned only starting material.

Encouraged by the successful isolation of the di-substituted **4.2**, the synthesis of tri-substituted $Li[HAl(mt)_3]$ **4.3** was investigated (Scheme 4.11). Treatment of three equivalents of Hmt with $LiAlH_4$ in tetrahydrofuran resulted in effervescence and the formation of a white precipitate of poor solubility in tetrahydrofuran and C_6D_6. Compound **4.3** had slightly better solubility in d_8-toluene, where the ^1H NMR spectrum contained a singlet methyl resonance of **4.3** (δ_H = 2.90) and olefinic protons at δ_H = 5.50 and 5.70 as broad singlets. As the resonances of methimazole are located at similar chemical shifts, the assignment of **4.3** was not definitive by ^1H NMR spectroscopy.

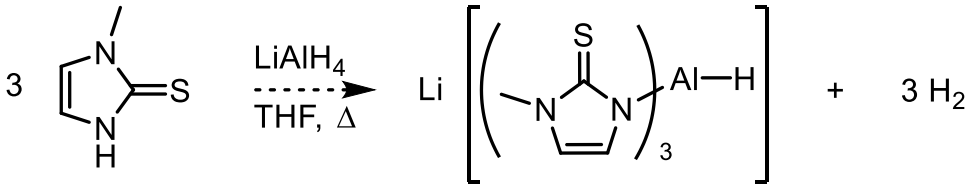

4.3

Scheme 4.11: Attempted synthesis of $Li[HAl(mt)_3]$ ligand.

Crystals grown from a tetrahydrofuran solution of **4.3** yielded microcrystalline solids that were too small for an X-ray diffraction study. The mass spectra of **4.3** returned a series of unidentifiable peaks and given the similar occurrence for disubstituted **4.2**, the absence of useful data from mass spectrometry is not a reliable assessment of the success of the synthesis. While tri-substituted **4.3** is expected to be less reactive than **4.2**, the ligand is nevertheless susceptible to oxygen and moisture and a solid sample of

4.3 in air progressively becomes pink over six hours. As the confirmation of **4.3** *via* crystallographic and spectroscopic means was unsuccessful, efforts were directed towards capturing the ligand within a metal coordination sphere.

The first metallaboratrane, [Ru{κ^4-*B,S,S',S''*-B(mt)$_3$}(CO)(PPh$_3$)], was isolated from ruthenium σ-organyl precursors [Ru(CH=CHR)Cl(CO)(PPh$_3$)$_2$] (R = Ph, CPh$_2$OH, C$_6$H$_4$Me-4) and Na[HB(mt)$_3$].[42] It was anticipated that similar reactivity might be observed with the hypothesised aluminium ligand **4.3**. Treatment of [Ru(CH=CHPh)Cl(CO)(PPh$_3$)$_2$] with **4.3** resulted in a mixture of complexes within 30 minutes that were observed at δ_P = 25.7 (broad), 31.8 (broad) and 42.0 (sharp singlet) in the $^{31}P\{^1H\}$ NMR spectrum. The signal at δ_P = 42.0 was consistent with complex [Ru(CH=CHPh)(mt)(CO)(PPh$_3$)$_2$] reported by Wilton-Ely.[45]

Attempts to isolate the complexes giving rise to the broad resonances encouraged further conversion into this side product. This was observed when the reaction was trialled with various solvents (benzene, THF, Et$_2$O), different reaction times and scales (NMR to preparative). The methodologies employed thus far have proven unsuccessful in confirming the existence of the proposed ligand. Given that *trans* disposition of aluminium and phosphorus centres in the targeted metallaluminatrane [Ru{κ^4-*Al,S,S',S''*-Al(mt)$_3$}(CO)(PPh$_3$)] might be expected to result in quadrupolar broadening of the ^{31}P resonances, the observation of unidentified intermediates giving rise to broadened resonances at δ_P = 25.7 and 31.8 remains tantalising.

4.3 Reactivity of Li[H$_2$Al(mt)$_2$] with Metal Precursors

4.3.1 Ruthenium

Given the extensive library of Bm$^{R'}$ ruthenium(II) complexes and the synthesis of complexes in Chapters 2 and 3, coordination of **4.2** was first investigated with various ruthenium(II) substrates.

The complex [RuH(CO)(PPh$_3$){κ^3-*H,S,S'*-H$_2$B(mt)$_2$}] **2.1** (Chapter 2) features a remarkably robust 3c2e BHRu interaction. Therefore, the synthesis of the analogous aluminium based complex [RuH(CO)(PPh$_3$){κ^3-*H,S,S'*-H$_2$Al(mt)$_2$}] **4.4** was explored (Scheme 4.12). Within 30 minutes of the reaction between Li[H$_2$Al(mt)$_2$].THF and [RuHCl(CO)(PPh$_3$)$_3$] (Scheme 4.12a), broad resonances at δ_H = –7.70 (apparent singlet) and δ_H = –9.45

(apparent doublet) were observed in the ^{1}H NMR spectrum. Additionally, the presence of complex $[RuH_2(CO)(PPh_3)_3]$ **4.4x** was also inferred from the spectrum. The broad signals were postulated as the respective Al–H–Ru and Ru–H interactions of complex **4.4** (Figure 4.3). The broadening of these resonances was attributed to the quadrupolar nature of aluminium influencing the aluminium bound hydrides. Alternatively, the broadened resonances might reflect the occurrence of fluxional processes, such as the swapping of Al–H in the 3c2e bonding to ruthenium. However, the absence of fluxional processes in the analogous boron complex **2.1** would suggest otherwise.

The corresponding $^{31}P\{^{1}H\}$ NMR resonance of the desired product was located at δ_P = 51.0 and confirmed by two dimensional $^{1}H^{31}P$ experiments. Consistent with the broad signals observed in the ^{1}H NMR spectrum, the $^{31}P\{^{1}H\}$ resonance is similarly broad (h.h.w. = 19 Hz) when compared to that of $[Ru(Ph)Cl(CO)(PPh_3)_2]$ (h.h.w. = 14 Hz).

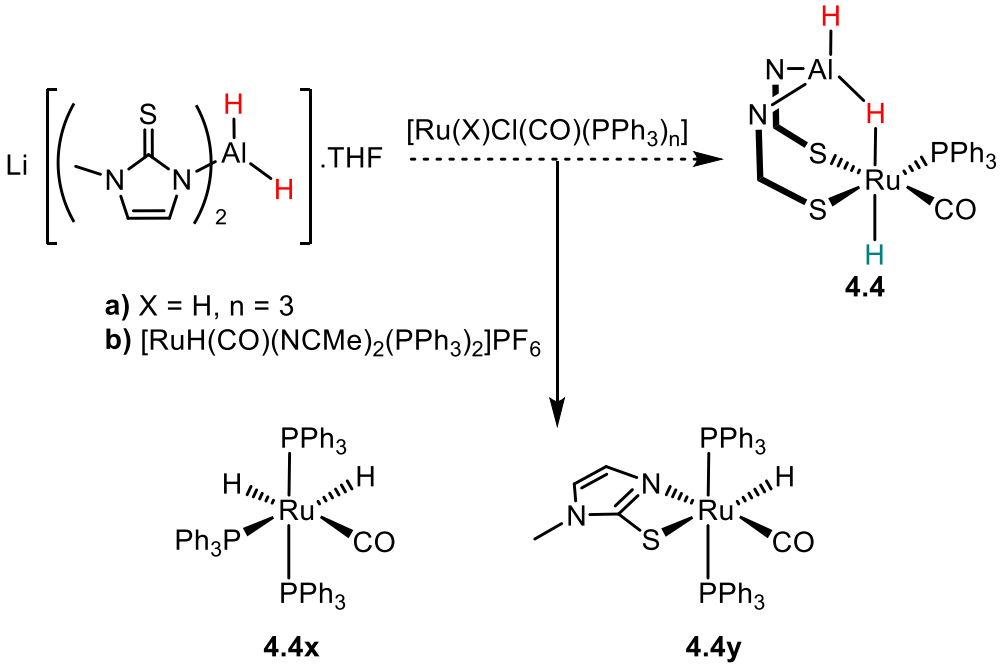

Scheme 4.12: Reaction of $Li[H_2Al(mt)_2].THF$ with Ru(II) precursors towards the synthesis of **4.4**. Actual products obtained were **4.4x** and **4.4y**.

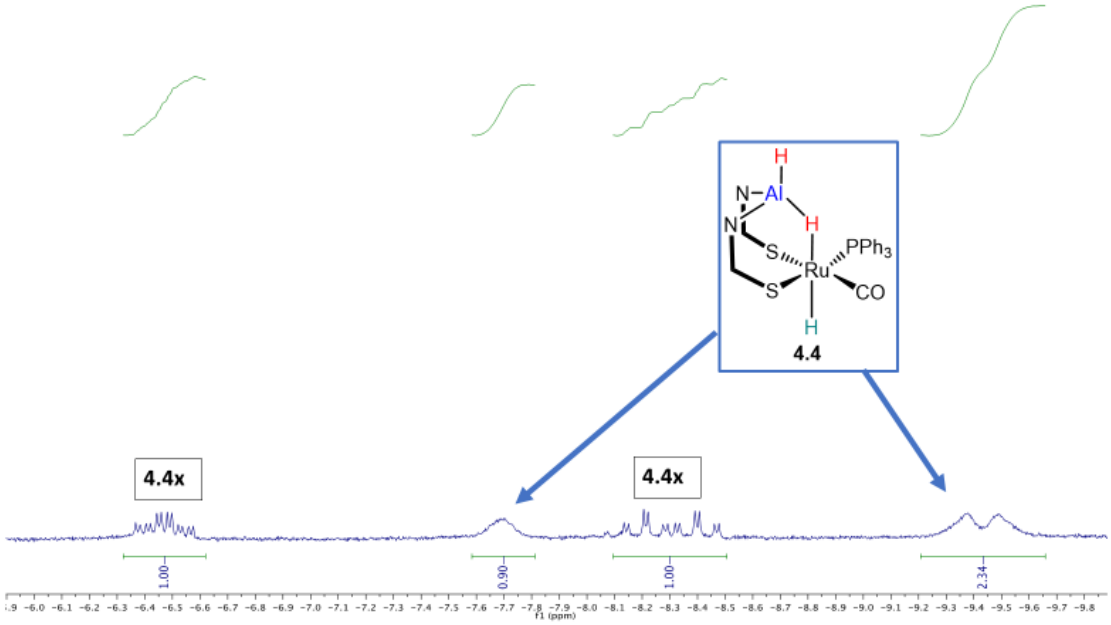

Figure 4.3: Coordination of $Li[H_2Al(mt)_2].THF$ to $[RuHCl(CO)(PPh_3)_3]$, hydride region of the crude NMR (C_6D_6), taken at 30 minutes.

The hypothesised complex **4.4** appears to be a kinetic product of poor stability, as evident by the disappearance of the resonances at δ_H = –7.70 and –9.45 in the same NMR sample taken at one hour. Instead the sample was mainly populated by two hydride complexes that were identified as **4.4x** and $[RuH(\kappa^2\text{-}N,S\text{-mt})(CO)(PPh_3)_2]$ **4.4y** *via* comparison of ^1H and $^{31}P\{^1H\}$ NMR data with literature values reported by Wilkinson[43] and Wilton-Ely, respectively.[45] The two hydride environments in **4.4x** exhibited characteristic splitting patterns from coupling to the *cis* hydride, and the ^{31}P nuclei from the two PPh_3 environments. The hydride *trans* to PPh_3 resonated as a double of triplet of doublets (δ_H = –8.3, $^2J_{HP}$ = 74, $^2J_{HP}$ = 29, $^2J_{HH}$ = 6 Hz) while the hydride *trans* to CO was a triplet of doublet of triplets (δ_H = –6.5, $^2J_{HP}$ = 31, $^2J_{HP}$ = 16, $^2J_{HH}$ = 6 Hz). Similarly, two resonances in the $^{31}P\{^1H\}$ NMR spectrum of the reaction, a triplet (δ_P = 45.9, $^2J_{PP}$ = 18 Hz, *cis* PPh_3) and doublet (δ_P = 58.0, $^2J_{PP}$ = 18 Hz, *trans*-disposed PPh_3) provided further support of the presence of side product **4.4x**.

The formation of complex **4.4y** in the reaction mixture was likewise determined *via* ^1H (δ_H hydride = –12.16, $^2J_{HP}$ = 20 Hz) and $^{31}P\{^1H\}$ (δ_P = 49.9) NMR assignments. Complexes **4.4x** and **4.4y** feature as two possible decomposition products of **4.2** in the presence of the $[RuHCl(CO)(PPh_3)_3]$ precursor. The higher reactivity of **4.2** compared to the boron analogue $Na[H_2B(mt)_2]$ is shown by the ease of coordination, where $[RuH(CO)(PPh_3)\{\kappa^3\text{-}H,S,S'\text{-}H_2Al(mt)_2\}]$ **4.4** transiently forms at room temperature while

[RuH(CO)(PPh_3){κ^3-*H,S,S'*-$H_2B(mt)_2$}] **2.1** was prepared *via* a 15 minute reflux in tetrahydrofuran. Unlike isolable **2.1**, complex **4.4** does not persist in solution and eluded isolation.

The ruthenium precursor [RuH(CO)$(NCMe)_2(PPh_3)_2$]PF_6 **4.5** was used to facilitate the formation of **4.4**, as it was envisaged that the more labile acetonitrile ligands (compared to PPh_3) would be easily displaced to allow for complex formation. Complex **4.5** was synthesised from [RuHCl(CO)$(PPh_3)_3$] using similar procedures to Roper's [RuH(CO)$(NCMe)_2(PPh_3)_2$]ClO_4 analogue.[46] Upon reaction of **4.5** with Li[$H_2Al(mt)_2$].THF (Scheme 4.12b), the appearance of side products **4.4x** (minor) and **4.4y** (major) was again evident from NMR spectral data. The persistence of decomposition product **4.4y** was further substantiated through an X-ray diffraction study (Figure 4.4). Although spectroscopic details of **4.4y** are available in literature,[45] the molecular structure has not been reported. The N1–Ru1–S1 chelate bite angle of 65.92(9)° in **4.4y** is analogous to Wilton-Ely's ruthenium derivatives featuring various co-ligands (65.69(5)–66.43(5) Å).[45]

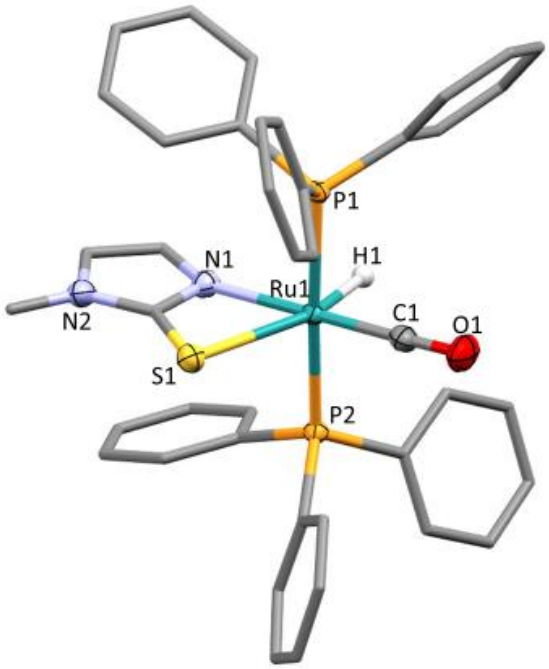

Figure 4.4: Molecular structure of [RuH(κ^2-*N,S*-mt)(CO)$(PPh_3)_2$] **4.4y**.2.5C_6H_6 (solvent omitted, organic hydrogen atoms omitted, phenyl and methimazolyl groups simplified, displacement ellipsoids shown at 50% probability). Selected bond lengths (Å) and angles (°): Ru1–S1 2.6064(11), Ru1–N1 2.158(3), Ru1–H1 1.57(5), Ru1–C1 1.817(4), Ru1–P1 2.3403(10), Ru1–P2 2.3392(10), P1–Ru1–P2 175.97(4), S1–Ru1–H1 158.3(17), N1–Ru1–C1 178.76(15), S1–Ru1–N1 65.92(9), N1–Ru1–H1 92.4(17), C1–Ru1–H1 88.8(17), S1–Ru1–C1 112.97(13), S1–Ru1–P1 93.46(4), S1–Ru1–P2 90.40(4).

The observation of **4.4** as a transient species *en route* to more thermodynamically stable **4.4x** and **4.4y** implies the presence of an unsustained Al–H–Ru 3c2e interaction that potentially leads to Al–H activation. Thus, investigations into the synthesis of the ruthenaaluminatrane analogue, [Ru{κ^3-*Al,S,S'*-AlH(mt)$_2$}(CO)(PPh$_3$)], of the ruthenaboratrane **3.1** (Chapter 3) were performed. As the synthesis of **3.1** from [Ru(X)Cl(CO)(PPh$_3$)$_2$] (X = Ph, CH=CHPh) was facile and occurred spontaneously at room temperature, the same conditions were applied to the synthesis of **4.6** (Scheme 4.13). Treatment of [Ru(Ph)Cl(CO)(PPh$_3$)$_2$] with **4.2** in C_6D_6 under an atmosphere of argon produced a mixture of complexes **4.4x** and **4.4y** within 30 minutes, which were identified *via* ^{1}H and ^{31}P{^{1}H} NMR (Scheme 4.13c). Similar reactivity was observed of **4.2** with [Ru(CH=CHPh)Cl(CO)(PPh$_3$)$_2$] (Scheme 4.13d). These results again suggest the degradation of the Li[H$_2$Al(mt)$_2$] ligand, serving as both a hydride and methimazolide donor. The ratio of complexes **4.4x** and **4.4y** from the reactions discussed thus far are summarised in Table 4.1.

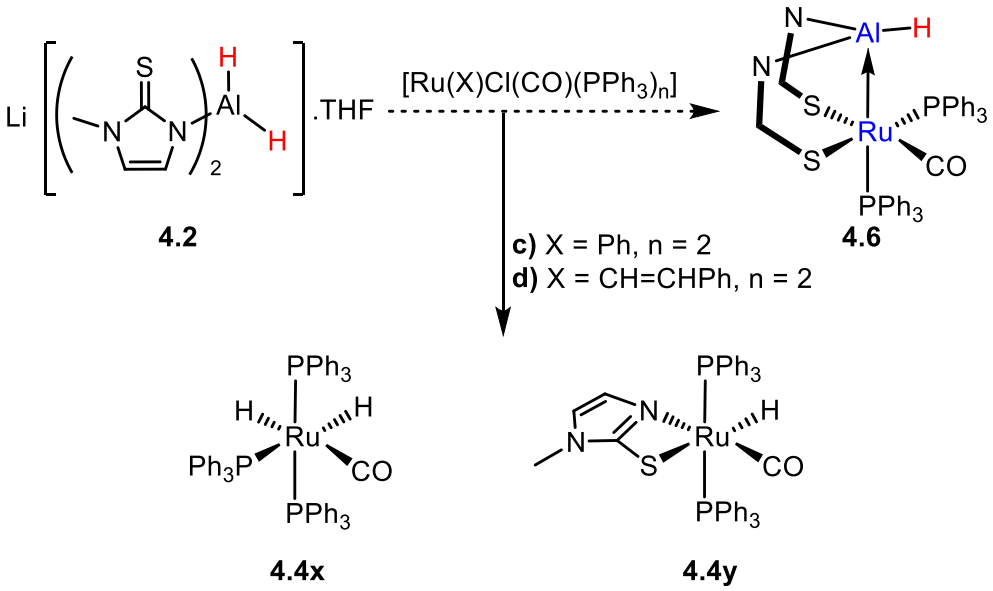

Scheme 4.13: Reaction of Li[H$_2$Al(mt)$_2$].THF with Ru(II) precursors towards synthesis of **4.6**. Actual products obtained were **4.4x** and **4.4y**.

Ru(II) Precursors	Ratio of 4.4x : 4.4y	Time taken (hour)
[RuHCl(CO)(PPh$_3$)$_3$]	8.4 : 1	1
[RuH(CO)(NCMe)$_2$(PPh$_3$)$_2$]PF$_6$	0 : 1	0.5
[Ru(Ph)Cl(CO)(PPh$_3$)$_2$]	1.8 : 1	0.5
[Ru(CH=CHPh)Cl(CO)(PPh$_3$)$_2$]	0.4 : 1	0.5

Table 4.1: Reaction outcomes of Li[H$_2$Al(mt)$_2$].THF with Ru(II) precursors.

From these preliminary investigations into the reactivity of $Li[H_2Al(mt)_2].THF$ with ruthenium(II) precursors, a few generalisations can be made. The aluminium pro-ligand **4.2** is considerably more reactive and less stable than the boron analogue $Na[H_2B(mt)_2]$, as observed through the decomposition of the ligand into side products **4.4x** and **4.4y**. One proposed decomposition pathway involves the anionic $[H_2Al(mt)_2]^-$ as a reducing agent, readily donating a hydride to an appropriate Lewis acid to liberate a neutral aluminium fragment with the potential to react further. Alternatively, the same hydride donation to the metal centre would occur from oxidative addition of the Al–H bond, an extreme consequence of the Al–H–M interaction as observed with the boron derivative. This process would be due to significant backbonding from the metal to the antibonding orbital of the Al–H bond of the free ligand or may occur following the coordination of the ligand. Another pathway of ligand degradation involves the cleavage of the Al–N bond to generate free mt^- that readily chelates to the ruthenium centre. Despite these hypotheses, the specific pathways to the formation of side products **4.4x** and **4.4y** are currently unknown; however, scrambling of the ligands does seem to be evident. Although not as facile as observed for $Li[H_2Al(mt)_2].THF$, the cleavage of poly(methimazolyl)borates to provide methimazolyl complexes is encountered occasionally.

4.3.2 Osmium

A general trend when progressing down a triad in the d-block is the increase in strength of transition metal-ligand bonds, which are consequently harder to cleave with later row transition metals. A celebrated example is the production of acetic acid through carbonylation of methanol catalysed by $[MI_2(CO)_2]^-$ (M = Rh, Monsanto; Ir, Cativa).[47] In the Monsanto process the rate determining step is the formation of M–L bonds in oxidative addition, whereas that for the Cativa process is the cleavage of M–L bonds in migratory insertion. Similarly, coordination of $[H_2B(mt)_2]^-$ to ruthenium occurred readily compared to osmium in the synthesis of **2.1** and **2.10** (15 minute reflux *cf.* 1.5 hour reflux). Therefore, to address the facile reactivity and subsequent decomposition encountered in the chemistry of $Li[H_2Al(mt)_2].THF$ with ruthenium(II) precursors, coordination to that of osmium(II) might be expected to provide complexes with greater stability and reduced kinetics with respect to bond cleavage.

The reaction of **4.2** with $[OsHCl(CO)(PPh_3)_3]$ produced similar product distribution to those previously discussed for the ruthenium analogue **4.4**. The ^1H and $^{31}P\{^1H\}$ NMR spectra at one hour contained the dihydride $[OsH_2(CO)(PPh_3)_3]$[48] **4.7x** and chelate $[OsH(\kappa^2\text{-}N,S\text{-mt})(CO)(PPh_3)_2]$[45] **4.7y** complexes as well as two promising broad resonances located at δ_H = –8.42 and δ_H = –11.19 in the ^1H NMR spectrum that may indicate the presence of $[OsH(CO)(PPh_3)\{\kappa^3\text{-}H,S,S'\text{-}H_2Al(mt)_2\}]$ **4.7** (Scheme 4.14). The associated $^{31}P\{^1H\}$ resonance could be detected as a broad signal at δ_P = 17.6, assigned *via* two dimensional $^1H^{31}P$ experiments. Complexes **4.7x** and **4.7y** were identified based on ^1H and $^{31}P\{^1H\}$ NMR resonances, consistent with data reported in literature.[45,48] The reaction was monitored by ^1H and $^{31}P\{^1H\}$ NMR spectroscopy over 24 hours and showed an increase in the side products **4.7x** and **4.7y** with the concomitant decrease of the broad signals over this time period. The persistence of the desired compound for up to 24 hours is consistent with the expected slower kinetics of 5d versus 4d transition metals.

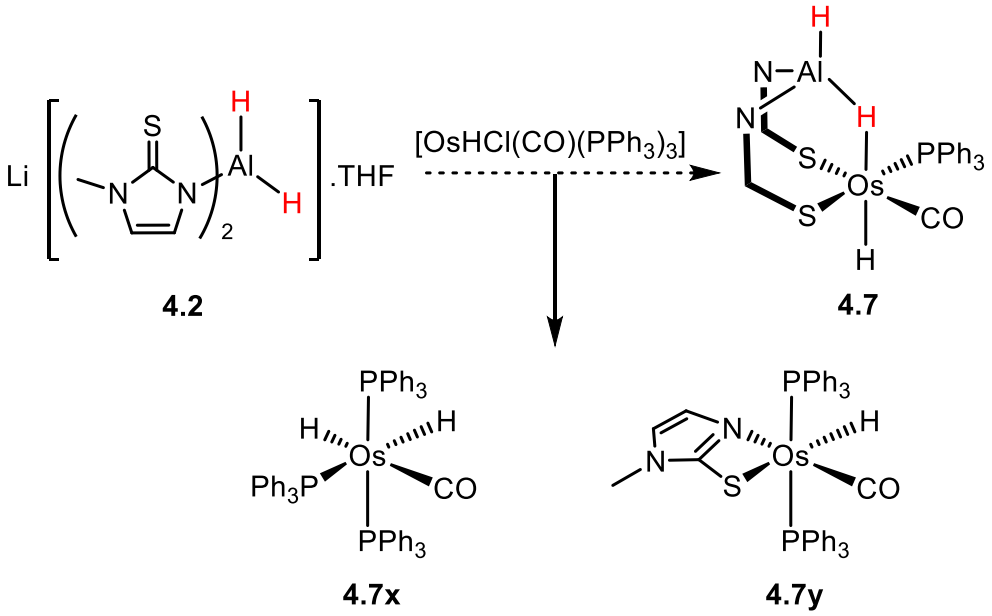

Scheme 4.14: Reaction of $Li[H_2Al(mt)_2].THF$ with $[OsHCl(CO)(PPh_3)_3]$ precursors in the attempted synthesis of **4.7**. Actual products observed include **4.7x** and **4.7y**.

Crystals isolated from a concentrated benzene solution of the crude mixture confirmed the formulation of **4.7y**, which was first synthesised by Wilton-Ely[45] *via* reaction of $[OsHCl(CO)(PPh_3)_3]$ with Hmt, however no X-ray data has been reported to date. The molecular structure of **4.7y** (Figure 4.5) supports the bidentate binding of the mt^- ligand through both S1 and N1 donor atoms, where the planarity of the ligand follows

from the contribution of the methyl-substituted nitrogen towards bonding in the methimazolyl ring. The methylimidazolethiolate chelate S1–Os1–N1 has a bite angle of similar value comparable to the ruthenium analogue in Figure 4.4 (65.61(4) Os *cf*. 65.92(9)° Ru) consistent with ruthenium and osmium having similar covalent radii.

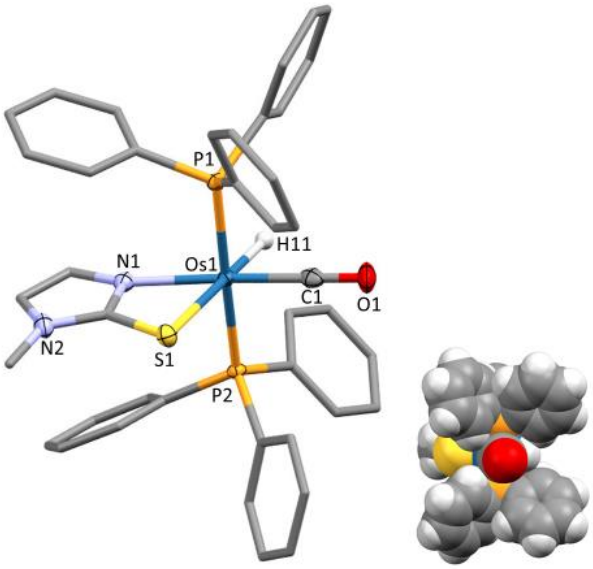

Figure 4.5: a) Molecular structure of [OsH(κ^2-*N,S*-mt)(CO)(PPh_3)$_2$] **4.7y**.2.5(C_6H_6) and space filling representation (solvent omitted, organic hydrogen atoms omitted, phenyl groups simplified, displacement ellipsoids shown at 50% probability). Selected bond lengths (Å) and angles (°): Os1–S1 2.596(3), Os1–N1 2.160(1), Os1–H11 1.700, Os1–C1 1.841(2), Os1–P1 2.340(4), Os1–P2 2.339(4), P1–Os1–P2 176.44(1), S1–Os1–H11 179.97, N1–Os1–C1 176.75(6), S1–Os1–N1 65.61(4), N1–Os1–H11 114.42, C1–Os1–H11 68.76, S1–Os1–C1 111.21(5), S1–Os1–P1 90.31(1), S1–Os1–P2 93.10(1).

The preparation of complex **4.7** was also explored on the preparative scale, independently, in diethyl ether and tetrahydrofuran. Decomposition of the complex into recognisable side products (**4.7x** and **4.7y**) was observed during the purification process at room temperature in each case.

The continued search for a suitable reaction partner for **4.2** turned to substrate [Os(Ph)Cl(CO)(PPh_3)$_2$] (Scheme 4.15) for the preparation of the osmaaluminatrane [Os{κ^3-*Al,S,S'*-AlH(mt)$_2$}(CO)(PPh_3)$_2$] **4.8**. The NMR scale reactions performed in C_6D_6 under argon showed consumption of both starting materials within 30 minutes, affording a mixture of products and free PPh_3 as observed in the $^{31}P\{^1H\}$ NMR spectrum (≈12 resonances). Amongst these resonances, those corresponding to the major product appeared independently as doublets at δ_P = 20.6 and 8.7 ($^2J_{PP}$ = 9.7 Hz), consistent with the two phosphorus environments expected for osmaaluminatrane **4.8**. The presence of

hydride containing complexes was evident by approximately nine broad resonances in the hydride region (δ_H <0) of the ^{1}H NMR spectrum, which was shown *via* ^{1}H^{31}P two-dimensional experiments to correlate to the minor resonances in the ^{31}P{^{1}H} NMR spectrum.

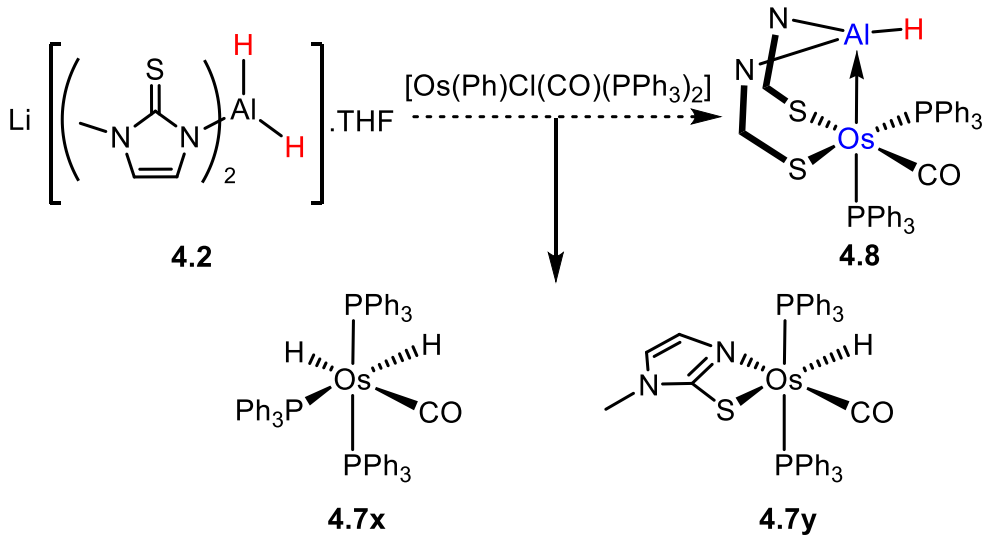

Scheme 4.15: Reaction of Li[H_2Al(mt)$_2$].THF with [Os(Ph)Cl(CO)(PPh_3)$_3$] in the attempted synthesis of **4.8**. Actual products observed include **4.7x** and **4.7y**.

Although the resonances postulated to correspond to **4.8** persisted at 1.5 hours, it was however accompanied by the unsurprising presence of side products **4.7x** and **4.7y**. Consistent with previous observations on the lack of endurance of the aluminium based complexes encountered with the **4.2** ligand, the sample degrades over 21 hours to the dihydride and chelate decomposition products **4.7x** and **4.7y**.

4.3.3 Other Metal Precursors

The metal substrates studied in this chapter thus far are of electron rich nature, being based on low-valent metal centres, while those with reduced electron density are yet to be explored. This naturally leads to the exploration of the reactivity of **4.2** with substrates bearing less electron density at the metal centre. Based on previous work by Santos[49] and Hill,[50] suitable rhenium and molybdenum metal precursors were chosen based on the established stability in the analogous NaBm derivatives.

On a preparative scale [Mo(CO)$_3$(η^6-C_7H_8)] was combined with a solution of **4.2** in THF in an attempt to generate the anion [Mo{H_2Al(mt)$_2$}(CO)$_3$]$^-$ for subsequent capture by $ClSnPh_3$ (Scheme 4.16). The resulting yellow supernatant from the combination of [Mo(CO)$_3$(η^6-C_7H_8)] with **4.2** was instantly accompanied by insoluble black solid

deposition. Numerous ν_{CO} bands were detected in the IR spectra of the supernatant fraction (ν_{CO} = 1807, 1824, 1917 cm^{-1}). Amongst these, none appeared to fall within similar values to those reported for the boron analogue $Na[Mo(CO)_3\{\kappa^3\text{-}H,S,S'\text{-}H_2B(mt)_2\}]^-$ (ν_{CO} = 1817, 1882, 2002 cm^{-1}).[51] However, bands at 1717 and 1782 cm^{-1} might be indicative of the presence of Al–H units.

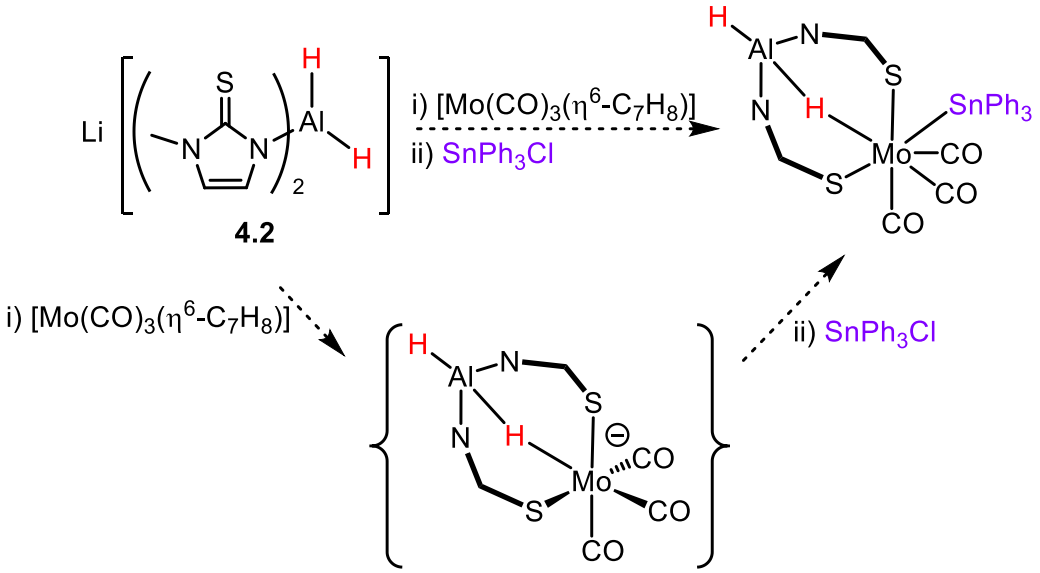

Scheme 4.16: Attempted synthesis of molybdenum stannyl complex, $[Mo(SnPh_3)(CO)_3\{\kappa^3\text{-}H,S,S'\text{-}H_2Al(mt^{Me})_2\}]$.

The supernatant fraction containing the postulated $Li[Mo(CO)_3\{\kappa^3\text{-}H,S,S'\text{-}H_2Al(mt)_2\}]$ salt was subsequently treated with $SnPh_3Cl$. An instantaneous colour change from yellow to orange occurred and several bands were observed in the IR spectrum, which likely corresponded to the anticipated product $[Mo(SnPh_3)(CO)_3\{\kappa^3\text{-}H,S,S'\text{-}H_2Al(mt)_2\}]$ (ν_{CO} = 1878, 1906, 2002, ν_{AlH} = 1719 cm^{-1}) and additional carbonyl containing by-products (ν = 1817 and 1940 cm^{-1}). Unfortunately, the precipitate obtained following purification had poor solubility in C_6D_6. Interpretation of the ^1H NMR spectrum obtained suggested that the products contained methimazole-based functionality but was absent of metal hydride units, thus disfavouring a complex with an Al–H–Mo interaction. Attempts to identify the products formed through crystallographic means were unsuccessful.

Coordination of $[H_2Al(mt)_2]$ to rhenium proved to be slightly more promising. The complex $[ReBr(CO)_3(THF)_2]$ was prepared by heating $[ReBr(CO)_5]$ in THF under reflux for 20 hours[52] and then was subsequently treated with a stoichiometric amount of **4.2** at –78°C (Scheme 4.17).

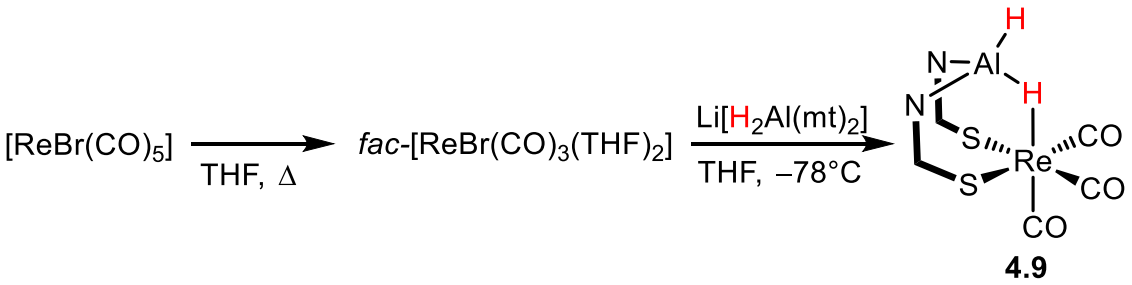

Scheme 4.17: Attempted synthesis of $[Re(CO)_3\{\kappa^3\text{-}H,S,S'\text{-}H_2Al(mt)_2\}]$.

The reaction was monitored by IR spectroscopy and the spectrum obtained following the addition of **4.2** contained absorptions at ν_{CO} = 1887 (broad) and 2008 cm^{-1}. There was an absence of aluminium-hydride ν_{AlH} and ν_{AlHRe} absorptions, which would be expected to occur at frequencies below 1800 cm^{-1}. The CO absorption bands are distinct from those of the precursor $[ReBr(CO)_3(THF)_2]$ (2029, 1915, 1894 cm^{-1}), and similar to Santos' $[Re(CO)_3\{\kappa^3\text{-}H,S,S'\text{-}H_2B(mt)_2\}]$ (1900 and 2000 cm^{-1}).[49] Poor solubility of the reaction mixture (in CD_2Cl_2 or C_6D_6) precluded the acquisition of good quality ^1H NMR spectra, however, interpretation of the spectrum obtained suggests that the crude contained a mixture of products. Crystals of differing morphology (red blocks and white needles) suitable for crystallographic analysis were obtained from a concentrated solution of the crude sample in benzene and were identified as $[Re_2(\mu\text{-}N,S\text{-}mt)_2(CO)_6(Hmt)_2]$ **4.9x** (Figure 4.6) and $[Re_2(\mu\text{-}N,S\text{-}mt)(\mu\text{-}S{:}\kappa^2\text{-}N,S\text{-}mt)(CO)_6(Hmt)_2]$ **4.9y** (Figure 4.7).

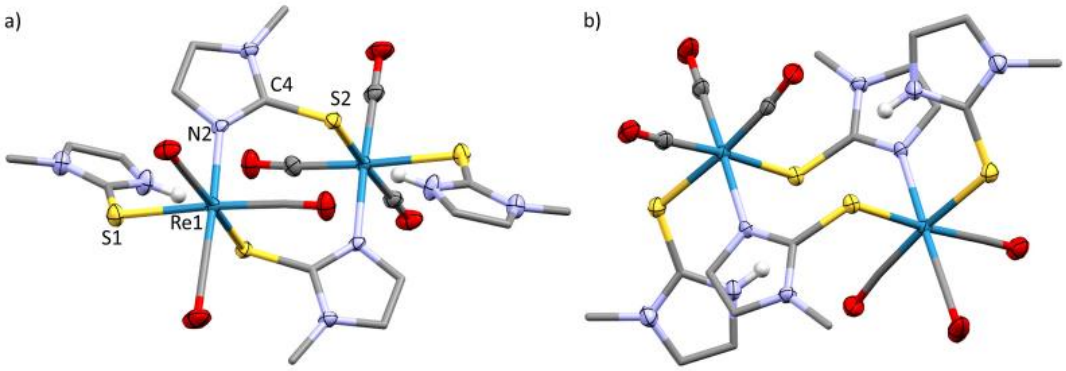

Figure 4.6: a) and b) Molecular structure of $[Re_2(\mu\text{-N,S-mt})_2(CO)_6(Hmt)_2]$ **4.9x**.0.5(C_6H_6) in two different orientations (CH hydrogens and solvent omitted, displacement ellipsoids shown at 50% probability). Selected bond lengths (Å) and angles (°): Re1–S1 2.545(1), Re1–S2 2.518(9), Re1–N2i 2.196(3), S2–C4 1.732(4), S1–Re1–S2 86.36(3), Re1–S2–C4 89.71(2), N2i–Re1–S2 88.99(9), Re1–N2–C4 130.4(3).

While no aluminium coordination is evident in structures **4.9x** and **4.9y**, they are nevertheless useful illustrations of the versatile modes of coordination of the mt^- ligand. The asymmetric unit of **4.9x** consists of a 'Re(mt)$(CO)_3$(Hmt)' fragment where a centre of inversion yields the symmetrical bimetallic rhenium complex **4.9x**. The methimazole-based unit binds in a monodentate (σ-S) manner while the methimazolyl groups bridge in a σ-S/σ-N fashion, each to a different rhenium centre. Monodentate coordination of Hmt is exemplified through the thione (S1) two-electron donor, with a longer rhenium-sulfur bond than the formally anionic bridged form (Re1–S1 2.545(1) *cf.* Re1–S2 2.518(9) Å). Both coordination modes have comparably longer rhenium-sulfur bond lengths than in the compact tridentate ligand of $[Re(CO)_3\{\kappa^3\text{-}H,S,S'\text{-}H_2B(mt)_2\}]$ (Re1–S1 2.486 Å).

In addition to the coordination modes described above, structure **4.9y** displays a third mode of mt^- bonding observed as chelation *via* nitrogen (N1) and sulfur (S3) donors to a common rhenium (Re1) centre while bridging through the sulfur (S3) atom to the second rhenium (Re2) centre. The versatile bonding exhibited by the sulfur atom results in elongation of the chelated Re1–S3 bond to 2.617(2) Å while the Re2–S3 bond length in **4.9y** resembles that of the thione coordination in **4.9x** (Re2–S3 2.545(2) **4.9y** and Re1–S1 2.545(1) Å **4.9x**).

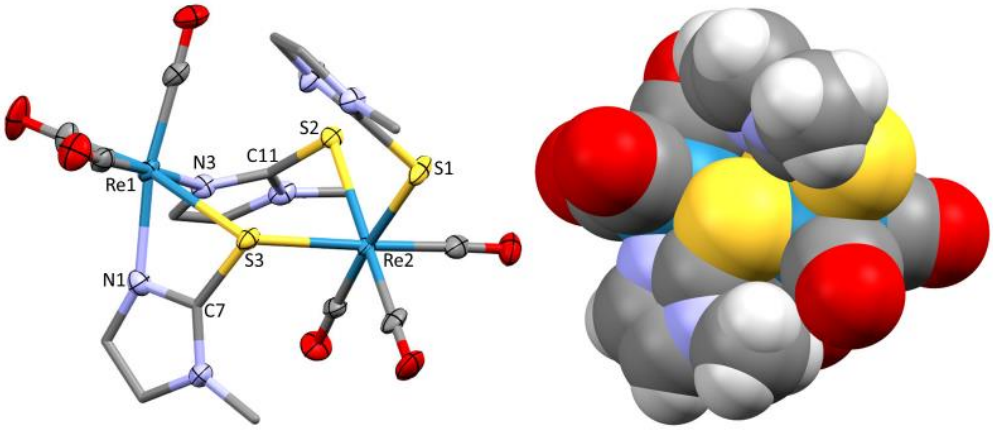

Figure 4.7: Molecular structure of $[Re_2(\mu\text{-}N,S\text{-}mt)(\mu\text{-}S{:}\kappa^2\text{-}N,S\text{-}mt)(CO)_6(Hmt)]$ **4.9y**.C_6H_6 and space filing representation (hydrogens and solvent omitted, groups simplified, displacement ellipsoids shown at 50% probability). Selected bond lengths (Å) and angles (°): Re1–S3 2.617(2), Re1–N1 2.182(6), S3–C7 1.751(7), Re1–N3 2.165(6), N3–C11 1.333(9), S2–C11 1.737(6), Re2–S2 2.520(2), Re2–S1 2.524(2), Re2–S3 2.545(2), S3–Re1–N1 64.96(2), Re1–N1–C7 103.3(5), S3–C7–N1 114.3(6), Re1–S3–C7 77.2(2), S3–Re1–N3 87.82(2), N1–Re1–N3 81.9(2), Re1–N3–C11 129.0(4), S2–C11–N3 127.1(5), Re2–S2–C11 99.4(2), S2–Re2–S3 85.28(6), S1–Re2–S3 91.93(6), S1–Re2–S2 89.37(6).

4.4 Future Work

The reactivity of $Li[H_2Al(mt)_2]$.THF has only been explored with second and third row transition metals featuring predominantly electron rich precursors and relying on ligand displacement (NCMe, PPh_3, THF, C_7H_8) for coordination of $Li[H_2Al(mt)_2]$. A consideration lies in the judicious choice of metal precursors where scrambling of ligands is less likely. The chloro-bridged dimers $[M_2Cl_2(Cp^*)_2]$ (M = Rh, Ir) and tetramer $[Ru_4Cl_4(Cp^*)_4]$ are examples of substrates featuring a robust Cp* unit occupying one face of the metal and a vacant coordination site upon cleavage of the chloro-bridge. This reduces the number of ligands available for scrambling while providing an available vacant site for coordination.

Coordination of $Li[H_2Al(mt)_2]$ to less electron rich metal substrates (group 4 and 5 transition metals) are presently unexplored and may offer a more compatible match should Hard Soft Acid Base considerations play a role. Similarly, little work has been directed to the first-row transition metals and main group metals, which provides many available avenues for investigation in the future.

4.5 Conclusion

The aluminium pro-ligand, Li[H_2Al(mt)$_2$].THF **4.2**, was successfully prepared and confirmed through spectroscopy and X-ray diffraction analysis. While the ligand can be easily and reliably prepared in high yield, subsequent coordination to metal precursors in groups 6–8 has failed to deliver complexes with an intact H_nAl(mt)$_2$ (n = 1, 2) ligand. In addition to the greater reactivity and lower stability of **4.2** compared to the well-behaved Na[H_2B(mt)$_2$] analogue, several generalisations can be drawn concerning the behaviour of **4.2** towards metal substrates. In competition with initial sulfur coordination, the pro-ligand retains sufficiently reactive Al–H bonds that it may serve as a hydride donor. Coordination of the aluminium functionality generates a thermolabile kinetic product that converts to known complexes of greater stability over time, devoid of the aluminium centre of interest. This conversion occurs with degradation of **4.2** to liberate free mt$^-$, which readily coordinates to the metal centre through various binding modes. Although the work with **4.2** herein has yet to afford stable aluminium containing complexes, the potential for reactivity with other elements of the periodic table remains an uncharted territory providing avenues for future research.

4.6 References

(1) Tanaka, R.; Yamashita, M.; Nozaki, K. *J. Am. Chem. Soc.* **2009**, *131*, 14168.
(2) Zurek, E.; Ziegler, T. *Prog. Polym. Sci.* **2004**, *29*, 107.
(3) Housecroft, C. E.; Sharpe, A. G. *Inorganic Chemistry*; Pearson Prentice Hall, 2005.
(4) Brunner, H.; Wailes, P. C.; Kaesz, H. D. *Inorg. Nucl. Chem. Lett.* **1965**, *1*, 125.
(5) Bruno, J. W.; Huffman, J. C.; Caulton, K. G. *J. Am. Chem. Soc.* **1984**, *106*, 444.
(6) Storr, A.; Thomas, B. S. *Can. J. Chem.* **1971**, *49*, 2504.
(7) Skupinski, W. A.; Huffman, J. C.; Bruno, J. W.; Caulton, K. G. *J. Am. Chem. Soc.* **1984**, *106*, 8128.
(8) Golden, J. T.; Peterson, T. H.; Holland, P. L.; Bergman, R. G.; Andersen, R. A. *J. Am. Chem. Soc.* **1998**, *120*, 223.
(9) Burlitch, J. M.; Leonowicz, M. E.; Petersen, R. B.; Hughes, R. E. *Inorg. Chem.* **1979**, *18*, 1097.
(10) Mayer, J. M.; Calabrese, J. C. *Organometallics* **1984**, *3*, 1292.
(11) Braunschweig, H.; Gruss, K.; Radacki, K. *Angew. Chem. Int. Ed.* **2007**, *46*, 7782.
(12) Braunschweig, H.; Radacki, K.; Schwab, K. *Chem. Commun.* **2010**, *46*, 913.
(13) Bauer, J.; Bertermann, R.; Braunschweig, H.; Gruss, K.; Hupp, F.; Kramer, T. *Inorg. Chem.* **2012**, *51*, 5617.
(14) Bauer, J.; Braunschweig, H.; Brenner, P.; Kraft, K.; Radacki, K.; Schwab, K. *Chem. Eur. J.* **2010**, *16*, 11985.
(15) Braunschweig, H.; Gruss, K.; Radacki, K. *Inorg. Chem.* **2008**, *47*, 8595.
(16) Braunschweig, H.; Gruss, K.; Radacki, K. *Angew. Chem. Int. Ed.* **2009**, *48*, 4239.
(17) Devillard , M.; Nicolas, E.; Ehlers, A. W.; Backs, J.; Mallet-Ladeira, S.; Bouhadir , G.; Slootweg, J. C.; Uhl, W.; Bourissou , D. *Chem. Eur. J.* **2015**, *21*, 74.

(18) Devillard, M.; Declercq, R.; Nicolas, E.; Ehlers, A. W.; Backs, J.; Saffon-Merceron, N.; Bouhadir, G.; Slootweg, J. C.; Uhl, W.; Bourissou, D. *J. Am. Chem. Soc.* **2016**, *138*, 4917.
(19) Heine, A.; Stalke, D. *Angew. Chem.* **1992**, *104*, 941.
(20) Gianopoulos, C. G.; Kirschbaum, K.; Mason, M. R. *Organometallics* **2014**, *33*, 4503.
(21) Qian, B.; Ward, D. L.; Smith, M. R., III *Organometallics* **1998**, *17*, 3070.
(22) Bonnier, C.; Piers, W. E.; Parvez, M.; Sorensen, T. S. *Chem. Commun.* **2008**, 4593.
(23) Welch, G. C.; Stephan, D. W. *J. Am. Chem. Soc.* **2007**, *129*, 1880.
(24) Stephan, D. W.; Erker, G. *Angew. Chem. Int. Ed.* **2010**, *49*, 46.
(25) Flynn, S. R.; Wass, D. F. *ACS Catal.* **2013**, *3*, 2574.
(26) Courtemanche, M.-A.; Larouche, J.; Legare, M.-A.; Bi, W.; Maron, L.; Fontaine, F.-G. *Organometallics* **2013**, *32*, 6804.
(27) Sircoglou, M.; Saffon, N.; Miqueu, K.; Bouhadir, G.; Bourissou, D. *Organometallics* **2013**, *32*, 6780.
(28) Derrah, E. J.; Sircoglou, M.; Mercy, M.; Ladeira, S.; Bouhadir, G.; Miqueu, K.; Maron, L.; Bourissou, D. *Organometallics* **2011**, *30*, 657.
(29) Sircoglou, M.; Mercy, M.; Saffon, N.; Coppel, Y.; Bouhadir, G.; Maron, L.; Bourissou, D. *Angew. Chem. Int. Ed.* **2009**, *48*, 3454.
(30) Sircoglou, M.; Bontemps, S.; Bouhadir, G.; Saffon, N.; Miqueu, K.; Gu, W.; Mercy, M.; Chen, C.-H.; Foxman, B. M.; Maron, L.; Ozerov, O. V.; Bourissou, D. *J. Am. Chem. Soc.* **2008**, *130*, 16729.
(31) Bontemps, S.; Bouhadir, G.; Gu, W.; Mercy, M.; Chen, C.-H.; Foxman, B. M.; Maron, L.; Ozerov, O. V.; Bourissou, D. *Angew. Chem. Int. Ed.* **2008**, *47*, 1481.
(32) Bontemps, S.; Bouhadir, G.; Dyer, P. W.; Miqueu, K.; Bourissou, D. *Inorg. Chem.* **2007**, *46*, 5149.
(33) Sircoglou, M.; Bouhadir, G.; Saffon, N.; Miqueu, K.; Bourissou, D. *Organometallics* **2008**, *27*, 1675.
(34) Snyder, C. J.; Heeg, M. J.; Winter, C. H. *Inorg. Chem.* **2011**, *50*, 9210.
(35) Sambade, D.; Parkin, G. *Polyhedron* **2017**, *125*, 219.
(36) Chong, K. S.; Rettig, S. J.; Storr, A.; Trotter, J. *Can. J. Chem.* **1977**, *55*, 4166.
(37) Cooper, D. A.; Rettig, S. J.; Storr, A.; Trotter, J. *Can. J. Chem.* **1986**, *64*, 1643.
(38) Takaya, J.; Iwasawa, N. *J. Am. Chem. Soc.* **2017**, *139*, 6074.
(39) Saito, T.; Hara, N.; Nakao, Y. *Chem. Lett.* **2017**, *46*, 1247.
(40) Hara, N.; Saito, T.; Semba, K.; Kuriakose, N.; Zheng, H.; Sakaki, S.; Nakao, Y. *J. Am. Chem. Soc.* **2018**, *140*, 7070.
(41) Hill, A. F.; Lee, S. B.; Park, J.; Shang, R.; Willis, A. C. *Organometallics* **2010**, *29*, 5661.
(42) Hill, A. F.; Owen, G. R.; White, A. J. P.; Williams, D. J. *Angew. Chem. Int. Ed.* **1999**, *38*, 2759.
(43) Hallman, P. S.; McGarvey, B. R.; Wilkinson, G. *J. Chem. Soc. A* **1968**, 3143.
(44) Rajasekharan-Nair, R.; Moore, D.; Chalmers, K.; Wallace, D.; Diamond, L. M.; Darby, L.; Armstrong, D. R.; Reglinski, J.; Spicer, M. D. *Chem. Eur. J.* **2013**, *19*, 2487.
(45) Wilton-Ely, J. D. E. T.; Honarkhah, S. J.; Wang, M.; Tocher, D. A.; Slawin, A. M. Z. *Dalton Trans.* **2005**, 1930.
(46) Cavit, B. E.; Grundy, K. R.; Roper, W. R. *J. Chem. Soc., Chem. Commun.* **1972**, 60.
(47) Jones, J. H. *Platinum Met. Rev.* **2000**, *44*, 94.
(48) Ahmad, N.; Robinson, S. D.; Uttley, M. F. *J. Chem. Soc., Dalton Trans.* **1972**, 843.
(49) Garcia, R.; Paulo, A.; Domingos, A.; Santos, I.; Ortner, K.; Alberto, R. *J. Am. Chem. Soc.* **2000**, *122*, 11240.
(50) Foreman, M. R. S. J.; Hill, A. F.; Smith, M. K.; Tshabang, N. *Organometallics* **2005**, *24*, 5224.
(51) Tshabang, N. PhD Thesis, The Australian National University, 2005.
(52) Roedel, J. N.; Wurzenberger, X.; Lorenz, I.-P. *Inorg. Chem. Commun.* **2008**, *11*, 829.

Chapter 5

Silane-based Pincer Ligands and Derived Complexes

5.1 Introduction

The ligands discussed within Chapters 2 to 4 of this thesis have generally shown preference for facial coordination on a metal. Within this chapter, focus turns to silicon-based pincer complexes that feature tridentate κ^3-*P,Si,P* frameworks, for their flexibility of coordination (*facial* or *meridional* modes). This field has been comprehensively discussed recently.[1,2] A summary of selected examples most relevant to the work to be discussed are highlighted herein.

5.1.1 Silane-based Tridentate Pro-ligands and Derived Complexes

The extensive range of silicon containing ligands was illustrated in Chapter 1. One subset of pincer ligands studied in the last two decades comprise tridentate κ^3-*P,Si,P* ligands, with selected developments summarised in Figure 5.1. The first examples of κ^3-*P,Si,P* ligands were pioneered by Stobart and co-workers in the early 90's, long before pincers became prevalent, and featured a flexible alkylic (**A**) or benzylic backbone (**B**).[3,4] Around the same time, the pro-ligand **C** was utilised by Handwerker and co-workers in investigations into reactivity with $Na_2[Cr(CO)_5]$.[5,6] A decade later, Turculet reported a similar ligand (**D**), of reduced flexibility compared to the frameworks developed by Stobart.[7] Further examples of diphosphinesilane pro-ligands such as **E**, have been investigated by the groups of Maron, Gabbaï, Amgoune and Bourissou.[8,9] The field was soon extended to feature more reactive secondary silanes (**F**). Comparatively less studied is the coordination chemistry involving the benzosiladiazole scaffold (**G**, **H**), which is abbreviated as ^{Ph}PNNP(SiHR) from here.[10,11]

Ligands **A**–**F** represent more structurally flexible systems than that of **G** and **H**. This is owing to the potential rotation about the Si–C bond for **A**–**F** relative to the Si locked within an N-Heterocyclic assembly in **G** and **H**. Furthermore, the planarised nitrogens in **G** and **H** ensure separation of the phosphine arms, and the consequential rigidity of the ligand framework is thus anticipated to favour meridional coordination.

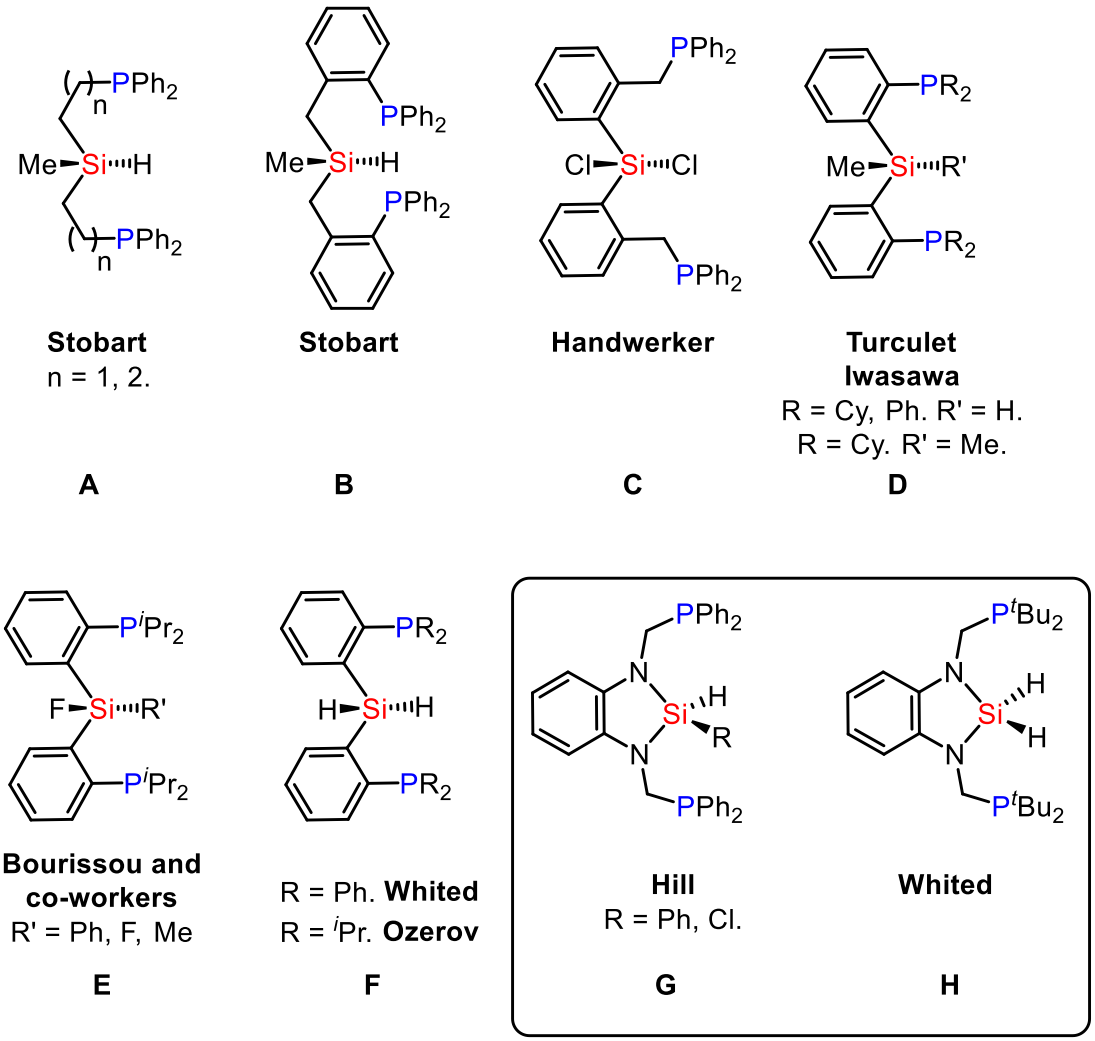

Figure 5.1: Summary of progressive silane ligand design.

Upon coordination of the silane pro-ligand to a metal precursor, the Si–H bond is prone towards chelate assisted activation (oxidative addition) by the metal, resulting in σ-silyl complexes. Where there is a choice of Si–H or Si–R (R = alkyl, aryl) activation, the former is typically observed, although Si–R activation can occur in the absence of a more reactive Si–H bond.[12]

The σ-silyl ligands are strong σ-donors, of comparable strength to σ-boryls,[13] and so can be used to stabilised metals in higher oxidation states.[14] The strong *trans* influence of the PSiP moiety may promote unusual reactivity and access to unconventional geometries with a vacant coordination site *trans* to the Si, such as the four-coordinate complex [RuX{SiMe($C_6H_4PCy_2$-2)$_2$}] **L5.1** (Figure 5.2).[15]

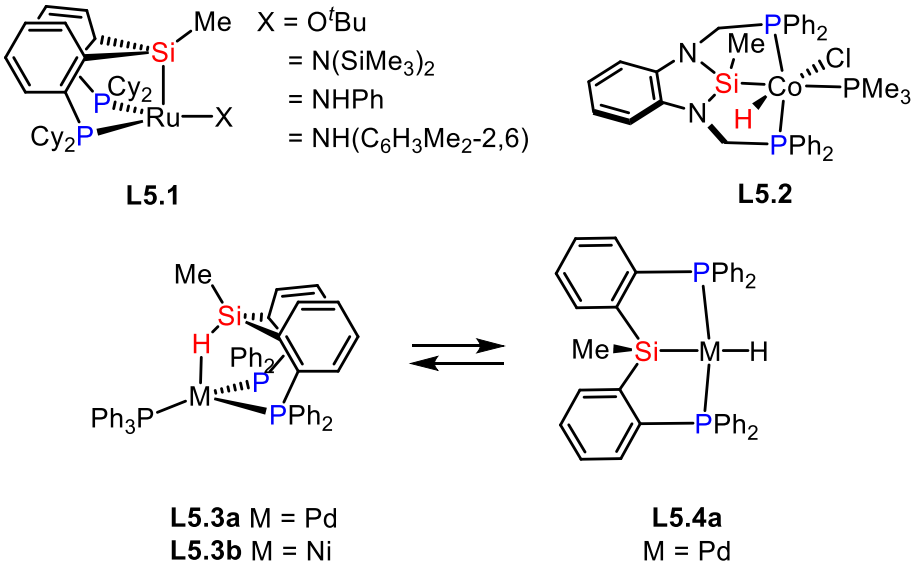

Figure 5.2: Selected examples of silyl-pincer complexes.

Additionally, the *trans*-labilising effect may facilitate extrusion of leaving groups in the *trans* position, which may be beneficial in catalysis. Catalytic applications include Kumada coupling reactions by [CoHCl{SiMe(NCH_2PPh_2)$_2$$C_6H_4$-1,2}($PMe_3$)] **L5.2** and hydrocarboxylation of allenes by [Pd{SiHMe($C_6H_4PPh_2$-2)$_2$}(PPh_3)] **L5.3a**.[16,17] The agostic η^2-(Si–H) interaction in **L5.3a** interconverts through Si–H activation to the palladium(II) hydride complex **L5.4a.** The balance between the η^2-(Si–H) and the metal hydride structural forms has been a topic for discussion. In particular, the cyclohexyl derivatives [M{SiHMe($C_6H_4PCy_2$-2)$_2$}] (M = Pd, Pt) were found through structural, spectroscopic and computational analysis to adopt a metal hydride form in solid state and solution.[18] Complex **L5.3a** predominately exists in the η^2-(Si–H) form, and is one of a few examples of mononuclear η^2-(Si–H) PSiP complexes.[19-22]

5.1.2 Geometric Variations of Silyl Complexes

The remarkable coordinative variation (*fac* or *mer*) of silyl ligands is reflected across the examples of silyl complexes in the literature. The coordination preference is usually dependent on the electronic nature of the metal centre and steric demands of the ligand. The examples depicted in Scheme 5.1 show *fac* binding of silane pro-ligand **D** to [$Rh_2Cl_2(COD)_2$], resulting in [Rh{SiCl($C_6H_4PPh_2$-2)$_2$}(COD)] **L5.5**, whereas reaction with [$PtCl_2$(COD)] yields [PtCl{SiH($C_6H_4P^iPr_2$-2)$_2$}] **L5.6** with *mer*-binding.[11,23] The *fac* coordination exhibited in **L5.5** is consistent with the preferred tetrahedral geometry of the sp^3-hybridised Si, whereas the d^8-Pt(II) electronic system may favour the square planar geometry of **L5.6**.

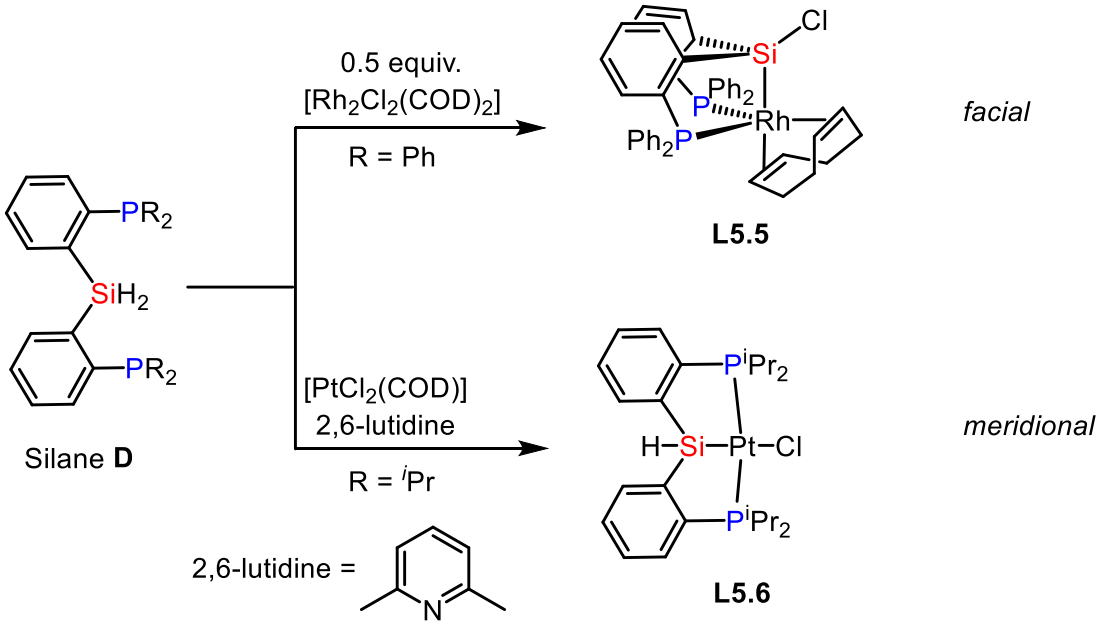

Scheme 5.1: Variation in coordination of silane pro-ligand **D** to rhodium and platinum precursors.

Where the co-ligand is another facially bound ligand, such as the arene in $[Ru\{SiMe(C_6H_4P^iPr_2\text{-}2)_2\}(C_6H_6)]^+$ **[L5.7]**$^+$ (Scheme 5.2), the PSiP ligand accommodates this by adopting *fac* coordination. However, upon replacement of the arene by acetonitrile ligands, the PSiP ligand readily converts to *mer* coordination in the complex $[Ru\{SiMe(C_6H_4P^iPr_2\text{-}2)_2\}(NCMe)_3]^+$ **[L5.8]**$^+$.[24]

The sterically demanding NSiN (NSiN = bis(8-quinolyl)methylsilyl) ligand in Scheme 5.2 prefers *fac* coordination to a metal centre but exhibits *mer* coordination in Tilley's d^8 [PtX{NSiN}] **L5.9** (X = halide, H, alkyl).[14] Whilst *mer* coordination satisfies the electronic requirements of d^8-Pt(II) in **L5.9** in adopting a square planar geometry, there is considerable ring strain associated with this coordination mode, as observed by the distorted tetrahedral geometry at Si. However, this ring strain is utilised to drive the subsequent bond activation of H_2 to form octahedral Pt(IV) $[PtH_2X\{NSiN\}]$ **L5.10**.

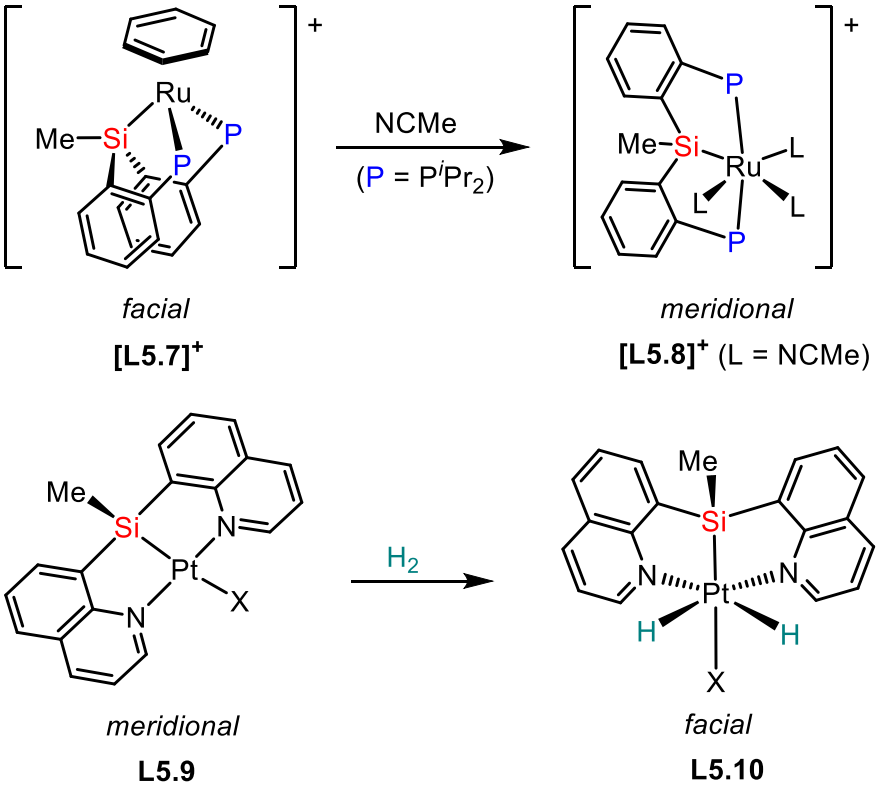

Scheme 5.2: Conversion between *fac*/*mer* coordination modes of PSiP ligands.

Conversion between *fac* and *mer* coordination has been noted in some cases. Complex $[IrH_3\{\kappa^3\text{-}Si,P,P'\text{-}SiMe(C_6H_4P^iPr_2\text{-}2)_2\}]^-$ in Figure 5.3 exists in an equilibrium between **[L5.11a]**$^-$ (*mer* coordinated) and **[L5.11b]**$^-$ (*fac* coordinated) that rapidly exchanges at temperatures above 260 K, and illustrates the ease of geometrical conversion.[25]

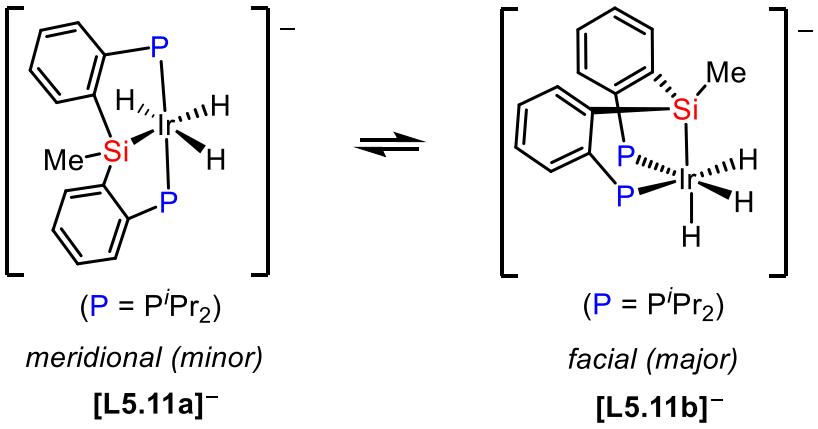

Figure 5.3: Equilibrium between **[L5.11a]**$^-$ and **[L5.11b]**$^-$.

PSiP complexes are commonly obtained as a mixture of non-interconverting diastereomers. Diastereomers are particularly prevalent when the ligand is *mer* coordinated, as the sp^3 hybridised silyl generates two inequivalent faces within the tridentate architecture. No interconversion was observed between diastereomers

L5.12a and **L5.12b** of complex [RuCl{SiPh(NCH$_2$PPh$_2$)$_2$C$_6$H$_4$-1,2}(CO)(PPh$_3$)] at room temperature.[10] Furthermore, the absence of the *fac*-isomer(s) is consistent with the expected increased rigidity of the ligand in **L5.12a**/**L5.12b** *cf.* that in the **L5.11a**/**L5.11b** set.

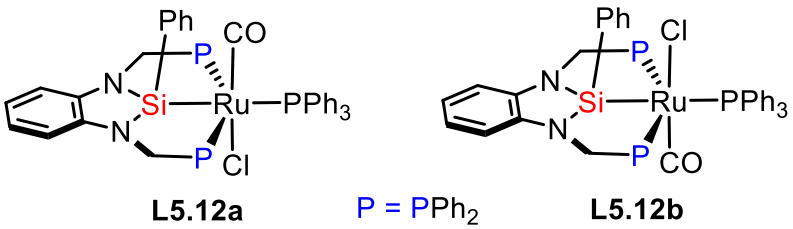

L5.12a P = PPh$_2$ **L5.12b**

Scheme 5.3: Mixture of non-interconverting diastereomers.

5.1.3 Chapter Aims

To date, examples of the coordination chemistry of pro-ligands ^{Ph}PNNP(SiHR) (R = Ph, Cl) (Figure 5.1, **G**) to metal precursors are relatively limited compared to that of more flexible frameworks. Investigations in this chapter will focus on the ligand synthesis of ^{Ph}PNNP(SiH$_2$), for which greater reactivity may be anticipated from two reactive Si–H bonds, and the coordination of ^{Ph}PNNP(SiHR) (R = Ph, Cl) to metal precursors of group 8 and 9. It was envisaged that the rigidity of the ^{Ph}PNNP(SiHR) (R = Ph, Cl) framework may allow access to *mer* coordinated complexes where the strong *trans* influence of silicon might engender unusual reactivity. Furthermore, the silicon in pro-ligands ^{Ph}PNNP(SiHR) are stabilised by π-donating nitrogens, rendering a PSiP silylene complex accessible.

5.2 N-Heterocyclic Pincer Ligands

5.2.1 Pincer Pro-ligands HRSi(NCH$_2$PPh$_2$)$_2$C$_6$H$_4$ (R = Ph, Cl, Me, H)

In 2014, Hill reported the first examples of benzosiladiazole HRSi(NCH$_2$PPh$_2$)$_2$C$_6$H$_4$ (R = Ph, Cl) (Scheme 5.4).[10] Condensation of R$_2$PCH$_2$OH with 1,2-diaminobenzene produces the precursor (NHCH$_2$PPh$_2$)$_2$C$_6$H$_4$-1,2, abbreviated as ^{Ph}PNNP, which upon treatment with an appropriate base and silane allows for the installation of a silicon group within the N-Heterocyclic assembly. Analogues containing H and Me substituents at Si have been recently reported by Whited[11] and Sun,[16] respectively. The latter was obtained through the same preparative route,

whereas H_2SiCl_2.TEEDA (TEEDA = *N,N,N',N'*-Tetraethylethylenediamine) was utilised as a source of H_2SiCl_2 to prepare the dihydrosilane analogue.

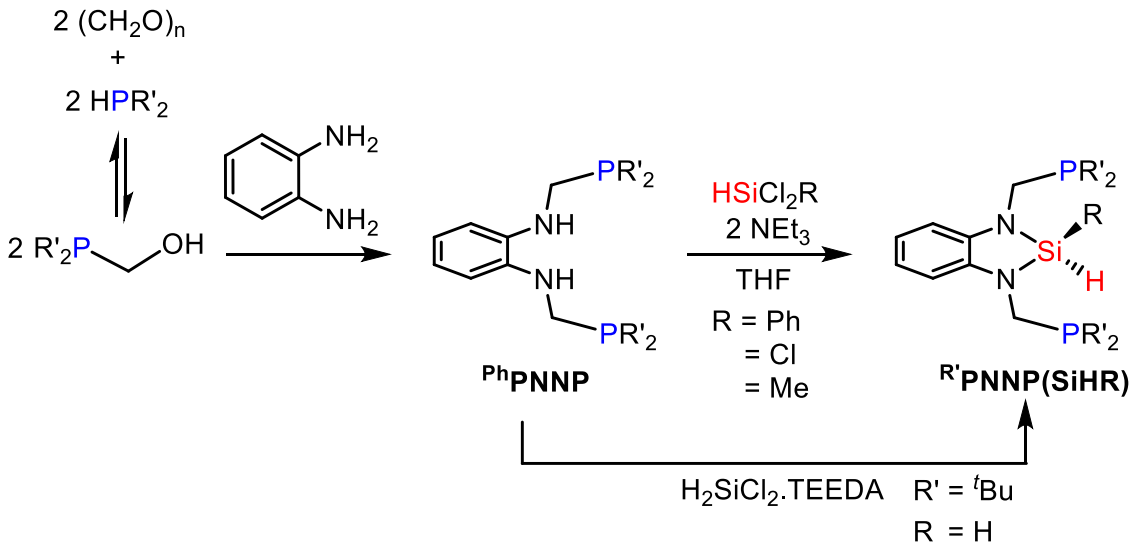

Scheme 5.4: Synthesis of N-Heterocyclic silicon pincer pro-ligands (TEEDA = *N,N,N',N'*-tetraethylethylenediamine).

5.2.2 Attempted Direct Synthesis of $H_2Si(NCH_2PPh_2)_2C_6H_4$

Using a similar protocol to the Whited group,[11] the preparation of ^{Ph}PNNP(SiH_2) was explored from the reaction between SiH_2Cl_2.TEEDA[26] and ^{Ph}PNNP[27] (Scheme 5.5), which were both synthesised following literature procedures.

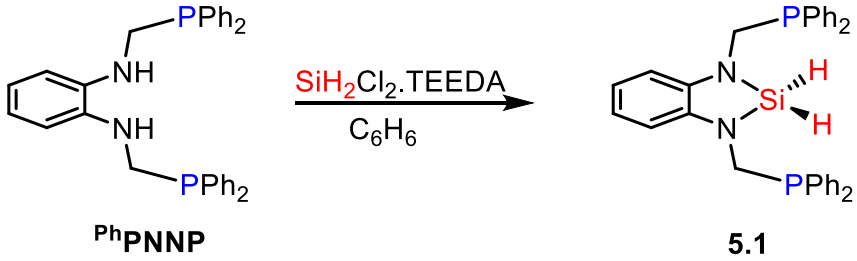

Scheme 5.5: Synthesis of $H_2Si(NCH_2PPh_2)_2C_6H_4$ **5.1**.

Reaction of equimolar amounts of ^{Ph}PNNP and SiH_2Cl_2.TEEDA in benzene for 1.5 hours resulted in a mixture of resonances in the $^{31}P\{^1H\}$ NMR spectrum associated with the starting material (–18.4 ppm), the ^{Ph}PNNP(SiHCl) analogue (–23.2 ppm) and the desired product ^{Ph}PNNP(SiH_2) **5.1** (–19.9 ppm). Compound ^{Ph}PNNP(SiHCl) was identified through comparison with an authentic sample, with key features including the methylene protons which are diastereotopic due to the tetrahedral geometry at silicon.[10]

In contrast, the methylene protons of **5.1** are chemically equivalent and appear as a doublet at δ_H = 3.78 ($^2J_{HP}$ = 2.4 Hz). This suggests that identical groups are bound to the silicon and supports the formation of **5.1**. In addition, the equivalent silyl hydrides resonate as a triplet at δ_H = 5.83 with a coupling constant of $^4J_{HP}$ = 3.8 Hz, similar in value to that of ^{Ph}PNNP(SiHCl) ($^4J_{HP}$ = 3.9 Hz). The resonance associated with **5.1** diminishes over 23 hours with the concurrent increase of the ^{Ph}PNNP(SiHCl) resonance. In each repetition of the reaction, the conversion of ^{Ph}PNNP to **5.1** did not reach completion and up to 30% of the starting material remained.

The reaction was repeated with two equivalents of SiH_2Cl_2.TEEDA to encourage full conversion of ^{Ph}PNNP to **5.1**. Analysis of the reaction by NMR spectroscopy after one hour showed compound **5.1** as the major product with ^{Ph}PNNP(SiHCl) as a 10% impurity. Slow conversion of **5.1** to ^{Ph}PNNP(SiHCl) was noted after leaving the mixture at room temperature for five days. Given the inevitable formation of ^{Ph}PNNP(SiHCl), attempts were made to isolate **5.1** within 30 minutes of the reaction. Whited's isolation of the ^{tBu}PNNP(SiH_2) analogue was achieved by lyophilisation, and thus the solution of **5.1** was similarly lyophilised using an acetonitrile/dry ice bath to yield a white solid. However, the $^{31}P\{^1H\}$ NMR spectrum revealed three resonances that corresponded to **5.1**, ^{Ph}PNNP(SiHCl) and an unidentified compound at δ_P = –23.9. Other attempts at purification included direct solvent removal under vacuum and washing with *n*-hexane. However, clean isolation of **5.1** proved difficult as a mixture of products was obtained in each case. From these results, it was inferred that **5.1** forms initially as a kinetic product and scrambling processes occur at Si between the silyl hydride and Cl groups of the $[TEEDAH_2]Cl_2$ by-product to generate ligands of greater thermodynamic stability.

Although compound **5.1** was not isolated, it could be generated cleanly *in situ* from two equivalents of SiH_2Cl_2.TEEDA. Therefore, efforts were directed towards preparing the ligand *in situ* and coordinating to rhodium precursors. Within 30 minutes of the reaction between Wilkinson's catalyst $[RhCl(PPh_3)_3]$ and **5.1**, the NMR spectra revealed full consumption of **5.1**, a large amount of free PPh_3 and complex $[RhHCl\{SiCl(NCH_2PPh_2)_2C_6H_4\text{-}1,2\}(PPh_3)]$ **5.4** in minor quantities (Scheme 5.6). Unfortunately, in all the precipitate and filtrate fractions following work-up only free PPh_3 was observed.

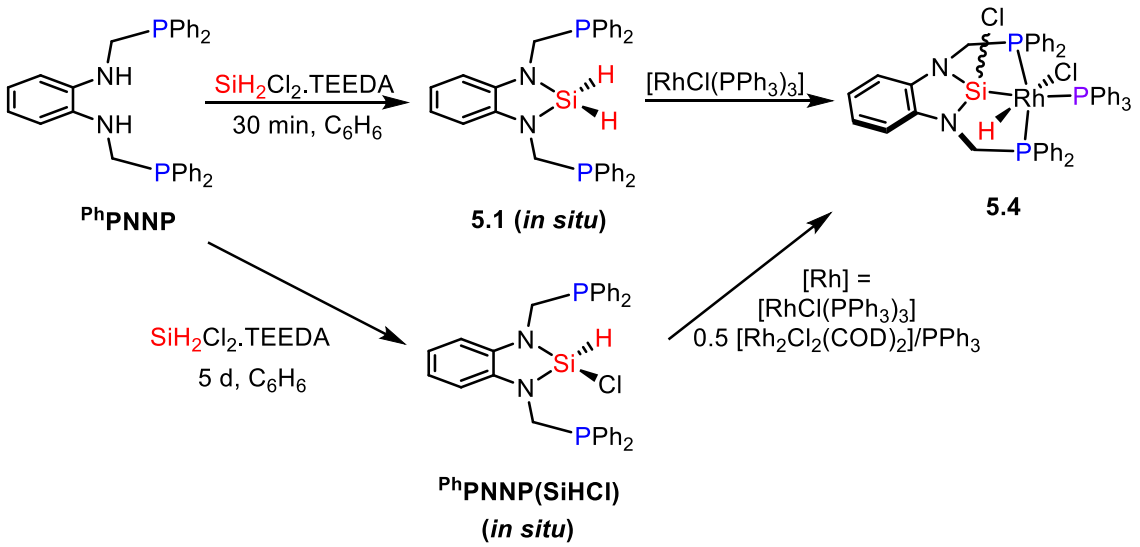

Scheme 5.6: Reactivity of **5.1** and ^{Ph}PNNP(SiHCl) generated *in situ* with rhodium precursors.

Interestingly, the same product was observed when the reaction was repeated with ^{Ph}PNNP(SiHCl) generated *in situ* from SiH_2Cl_2.TEEDA and ^{Ph}PNNP. This suggests that the presence of **5.4** from the reaction of **5.1** and $[RhCl(PPh_3)_3]$ may be due to reaction of $[RhCl(PPh_3)_3]$ with small quantities of ^{Ph}PNNP(SiHCl) that formed from ligand scrambling. This hypothesis was confirmed from the direct reaction of the ^{Ph}PNNP(SiHCl) ligand prepared from literature procedures[10] and $[RhCl(PPh_3)_3]$, the results and characterisation of which are discussed in Section 5.3.3.

Furthermore, as an alternative to the method outlined in Section 5.3.3, the synthesis of **5.4** was possible from the ^{Ph}PNNP(SiHCl) ligand generated *in situ* and rhodium precursors, $[RhCl(PPh_3)_3]$ or $[Rh_2Cl_2(COD)_2]$ followed by PPh_3 (at a 0.5:1 ratio). Two equivalents of PPh_3 were liberated when $[RhCl(PPh_3)_3]$ was used and thus required the sample to be purified through multiple washes with Et_2O. The second pathway allowed the controlled addition of PPh_3 eliminating the requirement for excessive washing. In both cases, the purification was made difficult by the persistence of the $[TEEDAH_2]Cl_2$ by-product following a number of work-up protocols including washing, extraction and trituration. Therefore, the methodology developed in Section 5.3.3 is the preferred pathway to **5.4**.

5.2.3 Attempted Synthesis of $H_2Si(NCH_2PPh_2)_2C_6H_4$ through Treatment of $HClSi(NCH_2PPh_2)_2C_6H_4$ with $Li[HBEt_3]$

From the previous section it was evident that H and Cl scrambling was a common occurrence in the attempted synthesis of **5.1** from the treatment of ^{Ph}PNNP with H_2SiCl_2.TEEDA. Therefore, an alternative pathway involving halogen replacement in ^{Ph}PNNP(SiHCl) was explored.

The preparation of ^{Ph}PNNP(SiHCl) was carried out following published procedures and the spectroscopic data were consistent with those reported.[10] Upon solvent removal of a concentrated solution of ^{Ph}PNNP(SiHCl) in benzene, colourless crystals formed which were suitable for X-ray diffraction analysis. The structure of ^{Ph}PNNP(SiHCl) has not been reported previously and is depicted in Figure 5.4.

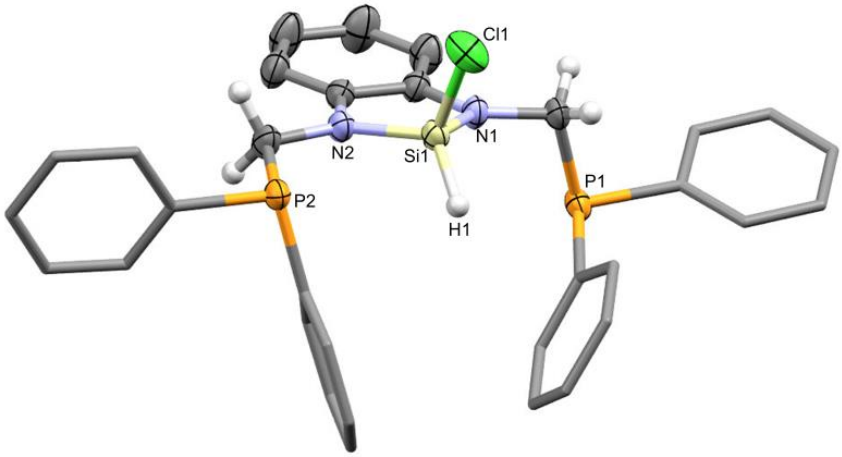

Figure 5.4: Molecular structure of ^{Ph}PNNP(SiHCl).C_6H_6 (solvent omitted, aryl hydrogen atoms omitted, phenyl groups simplified, displacement ellipsoids shown at 50% probability). Selected bond lengths (Å) and angles (°): Si1–H1 1.38(2), Si1–Cl1 2.0716(8), Si1–N1 1.7145(17), Si1–N2 1.7132(18), N2–Si1–N1 93.30(9), N2–Si1–H1 118.0(9), N2–Si1–Cl1 114.21(7), N1–Si1–Cl1 110.33(7), N1–Si1–H1 117.1(9), Cl1–Si1–H1 104.1(9).

The molecular structure contains a distorted tetrahedral geometry about the silicon with the N2–Si1–N1 angle compressed to 93.30(9)°, a substantial deviation from the ideal tetrahedral angle of 109.5°, but is necessary to accommodate Si within a planar five-membered ring. In contrast, the other angles within the tetrahedron are augmented slightly past the ideal value to 114.21(7)° and 110.33(7)° (N2–Si1–Cl1 and N1–Si1–Cl1 respectively). The reported molecular structure of the related phenyl derivative ^{Ph}PNNP(SiHPh) displays similar distortion about the silicon atom.[10]

The conversion of ^{Ph}PNNP(SiHCl) into ^{Ph}PNNP(SiH_2) was investigated by treatment of a solution of ^{Ph}PNNP(SiHCl) in THF with Li[$HBEt_3$]. It was envisaged that the use of Li[$HBEt_3$] could reduce H and Cl scrambling processes by trapping the chloride within the LiCl salt. The $^{31}P\{^1H\}$ NMR spectrum of an aliquot taken at 30 minutes revealed the presence of the expected product at δ_P = –19.9 (**5.1**) and an unidentified resonance at δ_P = –24.1 in roughly equal amounts. The two resonances persisted in the same ratio in the reaction at five hours and did not change with longer reaction times. Consistent with previous observations of decomposition during work-up (Section 5.2.2), solvent removal from the reaction mixture afforded scrambling of the desired product back to the starting material and the unidentified product. Further addition of Li[$HBEt_3$] reduced the mixture to the diamine ^{Ph}PNNP precursor.

Given the limited success encountered with the ^{Ph}PNNP(SiH_2) ligand, focus in this chapter was redirected to gaining an understanding of the reactivity of the more durable ligands, ^{Ph}PNNP(SiHCl) and ^{Ph}PNNP(SiHPh).

5.3 Group 9: Rh(III) and Ir(III) Complexes

5.3.1 Synthesis of [RhHCl{SiPh(NCH_2PPh_2)$_2C_6H_4$-1,2}(PPh_3)]

The reactivity of pro-ligand ^{Ph}PNNP(SiHPh) was investigated with [RhCl(CO)(PPh_3)$_2$], where the octahedral products of Si–H activation, [RhHCl{SiPh(NCH_2PPh_2)$_2C_6H_4$-1,2}(CO)] or [RhHCl{SiPh(NCH_2PPh_2)$_2C_6H_4$-1,2}(PPh_3)], might be anticipated. The formation of two complexes was noted in ^1H and $^{31}P\{^1H\}$ NMR spectra, and was formulated as diastereomers of [RhHCl{SiPh(NCH_2PPh_2)$_2C_6H_4$-1,2}(PPh_3)] **5.2** based off the multiplicity of the resonances, which were consistent with a complex featuring a PPh_3 co-ligand rather than CO (Scheme 5.7). For example, in the $^{31}P\{^1H\}$ NMR spectrum, the pincer PPh_2 groups of the major species resonated as a doublet of doublets (dd) with coupling to rhodium ($^1J_{PRh}$ = 113 Hz) and PPh_3 ($^2J_{PP}$ = 22 Hz); whereas the PPh_3 resonance of doublet of triplets (dt) couples to rhodium ($^1J_{PRh}$ = 84 Hz) and the PPh_2 groups ($^2J_{PP}$ = 22 Hz). Similar dt and dd splitting patterns were present for the minor product. Additionally, there was no evidence for the formation of [RhHCl{SiPh(NCH_2PPh_2)$_2C_6H_4$-1,2}(CO)] in the NMR spectral data, and the formation of **5.2** demonstrates the preferential coordination of PPh_3 over CO.

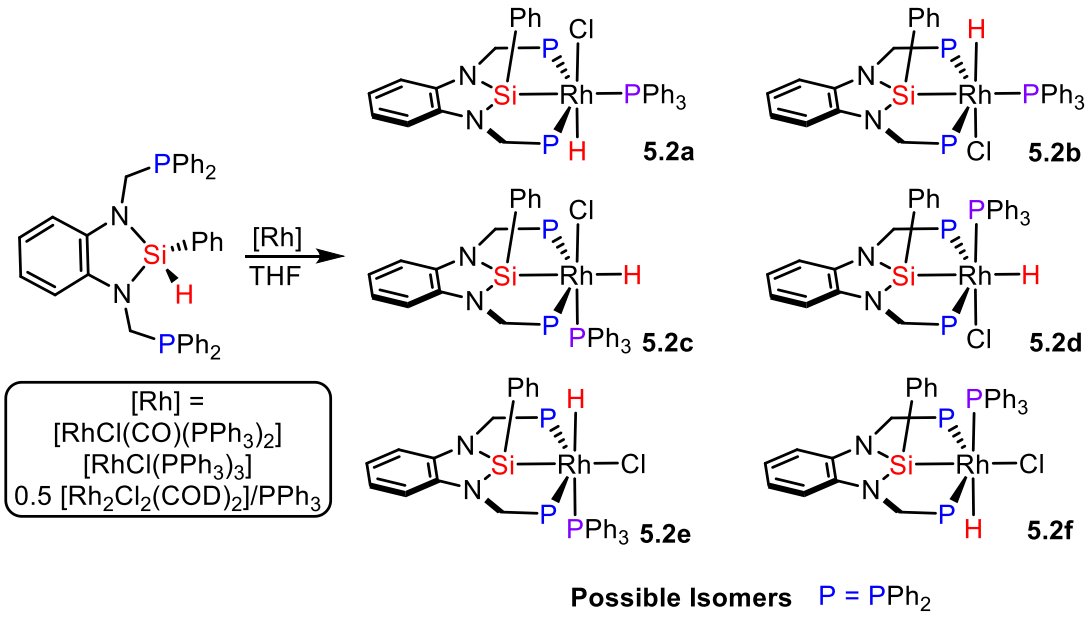

Scheme 5.7: Synthesis of **5.2** through reported procedures using $[RhCl(PPh_3)_3]$ and $[Rh_2Cl_2(COD)_2]/PPh_3$ (0.5:1)[10] and the new preparatory method from $[RhCl(CO)(PPh_3)_2]$. All six possible *mer*-diastereomers of **5.2** shown.

Although six diastereomers of **5.2** (Scheme 5.7) are conceivable from the various possible arrangements of the H, Cl and PPh_3 ligands and their position with respect to the silyl phenyl substituent (*syn*, *anti*), only two isomers of **5.2** are observed experimentally. To identify the two isomers formed in the reaction of ^{Ph}PNNP(SiHPh) and $[RhCl(CO)(PPh_3)_2]$, the hydride resonances were considered. While poor signal to noise ratio of the hydride resonance of the minor isomer occludes the determination of coupling constants, the hydride resonance of the major isomer showed doublet of doublet of triplet (ddt) multiplicity with coupling to rhodium ($^1J_{HRh}$ = 20.0 Hz), PPh_3 ($^2J_{HP}$ = 16.2 Hz) and the PPh_2 groups ($^2J_{HP}$ = 9.7 Hz).

The series of octahedral complexes of the form $[RhH(SiR_3)(SR')(PMe_3)_3]$ contains a hydride located *cis* to the *trans*-disposed PMe_3 groups and *trans* to the remaining PMe_3 ligand, and thus serves as a useful point of reference.[28] The magnitude of the ^{1}H-$^{31}PPh_3$ coupling constant in the major isomer of **5.2** ($^2J_{HP}$ = 16.2 Hz) falls within the range $^2J_{HP}$ = 14–18 Hz subtended by the *cis* ^{1}H-$^{31}PMe_3$ groups in $[RhH(SiR_3)(SR')(PMe_3)_3]$, whereas the *trans* ^{1}H-$^{31}PMe_3$ coupling constant is notably larger ($^2J_{HP}$ = 147–156 Hz).

Therefore, the major isomer of **5.2** was postulated to have *cis* H and PPh_3 ligands, eliminating diastereomers **5.2e** and **5.2f** in which these ligands are located *trans*. Furthermore, the formation of diastereomers **5.2c** and **5.2d** was envisaged to be

disfavoured due to the mutually *trans* positioning of H and Si groups, which are both strong σ-donors. From the process of elimination outlined thus far, the isomeric mixture of **5.2** was postulated as **5.2a** and **5.2b**. This mixture of isomers was isolated as a yellow solid in 70% yield.

Isomers **5.2a** and **5.2b** have previously been obtained through alternate syntheses involving rhodium precursors, $[RhCl(PPh_3)_3]$ or $[Rh_2Cl_2(COD)_2]/PPh_3$ (0.5:1), and ^{Ph}PNNP(SiHPh).[10] The spectral data of **5.2a** and **5.2b** derived from $[RhCl(CO)(PPh_3)_2]$ and ^{Ph}PNNP(SiHPh) are consistent with those reported from the alternative routes.

5.3.2 Synthesis of $[IrHCl\{SiPh(NCH_2PPh_2)_2C_6H_4\text{-}1,2\}(PPh_3)]$

The same preference for PPh_3 coordination over CO was observed for the iridium analogue. In the reaction of Vaska's complex *trans*-$[IrCl(CO)(PPh_3)_2]$ and ^{Ph}PNNP(SiHPh), an isomeric mixture of $[IrHCl\{SiPh(NCH_2PPh_2)_2C_6H_4\text{-}1,2\}(PPh_3)]$ **5.3** was formed in 60% yield (Scheme 5.8).

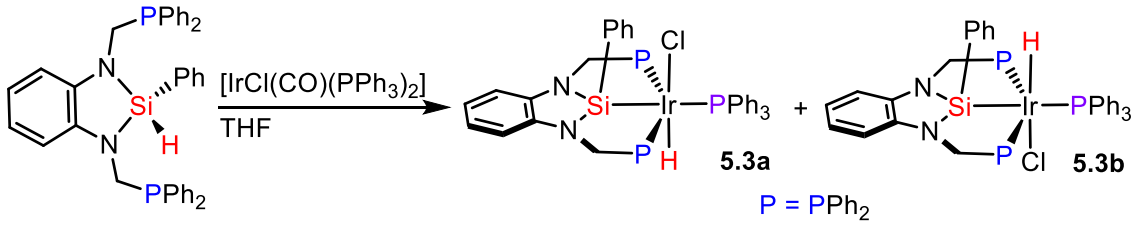

Scheme 5.8: Reaction of ^{Ph}PNNP(SiHPh) with Vaska's complex.

In contrast, reaction of Stobart's pro-ligand $HMeSi\{(CH_2)_3PPh_2\}_2$ (Figure 5.1, **A**) with Vaska's complex resulted in diastereomers of $[IrHCl\{SiMe((CH_2)_3PPh_2)_2\}(CO)]$, which illustrated preferential coordination of CO over PPh_3.[29] In the absence of an Si–H unit, such as in the difluorosilane pro-ligand $F_2Si(C_6H_4PPh_2\text{-}2)_2$, reaction with Vaska's complex leads to preferential Si–C σ-bond cleavage over Si–F activation.[30] This results in cleavage of the PSiP backbone forming complex $[IrCl\{SiF_2(C_6H_4PPh_2\text{-}2)\}(C_6H_4PPh_2\text{-}2)(CO)]$, and is one of a few examples of Si–C σ-bond cleavage processes of the $R'_2Si(C_6H_4PR_2\text{-}2)_2$ framework.[30,31]

Compared to **5.2a** and **5.2b**, the reaction of ^{Ph}PNNP(SiHPh) with $[IrCl(CO)(PPh_3)_2]$ was anticipated to proceed more slowly, as expected for the transition from a 4d to a 5d metal centre. An aliquot of the reaction mixture was taken after one hour to identify any intermediate complexes. However, the $^{31}P\{^1H\}$ NMR spectrum revealed an array of singlet resonances (≈7), and no intermediate could be discerned from the data obtained.

After 25 hours at room temperature, a mixture of isomers consisting of **5.3a** and **5.3b** was isolated as a pale yellow powder in a ratio of 1:8 based on ^{1}H NMR integration. With similar reasoning as used for the rhodium analogue (**5.2a/5.2b**), out of the six possible isomeric forms of **5.3**, diastereomers **5.3a** and **5.3b** that differ by the orientation of the phenyl group were inferred based off the hydride coupling constants. The hydride lies *cis* to the PPh_3 in both isomers, as inferred from the magnitude of the ^{1}H-$^{31}PPh_3$ coupling constants ($^{2}J_{HP\ (PPh3)}$ = Major: 15.4 Hz, Minor: 17.1 Hz). The magnitudes fall near the range reported for *cis* ^{1}H-$^{31}PMe_3$ coupling constants in complexes of the form $[IrHCl(CH_2COR)(PMe_3)_3]$ ($^{2}J_{HP}$ = 19–22 Hz).[32]

The rigidity of the ^{Ph}PNNP(SiHR) backbone encourages meridional coordination of the ^{Ph}PNNP(SiHPh) ligand to the metal centre. This chelation results in diastereotopic methylene protons H_a and H_b (Figure 5.5) that resonate at distinct environments (δ_H = 4.16 and δ_H = 4.84). The protons H_a and H_b commonly exhibit virtual coupling, where the strong coupling between the *trans*-disposed magnetically inequivalent diphenylphosphino phosphorus nuclei cause other nuclei to couple to them as if they were equidistant.[33] The coupling constant of the virtual triplet is therefore an intermediate between $^{2}J_{HP}$ and $^{4}J_{HP}$.

Although H_a and H_b are each two and four bonds away from the *trans*-disposed PPh_2, only one set of the protons in **5.3** show virtual coupling in the ^{1}H NMR spectrum. This manifests as a doublet of virtual triplets whereas the other environment is a doublet with an absence of virtual coupling. This is rationalised by the Karplus angular dependence of the methylene protons that are fixed within the ring system and suggests that virtual coupling occurs for the protons on one face of the ring, whereas the other set of protons where the J_{HP} coupling is absent likely has a dihedral angle close to 90°.[34,35] The phenomenon of virtual coupling is consistent with other complexes reported containing the ^{Ph}PNNP(SiHR) backbone and is a recurring feature in nearly many of the complexes synthesised in this chapter.[10]

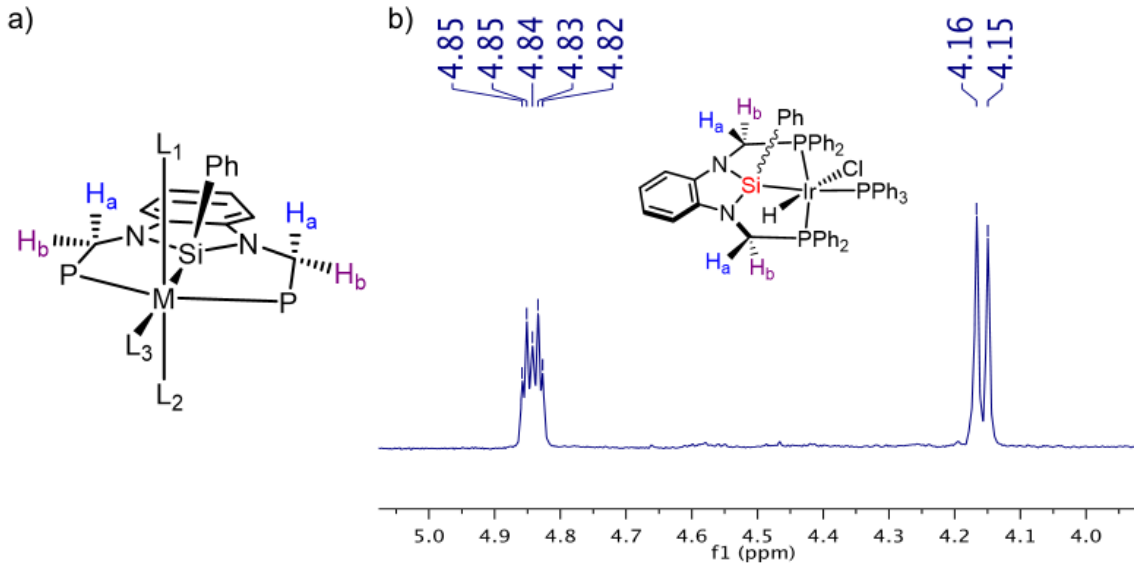

Figure 5.5: a) Meridional coordination of ^{Ph}PNNP(SiHPh) and b) virtual coupling in the ^{1}H NMR spectrum of **5.3**.

The formulation of the major isomer of **5.3** was further supported by distinct doublet and triplet resonances in the $^{31}P\{^{1}H\}$ NMR at the respective shifts δ_P = 27.0 and –1.81, where the nuclei in the two phosphorus environments $^{31}PPh_3$–$^{31}PPh_2$ couple with 18 Hz magnitude. The low solubility of the isomeric mixture precluded the acquisition of a $^{13}C\{^{1}H\}$ NMR spectrum with an adequate signal to noise ratio. However, of the resonances that were observed, the methylene carbon also displayed virtual coupling and appeared as a doublet of virtual triplets at 60.4 ppm ($^{2}J_{CP\ (PPh3)}$ = 8.0 and $^{2}J_{CP\ (PPh2)}$ = 20.0 Hz). The cross peak in the $^{1}H^{13}C$ HSQC experiments show the correlation of the two diastereotopic methylene proton environments to the same carbon resonance and provides further support for the assignment of the methylene resonance.

Additionally, the ^{29}Si signal of the major isomer of **5.3** resonates as a doublet of triplets at δ_{Si} = 88.3, with coupling to the phosphorus nuclei in distinct environments ($^{2}J_{SiP\ (PPh3)}$ = 126.5 and $^{2}J_{SiP\ (PPh2)}$ = 14.4 Hz). Although chemical shift values are available for numerous silyl pincer complexes in the literature, the coupling constants of ^{29}Si to neighbouring nuclei (particularly of $^{2}J_{SiP}$) are limited.

Notwithstanding electronic differences between iridium and ruthenium, Whited's complexes [RuH{SiR($C_6H_4PPh_2$-2)$_2$}(CO)(PPh_3)] (R = H, OTf) show $^{2}J_{SiP}$ values of similar magnitude to **5.3**. Consistent with **5.3**, the $^{2}J_{SiP}$ doublet coupling to PPh_3 was greater than the $^{2}J_{SiP}$ triplet coupling to PPh_2 (Whited: R = H: $^{2}J_{SiP\ (PPh3)}$ = 83 and $^{2}J_{SiP\ (PPh2)}$ = 15 Hz;

R = OTf: $^{2}J_{SiP\ (PPh3)}$ = 110 and $^{2}J_{SiP\ (PPh2)}$ = 19 Hz).[36] The larger *trans* ^{29}Si-^{31}PPh$_3$ coupling constant value than *cis* ^{29}Si-^{31}PPh$_2$ is a recurrent feature in the proceeding work.

5.3.3 Synthesis of [RhHCl{SiCl(NCH$_2$PPh$_2$)$_2$C$_6$H$_4$-1,2}(PPh$_3$)]

The complex [RhHCl{SiCl(NCH$_2$PPh$_2$)$_2$C$_6$H$_4$-1,2}(PPh$_3$)] **5.4** was observed in Section 5.2.2 in the reaction of rhodium precursors with the silane ligands formed *in situ*, ^{Ph}PNNP(SiHCl) and ^{Ph}PNNP(SiH$_2$). Here the direct reaction of ^{Ph}PNNP(SiHCl) and [RhCl(PPh$_3$)$_3$] afforded an isomeric mixture of complexes **5.4a** and **5.4b**, which was isolated in a combined yield of 68% (Scheme 5.9). The formation of **5.4** demonstrates the preferential oxidative addition of the Si–H bond over Si–Cl in the ligand ^{Ph}PNNP(SiHCl), consistent with its expected greater reactivity.

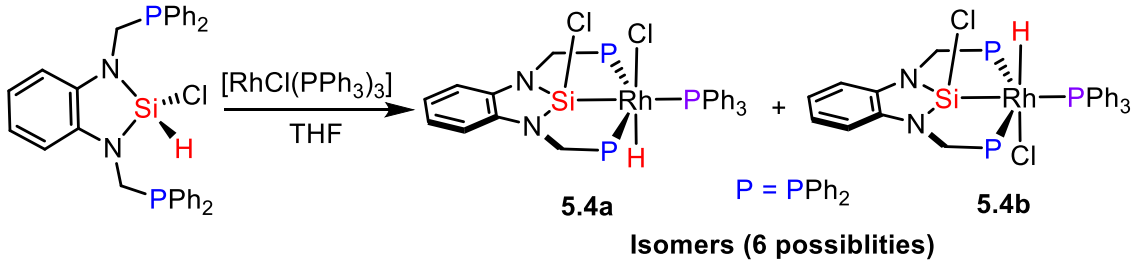

Scheme 5.9: Synthesis of **5.4a** and **5.4b** through reaction with Wilkinson's Catalyst.

The formulation of **5.4a** and **5.4b** was supported by spectroscopic data. The two diastereomers were observed in the ^{1}H and ^{31}P{^{1}H} NMR spectra at a ratio of 1:11 (C$_6$D$_6$) and 1:7 (CDCl$_3$), as assessed by ^{1}H NMR integration. The difference in ratio found in the solvents could be owing to the existence of the two isomers in a solvent dependent dynamic equilibrium, as was found for the phenyl analogues **5.2a**/**5.2b**.[10]

The hydride resonance of the major product of **5.4** was observed at –16.7 ppm in the ^{1}H NMR spectrum and exhibited a ddt splitting pattern consistent with coupling to rhodium, the triphenylphosphine and the diphenylphosphino nuclei ($^{1}J_{HRh}$ = 18.5, $^{2}J_{HP\ (PPh3)}$ = 15.4, $^{2}J_{HP\ (PPh2)}$ = 8.8 Hz). The coupling constants of the hydride signal at –19.4 ppm of the minor product could similarly be discerned. The resonance was resolved as a doublet of triplet of doublets (dtd) with coupling constants of $^{1}J_{HRh}$ = 18.4, $^{2}J_{HP\ (PPh2)}$ = 12.2 and $^{2}J_{HP\ (PPh3)}$ = 5.8 Hz respectively. Given the complexity of the hydride resonances of isomers of **5.4**, a ^{1}H{^{31}P} experiment was performed to confirm the magnitude of the rhodium hydride coupling constant ($^{1}J_{HRh}$) as 18.5 and 18.4 Hz (Figure 5.6).

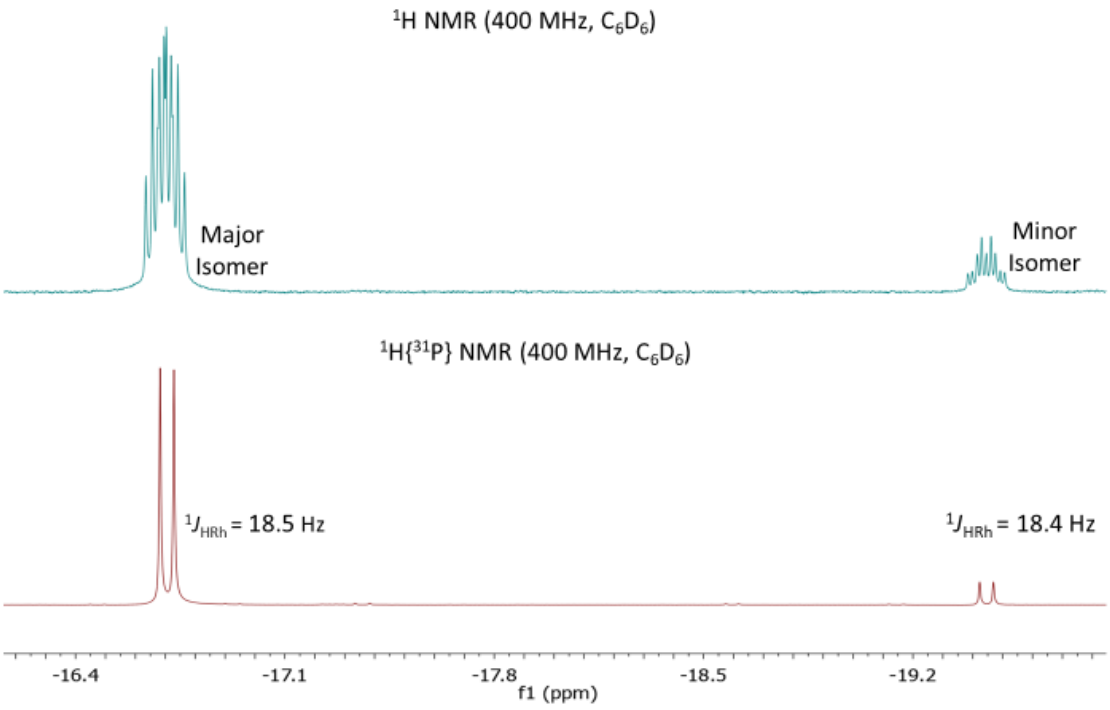

Figure 5.6: Simplification of the hydride resonances in isomers of **5.4** from the ^{1}H NMR spectrum to the ^{1}H{^{31}P} spectrum.

The presence of the hydride was further supported by a Rh–H stretching frequency of 2029 cm^{-1} in the IR spectrum. Consistent with the sets of complexes **5.2** and **5.3**, the methylene protons of the major isomer of **5.4** resonated in the ^{1}H NMR spectrum as a doublet and a doublet of virtual triplets at the respective shifts of 4.17 and 4.53 ppm. Both resonances contained a geminal $^2J_{HH}$ doublet coupling constant of 11.2 Hz, whilst one methylene proton environment exhibited virtual coupling to PPh_2 ($^2J_{HP}$ = 4.6 Hz). The isomers of **5.4** were also noted in the ^{31}P{^{1}H} NMR spectrum, with the major isomer displaying dt multiplicity for the triphenylphosphine co-ligand ($^1J_{PRh}$ = 91, $^2J_{PP}$ = 24 Hz) and dd for the diphenylphosphine ($^1J_{PRh}$ = 109, $^2J_{PP}$ = 24 Hz).

The limited solubility of **5.4** in C_6D_6 precluded the acquisition of a ^{13}C{^{1}H} NMR spectrum with a good signal to noise ratio. Characterisation was attempted in $CDCl_3$ but the complex displayed limited stability in this solvent. Therefore, all characterisation was performed in C_6D_6. To assess if the decomposition of **5.4** in $CDCl_3$ is due to hydride displacement with a chloride, a controlled displacement reaction was attempted using one equivalent of N-chlorosuccinimide. However, no reaction ensued after seven hours and at longer reaction times (26 hours) sample decomposition was observed as singlets at δ_P = 22.0, 29.1 and 41.4 in the ^{31}P{^{1}H} NMR spectrum.

Although the $^{13}C\{^{1}H\}$ spectrum of **5.4** was acquired over 20,000 scans (176 MHz spectrometer), only the methylene carbon resonances of the two isomers of **5.4** could be clearly discerned at 57.4 and 59.7 ppm. The ^{29}Si nuclei in the complex was found at 85.4 ppm in the $^{29}Si\{^{1}H\}$ NMR spectrum. Due to the expected complex ddt multiplicity, the resonance was broadened into the baseline and only the ^{29}Si-$^{31}PPh_3$ doublet coupling constant was determined with precision ($^{2}J_{SiP}$ = 190 Hz). Despite numerous attempts to obtain crystals of **5.4a**/**5.4b** suitable for X-ray diffraction, only precipitation of fine microcrystalline powder resulted.

5.3.4 Treatment of [RhHCl{SiCl(NCH$_2$PPh$_2$)$_2$C$_6$H$_4$-1,2}(PPh$_3$)] with PhLi

To explore reactivity at the silicon atom, particularly that of the Si–Cl bond, the mixture of complexes **5.4a**/**5.4b** was treated with excess phenyllithium in anticipation of chloride substitution to give the known complexes **5.2a**/**5.2b** (Figure 5.7). However, the ^{1}H and $^{31}P\{^{1}H\}$ NMR spectra of the reaction mixture were devoid of resonances associated with **5.2a**/**5.2b**. Instead the resonances observed were suggestive of a square planar complex [Rh{SiPh(NCH$_2$PPh$_2$)$_2$C$_6$H$_4$-1,2}(PPh$_3$)] **5.5** formed at 20% conversion, as well as starting material **5.4**.

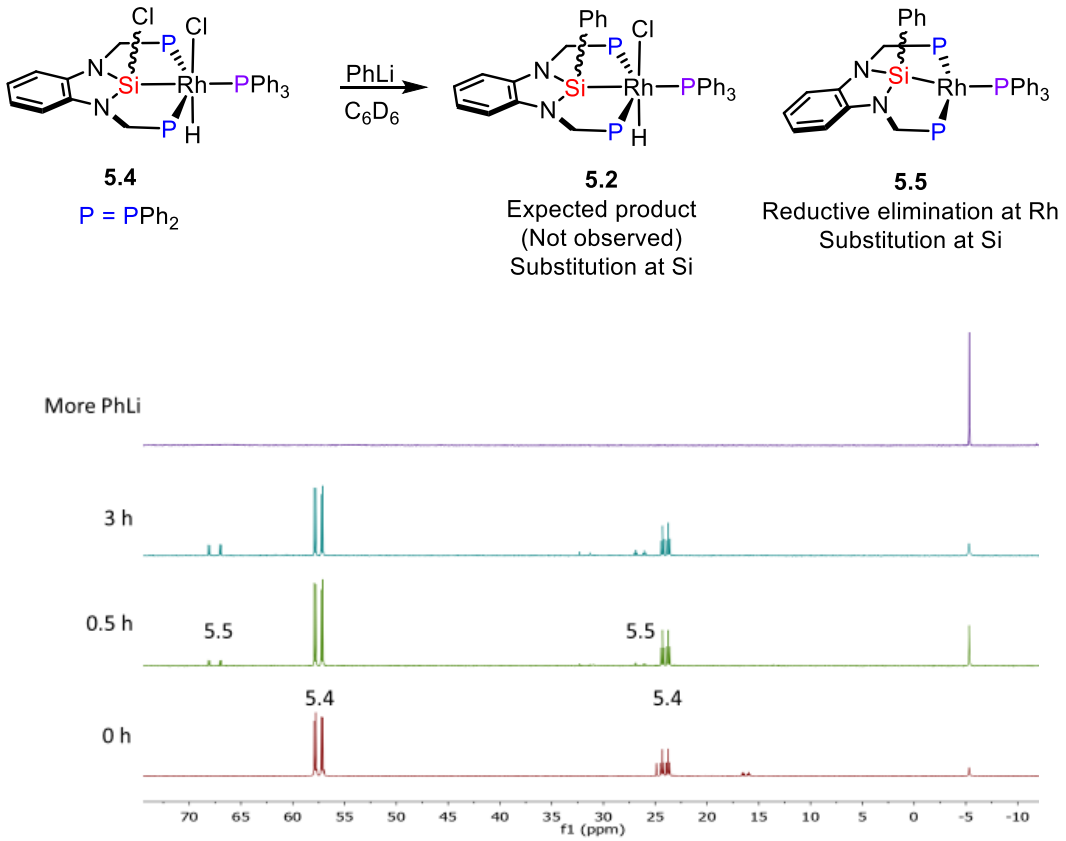

Figure 5.7: NMR scale conversion of [RhHCl{SiCl(NCH$_2$PPh$_2$)$_2$-C$_6$H$_4$-1,2}(PPh$_3$)] **5.4** to [Rh{SiPh(NCH$_2$PPh$_2$)$_2$-C$_6$H$_4$-1,2}(PPh$_3$)] **5.5** monitored by ^{31}P{^{1}H} (121 MHz) NMR spectroscopy in C$_6$D$_6$.

The formation of **5.5** was accompanied by the convergence of the independent resonances of **5.4a** and **5.4b** to a simpler spectrum. The PPh$_2$ pincer arms and PPh$_3$ co-ligand showed characteristic splitting in the ^{31}P{^{1}H} NMR at 68.6 ppm (dd, $^2J_{PRh}$ = 177, $^2J_{PP}$ = 21 Hz) and 27.5 (dt, $^2J_{PRh}$ = 133, $^2J_{PP}$ = 21 Hz) respectively. In contrast to the methylene proton environments of **5.4** (that resolve to d and dt^v), both environments in **5.5** displayed virtual coupling.

The formation of **5.5** involves the substitution of the silyl-chloride with phenyl and dehydrohalogenation of HCl. This selective conversion to **5.5** implies that dehydrohalogenation occurs more rapidly than nucleophilic substitution at the silicon. Attempts to encourage the reaction through further addition of phenyllithium resulted in complete reduction of the complex and only free triphenylphosphine was seen in the NMR spectrum. The fate of the PPh$_2$ groups of the pincer arm remains unknown as the spectrum was absent of the resonances from PPh$_2$Me (expected at δ_P = –27.1),[37] a product that might be anticipated from the decomposition and subsequent protonation of the pincer CH$_2$PPh$_2$ units.

Given the prevalence of established square planar complexes in catalysis by Group 9 transition metals (e.g., Wilkinson's $[RhCl(PPh_3)_3]$, Cavita's $[IrI_2(CO)_2]^-$), the preparation of $[Rh\{SiPh(NCH_2PPh_2)_2C_6H_4\text{-}1,2\}(PPh_3)]$ was pursued and is discussed in Section 5.4.

5.4 Group 9: Rh(I) Complexes

5.4.1 Synthesis of $[Rh\{SiPh(NCH_2PPh_2)_2C_6H_4\text{-}1,2\}(PPh_3)]$ from Treatment of $[RhHCl\{SiPh(NCH_2PPh_2)_2C_6H_4\text{-}1,2\}(PPh_3)]$ with Lithium Diisopropylamide

The formation of **5.5** from the dehydrohalogenation of **5.4a**/**5.4b** prompted investigations into the dehydrohalogenation of the related isomeric mixture **5.2a**/**5.2b** as a potential route to **5.5**. A suspension of **5.2a**/**5.2b** in C_6D_6 was treated with an excess of 0.5M solution of lithium diisopropylamide (LDA) in THF/*n*-hexane and monitored by ^1H and $^{31}P\{^1H\}$ NMR spectroscopy. The reaction progress in Figure 5.8 shows the slow, albeit clean dehydrohalogenation of the isomeric mixture **5.2a**/**5.2b** to **5.5** over 18 hours.

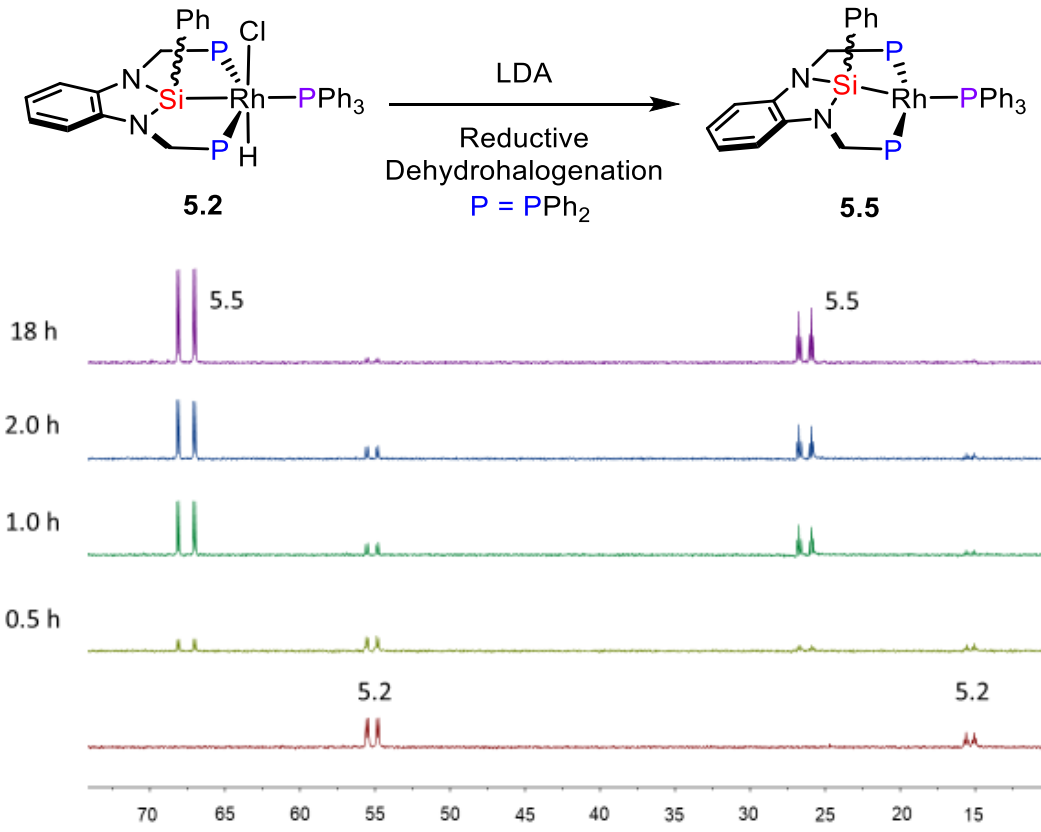

Figure 5.8: NMR scale conversion of $[RhHCl\{SiPh(NCH_2PPh_2)_2C_6H_4\text{-}1,2\}(PPh_3)]$ **5.2** to $[Rh\{SiPh(NCH_2PPh_2)_2C_6H_4\text{-}1,2\}(PPh_3)]$ **5.5** monitored by $^{31}P\{^1H\}$ (121 MHz) NMR spectroscopy in C_6D_6.

Whilst the conversion of **5.2a**/**5.2b** to **5.5** proceeded cleanly to completion on the NMR scale, the reaction only reached 20% conversion over 21 hours when repeated on a larger (150 mg) scale with a three-fold excess of LDA. The crude reaction mixture returned predominantly starting material as well as new resonances of unformulated products at δ_P = 63.7 (dd), 28.9 (dt) and 25.2 (dd).

5.4.2 Direct Synthesis of [Rh{SiPh(NCH$_2$PPh$_2$)$_2$C$_6$H$_4$-1,2}(PPh$_3$)]

The complexes discussed thus far feature complete saturation at an octahedral metal centre following Si–H activation. Judicious choice of a metal precursor bearing a suitable hydrogen acceptor was considered as a means to access to Rh(I) complexes with a low coordination number. Preliminary results from Dixon suggested the formation of **5.5** from the direct reaction of ^{Ph}PNNP(SiHPh) with [RhH(PPh$_3$)$_4$].[38]

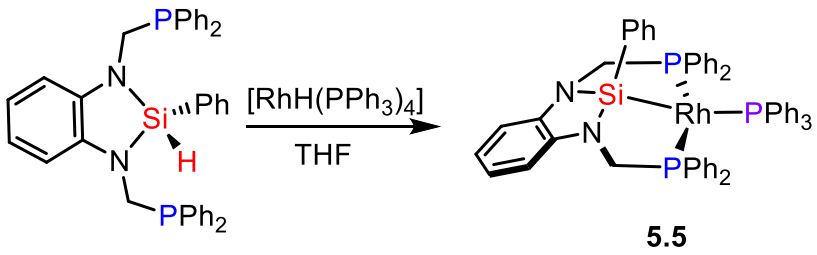

Scheme 5.10: Formation of complex **5.5** from [RhH(PPh$_3$)$_4$].

With minor modifications to Dixon's procedure, **5.5** was prepared (Scheme 5.10). The ^{1}H and ^{31}P{^{1}H} NMR spectra of the crude sample showed clean conversion to the proposed product and liberation of triphenylphosphine, which was washed out with diethyl ether to afford **5.5** in a modest 55% yield. The ^{1}H and ^{31}P{^{1}H} NMR data for **5.5** are consistent with those in Sections 5.3.4 and 5.4.1. The expected intermediate [RhH$_2$\{SiPh(NCH$_2$PPh$_2$)$_2$C$_6$H$_4$-1,2\}(PPh$_3$)] following Si–H activation was not observed spectroscopically, which suggests facile spontaneous reductive elimination of dihydrogen.

Coordinatively unsaturated square planar complexes have been reported to bind oxygen. An early example is the reversible oxygenation of Vaska's *trans*-[IrCl(CO)(PPh$_3$)$_2$] to [Ir(O$_2$)Cl(CO)(PPh$_3$)$_2$].[39] Complex **5.5** is extremely air sensitive, which is observed by a remarkably rapid colour change in the solid state from orange to green within 40 seconds upon exposure to the atmosphere. No oxygen adduct of **5.5** was detected in the ^{1}H and ^{31}P{^{1}H} NMR spectra of this green solid, regardless of whether the NMR was

prepared in air or under an argon atmosphere. Instead only triphenylphosphine oxide (δ_P = 25.0 in C_6D_6) was observed in the green solution, showing decomposition of **5.5** into $O{=}PPh_3$ and a rhodium species devoid of NMR detectable substituents (perhaps based on a paramagnetic d^7-Rh(II) species). Bubbling compressed air through an NMR solution of **5.5** produced the same results. The air sensitivity of complex **5.5** precluded the acquisition of suitable microanalytical data, however the formulation of the complex was confirmed by NMR and IR spectral data and mass spectrometry.

Furthermore, X-ray diffraction studies were performed to establish the structure of **5.5**. Crystals of a benzene solvate suitable for X-ray diffraction studies were obtained from a concentrated solution of **5.5** in benzene (Figure 5.9).

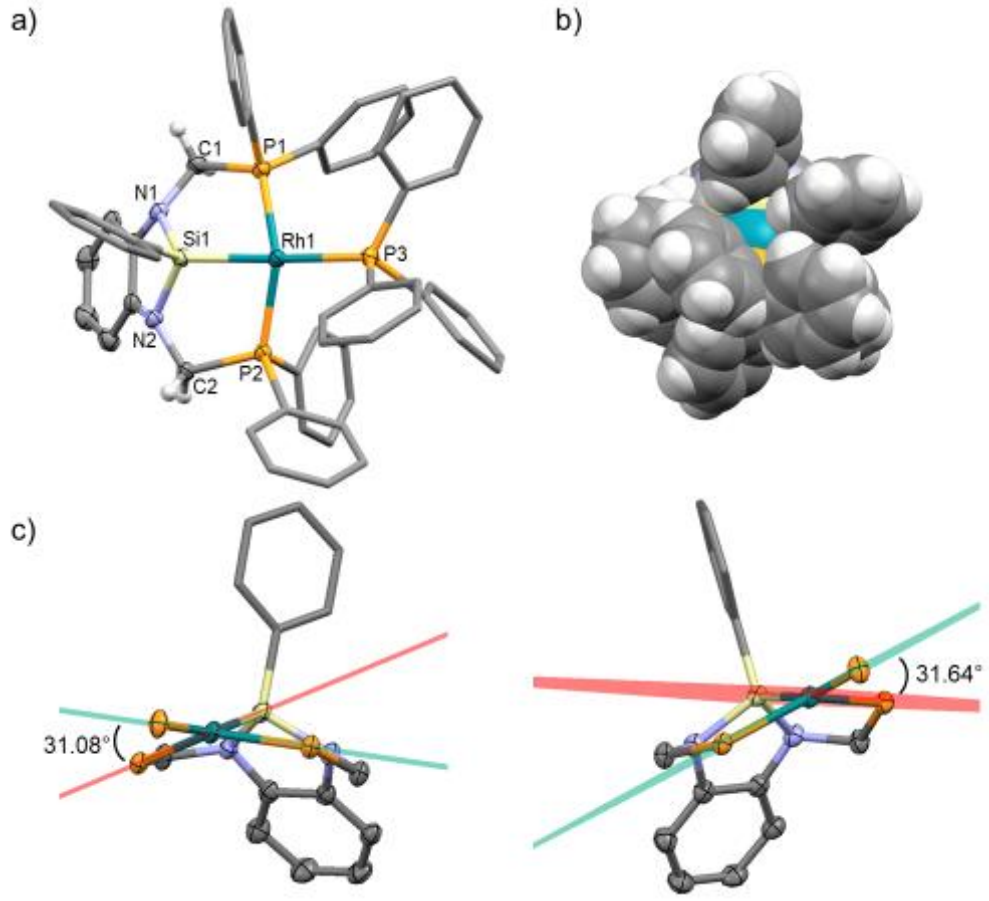

Figure 5.9: a) Molecular structure of [Rh{SiPh(NCH_2PPh_2)$_2C_6H_4$-1,2}(PPh_3)] **5.5**.C_6H_6 (aryl hydrogen atoms omitted, solvent omitted, phenyl groups simplified, displacement ellipsoids shown at 50% probability). Selected bond lengths (Å) and angles (°): Rh1–Si1 2.2610(7), Rh1–P3 2.3736(6), Rh1–P1 2.2523(6), Rh1–P2 2.2895(5), P1–Rh1–P2 142.66(2), P1–Rh1–P3 105.06(2), P2–Rh1–P3 103.98(2), Si1–N1–C1 115.9(1), Si1–N2–C2 115.8(1), Si1–Rh1–P1 77.87(2), Si1–Rh1–P2 80.54(2), Si1–Rh1–P3 164.24(2). b) Space-filling diagram of **5.5**. c) Simplified diagram with dihedral planes generated from Si1Rh1P1, P2Rh1P3 (left) and Si1Rh1P2, P1Rh1P3 (right).

The crystal structure of **5.5** reveals a significantly distorted square planar geometry about the rhodium, where the meridional coordination of the pincer ligand P1–Rh1–P2 is bent at 142.66(2)°, some 10° greater than the *transoidal* phosphines within the two crystallographic reports of complex [RhHCl{SiPh(NCH_2PPh_2)$_2C_6H_4$-1,2}(PPh_3)] (154.04(2)°–154.25(4)°).[10] The Si1–Rh1–P3 angle distorted at 164.24(2)° similarly deviates from the ideal 180° expected from square planar geometry. Thus, the coordination geometry of **5.5** lies between square planar and tetrahedral, and is quantified by the dihedral angles (δ) depicted in Figure 5.9c. The extent of the distortion from square planar ($\delta \approx 0°$) and tetrahedral ($\delta \approx 90°$) are determined as 31° (between the Si1Rh1P1 and the P2Rh1P3 planes) and 32° (between the Si1Rh1P1 and the P2Rh1P3 planes).

The puckered ring system demonstrates the delicate balance between the preferential tetrahedral geometry at silicon and the meridional coordination of the ligand (Figure 5.9c). The Rh–P bonds of the pincer (P1 and P2) are significantly shorter (54 e.s.d.) than that of the phosphine (P3) located *trans* to the silyl moiety, owing to the strong σ-donating properties of the silyl atom. The Rh1–Si1 bond length of 2.2610(7) Å in **5.5** is consistent with Whited's [Rh{SiCl($NCH_2P^tBu_2$)$_2C_6H_4$-1,2}(CO)] (*cf.* 2.2696(12) Å), and comparable to the d^6-octahedral analogues [RhHCl{SiPh(NCH_2PPh_2)$_2C_6H_4$-1,2}(PPh_3)] 2.3177(11) Å and [RhH(S_2CNEt_2){SiPh(NCH_2PPh_2)$_2C_6H_4$-1,2}] 2.2796(4) Å.[10,11]

The ^{29}Si nucleus of complex **5.5** was observed at 117.6 ppm as a doublet of doublet of triplets, representing the coupling of the ^{29}Si nucleus to rhodium ($^1J_{SiRh}$ = 31.1) and the two phosphines ($^2J_{SiP\ (PPh3)}$ = 104.2, $^2J_{SiP\ (PPh2)}$ = 24.5 Hz).

The synthesis of [Rh{SiCl(NCH_2PPh_2)$_2$-C_6H_4-1,2}(PPh_3)] **5.5a**, the silyl chloro analogue of **5.5**, was pursued through direct reaction of ^{Ph}PNNP(SiHCl) with [RhH(PPh_3)$_4$] (Scheme 5.11). Within one hour, the anticipated product was observed by the characteristic phosphine resonances at δ_P = 61.1 (dd, $^2J_{PRh\ (PPh3)}$ = 165, $^2J_{PP}$ = 26 Hz) and 27.2 (dt, $^2J_{PRh\ (PPh2)}$ = 136, $^2J_{PP}$ = 26 Hz) in the ^{31}P{^{1}H} NMR spectrum. The coupling constants were comparatively similar in magnitude to those of **5.5** ($^2J_{PRh\ (PPh3)}$ = 177, $^2J_{PRh\ (PPh2)}$ = 133, $^2J_{PP}$ = 21 Hz). Additionally, the two methylene proton environments of dt^v multiplicity were detected at δ_P = 3.80 ($^2J_{HH}$ = 12.6, $^2J_{HP}$ = 4.0 Hz) and 3.94 ($^2J_{HH}$ = 12.6, $^2J_{HP}$ = 2.2 Hz). Resonances corresponding to traces of **5.4** were observed in the crude

sample and increased, following work-up, to a 1:1 ratio of **5.5a** and **5.4**. The ESI(+) mass spectrum showed peaks consistent with **5.4**, whilst **5.5a** was not found.

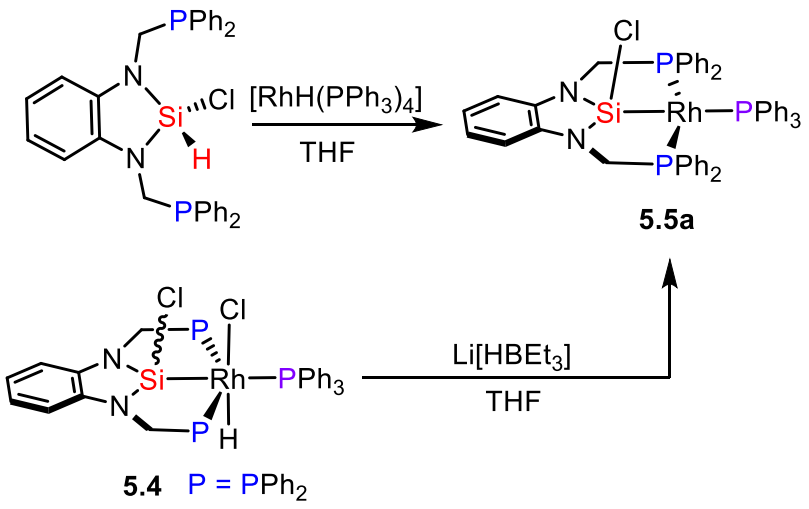

Scheme 5.11: Attempted synthesis of complex **5.5a** through two preparative routes.

Approaching the synthesis of **5.5a** through a dehydrohalogenative pathway from **5.4** and Li[HBEt$_3$] resulted in incomplete (50%) conversion and decomposition under longer reaction times (seven hours). This result is consistent with the dehydrohalogenation outcomes of partial conversion in the investigations on the preparation of **5.5**.

5.4.3 Reaction of [Rh{SiPh(NCH$_2$PPh$_2$)$_2$C$_6$H$_4$-1,2}(PPh$_3$)] with H$_2$

Three mechanistic pathways are possible for the formation of **5.5**, including a) oxidative addition/reductive elimination, b) σ-metathesis, and c) σ-complex assisted metathesis (σ-CAM) (Scheme 5.12).[40] The first involves Si–H activation of ^{Ph}PNNP(SiHPh) by [RhH(PPh$_3$)$_4$], followed by subsequent reductive elimination of dihydrogen. Alternatively, σ-metathesis of Rh–H and Si–H might proceed through a four-membered transition state, whilst the σ-CAM pathway involves discrete σ complexes as intermediates. A point of contrast between the oxidative addition/reductive elimination pathway (a) and that of metathesis (b and c) is the change in oxidation state, which varies by ±II in a) and remains constant in pathways b) and c).

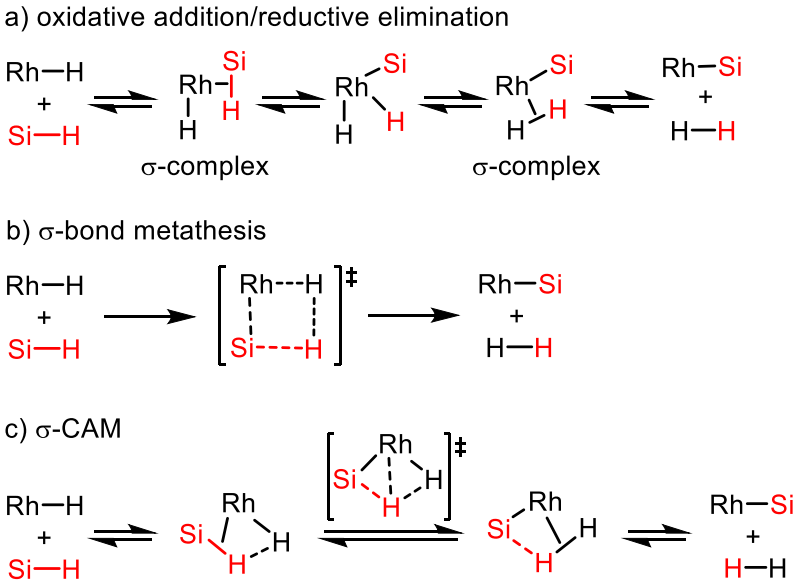

Scheme 5.12: Mechanistic pathways for conversion of Rh–H to Rh–Si (modified from a review by Perutz and Sabo-Etienne).[40] Here Rh–H and Si–H represent [RhH(PPh$_3$)$_4$] and ^{Ph}PNNP(SiHPh) respectively.

For the mechanism to proceed through pathway a), the generation of a vacant coordination site from 18 VE [RhH(PPh$_3$)$_4$] is required, which is likely to proceed through dissociation of PPh$_3$ given that [RhH(PPh$_3$)$_4$] exists in equilibrium with the tris(triphenylphosphino) analogue [RhH(PPh$_3$)$_3$].[41] Alternatively, pathways b) and c) might be possible with the coordinatively saturated [RhH(PPh$_3$)$_4$]. The dihydride species [RhH$_2${SiPh(NCH$_2$PPh$_2$)$_2$C$_6$H$_4$-1,2}(PPh$_3$)] was not observed as an intermediate in the reaction and thus the behaviour of **5.5** in a dihydrogen atmosphere was investigated.

Dihydrogen was bubbled into an NMR tube containing a solution of **5.5** in d$_8$-toluene. Broad resonances were observed in the ^{1}H and ^{31}P{^{1}H} NMR spectra obtained at 25°C, which were suggestive of an exchange process. A variable temperature NMR study was undertaken from –80°C to +80°C (Figure 5.10). In the low temperature range (–80 to –23°C, Figure 5.10) the presence of two hydride containing complexes at a ratio of 1:19 was observed. A minor product was observed as broad hydride multiplets at δ_H = –6.94 and –8.14 and the major product was located at δ_H = –8.71 and –8.89. The splitting pattern in all resonances was not well resolved and occluded accurate determination of the coupling constants. The resonances are broadened in the temperature range –23 –+20°C, whilst no resonances were observed in the hydride region at temperatures above +20°C. As broadening of all resonances takes place simultaneously, either the exchange constants for both complexes are coincidentally the

same or the two products are related by equilibrium. The process was reversible as lowering the temperature again to –60°C returned all hydride resonances in the same ratio as detected previously.

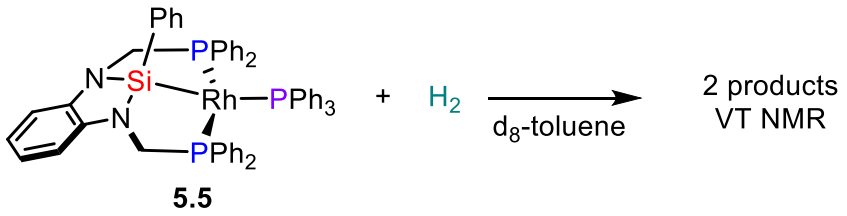

5.5

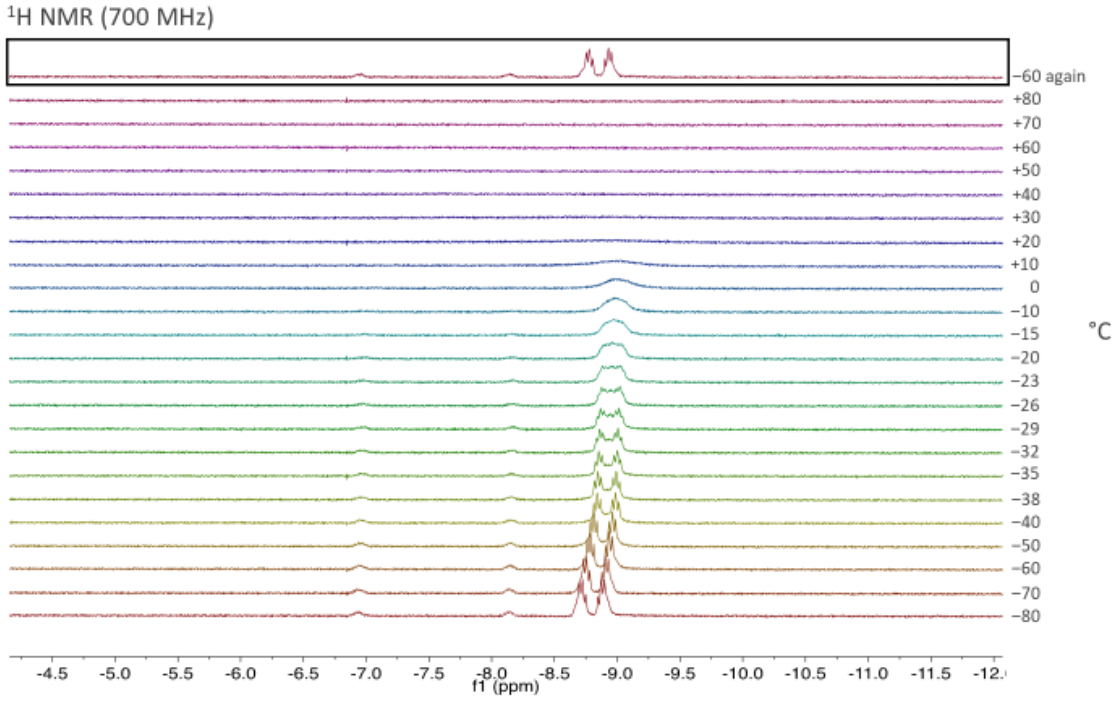

Figure 5.10: Variable Temperature NMR spectra of **5.5** in a dihydrogen atmosphere. ^{1}H (700 MHz) NMR spectroscopy in d_8-toluene. Hydride region shown.

Coordination of hydrogen to **5.5** could occur through two modes, as a dihydride with all terminal M–H bonds (classical) or bound as dihydrogen (non-classical). Hamilton and Crabtree demonstrated that the spin-lattice relaxation time (T_1) between the two modes of coordination differs by several orders of magnitude, with longer T_1 times for classical complexes (300+ ms) than nonclassical complexes (less than 100 ms).[42] Therefore, to determine the coordination mode of the hydrogen to **5.5**, the T_1 parameter was measured through the inversion recovery method. Due to the broadness of the resonances at temperatures above +10°C, experiments were carried out at –80°C for better resolution. At –80°C the T_1 value of the major product was determined as 2.378 seconds. The large T_1 value indicates dihydride coordination and the complex is

postulated as $[Rh(H)_2\{SiPh(NCH_2PPh_2)_2C_6H_4\text{-}1,2\}(PPh_3)]$ **5.6** rather than the dihydrogen σ-complex $[Rh(H_2)\{SiPh(NCH_2PPh_2)_2C_6H_4\text{-}1,2\}(PPh_3)]$. Although only a small amount of the minor product was present in the sample, the T_1 value was determined as 4.198 seconds (–80°C), fitting a classical dihydride coordination model.

The $^{31}P\{^1H\}$ NMR data are consistent with the identification of two products (Figure 5.11). At –80°C the minor product was detected at 72.5 (dd, $^1J_{PRh}$ = 114, $^2J_{PP}$ = 25 Hz) and 39.4 ppm (dt, $^1J_{PRh}$ = 90, $^2J_{PP}$ = 23 Hz), and the major product at 98.2 (dd, $^1J_{PRh}$ = 99, $^2J_{PP}$ = 21 Hz) and 37.3 (dt, $^1J_{PRh}$ = 94, $^2J_{PP}$ = 21 Hz). The $^1J_{PRh}$ coupling constants for $^{31}PPh_2$–^{103}Rh are of a similar value to the octahedral analogues (109 Hz **5.4** and 113 Hz **5.2**). Broadening was similarly observed with an increase in temperature. From the broad doublet at +80°C, a $^{31}PPh_3$-^{103}Rh coupling constant of 143 Hz was measured, whereas all other coupling could not be discerned. The absence of a resonance corresponding to free triphenylphosphine in the spectra allowed the exclusion of products without a triphenylphosphine co-ligand. Returning the sample to low temperature (–60°C) resulted in the reformation of both products as well as traces of **5.5**.

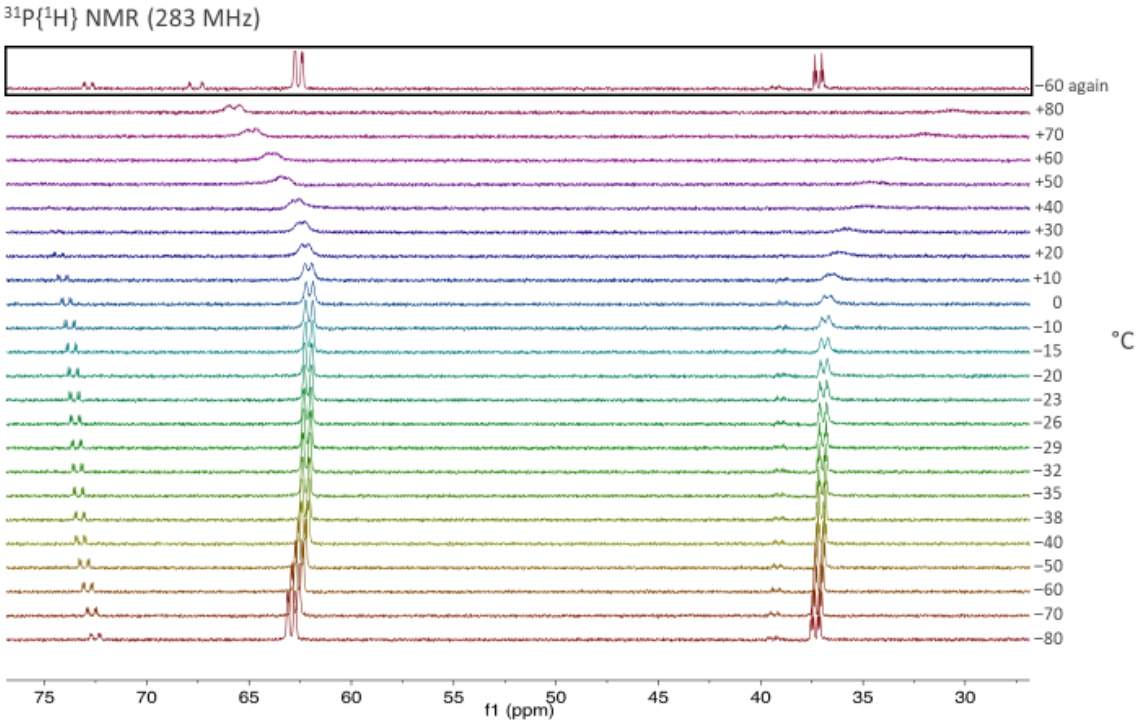

Figure 5.11: Variable Temperature NMR spectra of **5.5** under a dihydrogen atmosphere. $^{31}P\{^1H\}$ (283 MHz) NMR spectroscopy in d_8-toluene.

From the T_1 and the $^{31}P\{^1H\}$ NMR experiments it was inferred that the two products at low temperature (–80°C) are classical dihydride octahedral complexes. The dihydride isomers of **5.6** depicted in Scheme 5.13 are postulated as possible products from the reaction of **5.5** with H_2.

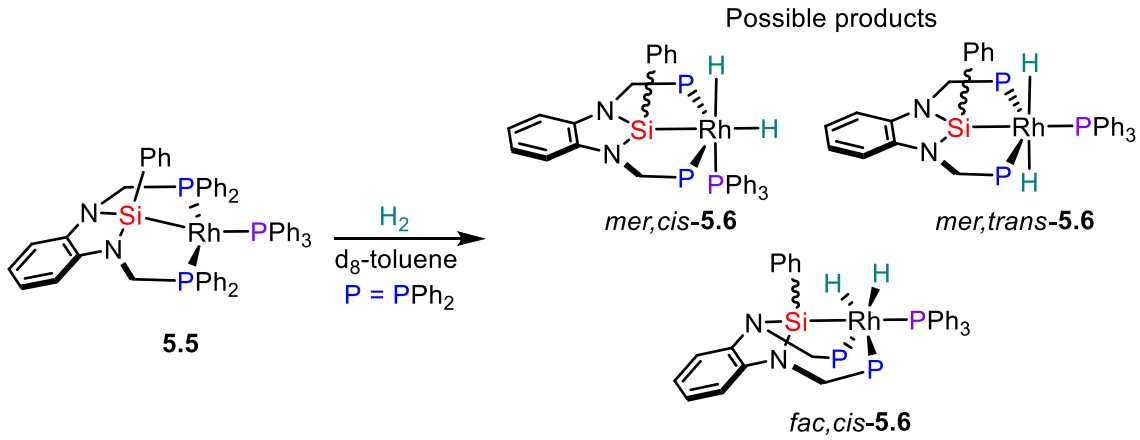

Scheme 5.13: Postulated products from the hydrogenation of **5.5**.

Roddick and co-workers showed the PCP ligand in $[Ir\{(P(CF_3)_2CH_2)_2C_6H_3\text{-}2,6\}(L)]$ ($L = P(C_2F_5)_2Me$, CO) readily fluctuated between *mer* and *fac* geometries upon reversible hydrogen coordination.[43] The resultant dihydride isomers include *mer,trans*, *mer,cis* and *fac,cis*, which was similarly applied to **5.6** in consideration of the products in Scheme 5.13. A *meridionally* coordinated PSiP ligand results in diastereomers where hydrides are located mutually *cis* or *trans* (*mer,cis*-**5.6** and *mer,trans*-**5.6** respectively). Although *facial* coordination of the benzosiladiazole PSiP ligand is uncommon, there are examples of five-coordinate cobalt complexes $[Co\{SiMe(NCH_2PPh_2)_2C_6H_4\text{-}1,2\}(PMe_3)_2]$ and $[CoI\{SiMe(NCH_2PPh_2)_2C_6H_4\text{-}1,2\}(PMe_3)]$ with *fac*-PSiP binding, however those of octahedral geometry have yet to be reported.[16] In addition to variations in the position of the dihydrides and geometric (*fac*/*mer*) factors, further diastereomers are possible depending on the orientation of the silyl phenyl group in each isomer of **5.6** shown in Scheme 5.13.

The hydride coupling constants in **5.6**, even at low temperature (–80°C), remain confounded by coupling to the many nearby nuclei (^{103}Rh, $^{31}PPh_3$, $^{31}PPh_2$, ^1H). The absence of well resolved hydride coupling constants precludes unambiguous assignment of the postulated isomers. Furthermore, attempts to isolate isomers of **5.6** have shown that decomposition occurs in the absence of a hydrogen atmosphere (when the sample was subjected to vacuum). This was noted by significant broadening of

resonances in the ^{1}H and $^{31}P\{^{1}H\}$ NMR spectra, suggesting that the complexes have sufficiently labile hydrogens such that a hydrogen atmosphere is required for their endurance. The reformation of **5.5** was not noted spectroscopically following the exposure of **5.6** to vacuum and instead decomposition was observed.

5.4.4 Synthesis of [Rh{SiPh(NCH$_2$PPh$_2$)$_2$C$_6$H$_4$-1,2}(CO)(PPh$_3$)]

It was envisaged that incorporation of π-acidic co-ligands capable of synergic bonding would alleviate electron density from the electron rich rhodium centre within complex **5.5**, thereby resulting in complexes of easier handling. The reaction of [RhH(CO)(PPh$_3$)$_3$][44] with ^{Ph}PNNP(SiHPh)[10] yielded [Rh{SiPh(NCH$_2$PPh$_2$)$_2$C$_6$H$_4$-1,2}(CO)(PPh$_3$)] **5.7** as the major product among a mixture of (≈ 10) complexes (Scheme 5.14). The mixture resisted purification despite numerous work-up protocols including washing and recrystallisation in various solvent combinations. Stabilisation by π-acceptor carbon monoxide in **5.7** results in a more stable, albeit still air sensitive, complex compared to **5.5**.

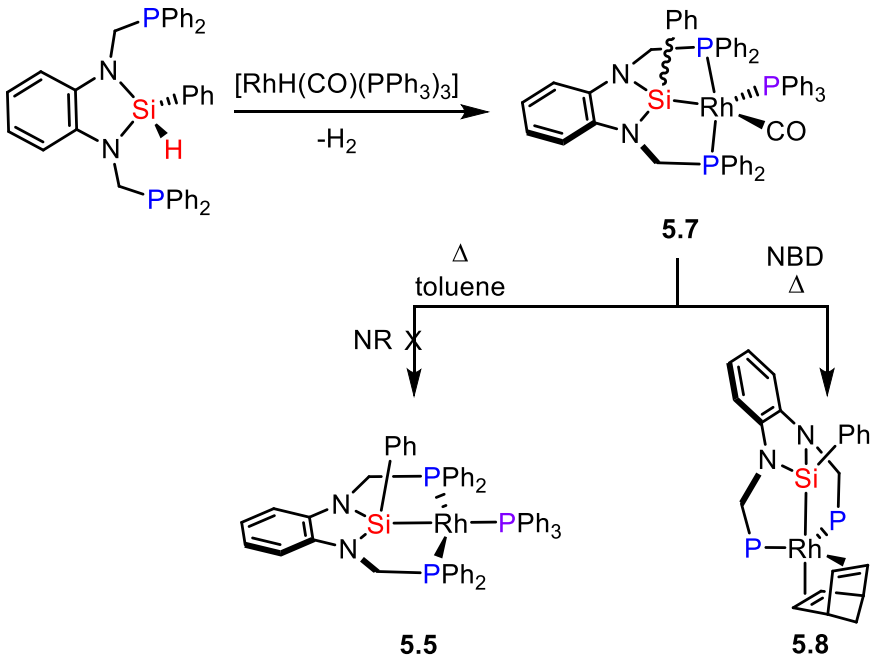

Scheme 5.14: Synthesis of **5.7** and subsequent thermal substitution reactions (NBD = norbornadiene).

Complex **5.7** was subjected to reflux in toluene to assess the lability of the PPh$_3$ or CO ligands, where the latter would lead to formation of **5.5**. This was performed in both a closed system (J-Young NMR tube, d$_8$-toluene, 100°C, five hours) and an open system (Schlenk flask, toluene, reflux, 20 hours). Both experiments returned the starting

material **5.7**, which implies that neither the CO or PPh_3 ligands are labile under thermal conditions and is also indicative of the remarkable thermal stability of the complex.

Although no thermal lability of **5.7** was noted, the CO and PPh_3 ligands can be displaced by norbornadiene (NBD) to afford the complex [Rh{SiPh(NCH_2PPh_2)$_2C_6H_4$-1,2}(C_7H_8)] **5.8**. Thermal reaction conditions (70°C, one hour) are required for the substitution to take place and no reaction was observed at room temperature. The conversion of **5.7** to **5.8** was accompanied by the simplification in the multiplicity of the resonances. The characteristic signals for **5.7** of dt at δ_P = 31.3 and dd at δ_P = 63.9 in the $^{31}P\{^1H\}$ NMR spectrum, converged to a doublet at δ_P = 70.4 ($^1J_{PRh}$ = 151 Hz) consistent with the displacement of PPh_3 to afford **5.8**. A cleaner and more facile preparatory method and characterisation of **5.8** is discussed in Section 5.4.6.

As the reaction of [RhH(CO)(PPh_3)$_3$] and ^{Ph}PNNP(SiHPh) towards the formation of **5.7** yields a mixture of products, alternative synthetic routes were pursued. The potential for square planar complexes to facilitate transformations *via* oxidative addition/reductive elimination processes led to the treatment of **5.5** with excess benzaldehyde in anticipation of the formation of complex **5.7** (Scheme 5.15).

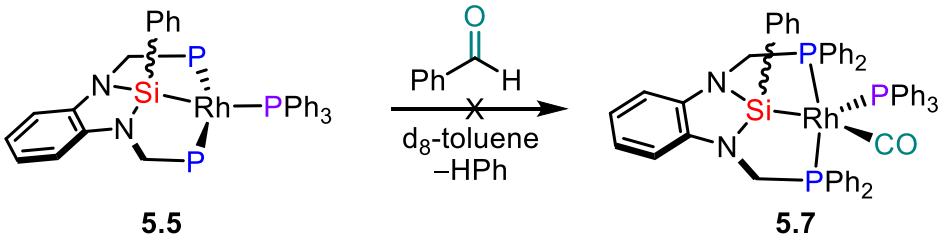

Scheme 5.15: Attempted synthesis of **5.7** through treatment of **5.5** with benzaldehyde.

No reaction was observed in the ^1H and $^{31}P\{^1H\}$ NMR spectra at room temperature. When the sample was subjected to a 15-minute reflux, the solution lightened from orange to yellow and the NMR spectra showed only free triphenylphosphine, suggesting decomposition. While **5.7** is thermally robust, **5.5** is comparatively less thermally stable. This may be a consequence of the ring strain of the biaxial pincer arms, as noted previously in the molecular structure of **5.5**, and a shortage of π-accepting co-ligands to stabilise the electron rich rhodium centre. Had the conversion of benzaldehyde been successful, liberated benzene would be anticipated as a by-product. Unfortunately, the abundance of aromatic proton resonances from the number of aromatic environments of **5.5** confounded identification of liberated benzene.

Since the introduction of CO to **5.5** using benzaldehyde was unsuccessful, direct treatment of **5.5** with CO was explored as a synthetic pathway to **5.7** (Scheme 5.16).

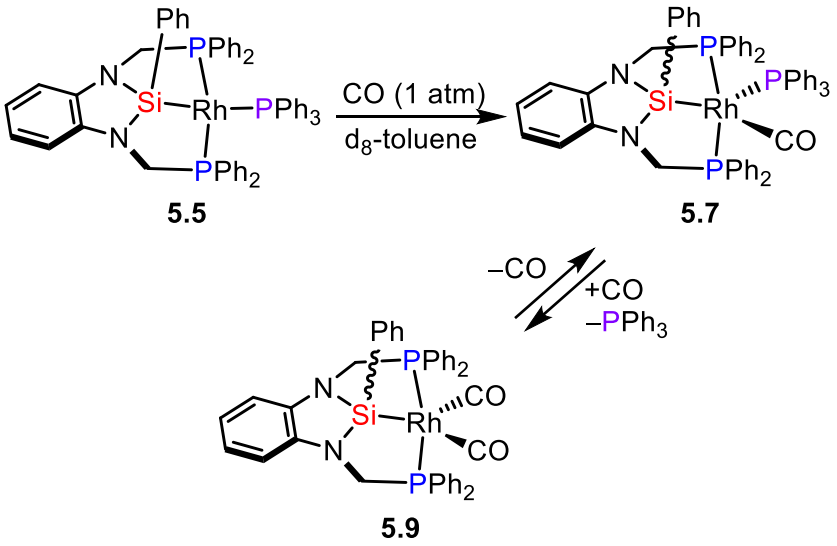

Scheme 5.16: Reactivity of **5.5** under an atmosphere of CO.

Carbon monoxide was bubbled through a solution of **5.5** in d_8-toluene for 5 minutes. The reaction was monitored by NMR spectroscopy and showed the presence of complex **5.7** as 10% of the sample (from ^{1}H NMR integration). The major product was identified as the dicarbonyl complex [Rh{SiPh(NCH$_2$PPh$_2$)$_2$C$_6$H$_4$-1,2}(CO)$_2$] **5.9**. Attempts to isolate [Rh{SiPh(NCH$_2$PPh$_2$)$_2$C$_6$H$_4$-1,2}(CO)$_2$] by solvent removal under Schlenk conditions led to the reformation of **5.7** (but not **5.5**) from re-coordination of the previously liberated triphenylphosphine present in the crude mixture (Scheme 5.16). The lability of the second carbonyl is consistent with Stobart's [RuCl{SiMe((CH$_2$)$_3$PPh$_2$)$_2$}(CO)$_2$] (*trans* CO) that decarbonylates under toluene reflux to the monocarbonyl analogue.[45] However, the analogous complex [RuH{SiMe((CH$_2$)$_3$PPh$_2$)$_2$}(CO)$_2$] (*cis* CO) was resistant to decarbonylation.[46] Additionally, examples of isolable dicarbonyl silyl pincer complexes are known in literature.[11,20] The *in situ* formation and characterisation of **5.9** is discussed in the next section.

The re-coordination of PPh$_3$ to **5.9** presents as a potential route to **5.7**. The synthesis of **5.7** was achieved in a one-pot reaction that involved generation of **5.5** *in situ* from ^{Ph}PNNP(SiHPh) and [RhH(PPh$_3$)$_4$], followed by treatment with CO to form **5.9**. The reaction mixture was subsequently subjected to vacuum to promote re-coordination of PPh$_3$ affording **5.7** in 65% yield (Scheme 5.17). The formulation of **5.7** was supported by NMR and IR spectroscopy and mass spectrometry.

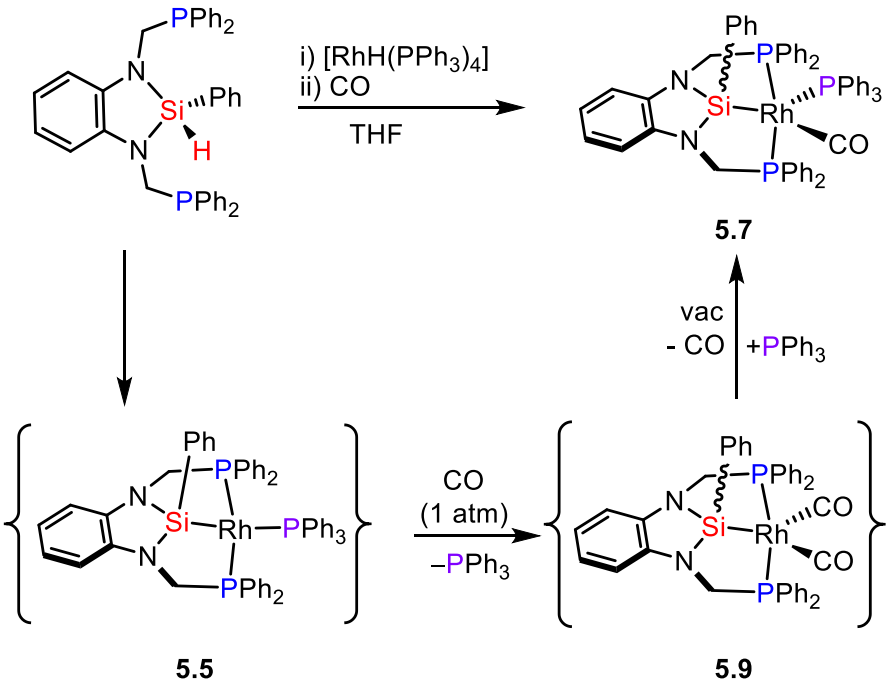

Scheme 5.17: Synthetic route to **5.7** *via in situ* generation of **5.5** and **5.9**.

The phenomenon of virtual coupling noted in the complexes discussed thus far was also observed in the ^{1}H NMR spectrum of **5.7**. One of the diastereotopic methylene proton environments was observed at δ_H = 4.47 as a doublet ($^{2}J_{HH}$ = 12.6 Hz), whereas the other was a doublet of virtual triplets at δ_H = 3.55 ($^{2}J_{HH}$ = 4.0, $^{2}J_{HP\ (PPh2)}$ = 13.2 Hz). The presence of virtual coupling suggested that the silyl ligand in complex **5.7** remains *mer* coordinated. In contrast, analogous reactions performed by Nakazawa with HMeSi($C_6H_4PPh_2$-2)$_2$ and MeRSi($C_6H_4PPh_2$-2)$_2$ (R = H, Et, aryl) showed *fac* coordination in all cases.[12] This difference in coordination mode is attributed to the geometric allowances of the more flexible MeSi($C_6H_4PPh_2$-2)$_2$ ligand compared to the rigid PhSi(NCH_2PPh_2)$_2C_6H_4$-1,2 framework.

Two phosphine environments were detected in the $^{31}P\{^{1}H\}$ NMR spectrum of **5.7**, with splitting patterns consistent with the *trans*-disposed phosphines of the pincer scaffold (dd) and the triphenylphosphine co-ligand (dt). Complexes **5.2** and **5.5** show similar multiplicity to **5.7** with both phosphines exhibiting coupling to rhodium and each other. However, the magnitude of $^{1}J_{PRh}$ for the PPh_2 and PPh_3 environments increase with decreasing coordination number from **5.2**, **5.7** to **5.5** (Figure 5.12). This effect is attributed to the proportion of s-character, as s-orbitals have finite electron density at the nucleus and make a large contribution to internuclear coupling. The complexes of decreasing coordination number **5.2**, **5.7** and **5.5** have the respective hybridisation and

increase in % s-character: sp^3d^2 (17%), sp^3d (20%), sp^2d (25%). Therefore, the six coordinate **5.2** has a remarkably smaller $^1J_{PRh}$ coupling constant than that of the five coordinate **5.7** and four coordinate **5.5**.

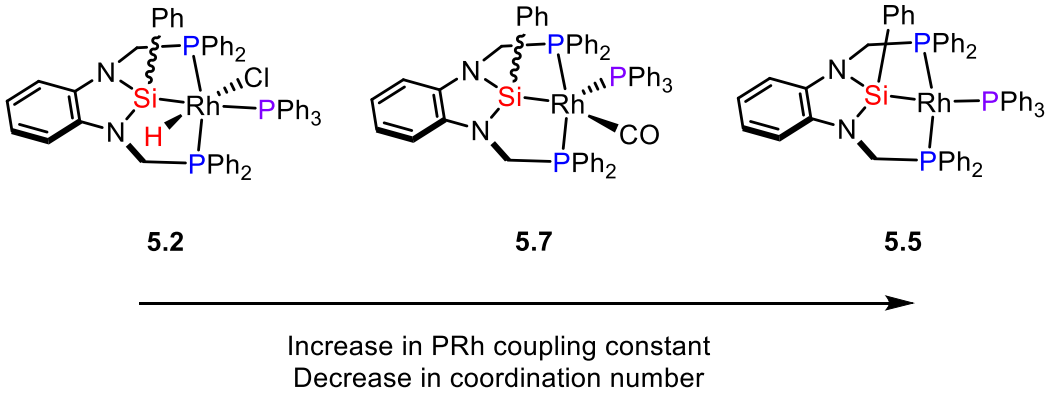

	dd (PPh_2)			dt (PPh_3)		
Complex	δ_P (ppm)	$^1J_{PRh}$	$^2J_{PP}$	δ_P (ppm)	$^1J_{PRh}$	$^2J_{PP}$
5.2	54.0	113	22	14.2	84	22
5.7	63.9	147	38	31.3	91	38
5.5	68.6	177	21	27.5	133	21

Figure 5.12: Comparison of the ^{31}P-^{103}Rh coupling constant value between complexes **5.2**, **5.7** and **5.5.**

5.4.5 *In situ* Synthesis and Characterisation of [Rh{SiPh(NCH$_2$PPh$_2$)$_2$C$_6$H$_4$-1,2}(CO)$_2$]

Whilst the isolation of complex **5.9** was precluded by the lability of the second CO ligand, the complex was characterised spectroscopically *in situ*, along with the triphenylphosphine by-product that was liberated during the reaction. Carbon monoxide was bubbled through a solution of **5.5** in C_6D_6, resulting in a colour change from orange to yellow-brown (Scheme 5.18).

Displacement of the PPh_3 co-ligand in **5.5** by CO afforded a simpler ^{29}Si resonance as an overlapping doublet of triplet at δ_{Si} = 102.3 (Figure 5.13), consistent with comparable coupling to rhodium and PPh_2 ($^1J_{SiRh}$ = 19.5 and $^2J_{SiP}$ = 19.6 Hz). The $^{31}P\{^1H\}$ NMR spectrum showed that the characteristic dd and dt coupling pattern of the starting material had evolved into a clean doublet at δ_P = 82.2 ($^1J_{PRh}$ = 145) and free PPh_3 (δ_P = –5.3).

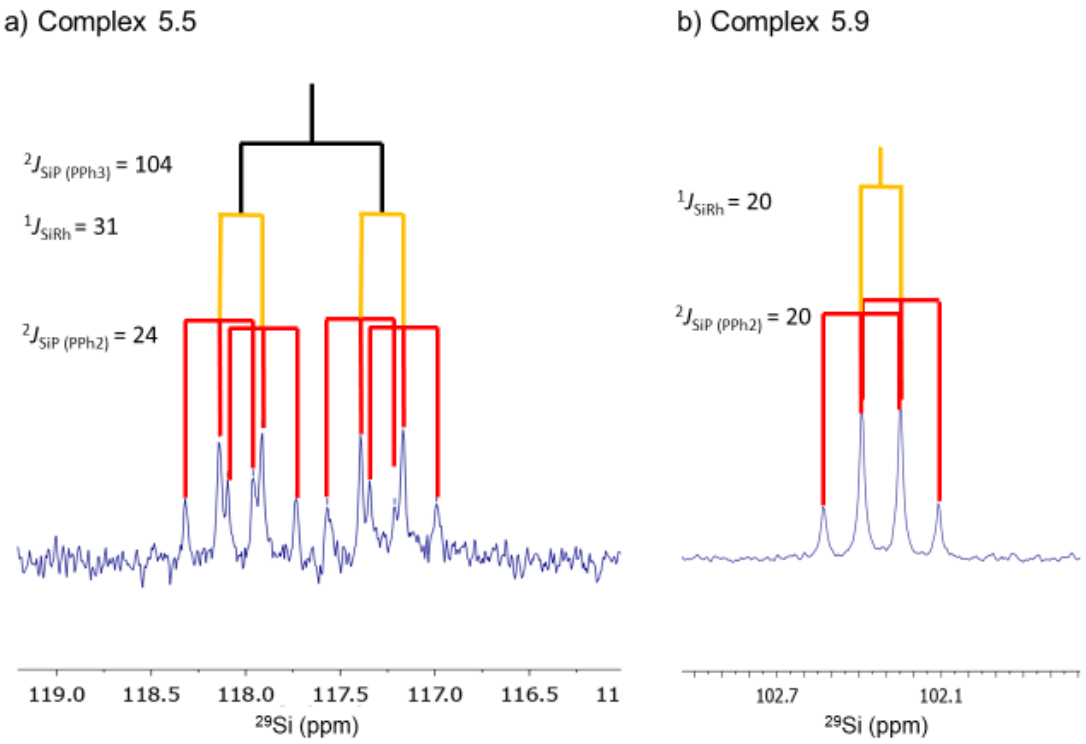

Figure 5.13: Simplification of the ^{29}Si resonance in the ^{29}Si NMR spectrum of a) **5.5** compared to b) **5.9** on ligand exchange with CO (coupling constants given in Hz).

The formulation of **5.9** was supported by two ν_{CO} stretching bands at 2018 and 1971 cm^{-1} in the THF solution IR spectrum. The ratio of the intensities of the ν_{sym} and ν_{asym} stretching modes was used to calculate the inter-carbonyl (OC–Rh–CO) angle, which was derived as 92° and suggests a *cis* relationship between the two carbonyls in **5.9**.[*47] Therefore, complex **5.9** was postulated to be in trigonal bipyramidal geometry (Scheme 5.18). The two carbonyls were also observed in the $^{13}C\{^1H\}$ spectrum at 198.5 ($^1J_{CRh}$ = 70.5, $^2J_{CP}$ = 30.8 Hz) and 201.4 ($^1J_{CRh}$ = 49.0, $^2J_{CP}$ = 14.9 Hz), with doublet coupling to rhodium and triplet coupling to the diphenylphosphino groups.

One potential way to isolate complex **5.9** without subjection to vacuum is through crystallisation. However, slow diffusion of *n*-pentane into a concentrated solution of **5.9** in benzene instead afforded the dimeric oxo-bridged complex **5.9x** (Figure 5.14), which shows the insertion of oxygen into the Rh–Si bond.

[*] The ratio of the two band intensities $\frac{I(sym)}{I(asym)}$, from the absorbance values (I_{sym} = 0.34 and I_{asym} = 0.37) in the IR spectrum of complex **5.9**, was calculated to be 0.92. This ratio was inputted into the following formula[47] to obtain the inter-carbonyl angle of 92°.

$$2\theta = 2\sqrt{arc\ cotan\ 0.92} = 92°$$

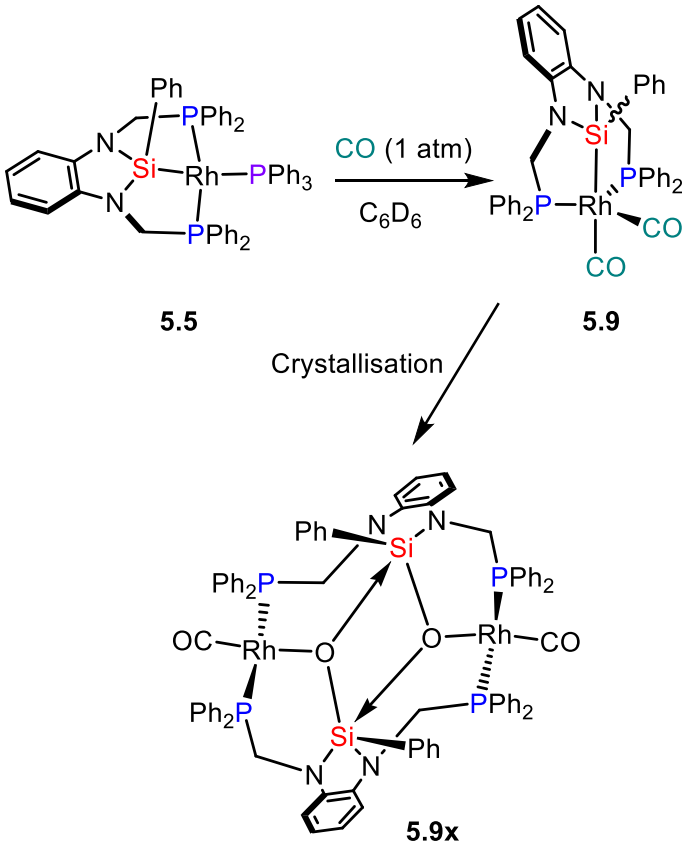

Scheme 5.18: Formation of **5.9** *in situ* in C_6D_6.

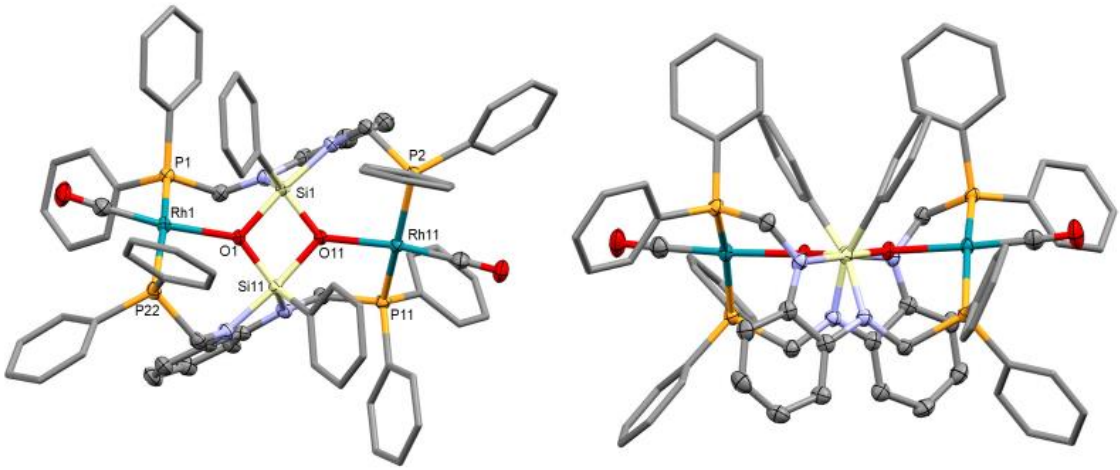

Figure 5.14: Molecular structure of **5.9x** (hydrogen atoms omitted, phenyl groups simplified, displacement ellipsoids shown at 50% probability). Selected bond lengths (Å) and angles (°): Rh1–O1 2.1029(15), Rh11–O11 2.0974(15), Si1–O1 1.8411(16), Si1–O11 1.6986(16), Si11–O1 1.6955(16), Si11–O11 1.8220(16), Rh1–P1 2.2866(6), Rh1–P22 2.3182(5), Rh11–P11 2.3057(6), Rh11–P2 2.3139(6), P1–Rh1–P22 163.52(2), P2–Rh11–P11 163.70(2), Rh1–O1–Si1 126.15(8), Rh1–O1–Si11 133.34(8), Rh11–O11–Si1 135.85(9), Rh11–O11–Si11 123.11(8), O1–S1–O11 78.75(7), O1–S11–O11 79.37(7).

The tetrameric [Si_2O_2] core is parallelogram shaped with two formal Si–O bonds (Si1–O11 1.6986(16) and Si11–O1 1.6955(16) Å) and two longer dative Si–O bonds (Si1–O1 1.8411(16) and Si11–O11 1.8220(16) Å). There are numerous examples in the literature of silane or silyl oxidation from adventitious water or oxygen. Comparative examples within pincer frameworks include silanoates in ruthenium and binuclear platinum complexes (Figure 5.15).[48,49] Mass spectrometry provided further support for the oxo-bridged species as the monomer of **5.9x** was detected at 755.0919 as $[M+2H]^{++}$.

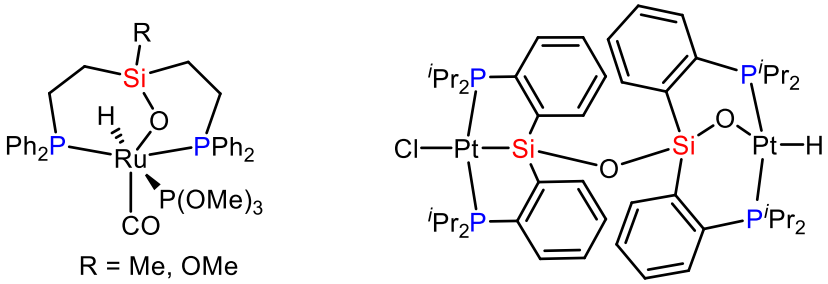

Figure 5.15: Examples of silanoate complexes (Si–O–M).

The molecular structure of **5.9x** shows square planar geometry about rhodium and trapping of oxygen. Thus, the synthesis of **5.9x** was explored by bubbling air through a solution of **5.9**, which was accompanied by a colour change from yellow to green within minutes. The decomposition of the complex was confirmed through NMR spectroscopy with triphenylphosphine oxide as the only detectable product.

5.4.6 Synthesis of [Rh{SiPh(NCH_2PPh_2)$_2C_6H_4$-1,2}(C_7H_8)]

Complex [Rh{SiPh(NCH_2PPh_2)$_2C_6H_4$-1,2}(C_7H_8)] **5.8** was previously identified in Section 5.4.4 from the reaction of **5.7** with NBD. A cleaner route to **5.8** includes the facile reaction between **5.5** and NBD. Although an isolated sample of **5.5** can be used in the reaction with NBD, it is not necessary as **5.5** can be generated and subsequently used *in situ* (as illustrated in the synthesis of carbonyl complex **5.7**, Section 5.4.4). This one-pot preparative methodology presents as a convenient method to access **5.5** without prior isolation and delicate air free work-up. Furthermore, the yield is not compromised from a one-pot procedure compared to the direct reaction pathway to **5.5** (with an isolated yield of 55%).

The formation of **5.5** *in situ* and subsequent addition of five equivalents of NBD afforded **5.8** in 63% yield (Scheme 5.19). The strong *trans*-labilising effect of the silyl moiety in **5.5** was evidenced by the facile substitution of the PPh_3 co-ligand (located *trans* to Si) with

NBD, which occurs readily at room temperature and reaches completion within 1.5 hours. In contrast, the preparation of **5.8** from carbonyl complex **5.7** (Section 5.4.4), required toluene reflux and implies that conversion of **5.7** to **5.8** is slower (kinetically less favourable) than of **5.5** to **5.8**. The substitution of both CO and PPh_3 ligands in **5.7** is expectedly less favourable than the displacement of the PPh_3 in **5.5** with NBD. This is especially so, as the bidentate olefins would be expected to confer more stability to the rhodium through chelation and π-stabilising properties than the single PPh_3 ligand of **5.5**.

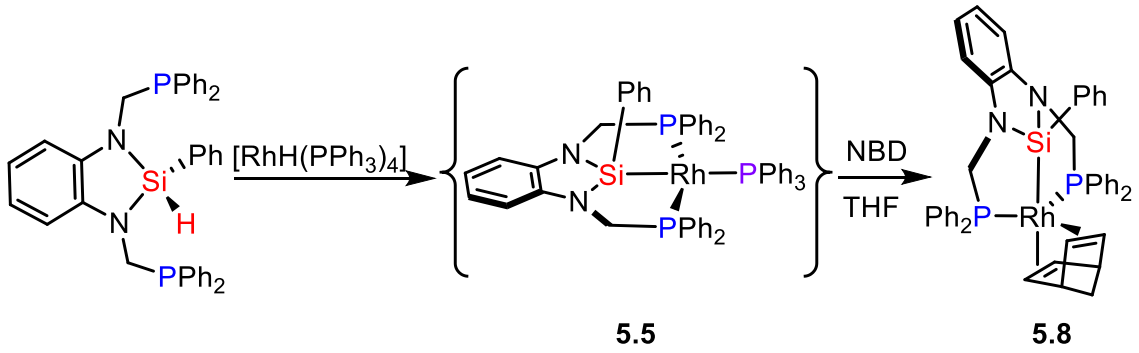

5.5 **5.8**

Scheme 5.19: *In situ* formation of **5.5** and reaction with norbornadiene to form **5.8**.

The formulation of **5.8** was confirmed by X-ray diffraction analysis (Figure 5.16). The molecular structure of **5.8** in Figure 5.16b features a trigonal bipyramidal arrangement with the angles of the equatorial ligands P1, P2 and C90/C91 summing to 360°. The Si1 and C93/C94 groups are the axial ligands.

The axial Rh1–C93/C94 bonds are significantly longer (80 e.s.d.) than the equatorial Rh1–C91/C90 bonds (average lengths 2.3478 *cf.* 2.1965 Å, respectively). This is to be expected given the greater amount of space available in the equatorial plane than in the axial position (≈120° between equatorial ligands *cf.* ≈90° between axial ligands to the equatorial plane). With all else equal, equatorial sites are preferred by sterically bulky ligands in a trigonal bipyramidal complex. An additional contribution to the elongated axial bond Rh1–C93/C94 might be considered as the strong *trans* influence of the σ-silyl donor, since it is anticipated that the silyl moiety would, to a first approximation, occupy more of the shared metal orbital than the corresponding *trans* ligand. The phenomenon is manifest as an elongation of the Rh1–C93/94 bonds that are located *trans* to the silyl, and consequently the reduced interaction between rhodium and the olefin leads to

stronger C=C (C93=C94) bonding. This is observed as a slightly shorter C=C bond in C93–C94 compared to C91–C90 (1.375 *cf.* 1.407 Å, 11 e.s.d.).

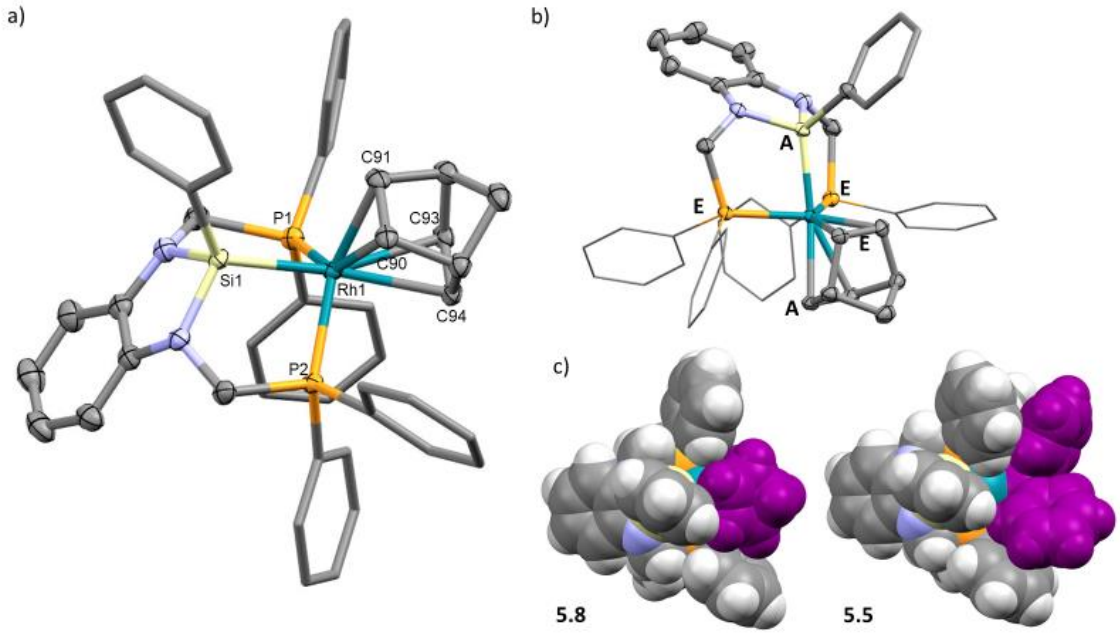

Figure 5.16: a) Molecular structure of [Rh{SiPh(NCH$_2$PPh$_2$)$_2$C$_6$H$_4$-1,2}(C$_7$H$_8$)] **5.8**.0.5(C$_6$H$_{14}$) (solvent omitted, hydrogen atoms omitted, phenyl groups simplified, displacement ellipsoids shown at 50% probability) Selected bond lengths (Å) and angles (°): Rh1–Si1 2.2826(5), Rh1–P1 2.3173(5), Rh1–P2 2.3266(5), Rh1–C90 2.1929(19), Rh1–C91 2.2000(19), Rh1–C93 2.3476(19), Rh1–C94 2.3479(19), C90–C91 1.407(3), C93–C94 1.375(3), P1–Rh1–P2 117.935(17), Si1–Rh1–C90 146.22(6), Si1–Rh1–C91 102.07(5), Si1–Rh1–C93 157.85(5), Si1–Rh1–C94 163.39(5). b) Emphasis on the trigonal bipyramidal geometry of **5.8**, A = axial and E = equatorial. c) Space-filling diagram comparison between **5.8** and **5.5** (NBD and PPh$_3$ in purple).

Complex **5.8** exhibited greater solid-state stability towards air than **5.5**, which is rationalised by the NBD ligand providing more steric shielding at the coordinatively saturated rhodium centre in **5.8** than the PPh$_3$ ligand in coordinatively unsaturated 16 VE **5.5**. The space filling diagrams in Figure 5.16c illustrate the contrasting exposure of the rhodium (green) centre. Furthermore, the molecular structure of **5.8** (Figure 5.16b) shows facial coordination of the silyl ligand. The angle subtended by the pincer phosphine donors (P1–Rh1–P2) in **5.8** of 117.935(17)° is close to the angle expected for equatorial ligands in trigonal bipyramidal geometry (120°), whereas the P–Rh–P angle in **5.5** is comparatively strained (142.66(2)°) and deviates from the angle expected for meridional ligands in square planar geometry (180°).

The related complexes [Rh{Si(OTf)((C$_6$H$_4$)PR$_2$)$_2$}(NBD)] (R = Ph, Cy) are similarly trigonal bipyramidal and *fac* coordinating with comparable P–Rh–P angles of 119.4° (Ph) and 122.8° (Cy).[50] However, for the benzosiladiazole scaffold, Sun's five-coordinate [Co{SiMe(NCH$_2$PPh$_2$)$_2$C$_6$H$_4$-1,2}(PMe$_3$)$_2$] and [CoI{SiMe(NCH$_2$PPh$_2$)$_2$C$_6$H$_4$-1,2}(PMe$_3$)] are the only other examples of *fac* coordinated PSiP with P–Co–P angles of 122.67(2) and 110.19(4)°, respectively.[16] The other complexes of this ligand system (on Fe, Co, Ru, Rh) adopt meridional coordination in preference, with the P–M–P angle spanning a range of 147.87–156.07(2)°.[10,11,16]

The departure from *trans*-disposed phosphine pincer arms was evidenced by the absence of virtual coupling in ^{1}H and ^{13}C{^{1}H} NMR spectroscopy. The virtual triplet coupling (dt^v) exhibited by the diastereotopic methylene protons of **5.5** was not observed in the ^{1}H NMR spectrum of **5.8**. Instead, the protons resonated as distinct doublet of doublets at δ_H = 4.20 and δ_H = 4.31 from the geminal coupling ($^2J_{HH}$ = 13.3 Hz) between the diastereotopic methylene proton environments and from ^{1}H-^{31}P coupling in each proton environment (determined as $^2J_{HP}$ = 7.0 and $^2J_{HP}$ = 4.9 Hz, respectively).

In addition, the appearance of the methylene carbon as a doublet at 60.9 ppm ($^1J_{CP}$ = 22.4 Hz) in the ^{13}C{^{1}H} NMR spectrum further demonstrated the absence of virtual coupling. The Si nucleus exhibited coupling to rhodium and phosphorus in the ^{29}Si{^{1}H} NMR spectrum, which appeared as a doublet of triplets at δ_{Si} = 95.2 (dt, $^1J_{SiRh}$ = 37.9, $^2J_{SiP}$ = 22.7 Hz). The ^{31}P{^{1}H} NMR spectrum comprised a simple doublet at δ_P = 70.4 with coupling to rhodium ($^1J_{PRh}$ = 151 Hz). The coupling constant is similar in magnitude to that of the five-coordinate complex **5.7** ($^1J_{PRh}$ = 147 Hz).

5.4.7 Reactivity of [Rh{SiPh(NCH$_2$PPh$_2$)$_2$C$_6$H$_4$-1,2}(PPh$_3$)] with R–C≡C–C≡C–R (R = Ph, SiMe$_3$)

The versatile reactivity of R-C≡C-C≡C-R (R = aryl) towards metal precursors has been widely investigated. In rhodium chemistry (Figure 5.17), Marder has demonstrated the participation of Ar-C≡C-C≡C-Ar (Ar = C$_6$H$_5$CF$_3$) in a versatile range of reactions including simple π-coordination to one (**I**) or two (**II**) rhodium centres or as a bridging ligand (**III**).[51] In addition, rhodacyclopentadiene complexes (**IV**) can be generated from the reductive coupling of two molecules of R-C≡C-C≡C-R.[52,53] If a hydrido-rhodium precursor is used then enynyl transition metal complexes are accessible (**V**) *via* alkyne hydrorhodation.[54]

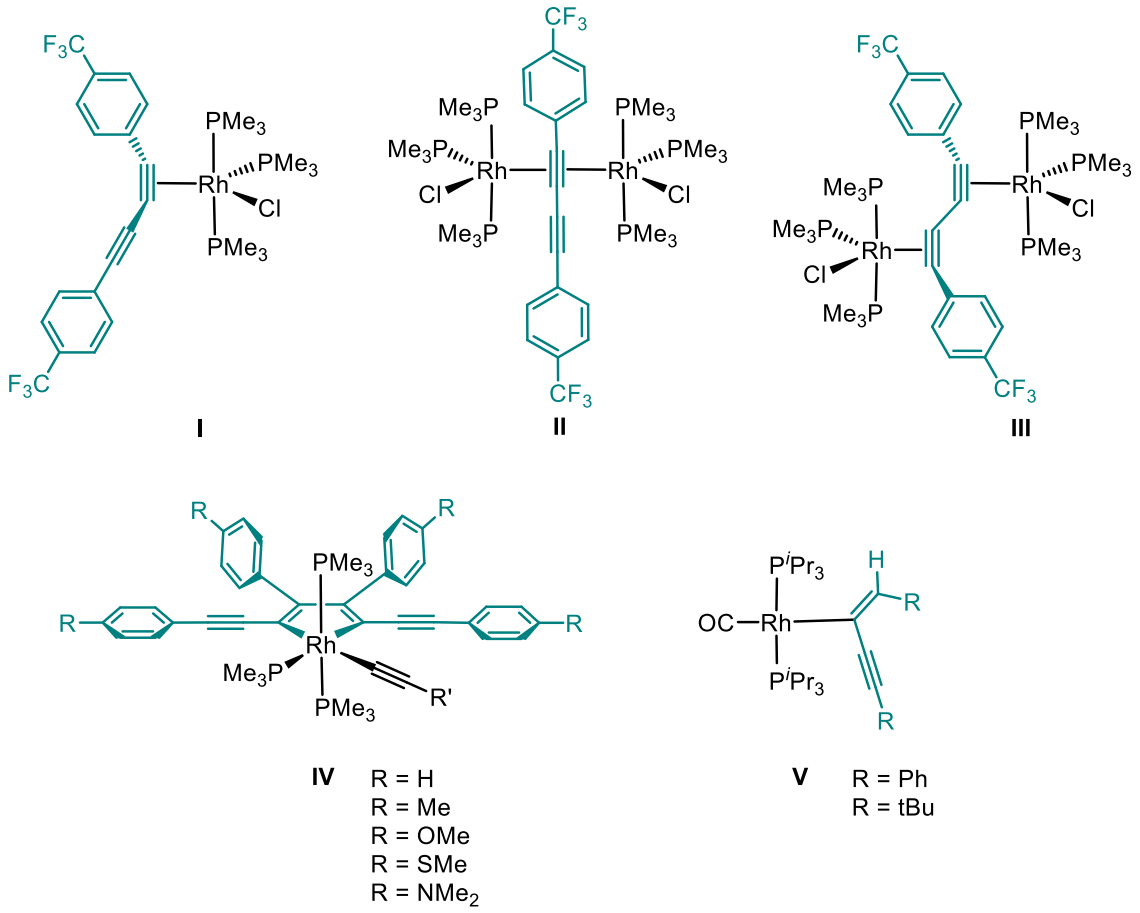

Figure 5.17: Products of coordination of R-C≡C-C≡C-R to rhodium precursors.

Given the formation of complexes **5.8** and **5.9** from the substitution of PPh_3 in **5.5**, it was envisaged that reductive coupling of Ph-C≡C-C≡C-Ph and concurrent displacement of the PPh_3 ligand might allow rhodacyclopentadiene formation. A facile reaction ensued between **5.5** and two equivalents of Ph-C≡C-C≡C-Ph, which was accompanied by an instantaneous colour change of the solution from orange to deep red.

The new product resonances observed at δ_P = 68.6 (dd) and 36.2 (dt) had splitting patterns consistent with the retention of both PPh_2 and PPh_3 environments at the rhodium. The magnitude of the ^{31}P-^{103}Rh coupling constants measured in the two environments were $^1J_{PRh}$ = 180 and 131 Hz, respectively. The values resemble those of **5.5** ($^1J_{PRh}$ = 177 and 133 Hz) and thus a four-coordinate geometry at rhodium was postulated.

The methylene proton resonances of **5.5** were shifted downfield to δ_H = 4.84 and 5.21 (d, $^2J_{HH}$ = 14.7 Hz), which show the loss of strong coupling between the two PPh_2 arms by the absence of virtual coupling. A distinct change of the Si environment was noted by the doublet at δ_{Si} = –16.0 with a ^{29}Si-^{103}Rh coupling constant of 4.2 Hz.

The simplicity of the ^{29}Si resonance and smaller magnitude of ^{29}Si-^{103}Rh coupling compared to the starting material (31 Hz **5.5**) and the other complexes in this chapter (20 Hz **5.9**, 38 Hz **5.8**) implies that the direct Si–Rh interaction has been replaced by a more distant communication between Si and Rh. This is further substantiated by the chemical shift of δ_{Si} = –16.0, which is in a similar region to that of the free ligand (δ_{Si} = –12.4, ^{Ph}PNNP(SiHPh)) and far upfield than those coordinated to rhodium synthesised in this work (δ_{Si} = 95.2–120.6).

Based on the collective NMR spectroscopic data, the product was formulated as [Rh{SiPh(NCH$_2$PPh$_2$)$_2$C$_6$H$_4$-1,2}(μ^2-*Si,Rh*-Ph-C=C-C≡C-Ph)PPh$_3$] **5.10a**. However, the regioisomer of **5.10a** was not confirmed due to a lack of information that could be gleaned in the ^{13}C{^{1}H} and two-dimensional NMR spectroscopy of the phenyl groups in Ph-C=C-C≡C-Ph. Identification of Ph-C=C-C≡C-Ph phenyl groups was confounded by the aromatic abundant PSiP backbone and PPh$_3$ co-ligand, which similarly resonate within the aromatic region of the ^{1}H and ^{13}C{^{1}H} spectra. Furthermore, all attempts to crystallise **5.10a** were unsuccessful. Thus, the regioisomer shown in Scheme 5.20 was postulated based on minimised steric repulsion between the phenyl moieties on the Si and olefin.

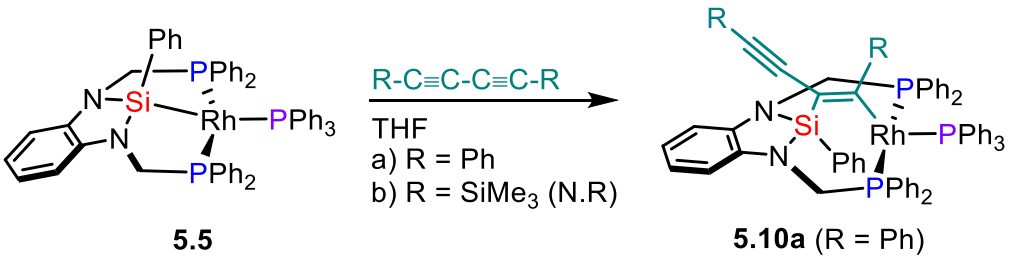

5.5 **5.10a** (R = Ph)

Scheme 5.20: Reactivity of **5.5** with R-C≡C-C≡C-R (R = Ph, SiMe$_3$).

Two minor products were observed as independent doublet of doublet resonances at δ_P = 72.4 ($^1J_{PRh}$ = 138 Hz, $^2J_{PP}$ = 22 Hz) and 70.0 ($^1J_{PRh}$ = 132 Hz, $^2J_{PP}$ = 23 Hz) with free PPh$_3$ present in similar quantities. The magnitudes of the $^1J_{PRh}$ coupling constants are similar to that of the five-coordinate complexes **5.7** ($^1J_{PRh}$ = 147 Hz) and **5.9** ($^1J_{PRh}$ = 145 Hz). Therefore, simple π-coordination of Ph-C≡C-C≡C-Ph and rhodacyclopentadiene are both possible formulations for the minor products. However, neither **5.10a** nor these products were detected by mass spectrometry. Repeating the reaction with one equivalent of Ph-C≡C-C≡C-Ph had no effect on the product distribution, showing preference for **5.10a** again as the major product.

To address the issue of regioselectivity in **5.10a**, the trimethylsilyl derivative (Me_3Si-C≡C-C≡C-$SiMe_3$) was used as it was anticipated that the methyl groups might serve as a spectroscopic handle to provide more insight into the regioselectivity of the reaction. However, in contrast to the facile reaction between **5.5** and Ph-C≡C-C≡C-Ph, treatment of **5.5** with Me_3Si-C≡C-C≡C-$SiMe_3$ showed no reaction at five minutes and the presence of only unreacted starting material was likewise noted at five hours by NMR spectroscopy. The characteristic orange colour of **5.5** persisted in the solution during the NMR experiments.

5.5 Group 8: Ruthenium and Osmium

Ruthenium complexes with a silyl (PSiP) ancillary are numerous in the literature, with contributions from the groups of Stobart,[29,45] Turculet,[7,15,55] Hill,[10] Martín and Sola,[24,56] and Whited.[36] In 2014, Hill reported the only example of a ^{Ph}PNNP(SiPh) supported ruthenium complex, [RuCl{SiPh(NCH_2PPh_2)$_2C_6H_4$-1,2}(CO)(PPh_3)] **L5.12**, formed from the reaction of ^{Ph}PNNP(SiHPh) and [Ru(R)Cl(CO)(PPh_3)$_2$] (R = Ph, CH=CHPh) (Scheme 5.21).[10]

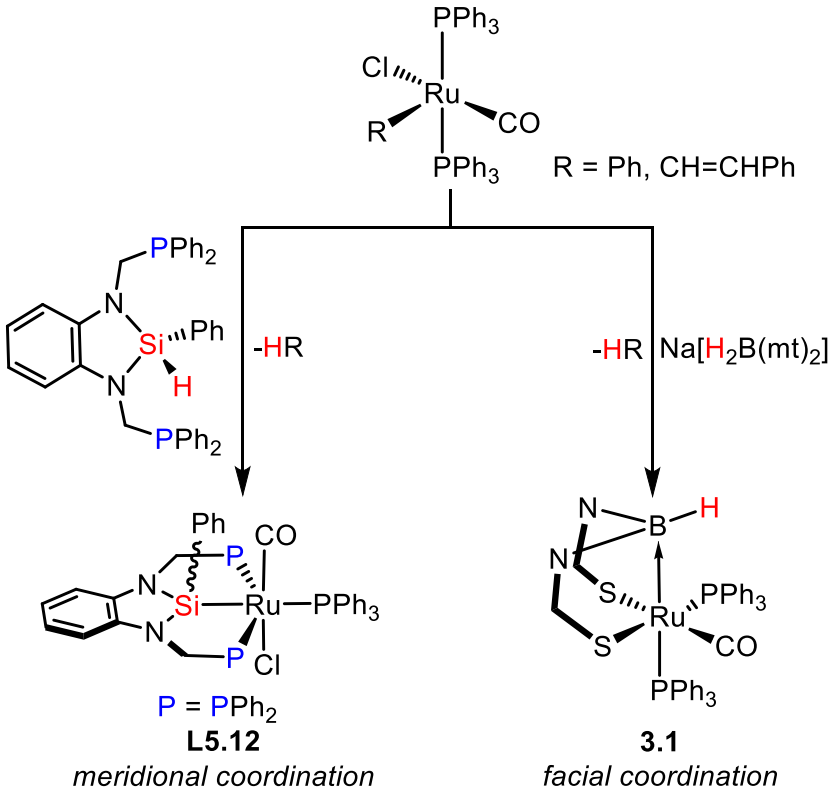

Scheme 5.21: Comparison of reactivity between [Ru(R)Cl(CO)(PPh_3)$_2$] (R = Ph, CH=CHPh) and ^{Ph}PNNP(SiHPh) or Na[$H_2B(mt)_2$].

The ruthenium precursor consists of a H-acceptor R group and was also a key feature in the formation of ruthenaboratrane **3.1** (Chapter 3), where R ultimately accepts a hydrogen from the $[H_2B(mt)_2]^-$ ligand. Similarly, complex **L5.12** is obtained from the extrusion of RH upon reaction between ^{Ph}PNNP(SiHPh) and $[Ru(R)Cl(CO)(PPh_3)_2]$ (R = Ph, CH=CHPh).

The coordination of ^{Ph}PNNP(SiRH) (R = Cl, Ph) to metal precursors in this chapter has typically involved Si–H activation. A previous report on the analogous borane ^{Ph}PNNP(BH) system has illustrated arrested B–H activation with η^2-B–H coordination in the formation of complexes $[MCl_2\{HB(NCH_2PPh_2)_2C_6H_4\text{-}1,2\}(PPh_3)]$ (M = Ru, Os) (Scheme 5.22).[57]

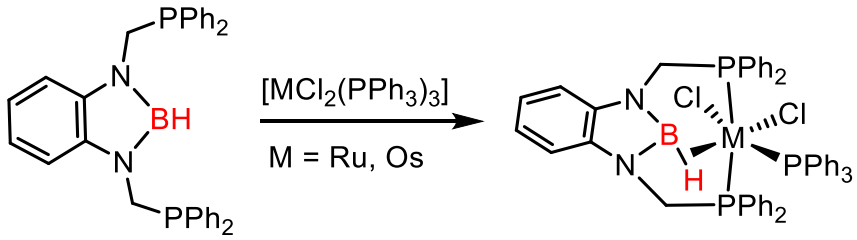

Scheme 5.22: Arrested B–H activation in σ-borane complexes $[MCl_2\{HB(NCH_2PPh_2)_2C_6H_4\text{-}1,2\}(PPh_3)]$ (M = Ru, Os).

To assess the potential of parallel reactivity of the ^{Ph}PNNP(SiHPh) ligand in arrested Si–H activation, reactions with precursors $[MCl_2(PPh_3)_3]$ (M = Ru, Os) were performed in the following section.

5.5.1 Synthesis of $[OsCl\{SiPh(NCH_2PPh_2)_2C_6H_4\text{-}1,2\}(PPh_3)]$

The reactivity of ^{Ph}PNNP(SiHPh) with $[MCl_2(PPh_3)_3]$ (M = Ru, Os) was investigated (Scheme 5.23). Consumption of the starting materials occurred within 1.5 hours in the reaction with $[RuCl_2(PPh_3)_3]$, but only a resonance from the liberated PPh_3 was observed by NMR spectroscopy. The reaction was monitored by NMR for 22 hours and consistently showed no evidence of further progress to identifiable organometallic products. No change was observed spectroscopically after work-up.

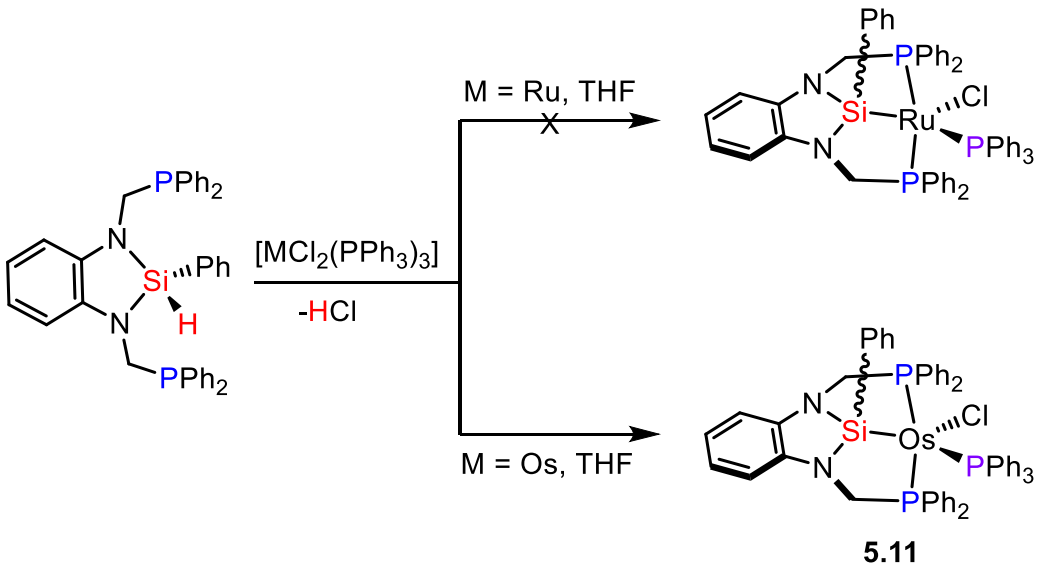

5.11

Scheme 5.23: Reaction of ^{Ph}PNNP(SiHPh) and $[MCl_2(PPh_3)_3]$ (M = Ru, Os).

More success was met in the reaction of ^{Ph}PNNP(SiHPh) with $[OsCl_2(PPh_3)_3]$ as the initial green solution rapidly changed to brown following solvation of both reactants. Within two hours, NMR spectra showed the consumption of starting materials and presence of $[OsCl\{SiPh(NCH_2PPh_2)_2C_6H_4\text{-}1,2\}(PPh_3)]$ **5.11**.

When the NMR scale reaction was monitored, the formation of **5.11** was accompanied by three hydride intermediates resonating in the range δ_H –9 to –13 in the ^{1}H NMR spectrum. This range is more upfield than those of η^2-Si–H bound complexes $[M\{SiHMe(C_6H_4PPh_2\text{-}2)_2\}(L)]$ (M = Ni, Pd, L = PMe_3; M = Ni, Pd, L = PPh_3; M = Ni, L = CO) spanning from δ_H 0.25 to –3.71. Therefore, it was postulated that the hydride intermediates resulted from a Si–H bond activation step. These intermediates subsequently disappeared over the course of a 30 minute reflux. The formation of **5.11** would appear to follow a similar mechanistic route to the complexes discussed in this chapter, involving Si–H activation in ^{Ph}PNNP(SiHPh) followed by extrusion, in this case, of HCl. When the reaction was repeated on the preparative scale, reaction completion was achieved from longer reaction times (three hours) at room temperature. The use of base (e.g. triethylamine) to facilitate the abstraction of HCl from the intermediate did not affect the time taken to reach completion.

No crystals suitable for X-ray diffraction analysis were obtained despite numerous attempts at various temperatures (–21°C, 0°C, 25°C), crystallisation methods (slow evaporation, liquid diffusion, vapour diffusion under nitrogen or argon atmosphere) and solvent combinations (benzene, toluene, THF, Et_2O, *n*-pentane, *n*-hexane). Nevertheless, the formulation of **5.11** was confirmed by NMR, IR and mass spectrometry. The virtual coupling of one of the diastereotopic methylene protons to the PPh_2 groups at δ_H = 4.33 ($^2J_{HP\ (PPh2)}$ = 4.7 Hz) supports the *transoidal* arrangement of the PPh_2 arms depicted in Scheme 5.23. The two phosphine environments were located at δ_P = –12.1 and 20.9 in the $^{31}P\{^1H\}$ NMR spectrum, with respective triplet and doublet ($^2J_{PP}$ = 16 Hz) multiplicity as expected for **5.11**. Additionally, the ^{29}Si nuclei couples to the two phosphine environments, appearing as a doublet of triplets at δ_{Si} = 85.4 ($^2J_{SiP\ (PPh3)}$ = 141.6, $^2J_{SiP\ (PPh2)}$ = 16.1 Hz). Consistent with complexes **5.2**–**5.7**, a larger ^{29}Si-$^{31}PPh_3$ coupling constant relative to ^{29}Si-$^{31}PPh_2$ was measured, suggesting a large Si–Os–P angle in **5.11**.

In contrast to rhodium and ruthenium, examples of osmium silyl pincer complexes are scarce. Literature examples predominantly comprise osmium clusters or monodentate silyl ligands bound to osmium. Thus, **5.11** is the first example of a PSiP based osmium(II) complex.

5.6 Conclusions

Novel silyl pincer complexes were obtained from the direct coordination of ^{Ph}PNNP(SiHR) (R = Cl, Ph) through Si–H activation to rhodium, iridium and osmium metal precursors. Diastereomers of rhodium(III) and iridium(III) complexes [MHCl{SiR(NCH_2PPh_2)$_2C_6H_4$-1,2}(PPh_3)] (R = Ph, M = Rh **5.2**, Ir **5.3**; R = Cl, M = Rh **5.4**) were obtained following Si–H activation. The rhodium(I) complexes [Rh{SiPh(NCH_2PPh_2)$_2C_6H_4$-1,2}(PPh_3)] **5.5** and [Rh{SiPh(NCH_2PPh_2)$_2C_6H_4$-1,2}(CO)(PPh_3)] **5.7** were accessible following extrusion of H_2. Rhodium(III) hydrido complexes were demonstrated to undergo dehydrohalogenation to provide rhodium(I) complexes.

Complex **5.5** was found to undergo various reactions including reversible coordination of hydrogen, alkyne coordination, and substitution reactions that afforded [RhH_2{$SiPh(NCH_2PPh_2)_2C_6H_4$-1,2}] **5.6**, [Rh{$SiPh(NCH_2PPh_2)_2C_6H_4$-1,2}(NBD)] **5.8** and [Rh{$SiPh(NCH_2PPh_2)_2C_6H_4$-1,2}$(CO)_2$] **5.9**. The lability of the second CO in **5.9** allowed an alternate pathway to monocarbonyl complex **5.7**. Coordination of ^{Ph}PNNP(SiHPh) to osmium provided the first example of a PSiP pincer osmium complex, [OsCl{$SiPh(NCH_2PPh_2)_2C_6H_4$-1,2}(PPh_3)] **5.11**.

5.7 Future Work

The work presented in this chapter has initiated investigations into rhodium(I) silyl complexes from a coordination chemistry perspective. Given the prominence of Rh(I) based catalyst systems, a direct application is envisaged in the screening of these complexes for catalytic activity. The strong σ-donating properties of silyls may be particularly adept at promoting faster oxidative addition by way of increasing electron density at the metal centre, while the *trans* influence of the silyl may direct reductive elimination processes. Additionally, the high reactivity of [Rh{$SiR(NCH_2PPh_2)_2C_6H_4$-1,2}(PPh_3)] **5.5** towards addition and ligand substitution shown in this chapter invites further exploration by future researchers.

A natural progression following the isolation of the osmium silyl complex **5.11**, is for extension to the ^{Ph}PNNP(SiHCl) scaffold. The Si–Cl bond of the coordinated ligand may provide access to rare silylene ($M=SiR_2$) complexes supported within a pincer system (Scheme 5.24). Examples of pincer type silylenes are scarce but have been implicated as transient intermediates on rhodium,[11,50] spectroscopically observed on chromium[5] and platinum,[23] and recently isolated on ruthenium.[36] The sp^2 planarity required by a silylene center may be enforced by the preference of the ^{Ph}PNNP(Si) scaffold for *mer* coordination. With access to pincer silylene complexes, the reactivity of the $M^{\delta-}=Si^{\delta+}$ unit could be investigated and compared to the unusual modes of reactivity reported for base-free silylenes.[58-69] Ultimately, the reactivity of the $M^{\delta-}=Si^{\delta+}$ unit could allow for their application in cooperative catalysis.

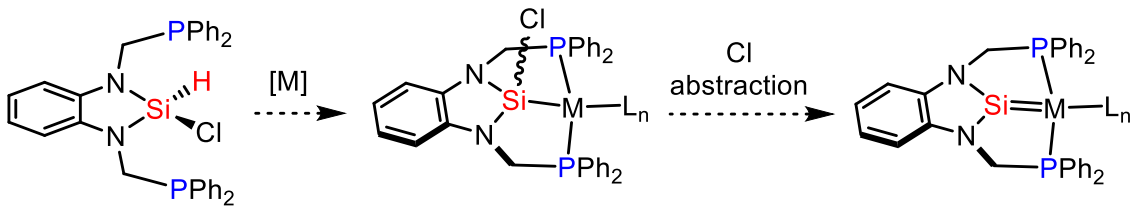

Scheme 5.24: Proposed route towards pincer silylene complexes.

5.8 References

(1) Simon, M.; Breher, F. *Dalton Trans.* **2017**, *46*, 7976.
(2) Sola, E. In *Pincer Compounds*; Morales-Morales, D., Ed.; Elsevier: 2018, p 401.
(3) Joslin, F. L.; Stobart, S. R. *Inorg. Chem.* **1993**, *32*, 2221.
(4) Gossage, R. A.; McLennan, G. D.; Stobart, S. R. *Inorg. Chem.* **1996**, *35*, 1729.
(5) Handwerker, H.; Paul, M.; Blümel, J.; Zybill, C. *Angew. Chem. Int. Ed. Engl.* **1993**, *32*, 1313.
(6) Handwerker, H.; Leis, C.; Probst, R.; Bissinger, P.; Grohmann, A.; Kiprof, P.; Herdtweck, E.; Bluemel, J.; Auner, N.; Zybill, C. *Organometallics* **1993**, *12*, 2162.
(7) MacInnis, M. C.; MacLean, D. F.; Lundgren, R. J.; McDonald, R.; Turculet, L. *Organometallics* **2007**, *26*, 6522.
(8) Gualco, P.; Lin, T.-P.; Sircoglou, M.; Mercy, M.; Ladeira, S.; Bouhadir, G.; Perez, L. M.; Amgoune, A.; Maron, L.; Gabbai, F. P.; Bourissou, D. *Angew. Chem. Int. Ed.* **2009**, *48*, 9892.
(9) Gualco, P.; Mercy, M.; Ladeira, S.; Coppel, Y.; Maron, L.; Amgoune, A.; Bourissou, D. *Chem. Eur. J.* **2010**, *16*, 10808.
(10) Dixon, L. S. H.; Hill, A. F.; Sinha, A.; Ward, J. S. *Organometallics* **2014**, *33*, 653.
(11) Whited, M. T.; Deetz, A. M.; Boerma, J. W.; DeRosha, D. E.; Janzen, D. E. *Organometallics* **2014**, *33*, 5070.
(12) Kameo, H.; Ishii, S.; Nakazawa, H. *Dalton Trans.* **2013**, *42*, 4663.
(13) Zhu, J.; Lin, Z.; Marder, T. B. *Inorg. Chem.* **2005**, *44*, 9384.
(14) Sangtrirutnugul, P.; Tilley, T. D. *Organometallics* **2008**, *27*, 2223.
(15) MacInnis, M. C.; McDonald, R.; Ferguson, M. J.; Tobisch, S.; Turculet, L. *J. Am. Chem. Soc.* **2011**, *133*, 13622.
(16) Xiong, Z.; Li, X.; Zhang, S.; Shi, Y.; Sun, H. *Organometallics* **2016**, *35*, 357.
(17) Takaya, J.; Iwasawa, N. *Organometallics* **2009**, *28*, 6636.
(18) Suh, H.-W.; Balcells, D.; Edwards, A. J.; Guard, L. M.; Hazari, N.; Mader, E. A.; Mercado, B. Q.; Repisky, M. *Inorg. Chem.* **2015**, *54*, 11411.
(19) Takaya, J.; Iwasawa, N. *Dalton Trans.* **2011**, *40*, 8814.
(20) Wu, S.; Li, X.; Xiong, Z.; Xu, W.; Lu, Y.; Sun, H. *Organometallics* **2013**, *32*, 3227.
(21) Kirai, N.; Takaya, J.; Iwasawa, N. *J. Am. Chem. Soc.* **2013**, *135*, 2493.
(22) Joost, M.; Mallet-Ladeira, S.; Miqueu, K.; Amgoune, A.; Bourissou, D. *Organometallics* **2013**, *32*, 898.
(23) DeMott, J. C.; Gu, W.; McCulloch, B. J.; Herbert, D. E.; Goshert, M. D.; Walensky, J. R.; Zhou, J.; Ozerov, O. V. *Organometallics* **2015**, *34*, 3930.
(24) Bernal, M. J.; Martín, M.; Sola, E. *Z. Anorg. Allg. Chem.* **2015**, *641*, 2122.
(25) Suárez, E.; Plou, P.; Gusev, D. G.; Martín, M.; Sola, E. *Inorg. Chem.* **2017**, *56*, 7190.
(26) Kloos, S. D.; Boudjouk, P. *Inorg. Synth.* **1998**, *32*, 294.
(27) Segawa, Y.; Yamashita, M.; Nozaki, K. *Organometallics* **2009**, *28*, 6234.
(28) Osakada, K.; Hataya, K.; Yamamoto, T. *Inorg. Chim. Acta* **1997**, *259*, 203.
(29) Brost, R. D.; Bruce, G. C.; Joslin, F. L.; Stobart, S. R. *Organometallics* **1997**, *16*, 5669.

(30) Kameo, H.; Kawamoto, T.; Sakaki, S.; Bourissou, D.; Nakazawa, H. *Chem. Eur. J.* **2016**, *22*, 2370.
(31) Mitton, S. J.; McDonald, R.; Turculet, L. *Angew. Chem. Int. Ed.* **2009**, *48*, 8568.
(32) Milstein, D.; Calabrese, J. C. *J. Am. Chem. Soc.* **1982**, *104*, 3773.
(33) Jenkins, J. M.; Shaw, B. L. *J. Chem. Soc. A* **1966**, 770.
(34) Karplus, M. *J. Chem. Phys.* **1959**, *30*, 11.
(35) Karplus, M. *J. Am. Chem. Soc.* **1963**, *85*, 2870.
(36) Whited, M. T.; Zhang, J.; Ma, S.; Nguyen, B. D.; Janzen, D. E. *Dalton Trans.* **2017**, *46*, 14757.
(37) Li, T.; Lough, A. J.; Morris, R. H. *Chem. Eur. J.* **2007**, *13*, 3796.
(38) Dixon, L. S. H. Honours Thesis, The Australian National University, 2012.
(39) Vaska, L. *Science* **1963**, *140*, 809.
(40) Perutz, R. N.; Sabo-Etienne, S. *Angew. Chem. Int. Ed.* **2007**, *46*, 2578.
(41) Dewhirst, K. C.; Keim, W.; Reilly, C. A. *Inorg. Chem.* **1968**, *7*, 546.
(42) Hamilton, D. G.; Crabtree, R. H. *J. Am. Chem. Soc.* **1988**, *110*, 4126.
(43) Adams, J. J.; Arulsamy, N.; Roddick, D. M. *Organometallics* **2011**, *30*, 697.
(44) Ahmad, N.; Levison, J. J.; Robinson, S. D.; Uttley, M. F. *Inorg. Synth.* **1974**, *15*, 45.
(45) Bushnell, G. W.; Casado, M. A.; Stobart, S. R. *Organometallics* **2001**, *20*, 601.
(46) Zhou, X.; Stobart, S. R. *Organometallics* **2001**, *20*, 1898.
(47) Cotton, F. A.; Wilkinson, G. In *Advanced Inorganic Chemistry*; Fifth Edition ed.; John Wiley and Sons Ltd: New York, 1988, p 1035.
(48) Korshin, E. E.; Leitus, G.; Shimon, L. J. W.; Konstantinovski, L.; Milstein, D. *Inorg. Chem.* **2008**, *47*, 7177.
(49) Stobart, S. R.; Zhou, X.; Cea-Olivares, R.; Toscano, A. *Organometallics* **2001**, *20*, 4766.
(50) Whited, M. T.; Deetz, A. M.; Donnell, T. M.; Janzen, D. E. *Dalton Trans.* **2016**, *45*, 9758.
(51) Ward, R. M.; Batsanov, A. S.; Howard, J. A. K.; Marder, T. B. *Inorg. Chim. Acta* **2006**, *359*, 3671.
(52) Rourke, J. P.; Batsanov, A. S.; Howard, J. A. K.; Marder, T. B. *Chem. Commun.* **2001**, 2626.
(53) Steffen, A.; Ward, R. M.; Tay, M. G.; Edkins, R. M.; Seeler, F.; van Leeuwen, M.; Palsson, L.-O.; Beeby, A.; Batsanov, A. S.; Howard, J. A. K.; Marder, T. B. *Chem. Eur. J.* **2014**, *20*, 3652.
(54) Werner, H.; Meyer, U.; Peters, K.; Von Schnering, H. G. *Chem. Ber.* **1989**, *122*, 2097.
(55) MacInnis, M. C.; Ruddy, A. J.; McDonald, R.; Ferguson, M. J.; Turculet, L. *Dalton Trans.* **2016**, *45*, 15850.
(56) Bernal, M. J.; Torres, O.; Martín, M.; Sola, E. *J. Am. Chem. Soc.* **2013**, *135*, 19008.
(57) Hill, A. F.; McQueen, C. M. A. *Organometallics* **2014**, *33*, 1977.
(58) Mitchell, G. P.; Tilley, T. D. *J. Am. Chem. Soc.* **1998**, *120*, 7635.
(59) Ochiai, M.; Hashimoto, H.; Tobita, H. *Organometallics* **2012**, *31*, 527.
(60) Watanabe, T.; Hashimoto, H.; Tobita, H. *J. Am. Chem. Soc.* **2006**, *128*, 2176.
(61) Klei, S. R.; Tilley, T. D.; Bergman, R. G. *Organometallics* **2002**, *21*, 4648.
(62) Mitchell, G. P.; Tilley, T. D. *J. Am. Chem. Soc.* **1997**, *119*, 11236.
(63) Lee, V. Y.; Aoki, S.; Yokoyama, T.; Horiguchi, S.; Sekiguchi, A.; Gornitzka, H.; Guo, J.-D.; Nagase, S. *J. Am. Chem. Soc.* **2013**, *135*, 2987.
(64) Watanabe, T.; Hashimoto, H.; Tobita, H. *J. Am. Chem. Soc.* **2007**, *129*, 11338.
(65) Fasulo, M. E.; Tilley, T. D. *Organometallics* **2012**, *31*, 5049.
(66) Glaser, P. B.; Tilley, T. D. *J. Am. Chem. Soc.* **2003**, *125*, 13640.
(67) Fasulo, M. E.; Lipke, M. C.; Tilley, T. D. *Chem. Sci.* **2013**, *4*, 3882.
(68) Grumbine, S. K.; Tilley, T. D. *J. Am. Chem. Soc.* **1994**, *116*, 6951.
(69) Wanandi, P. W.; Glaser, P. B.; Tilley, T. D. *J. Am. Chem. Soc.* **2000**, *122*, 972.

Chapter 6

Conclusions

A number of complexes featuring unconventional tridentate ligands with a central electropositive atom (boron, aluminium or silicon) have been synthesised.

The bis(methimazolyl)borate series [Ru(X)(CO)(PPh_3){κ^3-*H,S,S'*-$H_2B(mt)_2$}] (X = H, Cl, SePh, BCat, $SiCl_3$, $SiMe_3$) was synthesised to provide insight into how the 3c2e B–H–Ru interaction is influenced by the ligand in the *trans* position. Through analysis of collected spectroscopic and crystallographic data, a correlation between the σ-donating properties of the *trans* ligand and borohydride character of the B–H–Ru bridge was inferred. The stability of the B–H–Ru interaction was found to be dependent on the *trans* ligand. Elimination of X–H afforded the first ruthenaboratrane complex with two methimazolyl buttresses, [Ru{κ^3-*B,S,S'*-$BH(mt)_2$}(CO)(PPh_3)$_2$], for which a convenient one-pot synthesis was developed. Ligand exchange occurred readily at ruthenium with retention of the Ru→B bond, enabling derivatisation of the complex to access further examples of ruthenaboratrane complexes. Directing reactivity to the Ru→B bond proved difficult either leading to a plethora of products or no reaction. However, modification of the environment around boron could be a direction for further research, to access the σ-acceptor → σ-donor umpolung in borylene M=B moeities.

The preparation of aluminium-based ligands and complexes are underexplored compared to that of boron and silicon. The novel aluminium pro-ligand, Li[$H_2Al(mt)_2$].THF was found to be more reactive and less stable than the boron analogue, Na[$H_2B(mt)_2$], both as the free ligand and in the coordination sphere of metals. This is in part attributed to the highly electropositive nature of the aluminium. As complexes of bis(methimazolyl)aluminate were observed spectroscopically as transient species, finding the delicate combination of suitable metal and co-ligand environment to support the aluminium-based ligand remains a challenge for the future.

As the diagonal element of boron, silicon similarly has strong σ-donating properties that were observed crystallographically and in the reactivity of complexes featuring the *o*-phenylenediamine-based silyl $RSi(NCH_2PPh_2)_2C_6H_4$-1,2 (R = Cl, Ph) ligand. The ligand exhibited remarkable coordination flexibility, adopting *meridional* or *facial* modes to fit the environment around the metal centre. The rhodium(I) square planar complex [Rh{$SiPh(NCH_2PPh_2)_2C_6H_4$-1,2}(PPh_3)] showed rich ligand exchange reactivity and fluctional interaction with dihydrogen that might find application in small molecule activation processes.

Together these results show the versatility of unconventional tridentate ligands of boron, aluminium and silicon in coordination to metal precursors. The electropositive nature of the ligands renders unusual reactivity and unique interactions accessible.

Chapter 7

Experimental

7.1 General Experimental Procedures

All reactions were performed under a dry, oxygen-free N_2 atmosphere at room temperature using standard Schlenk, dry-box (argon) or vacuum line techniques, unless otherwise stated.

Solvents were degassed and distilled under dry nitrogen from suitable drying agents.

NMR spectra were obtained at 298 K on a Varian Mercury 300 (^{1}H: 300.1 MHz, ^{31}P: 121.5 MHz), a MR 400 (^{1}H: 399.8 MHz, ^{31}P: 161.8 MHz), a Bruker Avance 400 (^{1}H: 400.1 MHz, ^{11}B: 128.4 MHz, ^{13}C: 100.6 MHz, ^{27}Al: 104.3 MHz, ^{31}P: 162.0 MHz), a Bruker Avance 600 (^{1}H: 600.0 MHz, ^{13}C: 150.9 MHz), a Bruker Avance 700 (^{1}H: 700.2 MHz, ^{29}Si: 139.1 MHz, ^{13}C: 176.1 MHz, ^{31}P: 283.5 MHz), or Varian Mercury 800 (^{13}C: 201.2 MHz) spectrometers. Spectra were recorded at 298 K unless otherwise stated. ^{1}H chemical shift (δ) data were referenced to residual solvent peaks in deuterated solvent. ^{13}C chemical shift (δ) data were referenced to the resonances of the deuterated solvent. ^{31}P{^{1}H} and ^{27}Al{^{1}H} spectra were referenced to external 85% H_3PO_4 or $Al(acac)_3$ standards, respectively. Where applicable, data are reported as chemical shift (δ), multiplicity (s = singlet, d = doublet, dd = doublet of doublets, t = triplet, q = quartet, m = multiplet, t^{v} = virtual triplet), relative integral (for ^{1}H), coupling constant(s) (*J* in Hz) and assignment. The aromatic groups were reported as follows: ipso = $^{i}C_6H_5$, meta or ortho = $^{m/o}C_6H_5$, para = $^{p}C_6H_5$. The T_1 experiments were performed on a Bruker Avance 700 instrument with a standard 180°-τ-90° pulse sequence.

Infrared spectra were obtained with a Bruker Alpha FTIR with diamond plate Attenuated Total Reflectance sampling attachment, run at 4 cm^{-1} resolution. Solution infrared spectra were obtained using a Perkin-Elmer Spectrum One FT-IR Spectrometer. The strengths of IR absorptions are denoted by the abbreviations vs (very strong), s (strong), m (medium), w (weak), sh (shoulder), br (broad).

Low and high resolution Electro-spray ionisation mass spectrometry (MS-ESI) was carried out by the mass spectrometry unit at the ANU Research School of Chemistry. Data are expressed as *m/z*: mass [assignment]^{charge}. By virtue of the polar matrix employed (MeCN), peaks attributable to $[M - Cl]^+$ and $[M - Cl + NCMe]^+$ were commonly observed. Elemental microanalysis was performed by the microanalytical services of the London Metropolitan University. Crystallographic data were acquired using Enraf Nonius Kappa, Agilent SuperNova, and Agilent Xcalibur CCD diffractometers. Crystallography by Dr Jas Ward in the structure solve of **2.2x, 2.5x, ^{Ph}PNNP(SiHCl), 5.5** is

gratefully acknowledged. Preliminary results by Tshabang suggested the existence of complexes **3.10**, **3.11** and **3.12**.

The reagents $Na[H_2B(mt)_2]$,[1] SiH_2Cl_2.TEEDA,[2] $(HNCH_2PPh_2)_2C_6H_4$-1,2,[3] $H_2C(NCH_2PCy_2)_2C_{10}H_6$ and $H_2C(NCH_2PPh_2)_2C_{10}H_6$,[4] $[RuHCl(CO)(PPh_3)_3]$,[5] $[Ru(BCat)Cl(CO)(PPh_3)_2]$,[6] $[Ru(SiMe_3)Cl(CO)(PPh_3)_2]$,[7,8] $[Ru(Ph)Cl(CO)(PPh_3)_2]$,[9] $[Ru(CH=CHPh)Cl(CO)(PPh_3)_2]$,[10,11] $[OsHCl(CO)(PPh_3)_3]$,[12] $[Os(Ph)Cl(CO)(PPh_3)_2]$,[13] $[OsCl_2(PPh_3)_3]$,[14] $[ReBr(CO)_3(THF)_2]$,[15] $[RhCl(PPh_3)_3]$,[16] $[RhCl(CO)(PPh_3)_2]$,[17] $[RhH(CO)(PPh_3)_3]$,[5] $[RhH(PPh_3)_4]$,[5] $[Rh_2(\mu\text{-}Cl)_2(\eta^4\text{-}COD)_2]$,[18] $[Ir_2(\mu\text{-}Cl)_2(COE)_4]$,[19,20] $[IrCl(CO)(PPh_3)_2]$,[21] and $[Ru\{\kappa^4\text{-}B,S,S',S''\text{-}B(mt)_3\}(CO)(PPh_3)]$[22] were prepared according to literature procedures.

7.2 Synthetic Experimental Details

7.2.1 Bis(methimazolyl)borate Complexes of Ruthenium

Synthesis of $[RuH(CO)(PPh_3)\{\kappa^3\text{-}H,S,S'\text{-}H_2B(mt)_2\}]$ (2.1)

The complex $[RuHCl(CO)(PPh_3)_3]$ (2.01 g, 2.11 mmol) and $Na[H_2B(mt)_2]$ (0.551 g, 2.10 mmol) were heated under reflux in tetrahydrofuran (40 mL) for 15 min. During this time the mixture changed from pink to yellow and became less cloudy. The solvent was removed on the rotary evaporator. The solid was re-dissolved in dichloromethane and filtered through diatomaceous earth. The filtrate was slowly evaporated (adding ethanol to maintain a constant volume) to furnish a cream product. The resulting solid was collected on a sintered funnel, washed with ethanol (2 x 15 mL) and dried *in vacuo*. Yield: 1.02 g (1.60 mmol, 76%). IR (ATR): 1926 ν_{CO}, 2397 ν_{BH} cm^{-1}. IR (CH_2Cl_2): 1936 ν_{CO}, 2110 ν_{RuH}, 2201 ν_{BHRu}, 2399 ν_{BH} cm^{-1}. ^1H NMR (700 MHz, $CDCl_3$): δ_H = –12.22 (d, 1H, $^2J_{HP}$ = 23.1, RuH), –5.42 (br, 1H, BHRu), 3.10 (s, 3H, NCH_3), 3.57 (s, 3H, NCH_3), 6.35 (s, 1H, NCH=CH), 6.45 (s, 1H, NCH=CH), 6.62 (s, 1H, NCH=CH), 6.64 (s, 1H, NCH=CH), 7.10–7.12 (m, 3H, C_6H_5), 7.25–7.26 (m, 4H, C_6H_5), 7.27–7.31 (m, 2H, C_6H_5), 7.58–7.61 (m, 5H, C_6H_5), 7.70–7.73 (m, 1H, C_6H_5). $^{13}C\{^1H\}$ NMR (176 MHz, $CDCl_3$): Sample decomposed to $[RuCl(CO)(PPh_3)\{\kappa^3\text{-}H,S,S'\text{-}H_2B(mt)_2\}]$ **2.2** during the course of the data collection and had poor solubility in C_6D_6. $^{31}P\{^1H\}$ NMR (162 MHz, $CDCl_3$): δ_P = 56.7. $^{11}B\{^1H\}$ NMR (128 MHz, $CDCl_3$): δ_B = –5.52. MS-ESI(+) *m/z*: 631.0499 $[M - H]^+$. Calcd. for $C_{27}H_{27}{}^{11}BN_4OPS_2{}^{102}Ru$ = 631.0500.

Crystal data for $C_{27}H_{28}BN_4OPRuS_2$: M_w = 631.53, monoclinic, $P2_1/n$, a = 9.5785(2), b = 19.3036(4), c = 15.1080(3) Å, β = 98.727(2)°, V = 2761.12(5) Å^3, Z = 4, ρ_{calcd} = 1.519 Mgm^{-3}, μ(Mo $K\alpha$) = 0.81 mm^{-1}, T = 150(2) K, yellow prism, 0.74 x 0.50 x 0.43 mm, 7080 independent reflections. F^2 refinement, R = 0.025, wR = 0.052 for 6120 reflections ($I > 2.0\sigma(I)$, $2\theta_{max}$ = 60°), 343 parameters, 0 restraints, CCDC 1535756.

Synthesis of [RuCl(CO)(PPh$_3${κ^3-*H,S,S'*-H$_2$B(mt)$_2$}] (2.2)

A solution of [RuH(CO)(PPh$_3$){κ^3-*H,S,S'*-H$_2$B(mt)$_2$}] (**2.1**: 0.257 g, 0.41 mmol) in chloroform (10 mL) was heated under reflux for 1 h, observing a colour change from pale yellow to orange. After cooling, the solvent was removed under reduced pressure, and the residue was extracted with dichloromethane, filtered through diatomaceous earth and then diluted with an equal amount of ethanol. The solvent volume was reduced to afford a yellow precipitate. The fine yellow-orange product **2.2** was collected on a sintered funnel, washed with ethanol (2 × 10 mL) and dried in air. Yield: 0.112 g (0.168 mmol, 41%). Crystals suitable for crystallographic analysis were obtained from slow evaporation of a concentrated solution of **2.2** in chloroform over one day. IR (CH_2Cl_2): 1973 ν_{CO}, 2431 ν_{BH} cm^{-1}. IR (Nujol): 2442w ν_{BH}, 2011 ν_{BHRu}, 1963 ν_{CO} cm^{-1}. ^{1}H NMR (400 MHz, $CDCl_3$): δ_H = –18.11 (br, 1H, BHRu), 3.34 (s, 3H, CH_3), 3.56 (s, 3H, CH_3), 6.12 (s, 1H, NCH=CH), 6.38 (s, 1H, NCH=CH), 6.45 (s, 1H, NCH=CH), 6.62 (s, 1H, NCH=CH), 7.30–7.38 (m, 9H, C_6H_5), 7.69–7.70 (m, 6H, C_6H_5). ^{13}C{^{1}H} NMR (100 MHz, $CDCl_3$): δ_C = 34.5 (CH_3), 34.7 (CH_3), 120.1 (NCH=CH), 120.6 (NCH=CH), 121.4 (NCH=CH), 122.0 (NCH=CH), 127.8 (d, $^{2,3}J_{CP}$ = 9.8, $^{m/o}C_6H_5$), 129.7 (d, $^4J_{CP}$ = 2.3, $^pC_6H_5$), 134.1 (d, $^{2,3}J_{CP}$ = 9.8, $^{m/o}C_6H_5$), 134.9 (d, $^1J_{CP}$ = 44.7, $^iC_6H_5$), 164.6 (CS), 198.2 (d, $^2J_{CP}$ = 11.6, CO). ^{31}P{^{1}H} NMR (162 MHz, $CDCl_3$): δ_P = 36.3. ^{11}B{^{1}H} NMR (128 MHz, $CDCl_3$): δ_B = –7.36 (br). MS-ESI(+) *m/z*: = 689.0081 [M + Na]$^+$ Calcd. for $C_{27}H_{27}{}^{11}BN_4O^{23}NaPS_2{}^{35}Cl^{102}Ru$ = 689.0087; 631.0500 [M – Cl]$^+$. Calcd. for $C_{27}H_{27}{}^{11}BN_4OPS_2{}^{102}Ru$ 631.0500. Anal. Found: C, 46.37; H, 4.24; N, 7.03%. Calcd. For $C_{27}H_{27}BClN_4OPRuS_2$: C, 48.70; H, 4.09; N, 8.41%.

Crystal data for $C_{27}H_{27}BClN_4OPRuS_2.CHCl_3$: M_w = 785.35, monoclinic, $P2_1/n$, a = 9.7110(1), b = 17.5876(2), c = 19.2544(2) Å, β = 100.042(1)°, V = 3238.14(3) Å^3, Z = 4, ρ_{calcd} = 1.611 Mgm^{-3}, μ(Cu $K\alpha$) = 8.88 mm^{-1}, T = 150(2) K, yellow block, 0.12 x 0.08 x 0.04

mm, 6,537 independent reflections. F^2 refinement, R = 0.027, wR = 0.069 for 6,163 reflections ($I > 2.0\sigma(I)$, $2\theta_{max}$ = 144°), 385 parameters, 0 restraints, CCDC 1535758.

Crystal data for $[Ru_2(\mu\text{-S-mtH})(\mu\text{-mt})Cl_2(CO)_2(PPh_3)_2]$ **2.2x** side product $C_{46}H_{41}Cl_2N_4O_2P_2Ru_2S_2$: M_w = 1080.93, orthorhombic, $P2_12_12_1$, a = 11.1859(1), b = 15.0067(1), c = 30.1526(1) Å, V = 5061.52(6) Å^3, Z = 4, ρ_{calcd} = 1.418 Mgm^{-3}, μ(Cu $K\alpha$) = 7.48 mm^{-1}, T = 150(2) K, red prism, 0.22 x 0.18 x 0.12 mm, 10218 independent reflections. F^2 refinement, R = 0.019, wR = 0.049 for 10155 reflections ($I > 2.0\sigma(I)$, $2\theta_{max}$ = 144°), 586 parameters, 120 restraints.

Synthesis of [Ru(SePh)(CO)(PPh_3){κ^3-*H,S,S'*-$H_2B(mt)_2$}] (2.3)

(a) A solution of [RuH(CO)(PPh_3){κ^3-*H,S,S'*-$H_2B(mt)_2$}] (**2.1**: 0.200 g, 0.317 mmol) and PhSeSePh (0.100 g, 0.320 mmol) in tetrahydrofuran (20 mL) was stirred for 24 h. The pink precipitate was filtered from the deep red filtrate. The filtrate was concentrated on the rotary-evaporator and recrystallized from a mixture of dichloromethane/ethyl acetate/*n*-hexane in air to afford deep red crystals, which were collected on a sintered frit, washed with *n*-hexane (2 x 10 mL) and dried *in vacuo*. Yield: 0.165 g (0.210 mmol, 66%). Crystals suitable for crystallographic analysis were obtained from slow evaporation of a concentrated solution of **2.3** in chloroform/ethyl acetate over one day. IR (ATR): 1945 ν_{CO}, 2051 ν_{BHRu}, 2411 ν_{BH} cm^{-1}. ^{1}H NMR (400 MHz, $CDCl_3$): δ_H = –12.00 (br, 1H, BHRu), 3.20 (s, 3H, NCH_3), 3.42 (s, 3H, NCH_3), 6.19 (s, 1H, NCH=CH), 6.30 (s, 1H, NCH=CH), 6.39 (s, 1H, NCH=CH), 6.57 (s, 1H, NCH=CH), 6.95–6.99 (m, 2H, C_6H_5), 7.03–7.05 (m, 1H, C_6H_5), 7.23–7.26 (m, 4H, C_6H_5), 7.31–7.33 (m, 4H, C_6H_5), 7.54–7.59 (m, 7H, C_6H_5), 7.69–7.71 (m, 2H, C_6H_5). ^{13}C{^{1}H} NMR (100 MHz, $CDCl_3$): δ_C = 34.4 (CH_3), 34.6 (CH_3), 120.3 (NCH=CH), 120.8 (NCH=CH), 121.9 (NCH=CH), 125.0 (NCH=CH), 127.0 (d, $^{2,3}J_{CP}$ = 9.7, $^{m/o}C_6H_5$), 127.1 (SeC_6H_5), 127.8 (SeC_6H_5), 129.5 (d, $^4J_{CP}$ = 2.3, $^pC_6H_5$), 134.2 (d, $^{2,3}J_{CP}$ = 9.5, $^{m/o}C_6H_5$), 134.5 (d, $^1J_{CP}$ = 43.8, $^iC_6H_5$), 136.9 (SeC_6H_5), 138.0 (SeC_6H_5), 165.2 (CS), 166.9 (CS), 200.1 (d, $^2J_{CP}$ = 12.5, CO). ^{31}P{^{1}H} NMR (162 MHz, $CDCl_3$): δ_P = 39.7. ^{11}B{^{1}H} NMR (128 MHz, $CDCl_3$): δ_B = –5.50. MS-ESI(+) *m/z*: 788.0086 $[M]^+$. Calcd. for $C_{33}H_{32}{}^{11}BN_4OPS_2{}^{102}Ru^{80}Se$ = 788.0057. Anal. Found: C, 50.30; H, 3.96, N, 7.04. Calcd. for $C_{33}H_{32}BN_4OS_2PRuSe$: C, 50.39; H, 4.10; N, 7.12%.

Crystal data for $C_{33}H_{32}BN_4OPRuS_2Se$: M_w = 786.59, orthorhombic, *Pbca*, *a* = 19.9088(5), *b* = 15.9847(4), *c* = 20.7366(5) Å, *V* = 6599.14(16) Å^3, *Z* = 8, ρ_{calcd} = 1.583 Mgm^{-3}, μ(Mo *K*α) = 1.79 mm^{-1}, *T* = 150(2) K, orange plate, 0.26 x 0.15 x 0.05 mm, 8888 independent reflections. F^2 refinement, *R* = 0.048, *wR* = 0.104 for 6297 reflections ($I > 2.0\sigma(I)$, $2\theta_{max}$ = 60°), 403 parameters, 0 restraints, CCDC 1539734.

(b) In an NMR tube, a mixture of [RuH(CO)(PPh_3){κ^3-*H,S,S'*-$H_2B(mt)_2$}] (**2.1**: 0.015 g, 0.024 mmol) and grey selenium (0.004 g, 0.051 mmol) in $CDCl_3$ (0.5 mL) was monitored for 21 h by NMR spectroscopy. The ^{1}H and ^{31}P{^{1}H} NMR spectra showed no reaction between the reagents and instead slow conversion of [RuH(CO)(PPh_3){κ^3-*H,S,S'*-$H_2B(mt)_2$}] to [RuCl(CO)(PPh_3){ κ^3-*H,S,S'*-$H_2B(mt)_2$}] was observed.

Synthesis of [Ru(BCat)(CO)(PPh_3){κ^3-*H,S,S'*-$H_2B(mt)_2$}] (2.4)

A mixture of [Ru(BCat)Cl(CO)(PPh_3)$_2$] (0.203 g, 0.251 mmol) and Na[$H_2B(mt)_2$] (0.066 g, 0.25 mmol) was stirred in tetrahydrofuran (20 mL) at room temperature for 25 h. The solvent was removed on the rotary evaporator and the resulting residue was dissolved in dichloromethane, filtered through diatomaceous earth and then diluted with an equal volume of ethanol. The solution was slowly concentrated on a rotary evaporator to afford a pale yellow precipitate, which was collected on a sintered funnel and washed with ethanol (2 x 10 mL) and *n*-pentane. Yield: 0.139 g (0.180 mmol, 72%). IR (CH_2Cl_2): 2401 ν_{BH}, 2193 ν_{BHRu}, 1947 ν_{CO} cm^{-1}. IR (ATR): 1939 ν_{CO} cm^{-1}. ^{1}H NMR (400 MHz, $CDCl_3$): δ_H = –3.09 (br, 1H, BHRu), 3.15 (s, 3H, CH_3), 3.54 (s, 3H, CH_3), 6.33 (d, 1H, $^3J_{HH}$ = 1.5, NCH=CH), 6.50 (d, 1H, $^3J_{HH}$ = 1.6, NCH=CH), 6.65 (s, 2H, NCH=CH), 6.80–6.83 (m, 2H, C_6H_4), 7.00–7.02 (m, 2H, C_6H_4), 7.15–7.17 (m, 9H, C_6H_5), 7.50–7.54 (m, 6H, C_6H_5). ^{13}C{^{1}H} NMR (100 MHz, $CDCl_3$): δ_C = 34.5 (CH_3), 34.9 (CH_3), 110.8 [$C^{2,5}(C_6H_4)$], 120.2 [$C^{3,4}(C_6H_4)$], 120.1 (NCH=CH), 121.3 (NCH=CH), 121.4 (NCH=CH), 121.5 (NCH=CH), 127.4 (d, $^{2,3}J_{CP}$ = 9.6, $^{m/o}C_6H_5$), 129.0 (d, $^4J_{CP}$ = 2.2, $^pC_6H_5$), 133.7 (d, $^{2,3}J_{CP}$ = 10.3, $^{m/o}C_6H_5$), 135.9 (d, $^1J_{CP}$ = 44.2, $^iC_6H_5$), 150.6 [$C^{1,6}(C_6H_4)$], 164.5 (CS), 165.4 (CS), 200.5 (d, $^2J_{PC}$ = 12.8, CO). ^{31}P{^{1}H} NMR (162 MHz, $CDCl_3$): δ_P = 47.2. ^{11}B{^{1}H} NMR (128.4 MHz, $CDCl_3$): δ_B = –5.4 (BH_2), 52.3 (BCat). ^{11}B NMR (128 MHz, $CDCl_3$) δ_B = –4.98, 53.5 (BCat). MS-ESI(+): *m/z* = 773.0702 [M + Na]$^+$. Calcd. for $C_{33}H_{31}{}^{11}B_2N_4O_3P^{102}Ru^{23}NaS_2$: 773.0703; 750.0806

$[M]^+$ Calcd. for $C_{33}H_{31}{}^{11}B_2N_4O_3PS_2{}^{102}Ru$ 750.0805. Anal. Found: C, 52.63; H, 3.94, N, 7.39. Calcd. for $C_{33}H_{31}B_2N_4O_3PRuS_2$: C, 52.89; H, 4.17; N, 7.48%.

Synthesis of $[Ru(SiCl_3)Cl(CO)(PPh_3)_2]$ (2.5a)

The following procedure is based on that published for the corresponding osmium analogue.[7] Trichlorosilane (0.50 mL, 6.20 mmol) was added drop-wise to a suspension of $[RuHCl(CO)(PPh_3)_3]$ (2.00 g, 2.10 mmol) in toluene (100 mL). The reaction mixture was heated to 60°C with stirring for 30 min. The solvent was reduced *in vacuo* to approximately 10 mL and *n*-hexane (20 mL) was added to afford a yellow, fine, crystalline product, which was isolated by cannula filtration and dried *in vacuo*. Yield: 1.474 g (1.79 mmol, 85%). IR (ATR): 1989 ν_{CO} cm^{-1}. ^1H NMR (400 MHz, C_6D_6): δ_H = 7.01–7.86 (m, 30H, C_6H_5). $^{13}C\{^1H\}$ NMR (100 MHz, C_6D_6): δ_C = 128.7 (t, $^{2,3}J_{CP}$ = 4.9, $^{m/o}C_6H_5$), 130.8 ($^pC_6H_5$), 131.2 (t, $^1J_{CP}$ = 23.4, $^iC_6H_5$), 135.2 (d, $^{2,3}J_{CP}$ = 5.5, $^{m/o}C_6H_5$), 198.7 (t, $^2J_{CP}$ = 12.5, CO). $^{31}P\{^1H\}$ NMR (162 MHz, C_6D_6): δ_P = 34.8. MS-ESI(+) *m/z*: 829.9882 $[M - Cl + CH_3CN]^+$ Calcd. for $C_{39}H_{33}NOSiP_2{}^{35}Cl_2{}^{37}Cl{}^{102}Ru$: 829.9886; 827.9908 $[M - Cl + CH_3CN]^+$. Calcd. for $C_{39}H_{33}NOSiP_2{}^{35}Cl_3{}^{102}Ru$: 827.9916. Anal. Calc. for $C_{37}H_{30}Cl_4OP_2SiRu$: C, 53.96; H, 3.67%. Anal Found: C, 54.07; H, 3.73%

Synthesis of $[Ru(SiCl_3)(CO)(PPh_3)\{\kappa^3$-*H,S,S'*-$H_2B(mt)_2\}]$ (2.5)

A mixture of $[Ru(SiCl_3)Cl(CO)(PPh_3)_2]$ (**2.5a**: 0.100 g, 0.12 mmol) and $Na[H_2B(mt)_2]$ (0.032 g, 0.12 mmol) was stirred in tetrahydrofuran (10 mL) at room temperature for 2 h. The solvent was removed *in vacuo* and the yellow residue was re-dissolved in dichloromethane, filtered through diatomaceous earth and *n*-hexane (10 mL) was added to afford a yellow precipitate, which was isolated *via* filtration, washed with *n*-hexane (2 × 10 mL) and dried *in vacuo*. Yield: 0.056 g (0.073 mmol, 61%). IR (Nujol): 2416 ν_{BH}, 2042 ν_{BHRu}, 1970 ν_{CO} cm^{-1}. ^1H NMR (400 MHz, C_6D_6): δ_H = –5.74 (br, 1H, BHRu), 2.42 (s, 3H, NCH_3), 2.58 (s, 3H, NCH_3), 5.34 (d, 1H, $^3J_{HH}$ = 2.0, NCH=CH), 5.56 (d, 1H, $^3J_{HH}$ = 2.0, NCH=CH), 5.78 (d, 1H, $^3J_{HH}$ = 2.0, NCH=CH), 6.08 (d, 1H, $^3J_{HH}$ = 2.0, NCH=CH), 6.94–7.05, (m, 18H, C_6H_5). $^{31}P\{^1H\}$ NMR (162 MHz, C_6D_6): δ_P = 40.7. $^{11}B\{^1H\}$ NMR (128 MHz, C_6D_6): δ_B = –4.7. MS-ESI(+) *m/z*: 737.1429 $[M - 2Cl + CH_3CN]^+$. Calcd. for $C_{29}H_{30}BClN_5OPRuS_2Si$

737.0389. Anal. Found: C, 46.33; H, 4.06, N, 6.92. Calcd. for $C_{27}H_{27}BCl_3N_4OS_2PRuSi.C_6H_6$: C, 47.01; H, 3.95; N, 6.65%.

The complex **2.5** decomposes in dichloromethane/ethanol to afford *inter alia* the binuclear complex $[Ru_2(\mu\text{-Hmt})_2Cl_4(CO)_2(PPh_3)_2]$ (**2.5x**), which was characterised crystallographically. *Crystal data for* **2.5x**: $C_{46}H_{42}Cl_4N_4O_2P_2Ru_2S_2$, M_w = 1152.83, monoclinic, $P2_1/c$, a = 15.3765(2), b = 9.48940(1), c = 16.8296(3) Å, β = 106.263(2)°, V = 2357.41(6) Å^3, Z = 2, ρ_{calcd} = 1.624 Mgm^{-3}, μ(Cu $K\alpha$) = 9.09 mm^{-1}, T = 150(2) K, orange plate, 0.28 × 0.13 × 0.05 mm, 4750 independent reflections. F^2 refinement, R = 0.028, wR = 0.073 for 4345 reflections ($I > 2.0\sigma(I)$, $2\theta_{max}$ = 140°), 284 parameters, 0 restraints, CCDC 1540167.

Synthesis of $[Ru(SiMe_3)(CO)(PPh_3)\{\kappa^3\text{-}H,S,S'\text{-}H_2B(mt)_2\}]$ (2.6)

A mixture of $[Ru(SiMe_3)Cl(CO)(PPh_3)_2]$ (0.200 g, 0.262 mmol) and $Na[H_2B(mt)_2]$ (0.070 g, 0.267 mmol) was stirred in tetrahydrofuran (20 mL) at room temperature for 4 h. The solvent was reduced *in vacuo*, and *n*-hexane (10 mL) was added to afford a yellow precipitate, which was isolated *via* filtration, washed with *n*-hexane (2 × 10 mL) and dried *in vacuo*. Yield: 0.052 g (0.073 mmol, 39%). IR (ATR): 2389 ν_{BH}, 2197 ν_{BHRu}, 1906 ν_{CO} cm^{-1}. ^{1}H NMR (400 MHz, $CDCl_3$): δ_H = –3.50 (br, 1H, BHRu), 0.21 (s, 9H, $SiCH_3$), 3.13 (s, 3H, NCH_3), 3.60 (s, 3H, NCH_3), 6.26 (d, 1H, $^3J_{HH}$ = 2.0, NCH=CH), 6.34 (d, 1H, $^3J_{HH}$ = 2.1, NCH=CH), 6.55 (d, 1H, $^3J_{HH}$ = 2.1, NCH=CH), 6.63 (d, 1H, $^3J_{HH}$ = 2.0, NCH=CH), 7.24–7.26 (m, 7H, C_6H_5), 7.33 (br s, 1H, C_6H_5), 7.55–7.60 (m, 7H, C_6H_5). ^{13}C{^{1}H} NMR (100 MHz, $CDCl_3$): δ_C = 8.2 ($SiCH_3$), 34.4 (NCH_3), 34.9 (NCH_3), 119.8 (NCH=CH), 120.9 (NCH=CH), 121.0 (NCH=CH), 121.4 (NCH=CH), 127.3 (d, $^{2,3}J_{CP}$ = 9.4, $^{m/o}C_6H_5$), 129.0 (d, $^4J_{CP}$ = 2.3, $^pC_6H_5$), 134.2 (d, $^{2,3}J_{CP}$ = 10.0, $^{m/o}C_6H_5$), 136.6 (d, $^1J_{CP}$ = 41.4, $^iC_6H_5$), 165.4 (CS), 166.2 (CS), 202.7 (s, CO). ^{31}P{^{1}H} NMR (162.0 MHz, $CDCl_3$): δ_P = 48.7. ^{11}B NMR (128 MHz, $CDCl_3$): δ_B = –4.81 (br). ^{11}B{^{1}H} NMR (128 MHz, $CDCl_3$): δ_B = –4.51 (br). MS-ESI(+) *m/z*: 768.1137 $[M + Na + CH_3CN]^+$. Calcd. for $C_{32}H_{39}BNaN_5OPRuS_2Si$ 768.1137. MS-ESI(+) *m/z*: 704.0968 $[M]^+$. Calcd. for $C_{30}H_{36}{}^{11}BN_4OSiPS_2{}^{102}Ru$ 704.0974. Anal. Found: C, 51.25; H, 5.27, N, 7.83. Calcd. for $C_{30}H_{36}BN_4OS_2PRuSi$: C, 51.20; H, 5.16; N, 7.96%

Reaction of $Na[H_2B(mt)_2]$ with $[Ru(Ph)Cl(CO)(PPh_3)_2]$; Observation of $[Ru(Ph)(CO)(PPh_3)\{\kappa^3\text{-}H,S,S'\text{-}H_2B(mt)_2\}]$ (2.7)

In an NMR tube, $Na[H_2B(mt)_2]$ (0.005 g, 0.019 mmol), $[Ru(Ph)Cl(CO)(PPh_3)_2]$ (0.015 g, 0.020 mmol) and $CDCl_3$ (0.5 mL) were combined and the mixture monitored by $^{31}P\{^1H\}$ and ^1H NMR spectroscopy. At 9 min, a major singlet resonance was observed at 46.4 ppm in the $^{31}P\{^1H\}$ NMR spectrum as well as minor peaks at 52.7 and 19.3 ppm. The latter resonances increased in intensity with the decrease in the former over 60 h at room temperature. The $[Ru(Ph)(CO)(PPh_3)\{\kappa^3\text{-}H,S,S'\text{-}H_2B(mt)_2\}]$ **2.7** intermediate was observed in mass spectrometry taken at t ≈ 0. Both the intermediate **2.7** and eventually major product $[Ru\{\kappa^3\text{-}B,S,S'\text{-}BH(mt)_2\}(CO)(PPh_3)_2]$ (Ru→B) (**3.1**) were observed *via* IR spectroscopy at t ≈ 0. MS-ESI(+) *m/z*: 731.0783 $[M + Na]^+$. Calcd. for $C_{33}H_{32}{}^{11}BN_4O^{23}NaPS_2{}^{102}Ru$: 731.0789. IR ($CH_2Cl_2$, **2.7**): 2092 ν_{BHRu}, 1934 ν_{CO} cm^{-1}. IR (CH_2Cl_2, **3.1**): 2398 ν_{BH}, 1901 ν_{CO} cm^{-1}. $^{11}B\{^1H\}$ NMR (128 MHz, $CDCl_3$): δ_B = –6.59 (**2.7**), 4.09 (**3.1**).

Reaction of $Na[H_2B(mt)_2]$ with $[Ru(CH=CHPh)Cl(CO)(PPh_3)_2]$; Observation of $[Ru(CH=CHPh)(CO)(PPh_3)\{H_2B(mt)_2\}]$ (2.8)

In an NMR tube, $Na[H_2B(mt)_2]$ (0.005 g, 0.019 mmol), $[Ru(CH=CHPh)Cl(CO)(PPh_3)_2]$ (0.015 g, 0.019 mmol) and $CDCl_3$ (0.5 mL) were combined and the mixture monitored by $^{31}P\{^1H\}$ and ^1H NMR spectroscopy. Within 5 min, numerous resonances (>8) were observed in the $^{31}P\{^1H\}$ NMR spectrum (main resonance at δ_P 44.9) and broad hydride resonances at δ_H –6.6 and –8.5 in the ^1H NMR spectrum. The presence of free styrene could not be ascertained due to the abundance of resonances in the aromatic region. Over the next 24 h broad resonances at δ_P 52.7 and 19.3 increased in intensity suggesting the formation of $[Ru\{\kappa^3\text{-}B,S,S'\text{-}BH(mt)_2\}(CO)(PPh_3)_2]$ (Ru→B) (**3.1**). Both the intermediate $[Ru(CH=CHPh)(CO)(PPh_3)\{\kappa^3\text{-}H,S,S'\text{-}H_2B(mt)_2\}]$ (**2.8**) and eventually major product **3.1** were observed *via* mass spectrometry and IR spectroscopy at t ≈ 0. MS-ESI(+) *m/z*: 757.0950 $[M_{int} + Na]^+$. Calcd. for $C_{35}H_{34}{}^{11}BN_4O^{23}NaPS_2{}^{102}Ru$: 757.0946; 1491.1986 $[2M_{int} + Na]^+$. Calcd. for $C_{70}H_{68}{}^{11}B_2N_8O_2{}^{23}NaP_2S_4{}^{102}Ru_2$: 1491.1994. 893.1412 $[M_{prod} + H]^+$. Calcd. for $C_{45}H_{42}{}^{11}BN_4OP_2S_2{}^{102}Ru$: 893.1412. IR ($CH_2Cl_2$, **2.8**): 2089 ν_{BHRu},

1943 ν_{CO} cm^{-1}. IR (CH_2Cl_2, **3.1**): 2396 ν_{BH}, 1900 ν_{CO} cm^{-1}. $^{11}B\{^1H\}$ NMR (128 MHz, $CDCl_3$): δ_B = –5.82 (**2.8**), 4.53 (**3.1**).

Synthesis of [OsH(CO)(PPh_3){κ^3-*H,S,S'*-$H_2B(mt)_2$}] (2.9)

A mixture of [OsHCl(CO)(PPh_3)$_3$] (0.199 g, 0.234 mmol) and Na[$H_2B(mt)_2$] (0.068 g, 0.258 mmol) was combined in tetrahydrofuran (20 mL). The mixture was heated under reflux with stirring for 1.5 h, allowed to cool, and the solvent was removed on the rotary evaporator. The crude residue was dissolved in dichloromethane, filtered through diatomaceous earth, diluted with ethanol (equivalent volume) and concentrated on the rotary evaporator to afford a white precipitate, which was collected on a sintered funnel. The white solid was washed with ethanol (2 x 10 mL) and *n*-pentane. Yield: 0.123 g (0.171 mmol, 73%). IR (ATR): 2399 ν_{BH}, 1952 ν_{OsH}, 1906 ν_{CO} cm^{-1}. IR (CH_2Cl_2): 2408 ν_{BH}, 1955 ν_{OsH}, 1915 ν_{CO} cm^{-1}. ^1H NMR (400 MHz, $CDCl_3$): δ_H = –13.23 (d, 1H, $^2J_{HP}$ = 18.2, OsH), –6.82 (br, 1H, OsHB), 3.07 (s, 3H, CH_3), 3.55 (s, 3H, CH_3), 6.44 (d, 1H, $^3J_{HH}$ = 2.0, NCH=CH), 6.50 (d, 1H, $^3J_{HH}$ = 1.9, NCH=CH), 6.63 (d, 1H, $^3J_{HH}$ = 2.0, NCH=CH), 6.83 (d, 1H, $^3J_{HH}$ = 1.9, NCH=CH), 7.23–7.26 (m, 9H, C_6H_5), 7.54–7.59 (m, 6H, C_6H_5). $^{13}C\{^1H\}$ NMR (100 MHz, $CDCl_3$): δ_C = 34.1 (CH_3), 34.6 (CH_3), 120.9 (NCH=CH), 121.0 (NCH=CH), 121.4 (NCH=CH), 122.5 (NCH=CH), 127.3 (d, $^{2,3}J_{CP}$ = 9.7, $^{m/o}C_6H_5$), 129.0 (d, $^4J_{CP}$ = 2.3, $^pC_6H_5$), 134.1 (d, $^{2,3}J_{CP}$ = 10.1, $^{m/o}C_6H_5$), 136.9 (d, $^1J_{CP}$ = 50.2, $^iC_6H_5$), 167.4 (CS), 170.6 (CS), 182.2 (d, $^2J_{CP}$ = 9.7, CO). $^{31}P\{^1H\}$ NMR (162 MHz, $CDCl_3$): δ_P = 19.7. $^{11}B\{^1H\}$ NMR (128 MHz, $CDCl_3$): δ_B = –6.42. ^{11}B NMR (128 MHz, $CDCl_3$): δ_B = –6.47 (br s). MS(+)-ESI *m/z* = 745.1048 $[M + Na]^+$ Calcd. For $C_{27}H_{28}{}^{11}BN_4O^{23}NaPS_2{}^{192}Os$ = 745.1048; 721.1072 $[M – H]^+$. Calcd. for $C_{27}H_{27}{}^{11}BN_4OPS_2{}^{192}Os$ = 721.1072. Anal. Found: C, 44.50; H, 3.76, N, 7.62. Calcd. for $C_{27}H_{28}BN_4OOsPS_2$: C, 45.00; H, 3.92; N, 7.77%.

7.2.2 Poly(methimazolyl)borane Complexes of Ruthenium

Synthesis of [Ru{κ³-*B,S,S'*-BH(mt)₂}(CO)(PPh₃)₂] (Ru→B) (3.1)

Method 1: A suspension of [Ru(Ph)Cl(CO)(PPh$_3$)$_2$] (0.500 g, 0.65 mmol) and Na[H$_2$B(mt)$_2$] (0.175, 0.67 mmol) in diethyl ether (50 mL) was stirred for 15 h, by which time the suspension had lightened from an orange colour to beige. The solvent was removed *in vacuo* and the resulting residue was re-dissolved in dichloromethane (30 mL). The filtrate was transferred to another Schlenk flask by cannula filtration. An equal volume of ethanol was added, and the solvent was removed slowly under reduced pressure to afford a beige precipitate that was filtered and dried under high vacuum. Yield: 0.198 g (0.222 mmol, 34%).

Method 2: A suspension of [RuHCl(CO)(PPh$_3$)$_3$] (1.000 g, 1.05 mmol) and phenylacetylene (0.3 mL, 2.73 mmol) in dichloromethane (35 mL) was stirred for 1.5 h, by which time the solution had turned a deep red colour and Na[H$_2$B(mt)$_2$] (0.275 g, 1.05 mmol) was added. The reaction was stirred for a further 18 h, and the filtrate isolated by cannula filtration. The solvent was concentrated *in vacuo* to ≈5 mL. Diethyl ether (20 mL) was added to the yellow oily residue, to afford a pale yellow solid that was isolated by cannula filtration. Petroleum ether was added and the solid collected on a sintered funnel, washed with diethyl ether and petroleum ether, then dried under high vacuum. Yield: 0.570 g (0.639 mmol, 61%). Crystals suitable for crystallographic analysis were obtained from slow evaporation of a concentrated solution of **3.1** in diethyl ether over one day.

IR (ATR): 2316 ν_{BH}, 1893 ν_{CO} cm^{-1}. IR (CH_2Cl_2): 2397 ν_{BH}, 1899 ν_{CO} cm^{-1}. ^{1}H NMR (400 MHz, $CDCl_3$): δ_H = 3.07 (s, 3H, CH_3), 3.33 (s, 3H, CH_3), 4.07 (v. br s, 1H, BH), 6.04 (d, 1H, $^3J_{HH}$ = 1.8, NCH=CH), 6.15 (d, 1H, $^3J_{HH}$ = 1.8, NCH=CH), 6.50 (d, 1H, $^3J_{HH}$ = 1.7, NCH=CH), 6.58 (d, 1H, $^3J_{HH}$ = 1.8, NCH=CH), 6.97–7.07 (m, 9H, C_6H_5), 7.22–7.26 (m, 9H, C_6H_5), 7.40–7.47 (m, 12H, C_6H_5). ^{13}C{^{1}H} NMR (176 MHz, $CDCl_3$): δ_C = 33.7 (CH_3), 34.1 (CH_3), 119.8 (NCH=CH), 120.3 (NCH=CH), 120.7 (NCH=CH), 120.9 (NCH=CH), 126.4 (d, $^{2,3}J_{CP}$ = 8.8, $^{m/o}C_6H_5$), 127.5 (br, $^{m/o}C_6H_5$ PPh_3 *trans* to B), 128.1 (d, $^4J_{CP}$ = 1.8, $^pC_6H_5$), 128.5 ($^pC_6H_5$ PPh_3 *trans* to B), 134.3 (d, $^{2,3}J_{CP}$ = 14.1, $^{m/o}C_6H_5$ PPh_3 *trans* to B), 134.5 (d, $^{2,3}J_{CP}$ = 8.8, $^{m/o}C_6H_5$), 137.1 (d, $^1J_{CP}$ = 19.4, $^iC_6H_5$ PPh_3 *trans* to B), 137.9 (d, $^1J_{CP}$ = 40.5, $^iC_6H_5$), 163.6 (CS), 164.8 (CS), 208.5 (d, $^2J_{CP}$ = 15.6, CO). ^{31}P{^{1}H} NMR (162 MHz, $CDCl_3$): δ_P = 52.7 (br s, PPh_3 *trans* to S), 19.3 (br s, PPh_3 *trans* to B). ^{11}B{^{1}H} NMR (128 MHz,

$CDCl_3$): δ_B = 4.12 (br s). ^{11}B NMR (128 MHz, $CDCl_3$): δ_B = 3.81 (br s). MS-ESI(+) *m/z*: 895.2 $[M - CO + OMe]^+$. Accurate mass: found 895.1592 $[M - CO + OMe]^+$, Calcd. for $C_{45}H_{44}{}^{11}BN_4OP_2S_2{}^{102}Ru$ 895.1568. Anal. found: C, 60.52; H, 4.77; N, 6.13%. Calcd. for $C_{45}H_{41}BN_4OP_2RuS_2$: C, 60.61; H, 4.63; N, 6.28%.

At 185K. Crystal data for $C_{45}H_{41}BN_4OP_2RuS_2.C_4H_{10}O$: M_w = 965.93, monoclinic, *P* $2_1/n$, *a* = 12.2007(3) Å, *b* = 24.2676(5) Å, *c* = 15.8232(3) Å, β = 99.4773(19) °, *V* = 4621.02(9) Å^3, Z = 4, ρ_{calcd} = 1.388 Mg m^{-3}, μ(Mo *K*α) = 0.54 mm^{-1}, *T* = 185(2) K, clear pale yellow block, 0.14 x 0.10 x 0.06 mm, 10695 independent reflections. F^2 refinement, *R* = 0.037, *wR* = 0.070 for 8455 reflections ($I > 2.0\sigma(I)$, $2\theta_{max}$ = 60°), 553 parameters, 0 restraints.

At 150K. Crystal data for $C_{45}H_{41}BN_4OP_2RuS_2.C_4H_{10}O$: M_w = 965.93, monoclinic, *P*$2_1/n$, *a* = 12.2141(1) Å, *b* = 24.2890(2) Å, *c* = 15.8351(1) Å, β = 99.4996(7)°, *V* = 4633.35 (3) Å^3, Z = 4, ρ_{calcd} = 1.385 Mg m^{-3}, μ(Cu *K*α) = 4.57 mm^{-1}, *T* = 150(2) K, clear pale yellow block, 0.12 x 0.08 x 0.08 mm, 9370 independent reflections. F^2 refinement, *R* = 0.023, *wR* = 0.058 for 9370 reflections ($I > 2.0\sigma(I)$, $2\theta_{max}$ = 144°), 553 parameters, 0 restraints.

Side product crystal [Ru(Ph)(κ^2-*N,S*-mt)(CO)(PPh_3)$_2$] **3.1x**

Crystal data for $C_{47}H_{40}N_2OP_2RuS$: M_w = 843.93, monoclinic, *P* $2_1/n$, *a* = 13.1748(1), *b* = 18.1695(1), *c* = 17.5732(1) Å, β = 110.7668(8)°, *V* = 3933.36(2) Å^3, Z = 4, ρ_{calcd} = 1.425 Mg m^{-3}, μ(Cu *K*α) = 4.79 mm^{-1}, *T* = 150(2) K, clear light yellow needle, 0.22 x 0.05 x 0.04 mm, 7972 independent reflections. F^2 refinement, *R* = 0.024, *wR* = 0.062 for 7260 reflections ($I > 2.0\sigma(I)$, $2\theta_{max}$ = 60°), 487 parameters, 0 restraints.

Side product crystal [Ru(C≡CPh)(CO)(PPh_3){κ^3-*H,S,S'*-$H_2B(mt)_2$}] **3.1y**

Crystal data for $C_{35}H_{32}BN_4OPRuS_2.CHCl_3$: M_w = 850.98, triclinic, *P*-1 (No.2), *a* = 9.9810(7), *b* = 11.0018(6), *c* = 19.3279(8) Å, α = 73.725(4)°, β = 82.147(4)°, γ = 65.670(6)°, *V* = 1855.8(2) Å^3, Z = 2, ρ_{calcd} = 1.523 Mg m^{-3}, μ(Cu *K*α) = 7.15 mm^{-1}, *T* = 150(2) K, yellow prism, 0.11 x 0.08 x 0.04 mm, 7474 independent reflections. F^2 refinement, *R* = 0.032, *wR* = 0.083 for 6775 reflections ($I > 2.0\sigma(I)$, $2\theta_{max}$ = 144°), 450 parameters, 0 restraints.

Reaction of [Ru{κ³-*B,S,S'*-BH(mt)₂}(CO)(PPh₃)₂] (Ru→B) and HCl (3.2)

An ethereal solution of hydrogen chloride (0.25 mL, 1M, 0.25 mmol) was added to a stirred solution of **3.1** (0.200 g, 0.22 mmol) in tetrahydrofuran for 24 h. The $^{31}P\{^{1}H\}$ NMR revealed a mixture of products at 55.2, 50.0, 45.2, 35.7, 28.1, 19.1 and free triphenylphosphine. The solvent was removed using a rotary evaporator and the orange residue was recrystallized from chloroform and *n*-pentane. The crystals were collected on a sintered frit and dried in air to give a mixture of the products below. Combined yield: 0.073 g.

First side product $[RuCl_2(CO)(PPh_3)_2(Hmt)]$ **3.2x**:

MS-ESI(+) *m/z*: 803.1 $[M - Cl]^+$, 844.1 $[M - Cl + MeCN]^+$. Accurate mass: found 803.0754 $[M - Cl]^+$, Calcd. for $C_{41}H_{36}N_2OCl_2P_2S^{102}Ru$ 803.0750; found 844.1021 $[M - Cl + MeCN]^+$, Calcd. for $C_{43}H_{39}N_3OClP_2S^{102}Ru$ 844.1016.

Crystal data for $C_{41}H_{36}Cl_2N_2OP_2RuS.CHCl_3$: M_w = 958.11, monoclinic, $P2_1/c$, a = 11.5279(1), b = 20.9802(1), c = 18.3591(2) Å, V = 4222.02(5) Å^3, Z = 4, ρ_{calcd} = 1.507 Mg m^{-3}, μ(Cu $K\alpha$) = 7.38 mm^{-1}, T = 150(2) K, orange needle, 0.18 x 0.05 x 0.05 mm, 8525 independent reflections. F^2 refinement, R = 0.031, wR = 0.078 for 7799 reflections ($I > 2.0\sigma(I)$, $2\theta_{max}$ = 144°), 490 parameters, 0 restraints.

Second side product $[RuCl_2(CO)(PPh_3)(Hmt)_2]$ **3.2y**:

Washing the isolated mixture with chloroform and filtering under vacuum suction afforded a second product. IR (ATR): 3028 ν_{CH}, 1961 ν_{CO} cm^{-1}. ^{1}H NMR (400 MHz, $CDCl_3$): δ_H = 3.42 (s, 6H, CH_3), 6.61 (t, 2H, $^3J_{HH}$ = 2.3, NCH=CH), 6.75 (t, 2H, $^3J_{HH}$ = 2.4, NCH=CH), 7.30–7.33 (m, 9H, C_6H_5), 7.79–7.82 (m, 6H, C_6H_5), 12.92 (br s, 2H, NH). $^{13}C\{^1H\}$ NMR (100 MHz, $CDCl_3$): δ_C = 34.2 (CH_3), 115.2 (NCH=CH), 119.5 (NCH=CH), 127.6 (d, $^{2,3}J_{CP}$ = 10.0, $^{m/o}C_6H_5$), 129.7 (d, $^4J_{CP}$ = 3.0, $^pC_6H_5$), 133.8 (d, $^1J_{CP}$ = 48.3, $^iC_6H_5$), 134.5 (d, $^{2,3}J_{CP}$ = 9.1, $^{m/o}C_6H_5$), 158.1 (CS). $^{31}P\{^1H\}$ NMR (162 MHz, $CDCl_3$): δ_P = 45.1. MS-ESI(+) *m/z*: 689.1 $[M - H]^+$, 655.0 $[M - Cl]^+$. Accurate mass: found 655.0102 $[M - Cl]^+$, Calcd. for $C_{27}H_{27}N_4OClPS_2{}^{102}Ru$ 655.0104.

Crystal data for $C_{27}H_{27}Cl_2N_4OPRuS_2$: M_w = 690.58, monoclinic, *Cc*, a = 9.2352(4), b = 16.5996(6), c = 18.7713(7) Å, β = 94.733(4)°, V = 2867.84(19) Å^3, Z = 4, ρ_{calcd} = 1.599 Mg m^{-3}, μ(Mo $K\alpha$) = 0.96 mm^{-1}, T = 150(2) K, yellow block, 0.18 x 0.12 x 0.06 mm, 5442

independent reflections. F^2 refinement, R = 0.029, wR = 0.065 for 5212 reflections ($I > 2.0\sigma(I)$, $2\theta_{max}$ = 144°), 345 parameters, 2 restraints.

Synthesis of [Ru{κ³-*B,S,S'*-BH(mt)₂}(CO)₂(PPh₃)] (Ru→B) (3.3)

Carbon monoxide (1 atm) was bubbled through a stirred solution of **3.1** (0.205 g, 0.23 mmol) in dichloromethane for 15 min. The solvent was removed *in vacuo* to give a yellow residue, which was then suspended in diethyl ether (10 mL). The yellow solid was isolated by cannula filtration, washed with *n*-pentane (20 mL) and dried under vacuum. Yield: 0.079 g (0.120 mmol, 52%). Crystals suitable for crystallographic analysis were obtained from slow evaporation of a concentrated solution of **3.3** in chloroform/*n*-pentane over one day. IR (ATR): 2344 ν_{BH}, 1984, 1913 ν_{CO} cm^{-1}. ^{1}H NMR (700 MHz, $CDCl_3$): δ_H = 3.43 (s, 6H, CH_3), 6.62 (s, 2H, NCH=CH), 6.69 (s, 2H, NCH=CH), 7.36–7.39 (m, 9H, C_6H_5), 7.52–7.55 (m, 6H, C_6H_5). ^{13}C{^{1}H} NMR (176 MHz, $CDCl_3$): δ_C = 34.4 (CH_3), 120.9 (NCH=CH), 122.1 (NCH=CH), 128.3 (d, $^{2,3}J_{CP}$ = 8.8, $^{m/o}C_6H_5$), 129.4 (d, $^4J_{CP}$ = 1.2, $^pC_6H_5$), 133.6 (d, $^{2,3}J_{CP}$ = 13.2, $^{m/o}C_6H_5$), 136.3 (d, $^1J_{CP}$ = 27.1, $^iC_6H_5$), 163.9 (d, $^3J_{CP}$ = 20.2, CS), 202.9 (d, $^2J_{CP}$ = 2.4, CO). ^{31}P{^{1}H} NMR (162 MHz, $CDCl_3$): δ_P = 20.1. ^{11}B NMR (128 MHz, $CDCl_3$): δ_B = 2.97 (br s). MS-ESI(+) *m/z*: 648.1 $[M - B]^+$, 659.0 $[M + H]^+$. Accurate mass: found 659.0441 $[M + H]^+$, Calcd. for $C_{28}H_{27}{}^{11}BN_4O_2PS_2{}^{102}Ru$ 659.0450. Anal. found: C, 51.29; H, 3.95; N, 8.37%. Calcd. for $C_{28}H_{26}BN_4O_2PRuS_2$: C, 51.15; H, 3.99; N, 8.52%.

Crystal data for $C_{28}H_{26}BN_4O_2PRuS_2.CHCl_3$: M_w = 776.90, monoclinic, $P2_1/c$, a = 9.7228(1), b = 18.6012(1), c = 17.8876(1) Å, V = 3205.42(2) Å^3, Z = 4, ρ_{calcd} = 1.610 Mg m^{-3}, μ(Cu $K\alpha$) = 8.24 mm^{-1}, T = 150(2) K, yellow trapezoid, 0.31 x 0.25 x 0.16 mm, 6486 independent reflections. F^2 refinement, R = 0.029, wR = 0.078 for 7799 reflections ($I > 2.0\sigma(I)$, $2\theta_{max}$ = 144°), 391 parameters, 0 restraints.

Synthesis of [Ru{κ³-*B,S,S'*-BH(mt)₂}(CO)(PMe₂Ph)(PPh₃)] (Ru→B) (3.4)

A solution of **3.1** (0.203 g, 0.23 mmol) and PMe_2Ph (0.1 mL, 0.70 mmol) in tetrahydrofuran (20 mL) was stirred for 4 h. The solvent was removed *in vacuo* to give an oily orange residue and diethyl ether (20 mL) was added to afford a pale yellow solid

that was isolated by cannula filtration. The solid was suspended in *n*-pentane and collected on a sinter funnel, washed with *n*-pentane, then dried under high vacuum. Yield: 0.059 g (0.077 mmol, 34%). IR (ATR): 3044 ν_{CH}, 2363 ν_{BH}, 1890 ν_{CO} cm^{-1}. IR (THF): 2337 ν_{BH}, 1902 ν_{CO} cm^{-1}. ^{1}H NMR (400 MHz, $CDCl_3$): δ_H = 1.28 (d, 3H, $^{2}J_{HP}$ = 5.5, PCH_3), 1.43 (d, 3H, $^{2}J_{HP}$ = 5.3, PCH_3), 3.00 (s, 3H, NCH_3), 3.43 (s, 3H, NCH_3), 6.19 (d, 2H, $^{3}J_{HH}$ = 2.6, NCH=CH), 6.60 (s, 2H, NCH=CH), 7.07–7.13 (m, 9H, C_6H_5), 7.30–7.52 (m, 14H, C_6H_5). $^{13}C\{^{1}H\}$ NMR (176 MHz, $CDCl_3$): δ_C = Decomposition in $CDCl_3$ confounded the acquirement of $^{13}C\{^{1}H\}$ NMR data. $^{31}P\{^{1}H\}$ NMR (162 MHz, $CDCl_3$): δ_P = 56.9 (d, $^{1}J_{PC}$ = 11.3, PMe_2Ph), –17.2 (br s, PPh_3). $^{11}B\{^{1}H\}$ NMR (128 MHz, $CDCl_3$): δ_B = 5.13 (br s). ^{1}H NMR (400 MHz, CD_2Cl_2): δ_H = 1.25 (d, 3H, $^{2}J_{HP}$ = 5.5, PCH_3), 1.38 (d, 3H, $^{2}J_{HP}$ = 5.3, PCH_3), 2.97 (s, 3H, NCH_3), 3.49 (s, 3H, NCH_3), 6.19 (d, 1H, $^{3}J_{HH}$ = 1.4, NCH=CH), 6.27 (s, 1H, NCH=CH), 6.63 (d, 1H, $^{3}J_{HH}$ = 1.5, NCH=CH), 6.67 (s, 1H, NCH=CH), 7.07–7.16 (m, 9H, C_6H_5), 7.31–7.48 (m, 14H, C_6H_5). $^{31}P\{^{1}H\}$ NMR (162 MHz, CD_2Cl_2): δ_P = 56.2 (br s), –17.7 (br s, PPh_3). MS-ESI(+) *m/z*: 769.1 $[M + H]^+$. Accurate mass: found 769.1099 $[M + H]^+$, Calcd. for $C_{35}H_{38}ON_4{}^{11}BP_2S_2{}^{102}Ru$ 769.1093. Anal. found: C, 55.29; H, 5.02; N, 7.13%. Calcd. for $C_{35}H_{37}BN_4OP_2RuS_2$: C, 54.76; H, 4.86; N, 7.30%.

Synthesis of [Ru{κ³-*B,S,S'*-BH(mt)₂}(CO)(PMe₂Ph)₂] (Ru→B) (3.5)

A solution of **3.1** (0.200 g, 0.22 mmol) and PMe_2Ph (0.3 mL, 2.71 mmol) in tetrahydrofuran (20 mL) was heated under reflux for 18 h. The solvent was reduced to 3 mL and diethyl ether (10 mL) and *n*-pentane (15 mL) was added to afford a pale yellow solid that was isolated by cannula filtration and dried under high vacuum. Yield: 0.079 g (0.123 mmol, 55%). Crystals suitable for crystallographic analysis were obtained from slow evaporation of a concentrated solution of **3.5** in tetrahydrofuran/diethyl ether/*n*-pentane over one day. IR (ATR): 2298 ν_{BH}, 1877 ν_{CO} cm^{-1}. IR (THF): 2323 ν_{BH}, 1902 ν_{CO} cm^{-1}. ^{1}H NMR (700 MHz, $CDCl_3$): δ_H = 1.27 (d, 3H, $^{2}J_{HP}$ = 8.6, PCH_3), 1.38 (d, 3H, $^{2}J_{HP}$ = 5.0, PCH_3), 1.43 (d, 3H, $^{2}J_{HP}$ = 5.4, PCH_3), 1.48 (d, 3H, $^{2}J_{HP}$ = 8.4, PCH_3), 3.40 (s, 3H, NCH_3), 3.44 (s, 3H, NCH_3), 6.48 (d, 1H, $^{3}J_{HH}$ = 1.6, NCH=CH), 6.53 (s, 1H, NCH=CH), 6.58 (s, 1H, NCH=CH), 6.65 (d, 1H, $^{3}J_{HH}$ = 1.7, NCH=CH), 7.09–7.13 (m, 3H, C_6H_5), 7.20–7.22 (m, 2H, C_6H_5), 7.26–7.28 (m, 1H, C_6H_5), 7.31–7.33 (m, 2H, C_6H_5), 7.43–7.46 (m, 2H, C_6H_5). $^{13}C\{^{1}H\}$ NMR (176 MHz, $CDCl_3$): δ_C = 15.6 (dd, $^{1}J_{CP}$ = 31.2, $^{3}J_{CP}$ = 3.3, PCH_3), 16.3 (d, $^{1}J_{CP}$ = 13.6, PCH_3), 18.6 (dd, $^{1}J_{CP}$ = 32.3, $^{3}J_{CP}$ = 4.2, PCH_3), 19.4 (d, $^{1}J_{CP}$ = 16.2, PCH_3), 34.1

(NCH_3), 34.1 (NCH_3), 120.6 (d, $^4J_{CP}$ = 8.4, NCH=CH) overlapping with 120.6 (d, $^4J_{CP}$ = 7.6, NCH=CH), 121.1 (NCH=CH), 121.5 (NCH=CH), 127.3 (d, $^{2,3}J_{CP}$ = 8.2, $^{m/o}C_6H_5$), 128.0 (d, $^{2,3}J_{CP}$ = 7.7, $^{m/o}C_6H_5$), 127.6 ($^pC_6H_5$), 127.8 ($^pC_6H_5$), 129.3 (d, $^{2,3}J_{CP}$ = 7.8, $^{m/o}C_6H_5$), 129.7 (d, $^{2,3}J_{CP}$ = 11.4, $^{m/o}C_6H_5$), 143.2 (dd, $^1J_{CP}$ = 35.1, $^3J_{CP}$ = 5.9, $^iC_6H_5$), 143.3 (d, $^1J_{CP}$ = 20.7, $^iC_6H_5$), 165.0 (d, $^3J_{CP}$ = 23.7, CS), 165.3 (d, $^3J_{CP}$ = 20.2, CS), 207.7 (dd, $^2J_{CP}$ = 15.5, $^2J_{CP}$ = 3.3, CO). ^{31}P NMR (283 MHz, $CDCl_3$): δ_P = 14.5 (br m, coupling not resolved, PMe_2Ph *trans* to S), –16.4 (br s, PMe_2Ph *trans* to B). $^{31}P\{^1H\}$ NMR (283 MHz, $CDCl_3$): δ_P = 14.5 (d, $^1J_{PC}$ = 12.3, PMe_2Ph *trans* to S), –16.4 (br s, PMe_2Ph *trans* to B). ^{11}B NMR (128 MHz, $CDCl_3$): δ_B = 5.00 (br s). MS-ESI(+) *m/z*: 633.0 $[M - B]^+$. Accurate mass: found 1311.1317 $[2M + Na]^+$, Calcd. for $C_{50}H_{66}{}^{11}B_2N_8O_2{}^{23}NaP_4S_4{}^{102}Ru_2$ 1311.1313. Anal. found: C, 46.57; H, 5.28; N, 8.63%. Calcd. for $C_{25}H_{33}BN_4OP_2RuS_2$: C, 46.66; H, 5.17; N, 8.71%.

Crystal data for $C_{25}H_{33}BN_4OP_2RuS_2$: M_w = 643.52, orthorhombic, *Pbca*, *a* = 8.5565(1), *b* = 18.5822(2), *c* = 36.1544(3) Å, *V* = 5748.50(5) Å^3, Z = 8, ρ_{calcd} = 1.487 Mg m^{-3}, μ(Cu *K*α) = 7.03 mm^{-1}, *T* = 150(2) K, clear colourless block, 0.19 x 0.10 x 0.05 mm, 5806 independent reflections. F^2 refinement, *R* = 0.039, *wR* = 0.098 for 5659 reflections ($I > 2.0\sigma(I)$, $2\theta_{max}$ = 144°), 328 parameters, 0 restraints.

Synthesis of [Ru{κ^3-*B,S,S'*-BH(mt)$_2$}(CO){P(OMe)$_3$}$_2$] (Ru→B) (3.6)

A solution of **3.1** (0.202 g, 0.22 mmol) and $P(OMe)_3$ (0.1 mL, 0.85 mmol) in tetrahydrofuran (20 mL) was stirred for 18 h. The solvent was removed *in vacuo* and diethyl ether (10 mL) and *n*-pentane (15 mL) was added to afford a pale yellow solid that was isolated by cannula filtration and dried under high vacuum. Yield: 0.041 g (0.067 mmol, 30%). Crystals suitable for crystallographic analysis were obtained from slow evaporation of a concentrated solution of **3.6** in chloroform/*n*-pentane over one day. IR (ATR): 2358 ν_{BH}, 1921 ν_{CO} cm^{-1}. IR (THF): 2244 ν_{BH}, 1934 ν_{CO} cm^{-1}. ^{1}H NMR (700 MHz, $CDCl_3$): δ_H = 3.49 (s, 3H, NCH_3), 3.49 (s, 3H, NCH_3), 3.56 (d, 9H, $^3J_{HP}$ = 10.8, OCH_3), 3.67 (d, 9H, $^3J_{HP}$ = 11.1, OCH_3), 6.62 (d, 2H, $^4J_{HP}$ = 6.6, NCH=CH), 6.69 (dd, 2H, $^4J_{HP}$ = 8.1, $^3J_{HH}$ = 1.8, NCH=CH). $^{13}C\{^1H\}$ NMR (176 MHz, $CDCl_3$): δ_C = 34.2 (NCH_3), 34.3 (NCH_3), 50.8 [br, $P(OCH_3)_3$ *trans* to B], 52.0 [d, $^2J_{CP}$ = 5.9, $P(OCH_3)_3$ *trans* to S], 120.9 (d, $^4J_{CP}$ = 4.2, NCH=CH), 121.0 (d, $^4J_{CP}$ = 4.1, NCH=CH), 121.5 (d, $^4J_{CP}$ = 1.2, NCH=CH), 121.6 (NCH=CH), 165.3 (d, $^3J_{CP}$ = 24.3, CS), 166.9 (d, $^3J_{CP}$ = 28.4, CS), 207.7 (dd, $^2J_{CP}$ = 18.8, $^2J_{CP}$ = 5.5, CO).

$^{31}P\{^{1}H\}$ NMR (162 MHz, $CDCl_3$): δ_P = 151.1 [d, $^{2}J_{PC}$ = 19.4, $P(OMe)_3$ *trans* to S], 153.7 [br s, $P(OMe)_3$ *trans* to B]. ^{31}P NMR (162 MHz, $CDCl_3$): δ_P = 151.1 [m, $^{2}J_{PC}$ = 10.5, $P(OMe)_3$ *trans* to S], 153.7 [br s, $P(OMe)_3$ *trans* to B]. ^{11}B NMR (128 MHz, $CDCl_3$): δ_B = 3.62 (br s). $^{11}B\{^{1}H\}$ NMR (128 MHz, $CDCl_3$): δ_B = 3.80 (br s). MS-ESI(+) *m/z*: 617.0 $[M + H]^+$. Accurate mass: found 617.0166 $[M + H]^+$, Calcd. for $C_{15}H_{29}{}^{11}BN_4O_7P_2S_2{}^{102}Ru$ 617.0162. Anal. found: C, 29.35; H, 4.71; N, 8.98%. Calcd. for $C_{15}H_{29}BN_4O_7P_2RuS_2$: C, 29.28; H, 4.75; N, 9.10%.

Crystal data for $C_{45}H_{87}B_3N_{12}O_{21}P_6Ru_3S_6$: M_w = 1846.13, triclinic, *P*-1 (No.2), *a* = 9.4439(1), *b* = 15.2581(3), *c* = 26.4419(4) Å, α = 93.1670(14)°, β = 92.0931(12)°, γ = 93.9263(13)°, *V* = 3792.32(6) $Å^3$, Z = 2, ρ_{calcd} = 1.617 Mg m^{-3}, μ(Cu *K*α) = 8.14 mm^{-1}, *T* = 150(2) K, colourless needles, 0.42 x 0.06 x 0.04 mm, 15286 independent reflections. F^2 refinement, *R* = 0.038, *wR* = 0.098 for 13859 reflections ($I > 2.0\sigma(I)$, $2\theta_{max}$ = 144°), 914 parameters, 0 restraints.

Synthesis of [Ru{κ^3-*B,S,S'*-BH(mt)$_2$}(CO)(Z-Ph$_2$PCH=CHPPh$_2$)] (Ru→B) (3.8)

A solution of **3.1** (0.200 g, 0.22 mmol) and Z-PPh_2CH=$CHPPh_2$ (0.090 g, 0.22 mmol) in tetrahydrofuran (20 mL) was heated under reflux for 43 h. The solvent was removed *in vacuo* and diethyl ether was added to the orange residue to give a yellow solid that was isolated by cannula filtration. The solid was redissolved in tetrahydrofuran and layered with *n*-pentane. The filtrate was decanted to afford a yellow precipitate that was dried in air. Yield: 0.042 g (0.055 mmol, 24%). Crystals suitable for crystallographic analysis were obtained from vapour diffusion of *n*-pentane into a concentrated solution of **3.8** in acetone over one day. IR (ATR): 2354 ν_{BH}, 1905 ν_{CO} cm^{-1}. IR (THF): 2338 ν_{BH}, 1923 ν_{CO} cm^{-1}. ^{1}H NMR (700 MHz, $CDCl_3$): δ_H = 2.68 (s, 3H, NCH_3), 3.55 (s, 3H, NCH_3), 6.15 (s, 1H, NCH=CH), 6.51 (s, 1H, NCH=CH), 6.66 (s, 1H, NCH=CH), 6.73 (s, 1H, NCH=CH), 6.97 (br m, 3H, C_6H_5), 7.04–7.07 (m, 2H, C_6H_5), 7.22–7.24 (m, 1H, C_6H_5), 7.28–7.47 (m, 9H, C_6H_5), 7.71–7.79 (m, 3H, C_6H_5), 7.90–7.92 (m, 1H, PCH=CHP), 7.97–7.99 (m, 1H, PCH=CHP), 8.04–8.06 (m, 2H, C_6H_5). $^{13}C\{^{1}H\}$ NMR (151 MHz, $CDCl_3$): δ_C = 33.3 (NCH_3), 34.3 (NCH_3), 120.4 (NCH=CH) overlapping with 120.5 (d, $^{4}J_{CP}$ = 3.0, NCH=CH), 120.8 (d, $^{4}J_{CP}$ = 3.0, NCH=CH), 121.7 (NCH=CH), 125.7 (d, $^{2,3}J_{CP}$ = 9.6, $^{m/o}C_6H_5$), 127.4 ($^{p}C_6H_5$), 128.0 (d, $^{2,3}J_{CP}$ = 9.4, $^{m/o}C_6H_5$), 128.4 (d, $^{2,3}J_{CP}$ = 8.8, $^{m/o}C_6H_5$), 128.5 (d, $^{2,3}J_{CP}$ = 8.4, $^{m/o}C_6H_5$), 128.7 ($^{p}C_6H_5$), 129.4 ($^{p}C_6H_5$), 129.6 ($^{p}C_6H_5$), 131.1 (d, $^{2,3}J_{CP}$ = 8.5, $^{m/o}C_6H_5$), 131.6 (d, $^{2,3}J_{CP}$ = 13.2,

$^{m/o}C_6H_5$), 133.0 (d, $^{2,3}J_{CP}$ = 14.6, $^{m/o}C_6H_5$), 133.4 (d, $^{2,3}J_{CP}$ = 9.8, $^{m/o}C_6H_5$), 135.5 (dd, $^{1}J_{CP}$ = 44.1, $^{3}J_{CP}$ = 4.5, $^{i}C_6H_5$), 137.0 (d, $^{1}J_{CP}$ = 9.1, $^{i}C_6H_5$), 137.2 (d, $^{1}J_{CP}$ = 16.2, $^{i}C_6H_5$), 139.5 (d, $^{1}J_{CP}$ = 27.2, $^{i}C_6H_5$), 148.1 (dd, $^{1}J_{CP}$ = 26.6, $^{2}J_{CP}$ = 26.6, PCH=CHP), 149.0 (dd, $^{1}J_{CP}$ = 35.8, $^{2}J_{CP}$ = 45.5, PCH=CHP), 164.5 (d, $^{3}J_{CP}$ = 22.7, CS), 166.1 (d, $^{3}J_{CP}$ = 19.6, $^{3}J_{CP}$ = 1.5, CS), 206.9 (d, $^{2}J_{CP}$ = 10.6, CO). $^{31}P\{^{1}H\}$ NMR (162 MHz, $CDCl_3$): δ_P = 70.6 (d, $^{2}J_{PC}$ = 8.1, PPh_2 *trans* to S), 50.8 (br s, PPh_2 *trans* to B). ^{11}B NMR (128 MHz, $CDCl_3$): δ_B = 5.05 (br s). MS-ESI(+) *m/z*: 765.1 $[M + H]^+$. Accurate mass: found 765.0785 $[M + H]^+$, Calcd. for $C_{35}H_{34}{}^{11}BN_4OP_2S_2{}^{102}Ru$ 765.0780. Anal. found: C, 54.97; H, 4.30; N, 7.22%. Calcd. for $C_{35}H_{33}BN_4OP_2RuS_2$: C, 55.05; H, 4.36; N, 7.34%.

Crystal data for $C_{35}H_{33}BN_4OP_2RuS_2$: M_w = 763.63, triclinic, *P*-1 (No.2), *a* = 10.4568(5), *b* = 12.4325(5), *c* = 15.9030(7) Å, α = 68.191(4)°, β = 82.434(4)°, γ = 71.916(4)°, *V* = 1824.35(8) Å^3, Z = 2, ρ_{calcd} = 1.390 Mg m^{-3}, μ(Cu *K*α) = 5.64 mm^{-1}, *T* = 150(2) K, yellow block, 0.21 x 0.14 x 0.07 mm, 7333 independent reflections. F^2 refinement, *R* = 0.037, *wR* = 0.101 for 6926 reflections ($I > 2.0\sigma(I)$, $2\theta_{max}$ = 144°), 418 parameters, 0 restraints.

Attempted synthesis of $[Ru\{\kappa^3\text{-}B,S,S'\text{-}B(mt)_2\}(CO)(PPh_3)_2]PF_6$ (3.9)

A solution of **3.1** (0.100 g, 0.112 mmol) and $[CPh_3]PF_6$ (0.037 g, 0.095 mmol) in tetrahydrofuran (10 mL) was stirred for 24 h. The solvent was removed *in vacuo* and diethyl ether (10 mL) was added to afford an orange precipitate that was isolated *via* cannula filtration. Crude mixture: IR (THF): 1931 ν_{CO}, 1972 ν_{CO} cm^{-1}. $^{31}P\{^{1}H\}$ NMR (162 MHz, C_6D_6): δ_P = 39.6 (br s), –142.9 ($^{1}J_{PF}$ = 713.9, PF_6), –5.3 (br s, PPh_3). The orange precipitate had poor solubility in C_6D_6. $^{31}P\{^{1}H\}$ NMR (162 MHz, $CDCl_3$): δ_P = 43.8, 39.0 (br s), 35.3, 26.2, 24.9, –144.3 ($^{1}J_{PF}$ = 714.7, PF_6), –5.3 (PPh_3).

Crystals of $[RuF(CO)(PPh_3)_2(Hmt)_2]PF_6$ **3.9x** suitable for crystallographic analysis were obtained from slow evaporation of a concentrated solution of **3.9** in benzene/*n*-pentane over one day. *Crystal data for* $C_{45}H_{42}FN_4OP_2RuS_2.F_6P.C_6H_6$: M_w = 1124.03, monoclinic, $P2_1/c$, *a* = 14.5664(1), *b* = 15.1058(1), *c* = 23.6542(2) Å, *V* = 5016.47(7) Å^3, Z = 4, ρ_{calcd} = 1.488 Mg m^{-3}, μ(Cu *K*α) = 4.80 mm^{-1}, *T* = 150(2) K, yellow block, 0.18 x 0.11 x 0.07 mm, 10144 independent reflections. F^2 refinement, *R* = 0.044, *wR* = 0.104 for 9278 reflections ($I > 2.0\sigma(I)$, $2\theta_{max}$ = 144°), 729 parameters, 96 restraints.

Synthesis of [Ru{κ⁴-*B,S,S',S''*-B(mt)₃}(CO)(PMe₂Ph)] (Ru→B) (3.10)

A solution of [Ru{κ⁴-*B,S,S',S''*-B(mt)₃}(CO)(PPh₃)] (0.200 g, 0.27 mmol) and PMe_2Ph (0.1 mL, 0.70 mmol) in tetrahydrofuran (20 mL) was stirred for 2 h. The yellow solution was concentrated to 3 mL and diethyl ether (10 mL) was added to afford a pale green precipitate. The solid was suspended in petroleum ether and collected on a sintered frit and dried *in vacuo*. Yield: 0.066 g (0.089 mmol, 40%). Crystals suitable for crystallographic analysis were obtained from slow evaporation of a concentrated solution of **3.10** in dichloromethane/*n*-pentane over one day. IR (ATR): 3115, 2970 ν_{CH}, 1882 ν_{CO} cm^{-1}. ^1H NMR (700 MHz, $CDCl_3$): δ_H = 1.75 (d, 6H, $^2J_{HP}$ = 4.7, PCH_3), 3.40 (s, 9H, NCH_3), 6.39 (s, 1H, NCH=CH), 6.54 (s, 1H, NCH=CH), 6.68 (s, 2H, NCH=CH), 6.97 (s, 2H, NCH=CH), 7.26–7.28 (m, 1H, C_6H_5), 7.36–7.38 (m, 2H, C_6H_5), 7.68–7.70 (m, 2H, C_6H_5). $^{13}C\{^1H\}$ NMR (176 MHz, $CDCl_3$): δ_C = 18.6 (d, $^1J_{CP}$ = 15.8, PCH_3), 33.7 (2C NCH_3), 34.2 (1C NCH_3), 116.5 (d, $^4J_{CP}$ = 2.3, 1C NCH=CH), 116.6 (d, $^4J_{CP}$ = 1.7, 2C NCH=CH), 122.2 ($^pC_6H_5$), 128.0 (1C NCH=CH), 128.1 (2C NCH=CH), 128.0 (d, $^{2,3}J_{CP}$ = 7.9, $^{m/o}C_6H_5$), 130.3 (d, $^{2,3}J_{CP}$ = 12.3, $^{m/o}C_6H_5$), 142.2 (d, $^1J_{CP}$ = 19.4, $^iC_6H_5$), 166.8 (d, $^3J_{CP}$ = 22.9, 1C CS), 170.1 (d, $^3J_{CP}$ = 17.6, 2C CS), 206.7 (d, $^2J_{CP}$ = 5.3, CO). $^{31}P\{^1H\}$ NMR (283 MHz, $CDCl_3$): δ_P = –13.3 (br s). ^{11}B NMR (128 MHz, $CDCl_3$): δ_B = 15.4 (br s). MS-ESI(+) *m/z*: 618.0 $[M]^+$. Accurate mass: found 618.0201 $[M]^+$, Calcd. for $C_{21}H_{26}{}^{11}BN_6OPS_3{}^{102}Ru$ 618.0204; found 641.0121 $[M + Na]^+$, Calcd. for $C_{21}H_{26}{}^{11}BN_6O^{23}NaPS_3{}^{102}Ru$ 641.0102; found 1258.0226 $[M – H + Na]^+$, Calcd. for $C_{42}H_{51}{}^{11}B_2N_{12}O_2{}^{23}NaP_2S_6{}^{102}Ru_2$ 1258.0228. Anal. found: C, 40.91; H, 4.18; N, 13.49%. Calcd. for $C_{21}H_{26}BN_6OPRuS_3$: C, 40.85; H, 4.24; N, 13.61%.

Crystal data for $C_{21}H_{26}BN_6OPRuS_3$: M_w = 617.53, monoclinic, $P2_1/c$, a = 14.4644(2), b = 14.2915(2), c = 13.0253(1) Å, β = 102.2830(13)°, V = 2630.93(2) $Å^3$, Z = 4, ρ_{calcd} = 1.559 Mg m^{-3}, μ(Cu $K\alpha$) = 7.84 mm^{-1}, T = 150(2) K, yellow block, 0.39 x 0.19 x 0.09 mm, 5301 independent reflections. F^2 refinement, R = 0.035, wR = 0.095 for 4954 reflections ($I > 2.0\sigma(I)$, $2\theta_{max}$ = 144°), 307 parameters, 42 restraints, CCDC 1874175.

Improved Synthesis of [Ru{κ⁴-*B,S,S',S''*-B(mt)₃}(CO){P(OMe)₃}] (Ru→B) (3.11)

A solution of [Ru{κ⁴-*B,S,S',S''*-B(mt)₃}(CO)(PPh₃)] (0.202 g, 0.27 mmol) and $P(OMe)_3$ (0.2 mL, 1.64 mmol) in tetrahydrofuran (20 mL) was heated to reflux for 16 h. The bright yellow precipitate was separated from the supernatant by cannula filtration, washed

with *n*-pentane and dried *in vacuo*. Yield: 0.080 g (0.133 mmol, 49%). IR (ATR): 3114, 2939 ν_{CH}, 1894 ν_{CO} cm^{-1}. ^{1}H NMR (400 MHz, $CDCl_3$): δ_H = 3.48, 3.49 (2 x s overlapping resonances, 9H, NCH_3), 3.68 (d, 9H, $^{3}J_{HP}$ = 11.5, OMe), 6.41 (d, 1H, $^{3}J_{HH}$ = 2.0, NCH=CH), 6.60 (t, 1H, $^{3}J_{HH}$ = 1.7, NCH=CH), 6.75 (s, NCH=CH), 6.99 (d, 2H, $^{3}J_{HH}$ = 2.0, NCH=CH). $^{13}C\{^{1}H\}$ NMR (176 MHz, $CDCl_3$): δ_C = 33.8 (2C NCH_3), 34.3 (1C NCH_3), 50.8 (OCH_3), 116.6 (d, $^{4}J_{CP}$ = 3.2, 1C NCH=CH), 116.7 (d, $^{4}J_{CP}$ = 2.6, 2C NCH=CH), 122.5 (2C NCH=CH), 122.7 (1C NCH=CH), 167.3 (d, $^{3}J_{CP}$ = 27.2, 1C CS), 171.0 (d, $^{3}J_{CP}$ = 22.1, 2C CS), 206.0 (d, $^{2}J_{CP}$ = 7.1, CO). $^{31}P\{^{1}H\}$ NMR (283 MHz, $CDCl_3$): δ_P = 159.1 (br s). ^{11}B NMR (128 MHz, $CDCl_3$): δ_B = 15.4 (br s). MS-ESI(+) *m/z*: 604.0 $[M]^+$, 627.0 $[M + Na]^+$. Accurate mass: found 603.9898 $[M]^+$, Calcd. for $C_{16}H_{24}{}^{11}BN_6O_4PS_3{}^{102}Ru$ 603.9895; found 626.9792 $[M + Na]^+$, Calcd. for $C_{16}H_{24}{}^{11}BN_6O_4{}^{23}NaPS_3{}^{102}Ru$ 626.9793; found 1230.9668 $[2M + Na]^+$, Calcd. for $C_{32}H_{48}{}^{11}B_2N_{12}O_8{}^{23}NaP_2S_6{}^{102}Ru_2$ 1230.9688. Anal. found: C, 31.94; H, 4.12; N, 13.84%. Calcd. for $C_{16}H_{24}BN_6O_4PRuS_3$: C, 31.85; H, 4.01; N, 13.93%.

Synthesis of [Ru{κ⁴-*B,S,S',S''*-B(mt)₃}(CO)(PCy₃)] (Ru→B) (3.12)

A solution of [Ru(Ph)Cl(CO)$(PCy_3)_2$] (0.200 g, 0.18 mmol) and Na{$HB(mt)_3$} (0.066 g, 0.18 mmol) in dichloromethane (10 mL) was stirred for 3.5 h. The yellow filtrate was separated from the NaCl by-product *via* cannula filtration and the solvent of the filtrate was removed *in vacuo*. The yellow residue was redissolved in a minimum amount of dichloromethane (2 mL) and *n*-hexane (20 mL) was added to afford a yellow precipitate, which was isolated by cannula filtration, further washed with *n*-hexane (20 mL) and dried under high vacuum. Yield: 0.109 g (0.143 mmol, 80%). Crystals suitable for crystallographic analysis were obtained from slow evaporation of a concentrated solution of **3.12** in dichloromethane/*n*-pentane over one day. IR (ATR): 2923, 2847 ν_{CH}, 1871 ν_{CO} cm^{-1}. ^{1}H NMR (700 MHz, $CDCl_3$): δ_H = 1.30–2.07 (sets of m, 36H overlap with hexane resonance, PCy_3), 3.46 (s, 3H, NCH_3), 3.48 (s, 6H, NCH_3), 6.37 (d, 1H, $^{3}J_{HH}$ = 2.1, NCH=CH), 6.50 (d, 1H, $^{3}J_{HH}$ = 1.7, NCH=CH), 6.70 (d, 2H, $^{3}J_{HH}$ = 1.8, NCH=CH), 6.99 (d, 2H, $^{3}J_{HH}$ = 2.0, NCH=CH). $^{13}C\{^{1}H\}$ APT NMR (100 MHz, $CDCl_3$): δ_C = 26.9 (CH_2 of C_6H_{11}), 28.1 (d, $^{2}J_{CP}$ = 9.4, CH_2 of C_6H_{11}), 29.9 (d, $^{2}J_{CP}$ = 2.2, CH_2 of C_6H_{11}), 33.9 (2C NCH_3), 34.4 (1C NCH_3), 35.3 (d, $^{1}J_{CP}$ = 6.3, CH of C_6H_{11}), 116.3 (d, $^{4}J_{CP}$ = 1.8, 1C NCH=CH), 116.5 (d, $^{4}J_{CP}$ = 1.2, 2C NCH=CH), 121.9 (2C NCH=CH), 122.0 (1C NCH=CH), 166.8 (d, $^{3}J_{CP}$ = 17.8, 1C CS), 171.0 (d, $^{3}J_{CP}$ = 13.5, 2C CS), 208.2 (CO). $^{31}P\{^{1}H\}$ NMR (283 MHz, $CDCl_3$): δ_P = 28.2

(br s). ^{11}B NMR (128 MHz, $CDCl_3$): δ_B = 15.4 (br s). MS-ESI(+) *m/z*: 760.2 $[M]^+$, 783.2 $[M + Na]^+$. Accurate mass: found 760.1951 $[M]^+$, Calcd. for $C_{31}H_{48}{}^{11}BN_6OPS_3{}^{102}Ru$ 760.1926; found 783.1813 $[M + Na]^+$, Calcd. for $C_{31}H_{48}{}^{11}BN_6O^{23}NaPS_3{}^{102}Ru$ 783.1824. Anal. found: C, 46.80; H, 6.09; N, 12.32%. Calcd. for $C_{31}H_{48}BN_6OPRuS_3$: C, 49.01; H, 6.37; N, 11.06%.

Crystal data for $C_{31}H_{48}BN_6OPRuS_3.CH_2Cl_2$: M_w = 844.75, triclinic, *P*-1 (No.2), *a* = 11.5008(5), *b* = 12.1448(5), *c* = 14.2700(4) Å, α = 82.893(3), β = 81.948(3), γ = 75.012(4)°, *V* = 1898.38(5) Å^3, Z = 2, ρ_{calcd} = 1.478 Mg m^{-3}, μ(Cu *K*α) = 6.86 mm^{-1}, *T* = 150(2) K, colourless needle, 0.28 x 0.06 x 0.04 mm, 7649 independent reflections. F^2 refinement, *R* = 0.041, *wR* = 0.106 for 6878 reflections ($I > 2.0\sigma(I)$, $2\theta_{max}$ = 144°), 442 parameters, 0 restraints, CCDC 1874176.

7.2.3 Investigation of Aluminium-based Pro-ligands and Complexes

Synthesis of Li[$H_2Al(NCH_2PPh_2)_2C_6H_4$-1,2)] (4.1a) or $HAl(NCH_2PPh_2)_2C_6H_4$-1,2 (4.1b)

A solution of $LiAlH_4$ in tetrahydrofuran (0.52 mL, 2M, 1.04 mmol) was added dropwise to a stirred solution of ^{Ph}PNNP (0.500 g, 1.05 mmol) in tetrahydrofuran (10 mL) at –78°C for 15 min. The solution turned from clear to pale yellow upon warming to room temperature. Solvent removal *in vacuo* resulted in a yellow oil. IR (ATR): 1712 ν_{AlH} cm^{-1}. ^{1}H NMR (400 MHz, C_6D_6): δ_H = 3.55 (br s, 4H, NCH_2P), 6.77–6.79 (m, 2H, C_6H_4), 6.95–7.06 (m, 17H, C_6H_4 and C_6H_5), 7.27–7.32 (m, 9H, C_6H_4). ^{13}C{^{1}H} NMR (100 MHz, C_6D_6): δ_C = 46.7 (s, NCH_2P), 106.8 [$C^{2,5}(C_6H_4)$], 115.2 [$C^{3,4}(C_6H_4)$], overlapping peaks 128.6–128.7 ($^{o/m}C_6H_5$), 133.1 ($^1J_{CP}$ = 17.4, $^iC_6H_5$), 138.5 ($^pC_6H_5$), 143.5 [$C^{1,6}(C_6H_4)$]. ^{31}P{^{1}H} NMR (162 MHz, C_6D_6): δ_P = −19.7. ^{27}Al (104 MHz, C_6D_6): δ_{Al} = 103.7. MS-ESI(+/-) *m/z*: no identifiable peaks were observed by mass spectrometry. Attempts to obtain a crystal suitable for crystallographic analysis resulted in decomposition of the compound to starting material (^{Ph}PNNP).

Synthesis of Li[{$H_2Al(mt)_2$}].THF (4.2)

A solution of $LiAlH_4$ in tetrahydrofuran (4.0 mL, 2M, 8 mmol) was added dropwise to a stirred solution of Hmt (2.00 g, 17.5 mmol) in tetrahydrofuran (50 mL) at –78°C. The reaction was warmed to room temperature and stirred for 3 h, which produced a clear solution accompanied by effervescence. The solvent was removed under reduced

pressure to produce a clear oil that became a crystalline white solid overnight. Yield: 2.60 g (7.80 mmol, 97%). Crystals of a tetrahydrofuran solvate suitable for crystallographic analysis were obtained from concentration of **4.2** under reduced pressure in tetrahydrofuran. IR (ATR): 3109 ν_{CH}, 1815 ν_{AlH} cm^{-1}. IR (THF): 1800 br ν_{AlH} cm^{-1}. ^{1}H NMR (400 MHz, C_6D_6): δ_H = 3.03 (s, 6H, CH_3), 4.72 (br s, 1H, AlH), 5.91 (d, 2H, $^{3}J_{HH}$ = 2.0, NCH=CH), 6.71 (s br, 2H, NCH=CH). $^{13}C\{^{1}H\}$ NMR (100 MHz, C_6D_6): δ_C = 34.2 (CH_3), 119.6 (NCH=CH), 121.5 (NCH=CH), 165.1 (CS). ^{27}Al (104 MHz, C_6D_6): δ_{Al} = 126.9. MS-ESI(–) *m/z*: Unidentifiable peaks and no molecular ion was detected due to the sensitivity of the compound in solution. Anal. found: C, 31.55; H, 5.99; N, 16.79%. Calcd. for $C_8H_{12}AlLiN_4S_2$: C, 36.64; H, 4.61; N, 21.36%. Given the air and moisture sensitivity of **4.2**, decomposition *en route* to the microanalytical facility in London is likely despite the rigorous precautions taken to ensure the samples are kept under inert atmosphere during transport.

Crystal data for $C_8H_{12}AlLiN_4S_2.(C_4H_8O)$: M_w = 334.37, monoclinic, $P2_1/n$, a = 9.3334(2), b = 16.4534(3), c = 11.8672(2) Å, β = 111.568(2) Å, V = 1694.80(6) $Å^3$, Z = 4, ρ_{calcd} = 1.310 Mg m^{-3}, μ(Cu $K\alpha$) = 3.36 mm^{-1}, T = 150(2) K, white block, 0.14 x 0.09 x 0.05 mm, 3346 independent reflections. F^2 refinement, R = 0.032, wR = 0.080 for 3076 reflections ($I > 2.0\sigma(I)$, $2\theta_{max}$ = 144°), 196 parameters, 0 restraints.

Attempted synthesis of Li[HAl(mt)$_3$] (4.3) and reactivity with [Ru(CH=CHPh)Cl(CO)(PPh$_3$)$_2$]

A solution of $LiAlH_4$ in tetrahydrofuran (1.0 mL, 2M, 2 mmol) was added dropwise to a stirred solution of Hmt (0.841 g, 7.37 mmol) in tetrahydrofuran (9 mL) at room temperature. The pink solution became clear within 10 min and was accompanied by effervescence and the precipitation of white powder. The reaction mixture was heated at reflux for 19 h. The white precipitate was isolated from the supernatant through cannula filtration and dried *in vacuo*. Yield: 0.718 g (0.96 mmol, 96%).^{1}H NMR (400 MHz, $CD_3C_6D_5$): δ_H = 2.90 (s, 9H, CH_3), 5.50 (br s, 3H, NCH=CH), 5.70 (br s, 3H, NCH=CH). ^{1}H NMR (400 MHz, C_6D_6): δ_H = 2.91 (s, 9H, CH_3), 5.45 (d, 3H, $^{3}J_{HH}$ = 1.9, NCH=CH), 5.72 (d, 3H, $^{3}J_{HH}$ = 1.8, NCH=CH). MS-ESI(–) *m/z*: Unidentifiable peaks and no molecular ion detected due to the sensitivity of the compound in solution.

A mixture of [Ru(CH=CHPh)Cl(CO)(PPh_3)$_2$] (0.005 g, 0.006 mmol) and Li[HAl(mt)$_3$] (0.015 g, 0.040 mmol) was combined in d_6-benzene (0.5 mL) in the argon box. At 30 min a mixture of products was observed in the ^{1}H and ^{31}P{^{1}H} NMR spectra. ^{31}P{^{1}H} NMR (162 MHz, C_6D_6): δ_P = 25.7 (br s), 31.8 (br s), 42.0 ([Ru(CH=CHPh)(mt)(CO)(PPh_3)$_2$][23]).

Attempted synthesis of [RuH(CO)(PPh_3){κ^3-*H,S,S'*-H_2Al(mt)$_2$}] (4.4)

From ruthenium precursor [RuHCl(CO)(PPh_3)$_3$]:

A mixture of [RuHCl(CO)(PPh_3)$_3$] (0.015 g, 0.016 mmol) and Li[H_2Al(mt)$_2$].THF (0.005 g, 0.015 mmol) was combined in d_6-benzene (0.5 mL) in the argon box. The white suspension rapidly became pale yellow. At 30 min a mixture of [RuH_2(CO)(PPh_3)$_3$][24] **4.4x**, PPh_3, and the postulated product **4.4** was observed in the ^{1}H and ^{31}P{^{1}H} NMR spectra. **4.4**: ^{1}H NMR (400 MHz, C_6D_6): δ_H = –9.45 (br d, 2H, AlHRu), –7.70 (br s, 1H, RuH), 3.11 (s, 6H, NCH_3), 5.85 (d, 2H, $^3J_{HH}$ = 1.8, NCH=CH), 5.87 (d, 2H, coupling not resolved, NCH=CH), 6.82–7.04 (m, 88H, C_6H_5 in the mixture), 7.29–7.53 (m, 62H, C_6H_5 in the mixture). ^{31}P{^{1}H} NMR (162 MHz, C_6D_6): δ_P = 51.0. At 1 h the ^{1}H NMR spectra only showed resonances corresponding to **4.4x** and [RuH(κ^2-*N,S*-mt)(CO)(PPh_3)$_2$][23] **4.4y**.

From ruthenium precursor [RuH(CO)($NCMe$)$_2$(PPh_3)$_3$]PF_6:

A mixture of [RuH(CO)($NCMe$)$_2$(PPh_3)$_2$]PF_6 (0.015 g, 0.017 mmol) and Li[H_2Al(mt)$_2$].THF (0.008 g, 0.024 mmol) was combined in d_6-benzene (0.5 mL) in the argon box. The white suspension rapidly became pale yellow. Crystals of **4.4y** suitable for crystallographic analysis were obtained from slow evaporation in benzene over one day.

4.4y: *Crystal data* for $C_{41}H_{36}N_2ORuP_2S.2.5(C_6H_6)$: M_w = 953.05, monoclinic, $P2_1/n$, a = 14.4371(4), b = 20.3397(4), c = 16.6926(4) Å, β = 105.251(3)°, V = 4729.1(2) Å^3, Z = 4, ρ_{calcd} = 1.353 Mg m^{-3}, μ(Mo $K\alpha$) = 0.49 mm^{-1}, T = 150(2) K, colourless block, 0.15 x 0.11 x 0.10 mm, 11525 independent reflections. F^2 refinement, R = 0.058, wR = 0.145 for 7063 reflections ($I > 2.0\sigma(I)$, $2\theta_{max}$ = 60°), 573 parameters, 0 restraints.

Synthesis of [RuH(CO)($NCMe$)$_2$(PPh_3)$_2$]PF_6 (4.5)

In a 100 mL flask, [RuHCl(CO)(PPh_3)$_3$] (2.00 g, 2.10 mmol) and $NaPF_6$ (0.388 g, 2.31 mmol) were suspended in degassed acetonitrile (50 mL) and heated at reflux for 1 h. The pink suspension became a pale yellow solution. The flask was cooled to room temperature, filtered through diatomaceous earth in air and washed with acetonitrile and then dichloromethane. The solution was evaporated to dryness on a rotary evaporator.

The compound was dissolved in acetonitrile (30 mL) and ethanol (20 mL) was added. The solution was concentrated to half volume, more ethanol (20 mL) was added and concentrated again using the rotary evaporator to reduce the overall volume to 10 mL. The target compound was isolated by Buchner filtration, washed with ethanol and collected as a white powder. Yield: 1.586 g (1.80 mmol, 86%). Crystals suitable for crystallographic analysis were obtained from slow evaporation of a concentrated solution of **4.5** in chloroform over several days. IR (ATR): 3053 ν_{CH}, 1944 ν_{CO} cm^{-1}. ^{1}H NMR (400 MHz, C_6D_6): δ_H = −12.99 (t, 1H, $^{2}J_{HP}$ = 17.6, RuH), 1.36 (s, 3H, CH_3CN), 1.73 (s, 3H, CH_3CN), 7.45–7.58 (m, 30H, C_6H_5). $^{13}C\{^{1}H\}$ NMR (100 MHz, C_6D_6): δ_C = 2.25 (CH_3), 2.35 (CH_3), 123.9 (CN), 124.6 (CN), 128.7 (t, $^{2}J_{CP}$ = 4.8, $^{o}C_6H_5$), 130.5 ($^{p}C_6H_5$), 132.2 (t, $^{1}J_{CP}$ = 22.3, $^{i}C_6H_5$), 134.1 (t, $^{3}J_{CP}$ = 5.9, $^{m}C_6H_5$), 202.3 (t, $^{2}J_{CP}$ = 13.5, CO). $^{31}P\{^{1}H\}$ NMR (162 MHz, C_6D_6): δ_P = 46.1 (PPh_3), −144.4 (septet, $^{1}J_{PF}$ = 713.2, PF_6). MS-ESI(+) *m/z*: 737.1 $[M]^+$. Accurate mass: found 737.1414 $[M]^+$, Calcd. for $C_{41}H_{37}N_2OP_2{}^{102}Ru$ 737.1425. Anal. found: C, 56.02; H, 4.35; N, 3.13%. Calcd. for $C_{41}H_{37}N_2F_6OP_3Ru$ C, 55.85; H, 4.23; N, 3.18%. The analogous ClO_4 salt has been described previously.[25]

Crystal data for $C_{41}H_{37}N_2OP_2Ru.F_6P$: M_w = 881.74, monoclinic, $P2_1/m$, a = 9.253(1), b = 21.921(1), c = 10.412(1) Å, β = 110.985(2)°, V = 1971.67(2) $Å^3$, Z = 2, ρ_{calcd} = 1.485 Mg m^{-3}, μ(Cu $K\alpha$) = 1.54 mm^{-1}, T = 150(2) K, colourless block, 0.14 x 0.10 x 0.06 mm, 4000 independent reflections. F^2 refinement, R = 0.045, wR = 0.122 for 3977 reflections ($I > 2.0\sigma(I)$, $2\theta_{max}$ = 144°), 266 parameters, 22 restraints.

Attempted synthesis of [OsH(CO)(PPh_3){κ^3-*H,S,S'*-$H_2Al(mt)_2$}] (4.7)

A suspension of [OsHCl(CO)(PPh_3)$_3$] (0.570 g, 0.547 mmol) and Li[$H_2Al(mt)_2$].THF (0.250 g, 0.748 mmol) in diethyl ether (15 mL) was stirred for 2 h. The solvent was concentrated down to half volume and *n*-hexane was added to afford a white precipitate that was isolated *via* cannula filtration. The sample was dried *in vacuo*. The ^{1}H and $^{31}P\{^{1}H\}$ NMR of the white solid contained a mixture of [OsH_2(CO)(PPh_3)$_3$] **4.7x**,[26] [OsH(κ^2-*N,S*-mt)(CO)(PPh_3)$_2$] **4.7y**[23] and PPh_3. See text (Section 4.3.2) for a description of the experiment performed on the NMR scale.

Crystals of **4.7y** suitable for crystallographic analysis were obtained from slow evaporation of the crude solution in benzene at 25°C over several days.

4.7y: *Crystal data* for $C_{41}H_{36}N_2OOsP_2S.2.5(C_6H_6)$: M_w = 1052.25, monoclinic, $P2_1/n$, a = 14.4328(1), b = 20.3571(1), c = 16.6528(1) Å, β = 105.3879(4)°, V = 4717.36(3) Å^3, Z = 4, ρ_{calcd} = 1.482 Mg m^{-3}, μ(Cu $K\alpha$) = 6.48 mm^{-1}, T = 150(2) K, colourless block, 0.20 x 0.12 x 0.04 mm, 9329 independent reflections. F^2 refinement, R = 0.017, wR = 0.043 for 9063 reflections ($I > 2.0\sigma(I)$, $2\theta_{max}$ = 144°), 568 parameters, 0 restraints.

Attempted synthesis of [Os{κ^3-*Al,S,S'*-AlH(mt)$_2$}(CO)(PPh$_3$)$_2$] (Os→Al) (4.8)

A mixture of [Os(Ph)Cl(CO)(PPh$_3$)$_2$] (0.015 g, 0.018 mmol) and Li[H$_2$Al(mt)$_2$].THF (0.005 g, 0.015 mmol) was combined in d$_6$-benzene (0.5 mL) in the argon box. The white suspension rapidly became pale yellow. At 30 min a mixture of products including PPh$_3$ and the postulated product **4.8** was observed in the $^{31}P\{^1H\}$ NMR spectra. $^{31}P\{^1H\}$ NMR (162 MHz, C_6D_6): δ_P = 4.6, 5.4, 8.7, 10.2, 12.7, 13.4, 17.2, 17.7, 18.4, 20.7, 21.3, 21.6. **4.8**: δ_P = 8.7 ($^2J_{PP}$ = 9.7 Hz), 20.6 ($^2J_{PP}$ = 9.7 Hz). At 21 h the ^1H and $^{31}P\{^1H\}$ NMR spectra contained resonances associated with **4.7x** and **4.7y** (1:1 ratio).

Attempted synthesis of [Re(CO)$_3${κ^3-*Al,S,S'*-H$_2$Al(mt)$_2$}] (4.9)

A solution of [ReBr(CO)$_5$] (0.028 g, 0.069 mmol) in tetrahydrofuran (2 mL) was brought to reflux for 20 h to provide [ReBr(CO)$_3$(THF)$_2$] (1894, 1915, 2029 ν_{CO} cm^{-1}). The solution was cooled to –78°C and Li[H$_2$Al(mt)$_2$].THF (0.030 g, 0.093 mmol) in tetrahydrofuran (3 mL) was added to the rapidly stirred solution. The reaction was stirred at –78°C for 30 min then warmed to room temperature and stirred for 20 min. The reaction was monitored by IR spectroscopy (br 1887, 2008 ν_{CO} cm^{-1}). The white product had extremely poor solubility in C_6D_6 and CD_2Cl_2. Several crystallisations were set-up to clarify the product formed. Crystals of a benzene solvate suitable for crystallographic analysis were obtained from slow evaporation of the crude solution in benzene at 25 °C over several days. The crystals solved as the side products below.

[Re$_2$(μ-N,S-mt)$_2$(CO)$_6$(Hmt)$_2$] **4.9x** *Crystal data* for $C_{11}H_{11}N_4O_3ReS_2.0.5(C_6H_6)$: M_w = 536.62, monoclinic, $C2/c$, a = 10.1931(1), b = 20.4062(2), c = 16.6968(2) Å, β = 92.2009(9)°, V = 3470.41(4) Å^3, Z = 8, ρ_{calcd} = 2.054 Mg m^{-3}, μ(Mo $K\alpha$) = 7.26 mm^{-1}, T = 150(2) K, red block, 0.15 x 0.12 x 0.08 mm, 4608 independent reflections. F^2 refinement, R = 0.022, wR = 0.047 for 4603 reflections ($I > 2.0\sigma(I)$, $2\theta_{max}$ = 60°), 222 parameters, 8 restraints.

$[Re_2(\mu\text{-N,S-mt})(\mu\text{-S:}\kappa^2\text{-}N,S\text{-mt})(CO)_6(Hmt)_2]$ **4.9y** *Crystal data* for $C_{18}H_{16}N_6O_6Re_2S_3.(C_6H_6)$: M_w = 959.07, monoclinic, *I*2/*c*, *a* = 21.3801(5), *b* = 9.7464(2), *c* = 28.7542(10) Å, β = 105.314(3)°, *V* = 5779.0(2) Å^3, Z = 8, ρ_{calcd} = 2.205 Mg m^{-3}, μ(Mo *K*α) = 8.64 mm^{-1}, *T* = 150(2) K, white block, 0.13 x 0.10 x 0.05 mm, 6562 independent reflections. F^2 refinement, *R* = 0.043, *wR* = 0.076 for 6560 reflections ($I > 2.0\sigma(I)$, $2\theta_{max}$ = 60°), 371 parameters, 46 restraints.

7.2.4 Silane-based Pincer Ligands and Derived Complexes

Observation of $H_2Si(NCH_2PPh_2)_2C_6H_4$-1,2 (5.1)

A solution of SiH_2Cl_2.TEEDA (0.196 g, 0.717 mmol) in benzene (4 mL) was added dropwise into a stirred solution of ^{Ph}PNNP (0.124 g, 0.246 mmol) in benzene (4 mL). The resulting suspension was stirred for 30 min. The filtrate was isolated by cannula filtration and frozen at –40°C, and lyophilised to produce a mixture of **5.1** and ^{Ph}PNNP(SiHCl). ^{1}H NMR (400 MHz, C_6D_6): **5.1**: δ_H = 3.78 (d, 4H, $^2J_{HP}$ = 2.4, NCH_2P), 5.83 (t, 2H, $^4J_{HP}$ = 3.8, SiH_2), 6.91–7.35 (m, C_6H_5 and C_6H_4). $^{31}P\{^1H\}$ NMR (162 MHz, C_6D_6): δ_P = –19.9.

Crystal structure of $HClSi(NCH_2PPh_2)_2C_6H_4$-1,2 (^{Ph}PNNP(SiHCl))

Compound $HClSi(NCH_2PPh_2)_2C_6H_4$-1,2 was synthesized following literature procedures. Upon solvent removal of a concentrated solution of ^{Ph}PNNP(SiHCl) in benzene, clear crystals formed which were suitable for X-ray diffraction analysis:

Crystal data for $C_{32}H_{29}ClN_2P_2Si.C_3H_3$: M_w = 606.10, monoclinic, $P2_1/c$, *a* = 9.1710(2), *b* = 26.2924(7), *c* = 13.8164(3) Å, β = 109.276(3)°, *V* = 3144.74(14) Å^3, Z = 4, ρ_{calcd} = 1.280 Mg m^{-3}, μ(Cu *K*α) = 2.61 mm^{-1}, *T* = 150(2) K, colourless block, 0.16 x 0.09 x 0.04 mm, 6098 independent reflections. F^2 refinement, *R* = 0.048, *wR* = 0.105 for 5105 reflections ($I > 2.0\sigma(I)$, $2\theta_{max}$ = 144°), 446 parameters, 96 restraints.

Synthesis of $[RhHCl\{SiPh(NCH_2PPh_2)_2C_6H_4\text{-}1,2\}(PPh_3)]$ (5.2)

A mixture of $[RhCl(CO)(PPh_3)_2]$ (0.200 g, 0.289 mmol) and ^{Ph}PNNP(SiHPh) (0.176 g, 0.289 mmol) was dissolved in tetrahydrofuran (15 mL) and stirred for 6 h. The solvent was removed *in vacuo* and diethyl ether (18 mL) was added to the residue before being

vigorously stirred for 5 min. The resulting pale yellow precipitate was isolated by cannula filtration and dried *in vacuo*. The mixture of diastereomers (**5.2a**/**5.2b**) was obtained in a ratio of 1:3 based off ^{1}H NMR integration. Yield: 0.203 g (0.201 mmol, 70%). Data were consistent with those previously reported obtained *via* a different route.[3] IR (ATR): 3049 ν_{CH}, 2033 ν_{RhH} cm^{-1}. ^{1}H NMR (400 MHz, C_6D_6): Major isomer: δ_H = –17.2 (ddt, 1H, $^{1}J_{HRh}$ = 20.0, $^{2}J_{HP\ (PPh3)}$ = 16.2, $^{2}J_{HP\ (PPh2)}$ = 9.7, RhH), 4.25 (d, 2H, $^{2}J_{HH}$ = 12.0, NCH_aH_bP), 4.53 (dt^{v}, 2H, $^{2}J_{HH}$ = 11.7, $^{2}J_{HP}$ = 4.8, NCH_aH_bP), 6.58–7.97 (m, 78H, C_6H_5 and C_6H_4)[*]. Hydride of minor isomer: –19.2 (expected dtd coupling not well resolved, 1H, RhH). ^{13}C{^{1}H} APT NMR (100 MHz, C_6D_6): δ_C = The 1D ^{13}C{^{1}H} APT spectrum showed poor signal to noise and not all resonances could be unambiguously identified. Resonances identified: 58.6 (m, NCH_2P), 113.2 [$C^{2,5}(C_6H_4)$], 120.1 [$C^{3,4}(C_6H_4)$], 127.0–136.7 (C_6H_5, from a combination of **5.2a**/**5.2b**), 149.5 [$C^{1,6}(C_6H_4)$]. ^{31}P{^{1}H} NMR (162 MHz, C_6D_6): Major isomer: δ_P = 14.2 (dt, $^{1}J_{PRh}$ = 83.9, $^{2}J_{PP}$ = 21.7, PPh_3), 54.0 (dd, $^{1}J_{PRh}$ = 113.1, $^{2}J_{PP}$ = 22.0, PPh_2); Minor isomer: 13.2 (dt, $^{1}J_{PRh}$ = 78.2, $^{2}J_{PP}$ = 20.2, PPh_3), 57.2 (dd, $^{1}J_{PRh}$ = 118.9, $^{2}J_{PP}$ = 20.2, PPh_2). MS-ESI(+) *m/z*: 1009.2 $[M + H]^+$. Accurate mass: found 1009.1697 $[M + H]^+$, Calcd. for $C_{56}H_{50}N_2SiP_3{}^{35}Cl^{103}Rh$ 1009.1700. Anal. found: C, 61.86; H, 4.79; N, 3.56%. Calcd. for $C_{56}H_{49}ClN_2P_3RhSi$: C, 66.64; H, 4.89; N, 2.78%.[†]

Synthesis of [IrHCl{SiPh(NCH_2PPh_2)$_2$$C_6H_4$-1,2}($PPh_3$)] (5.3)

A mixture of [IrCl(CO)(PPh_3)$_2$] (0.201 g, 0.258 mmol) and ^{Ph}PNNP(SiHPh) (0.158 g, 0.260 mmol) was dissolved in tetrahydrofuran (20 mL) and stirred for 25 h. The solvent was removed *in vacuo* and diethyl ether (15 mL) was added to the residue before being vigorously stirred for 5 min resulting in a pale yellow precipitate consisting of two isomers (**5.3a**/**5.3b**) in a 1:8 ratio, which was isolated by cannula filtration and dried *in vacuo*. Yield: 0.170 g (0.155 mmol, 60%). IR (ATR): 3049 ν_{CH}, 2166 ν_{IrH} cm^{-1}. ^{1}H NMR (700 MHz, C_6D_6): Major isomer: δ_H = –20.7 (dt, 1H, $^{2}J_{HP\ (PPh3)}$ = 15.4, $^{2}J_{HP\ (PPh2)}$ = 9.8, IrH), 4.16 (d, 2H, $^{2}J_{HH}$ = 11.9, NCH_2P), 4.84 (dt^{v}, 2H, $^{2}J_{HH}$ = 11.9, $^{2}J_{PH\ (PPh2)}$ = 4.9, NCH_2P), 6.70–7.38

[*] The integrals in the aromatic region of the ^{1}H NMR are confounded by the overlapping resonances for the two isomers and overlap with the NMR solvent (C_6D_6), such that a larger than expected proton integration is measured.

[†] Inexplicably, multiple attempts to obtain consistent elemental microanalytical data for a number of the silicon pincer complexes resulted in data that were consistently lower in %C and higher in %N, which might be a result of the formation of refractory silicon nitride during incomplete combustion analysis.

(m, 44H, C_6H_5 and C_6H_4). Hydride of minor isomer: δ_H = –22.6 (dt, $^2J_{HP\ (PPh3)}$ = 17.1, $^2J_{HP\ (PPh2)}$ = 7.8). $^{13}C\{^1H\}$ NMR (201 MHz, C_6D_6): δ_C = Due to poor solubility of **5.3** in C_6D_6, the 1D $^{13}C\{^1H\}$ spectrum acquired over 20,000 scans showed poor signal to noise ratio and not all resonances could be unambiguously identified or observed. Resonances identified: 60.4 (dt^v, $^2J_{CP\ (PPh3)}$ = 8.0, $^2J_{CP\ (PPh2)}$ = 20.0, NCH_2P), 113.5 [$C^{2,5}(C_6H_4)$], 119.9 [$C^{3,4}(C_6H_4)$], 127.6–128.3 (C_6H_5 carbon environments could not be unambiguously assigned due to overlap with the solvent resonance), 129.2–136.6 (C_6H_5), 143.0 [$C^{1,6}(C_6H_4)$], 150.0 (C_6H_5). ^{29}Si NMR (139 MHz, C_6D_6): δ_{Si} = 88.3 (dt, $^2J_{SiP\ (PPh3)}$ = 126.5, $^2J_{SiP\ (PPh2)}$ = 14.4). $^{31}P\{^1H\}$ NMR (283 MHz, C_6D_6): δ_P = –1.81 (t, $^2J_{PP}$ = 17.4, PPh_3), 27.0 (d, $^2J_{PP}$ = 17.8, PPh_2). MS-ESI(+) *m/z*: 1099.2 $[M + H]^+$, 1063.3 $[M – Cl]^+$. Accurate mass: found 1099.2275 $[M + H]^+$, Calcd. for $C_{56}H_{50}N_2SiP_3{}^{35}Cl{}^{193}Ir$ 1099.2274, found 1063.2500 $[M – Cl]^+$, Calcd. for $C_{56}H_{49}N_2SiP_3{}^{193}Ir$ 1063.2507. Anal. found: C, 61.08; H, 4.40; N, 2.69%. Calcd. for $C_{56}H_{49}ClN_2IrP_3Si$: C, 61.22; H, 4.50; N, 2.55%.

Synthesis of [RhHCl{SiCl(NCH_2PPh_2)$_2C_6H_4$-1,2}(PPh_3)] (5.4)

Method 1: A suspension of ^{Ph}PNNP (0.124 g, 0.246 mmol) and SiH_2Cl_2.TEEDA (0.196 g, 0.717 mmol) in benzene (8 mL) was stirred for 5 days. The supernatant was transferred *via* cannula filtration to a flask containing $[Rh_2Cl_2(COD)_2]$ (0.049 g, 0.099 mmol), which was stirred for 2.5 h and then PPh_3 (0.052 g, 198 mmol) was added as a solid and stirred for a further 6 h. The solvent was removed *in vacuo* to give a brown solid that was suspended in benzene (1 mL) and *n*-pentane (11 mL) was added. The light brown solid was isolated *via* cannula filtration. However, the side product $[TEEDAH_2]Cl_2$ persisted and therefore an alternative preparatory route (method 2) was used. ^1H NMR (400 MHz, C_6D_6): δ_H = –16.7 (ddt, 1H, $^1J_{HRh}$ = 18.2, $^2J_{HP\ (PPh3)}$ = 15.6, $^2J_{HP\ (PPh2)}$ = 8.8, RhH), 4.17 (d, $^2J_{HH}$ = 11.3, 2H, NCH_aH_bP), 4.52 (dt^v, $^2J_{HH}$ = 11.3, $^2J_{HP}$ = 4.7, 2H, NCH_aH_bP), 6.67–7.13 (m, 60H, C_6H_5 and C_6H_4), 7.28–7.31 (m, 11H, C_6H_5 and C_6H_4), 7.78–7.81 (m, 8H, C_6H_5 and C_6H_4). $^{31}P\{^1H\}$ NMR (162 MHz, C_6D_6): δ_P = 24.2 (dt, $^1J_{PRh}$ = 90.9, $^2J_{PP}$ = 24.4, PPh_3), 58.1 (dd, $^1J_{PRh}$ = 108.8, $^2J_{PP}$ = 24.2, PPh_2).

Method 2: A suspension of $[RhCl(PPh_3)_3]$ (0.209 g, 0.226 mmol) and ^{Ph}PNNP(SiHCl) (0.123 g, 0.217 mmol) in tetrahydrofuran (20 mL) was stirred for 6 h. The solvent was removed *in vacuo* and the resulting red residue triturated with benzene/*n*-pentane,

then washed with diethyl ether. The beige precipitate was dried *in vacuo* to afford a mixture of isomers (**5.4a**/**5.4b**) in a ratio of 1:11. Yield: 0.148 g (0.147 mmol, 68%). IR (ATR): 3052 ν_{CH}, 2029 ν_{RhH} cm^{-1}. ^{1}H NMR (700 MHz, C_6D_6): Major isomer: δ_H = –16.7 (ddt, 1H, $^{1}J_{HRh}$ = 18.5, $^{2}J_{HP\ (PPh3)}$ = 15.4, $^{2}J_{HP\ (PPh2)}$ = 8.8, RhH), 4.17 (d, 2H, $^{2}J_{HH}$ = 11.2, NCH_aH_bP), 4.53 (dt^{v}, 2H, $^{2}J_{HH}$ = 11.2, $^{2}J_{HP}$ = 4.6, NCH_aH_bP), 6.54–6.56 (m, 1H, C_6H_5 and C_6H_4), 6.68–6.79 (m, 9H, C_6H_5 and C_6H_4), 6.85–6.89 (m, 6H, C_6H_5 and C_6H_4), 7.03–7.18 (m, 18H, C_6H_5 and C_6H_4), 7.30–7.33 (m, 4H, C_6H_5 and C_6H_4), 7.38–7.40 (m, 1H, C_6H_5 and C_6H_4), 7.71–7.72 (m, 1H, C_6H_5 and C_6H_4), 7.78–7.81 (m, 4H, C_6H_5 and C_6H_4). Hydride of minor isomer: –19.4 (dtd, 1H, $^{1}J_{HRh}$ = 18.4, $^{2}J_{HP\ (PPh2)}$ = 12.2, $^{2}J_{HP\ (PPh3)}$ = 5.8, RhH). $^{13}C\{^{1}H\}$ NMR (176 MHz, C_6D_6): δ_C = Due to poor solubility of **5.4** in C_6D_6, the $^{13}C\{^{1}H\}$ NMR spectrum was of poor signal to noise ratio and not all resonances could be unambiguously identified and observed. Resonances identified: 57.4 (dt^{v}, $^{2}J_{CRh}$ = 5.9, $^{1,3}J_{CP}$ = 18.2, NCH_2P), 59.7 (br m, NCH_2P, other isomer), 112.2, 113.3 ([$C^{2,5}(C_6H_4)$], both isomers), 119.7, 120.2 ([$C^{3,4}(C_6H_4)$], both isomers), 127.7–128.4 (carbon environments could not be unambiguously assigned due to overlap with the solvent resonance), 128.6–135.8 (C_6H_5), 143.9 (br, [$C^{1,6}(C_6H_4)$]), 147.7 (C_6H_5). ^{29}Si NMR (139 MHz, C_6D_6): δ_{Si} = 85.4 (some combination of dddt expected but not well resolved, $^{2}J_{SiP\ (PPh3)}$ = 190). $^{31}P\{^{1}H\}$ NMR (283 MHz, C_6D_6): δ_P = 24.7 (dt, $^{1}J_{PRh}$ = 90.6, $^{2}J_{PP}$ = 24.4, PPh_3), 58.1 (dd, $^{1}J_{PRh}$ = 108.8, $^{2}J_{PP}$ = 24.2, PPh_2). MS-ESI(+) *m/z*: 968.2 $[M + H]^+$, 933.2 $[M - Cl]^+$. Accurate mass: found 967.0989 $[M + H]^+$, Calcd. for $C_{50}H_{45}N_2SiP_3{}^{35}Cl_2{}^{103}Rh$ 967.0997. Anal. found: C, 54.32; H, 4.37; N, 3.35%. Calcd. for $C_{50}H_{44}N_2P_3RhSiCl$: C, 62.06; H, 4.58; N, 2.89%.[†]

Synthesis of [Rh{SiPh(NCH_2PPh_2)$_2$$C_6H_4$-1,2}($PPh_3$)] (5.5)

A mixture of [$RhH(PPh_3)_4$] (0.205 g, 0.178 mmol) and ^{Ph}PNNP(SiHPh) (0.107 g, 0.176 mmol) was dissolved in tetrahydrofuran (15 mL) and stirred for 1.5 h. The solvent was removed *in vacuo* and diethyl ether (18 mL) was added to the residue before being sonicated then vigorously stirred for 5 min, resulting in the formation of an orange solid. The orange precipitate was isolated by cannula filtration and dried *in vacuo*. Yield: 0.096 g (0.099 mmol, 55%). IR (ATR): 3047 ν_{CH}, 1476, 1433 $\nu_{C=C}$ cm^{-1}. ^{1}H NMR (700 MHz, C_6D_6): δ_H = 4.01 (dt^{v}, 2H, $^{2}J_{HH}$ = 13.4, triplet not resolved, NCH_2P), 4.36 (dt^{v}, 2H, $^{2}J_{HH}$ = 12.9, triplet not resolved, NCH_2P), 7.25–6.71 (m, 42H, C_6H_5 and C_6H_4), 7.87 (d, 2H, C_6H_5). $^{13}C\{^{1}H\}$ NMR (176 MHz, C_6D_6): δ_C = 61.3 (br m, NCH_2P), 112.2 [$C^{2,5}(C_6H_4)$],

118.8 [$C^{3,4}(C_6H_4)$], 127.7–129.4 (carbon environments could not be unambiguously assigned due to overlap with the solvent resonance, C_6H_5), 128.7 (C_6H_5), 128.8 (C_6H_5), 128.9 (C_6H_5), 132.6 (t^v, $^2J_{CP}$ = 6.2, $^oC_6H_5$ [PPh_2], 133.5 (t^v, $^3J_{CP}$ = 6.7, $^mC_6H_5$ [PPh_2]), 134.3 (d, $^2J_{CP}$ = 14.1, $^oC_6H_5$ [PPh_3]), 134.9 (CH SiPh), 137.7 (t^v, $^1J_{CP}$ = 14.5, $^iC_6H_5$ [PPh_2], 137.7 (d, $^1J_{CP}$ = 25.7, $^iC_6H_5$ [PPh_3], 138.1 (t^v, $^1J_{CP}$ = 13.0, $^iC_6H_5$ [PPh_2], 144.1 [$C^{1,6}(C_6H_4)$], 146.1 (C_6H_5). ^{29}Si NMR (139 MHz, C_6D_6): δ_{Si} = 117.6 (ddt, $^2J_{SiP\ (PPh3)}$ = 104.2, $^1J_{SiRh}$ = 31.1, $^2J_{SiP\ (PPh2)}$ = 24.5). $^{31}P\{^1H\}$ NMR (283 MHz, C_6D_6): δ_P = 27.5 (dt, $^1J_{PRh}$ = 133.0, $^2J_{PP}$ = 21.3, PPh_3), 68.6 (dd, $^1J_{PRh}$ = 176.9, $^2J_{PP}$ = 21.4, PPh_2). MS-ESI(+) *m/z* Accurate mass: found 973.1937 $[M + H]^+$, Calcd. for $C_{56}H_{49}N_2SiP_3{}^{103}Rh$ 973.1933; found 1014.2178 $[M + CH_3CN]^+$, Calcd. for $C_{58}H_{52}N_3SiP_3{}^{103}Rh$ 1014.2198. Despite the usual precautions in packaging the sample under an inert atmosphere for microanalysis, the air sensitivity of **5.5** prevented collection of suitable microanalytical data. The best data is reported here. Anal. found: C, 64.08; H, 5.33; N, 3.04%. Calcd. for $C_{56}H_{48}N_2P_3RhSi$: C, 69.13; H, 4.97; N, 2.88%.

Crystal data for $C_{56}H_{48}N_2P_3RhSi.0.75(C_6H_6)$: M_w = 1031.45, triclinic, *P*-1 (No.2), *a* = 12.4122(2), *b* = 12.9208(2), *c* = 18.9027(3) Å, α = 74.5369(15)°, β = 84.7732(15)°, γ = 67.4925(17)°, *V* = 2699.05(9) Å^3, Z = 2, ρ_{calcd} = 1.269 Mg m^{-3}, μ(Cu *K*α) = 3.91 mm^{-1}, *T* = 150(2) K, orange block, 0.19 x 0.13 x 0.04 mm, 10542 independent reflections. F^2 refinement, *R* = 0.031, *wR* = 0.083 for 9954 reflections ($I > 2.0\sigma(I)$, $2\theta_{max}$ = 144°), 652 parameters, 120 restraints.

Variable Temperature NMR study of [Rh{SiPh(NCH_2PPh_2)$_2C_6H_4$-1,2}(PPh_3)] + H_2 (5.6) See Figures 5.10 and 5.11.

With a needle attached to a balloon, dihydrogen (1 atm) was bubbled into an NMR solution of **5.5** in d_8-toluene (0.5 mL) for 2 min. A variable temperature NMR study of **5.6** was performed from –80 to +80°C. ^{1}H NMR (700 MHz, $C_6D_5CD_3$, –80°C): δ_H = Major: –8.71, –8.89 (m, 1H x 2, coupling not resolved, 2 x Rh–H), 3.95 (d, 2H, $^2J_{HH}$ = 12.5, NCH_2P), 4.13 (coupling not resolved, 2H, NCH_2P), 6.53–7.72 (m, 49H of combined isomers, expect 39H for one isomer, C_6H_5 and C_6H_4), 8.65–8.66 (m, 2H, C_6H_5). Hydride of minor product: –6.94, –8.14 (br m, 1H x 2, H x 2). $^{31}P\{^1H\}$ NMR (283 MHz, $C_6D_5CD_3$, –80°C): δ_P = Major: 37.3 (dt, $^1J_{PRh}$ = 93.6, $^2J_{PP}$ = 21.0), 98.2 (dd, $^1J_{PRh}$ = 98.7, $^2J_{PP}$ = 21.2). Minor: 39.4 (dt, $^1J_{PRh}$ = 90.4, $^2J_{PP}$ = 23.4), 72.5 (dd, $^1J_{PRh}$ = 113.9, $^2J_{PP}$ = 24.9).

Synthesis of [Rh{SiPh(NCH$_2$PPh$_2$)$_2$C$_6$H$_4$-1,2}(CO)(PPh$_3$)] (5.7)

Method 1: A solution of [RhH(CO)(PPh$_3$)$_3$] (0.200 g, 0.218 mmol) and ^{Ph}PNNP(SiHPh) (0.133 g, 0.218 mmol) in tetrahydrofuran (20 mL) was stirred for 48 h. The supernatant was isolated *via* cannula filtration and the solvent of the filtrate was removed in *vacuo*. The neon yellow residue was stirred in *n*-hexane (40 mL) to yield a bright yellow powder, which was isolated *via* cannula filtration and dried *in vacuo*. The powder consisted of a mixture observed as ≈10 resonances in the ^{31}P{^{1}H} NMR spectrum, with **5.7** as the major product (*ca* 50% of the total phosphorus content). Yield: 0.167 g (0.167 mmol, 77%). IR (ATR): 3051 ν_{CH}, 1970, 1931 ν_{CO} cm^{-1}. IR (THF): 1971, 1934 ν_{CO} cm^{-1}. ^{31}P{^{1}H} NMR (162 MHz, C$_6$D$_6$): δ_P = 31.3 (dt, $^1J_{PRh}$ = 91.1, $^2J_{PP}$ = 38.2, PPh$_3$), 63.9 (dd, $^1J_{PRh}$ = 147.0, $^2J_{PP}$ = 38.1, PPh$_2$). MS-ESI(+) *m/z*: 867.2 [M – CO – Ph – Si]$^+$. Accurate mass: found 1014.2192 [M – CO + H + MeCN]$^+$, Calcd. for C$_{58}$H$_{52}$N$_3$SiP$_3$^{103}Rh 1014.2198, found 973.1933 [M – CO + H]$^+$, Calcd. for C$_{56}$H$_{49}$N$_2$SiP$_3$^{103}Rh 973.1933.

Method 2: A solution of **5.5** was generated *in situ* from the reaction of [RhH(PPh$_3$)$_4$] (0.200 g, 0.173 mmol) and ^{Ph}PNNP(SiHPh) (0.110 g, 0.181 mmol) stirred in tetrahydrofuran (20 mL) for 2 h. Carbon monoxide (1 atm) was bubbled into the solution for 10 min until the colour of the solution changed from orange to light brown. The solvent was removed *in vacuo* to give a green-yellow residue, which was suspended and stirred in *n*-pentane (25 mL) for 2 d and the precipitate was isolated *via* cannula filtration and dried *in vacuo*. Yield: 0.112 g (0.112 mmol, 65%). IR (ATR): 3045 ν_{CH}, 1937 ν_{CO} cm^{-1}. IR (THF): 1945 ν_{CO} cm^{-1}. ^{1}H NMR (400 MHz, C$_6$D$_6$): δ_H = 3.55 (dt^v, 2H, $^2J_{HH}$ = 4.0, $^2J_{HP}$ = 13.2, NCH$_2$P), 4.47 (d, 2H, $^2J_{HH}$ = 12.6, NCH$_2$P), 6.53–7.09 (m, 40H, C$_6$H$_5$ and C$_6$H$_4$), 7.29–7.39 (m, 7H, C$_6$H$_5$ and C$_6$H$_4$), 8.03–8.06 (m, 2H, C$_6$H$_5$). ^{13}C{^{1}H} NMR (100 MHz, C$_6$D$_6$): δ_C = 61.9 (dt^v, $^2J_{CRh}$ = 10.3, $^1J_{CP}$ = 8.7, NCH$_2$P), 113.1 [C^{2,5}(C$_6$H$_4$)], 119.1 [C^{3,4}(C$_6$H$_4$)], 127.0–144.5 (C$_6$H$_5$), 145.2 [C^{1,6}(C$_6$H$_4$)], 201.7 (coupling not resolved, CO). ^{31}P{^{1}H} NMR (162 MHz, C$_6$D$_6$): δ_P = 31.3 (dt, $^1J_{PRh}$ = 91.0, $^2J_{PP}$ = 38.0, PPh$_3$), 63.9 (dd, $^1J_{PRh}$ = 146.7, $^2J_{PP}$ = 38.2, PPh$_2$). ^{29}Si NMR (139 MHz, C$_6$D$_6$): δ_{Si} = 95.1 (ddt, $^2J_{SiP\,(PPh3)}$ = 120.6, $^1J_{SiRh}$ = 22.4, $^2J_{SiP\,(PPh2)}$ = 21.8). MS-ESI(+) *m/z*: 867.2 [M – CO – Ph – Si]$^+$. Accurate mass: found 1001.1882 [M + H]$^+$, Calcd. for C$_{57}$H$_{49}$N$_2$OSiP$_3$^{103}Rh 1001.1882, found 1000.1836 [M]$^+$, Calcd. for C$_{57}$H$_{48}$N$_2$OSiP$_3$^{103}Rh 1000.1804. Anal. found: C, 68.32; H, 4.93; N, 2.74%. Calcd. for C$_{57}$H$_{48}$N$_2$OP$_3$RhSi: C, 68.40; H, 4.83; N, 2.80%.

Synthesis of [Rh{SiPh(NCH$_2$PPh$_2$)$_2$C$_6$H$_4$-1,2}(C$_7$H$_8$)] (5.8)

A solution of **5.5** was generated *in situ* from the reaction of [RhH(PPh$_3$)$_4$] (0.200 g, 0.173 mmol) and ^{Ph}PNNP(SiHPh) (0.112 g, 0.184 mmol) stirred in tetrahydrofuran (15 mL) for 2 h. Norbornadiene (0.10 mL, 0.983 mmol) was added to this solution and stirred for 18 h. The brown residue was stirred in *n*-pentane for 24 h and the precipitate was isolated *via* cannula filtration, washed further with *n*-pentane and then dried *in vacuo*. Yield: 0.088 g (0.110 mmol, 63%). Crystals suitable for X-ray diffraction analysis were obtained from slow evaporation of a concentrated solution of **5.8** in *n*-hexane. IR (ATR): 2840–3070 ν_{CH}, 1474, 1429 $\nu_{C=C}$ cm^{-1}. ^{1}H NMR (700 MHz, C$_6$D$_6$): δ_H = 0.88–0.90 (m, 2H, CH$_2$ C$_7$H$_8$), 2.60 (br s, 2H, bridgehead C$_7$H$_8$), 3.10 (br s, HC=CH), 4.20 (dd, 2H, $^2J_{HH}$ = 13.3, $^2J_{HP}$ = 7.0, NCH$_a$H$_b$P), 4.31 (dd, 2H, $^2J_{HH}$ = 13.3, $^2J_{HP}$ = 4.9, NCH$_a$H$_b$P), 4.55 (s, 2H, HC=CH), 6.67 (s, 4H, C$_6$H$_4$), 6.71–6.72 (m, 4H, C$_6$H$_5$), 6.80–6.81 (m, 2H, C$_6$H$_5$), 6.91–6.93 (m, 4H, C$_6$H$_5$), 7.08–7.10 (m, 2H, C$_6$H$_5$), 7.15–7.17 (m, 5H, C$_6$H$_5$), 7.26–7.28 (m, 2H, C$_6$H$_5$), 7.66–7.71 (m, 6H, C$_6$H$_5$). ^{13}C{^{1}H} NMR (176 MHz, C$_6$D$_6$): δ_C = 42.2–42.3 (m, HC=CH *trans* to P), 47.5 (CH C$_7$H$_8$), 60.9 (d, $^1J_{CP}$ = 22.4, NCH$_2$P), 63.9 (CH$_2$ C$_7$H$_8$), 75.0 (s, HC=CH *trans* to Si), 114.5 [C^{2,5}(C$_6$H$_4$)], 119.6 [C^{3,4}(C$_6$H$_4$)], 127.9–128.5 (carbon environments could not be unambiguously assigned due to overlap with the solvent resonance, C$_6$H$_5$), 128.5 (C$_6$H$_5$), 128.9 (C$_6$H$_5$), 131.5–131.6 (m, $^{o/m}$C$_6$H$_5$ [PPh$_2$]), 133.2 ($^{o/m}$C$_6$H$_5$ [SiPh]), 133.2–133.3 (m, $^{o/m}$C$_6$H$_5$ [PPh$_2$]), 138.7–138.8 (br m, C$_6$H$_5$ [PPh$_2$]), 141.1 (d, $^1J_{CSi}$ = 3.0, [Si(^{i}C$_6$H$_5$)]), 143.9–144.1 (br m, C$_6$H$_5$ [PPh$_2$]), 146.8 [C^{1,6}(C$_6$H$_4$)]. ^{29}Si NMR (139 MHz, C$_6$D$_6$): δ_{Si} = 95.2 (dt, $^1J_{SiRh}$ = 37.9, $^2J_{SiP}$ = 22.7). ^{31}P{^{1}H} NMR (283 MHz, C$_6$D$_6$): δ_P = 70.4 (d, $^1J_{PRh}$ = 150.8). MS-ESI(+) *m/z*: 825.1 [M + Na]$^+$. Accurate mass: found 825.1451 [M + Na]$^+$, Calcd. for C$_{45}$H$_{41}$N$_2$^{23}NaSiP$_2$Rh 825.1467. Anal. found: C, 67.23; H, 5.29; N, 3.42%. Calcd. for C$_{45}$H$_{41}$N$_2$P$_2$RhSi: C, 67.33; H, 5.15; N, 3.49%.

Crystal data for C$_{45}$H$_{41}$N$_2$P$_2$RhSi.0.5(C$_6$H$_{14}$): M_w = 845.86, monoclinic, *P*2/*n*, *a* = 16.5467(2), *b* = 14.3997(1), *c* = 18.2036(2) Å, β = 111.6280(12) Å, *V* = 4031.96(4) Å^3, Z = 4, ρ_{calcd} = 1.393 Mg m^{-3}, μ(Cu *K*α) = 4.73 mm^{-1}, *T* = 150(2) K, yellow plate, 0.20 x 0.19 x 0.04 mm, 8146 independent reflections. F^2 refinement, *R* = 0.029, *wR* = 0.080 for 7782 reflections ($I > 2.0\sigma(I)$, $2\theta_{max}$ = 144°), 487 parameters.

Synthesis of [Rh{SiPh(NCH$_2$PPh$_2$)$_2$C$_6$H$_4$-1,2}(CO)$_2$] *in situ* (5.9)

Generation of **5.9** *in situ* and characterisation: With a needle attached to a balloon, carbon monoxide (1 atm) was bubbled into an NMR solution of **5.5** (0.015 g, 0.015 mmol) in d_8-toluene (0.5 mL) for 5 min. The solution changed from orange to yellow over the course of the reaction. IR (THF): 2018 ν_{CO}, 1971 ν_{CO} cm^{-1}. ^{1}H NMR (700 MHz, $C_6D_5CD_3$): δ_H = 3.74 (s, 2H, NCH_2P), 4.42 (d, 2H, $^2J_{HH}$ = 12.6, NCH_2P), 6.63–6.87 (m, 14H, C_6H_5 and C_6H_4), 6.97–7.09 (m, 16H, C_6H_5 and C_6H_4), 7.33 (br s, 5H, C_6H_5 and C_6H_4), 7.69–7.75 (m, 5H, C_6H_5 and C_6H_4). ^{31}P{^{1}H} NMR (283 MHz, $C_6D_5CD_3$): δ_P = 82.2 (d, $^1J_{PRh}$ = 145.4). ^{1}H NMR (700 MHz, C_6D_6): δ_H = 3.79 (dt^v, 2H, $^2J_{HH}$ = 14.1, $^2J_{HP}$ = 5.0, NCH_2P), 4.42 (d, 2H, $^2J_{HH}$ = 13.8, NCH_2P), 6.64–6.66 (m, 4H, C_6H_5 and C_6H_4), 6.73–6.74 (m, 6H, C_6H_5 and C_6H_4), 6.82–6.83 (m, 2H, C_6H_5 and C_6H_4), 6.92–6.93 (m, 3H, C_6H_5 and C_6H_4), 7.03–7.09 (m, 16H, C_6H_5 and C_6H_4), 7.13–7.15 (m, 2H, C_6H_5 and C_6H_4), 7.39 (br s, 6H, C_6H_5 and C_6H_4), 7.75–7.76 (m, 5H, C_6H_5 and C_6H_4). ^{13}C{^{1}H} NMR (176 MHz, C_6D_6): δ_C = 58.4 (t, $^1J_{CP}$ = 8.4, NCH_2P), 114.3 [$C^{2,5}(C_6H_4)$], 119.8 [$C^{3,4}(C_6H_4)$], 128.0–129.4 (some C_6H_5 resonances are obscured by the solvent), 130.3 (C_6H_5), 130.7 (t, $^{2/3}J_{CP}$ = 6.2, $^{o/m}C_6H_5$), 132.4 (d, $^{4/5}J_{CP}$ = 9.6, [Si($^{m/o}C_6H_5$)]), 133.5 (t, $^{2/3}J_{CP}$ = 7.9, $^{o/m}C_6H_5$), 138.4 (t, $^3J_{CP}$ = 18.4, [Si($^iC_6H_5$)]), 139.6 (t, $^{4/5}J_{CP}$ = 11.4, [Si($^{m/o}C_6H_5$)]), 143.1 [Si($^pC_6H_5$)]), 144.4 [$C^{1,6}(C_6H_4)$], 198.5 (dt, $^1J_{CRh}$ = 70.5, $^2J_{CP}$ = 30.8, CO), 201.4 (dt, $^1J_{CRh}$ = 49.0, $^2J_{CP}$ = 14.9, CO). ^{31}P{^{1}H} NMR (283 MHz, C_6D_6): δ_P = 81.7 (d, $^1J_{PRh}$ = 145.7). ^{29}Si NMR (139 MHz, C_6D_6): δ_{Si} = 102.3 (dt, $^1J_{SiRh}$ = 19.5, $^2J_{SiP}$ = 19.6).

A siloxybridged dimer was observed *via* a crystallographic study and MS-ESI(+). MS-ESI(+) *m/z*: 755.1 [M+2H]$^{++}$. Accurate mass: found 755.0919 [M+2H]$^{++}$, Calcd. for $C_{79}H_{68}N_4O_4Si_2P_4{}^{103}Rh_2$ 755.0914. Crystals for X-ray diffraction were obtained from slow diffusion of *n*-pentane into a concentrated solution of **5.9** in toluene.

Crystal data for **5.9x** $C_{78}H_{66}N_4O_4P_4Rh_2Si_2$: M_w = 1509.28, triclinic, *P*-1 (No.2), *a* = 13.0331(1), *b* = 16.3219(2), *c* = 18.4849(3) Å, α = 75.4827(12)°, β = 82.5524(10)°, γ = 85.6010(9)°, *V* = 3770.53(6) Å^3, Z = 2, ρ_{calcd} = 1.329 Mg m^{-3}, μ(Cu *K*α) = 5.04 mm^{-1}, *T* = 150(2) K, yellow block, 0.32 x 0.15 x 0.11 mm, 15203 independent reflections. F^2 refinement, *R* = 0.038, *wR* = 0.106 for 14123 reflections ($I > 2.0\sigma(I)$, $2\theta_{max}$ = 144°), 847 parameters, 0 restraints.

Synthesis of [Rh{SiPh(NCH$_2$PPh$_2$)$_2$C$_6$H$_4$-1,2}(PhC≡C-C≡CPh)(PPh$_3$)] (5.10a)

In the argon box, a mixture of **5.5** (0.015 g, 0.015 mmol) and Ph–C≡C–C≡C–Ph (0.006 g, 0.030 mmol) was dissolved in C_6D_6 (0.5 mL) and mixed thoroughly with a pipette before transferring into an NMR tube. A red solution resulted instantly, and the NMR spectrum was measured 10 min after its preparation. IR (THF): 1594 $\nu_{C=C}$ cm^{-1}. ^{1}H NMR (700 MHz, C_6D_6): δ_H = 4.84 (d, 2H, $^2J_{HH}$ = 14.8, NCH$_a$H$_b$P), 5.21 (d, 2H, $^2J_{HH}$ = 14.7, NCH$_a$H$_b$P), 6.54–7.51 (m, 77H, 54H expected, C_6H_5 and C_6H_4). ^{29}Si NMR (139 MHz, C_6D_6): δ_{Si} = –16.0 (d, $^3J_{SiRh}$ = 4.2). ^{31}P{^{1}H} NMR (283 MHz, C_6D_6): δ_P = 36.2 (dt, $^1J_{PRh}$ = 131.0, $^2J_{PP}$ = 34.0, PPh$_3$), 68.6 (dd, $^1J_{PRh}$ = 179.8, $^2J_{PP}$ = 34.0, PPh$_2$). Two minor products were also noted as *ca* 9% of the total phosphorus content and persisted following workup involving an *n*-hexane wash. δ_P = 72.4 ($^1J_{PRh}$ = 137.9, $^2J_{PP}$ = 21.6) and 70.0 ($^1J_{PRh}$ = 131.8, $^2J_{PP}$ = 22.9).

Synthesis of [OsCl{SiPh(NCH$_2$PPh$_2$)$_2$C$_6$H$_4$-1,2}(PPh$_3$)] (5.11)

A mixture of [OsCl$_2$(PPh$_3$)$_3$] (0.100 g, 0.095 mmol) and ^{Ph}PNNP(SiHPh) (0.058 g, 0.095 mmol) was dissolved in tetrahydrofuran (10 mL) and stirred for 3 h. The solvent was removed *in vacuo* to give a gummy dark residue that was triturated with benzene (4 mL) and *n*-hexane (6 mL). The pale brown precipitate was isolated by cannula filtration, washed with a further portion of *n*-hexane and dried *in vacuo*. Yield: 0.047 g (0.043 mmol, 45%). IR (ATR): 3052 ν_{CH} cm^{-1}. ^{1}H NMR (700 MHz, C_6D_6): δ_H = 4.25 (d, 2H, $^2J_{HH}$ = 11.9, NCH$_2$P), 4.33 (dt^v, 2H, $^2J_{HH}$ = 11.9, $^2J_{HP\ (PPh2)}$ = 4.7, NCH$_2$P), 6.67–6.69 (m, 5H, C_6H_4 and C_6H_5), 6.80–7.07 (sets of m, 48H, C_6H_4 and C_6H_5), 7.31–7.48 (m, 15H, C_6H_4 and C_6H_5). ^{13}C{^{1}H} NMR (176 MHz, C_6D_6): δ_C = 58.0 (dt, $^2J_{CP\ (PPh3)}$ = 4.9, $^2J_{CP\ (PPh2)}$ = 20.4, NCH$_2$P), 113.5 [C^{2,5}(C_6H_4)], 120.0 [C^{3,4}(C_6H_4)], 128.6–135.7 (C_6H_5), 148.4 [C^{1,6}(C_6H_4)]. ^{31}P{^{1}H} NMR (283 MHz, C_6D_6): δ_P = –12.1 (t, $^2J_{PP}$ = 15.9, PPh$_3$), 20.9 (d, $^2J_{PP}$ = 15.8, PPh$_2$). ^{29}Si NMR (139 MHz, C_6D_6): δ_{Si} = 85.4 (dt, $^2J_{SiP\ (PPh3)}$ = 141.6, $^2J_{SiP\ (PPh2)}$ = 16.1). MS-ESI(+) *m/z*: 1097.2 [M + H]$^+$. Accurate mass: found 1097.2173 [M + H]$^+$, Calcd. for $C_{56}H_{49}N_2SiP_3{}^{35}Cl^{192}Os$ 1097.2181. Anal. found: C, 54.23; H, 4.17; N, 3.39%. Calcd. for $C_{56}H_{48}ClN_2P_3OsSi$: C, 61.39; H, 4.42; N, 2.56%.[†]

7.2.5 Appendix: Perimidine-based N-Heterocyclic Pincer Complexes

Synthesis of *trans*-[$IrH_2Cl\{C(NCH_2PCy_2)_2C_{10}H_6\}$] (*trans*-A.1)

A solution of $[Ir_2(\mu\text{-}Cl)_2(COE)_4]$ (0.102 g, 0.114 mmol) and $H_2C(NCH_2PCy_2)_2C_{10}H_6$ (0.132 g, 0.223 mmol) in toluene (10 mL) was stirred at room temperature for 4 h. The volatiles were removed under reduced pressure, and the residue washed with diethyl ether and dried *in vacuo*. Yield: 0.117 g (0.143 mmol, 64%). IR (ATR): 2917, 2848 ν_{CH}, 1772 ν_{IrH}, 1582 ν_{aromCC} cm^{-1}. ^1H NMR (400 MHz, C_6D_6): δ_H = –6.96 (t, 2H, $^2J_{HP}$ = 15.8, IrH), 1.53–2.07 (sets of m, 51H, C_6H_{11} overlapping with residual toluene), 3.70 (br s, 4H, PCH_2N), 6.31 (d, 2H, $^3J_{HH}$ = 7.6, $C_{10}H_6$), 7.08–7.13 (m, 2H, $C_{10}H_6$), 7.22–7.24 (m, 2H, $C_{10}H_6$). $^{13}C\{^1H\}$ NMR (100 MHz, C_6D_6): δ_C = 26.6 (C_6H_{11}), 27.2 (t^v, J_{CP} = 6.5, C_6H_{11}), 27.9 (C_6H_{11}), 29.0 (C_6H_{11}), 34.4 (t^v, J_{CP} = 15.3, C_6H_{11}), 53.6 (t^v, J_{CP} = 14.7, PCH_2), 106.3 ($C_{10}H_6$), 117.7 [$^4C(C_{10}H_6)$], 120.4 ($C_{10}H_6$), 121.3 [$^4C(C_{10}H_6)$], 134.8 (t^v, $^{3,5}J_{CP}$ = 6.5, [$C^{1,8}(C_{10}H_6)$]), 193.3 (Ir=C, identified from $^1H^{13}C$ HMBC experiments). $^{31}P\{^1H\}$ NMR (162 MHz, C_6D_6): 27.3. MS-ESI(+) *m/z*: 817.3 $[M - H]^+$. Accurate Mass: Found 817.3148 $[M - H]^+$, Calcd. for $C_{37}H_{55}N_2{}^{35}Cl^{193}IrP_2$ 817.3153; Found 819.3112 $[M - H]^+$, Calcd. for $C_{37}H_{55}N_2{}^{37}Cl^{193}IrP_2$ 819.3123. Anal. Found: C, 54.26; H, 6.89; N, 3.51%. Calcd. for: $C_{37}H_{56}ClIrN_2P_2$, 54.30; H, 6.90; N, 3.42%.

Observation of [$IrCl\{C(NCH_2PCy_2)_2C_{10}H_6\}$] (A.2)

A solution of $[Ir_2(\mu\text{-}Cl)_2(COE)_4]$ (0.201 g, 0.224 mmol) and $H_2C(NCH_2PCy_2)_2C_{10}H_6$ (0.264 g, 0.447 mmol) in toluene (20 mL) was heated at 70°C for 40 h. The volatiles were removed under reduced pressure, and the residue suspended in diethyl ether. The yellow-brown solid, which contained a mixture of (≈4) products, was isolated *via* cannula filtration and dried *in vacuo*. Complex **A.2** was identified as the major product in the mixture by ^{31}P NMR integration. $^1H^{13}C$ HMBC (100 MHz, C_6D_6): δ_C = 188.2 (δ_H = 3.30) (Ir=C, coupling not resolved). $^{31}P\{^1H\}$ NMR (162 MHz, $CDCl_3$) of the mixture: δ_P = –1.9, 1.8, 4.6, 37.5 (**A.2**). MS-ESI(+) *m/z*: 817.3 $[M + H]^+$. Accurate Mass: Found 819.3121 $[M + H]^+$, Calcd. for $C_{37}H_{55}N_2P_2{}^{37}Cl^{193}Ir$ 819.3134.

Synthesis of *cis*-[IrHCl$_2${C(NCH$_2$PCy$_2$)$_2$C$_{10}$H$_6$}] (*cis*-A.3)

A solution of [Ir$_2$(μ-Cl)$_2$(COE)$_4$] (0.101 g, 0.113 mmol) and H$_2$C(NCH$_2$PCy$_2$)$_2$C$_{10}$H$_6$ (0.132 g, 0.223 mmol) in toluene (10 mL) was stirred at room temperature for 4 h. The volatiles were removed under reduced pressure, and chloroform (1 mL) was added, instantly producing a dark brown solution that was stirred overnight. The solvent was removed, and the brown precipitate was washed with *n*-pentane and dried *in vacuo*. Yield: 0.156 g (0.183 mmol, 82%). IR (ATR): 2920, 2849 ν_{CH}, 1636 ν_{IrH}, 1585 ν_{aromCC} cm^{-1}. ^{1}H NMR (400 MHz, CDCl$_3$): δ_H = –18.98 (t, 1H, $^2J_{HP}$ = 12.4, IrH), 1.58–2.98 (set of m, 44H, C$_6$H$_{11}$), 4.04 (d, 2H, $^2J_{HH}$ = 13.0, PCH$_a$H$_b$N), 4.38 (d, 2H, $^2J_{HH}$ = 13.0, PCH$_a$H$_b$N), 6.82 (d, 2H, $^3J_{HH}$ = 7.5, C$_{10}$H$_6$), 7.35–7.44 (m, 4H, C$_{10}$H$_6$). ^{13}C{^{1}H} NMR (100 MHz, CDCl$_3$): δ_C = 26.2 (C$_6$H$_{11}$), 26.7 (t^v, $^2J_{CP}$ = 6.6, C$_6$H$_{11}$), 26.9 (t^v, $^2J_{CP}$ = 5.1, C$_6$H$_{11}$), 27.2 (t^v, $^2J_{CP}$ = 5.3, C$_6$H$_{11}$), 27.3 (t^v, $^2J_{CP}$ = 6.5, C$_6$H$_{11}$), 27.7 (C$_6$H$_{11}$), 27.9 (C$_6$H$_{11}$), 28.0 (C$_6$H$_{11}$), 29.6 (C$_6$H$_{11}$), 32.6 (t^v, $^1J_{PC}$ = 14.8, C$_6$H$_{11}$), 35.1 (t^v, $^1J_{CP}$ = 13.8, C$_6$H$_{11}$), 53.0 (t^v, $^{1,3}J_{CP}$ = 15.3, PCH$_2$), 106.7 (C$_{10}$H$_6$), 118.7 [^{4}C(C$_{10}$H$_6$)], 121.5 (C$_{10}$H$_6$), 128.3 (C$_{10}$H$_6$), 134.1 (t^v, $^4J_{CP}$ = 3.7, [C^{1,8}(C$_{10}$H$_6$)]), 134.4 [^{4}C(C$_{10}$H$_6$)], 187.2 (Ir=C, coupling not resolved). ^{31}P{^{1}H} NMR (162 MHz, CDCl$_3$): 16.1. MS-ESI(+) *m/z*: 817.3 [M – Cl]$^+$, 858.3 [M – Cl + MeCN]$^+$. Accurate Mass: Found 860.3394 [M – Cl + MeCN]$^+$, Calcd. for C$_{39}$H$_{58}$N$_3$P$_2$^{37}Cl^{193}Ir 860.3394. Anal. Found: C, 52.11; H, 6.40; N, 3.36%. Calcd. for: C$_{37}$H$_{55}$Cl$_2$IrN$_2$P$_2$, 52.10; H, 6.50; N, 3.28%.

Crystals of [IrCl$_3${C(NCH$_2$PCy$_2$)$_2$C$_{10}$H$_6$}] **A.3a**.(C$_6$H$_6$)$_2$ suitable for X-ray diffraction analysis were obtained from slow evaporation of a concentrated solution of ***cis*-A.3** in benzene. *Crystal data for* **A.3a**.(C$_6$H$_6$)$_2$ C$_{37}$H$_{54}$Cl$_3$IrN$_2$P$_2$.2(C$_6$H$_6$): Mw = 1043.60, triclinic, *P*-1 (No.2), *a* = 12.3051(3), *b* = 13.4628(4), *c* = 14.1870(3) Å, α = 98.375(2)°, β = 94.854(2)°, γ = 100.425(2) °, *V* = 2271.87(5) Å^3, Z = 2, ρ_{calcd} = 1.525 Mg m^{-3}, μ(Cu Kα) = 8.25 mm^{-1}, T = 150(2) K, clear intense yellow block, 0.17 x 0.16 x 0.10 mm, 8912 independent reflections. F^2 refinement, R = 0.041, wR = 0.116 for 8116 reflections (I > 2.0σ(I), 2θ_{max} = 148°), 514 parameters, 48 restraints, CCDC 1579232.

Synthesis of $[IrH_3\{C(NCH_2PPh_2)_2C_{10}H_6\}]$ (A.4)

The complex $[IrCl\{C(NCH_2PPh_2)_2C_{10}H_6\}]$ (0.078 g, 0.098 mmol) and $NaBH_4$ (0.039 g, 1.03 mmol) were stirred in methanol/toluene (2:7 mL) for 3 days. The solvent was removed under reduced pressure and methanol (10 mL) was added to give a beige precipitate. The precipitate was isolated *via* cannula filtration, washed with *n*-pentane and dried *in vacuo*. Yield 0.058 g (0.073 mmol, 77%). IR (ATR): 3046 ν_{CH}, 1963, 1739 ν_{IrH} cm^{-1}. ^1H NMR (700 MHz, C_6D_6): δ_H = –10.65 (tt, 1H, $^2J_{HH}$ = 7.1, $^2J_{HP}$ = 13.9, IrH), –9.95 (dt, 2H, $^2J_{HH}$ = 7.0, $^2J_{HP}$ = 14.1, IrH), 4.64 (4H, PCH_2N), 6.20 (d, 2H, $^3J_{HH}$ = 7.8, $C_{10}H_6$), 6.98–7.07 (m, 15H, $C_{10}H_6$ and C_6H_5), 7.21–7.22 (m, 3H, $C_{10}H_6$ and C_6H_5), 8.09–8.10 (m, 6H, C_6H_5 and $C_{10}H_6$). $^{13}C\{^1H\}$ NMR (100 MHz, C_6D_6): δ_C = Due to poor solubility of **A.4**, satisfactory 1-D and 2-D spectra could not be obtained. $^{31}P\{^1H\}$ NMR (162 MHz, C_6D_6): 20.4. MS-ESI(+) *m/z*: 759.2 $[M - H]^+$. Accurate mass: Found 759.1672 $[M - H]^+$, Calcd. for $C_{37}H_{32}N_2P_2{}^{193}Ir$ 759.1670; Found 800.1935 $[M + MeCN - H]^+$, Calcd. for $C_{39}H_{35}N_3P_2{}^{193}Ir$ 800.1936. Although the formulation of **A.4** is supported by spectroscopic and spectrometric techniques, consistent elemental analytical data was not obtained. The best result out of numerous attempts is reported. Anal. Found: C, 53.28; H, 4.37; N, 3.41%. Calcd. for $C_{37}H_{33}IrN_2P_2$: C, 58.49; H, 4.38; N, 3.69%.

7.3 References

(1) Foreman, M. R. S. J.; Hill, A. F.; Tshabang, N.; White, A. J. P.; Williams, D. J. *Organometallics* **2003**, *22*, 5593.
(2) Kloos, S. D.; Boudjouk, P. *Inorg. Synth.* **1998**, *32*, 294.
(3) Dixon, L. S. H.; Hill, A. F.; Sinha, A.; Ward, J. S. *Organometallics* **2014**, *33*, 653.
(4) Hill, A. F.; McQueen, C. M. A. *Organometallics* **2014**, *33*, 1909.
(5) Ahmad, N.; Levison, J. J.; Robinson, S. D.; Uttley, M. F. *Inorg. Synth.* **1974**, *15*, 45.
(6) Irvine, G. J.; Roper, W. R.; Wright, L. J. *Organometallics* **1997**, *16*, 2291.
(7) Clark, G. R.; Rickard, C. E. F.; Roper, W. R.; Salter, D. M.; Wright, L. J. *Pure Appl. Chem.* **1990**, *62*, 1039.
(8) Marciniec, B.; Pietraszuk, C. *Organometallics* **1997**, *16*, 4320.
(9) Bohle, D. S.; Clark, G. R.; Rickard, C. E. F.; Roper, W. R.; Wright, L. J. *J. Organomet. Chem.* **1988**, *358*, 411.
(10) Torres, M. R.; Vegas, A.; Santos, A.; Ros, J. *J. Organomet. Chem.* **1986**, *309*, 169.
(11) Werner, H.; Meyer, U.; Peters, K.; Von Schnering, H. G. *Chem. Ber.* **1989**, *122*, 2097.
(12) Collins, T. J.; Grundy, K. R.; Roper, W. R. *J. Organomet. Chem.* **1982**, *231*, 161.
(13) Rickard, C. E. F.; Roper, W. R.; Taylor, G. E.; Waters, J. M.; Wright, L. J. *J. Organomet. Chem.* **1990**, *389*, 375.
(14) Elliott, G. P.; McAuley, N. M.; Roper, W. R. *Inorg. Synth.* **1989**, *26*, 184.
(15) Roedel, J. N.; Wurzenberger, X.; Lorenz, I.-P. *Inorg. Chem. Commun.* **2008**, *11*, 829.
(16) Osborn, J. A.; Wilkinson, G. *Inorg. Synth.* **1967**, *10*, 67.

(17) Evans, D.; Osborn, J. A.; Wilkinson, G. *Inorg. Synth.* **1968**, *11*, 99.
(18) Giordano, G.; Crabtree, R. H. *Inorg. Synth.* **1979**, *19*, 218.
(19) Van der Ent, A.; Onderdelinden, A. L. *Inorg. Synth.* **1973**, *14*, 92.
(20) Herde, J. L.; Lambert, J. C.; Senoff, C. V. *Inorg. Synth.* **1974**, *15*, 18.
(21) Collman, J. P.; Sears, C. T., Jr.; Kubota, M. *Inorg. Synth.* **1990**, *28*, 92.
(22) Hill, A. F.; Owen, G. R.; White, A. J. P.; Williams, D. J. *Angew. Chem. Int. Ed.* **1999**, *38*, 2759.
(23) Wilton-Ely, J. D. E. T.; Honarkhah, S. J.; Wang, M.; Tocher, D. A.; Slawin, A. M. Z. *Dalton Trans.* **2005**, 1930.
(24) Hallman, P. S.; McGarvey, B. R.; Wilkinson, G. *J. Chem. Soc. A* **1968**, 3143.
(25) Cavit, B. E.; Grundy, K. R.; Roper, W. R. *J. Chem. Soc., Chem. Commun.* **1972**, 60.
(26) Ahmad, N.; Robinson, S. D.; Uttley, M. F. *J. Chem. Soc., Dalton Trans.* **1972**, 843.

Appendix

Perimidine-based N-Heterocyclic Pincer Complexes

The work described in this appendix has recently appeared in publication.

Iridium complexes of perimidine-based N-heterocyclic carbene pincer ligands *via* aminal C–H activation

By Hill, Anthony F.; Ma, Chenxi; McQueen, Caitlin. M. A.; Ward, Jas.

Dalton Transactions, **2018**, 47, 1577–1587.

A.0 Preamble

Coordination of the dihydropermidine pro-ligand $H_2C(NCH_2PPh_2)_2C_{10}H_6$-1,8 ($^{Ph}PCH_2P$) to iridium was investigated by the author in 2014 (Honours year); the results of which are detailed in the introduction here (Section A.1, Scheme A.2). The analogous pro-ligand $H_2C(NCH_2PCy_2)_2C_{10}H_6$-1,8 ($^{Cy}PCH_2P$) with dicyclohexylphosphine pincer arms has been found to exhibit different reactivity on ruthenium compared to $^{Ph}PCH_2P$.[1] Therefore, reaction of the $^{Cy}PCH_2P$ pro-ligand with iridium precursors was explored in this chapter. Additional complexes to complete the comparative story between the reactivity of $^{Cy}PCH_2P$ and $^{Ph}PCH_2P$ are described here.

A.1 Introduction

A.1.1 N-Heterocyclic Carbenes

N-Heterocyclic Carbene (NHC) ligands have been thoroughly explored as ancillaries in catalyst design.[2,3] The inherently strong metal-NHC bond, enhanced σ-donor properties[4,5] and reduced propensity for dissociation[6] make NHC ligands an attractive alternative to phosphine ligands. Despite the strong metal-NHC bonding, numerous decomposition pathways have been noted.[7,8] Therefore, the incorporation of NHCs within the tridentate pincer framework might be expected to confer additional stabilisation.

The majority of NHCs are based on five-membered heterocycle rings such as imidazole **A** (Figure A.1), while there are relatively fewer examples with the perimidine framework **B**. Expanding the ring size from five (**A**) to six (**B**) results in a decrease of the α angle (Figure A.1), directing the amine R substituents closer to the metal. Additionally, the enhanced σ-basicity of NHC **B** compared to **A** has been demonstrated,[9-11] and complexes of **B** have found to be effective catalysts.[12,13]

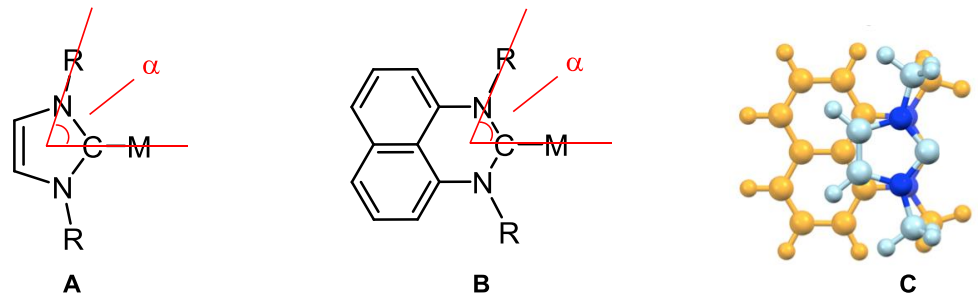

Figure A.1: N-Heterocyclic carbene ligands with **A**) imidazole-based (α ≈ 72°) and **B**) perimidine-based (α ≈ 60°) and **C**) superposition of both.

A.1.2 Dihydroperimidine-derived Pincer Complexes

There has been an increasing number of reports of pincer complexes based on the dihydropermidine framework, $H_2C(NCH_2PR_2)_2C_{10}H_6$-1,8 (R = Cy, Ph) ($^{R}PCH_2P$).[14] The installation of NHC complexes typically involve activation of cationic azolium precursors (Chapter 1, Section 1.2.2.1).[15] The first examples of $^{R}PCH_2P$ (R = Cy, Ph) ligation were reported on rhodium and iridium (Scheme A.1), resulting from the less conventional C–H activation of the central aminal group.[14]

The formation of [RhCl{$C(NCH_2PR_2)_2C_{10}H_6$}] (R = Cy **LA.1a**, Ph **LA.1b**) follows from facile double C–H activation and subsequent reductive elimination of H_2. In contrast, the reaction of $^{Cy}PCH_2P$ and Vaska's *trans*-[IrCl(CO)(PPh_3)$_2$] stalled at single C–H activation to afford the perimidinyl complex [IrHCl{$CH(NCH_2PCy_2)_2C_{10}H_6$}(CO)] **LA.3**. The remaining C–H bond could subsequently be activated by use of silver salts in Ir–H abstraction to produce complex [IrHCl{$C(NCH_2PCy_2)_2C_{10}H_6$}(CO)]$^+$ **LA.4** following migration of the perimidinyl hydrogen to the iridium centre.

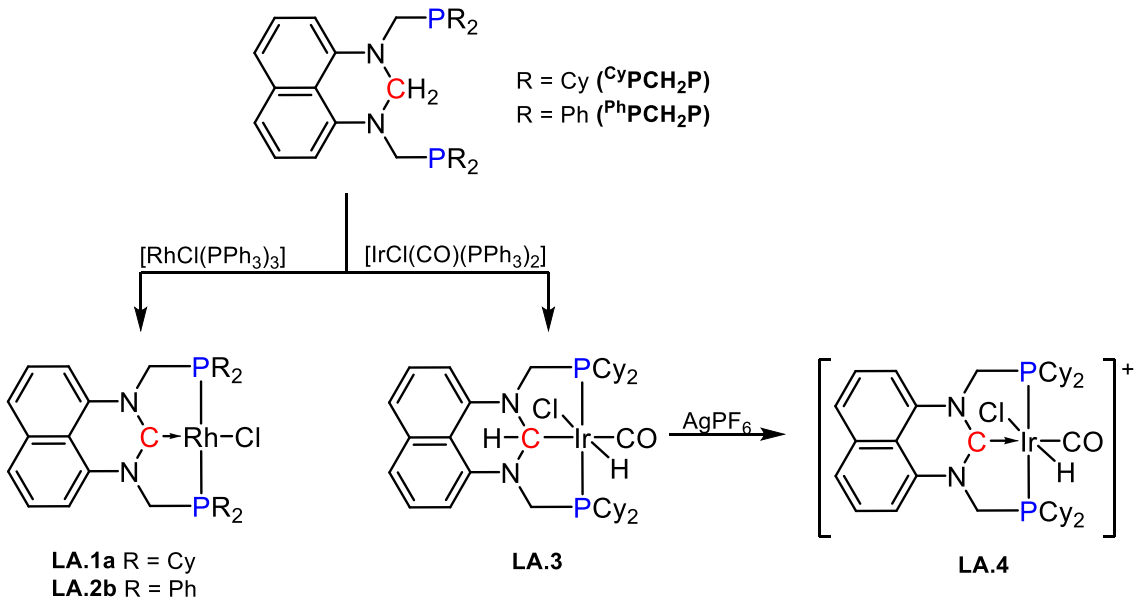

Scheme A.1: Previous reactivity of $^{R}PCH_2P$ (R = Cy, Ph) with rhodium and iridium precursors.

Subsequent research has demonstrated the coordination of $^{R}PCH_2P$ (R = Cy, Ph) onto ruthenium, osmium, nickel and gold.[1,16,17] The mode of coordination (i.e., the degree of C–H activation) has varied across these complexes, and thus, the factors governing metal induced C–H activation remain to be more clearly delineated. Whilst the formation of **LA.2b** occurs quickly, investigations into the iridium analogue previously carried out by

the author has demonstrated reduced propensity for C–H activation.[18] The combination of $^{Ph}PCH_2P$ and $[Ir_2Cl_2(COD)_2]$ yields an isolable non C–H activated intermediate, $[IrCl\{CH_2(NCH_2PPh_2)_2C_{10}H_6\}(COD)]$ **LA.5** (Scheme A.2). Halide abstraction of **LA.5** resulted in single C–H activation to $[IrH\{CH(NCH_2PPh_2)_2C_{10}H_6\}(COD)]^+$ **LA.5**, whereas double C–H activation was thermally induced to afford **LA.6** as the iridium analogue of **LA.2b**.

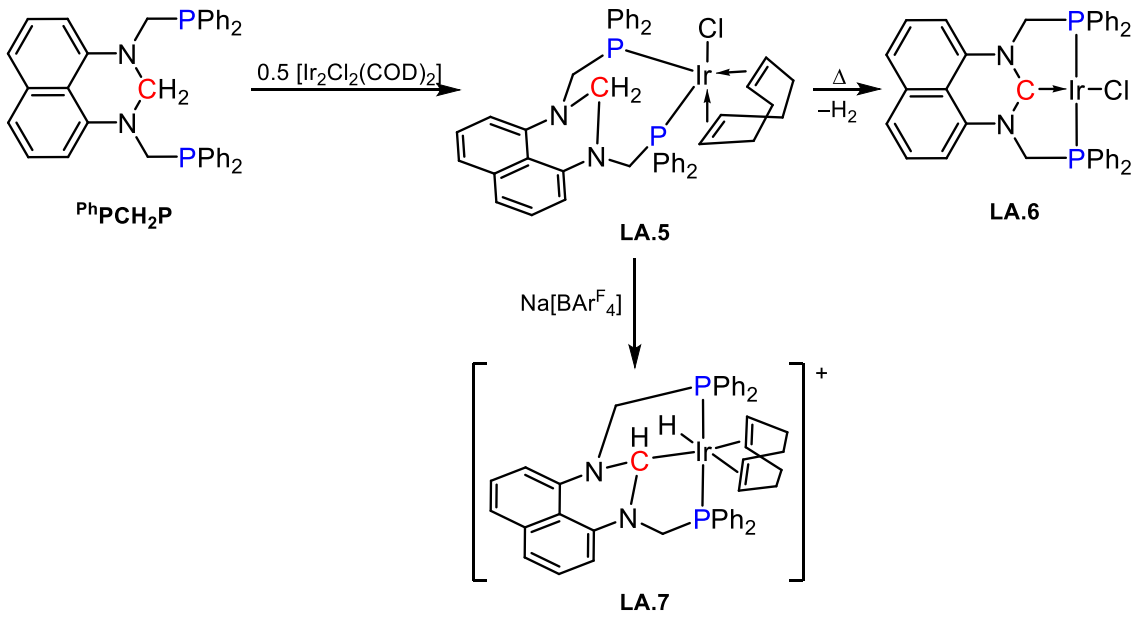

Scheme A.2: Previous exploration of the reactivity of $^{Ph}PCH_2P$ with $[Ir_2Cl_2(COD)_2]$ and subsequent C–H activation processes.

The intriguing difference in propensity for C–H activation was further noted in preliminary unpublished results by McQueen[19], which suggested the formation of *trans*-$[IrH_2Cl\{C(NCH_2PCy_2)_2C_{10}H_6\}]$ *trans*-**A.1** from $^{Cy}PCH_2P$ and $[Ir_2Cl_2(COE)_4]$. Therefore, the preparation of *trans*-**A.1** was revisited and the reactivity subsequently explored to better understand the facility and mechanism of chelate-assisted C–H activation processes.

A.2 Iridium Complexes of Perimidine-based NHC Pincer ligands

A.2.1 Reactivity of *trans*-$[IrH_2Cl\{C(NCH_2PCy_2)_2C_{10}H_6\}]$

Whilst complex *trans*-**A.1** was observed spectroscopically by McQueen, the reported microanalytical analysis did not support its formulation.[19] Based on McQueen's procedure, complex *trans*-**A.1** was prepared in this work and obtained in 64% yield from the reaction of $^{Cy}PCH_2P$ and $[Ir_2Cl_2(COE)_4]$ (1:0.5) in toluene for four hours at room

temperature (Scheme A.3). The reaction completion was noted spectroscopically at 30 minutes and illustrates the facile formation of *trans*-**A.1**. The formulation of *trans*-**A.1** was inferred from spectroscopic data consistent with previously reported, and further supported by satisfactory microanalytical data.

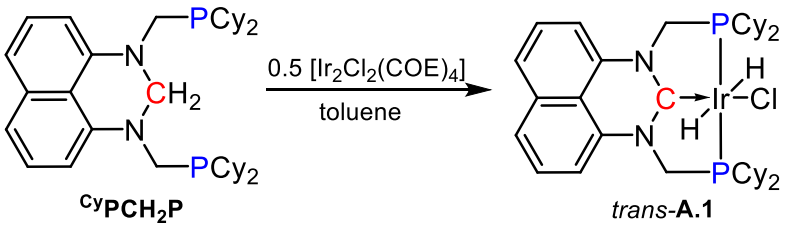

$^{Cy}PCH_2P$ *trans*-**A.1**

Scheme A.3: Synthesis of *trans*-**A.1** modified from McQueen's procedure.

In contrast to the spontaneous reductive elimination of H_2 following the presumed formation of the analogous rhodium complex **LA.1a**, the persistence of the hydrides of *trans*-**A.1** is evident in the solid-state IR spectrum by the low ν_{IrH} frequency of 1772 cm^{-1}, which is characteristic of *trans*-IrH_2 geometry (typically 1700–1800 cm^{-1})[20]. Furthermore, the hydrides are evident in the ^1H NMR spectroscopy as a triplet that integrates as two protons (δ_H = –6.96, $^2J_{HP}$ = 15.8 Hz).

Given that the conversion of non C–H activated **LA.5** to square planar **LA.6** (Scheme A.2) occurs through thermally induced double C–H activation and subsequent reductive elimination, a solution of *trans*-**A.1** was similarly subjected to elevated temperature (70°C) with prolonged heating (40 hours) (Scheme A.4). The desired iridium(I) complex [IrCl{$C(NCH_2PCy_2)_2C_{10}H_6$}] **A.2** was observed spectroscopically with the carbene resonance found at δ_C = 188 through $^1H^{13}C$ HMBC experiments. The formation of **A.2** was also supported by mass spectrometry, the results of which were distinct from those for **A.1**.

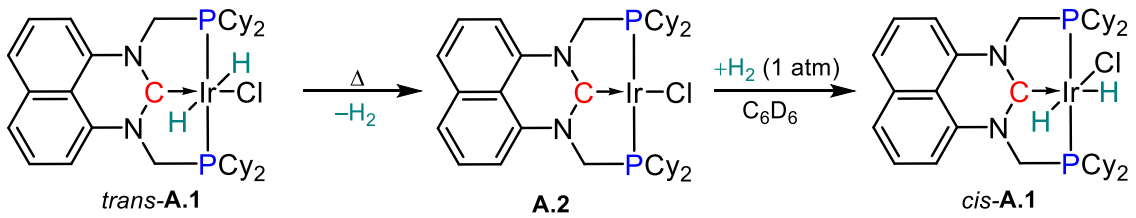

trans-**A.1** **A.2** *cis*-**A.1**

Scheme A.4: Reactivity of *trans*-**A.1**.

Although complex **A.2** eluded clean isolation despite numerous purification attempts, its subsequent reactivity with H_2 (1 atmosphere at room temperature) indicated the formation of the *cis* isomer of **A.1** (Scheme A.4). The *cis*-**A.1** geometry of the complex was noted by two characteristic distinct hydride resonances of doublet of triplet multiplicity at δ_H = –8.78 ($^2J_{HH}$ = 8.0, $^2J_{HP}$ = 15.4 Hz) and δ_H = –20.9 ($^2J_{HH}$ = 8.0, $^2J_{HP}$ = 14.9 Hz). Complex *trans*-**A.1** was only observed in trace amounts, indicating a preference for the formation of the *cis* isomer, as would be expected if the reaction were to proceed *via* a dihydrogen σ-complex.

A.2.2 Synthesis of *cis*-[IrHCl$_2${C(NCH$_2$PCy$_2$)$_2$C$_{10}$H$_6$}]

Dissolution of *trans*-**A.1** in $CHCl_3$ resulted in clean conversion to *cis*-[IrHCl$_2${C(NCH$_2$PCy$_2$)$_2$C$_{10}$H$_6$}] *cis*-**A.3**, which was isolated in high yield (82%) (Scheme A.5). This was indicated by the upfield shift of the *trans*-**A.1** hydride resonance (δ_H = –6.96, $^2J_{HP}$ = 15.8 Hz) to a triplet at δ_H = –18.98 ($^2J_{HP}$ = 12.4 Hz) that integrates for one proton. This implies the selective displacement of one of the hydrides in *trans*-**A.1** by a chloride. Furthermore, the NCH$_2$P methylene groups were observed as two diastereotopically distinct resonances in the ^{1}H NMR spectrum, suggesting a *cis*-IrCl$_2$ geometry in *cis*-**A.3**. The NHC remained intact during formation of *cis*-**A.3** and the carbene carbon was detected at δ_C = 187 *via* ^{1}H^{13}C HMBC experiments.

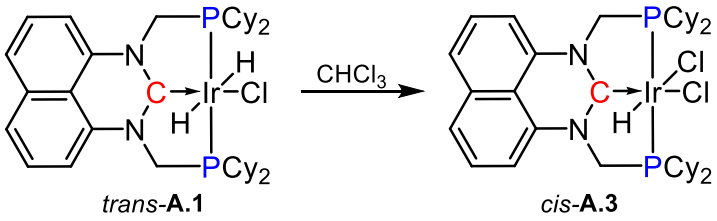

trans-**A.1** *cis*-**A.3**

Scheme A.5: Synthesis of *cis*-**A.3**.

The formation of *cis*-**A.3** proceeded quickly within 30 minutes of solvation in chloroform with no identifiable intermediates detectable by NMR spectroscopy. Therefore, reaction of ^{Cy}PCH$_2$P with the less reactive iridium dimer [Ir$_2$Cl$_2$(COD)$_2$] was explored. An equimolar amount of the two reagents in C_6D_6 was monitored over 38 hours. As depicted in Figure A.2, the gradual consumption of ^{Cy}PCH$_2$P (δ_P = –18.78) over 18 hours was accompanied by the formation of a mixture of three species identified as *trans*-**A.1**, *cis*-**A.3** and **A.2**. At room temperature *trans*-**A.1** appears in minute amounts, whereas the reaction was significantly progressed to *cis*-**A.3** and **A.2** by heating at 60°C.

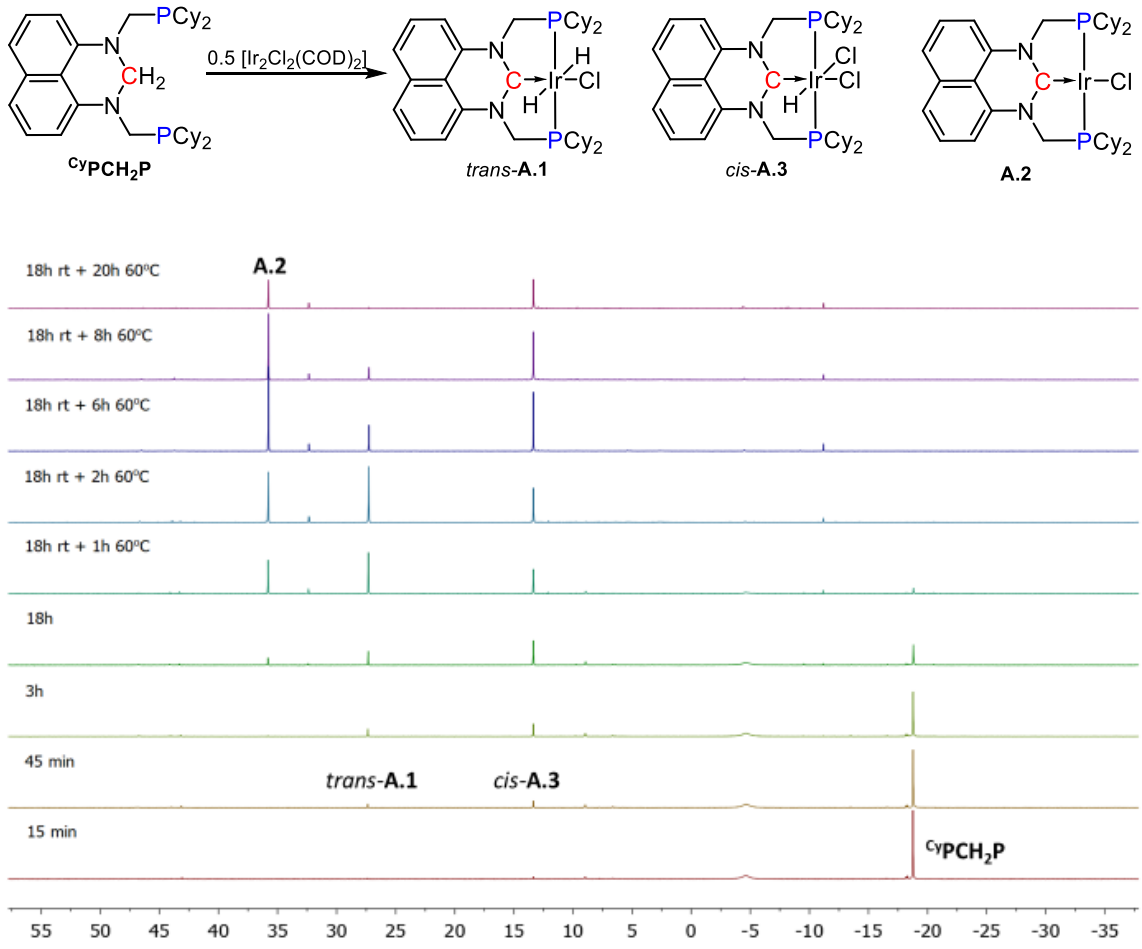

Figure A.2: Reaction of $^{Cy}PCH_2P$ and $[Ir_2Cl_2(COD)_2]$ in C_6D_6 monitored by $^{31}P\{^1H\}$ (121 MHz) NMR spectroscopy.

Although none of the products shown in Figure A.2 could be isolated cleanly, crystals obtained from the crude reaction mixture afforded $[IrCl_3\{C(NCH_2PCy_2)_2C_{10}H_6\}]$ **A.3a** (Figure A.3). The Ir–Cl bond disposed trans to the carbene is notably elongated relative to those of the *trans*-$IrCl_2$ unit (Ir1–Cl1 2.417(1) Å *cf.* Ir1–Cl2 2.328(2) and Ir1–Cl3 2.335(2) Å).

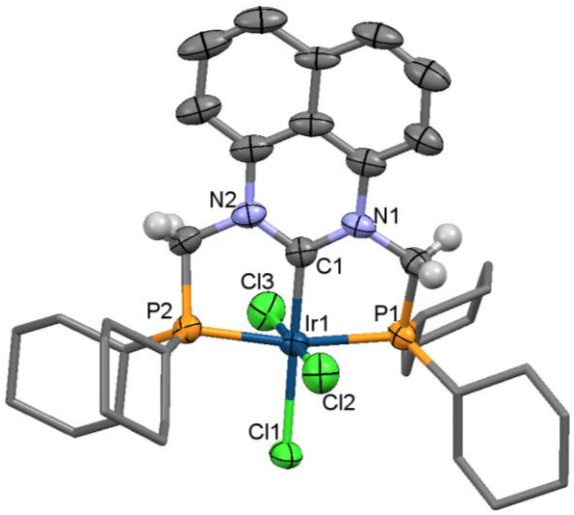

Figure A.3: Molecular structure of $[IrCl_3\{C(NCH_2PCy_2)_2C_{10}H_6\}]$ **A.3a**.$2C_6H_6$ (cyclohexyl and naphthyl hydrogen atoms omitted, displacement ellipsoids shown at 50% probability). Selected bond lengths (Å) and angles (°): Ir1–C1 1.986(5), Ir1–P1 2.307(12), Ir1–P2 2.307(12), Ir1–Cl1 2.417(12), Ir1–Cl2 2.328(17), Ir1–Cl3 2.335(16), C1–N1 1.356(6), C1–N2 1.358(6), C1–Ir1–P1 84.27(15), C1–Ir1–P2 84.04(15), P1–Ir1–P2 168.29(4).

Intentional synthesis of **A.3a** was attempted from the displacement of the hydride in *cis*-**A.3** with various chlorinating agents. However, treatment of *cis*-**A.3** with HCl, $CHCl_3$ or CCl_4 returned only starting material and reaction with *N*-chlorosuccinimide resulted in an inseparable mixture.

A.2.3 Synthesis of $[IrH_3\{C(NCH_2PPh_2)_2C_{10}H_6\}]$

The work discussed thus far demonstrates the propensity of perimidine NHC iridium complexes to support an octahedral geometry and the +III(d^6) oxidation number. Investigations were continued using the $^{Ph}PCH_2P$ framework where circumstantial evidence has previously suggested that C–H activation is less prone with the less electron releasing PPh_2 pincer arms than PCy_2. For example, the reaction of $[RuCl_2(PPh_3)_3]$ with $^{Cy}PCH_2P$ yields the NHC ruthenium complexes $[RuCl_2\{\kappa^3\text{-}C,P,P'\text{-}C(NCH_2PCy_2)_2C_{10}H_6\}(L)]$ (L = PPh_3, THF), while with $^{Ph}PCH_2P$ the non C–H activated complex $[RuCl_2\{\kappa^3\text{-}N,P,P'\text{-}CH_2(NCH_2PPh_2)_2C_{10}H_6\}(PPh_3)]$ was obtained.[1] Similarly, the aminal methylene group remains intact in complex $[IrCl(\eta^4\text{-COD})\{\kappa^2\text{-}P,P'\text{-}CH_2(NCH_2PPh_2)_2C_{10}H_6\}]$ **LA.5** formerly obtained from the reaction of $^{Ph}PCH_2P$ and $[Ir_2Cl_2(COD)_2]$ at room temperature (Scheme A.2).

Thus, the combination of $^{Ph}PCH_2P$ with the more reactive substrate $[Ir_2Cl_2(COE)_4]$ might be expected to better encourage C–H activation processes. Whilst the *trans*-**A.1** formed cleanly and quickly, the analogous reaction between $^{Ph}PCH_2P$ and $[Ir_2Cl_2(COE)_4]$ resulted in a mixture of products at room temperature, and subsequent conversion to **LA.6** upon heating (50°C) for 42 hours (Scheme A.6). A mixture of hydride complexes was noted in the ^1H NMR spectrum, which persisted at elevated temperatures and no complexes were isolated from the intractable mixture.

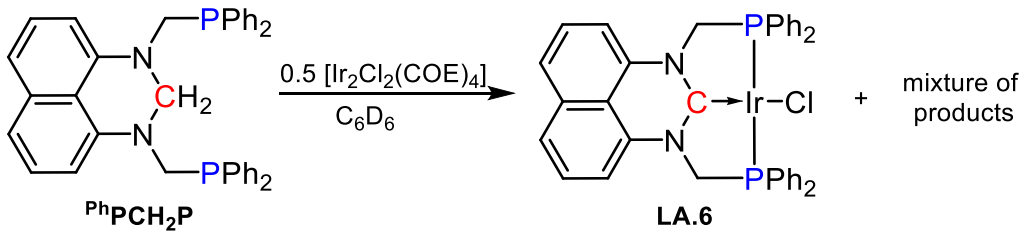

$^{Ph}PCH_2P$ **LA.6**

Scheme A.6: Reaction of $^{Ph}PCH_2P$ and $[Ir_2Cl_2(COE)_4]$.

Given the facile reactivity of square planar **A.2** with H_2, the analogous reaction with the phenyl variant **LA.6** was envisaged as an alternative approach of accessing the ^{Ph}PCP analogues of *trans*/*cis*-**A.1.** However, bubbling of H_2 into a solution of **LA.6** returned starting material unchanged. This may be owing to the less electron rich iridium(I) centre in **LA.6**, compared to complex **A.2** with electron donating PCy_2 groups. However, Vaska's complex *trans*-$[IrCl(CO)(PPh_3)_2]$, which has a less electron rich metal centre readily adds H_2.

The introduction of hydrides to metal centres can in many cases be achieved by using group 13 metal hydride donors such as sodium borohydride. The coordination of BH_4^- as an intact tetrahydroborate was exemplified in complex $[IrH(\kappa^2\text{-}H,H\text{-}H_2BH_2)\{\kappa^2\text{-}P,P,Si\text{-}SiMe(C_6H_4\text{-}2\text{-}P^iPr_2)_2\}]$, which evolves to the dihydride complex $[IrH_2\{\kappa^3\text{-}P,P,Si\text{-}SiMe(C_6H_4\text{-}2\text{-}P^iPr_2)_2\}(CO)]$ in methanol/toluene.[21] Treatment of **LA.6** with excess $NaBH_4$ provided $[IrH_3\{C(NCH_2PPh_2)_2C_{10}H_6\}]$ **A.4** (Scheme A.7) in 77% yield and is the first example of a trihydrido PCP pincer complex.

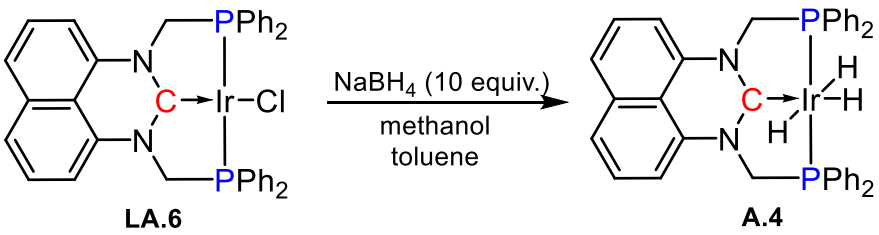

LA.6 **A.4**

Scheme A.7: Synthesis of **A.4**.

The formulation of **A.4** as a trihydride was supported by two resonances appearing in the hydride region as a doublet of triplets at δ_H = –9.95 (2H) and triplet of triplets at δ_H = –10.65 (1H), each with coupling constants of $^2J_{HH}$ = 7.1 and $^2J_{HP}$ = 14.1 Hz. The magnitude of the coupling constants are similar to that of complex [IrH_3{κ^3-*N,P,P'*-$(CH_2P^iPr_2)_2C_5H_3N$}] reported by Nozaki and co-workers ($^2J_{HH}$ = 5, $^2J_{HP}$ = 15 and 17 Hz).[22] Additionally, two ν_{IrH} bands at 1963 and 1739 cm^{-1} were observed in the IR spectrum of **A.4**, consistent with ν_{IrH} 2131 and 1678 cm^{-1} found for complex [IrH_3{κ^3-*N,P,P'*-$(CH_2P^iPr_2)_2C_5H_3N$}].

Successive displacement of the hydride ligands with chloride was achieved from a sample of **A.4** in $CDCl_3$ over three days (Figure A.4). Within two hours both the single and double chloride substituted products *cis*-[IrH_2Cl{$C(NCH_2PPh_2)_2C_{10}H_6$}] *cis*-**A.4a** and *cis*-[$IrHCl_2${$C(NCH_2PPh_2)_2C_{10}H_6$}] *cis*-**A.4b** were present in the ^1H and $^{31}P\{^1H\}$ NMR spectra. The *cis*-IrH_2 geometry of *cis*-**A.4a** was evident by two distinct doublet of triplet resonances at δ_H = –8.73 ($^2J_{HH}$ = 4.2, $^2J_{HP}$ = 15.2 Hz) and δ_H = –20.25 ($^2J_{HH}$ = 4.0, $^2J_{HP}$ = 16.4 Hz). In comparison, the monohydride of *cis*-**A.4b** resonated as a triplet at δ_H = –17.73 ($^2J_{HP}$ = 14.4 Hz). The conversion of *cis*-**A.4a** to *cis*-**A.4b** proceeded slowly and reaction completion was reached after 72 hours. The independent hydride displacement reactions of *cis*-**A.4a** and *trans*-**A.1** in chloroform both result in dichloro iridium(III) products. However, conversion of *trans*-**A.1** to *cis*-**A.3** proceeds substantially faster than the formation of *cis*-**A.4b** from *cis*-**A.4a**.

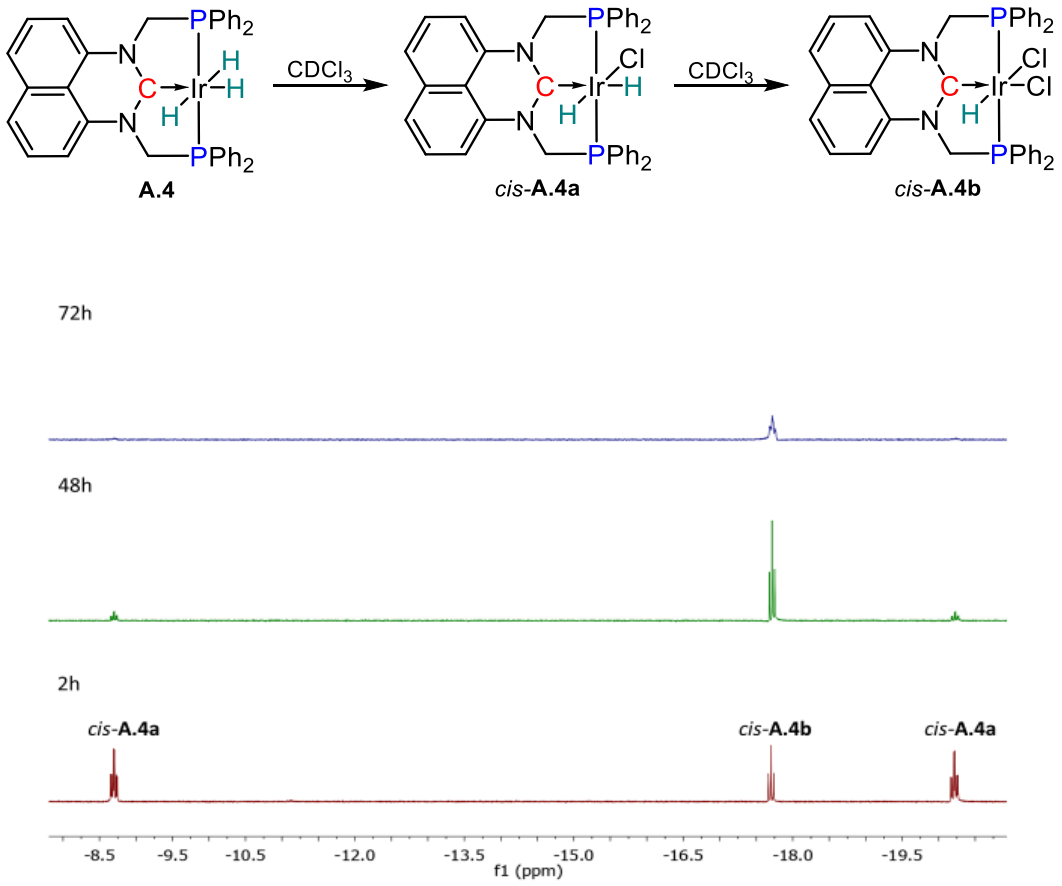

Figure A.4: Conversion of **A.4** to *cis*-**A.4a** and *cis*-**A.4b** in $CDCl_3$, observed by ^1H (400 MHz) NMR spectroscopy. Hydride region shown.

A.3 Conclusion

Further examples of perimidine based NHC iridium complexes are reported and provided insight into the factors governing C–H activation and subsequent reactivity of the complexes. Installation of the $^{Cy}PCH_2P$ ligand on iridium proceeds favourably through C–H activation with regioselectivity of the resulting complex (*trans*-$[IrH_2Cl\{C(NCH_2PCy_2)_2C_{10}H_6\}]$ *trans*-**A.1**), which hinders subsequent reductive elimination processes. Whilst the square planar ^{Cy}PCP complex ($[IrCl\{C(NCH_2PCy_2)_2C_{10}H_6\}]$ **A.2**) readily reacted with dihydrogen to form isomers *trans*/*cis*-**A.1**, the less electron rich ^{Ph}PCP complex ($[IrCl\{C(NCH_2PPh_2)_2C_{10}H_6\}]$ **LA.6**) was reluctant to oxidatively add dihydrogen. However, the iridium(III) hydride complexes of both ligand frameworks were susceptible to hydride substitution reactions, ultimately affording the *cis*-chloro complexes $[IrHCl_2\{C(NCH_2PR_2)_2C_{10}H_6\}]$ (R = Cy *cis*-**A.3**, Ph *cis*-**A.4b**).

A.4 Future Work

The complexes synthesised here showed reactivity directed at the coordination site of the metal, which further illustrated the concept of NHCs as spectator ligands with innocent Ir=C carbene units. On the contrary, reactions at the M=C bond are intriguing for potential reversible C–H activation (i.e. hydrogenation of M=C). This has been elegantly demonstrated by Piers in bis(2-phosphinoaryl)methane systems with Ir=C reactivity towards H_2 and epoxidation.[23-26] Thus, further understanding of the factors controlling chelate assisted C–H activation may arise should the Ir=C unit participate in reactions.

A.5 References

(1) Hill, A. F.; McQueen, C. M. A. *Organometallics* **2014**, *33*, 1909.
(2) Wang, W.; Cui, L.; Sun, P.; Shi, L.; Yue, C.; Li, F. *Chem. Rev.* **2018**.
(3) Froese, R. D. J.; Lombardi, C.; Pompeo, M.; Rucker, R. P.; Organ, M. G. *Acc. Chem. Res.* **2017**, *50*, 2244.
(4) Dorta, R.; Stevens, E. D.; Scott, N. M.; Costabile, C.; Cavallo, L.; Hoff, C. D.; Nolan, S. P. *J. Am. Chem. Soc.* **2005**, *127*, 2485.
(5) Chianese, A. R.; Li, X.; Janzen, M. C.; Faller, J. W.; Crabtree, R. H. *Organometallics* **2003**, *22*, 1663.
(6) Cavallo, L.; Correa, A.; Costabile, C.; Jacobsen, H. *J. Organomet. Chem.* **2005**, *690*, 5407.
(7) Crudden, C. M.; Allen, D. P. *Coord. Chem. Rev.* **2004**, *248*, 2247.
(8) Praetorius, J. M.; Crudden, C. M. *RSC Catal. Ser.* **2011**, *6*, 77.
(9) Bazinet, P.; Yap, G. P. A.; Richeson, D. S. *J. Am. Chem. Soc.* **2003**, *125*, 13314.
(10) Bazinet, P.; Ong, T.-G.; O'Brien, J. S.; Lavoie, N.; Bell, E.; Yap, G. P. A.; Korobkov, I.; Richeson, D. S. *Organometallics* **2007**, *26*, 2885.
(11) Herrmann, W. A.; Schütz, J.; Frey, G. D.; Herdtweck, E. *Organometallics* **2006**, *25*, 2437.
(12) Özdemir, İ.; Alıcı, B.; Gürbüz, N.; Çetinkaya, E.; Çetinkaya, B. *J. Mol. Catal. A: Chem.* **2004**, *217*, 37.
(13) Tu, T.; Malineni, J.; Bao, X.; Dötz, K. H. *Adv. Synth. Catal.* **2009**, *351*, 1029.
(14) Hill, A. F.; McQueen, C. M. A. *Organometallics* **2012**, *31*, 8051.
(15) Peris, E. *Top. Organomet. Chem.* **2007**, *21*, 83.
(16) McQueen, C. M. A.; Hill, A. F.; Ma, C.; Ward, J. S. *Dalton Trans.* **2015**, *44*, 20376.
(17) Krieck, S.; Schulze, D.; Goerls, H.; Westerhausen, M. *Z. Naturforsch., B: J. Chem. Sci.* **2014**, *69*, 1299.
(18) Ma, C. Honours Thesis, The Australian National University, 2014.
(19) McQueen, C. M. A. PhD thesis, The Australian National University, 2013.
(20) Malatesta, L.; Caglio, G.; Angoletta, M. *J. Chem. Soc.* **1965**, 6974.
(21) Suárez, E.; Plou, P.; Gusev, D. G.; Martín, M.; Sola, E. *Inorg. Chem.* **2017**, *56*, 7190.
(22) Tanaka, R.; Yamashita, M.; Nozaki, K. *J. Am. Chem. Soc.* **2009**, *131*, 14168.
(23) Burford, R. J.; Piers, W. E.; Parvez, M. *Organometallics* **2012**, *31*, 2949.
(24) Burford, R. J.; Piers, W. E.; Ess, D. H.; Parvez, M. *J. Am. Chem. Soc.* **2014**, *136*, 3256.
(25) Doyle, L. E.; Piers, W. E.; Borau-Garcia, J. *J. Am. Chem. Soc.* **2015**, *137*, 2187.
(26) Doyle, L. E.; Piers, W. E.; Borau-Garcia, J.; Sgro, M. J.; Spasyuk, D. M. *Chem. Sci.* **2016**, *7*, 921.